Universität Potsdam

Potsdam University Press

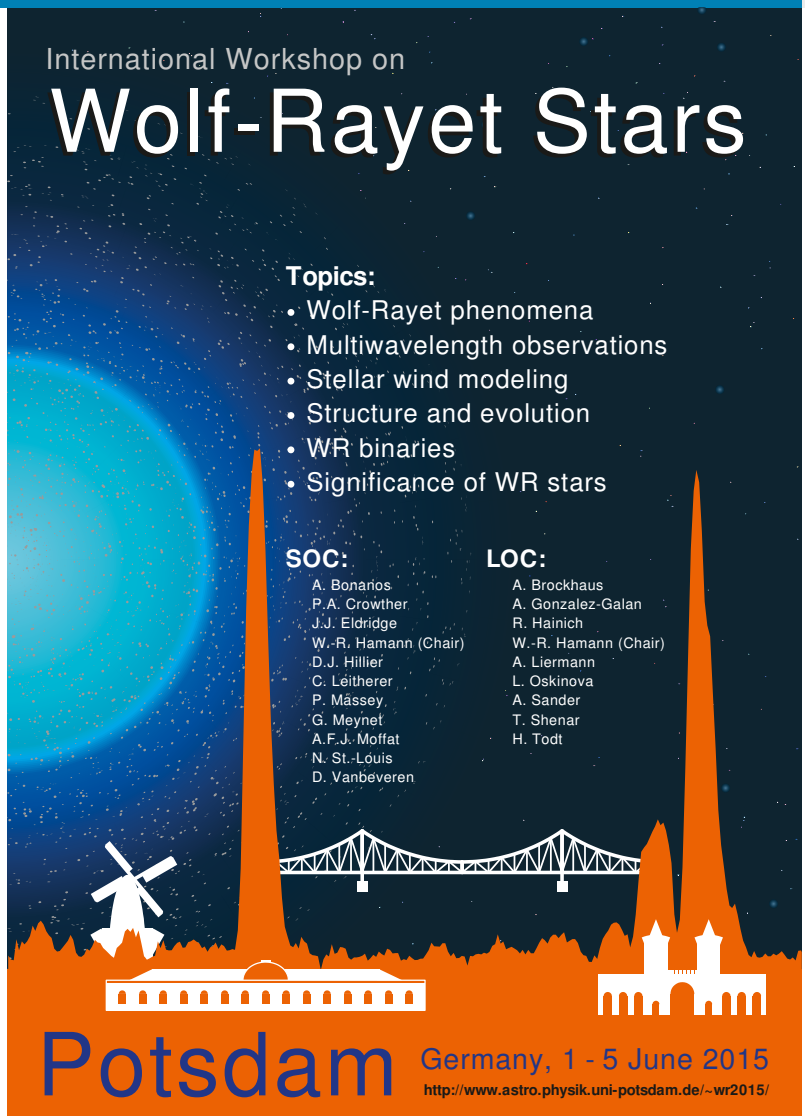

Wolf-Rainer Hamann | Andreas Sander | Helge Todt (Eds.)

Wolf-Rayet Stars

Proceedings of an International Workshop held in Potsdam, Germany, 1.–5. June 2015

University of Potsdam

Wolf-Rayet Stars

Wolf-Rainer Hamann | Andreas Sander | Helge Todt (Eds.)

Wolf-Rayet Stars

Proceedings of an International Workshop held
in Potsdam, Germany, 1.–5. June 2015

Potsdam University Press

Bibliographic information published by the Deutsche Nationalbibliothek
The Deutsche Nationalbibliothek lists this publication in the Deutsche Nationalbibliografie; detailed bibliographic data are available in the Internet at http://dnb.dnb.de.

Potsdam University Press 2016
http://verlag.ub.uni-potsdam.de/

Am Neuen Palais 10, 14469 Potsdam
Tel.:+49 (0)331 977 2533/ Fax: 2292
E-Mail: verlag@uni-potsdam.de

Published online at the Institutional Repository of the University of Potsdam:
URN urn:nbn:de:kobv:517-opus4-84268
http://nbn-resolving.de/urn:nbn:de:kobv:517-opus4-84268

Abstract

Nearly 150 years ago, the French astronomers Charles Wolf and Georges Rayet described stars with very conspicuous spectra that are dominated by bright and broad emission lines. Meanwhile termed *Wolf-Rayet Stars* after their discoverers, those objects turned out to represent important stages in the life of massive stars.

As the first conference in a long time that was specifically dedicated to Wolf-Rayet stars, an international workshop was held in Potsdam, Germany, from 1. – 5. June 2015. About 100 participants, comprising most of the leading experts in the field as well as as many young scientists, gathered for one week of extensive scientific exchange and discussions. Considerable progress has been reported throughout, e.g. on finding such stars, modeling and analyzing their spectra, understanding their evolutionary context, and studying their circumstellar nebulae. While some major questions regarding Wolf-Rayet stars still remain open 150 years after their discovery, it is clear today that these objects are not just interesting stars as such, but also keystones in the evolution of galaxies.

These proceedings summarize the talks and posters presented at the Potsdam Wolf-Rayet workshop. Moreover, they also include the questions, comments, and discussions emerging after each talk, thereby giving a rare overview not only about the research, but also about the current debates and unknowns in the field. The Scientific Organizing Committee (SOC) included Alceste Bonanos (Athens), Paul Crowther (Sheffield), John Eldridge (Auckland), Wolf-Rainer Hamann (Potsdam, Chair), John Hillier (Pittsburgh), Claus Leitherer (Baltimore), Philip Massey (Flagstaff), George Meynet (Geneva), Tony Moffat (Montréal), Nicole St-Louis (Montréal), and Dany Vanbeveren (Brussels).

List of participants

Aldoretta, Emily	Universite de Montreal, Canada
Aliçavus, Fahri	Çanakkale Onsekiz Mart University, Physics Depertmant, Turkey, Turkey
Arthur, Jane	Centro de Radioastronomia y Astrofisica, UNAM, Mexico
Becker, Alexander	Astronomical Institute of the Ruhr-University Bochum, Germany
Beradze, Sopia	Abastumani Astrophysical Observatory, Ilia State University, Georgia
Bestenlehner, Joachim	Max Planck Institute for Astronomy, Germany
Bibby, Joanne	University of Central Lancashire, United Kingdom
Bomans, Dominik	Astronomical Institute of the Ruhr-University Bochum, Germany
Calderón Espinoza, Diego	Instituto de Astrofísica, Pontificia Universidad Católica de Chile, Chile
Chené, André-Nicolas	Gemini Observatory, USA
Cherchneff, Isabelle	Basel University, Switzerland
Conti, Peter	JILA, Boulder CO, USA
Corcoran, Michael	USRA & NASA-GSFC, USA
Crowther, Paul	University of Sheffield, UK
Dessart, Luc	Observatoire de la Cote d'Azur, France
Dwarkadas, Vikram	University of Chicago, USA
Eldridge, John	The University of Auckland, New Zealand
Eversberg, Thomas	Schnörringen Telescope Science Institute (STScI), Germany
Falceta-Gonçalves, Diego	Univ. of St Andrews, United Kingdom
Georgy, Cyril	Keele University, United Kingdom
González-Galán, Ana	University of Potsdam, Germany
Gormaz-Matamala, Alex	Universidad de Concepción, Chile
Gosset, Eric	Institut d'Astrophysique, Liege University, Belgique
Grassitelli, Luca	Argelander Institute for Astronomy, Germany
Groh, Jose	Geneva Observatory, Switzerland
Gräfener, Götz	Armagh Observatory, United Kingdom
Guerrero, Martín A	IAA, Spain
Gull, Ted	NASA/GSFC, USA
Gómez-González, Víctor	INAOE, Tonantzintla, Puebla, México
Hainich, Rainer	University of Potsdam, Germany
Hamaguchi, Kenji	NASA@GSFC & UMBC, USA
Hamann, Wolf-Rainer	University Potsdam, Germany, Germany
Hendrix, Tom	CmPA, KU Leuven, Belgium
Hillier, D. John	University of Pittsburgh, USA
Hoffman, Jennifer L.	University of Denver, USA
Huenemoerder, David	MIT, United States
Ignace, Richard	East Tennessee State University, USA
Kanarek, Graham	Columbia University / American Museum of Natural History, USA
Kehrig, Carolina	Instituto de Astrofisica de Andalucia (IAA-CSIC), Spain
Kochiashvili, Nino	Abastumani Astrophysical Observatory, Ilia State University, Georgia
Koenigsberger, Gloria	UNAM- Instituto de Ciencias Fisicas, Mexico
Kourniotis, Michalis	National Observatory of Athens, Greece
Kubátová, Brankica	Astronomical Institute Ondrejov, Czech Republic
Küker, Manfred	Leibniz-Institut für Astrophysik Potsdam, Germany
Langer, Norbert	Uni Bonn, Germany
Leitherer, Claus	STScI, USA
Leyder, Jean-Christophe	European Space Agency (ESA), Spain
Liermann, Adriane	AIP, Germany
Lynas-Gray, Anthony Eugene	University of Oxford, UK
Madura, Thomas	NASA Goddard Space Flight Center, USA
Marston, Anthony	ESA, Spain
Maryeva, Olga	Special Astrophysical observatory, Russia, Russia
Massey, Philip	Lowell Observatory, USA
McClelland, Liam	University of Auckland, Department of Physics, New Zealand
Mesa-Delgado, Adal	Pontificia Universidad Católica de Chile, Chile
Meynet, Georges	Geneva Observatory, University of Geneva, Switzerland
Miller Bertolami, Marcelo Miguel	Max Planck Institute for Astrophysics, Germany

Miszalski, Brent	SAAO, South Africa
Moffat, Anthony (Tony)	Universite de Montreal, Canada
Mohamed, Shazrene	South African Astronomical Observatory, South Africa
Morris, Patrick	Caltech, US
Muñoz, Melissa	Université de Montréal, Canada
Najarro, Francisco	CAB, CSIC-INTA , Spain
Nebot, Ada	Observatoire Astronomique de Strasbourg, France
Neugent, Kathryn	Lowell Observatory, USA
Oskinova, Lidia	University of Potsdam, Germany
Pablo, Herbert	University of Montreal, H3S 2C4
Pollock, Andy	Computer & Scientific Co. Ltd., England
Ramírez Alegría, Sebastian	Universidad de Valparaiso / MAS, Chile
Reyes-Pérez, Jonnathan	Instituto de Astronomia, UNAM, Mexico
Reyes Iturbide, Jorge	Instituto de Ciencias Nucleares (Universidad Nacional De México), Mexico
Ro, Stephen	University of Toronto, Canada
Roman-Lopes, Alexandre	Universidad de La Serena, Chile
Rosslowe, Christopher	University of Sheffield, United Kingdom
Russell, Christopher	NASA GSFC, USA
Sander, Andreas	University of Potsdam, Germany
Sanyal, Debashis	Argelander Institut für Astronomie, Universität Bonn, Germany
Schnurr, Olivier	Leibniz-Institut f. Astrophysik Potsdam (AIP), Germany
Shacham, Tomer	Jerusalem, Israel
Shenar, Tomer	University of Potsdam, Germany
Sokal, Kimberly	University of Virginia, U.S.A.
Srivastava, Shweta	Physical Research Laboratory, Ahmedabad, India, India
St-Louis, Nicole	Université de Montréal, Canada
Steinke, Martin	University Potsdam, Germany
Sugawara, Yasuharu	Chuo University, Japan
Szécsi, Dorottya	Argelander-Institut für Astronomie, Bonn, Germany, Germany
Toalá, Jesús A.	Instituto de Astrofisica de Andalucia - CSIC, Spain
Todt, Helge	University of Potsdam, Germany
Tramper, Frank	University of Amsterdam, Netherlands
Vanbeveren, Dany	K.U.Leuven and Vrije Universiteit Brussel, Belgium
Vink, Jorick	Armagh Observatory, UK
Walsh, Jeremy	ESO, Germany
Weis, Kerstin	Astronomisches Institut, Ruhr-Universität Bochum, Germany
Williams, Peredur	Royal Observatory Edinburgh, United Kingdom
Wofford, Aida	Institut d'Astrophysique de Paris, France

Table of Contents

Opening 11

A. F. J. Moffat
General overview of Wolf-Rayet stars 13

WR surveys 19

P. A. Crowther
Wolf-Rayet content of the Milky Way 21
A. P. Marston, J. Mauerhan, P. W. Morris, S. Van Dyk
Finding Wolf-Rayet Stars in the Milky Way: Inputs to Star Formation and Stellar Evolution 27
A. Roman-Lopes, G. A. P. Franco, D. Sanmartin
SOAR Near-Infrared and Optical Survey of OIf* and OIf*/WN Stars in the Periphery of Galactic Massive Star Forming Regions 31
P. Massey, K. F. Neugent, N. I. Morrell
Finding Wolf-Rayet Stars in the Local Group 35
V. M. A. Gómez-González, Y. D. Mayya, D. Rosa-González
Detection and Characterization of Wolf-Rayet stars in M81 with GTC/OSIRIS spectra and HST images 43
A. Becker, D. J. Bomans, K. Weis
Finding new Wolf-Rayet stars in the Magellanic Clouds 47
D. J. Bomans, A. Becker, B. Kleemann, K. Weis, A. Pasquali
Luminous Wolf-Rayet stars at low metallicity 51
C. Kehrig, J. M. Vílchez, E. Pérez-Montero, J. Iglesias-Páramo, J. Brinchmann, P. A. Crowther, F. Durret, D. Kunth
PopIII-star siblings in IZw18 and metal-poor WR galaxies unveiled from integral field spectroscopy 55
S. Srivastava, C. Kehrig, N. G. Kantharia, E. Pérez-Montero, J. M. Vílchez, J. Iglesias-Páramo, P. Janardhan
A 2D view of Wolf-Rayet Galaxies 59

WR spectroscopy and polarimetry 63

D. J. Hillier
Spectrum formation in Wolf-Rayet stars 65
T. Eversberg, E. J. Aldoretta, J. H. Knapen, A. F. J. Moffat, T. Morel, T. Ramiaramanantsoa, G. Rauw, N. D. Richardson, N. St-Louis, M. Teodoro
World-wide amateur observations - A viable future of massive star research 71
E. J. Aldoretta, N. St-Louis, N. D. Richardson, A. F. J. Moffat, T. Eversberg, G. M. Hill
The Results of the 2013 Pro-Am Wolf-Rayet Campaign 75
N. St-Louis
Studying Large and Small Scale Wind Asymmetries with Spectroscopy and Polarimetry . . 79
J. L. Hoffman, J. R. Lomax
Structure and fate of binary WR stars: Clues from spectropolarimetry 85

WR spectral analysis, parameters, and wind theory 89

W.-R. Hamann
Wind models and spectral analyses 91
A.-N. Chené, D. Wyrick, J. Borissova, M. Kuhn, A. Hervé, S. Ramírez Alegría, C. Bonatto, J.-C. Bouret, R. Kurtev
Improving distances to Galactic Wolf-Rayet stars 97
K. F. Neugent, P. Massey, D. J. Hillier, N. I. Morrell
The Discovery and Physical Parameterization of a New Type of Wolf-Rayet Star 101

C. K. Rosslowe, P. A. Crowther, J. S. Clark, I. Negueruela
Physical properties of the WR stars in Westerlund 1 . . . 105
F. Tramper, S. M. Straal, D. Sanyal, H. Sana, A. de Koter, G. Gräfener, N. Langer, J. S. Vink, S. E. de Mink, L. Kaper
Massive Wolf-Rayet stars on the verge to explode: the properties of the WO stars . . . 109
F. Najarro, D. de la Fuente, T. R. Geballe, D. F. Figer, D. J. Hillier
The WR population in the Galactic Center . . . 113
R. Hainich, U. Rühling, D. Pasemann, W.-R. Hamann
The WN population in the Magellanic Clouds . . . 117
M. Kourniotis, A. Bonanos, F. Najarro
Accurate parameters of massive binaries in the Danks clusters . . . 121
B. Kubátová, W.-R. Hamann, H. Todt, A. Sander, M. Steinke, R. Hainich, T. Shenar
Macroclumping in WR136 . . . 125
A. Liermann
Evolution of Wolf-Rayet spectra . . . 129
J. S. Vink
The True origin of Wolf-Rayet stars . . . 133
A. Sander, W.-R. Hamann, R. Hainich, T. Shenar, H. Todt
Hydrodynamic modeling of massive star atmospheres . . . 139
M. Küker
Magnetopsheres of massive stars . . . 143

Eta Car, LBVs . . . 147

T. R. Gull
Eta Carinae: Many Advances .... Even More Puzzles . . . 149
P. W. Morris
Measuring η Carinae's High Mass Ejecta in the Infrared and Sub-millimeter . . . 155
K. Hamaguchi, M. F. Corcoran
Extremely Hard X-ray Emission from η Car Observed with XMM-Newton and NuSTAR around [1.5mm] Periastron in 2014.6 . . . 159
T. I. Madura, N. Clementel, T. R. Gull, C. J. H. Kruip, J.-P. Paardekooper, V. Icke
3D hydrodynamical and radiative transfer modeling of η Carinae's colliding winds . . . 163
K. Weis
Family ties of WR to LBV nebulae yielding clues for stellar evolution . . . 167
G. Koenigsberger
HD5980: wind collisions and binary star evolution . . . 171

Structure & Evolution of WR stars . . . 175

J. J. Eldridge, L. A. S. McClelland, L. Xiao, E. R. Stanway, J. Bray
The importance of getting single-star and binary physics correct. . . . 177
G. Meynet, C. Georgy, A. Maeder, S. Ekström, J. H. Groh, F. Barblan, H. F. Song, P. Eggenberger
Physics of massive stars relevant for the modeling of Wolf-Rayet populations . . . 183
D. Szécsi, N. Langer, D. Sanyal, C. J. Evans, J. M. Bestenlehner, F. Raucq
Do rapidly-rotating massive stars at low metallicity form Wolf–Rayet stars? . . . 189
T. Shenar, W.-R. Hamann, H. Todt
The impact of rotation on the line profiles of Wolf-Rayet stars . . . 193
L. A. S. McClelland, J. J. Eldridge
Helium stars: Towards an understanding of Wolf–Rayet evolution . . . 197
L. Grassitelli, N. Langer, D. Sanyal, L. Fossati, J. M. Bestenlehner
Instabilities in the envelope of Wolf-Rayet stars . . . 201
H. Pablo, A. F. J. Moffat
WR Time Series Photometry: A Forest of Possibilities . . . 205
T. Shacham, I. Idan, N. J. Shaviv
A new mechanism for long long-term pulsations of hot stars? . . . 209
D. Sanyal, T. J. Moriya, N. Langer
Envelope inflation in Wolf-Rayet stars and extended supernova shock breakout signals . . . 213

D. Vanbeveren, N. Mennekens
Massive star population synthesis with binaries . . . 217
M. Munoz, A. F. J. Moffat, G. M. Hill, N. D. Richardson, H. Pablo
The missing Wolf-Rayet X-ray binary systems . . . 225
C. Georgy, S. Ekström, R. Hirschi, G. Meynet, J. H. Groh, P. Eggenberger
Wolf-Rayet stars as an evolved stage of stellar life . . . 229
A. Wofford, S. Charlot, J. J. Eldridge
Properties of LEGUS Clusters Obtained with Different Massive-Star Evolutionary Tracks. 233
J. H. Groh
The end stages of massive star evolution: WR stars as SN Ibc progenitors . . . 237
N. Langer, D. Sanyal, L. Grassitelli, D. Szécsi
The stellar Eddington limit . . . 241
L. Dessart
Wolf-Rayet stars as supernova progenitors . . . 245

WR-type central stars of PNe . . . 251

H. Todt, W.-R. Hamann
Wolf-Rayet central stars of planetary nebulae . . . 253
B. Miszalski, R. Manick, V. McBride
Post-common-envelope Wolf-Rayet central stars of planetary nebulae . . . 259
M. A. Guerrero
Planetary nebulae and Their Central Stars in X-rays . . . 263

WR colliding winds, dust . . . 267

I. Cherchneff
Dust formation in carbon-rich Wolf-Rayet colliding winds . . . 269
P. M. Williams, K. A. van der Hucht
The colliding-wind WC9+OB system WR 65 and dust formation by WR stars . . . 275
T. Hendrix, R. Keppens
Modelling colliding wind binaries in 2D . . . 279
S. Mohamed, J. Mackey, N. Langer, Ph. Podsiadlowski
Shaping the outflows of Wolf-Rayet stars . . . 283
D. Falceta-Gonçalves
Magnetic fields, non-thermal radiation and particle acceleration in colliding winds of WR-O stars . . . 289

X-rays and WR stars . . . 293

L. M. Oskinova
X-ray emission from single WR stars . . . 295
D. Huenemoerder, K. Gayley, W.-R. Hamann, R. Ignace, J. Nichols, L. M. Oskinova, A. M. T. Pollock, N. Schulz
High Resolution X-Ray Spectra of WR 6 . . . 301
E. Gosset
Studies of WR+O colliding-wind binaries . . . 305
C. M. P. Russell, M. F. Corcoran, J. Cuadra, S. P. Owocki, Q. D. Wang, K. Hamaguchi, Y. Sugawara, A. M. T. Pollock, T. R. Kallman
Hydrodynamic and radiative transfer modeling of X-ray emission from colliding WR winds: WR 140 & the Galactic center . . . 309

WR nebulae . . . 313

S. J. Arthur
Wolf-Rayet nebulae and the wind-interstellar medium interaction . . . 315
J. Reyes-Pérez, C. Morisset, M. Penã, A. Mesa-Delgado
A consistent spectral model of WR 136 and its associated bubble NGC 6888 . . . 321

A. Mesa-Delgado, C. Esteban, J. García-Rojas
Ring Nebulae: Tracers of the CNO Nucleosynthesis . . . 325
V. V. Dwarkadas, D. Rosenberg
X-ray Emission from Ionized Wind-Bubbles around Wolf-Rayet Stars . . . 329
J. A. Toalá, M. A. Guerrero, Y.-H. Chu, S. J. Arthur, R. A. Gruendl
Diffuse X-ray Emission within Wolf-Rayet Nebulae . . . 333
K. R. Sokal, K. E. Johnson, P. Massey, R. Indebetouw
The importance of Wolf-Rayet ionization and feedback on super star cluster evolution . . . 337
J. R. Walsh, A. Monreal-Ibero, J. M. Vílchez, E. Pérez-Montero, J. Iglesias-Páramo, C. Sandin, M. Relaño, R. Amorín
The Wolf-Rayet Population and ISM Interaction in Nearby Starburts . . . 341

Closing session . . . 345

P. S. Conti
Concluding Remarks . . . 347

Posters . . . 351

S. Beradze, N. Kochiashvili, R. Natsvlishvili, I. Kochiashvili, E. Janiashvili, T. Urushadze, M. Vardosanidze
P Cygni and its Observations at the Abastumani Observatory . . . 353
J. M. Bestenlehner
Stellar parameters from photometric data for fainter and more distant Wolf-Rayet stars . . 354
J. Bibby, M. Shara, D. Zurek, P. A. Crowther, A. F. J. Moffat, L. Drissen, M. Wilde
The Distribution of Massive Stars in M101 . . . 355
D. Calderón, A. Ballone, J. Cuadra, M. Schartmann, A. Burkert, S. Gillessen
Formation of the infalling Galactic Centre cloud G2 by collision of stellar winds . . . 356
A. C. Gormaz-Matamala, A. Hervé, A.-N. Chené, M. Curé, R. E. Mennickent
Results Of The Spectroscopic Analysis Of WR6 Using CMFGEN . . . 357
R. Ignace, J. A. Toalá, L. M. Oskinova
Inversion of Intensity Profiles for Bubble Emissivity . . . 358
G. Kanarek, M. Shara, J. Faherty, D. Zurek, A. F. J. Moffat
New Galactic Wolf-Rayet Stars . . . 359
N. Kochiashvili, S. Beradze, I. Kochiashvili, R. Natsvlishvili, M. Vardosanidze
New Photometric Observations of P Cygni . . . 360
O. Maryeva, V. F. Polcaro, C. Rossi, R. Viotti
Modeling of spectral variability of Romano's star . . . 361
S. Ramírez Alegría, A.-N. Chené, J. Borissova, R. Kurtev, C. Navarro, M. Kuhn, J. A. Carballo-Bello
A not so massive cluster hosting a very massive star . . . 362
J. Reyes-Iturbide, P. F. Velázquez, M. Rosado
3D numerical model for NGC 6888 Nebula . . . 363
S. Ro, C. D. Matzner
Envelope Inflation or Stellar Wind? . . . 364
M. Steinke, L. M. Oskinova, W.-R. Hamann, A. Sander
The Wolf-Rayet stars WR102c and 102ka and their isolation . . . 365
Y. Sugawara, Y. Tsuboi, Y. Maeda, A. M. T. Pollock, P. M. Williams
The Swift monitoring of the colliding wind binary WR 21a . . . 366

Opening

Wolf-Rayet Stars
W.-R. Hamann, A. Sander, H. Todt, eds.
Potsdam: Univ.-Verlag, 2015
URL: http://nbn-resolving.de/urn:nbn:de:kobv:517-opus4-84268

General overview of Wolf-Rayet stars

A. F. J. Moffat
Université de Montréal, Canada

Although we all use the name Wolf-Rayet to refer to specific groups of stars, "Wolf-Rayet" *per se* is really an astrophysical phenomenon of fast-moving, hot plasma, normally expanding around a hot star. However, expediency demands that we follow established traditions by referring to three specific kinds of WR stars: (1) cWR, "classical" He-burning descendants of massive, O-type stars, presumably all of which pass through a WR stage; (2) WNh, the most massive and luminous hydrogen-rich main-sequence stars with strong winds; and (3) [WR], the central stars of some 15 % of Planetary Nebulae. Wolf-Rayet stars are the epitome of relatively stable stars with the highest mass-loss rates for their kind. It behooves us to understand the what, how and why of this circumstance, along with its manyfold and fascinating consequences.

1 Dedication

This talk is devoted to my first real WR contact and inspiration: Lindsey F. Smith. I first encountered Lindsey in 1968 when I was a doctoral student in Bonn, Germany, where she gave a colloquium on her freshly-minted Australian PhD thesis work with Bengt Westerlund on WR stars. We also met at various places thereafter, including the Elba IAU Symposium 163 on hot luminous stars in 1994, where on the banquet dance-floor I was able to convince her that "See, Lindsey, they *do* rotate after all!" I also salute "Wolf-Rayet" Hamann, our PoWRful Prussian-based hot-star king, who took the lead in organizing this extraordinary workshop. And finally, I cannot forget that 1867 was a great year, marked by the discovery at l'Observatoire de Paris of the first three WR stars (WR134, 135 & 137 in Cygnus) and by the creation of my home country.

2 WR stars in context

The upper CMD for massive stars is a rather peculiar place, with boundaries in which "allowed" stars can lie, defining a relatively small area (de Jager 1980), from the nearly vertical line at $\log(T_{\rm eff}) \approx 3.5$, i.e. the Hayashi limit to the red with $R \approx 1000 R_\odot$; the also nearly vertical line at $\log(T_{\rm eff}) \approx 5.0$, i.e. the He-burning main-sequence (MS) to the blue; and the Humphreys-Davidson (H-D) limit at a maximum ($\sim$ Eddington) luminosity corresponding to $\log(L/L_\odot) \approx 6.3$. The lower boundary for massive stars ($> 8 M_\odot$) is at $\log(L/L_\odot) \approx 3.5$. Only the degenerate bluer cooling sequences of very hot, but much lower-mass, white dwarfs (WDs) and neutron stars (NSs) lie outside this region. The He-burning massive WR stars are expected to occupy the extreme blue of this zone with $R \approx 1 R_\odot$, but as we'll see only few of them appear to have actually reached that far coming from the right.

While mass loss is crucial in determining the evolution for all massive stars at all stages above $M_{\rm i} \sim 20 M_\odot$, it is especially important as such stars leave the MS and their outer layers puff up towards the H-D limit (while the core shrinks) or later, when its wind-bared core becomes a more compact and hotter WR star, believed to be the ultimate fate of all such stars. B-type stars in the range $8 - 20 M_\odot$ lose less mass, but when they do, it is mainly as supergiants, especially in the RSG stage, where they also explode as type II (H-rich) supernovae. WR stars are believed to explode as type Ib (from H-poor WN) or Ic (from H- and relatively He-poor WC/WO) supernovae. For a typical massive star, the most important stages (especially regarding wind interactions) are:

1. first as a MS O-star (long time, fast wind), culminating in the post-MS SG stage as
2. an LBV stage (short time, slow wind), with RSG instead of LBV in the lowest part of this mass range, then
3. a WR stage (moderate time, fast wind), then
4. SN (ultra-short time and fast wind), ending in most cases as
5. a BH (essentially for infinite time, virtually no wind), or perhaps magnetars (= highly magnetic, slowly rotating NSs) in some cases.

For massive stars, thermonuclear fusion occurs in successively hotter and more compact regions from sequential "burning" of H, He, C, Ne, O and Si, finally to produce Fe, which immediately leads to a core-collapse implosion. After He-burning, a CMD is not useful, since the core evolves ever faster than the surface. Hence, the last visible stage before the SN is as a WR star, probably WC or WO in most cases, if they reach that far before their cores collapse.

While their progenitor O stars have spectra with relatively narrow photospheric absorption lines, the strongest of which reach an equivalent width (EW) up to several Å, WR stars reveal giant emission lines even in the optical domain, with EW up to ≈ 1000Å, arising in projected radial velocities from various layers of the rapidly expanding wind. Sample *optical* spectra, often considered key in distinguishing WR

vs O stars, are shown in Crowther (2007) for both the WN (ranging from hot to cold: WN2-9, with CNO-cycle products of H-fusion reaching the surface and wind) and the WC (ranging over WC4-9, with triple-alpha products of He-fusion) sequences. Interestingly, WC stars form a more homogeneous sequence with regards to their fundamental properties as a function of wind temperature or spectral subtype, than do WN stars. WC stars are followed by WO stars (WO1-4), with either enhanced oxygen and/or hotter temperature (see below).

In this context I do recall once having an amusing moment during an evaluation site visit to our observatory (Observatoire du Mont-Mégantic, in Québec province) in 1988, where I was observing spectra of WR stars with a student. The external examiner, Robert Wagoner, a well-known SN expert, now emeritus at Stanford, happened to glance at one of our freshly obtained spectra and exclaim "Wow, what SN is that?" Our explanation that it was "only" a WR star created no lack of enthusiasm on his behalf, but I still wonder if our observatory grant only remained proportional to the width of the spectral lines!

So far, I've treated WR as only massive stars. In reality, as has been pointed out previously on various occasions, "WR" is really a phenomenon of strong, broad emission lines from a hot, expanding plasma, involving three recognized situations:

1. Classical He-rich cWR stars = evolved He-burning, pre-SN Ib,c stars of $M_{\rm i} \sim 25 - 100+?$ $M_\odot$ (types WN, WC, WO).

2. Central stars of planetary nebulae (CSPN) - [WR], relatively massive post AGB stars ($\sim$15 %).

3. Main Sequence H-rich WNh stars of $M_{\rm i} \sim 80 - 300$ $M_\odot$.

We normally only see a stellar photosphere for stars in the third line above, while all massive stars above $M_{\rm i} \sim 25 M_\odot$ pass through a cWR phase, apparently regardless of initial metallicity (at least down to observed limits around 0.01 solar), which however, does have an effect on the wind and thus emission-line strengths.

How can such vastly different stars have similar normalized emission measures (NEM)? This was first realized by Schmutz et al. (1989), who showed that NEM can be expressed as a volume integral of density-squared per unit stellar surface, i.e.

NEM $\sim V\rho^2/R_\star^2$, so with $V \sim R_\star^3$ and $\dot{M}\sqrt{D} \sim R_\star^2 v_\infty \rho$: NEM $\sim \dot{M}^2 D/(R_\star^3 v_\infty^2)$.

Thus, for D = const. ($\sim$ 10) and v_∞ = const. ($\sim$ 2500km/s), $\sqrt{\rm NEM} \sim \dot{M}/R_\star^{3/2}$, which is listed in Table 1 for typical parameters of the three kinds of WR stars.

Tab. 1: Typical parameters for the three families of WR stars ([WR] for Abell 48: (Todt et al. 2013))

Type	$R_\star/R_\odot$	$\dot{M}/10^5 M_\odot$/yr	$\sqrt{\rm NEM}$
WNLh	15	10	0.017
cWR	3	1.0	0.019
[WR]	0.5	0.05	0.014

Remarkably, these 3 types do show very similar NEM and thus spectra, although line-width could be a distinguishing factor in some cases (Smith & Aller 1971).

Another puzzle with a less obvious solution is how cWR stars can have mass-loss rates that are typically 10 times higher than their progenitor O stars, despite their similar (or even slightly reduced) luminosities, which are normally believed to provide the radiation pressure needed to drive their winds, whether WR or O. One simple answer is that the theoretical (from internal models; external spectral fitting requires a rather uncertain extrapolation) radii of cWR stars are typically a factor 10 smaller than those of O stars. Thus, for flux conservation $L = 4\pi\sigma R^2 T_\star^4$, $T_\star$(cWR) $\sim \sqrt{10}\ T_{\rm eff}$(O) $\sim$ 100kK, taking a typical $T_{\rm eff}$(O) $\sim$ 30kK. Therefore, at higher surface temperatures, there is relatively much more UV flux and thus more driving from ambient-ISM-provided Fe, with its complex atomic structure and forests of mainly UV-lines from Fe II through IV. [Note that the metallicity dependence $\dot{M} \sim Z^{0.7}$ is similar, although not identical, for both O- and WR-stars (Vink & de Koter 2005).] Thus, it is the high, stable $\dot{M}$ that distinguishes WR from their progenitor O stars.

As we'll see later in this meeting, another factor in explaining why WR stars have such high $\dot{M}$, despite their similar Ls to those of O stars is their tendency to approach their Eddington limits with inflated envelopes. However, this might ultimately be related to the above fundamental circumstance of WR stars having hot, compact radii with enhanced wind driving.

As for their evolution, most astronomers probably agree with the general scenario, which began with that of Conti (1975):
O $\rightarrow$ LBV (RSG) $\rightarrow$ WN $\rightarrow$ WC $\rightarrow$ SN Ib,c $\rightarrow$ BH (NS)

But there are now many different detailed scenarios, of which that of Crowther (2007) is my preferred, because it is simultaneously simple and plausible, for the following approximate mass ranges:

1. $M_{\rm i} >\sim 75\, M_\odot$:
   [O $\rightarrow$] WN(H-rich) $\rightarrow$ LBV $\rightarrow$ WN(H-poor) $\rightarrow$ WC $\rightarrow$ SN Ic

2. $M_{\rm i} \sim 40 - 75\, M_\odot$:
   O $\rightarrow$ LBV $\rightarrow$ WN(H-poor) $\rightarrow$ WC $\rightarrow$ SN Ic

3. $M_{\rm i} \sim 25 - 40\,M_\odot$:
   O → LBV/[RSG] → WN(H-poor) → SN Ib

(Note: In square brackets I have added possible modifications that may apply.)

In contrast, for stars with the next lower mass bracket, $M_{\rm i} \sim 10 - 25\,M_\odot$:
late-O/early-B → RSG → SN IIb, or bare He core if in a close binary, and some LBV may → SN IIn (Smith et al. 2007).

3 Some nagging questions

3.1 Are all WNE stars H-poor?

Answer: No, especially for lower ambient metallicity. A beautiful example is the single WN3ha (using the commonly accepted 3D classification system of Smith et al. 1996) star WR3 (in the outer Galaxy with Z like that found in the Magellanic Clouds, which contain many similar stars). Such stars often display weak lines with triangular profiles, believed to arise from lower mass-loss rates at low Z combined with rotationally induced meridional circulation. The principle parameters for WR3 from Marchenko et al. (2004) are: $\dot{M} = 2 \times 10^{-6} M_\odot/{\rm yr}, R_\star = 3.6\,R_\odot, R_{2/3} = 3.8\,R_\odot, \log(L/L_\odot) = 5.4, v_\infty = 2750\,{\rm km/s}, X_{\rm H} = 0.20, X_{\rm He} = 0.79, X_{\rm N} = 0.008$.

3.2 Are all WNL stars H-rich?

Answer: Again, no, contrary to common belief. A good example is the single Galactic star WR123 of type WN8o, i.e. lacking hydrogen. Along with four other Galactic runaways (WR64, 71, 93a and 148), WR123 is located over 500 pc from the Galactic plane (Rosslowe & Crowther 2015). On the other hand, the two runaway WN8h stars WR124 (surrounded by the "fireball" nebula M1-67, with $RV_{\rm pec} \sim 200\,{\rm km/s}$, although not too far from the Galactic plane) and WR148 (a close 4.2d single-line binary) do have hydrogen, like most stars of this kind. Note that WN8 stars are often found to be runaways for reasons that remain obscure at best.

On the other hand, all WN stars with high luminosity do appear to contain hydrogen (and designated WNh), since they are likely MS stars, in contrast with the He-burning cWR stars (see above).

3.3 Does intra-sequence evolution occur via the peeling-off scenario?

I.e. does one have WN9 → WN8 → WN7 → WN6 → WN5 → WN4 → WN3 → WN2, or WC9 → WC8 → WC7 → WC6 → WC5 → WC4, then → WO4→ WO3 → WO2 → WO1? In reality, a star does not need to follow the entire sequence and may transition from WN to WC or be interrupted by a SN explosion at any time in the sequence.

Answer: Yes, according to Smith & Hummer (1988) and Smith & Maeder (1991) for WC stars and Moffat (1995) for both WN and WC in limited sequences depending on the ambient metallicity, although with caveats. In addition, Moffat (1995) found that line widths have to match up at the transition from WN to WC, where the relatively rare transition WN/WC types are known to occur. More recently, however, Crowther (2007) showed that little intratype evolution occurs. This appears to be supported by the observed $f(Z)$ distribution of Galactic WR stars (van der Hucht 2001), where different subclasses tend to occupy different zones in Galactocentric distance (a proxy for metallicity Z), going from super-solar near the Galactic centre to LMC/SMC values in the outer Galaxy (1/2 – 1/4 solar). A good example here is that WC9 stars are only found in the inner Galaxy among all Local Group galaxies, where WR stars are formed at the highest Z. The main reason must be the enhanced opacity at higher ambient Z, since it is mainly Fe that drives the winds, more than the locally produced heavy elements He, N, C, O. However, there is a caveat to this, namely that poorly-determined distances may have smeared the Galactic distributions out, such that the true relation may be clearer than appears at first sight. Alternatively, if the smearing is not important, then there could indeed be some intra-sequence evolution. The astrometric satellite GAIA will hopefully straighten this out, with its vast improvement of distance determinations especially for WR stars. A recent study of abundances in WO stars may indeed suggest that peeling-off does occur, at least among these stars, after passing through a hotter WC stage (Tramper et al. 2015).

3.4 Do WR/O, WC/WN, WNL/WNE, WCL/WCE number ratios increase with Z?

Answer: No doubt, with lots of studies to back this up, both observational and theoretical. It's mainly a question of enhanced opacity (especially initial Fe), which allows more stars of lower mass to become WR. But what happens at extremely low Z ($\ll 0.01$ solar) remains to be seen.

3.5 Do all WRs start as O → Of → WNL?

Answer: This was first proposed by the wrap-up speaker at this meeting and is referred to as the Conti (1975) scenario. In reality, things have become a bit more complicated, as we have seen above and we'll see in the rest of this meeting.

3.6 What distinguishes [WR] from "normal" CSPN?

Answer: This remains a puzzle, but one idea I'd like to throw into the mix is: Stronger winds among post-AGB CSPN may possibly be due to smaller radii and higher $T_{\rm eff}$, as might be the case if [WR] stars are more massive and degenerate than most non-[WR] CSPN, something like comparing pop I cWR with their progenitor O stars (although not with respect to degeneracy). Note that [WN] stars have recently been found to exist (Miszalski et al. 2012), putting to rest the long-believed notion that all [WR] CSPN are [WC], albeit [WN] seems to be much rarer than [WC].

3.7 Does binarity affect cWR evolution?

Answer: Yes, but probably for close binaries only. From Kepler's 3rd law $M_1 + M_2 = a^3/P^2$ (for $M_\odot$, AU & yr), then with $a \sim 2R$ for two stars of similar radii, R, corresponding $\sim$ to the RLOF limit, and for a typical LBV, $R \sim 75\,R_\odot \sim 0.35$ AU, with $M_1 + M_2 \sim 70\,M_\odot$ for a modest system: $P_{\rm i} \lesssim 25$ d (unless there are huge outbursts). For a typical RSG, $R \sim 1000\,R_\odot \sim 5$ AU, $M_1 + M_2 \sim 50\,M_\odot$, one finds $P_{\rm i} \lesssim 4$ yr.

Note that the shortest-period cWR binaries, which must almost certainly have gone through RLOF are:

1. Cyg X-3, WN4-6 + cc, $P = 4.8\,{\rm h} = 0.20$ d (the only recognized WR + cc binary) (van Kerkwijk et al. 1996),

2. CQ Cep, WN6o + O, $P = 1.64$ d (Marchenko et al. 1995),

3. BAT99-32, WN6(h) + O, $P = 1.91$ d (Schnurr et al. 2008),

4. BAT99-39 = Br32, WC4 + O, $P = 1.92$ d (Bartzakos et al. 2001), thus putting to rest the suspicion that WC+O binaries have longer periods (L. F. Smith, priv. comm.).

Examples of rare massive RLOF W Ser systems in action possibly on their way to becoming WR+O systems include β Lyr, RY Scuti and more recently HDE 326823 (Richardson et al. 2011), for which $P = 6.1$ d, $e = 0.19$, $f(M) = 7\,M_\odot$. In this case, the visible star (which has a spectrum similar to that of a B-supergiant despite its low mass, $\sim 6\,M_\odot$) is the mass donor, and is transferring mass to a more massive gainer star of $\sim 30\,M_\odot$ that is enshrouded in a thick accretion torus.

4 Population I WR inventory and relevance for supernovae

The current number of known (i.e. spectroscopically confirmed) WR stars in the Galaxy now stands at 642 (June 2015: P.A. Crowther's on-line catalogue: http://pacrowther.staff.shef.ac.uk/WRcat/), somewhat short still of the expected 1900 total (Rosslowe & Crowther 2015). The number of known extragalactic WR stars is ca. 700 (Massey, priv. comm.), excluding unresolved WR galaxies, where severe crowding occurs.

The expected average time till the next core-collapse WR supernova in a random sample of N WR stars will be $t = \tau({\rm WR})/(2N) = 2 \times 10^5\,{\rm yr}/N$. Thus, for an average total WR lifetime $\tau({\rm WR}) \sim 0.4$ Myr, one has the results in Table 2:

Tab. 2: Time until next SN in a sample of N WR stars

N	t [yr]
10^3	200
10^4	20
10^5	2

Of course the last row is the most interesting, but requiring some 50 giant spirals each with 2000 WR. But if WR stars collapse into BHs taking everything with them without a SN, then the task of finding which WR stars have actually done this clearly becomes much more challenging, i.e. looking for missing WR stars without the signal of a preceding explosion.

Interestingly in this context, the proof that WN stars actually do explode as SN Ib and WC stars explode as SN-Ic in spiral galaxies, including e.g. NGC 7793, is intimated by their similar respective distributions (Bibby & Crowther 2010). Note that ~ 20 % of all SNe are of type Ib, c, with the majority (type II) coming from more numerous lower-mass RSG.

5 WR models: winds and internal structure

How have spectral models (mainly CMFGEN and PoWR) faired over the years? A sample PoWR model fit to the weak-line (requiring a less dramatic extrapolation down through the wind to the hydrostatic surface, and thus a more likely fit) WN5-w star WR61 (Hamann et al. 2006) exhibits a good, although not perfect fit. Even if the fit were perfect though, one always wonders about the uniqueness of the model, given the large number of parameters involved. Fortunately, due to proper inclusion

during the past decade of line blanketing, model atmospheres have become more realistic, with O stars now cooler and fainter, while WR stars are estimated to be hotter and brighter. In $M_{\rm v}$, WNL stars are always the brightest, while WNE stars become increasingly fainter for progressively hotter subtypes. But despite the large progression in $M_{\rm v}$ with subtype, all WNE have $L \sim$ const., due to enhanced bolometric corrections for hotter stars.

Overall, the position in the CMD of single Galactic WN stars follows a distinct trend with a few exceptions: those with H (mostly WNL) are brighter in bolometric luminosity L by 0.5 dex (factor 3) on average than those without H (mostly WNE). But still, a problem remains: Why are there not more WN on/near the He-ZAMS as expected from internal models? Model atmospheres carry a high degree of uncertainty due to the required extrapolation to what is considered something close to their hydrostatic core radii $R_\star$, assuming $\tau_\star = 20$ and $\beta = 1$.

Things appear to get even stranger when the WC model atmospheres are examined (Sander et al. 2012). While WC4 stars may lie close to the He-ZAMS, cooler WC stars lie further towards the H-ZAMS, with WC9 stars clearly lying apart from the remaining WC stars, essentially on the H-ZAMS at luminosity lower by ca. 0.2 dex than their WC4–8 cousins. Perhaps this is due to their lower initial mass, being formed at higher initial Z, which allows lower-mass stars to become WR, in this case eventually ending up as WC9, although why so far from the He-ZAMS?

Comparison of wind models with evolutionary models (Meynet & Maeder 2003) for two groups of initial rotation $V_{\rm rot}({\rm init}) = 0$ vs. 300 km/s shows that neither gives satisfactory agreement. The possibility of cooler cWR surface/wind models with inflated envelopes has been conjectured (Moriya et al. 2015), as will be discussed later in these proceedings. Ultimately one might need consistent models from basic principles starting with 10^{58} atoms + basic laws of physics! Of course that is a totally unrealistic pipe dream and we'll have to wait and see what gradually improved models bring as more realistic physics is included.

6 Conclusions

I originally wanted to zero in on a few topics in more detail, such as binaries, colliding winds and wind structures, but time and space limitations mean that I'll gladly defer to the excellent presentations to follow. Basically, I have given personal highlights, both subjective & not complete. E.g., not discussed much here have been: hybrid models (interiors + winds), abundances, ring nebulae, gamma rays, WR galaxies, etc. One thing is sure, though, and that is that future research will greatly benefit from highly advanced projects such as GAIA, JWST, EELT/TMT, Interferometry, and even pro-am collaborations.

And now let the real meeting begin!

References

Bartzakos, P., Moffat, A. F. J., & Niemela, V. S. 2001, MNRAS, 324, 33

Bibby, J. L., & Crowther, P. A. 2010, MNRAS, 405, 2737

Conti, P. S. 1975, Memoires of the Societe Royale des Sciences de Liege, 9, 193

Crowther, P. A. 2007, ARA&A, 45, 177

de Jager, C. 1980, Geophysics and Astrophysics Monographs, 19,

Hamann, W.-R., Gräfener, G., & Liermann, A. 2006, A&A, 457, 1015

Marchenko, S. V., Moffat, A. F. J., Eenens, P. R. J., Hill, G. M., & Grandchamps, A. 1995, ApJ, 450, 811

Marchenko, S. V., Moffat, A. F. J., Crowther, P. A., et al. 2004, MNRAS, 353, 153

Meynet, G., & Maeder, A. 2003, A&A, 404, 975

Miszalski, B., Crowther, P. A., De Marco, O., et al. 2012, MNRAS, 423, 934

Moffat, A. F. J. 1995, Wolf-Rayet Stars: Binaries; Colliding Winds; Evolution, 163, 213

Moriya, T. J., Sanyal, D., & Langer, N. 2015, A&A, 575, L10

Richardson, N. D., Gies, D. R., & Williams, S. J. 2011, AJ, 142, 201

Rosslowe, C. K., & Crowther, P. A. 2015, MNRAS, 447, 2322

Sander, A., Hamann, W.-R., & Todt, H. 2012, A&A, 540, A144

Schmutz, W., Hamann, W.-R., & Wessolowski, U. 1989, A&A, 210, 236

Schnurr, O., Moffat, A. F. J., St-Louis, N., Morrell, N. I., & Guerrero, M. A. 2008, MNRAS, 389, 806

Smith, L. F., & Aller, L. H. 1971, ApJ, 164, 275

Smith, L. F., & Hummer, D. G. 1988, MNRAS, 230, 511

Smith, L. F., & Maeder, A. 1991, A&A, 241, 77

Smith, L. F., Shara, M. M., & Moffat, A. F. J. 1996, MNRAS, 281, 163

Smith, N., Li, W., Foley, R. J., et al. 2007, ApJ, 666, 1116

Todt, H., Kniazev, A. Y., Gvaramadze, V. V., et al. 2013, MNRAS, 430, 2302

Tramper, F., Straal, S. M., Sanyal, D., et al. 2015, arXiv:1507.00839

van der Hucht, K. A. 2001, New A Rev., 45, 135

van Kerkwijk, M. H., Geballe, T. R., King, D. L., van der Klis, M., & van Paradijs, J. 1996, A&A, 314, 521

Vink, J. S., & de Koter, A. 2005, A&A, 442, 587

Peredur Williams: The figure comparing the ISO infrared co-added spectra of dust-making WCL stars with the PAH spectrum has corresponding emission features red-shifted by about 8000 km/s. This is greater than the outflow velocities of these stars or of the dust expansion velocities like that of the WR112 pinwheel. So these data do not show evidence for PAH emission in dust-making WCL stars.

Anthony (Tony) Moffat: The relative positions of the lines are consistent with each other and the strong red-shift can be understood in terms of published models in other contexts. A paper is in preparation on this and will be submitted soon.

WR surveys

Wolf-Rayet Stars
W.-R. Hamann, A. Sander, H. Todt, eds.
Potsdam: Univ.-Verlag, 2015
URL: http://nbn-resolving.de/urn:nbn:de:kobv:517-opus4-84268

Wolf-Rayet content of the Milky Way

P. A. Crowther
Dept of Physics & Astronomy, University of Sheffield, Sheffield S3 7RH, UK

An overview of the known Wolf-Rayet (WR) population of the Milky Way is presented, including a brief overview of historical catalogues and recent advances based on infrared photometric and spectroscopic observations resulting in the current census of 642 (v1.13 online catalogue). The observed distribution of WR stars is considered with respect to known star clusters, given that ≤20% of WR stars in the disk are located in clusters. WN stars outnumber WC stars at all galactocentric radii, while early-type WC stars are strongly biased against the inner Milky Way. Finally, recent estimates of the global WR population in the Milky Way are reassessed, with 1,200±100 estimated, such that the current census may be 50% complete. A characteristic WR lifetime of 0.25 Myr is inferred for an initial mass threshold of 25 $M_{\odot}$.

1 Historical overview and current census

Wolf-Rayet (WR) stars are the evolved descendents of massive stars, with two main flavours: Helium-rich WN stars displaying the products of core H burning and Carbon-rich WC stars displaying the products of core He burning (Crowther 2007). An overview of the number of WR stars in the Milky Way is provided. The Galactic census tripled between the 1st (Campbell 1894) and the 6th catalogues (van der Hucht 1981), a century later (Table 1), and subsequently doubled by the Annex to the 7th catalogue (van der Hucht 2006) owing to deep narrow-band optical surveys (Shara et al. 1999), the discovery of rich star clusters (Crowther et al. 2006) and infrared surveys of the Galactic Centre region (Figer et al. 2002). Over the past decade, the number has doubled again, primarily through surveys arising from the advent of large format infrared detectors, with the census totalling 642[1], comprising 357 WN stars, 8 WN/C stars, 273 WC stars and 4 WO stars.

Tab. 1: Historical catalogues of Galactic WR stars

Catalogue	Reference	Number
I	Campbell (1894)	55
II	Fleming & Pickering (1912)	108
III	Payne (1930)	92
IV	Roberts (1962)	123
V	Smith (1968)	127
VI	van der Hucht et al. (1981)	157
VII	van der Hucht (2001)	227
VII	Current census v1.13	642[1]

Two complementary initiatives have dominated this improvement since the annex to the 7th catalogue (van der Hucht 2006). Mike Shara and collaborators have employed narrow-band imaging of the Galactic plane at 2-2.3μm to identify 150+ WR stars from follow-up spectroscopy (Shara et al. 2012). Since this approach relies upon the contrast between emission lines and the adjacent continuum, systems which are dominated by hot dust or a companion in the K-band will not be identified. A second method exploiting the unusual near- to mid-IR broad-band colours of WR stars has been exploited by Schuyler Van Dyk, Pat Morris and collaborators has identified 100+ WR stars (Hadfield et al. 2007; Mauerhan et al. 2011). This approach has successfully identified dusty WR stars, but would also prove problematic for systems whose IR energy distribution is dominated by a companion star.

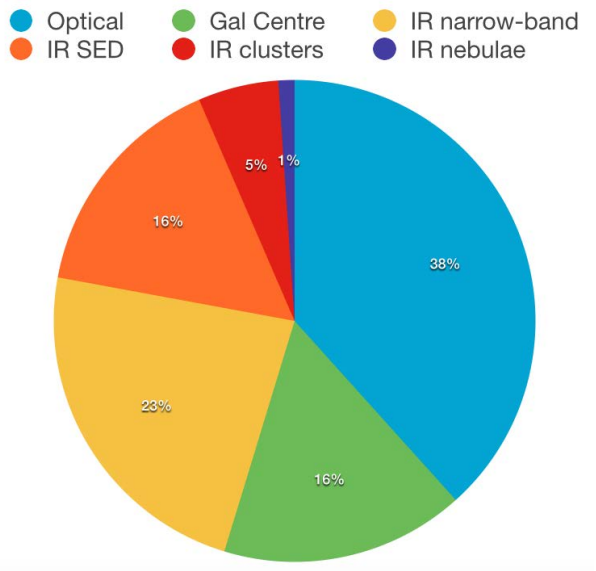

Fig. 1: Pie chart illustrating breakdown of discovery technique for WR stars in current census (v1.13 of online catalogue)

In addition, WR stars have been discovered from follow-up spectroscopy of members in star

[1]v1.13 of online WR catalogue http://pacrowther.staff.shef.ac.uk/WRcat/

clusters newly identified from IR surveys (e.g. Spitzer/GLIMPSE, VISTA/VVV) such as Chené et al. (2012). Other WR stars have been newly identified from follow-up spectroscopy of the ionizing stars in dusty mid-IR nebulae (Wachter et al. 2010). A chart illustrating the fraction of WR stars discovered by different techniques is illustrated in Fig. 1.

The binary frequency of O stars in young Galactic clusters is believed to be high: ∼71% will interact with a companion during their lifetime according to Sana et al. (2012). Since WR stars are the progeny of O stars, a high WR binary frequency will also be anticipated. The majority of searches for binarity in WR stars have been conducted via blue visual spectroscopic monitoring. Amongst the 25% of WR stars which are visually brighter than V=15 mag, 44 are close binaries (either SB1 or SB2), plus another 10 are dusty WC stars. It is now widely accepted that dusty WC stars are universally binary systems involving a WC star and an O star companion. Therefore, a strict lower limit to the binary frequency is 34% (= 54/160 stars). For comparison, a WR binary frequency of 38% (86/227) was estimated in the 7th WR catalogue (van der Hucht 2001), including long period systems (P > 1000 days) and X-ray bright systems - by way of example the X-ray bright system WR25 was subsequently identified as an SB1 by Gamen et al. (2006). These statistics undoubtedly represent lower limits to the WR binary frequency, although one would expect a lower binary frequency than for O stars since some WR stars will be merger products and others will become single following the (dynamical or post-supernova) disruption of initial binary systems.

2 WR stars and star clusters

If we adopt a lower mass limit to the production of WR stars of ∼25 $M_\odot$, and if massive stars only form in clusters, whose upper mass limit follows the relationship of Weidner et al. (2010), one would expect $10^3 M_\odot$ clusters to host the majority of WR stars. In reality only 27% of WR stars in the Milky Way are in known star clusters (Rosslowe & Crowther 2015). Of these, the majority of known WR stars in the Central Molecular Zone (CMZ) do lie within one of the three massive star clusters, the Arches, Quintuplet and the Galactic Centre cluster itself. Excluding the CMZ, only 18% of the WR stars located in the disk lie within star clusters. This is illustrated in Fig. 2.

Consequently, either the lower mass limit to the production of WR stars must be significantly lower (making birth clusters harder to identify), WR stars do not preferentially form in dense star clusters, or the majority of WR stars are no longer associated with their birth cluster.

OB stars are observed in a range of environments - low density star forming regions (e.g. ρ Oph), intermediate density OB associations such as Cyg OB2, and dense clusters such as NGC 3603. Indeed, the fraction of stars (of all masses) located in dense (Orion Nebula-like) clusters in the Solar Neighbourhood is <26% (Bressert et al. 2010). Wright et al. (2014) have established that massive stars in Cyg OB2 did not form in close proximity, nor in regions of higher density, so can form in regions of relatively low density.

Therefore, it is likely that typical massive stars arise from relatively loose OB associations, with only a small fraction born in dense star clusters, so the rarity of WR stars in star clusters naturally follows without resorting to a low threshold mass to the formation of WR stars or a high ejection frequency. This has relevance to the discussion of Smith & Tombleson (2015) regarding the relative masses of O, WR stars and Luminous Blue Variable (LBV) in the Large Magellanic Cloud from their spatial locations. One would expect relatively few O stars in close proximity to most WR stars/LBVs if the majority of massive stars originate in intermediate density environments, especially since most WR stars will arise from relatively modest ∼ $25 M_\odot$ progenitors.

3 Distribution of WR stars

Since the distance of the majority of Galactic WR stars is not well established, Rosslowe & Crowther (2015) have investigated the near-IR absolute magnitudes of different WR subtypes based on 108 stars whose distances have been estimated, either from cluster/association membership or other techniques. The spatial distribution of these, plus 246 field WR stars for which reliable spectral types have been obtained, are presented in Fig. 3.

Field WR populations include binary systems, providing the WR to OB light ratio can be estimated in the K-band or the WR star is thought to dominate the near-IR continuum flux. From a census of local (<3 kpc) WR systems, the WR star dominates the K-band flux in 82% of cases. In addition, dusty WC stars are omitted from this distribution because their K-band flux is typically dominated by hot dust rather than the WC continuum. For reference, dusty WC stars comprise ∼15% of the local (<3 kpc) WR population.

Generally, the near-IR classification of WR stars is rather coarser than at visible wavelengths. The majority of near-IR studies have followed the scheme of Crowther et al. (2006) who utilised IRTF/SpeX 1–5μm observations of ∼30 optically classified WR stars. In general robust near-IR classification requires observations at J, H and K, although the actual number of WN/C transition stars will be underestimated since no near-IR schemes have so far been implemented (efforts are currently underway to remedy this deficiency).

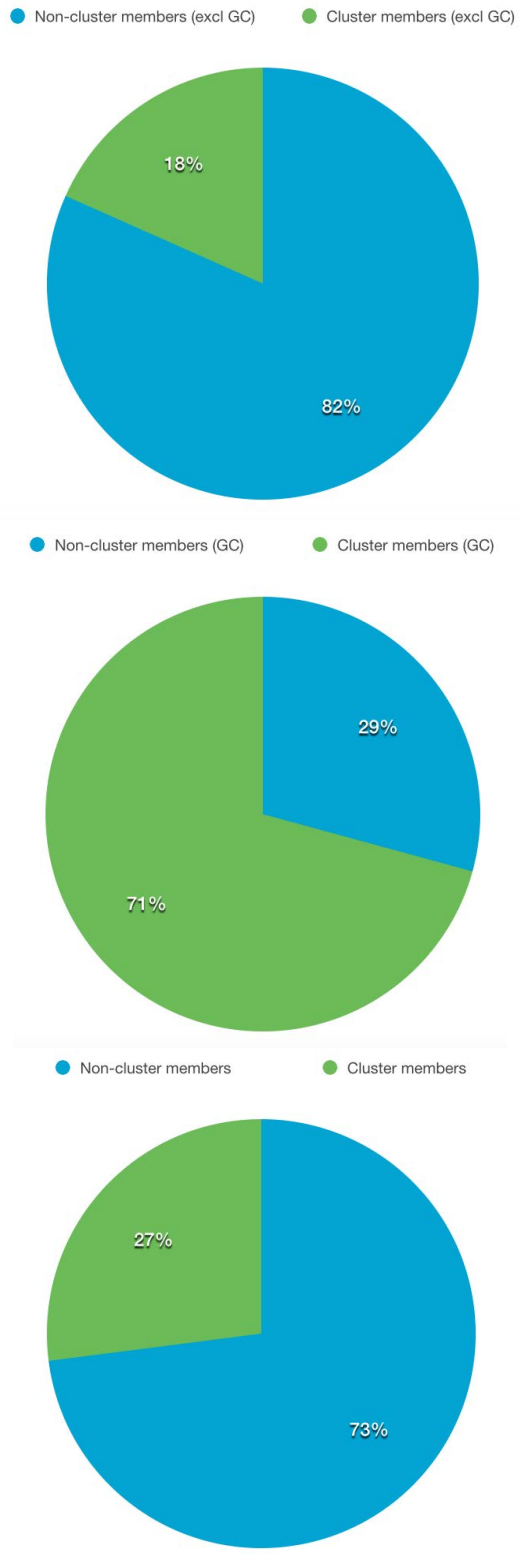

Fig. 2: Pie charts illustrating the fraction of Wolf-Rayet stars (v1.13 of catalogue) which are cluster members (green) or in the field (blue) for the Galactic disk (top), Galactic Centre region (middle) and combined pop (bottom).

The observed ratios of WR subtypes in the inner Galaxy at galactocentric distances of below 6 kpc (log O/H+12 $\sim$ 8.85), mid disk from 6–9 kpc (log O/H+12 $\sim$ 8.7) and outer disk beyond 9 kpc (log O/H + 12 $\sim$ 8.55) is presented in Table 2. Overall there is little variation between these regions with the exception of early to late WC stars, with the latter dominating in the inner disk owing to the metallicity dependence of WC classification diagnostics (Crowther et al. 2002). Incorporating results from the Magellanic Clouds, the observed WC to WN ratio is presented in Fig. 4, together with a variety of evolutionary predictions from single and binary models (see caption).

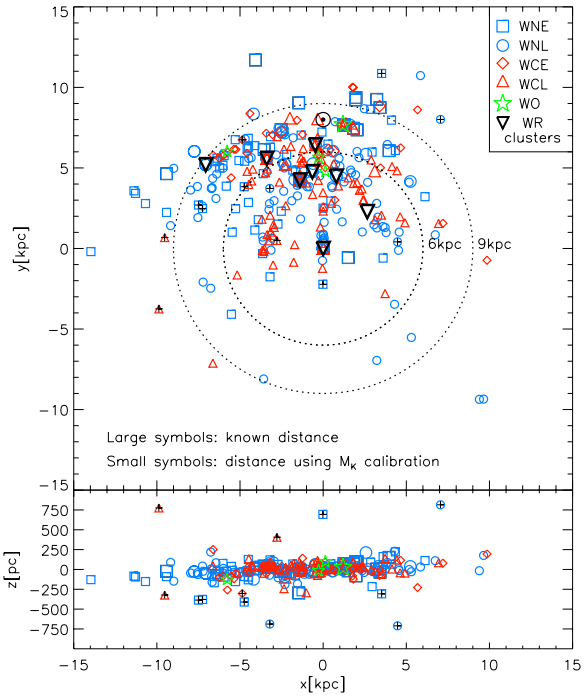

Fig. 3: Distribution of 354 WR stars in the Galactic disk from Rosslowe & Crowther (2015)

4 Global WR content

Various estimates of the global WR population in the Milky Way have been made, ranging from 1,200 (Maeder & Lequeux 1982) to 6,500 (van der Hucht 2001). We have constructed a toy model of the WR population in the Milky Way in an azimuthally symmetric disk following the radial HII distribution, atomic/molecular dust distribution and the observed WN/WC distribution (Rosslowe & Crowther 2015).

If we assume that the observed WR distribution is complete to K=8 mag (though see below), $\sim$550 WR

Tab. 2: WR subtype distribution in the Milky Way (Rosslowe & Crowther 2015) for three galacto-centric distances (R_{GC}).

Region	N(WR)	N(WC)/N(WN)	N(WC+d)/N(WN)	N(WCE)/N(WCL)
Inner ($R_{GC} < 6$ kpc)	187	0.51	0.69	0.05
Mid ($6 \leq R_{GC} \leq 9$ kpc)	132	0.53	0.73	1.0
Outer ($R_{GC} > 9$ kpc)	35	0.40	0.57	1.5

dominated stars in the Galactic disk reproduce the observed WR distribution. In addition, over 100 WR stars are currently known with $-2.5° \leq l \leq +3.5°$ so the total CMZ population may be as large as 250. Such a large population is surprising given that the CMZ accounts for perhaps 5% of the entire Milky Way star formation rate (Longmore et al. 2013), but the presence of three very massive clusters in the Galactic Centre region suggests WR stars may be disproportionately represented.

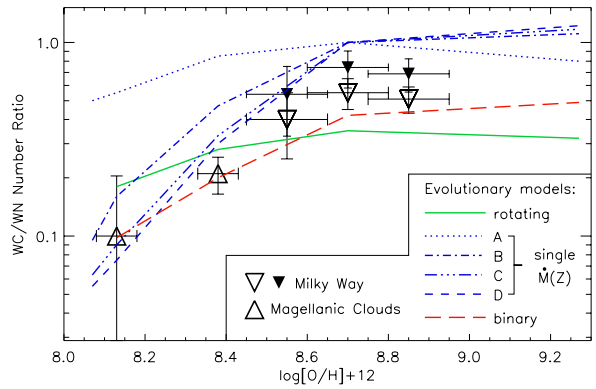

Fig. 4: Ratio of WC to WN stars in the Milky Way, for which dusty WC stars have been omitted (inverted open triangles) or included (inverted filled triangles), plus the Magellanic Clouds (open triangles) from Rosslowe & Crowther (2015). Predictions from rotating single star models (Meynet & Maeder 2005, green), binary models (Eldridge et al. 2008, red) and non-rotating single star models for various mass-loss metallicity dependencies (Eldridge & Vink 2006, blue) are also indicated.

A total of 550 + 250 = 800 stars would represent only 82% of the non-dusty WR population since 18% of systems are expected to be dominated by the WR companion in the K-band, so the non-dusty WR population inferred is ∼950. Finally, including dusty WC stars, which comprise 15% (150) of the whole population, we estimate N(WR) = 1,100, providing N(WCd)/N(WC) is uniform across all galactocentric radii. A histogram of the predicted JHK$_s$ magnitudes for this predicted WR population is presented in Fig. 5.

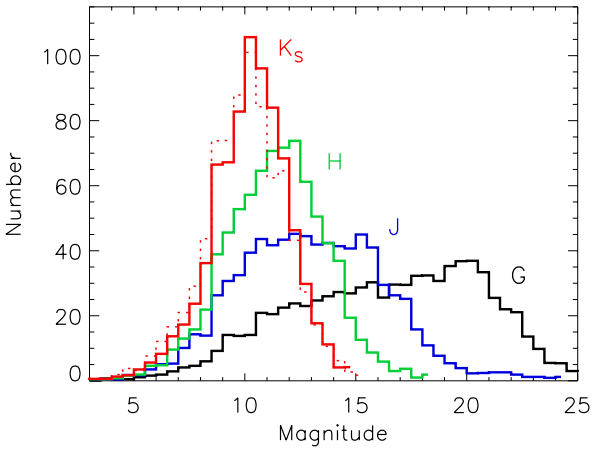

Fig. 5: Histogram of JHK$_s$ and GAIA G-band magnitudes predicted from the model WR population by Rosslowe & Crowther (2015).Thick lines represent populations consisting of WN and non-dusty WC stars, while the dotted-line illustrates a model population in which 28% of WC stars are dust-forming with $M_K = -6.95$ mag.

Based on this global WR population of 1,100, if the lower mass threshold to WR stars is $25M_\odot$, an average lifetime for the WR phase of 0.25 Myr is implied by the current Milky Way star formation rate of 1.9 $M_\odot$ yr^{-1} (Chomiuk & Povich 2011) and a standard Kroupa Initial Mass Function. This characteristic lifetime is in fair agreement with non-rotation evolutionary models, but is somewhat shorter than rotating model predictions (Georgy et al. 2012).

If the observed WR distribution is not complete to K=8 mag, the actual WR population will increase. By way of example, the two most recent additions to the on-line catalogue (v1.13) involve WR111-13[2], a WN6 star from Messineo et al. (2015) with K=8.02 mag and WR111-14, a WN7–8 star from Nebot Gómez-Morán et al. (2015) with K=7.7 mag. If the

[2]All WR stars discovered between the 6th catalogue and the Annex to the 7th catalogue follow the WRXXXa, WRXXXb nomenclature, whereas more recent additions utilise WRXXX-1, -2

WR-dominated disk population were 650 instead of 550, a global population of 1,300 would be inferred, so the current census may be 50% complete.

5 Summary

A brief overview of the Wolf-Rayet population in the Milky Way is presented. The current census of 642 (v1.13 of online catalogue) represents a doubling of the population since the Annex to the 7th WR catalogue only a decade ago, due to systematic searches from narrow-band surveys at 2μm and broad-band near to mid-IR surveys.

A strict lower limit to the binary fraction is 34% (SB1–2 systems plus dusty WC stars) for V< 15 mag, but the actual fraction will undoubtedly be significantly higher. Spectroscopic monitoring of WR stars in the near-IR is now feasible owing to multi-object IR integral field units (e.g. KMOS at ESO's VLT).

Excluding the Galactic Centre region, $\leq$20% of WR stars are located in star clusters, adding weight to the formation of most massive stars in OB associations, i.e. away from dense clusters. The current WR census may be 50% complete, in which case the average duration of the WR phase is 0.25 Myr for a lower mass limit of 25 $M_{\odot}$ to the formation of WR stars.

The majority of systems hosting WR stars are dominated by the He-rich component in the K-band, so these are fundamentally high luminosity (high mass) stars. In contrast, typical progenitors of stripped envelope core-collapse supernovae are relatively low mass stars, having transferred the majority of their H-rich envelope to a close companion. Such systems would not be recognised as conventional WR stars since the He-rich mass donor would be masked by the H-rich mass gainer at optical and near-IR wavelengths.

Finally, the online WR catalogue is maintained in Sheffield on a best efforts basis so authors are encouraged to provide Paul Crowther with preprints as soon as they are accepted for publication.

References

Bressert, E., Bastian, N., Gutermuth, R., et al. 2010, MNRAS, 409, L54

Campbell, W. W. 1894, Astronomy and Astro-Physics (formerly The Sidereal Messenger), 13, 448

Chené, A.-N., Borissova, J., Clarke, J. R. A., et al. 2012, A&A, 545, A54

Chomiuk, L. & Povich, M. S. 2011, AJ, 142, 197

Crowther, P. A. 2007, ARA&A, 45, 177

Crowther, P. A., Dessart, L., Hillier, D. J., Abbott, J. B., & Fullerton, A. W. 2002, A&A, 392, 653

Crowther, P. A., Hadfield, L. J., Clark, J. S., Negueruela, I., & Vacca, W. D. 2006, MNRAS, 372, 1407

Eldridge, J. J., Izzard, R. G., & Tout, C. A. 2008, MNRAS, 384, 1109

Eldridge, J. J. & Vink, J. S. 2006, A&A, 452, 295

Figer, D. F., Najarro, F., Gilmore, D., et al. 2002, ApJ, 581, 258

Fleming, W. P. S. & Pickering, E. C. 1912, Annals of Harvard College Observatory, 56, 165

Gamen, R., Gosset, E., Morrell, N., et al. 2006, A&A, 460, 777

Georgy, C., Ekström, S., Meynet, G., et al. 2012, A&A, 542, A29

Hadfield, L. J., van Dyk, S. D., Morris, P. W., et al. 2007, MNRAS, 376, 248

Longmore, S. N., Bally, J., Testi, L., et al. 2013, MNRAS, 429, 987

Maeder, A. & Lequeux, J. 1982, A&A, 114, 409

Mauerhan, J. C., Van Dyk, S. D., & Morris, P. W. 2011, AJ, 142, 40

Messineo, M., Clark, J. S., Figer, D. F., et al. 2015, ApJ, 805, 110

Meynet, G. & Maeder, A. 2005, A&A, 429, 581

Nebot Gómez-Morán, A., Motch, C., Pineau, F.-X., et al. 2015, MNRAS, 452, 884

Payne, C. H. 1930, Harvard Observatory Monographs, 3, 1

Roberts, M. S. 1962, AJ, 67, 79

Rosslowe, C. K. & Crowther, P. A. 2015, MNRAS, 447, 2322

Sana, H., de Mink, S. E., de Koter, A., et al. 2012, Science, 337, 444

Shara, M. M., Faherty, J. K., Zurek, D., et al. 2012, AJ, 143, 149

Shara, M. M., Moffat, A. F. J., Smith, L. F., et al. 1999, AJ, 118, 390

Smith, L. F. 1968, MNRAS, 138, 109

Smith, N. & Tombleson, R. 2015, MNRAS, 447, 598

van der Hucht, K. A. 2001, New A Rev., 45, 135

van der Hucht, K. A. 2006, A&A, 458, 453

van der Hucht, K. A., Conti, P. S., Lundstrom, I., & Stenholm, B. 1981, Space Sci. Rev., 28, 227

Wachter, S., Mauerhan, J. C., Van Dyk, S. D., et al. 2010, AJ, 139, 2330

Weidner, C., Kroupa, P., & Bonnell, I. A. D. 2010, MNRAS, 401, 275

Wright, N. J., Parker, R. J., Goodwin, S. P., & Drake, J. J. 2014, MNRAS, 438, 639

Dany Vanbeveren: In most of the WR+O binaries the O star is the brighter component. How many O-type stars could be WR+OB binaries but unrecognized because the WR star is too faint?

Paul Crowther: Indeed many WR+O systems are dominated by OB (supergiant) companions at optical wavelengths, but the IR continuum excess from dense WR winds tends to ensure that a fraction of such systems are WR dominated in K band. Still, we estimate 1/6 of nearby WR+O systems (<3 kpc) are dominated by companions (Rosslowe & Crowther 2015).

Ted Gull: Your presentation suggests a bias of detection for WC stars, especially in the IR. Please elucidate how WN stars are identified.

Paul Crowther: IR selected Wolf-Rayet stars span WC, WN subtypes since both subtypes possess K-band emission lines and a continuum excess at 1 – 10 μm with respect to "normal" stars.

Anthony (Tony) Moffat: Are the 24 WRs in Wd1 confirmed binaries (e.g. by periodic RV variations)?

Paul Crowther: Only a few have orbital periods from RV variations to date, although Simon Clark is using VLT/FLAMES to search for more. Still, many more Wd1 WR stars are likely to be binaries owing to either being dusty WC stars or bright X-ray emitters (or both), so a very high binary WR fraction can't be ruled out,

Wolf-Rayet Stars
W.-R. Hamann, A. Sander, H. Todt, eds.
Potsdam: Univ.-Verlag, 2015
URL: http://nbn-resolving.de/urn:nbn:de:kobv:517-opus4-84268

Finding Wolf-Rayet Stars in the Milky Way: Inputs to Star Formation and Stellar Evolution

A. P. Marston[1], J. Mauerhan[2], P. W. Morris[3] & S. Van Dyk[3]
[1]*European Space Astronomy Centre (ESAC), Spain*
[2]*University of California Berkeley, California, USA*
[3]*Infrared Processing and Analysis Center (IPAC), Caltech, California, USA*

The total population of Wolf-Rayet (WR) stars in the Galaxy is predicted by models to be as many as ∼6000 stars, and yet the number of catalogued WR stars as a result of optical surveys was far lower than this (∼200) at the turn of this century. When beginning our WR searches using infrared techniques it was not clear whether WR number predictions were too optimistic or whether there was more hidden behind interstellar and circumstellar extinction. During the last decade we pioneered a technique of exploiting the near- and mid-infrared continuum colours for individual point sources provided by large-format surveys of the Galaxy, including 2MASS and Spitzer/GLIMPSE, to pierce through the dust and reveal newly discovered WR stars throughout the Galactic Plane. The key item to the colour discrimination is via the characteristic infrared spectral index produced by the strong winds of the WR stars, combined with dust extinction, which place WR stars in a relatively depopulated area of infrared colour-colour diagrams. The use of the Spitzer/GLIMPSE 8μm and, more recently, WISE 22μm fluxes together with cross-referencing with X-ray measurements in selected Galactic regions have enabled improved candidate lists that increased our confirmation success rate, achieved via follow-up infrared and optical spectroscopy. To date a total of 102 new WR stars have been found with many more candidates still available for follow-up. This constitutes an addition of ∼16% to the current inventory of 642 Galactic WR stars. In this talk we review our methods and provide some new results and a preliminary review of their stellar and interstellar medium environments. We provide a roadmap for the future of this search, including statistical modeling, and what we can add to star formation and high mass star evolution studies.

1 Motivation for finding Wolf-Rayet stars in the Milky Way

At the start of our studies in 2003, we considered the distribution and numbers of Wolf-Rayet (WR) stars in the Milky Way. There were a number of motivating factors for finding more. A limited number of Wolf-Rayet stars were known, 227 in 2001, while around 20 times more than this were predicted to exist in the Galaxy (see van der Hucht (2001). Sample groups of particular WR subtypes made evolutionary studies more difficult. WR to O star and WN versus WC sublass ratios are key for stellar evolution model tests. These values and their variation across the Galaxy were unclear. WR population estimates are major constraints for predicted evolutionary lifetimes (e.g., Maeder et al. 2014; Shenar et al. 2014). While studies of a larger sample of WR star ejecta nebulae could also provide information on evolutionary sequences and linkages to other high mass stars such as Luminous Blue Variables (LBVs).

Since 2001 more than 400 new WR stars have been discovered in the Galaxy. Predominantly due to new techniques in the infrared. A slew of estimates indicate a total number in the Galaxy as being between 1200 and 6000 stars (Shara et al. 2009; Rosslowe & Crowther 2015). More than 100 of these new discoveries come directly or indirectly from our work. We describe our methods and we indicate how our work is expected to continue in the future.

2 Defining WR candidates

2.1 Spitzer/GLIMPSE survey candidates

The best means of finding new stellar populations in the Galaxy is via infrared observations. The GLIMPSE legacy program on board the *Spitzer Space Observatory* allowed 4-colour broadband infrared imaging between 3.6 and 8.0μm covering the whole Galactic plane between galactic latitudes of -1 and +1 degrees. The extracted GLIMPSE point source catalogue and associated 2MASS sources provide the potential for identifying previously obscured and distant stellar populations Benjamin et al. (2003). It also provides an unbiased sample across the galactic plane, not just covering the dense massive star clusters where many WR stars have been found previously.

Strong winds from WR stars are responsible for producing free-free emission which shows as an infrared excess in the spectral energy distribution (SED). Morris et al. (1993) showed the observed wavelength spectral index of WR stars is -2.95 ± 0.25, providing a shallower spectral index than that of a pure photosphere. With a limited range of spectral indices, there is a narrow range of possible in-

frared colours. Results from fields observed early in the GLIMPSE survey were used to distinguish candidate objects, including the field around Westerlund 2 and RCW49 (see Figure 1). Candidate WR stars were defined by those objects in the colour-colour plot box shown in Figure 1 which contained all previously known WR stars. A similar candidate selection process was done for two less remarkable parts of the Galaxy at longitudes of 312 and 321 degrees.

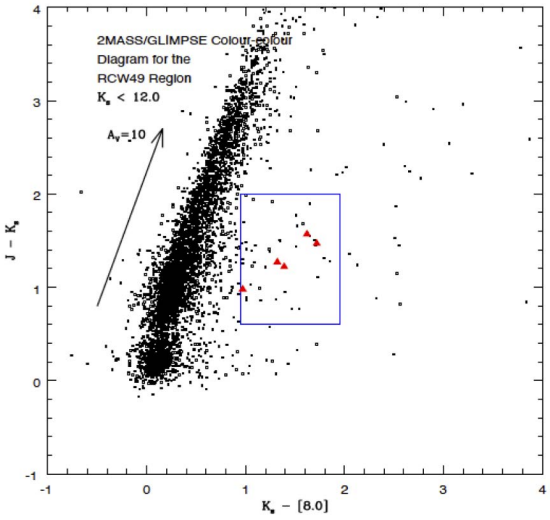

Fig. 1: Original colour-colour plot for objects in the RCW49 region for GLIMPSE identified objects with 2MASS K_s band magnitudes < 12.0, used in our NTT proposal. WR stars from the van der Hucht (2001) catalogue are shown as red triangles, while the blue box provides the boundary conditions used for identifying potential new WR candidates. A similar selection was done for 2x2 degree regions at galactic latitudes of 312 and 320 degrees. The reddening vector is based on Indebetouw et al. (2005).

Two main surprises of the work were: (a) the fact that WR stars were found well away from stellar clusters; (b) approximately 85% of all candidates showed emission lines, most of which appear to be lower mass Be stars.

2.2 Further WR discoveries

A larger followup of the galactic plane around l=312 degrees by Hadfield et al. (2007) provided 15 more WR star discoveries, while Mauerhan et al. (2011) provided a further 60 with somewhat improved candidate selection through GLIMPSE colour selections (see Figure 2).

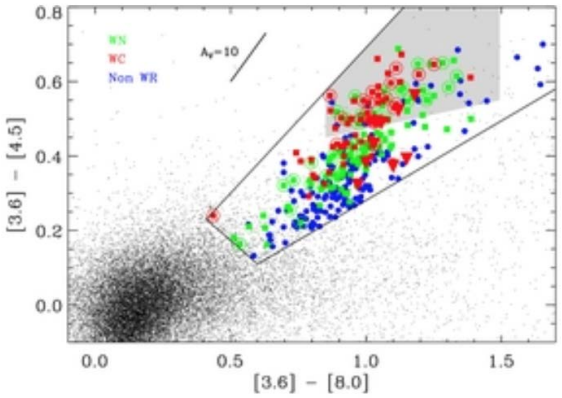

Fig. 2: WN and WC objects are seen in green and red in this colour-colour plot taken from Mauerhan et al. (2011). Candidate objects turning out not to be WR stars are shown blue. The gray shaded area indicates a 50%+ rate of WR detection from the candidate list. Dusty WC stars are shown by inverted red triangles.

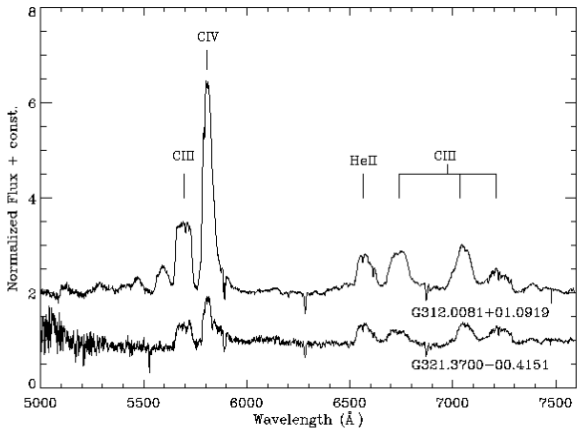

Fig. 3: CTIO/SOAR optical spectra taken by P. Morris and S. Van Dyk as confirmation to the SOFI near-infrared discoveries of WR60-5 and WR67-2.

2.3 Optical and Near-Infrared Spectra of WR candidates

Confirmation of WR candidates was achieved initially by near-infrared H and K band SOFI spectroscopy at the NTT on La Silla, Chile in 2004. Further optical spectroscopy of confirmed candidates was done in follow-up observations on the CTIO/SOAR telescope. Six WR stars have been discovered from this early work (see Marston et al. 2013; Roman-Lopes 2011b; Roman-Lopes 2011a; Roman-Lopes 2012). Optical spectra of two new WC stars found in this early work are shown in Figure 3.

2.4 Future candidate selection

We are currently looking into improving candidate selection criteria based on near- and mid-infrared colours (including MIPSGAL/Spitzer and WISE fluxes). We can start to make knowledge-based estimates of the probability/confidence level of and object's classification based on its colours. In this way we can potentially determine a statistical value of WR numbers in the galaxy – assuming a reasonable probability estimate is able to be done. To this end we have considered nearest-neighbour tests in infrared colour space. Potentially this could improve WR candidate identification considerably, but requires hypothesis testing via follow-up IR spectroscopic observations that we expect to make in the summer of 2015.

3 Followup of new WR stars - origins of isolated WR stars

Of the more than 100 WR stars discovered in follow-up spectroscopy of infrared colour-selected candidates, a large fraction of them are found well away from stellar clusters. In general, we have a bias against objects being found in clusters due to Spitzer confusion, our work therefore complements surveys such as those done in Westerlund 1 (Crowther et al. 2006). A number of new WR stars have been found towards the edges of stellar clusters (e.g. see Roman-Lopes 2011b; and the Danks clusters objects in Mauerhan et al. 2011). This hints at significant numbers of runaway stars from central dense stellar clusters.

Further out in the galaxy, a number of apparently isolated WR stars may well be scattered out from stellar clusters at earlier times (e.g., see Mackey et al. 2013) and indeed 25% of local O stars may be runaways (Blaauw 1993). GAIA results will help with determining proper motions of WR stars in the future.

But some objects appear too far from star forming areas to have been scattered from high density star forming sites within an average WR lifetime and suggest the possibility of *in situ* star formation, possibly associated with looser stellar associations. Although the lack of stellar clusters may simply be due to elusive lower mass clusters lost in infrared galactic confusion – "false negative clusters" Hanson et al. (2010).

4 Conclusions

Broad-band infrared colours have been successful in finding obscured and distant WR stars in our Galaxy. We plan to extend the work to better provide numbers and distributions of WR stars and their subclasses. Such information helps to constrain stellar evolutionary models of high mass stars and the current assumptions they make.

An alternative narrow-band infrared imaging technique, centred on the wavelengths of key spectral line features in WR spectra, has been performed in the Galactic plane and new WR discoveries have been reported in several papers including Shara et al. (2009) and Faherty et al. (2014).

Our studies show that WR stars are not all grouped in dense stellar clusters but many may be runaways or possibly created in relatively isolated regions or loose associations. Many of the objects also have nebulae (including a number of apparent ejecta nebulae) associated with them which provide a better statistical basis for the study of WR subclasses and ejecta plus timing of ejecta events.

References

Benjamin, R., Churchwell, E., Babler, B. L., et al. 2003, PASP, 115, 953

Blaauw, A. 1993, Massive Stars: Their Lives in the Interstellar Medium, ASP Conference Series, ed. J.P.Cassinelli & E. B.Churchwell, 35, 207

Crowther, P. A., Hadfield, L. J., Clark, J. S., Negueruela, I., & Vacca, W. D. 2006, MNRAS, 372, 1407

Faherty, J. K., Shara, M. M., Zurek, D., Kanarek, G., & Moffat, A. F. J. 2014, AJ, 147, 115

Hadfield, L. J., Van Dyk, S. D., Morris, P. W., et al. 2007, MNRAS, 376, 248

Hanson, M. M., Popescu, B., Larsen, S. S., & Ivanov, V. D. 2010, Highlights of Astronomy, 15, 794

Indebetouw, R., Mathis, J. S., Babler, B. L., et al. 2005, ApJ, 619, 931

Mackey, J., Langer, N., & Gvaramadze, V. V. 2013, MNRAS, 436, 859

Maeder, A., Przybilla, N., Nieva, M.-F., et al. 2014, A&A, 565, A39

Marston, A., Mauerhan, J. C., Van Dyk, S., Cohen, M., & Morris, P. 2013, Massive Stars: From α to Ω, held 10-14 June 2013 in Rhodes, Greece; Online at http://a2omega-conference.net, id167

Mauerhan, J. C., Van Dyk, S. D., & Morris, P. W. 2011, AJ, 142, A40

Morris, P. W., Brownsberger, K. R., Conti, P.-S., Massey, P., & Vacca, W. D. 1993, ApJ, 412, 324

Roman-Lopes, R. 2011a, ISRN Astronomy and Astrophysics, 2011, 632850

Roman-Lopes, R. 2011b, MNRAS, 410, 161

Roman-Lopes, R. 2012, MNRAS, 427, L65

Rosslowe, C. K. & Crowther, P. A. 2015, MNRAS, 447, 2322

Shara, M., Moffat, A. F. J., Gerke, J., et al. 2009, AJ, 138, 402

Shenar, T., Hamann, W.-R., & Todt, H. 2014, A&A, 562, A118

van der Hucht, K. A. 2001, New A Rev., 45, 135

Phil Massey: You've done well in eliminating false positives among your candidates, but what about false negatives? In other words, how sensitive are you to weak-lined WRs?

Anthony Marston: The broad-band selection technique should pick up all, since it depends on the free-free spectral index only (plus reddening) and *not* emission-line strength. So our only problem is recognizing the weak-lined WR stars in our candidate spectroscopy (as per narrow-band technique). Possible issues in spectroscopy are: hot dust emission, companion emission causing spectral feature dilution.

Lidia Oskinova: Integral field spectroscopy with SINFONI@ESO-VLT of an area around WR 102ka did not reveal a hidden low-mass cluster. It seems that some of the massive WRs are indeed quite isolated, just as you pointed out.

Anthony Marston: Thanks for this point, I am very aware of this case. We need to do a lot more work on possible isolated star formation (or massive star formation).

Anthony (Tony) Moffat: Tony (nice name, BTW), this is just a nit-pick, but on one of your opening slides you have O $\rightarrow$ RSG $\rightarrow$ WR for $M_{\rm i} = 25 - 40\,M_{\odot}$. But no one believes (does he?) that this happens; rather one has O $\rightarrow$ LBV $\rightarrow$ WR for such stars (just like the range $M_{\rm i} = 40 - 75\,M_{\odot}$), with only a few at the low-mass end going through a RSG stage.

Alexandre Roman Lopes: Concerning the "isolated formation" vs. "ejection" process, WR 67a is an interesting case. Do you have considered it in your studies? (Please see the figure with the cavity (NIR) and the "isolation" of the source.)

Anthony Marston: At present we have not properly looked at isolation and cluster ejection. It appears (at first glance) that these are both in the data. But this requires more checks and follow-up than we have done so far. WR 67a will be considered when we do this work.

Wolf-Rayet Stars
W.-R. Hamann, A. Sander, H. Todt, eds.
Potsdam: Univ.-Verlag, 2015
URL: http://nbn-resolving.de/urn:nbn:de:kobv:517-opus4-84268

SOAR Near-Infrared and Optical Survey of OIf* and OIf*/WN Stars in the Periphery of Galactic Massive Star Forming Regions

A. Roman-Lopes[1], G. A. P. Franco[2] & D. Sanmartin[3]
[1] *Universidad de La Serena, Chile*
[2] *Departamento de Física â "ICEx" UFMG, Caixa Postal 702, 30.123-970 Belo Horizonte, Brazil*
[3] *Southern Astrophysical Research Telescope (SOAR) Telescope, Chile*

In this contribution we present some preliminary results obtained from a SOAR-Goodman optical spectroscopic survey aimed to confirm the OIf* - OIf*/WN nature of a sample of Galactic candidates that were previously confirmed as massive stars based on near-infrared spectra taken with OSIRIS at SOAR. With only a few of such stars known in the Galaxy to date, our study significantly contributes to improve the number of known Galactic O2If* stars, as well as almost doubling the number of known members of the galactic sample of the rare type OIf*/WN.

1 The most massive hydrogen core burning stars

1.1 The earliest O-type stars and the OIf*/WN intermediate type

For a long time the O3 stars were considered to represent the most massive main-sequence stars. However, in the last decades it has become clear that some hydrogen-rich nitrogen sequence Wolf-Rayet stars are in reality extremely massive and luminous main-sequence stars (de Koter, Heap & Hubeny 1997; Schnurr et al. 2008; Smith & Conti 2008; Crowther et al. 2010), which because of their proximity to the Eddington limit present an emission-line spectrum at the beginning of their main-sequence evolution, mimicking the spectral appearance of classical WR stars. From the empirical determination of stellar masses of high-mass binary systems, and the use of state-of-the-art stellar models, it is now clear that such kind of massive stars probably belong to the OIf*/WN and WNH spectral types (Smith & Conti 2008; Crowther et al. 2010). This conclusion is supported by systematic studies of binaries made for example, by Schnurr et al. (2008) for R145 (in 30 Dor), Smith & Conti (2008) for WR25, Roman-Lopes (2013a) for WR22 (both in the Carina Nebula), Schnurr et al. (2009) for NGC3603-A1, Smith & Conti (2008); Bonanos et al. (2004), for WR20a (comprised of two O3If*/WN6-type stars with absolute masses of 83 and 82 M$\odot$), Roman-Lopes (2012) for WR21a (one WN6ha with an estimated minimum mass of 87 M$\odot$, and an early O-type secondary with a minimum mass of 53 M$\odot$), and more recently, Crowther et al. (2010) from the spectroscopic analyses of WNH stars located within the core of NGC 3603 and the 30 Doradus Nebula in the Large Magellanic Cloud. Indeed, some WNH stars in the core of 30 Doradus and NGC 3603 have computed initial masses in the range of 165-320M$\odot$, and 105-170M$\odot$, respectively.

The intermediate spectral type O3If*/WN6-A was introduced more than 30 years ago by Rauw et al. (1996) to classify the bright emission line star Sk-67 22 in the LMC, which shows intermediate spectra between those of HD93129A (the prototype of the O2If* class) and WR20aa (O2If*/WN5) (Figure 1). The OIf*/WN type can be distinguished from the OIf* and WNH types by the P-Cygni morphology of the Hβ line, since it is uniquely in absorption for O stars (including OIf* stars) and purely in emission for WN stars (Hadfield et al. 2007). New exemplars of the OIf*/WN spectral type were mainly found in the LMC, always consisting of bright massive objects (for more on this see for example, Walborn & Blades (1997); Melnick (1985); Crowther et al. (2010)). In the Galaxy, Roman-Lopes, Barba & Morrel (2011) and Roman-Lopes (2012, 2013a,b) using low-resolution SOAR-OSIRIS and NTT-SOFI NIR spectra, have identified five new exemplars of the type, whose Galactic sample possibly is still compound by less than 10 known exemplars to date.

1.2 Optical and near-IR spectroscopic classification

The classification of early-type stars has historically relied upon high quality blue visual spectra, to which UV morphological sequences have been added (e.g. Walborn 1982). With the advent of efficient detectors and large ground-based telescopes, the near-IR window has opened up (mainly the K-band) for spectral typing, albeit generally cruder with respect to optical spectroscopy (Gray & Corbaly 2009). This is especially relevant for highly obscured and distant emission line early-type stars, which have been discovered for example from near-IR narrow-band surveys (Crowther et al. 2006; Shara et al. 2009) and near to mid-IR spectral energy distributions (Hadfield et al. 2007).

In spite of the observational progress made during the last years, the number of known Galactic OIf*/WNH stars with studies in both, optical and near-IR domains is very small, only four! (WR20a,

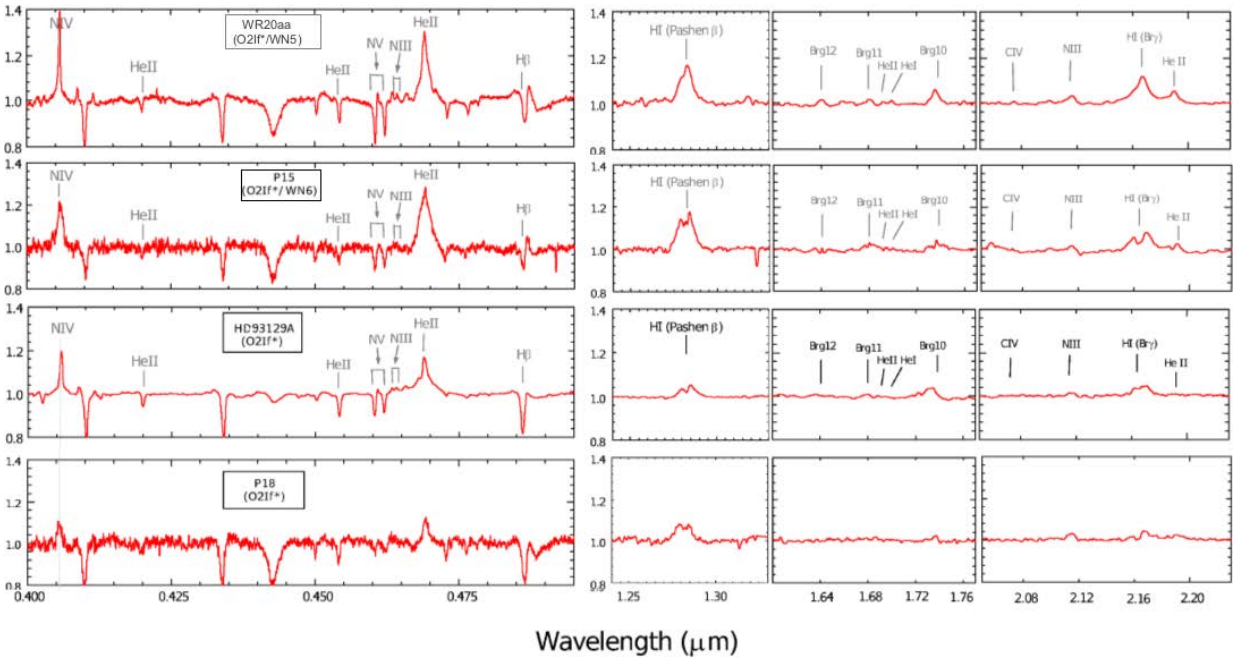

Fig. 1: Goodman and OSIRIS optical-NIR spectra of WR20aa (O2If*/WN5) and HD93129A (O2If*) taken at the SOAR telescope, together with the spectra taken for two (P15 and P18) newly discovered O2If* and O2If*/WN6 Galactic exemplars, with the main spectral lines indicated by labels. Despite the similar morphology, one can notice that the intensity of some key optical and NIR lines are quite different.

WR21a, WR25 - Crowther et al. (2010) and WR20aa - Roman-Lopes, Barba & Morrel (2011)). Considering that most (if not all) of the still unknown members of the OIf*/WNH Galactic population probably are going to be discovered (and properly studied) only from the use of NIR spectroscopic facilities, one relevant questions is, can we properly distinguish between Of, Of/WN and WN stars solely from near-IR spectroscopy? Before we can answer that, it is necessary to improve the number of known Galactic OIf*, OIf*/WNH and WNH stars with high quality optical and near-IR spectra.

2 Results

Here we present some results on our search for massive stars still unknown in the periphery of a sample of Galactic massive star regions. The 2MASS point sources there were studied based on a near-infrared selection criteria and from spectroscopic surveys aimed to determine their corresponding spectral types. From the related surveys, it was possible to successfully identify and classify at least four new Galactic O2If* stars, as well as a similar number of new Galactic exemplars of the intermediate OIf*/WN type.

2.1 SOAR observing runs and the OSIRIS and Goodman spectra

The NIR and optical spectroscopic data were obtained with the OSIRIS and Goodman instruments at the SOAR telescope during several runs from 2011 to 2015, with the data being taken on nights that in general presented good seeing conditions.

The NIR raw frames were reduced following standard reduction procedures, which are presented in details in Roman-Lopes (2009). The two-dimensional frames were sky-subtracted for each pair of images taken at two nod positions, followed by division of the resultant image by a master flat. The multiple exposures were combined, and then followed by one-dimensional extraction of the spectra. Also, the effects of the earth atmosphere in the NIR science spectra were corrected using J-, H- and K-band spectra of A-type stars, with the intrinsic hydrogen lines being carefully subtracted by modeling the observed line profiles through the use of Voigt profiles given by the SPLOT task on IRAF. The final NIR spectra were normalized through the fitting to the continuum emission observed in the associated wavelength range. On the other hand, the blue-optical Goodman spectra presented in this work were acquired using the 1.03" long slit with the 930 l/mm (M2 - 385-555nm) grating, which with the mentioned setup provides a maximum resolving

power R∼2100 (at 550nm). The reduction of the optical spectra was performed using standard techniques through the use of the packages (beside others) ONEDSPEC, TWODSPEC and APEXTRACT within IRAF. The one-dimensional spectra of the science targets were extracted from the two dimensional frames by summing pixels in the data range and subtracting off the background value for each column. The bad pixels were replaced through a linear interpolation of the removed data range, and the wavelength calibration was performed using Hg(Ar) + Ne lamp spectra. As was made in the case of the NIR spectroscopic observations, the final optical spectra were also normalized through the fitting of the continuum emission in the associated wavelength range.

2.2 Optical and NIR spectra of OIf*, OIf*/WNH and WNH candidates - two template cases

In Figure 1 it is shown the optical and near-infrared spectra of two Galactic stars of the O2If* (HD93129A) and O2If*/WN5 (WR20aa - Roman-Lopes, Barba & Morrel (2011)) types, together with the SOAR spectra taken for two new discoveries (P15 and P18) taken from our sample of new Galactic O2If* and OIf*/WN stars.

Regarding the O2If* sample, HD93129A together with MTT68 (Roman-Lopes 2013b) are probably the only two known Galactic exemplars of the class, with the former being considered the earliest, hottest, most massive and luminous O star in the Galaxy. Indeed, it is an extremely powerful X-ray source that has also an extremely powerful wind with a terminal velocity above 3000 km s^{-1}, and a mass-loss rate above 10^{-5} $M_{\odot}$ yr^{-1} (Cohen et al. 2011). From a direct comparison of the HD93129A's spectrograms with the optical and NIR SOAR spectra of P18, it is possible to conclude that P18 probably is the third known Galactic exemplar of the rare O2If* type. It is interesting to notice that the optical spectrogram of P18 presents a very intense DIB at 4427Å indicative of heavily optical reddening. In fact, the Goodman blue-optical spectrogram of P18 shown there was generate from the combination of 5 individual exposures of 1800s each, corresponding to about 2.5 hours of integration time at the SOAR telescope. On the other hand, the J-, H- and K-band spectrograms of P18 (also shown in Figure 1) are the results of the combination of 8 individual exposures of 90s each, and if we consider also the standard A0 star observed at the end of the science block (in order to suppress the telluric features imprinted on the original science spectra), the total integration time necessary to get the science + telluric sample corresponds to only 0.4 hours at the same telescope!

Finally in Figure 1 we also present the optical and near-infrared spectra of P15, which present the a very strong NIV 4058Å emission line much much stronger than the NIII emission lines around 4630-40Å , a feature typical of O2If* stars like HD93129A. On the other hand, the presence of a P-cygni profile in the Hβ line indicate that P15 is a new Galactic exemplar of the O2If*/WN6 type.

Acknowledgments

ARL thanks Nidia Morrel for very stimulating discussions about the classification of very massive stars in the optical and in the near-infrared, and from partial financial support of the DIULS Regular project PR15143.

References

Bonanos, A. Z., Stanek, K. Z., Udalski, A., Wyrzykowski, L., et al. 2004, ApJ, 611L, 33B

Cohen, David H., Gagné, Marc, Leutenegger, Maurice A., et al. 2011, MNRAS, 415, 3354

Crowther, Paul A., Hadfield, L. J., Clark, J. S., Negueruela, I.,et al. 2006, MNRAS, 372, 1407

Crowther, P. A., Schnurr, O., Hirschi, R., Yusof, N., Parker, R. J., et al. 2010, MNRAS, 408, 731

Crowther, P. A. & Walborn, N. R. 2011, MNRAS, 416, 1311

de Koter, A., Heap, S. R., Hubeny, I. 1997, ApJ, 477, 792

Gray, R. O., Corbally, C., J. 2009, Princeton University Press, 2009. ISBN: Ã978-0-691-12511-4

Hadfield, L. J., van Dyk, S. D., Morris, P. W., Smith, J. D., Marston, A. P., Peterson, D. E. 2007, MNRAS, 376, 248

Melnick, J. 1985 A&A 153, 235

Niemela V. S., Gamen R. C., Barbá R. H., Fernández Lajús E., Benaglia P., Solivella G. R., Reig P., Coe M. J., 2008, MNRAS,389, 1447

Rauw, G., Vreux, J.-M., Gosset, E. 1996, RMxAC, 5, 108

Rauw, G., De Becker, M., Nazé, Y., et al. 2004, A&A, 420, L9

Roman-Lopes, A. 2009, MNRAS, 398, 1368

Roman-Lopes, Barba, R. & Morrell, N. 2011, MNRAS, 416, 501

Roman-Lopes, A. 2012, MNRAS, 427, 65

Roman-Lopes, A. 2013a, MNRAS, 433, 712

Roman-Lopes, A. 2013b, MNRAS, 435, 73

Schnurr, O., Casoli, J., Chené, A.-N., Moffat, A. F. J., St-Louis, N. 2008, MNRAS, 389, 38

Schnurr, O., Moffat, A.F.J., Villar-Sbaffi, A., St-Louis, N., Morrell, N. 2009, MNRAS, 395, 823

Shara, M. M., Moffat, A. F. J., Gerke, J., Zurek, D., et al. 2009, AJ, 138, 402

Smith, N. & Conti, P. S. 2008, ApJ, 679, 1467

Walborn, N. R. 1982, ApJ, 254, L15

Walborn, N. & Blades, C. 1997, ApJS, 112, 457

Paco Najarro: Could you use the strength of the N IV 9–8 transition to distinguish between O I* and WN spectral class?

Alexandre Roman-Lopes: Thanks for the question. In my opinion, if one can successfully relate the strength of the observed H I Brackett recomlination line (relative to others in the same sequence) with the presence of the N IV emission line, that would probably be an interesting way to distinguish between those two spectral classes.

Geographical distribution of the participant's home institutes

Wolf-Rayet Stars
W.-R. Hamann, A. Sander, H. Todt, eds.
Potsdam: Univ.-Verlag, 2015
URL: http://nbn-resolving.de/urn:nbn:de:kobv:517-opus4-84268

Finding Wolf-Rayet Stars in the Local Group

P. Massey[1], K. F. Neugent[1], & N. I. Morrell[2]
[1]*Lowell Observatory, Flagstaff, AZ, USA*
[2]*Las Campanas Observatory, La Serena, Chile*

We summarize past and current surveys for WRs among the Local Group galaxies, emphasizing both the why and how. Such studies are invaluable for helping us learn about massive star evolution, and for providing sensitive tests of the stellar evolution models. But for such surveys to be useful, the completeness limits must be well understood. We illustrate that point by following the "evolution" of the observed WC/WN ratio in nearby galaxies. We end by examining our new survey for WR stars in the Magellanic Clouds, which has revealed a new type of WN star, never before seen.

1 Introduction

The motivation for WR surveys should be to improve our understanding of massive star evolution, and not just for the sake of adding a few more WRs to our lists. Stellar evolutionary modeling is hard, and there are numerous simplifications that our theoretician colleagues have had to adopt. How good are these approximations? Until we compare observations with the model predictions, we don't know. But, to succeed at this our surveys must be complete enough to be useful.

The basic premise of the "Conti scenario" (Conti 1975) is that a massive star strips off its H-rich outer layers through stellar winds, first revealing He and N, the products of the CNO cycle. If there is sufficient additional mass loss, then the star peels down far enough for us to see C and O, the productions of triple-α He burning. Today we would argue that this process is occasionally aided by Roche-lobe overflow in close binaries and/or episodic mass loss during the LBV stage (Smith & Owocki 2006), although whether these processes are important for most massive stars or not remains an open question.

These stellar winds are driven by radiation pressure in highly ionized metal lines, and hence the mass-loss rates are metallicity dependent. Since the nearby star-forming galaxies cover a range of 20× in metallicity (Massey 2003), these galaxies make ideal laboratories for studying massive star evolution as a function of metallicity.

We show in Fig. 1 an example of what we can learn from such studies. We have plotted the log of the relative number of RSGs and WRs against the metal abundance, measured from the oxygen content of H II regions, for four Local Group galaxies for which we believe the numbers are relatively complete. Note that this quantity changes by an order of magnitude over a similar change in metallicity. Maeder et al. (1980) was the first to suggest that this number ratio should be very sensitive to the (initial) metallicity of the stars, and that a comparison with observations would be a good test of the models.

If our surveys for WRs and other evolved stars are to be useful in learning about massive star evolution, we must be careful that they are complete, or at least that their limitations are well understood. To be useful, WR surveys must be sensitive enough to detect the weakest-lined WRs at the faintest magnitude limits one expects to find them, and be volume-limited, and not magnitude-limited.

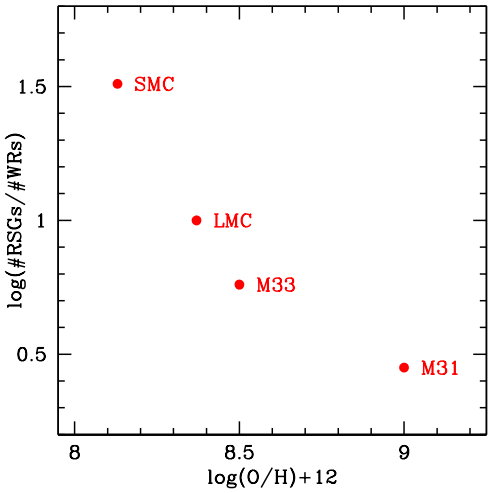

Fig. 1: We have counted the number of RSGs more luminous than $M_V \sim -5$ with $T_{\rm eff} < 4000$ and compared that to the number of WRs as a function of metallicity.

An advantage of using WRs in an external galaxy for such studies is that the stars all lie at essentially the same distances; thus the second criterion (being volume-limited) is automatically met. Sadly, studies of the WR content of the Milky Way do not share this, as distances are highly uncertain, greatly magnifying the problems with other selection effects. Nor is it clear what we learn by detecting a few WCs in more distant galaxies, so this review will be restricted to the WRs in Local Group.

2 Past Surveys for WRs

One of the testable predictions of massive star evolutionary models is the relative number of WC- and

WN-type WRs as a function of metallicity. In a completely mixed-age population (such as what we observe by averaging over many star-forming regions in a galaxy) we would naively expect this ratio to increase with metallicity according to the Conti Scenario, as at high metallicity we expect stars of somewhat lower masses will suffer sufficient mass-loss to become WC stars. At lower metallicities the mass limit for evolving to the WC stage should be higher. And indeed, when the first author was a graduate student, this was known to be the case, with the WC to WN ratio changing from about 1:7 in the low metallicity SMC and 1:1 in the Milky Way, while the LMC, at intermediate metallicity, had an intermediate ratio (1:4.5) (see e.g. Vanbeveren & Conti 1980). Shortly after that, Massey & Conti (1983a) confirmed that there was a galactrocentric gradient in the WC to WN ratio in M33, consistent, perhaps, with its metallicity gradient. And, our good colleagues (Moffat & Shara 1983, 1987) were busy discovering WRs in M31, almost all of WC type, again consistent (one might imagine) with M31's supersolar metallicity (Zaritsky et al. 1994).

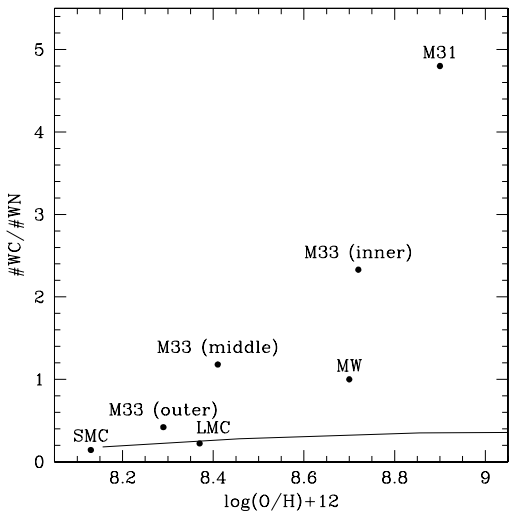

Fig. 2: The relative number of WC and WN stars as a function of metallicity as we knew from photographic studies, compared to the predictions of the Geneva evolutionary models from Meynet & Maeder (2005).

The problem came when one attempted to compare the actual numbers with the predictions of the stellar evolutionary models. Recall that the predicted ratio isn't simply due to the lowering of the mass limits with increased metallicities: the relative lifetimes of the WC and the WN stage also play a critical role. And when these are folded in with the mass limits, one finds a rather disturbing disagreement between the data (such as we knew it in the early 1980s) and the models, as Fig. 2 shows dramatically. (For convenience, we have adopted the predictions from the rotating models of Meynet & Maeder 2005, although we had nothing so advanced at the time.) We find that there is a factor of 13 difference between what the observations and models predict for the WC to WN ratio in M31! Clearly something was very wrong. Interpreted naively, this would suggest a horrendous problem with the model mass limits and/or WR lifetimes.

However, there was another possibility. The strongest optical emission line (C III λ4650) in WC-type WRs is, on average, much stronger than that of the strongest emission line (He II λ4686) in WN-type WRs (see, e.g., Massey et al. 1987; Conti & Massey 1989). What, then, if the surveys of the galaxies beyond the Magellanic Clouds were just very biased towards WCs? In all honesty, this thought did occur to us at the time; Massey & Conti (1983a) discuss this as a possibility, but conclude that the amount of incompleteness would have to be too great to explain the discrepancy even between the outer regions of M33 and the SMC/LMC.

2.1 A Brief Journey Through Time

To understand why the WC/WN ratios of the higher metallicities systems agreed so poorly with the models let us consider what we are calling the three eras of Local Group WR surveys.

The First Era: Photographic. The data in Fig. 2 came photographic surveys. These began with the Henry Draper Catalogue (1918–1924) and its extension (1925–1936), both general objective prism surveys which found many of the bright Galactic and LMC WRs. These were followed by general objective prism surveys of the Magellanic Clouds, (Sanduleak 1970; Azzopardi et al. 1975), which found not only OB stars but also a wealth of WRs. There followed the first searches specifically for WRs, namely Azzopardi & Breysacher (1979a,b, 1980). They did a very clever thing: they took photographic objective prism images of fields in the Magellanic Clouds, but added a 120Å wide filter that centered at 4650Å in order to isolate only objects with C III λ4650 and/or He II λ4686 emission. This had the advantage of cutting down on crowding, and also greatly reduced the sky contribution, allowing them to go much deeper than would otherwise have been possible. The photographic era ended with WR surveys being extended to the more distant members of the Local Group, M33 and M31. Wray & Corso (1972) used an on-band He II/C III filter and a continuum filter to take images of two fields in M33, identifying the first WRs beyond the Magellanic Clouds. The same technique was used by Massey & Conti (1983a) for a more extensive survey of M33, and by Moffat & Shara (1983, 1987) for two fields in M31.

The Second Era: Optimal filters and Small CCD fields. With the advent of CCDs, it was no longer necessary to blink on-band and off-band photographic plates trying to spot the change in brightness that would demark the presence of a WR star. Instead, quantitative photometry could be used to measure the brightness of all the objects on a CCD frame, and the magnitude differences compared to the photometric errors to find statistically significant candidates. Armandroff & Massey (1985) were the first to apply this technique, searching for WR stars in the nearby irregular galaxies NGC 6822 and IC 1613, as well as two test fields in M33. For this work they designed a new filter system, consisting of 50Å-wide bandpasses centered on C III λ4650, He II λ4686, and neighboring continuum at 4750Å. This system was designed to be optimized for the detection of WRs, using the extensive spectrophotometry of the normal (non-WR) stars from Jacoby et al. (1984) and WRs from Massey (1984) and Massey & Conti (1983b). They discovered three more WNs in NGC 6822 (Massey et al. 1987) in addition to the one previously known (Westerlund et al. 1983), but more importantly their study identified five new WN stars in a M33 field previously known only to contain six WCs and two WNs. (Compare Table 5 in Armandroff & Massey1985 to Table 2 in Massey et al. 1987.) Thus, in this one field the WC/WN ratio changed from 3.0 to 0.9. The significance of this was not immediately apparent, but further studies hammered home the point that the photographic studies had been woefully incomplete for WNs. In particular, Massey et al. (1986) surveyed eight small fields in M31 for WRs, identifying new WR candidates, many of which were subsequently spectroscopically confirmed as WRs (Massey et al. 1987; Armandroff & Massey 1991). Massey & Johnson (1998) extended these studies to include additional fields in M33, provided catalogs of all WRs beyond the Magellanic Clouds, and extensively discussed the selection biases against WNs. Their conclusion was that the photographic studies had been 50% incomplete for WNs, a number we might consider now to have been conservative. These studies also demonstrated the need for spectroscopic confirmation of any photometrically-detected WR candidates: none of the new IC 1613 WR candidates found by Armandroff & Massey (1985) turned out to be real. Similarly, Royer et al. (1998) designed their own photometric system aimed at identifying WRs, and used this to announce the discovery of the first WC9 stars detected in another galaxy (Royer et al. 2001). When observed spectroscopically, none of the WC9 candidates proved to be WRs (Crowther et al. 2003).

The Third Era: Large CCDs and Image Subtraction Techniques. Although CCDs were much more sensitive than photographic plates, and allowed quantitative assessment of the candidates, the early chips were *tiny* compared to plates, and the areal coverages about large enough to include a single OB association in one of these galaxies. The introduction of larger chips and mosaic cameras provided the means to finally complete surveys for WRs in M33 (Neugent & Massey 2011) and even M31 (Neugent et al. 2012a). Furthermore, our supernovae colleagues had spent years developing powerful image subtraction techniques. Combined with photometry, these greatly reduced the number of false positives we had typically experienced by just using photometry. (When one is considering 10,000 stars, a 3σ criterion will lead to 15 spurious detections!) With these deeper surveys what has happened to the large discrepancy with the models shown in Fig. 2? The improved data are shown in Fig. 3.

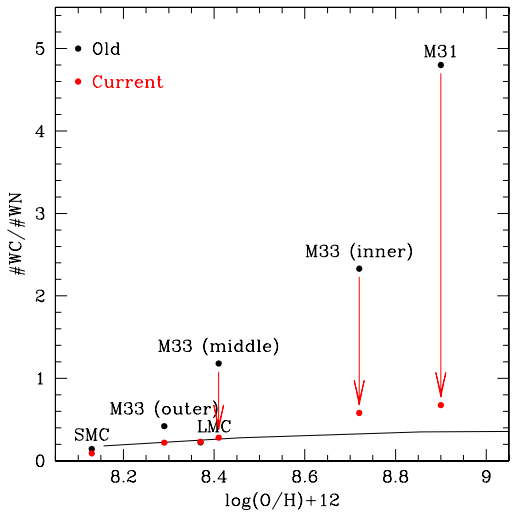

Fig. 3: The relative number of WC and WN stars as a function of metallicity as we know today (red) compared to the older data shown in Fig. 2. The agreement with the models is significantly improved!

What haven't we included in Fig. 3? First, we have ignored NGC 6822 and IC 1613 due to their very small number statistics: NGC 6822 has four WNs confirmed (Massey et al. 1987, and references therein). There is one WR star known in IC 1613; this is of WO-type. We have also not included any numbers for the Milky Way, as we suspect that these are still incomplete, and defining a volume-limited sample from the distances derived from spectral types to contain too many biases.

The galaxy most conspicuous by its absence is IC 10. IC 10 is a metal-poor (log O/H+12 ~8.3) irregular Local Group galaxy, chracterized as a starburst due to the surprising discovery of 15 WRs by Massey et al. (1992) and Massey & Armandroff (1995). This meant that IC 10 had $\sim$ 5$\times$ the surface density of WRs as the SMC, compa-

rable to that found in the most active OB associations (Massey & Holmes 2002). Even more surprising was that the WC/WN ratio in IC 10 was very high, ∼2, despite the fact that the metallicity was low; one would expect a value about 0.2. Although it seemed unlikely that the answer was that there were a very large number of WNs unaccounted for, nine of the additional candidates found by Royer et al. (2001) were spectroscopically confirmed by Crowther et al. (2003), demonstrating the incompleteness of the Massey et al. (1992) survey. Using deeper images, Massey & Holmes (2002) in fact found a large number of additional candidates, suggesting that the total WR population of IC 10 might be as large as 100! The WC/WN ratio to now down to 1.2, and many dozens of candidates still await spectroscopy.

What else have we learned from the study of WRs in nearby galaxies? For one thing, the relative number of early and late WNs change with metallicity, as does the the relative number of early and late WCs (Table 1). For the WCs we think we understand this purely as a metallicity effect on the spectral appearance (Crowther et al. 2002), but for the WNs, something more complicated is going on.

Tab. 1: Early and Late-Type WRs

Galaxy	log O/H +12	WNE/ WNL	WCE/ WCL
SMC	8.1	4.5	∞
M33out	8.3	4.4	∞
LMC	8.4	1.6	12
M33mid	8.4	1.2	1.8
M33in	8.7	0.9:	1.3
M31	8.9	1.2	0.4

3 A Modern Survey for WRs in the Magellanic Clouds

During the 2013 Rhodes meeting the three authors decided that we had to conduct a modern search for WRs in the Magellanic Clouds. Although the prevailing wisdom was that the WR content of the Clouds was mostly known, 7 new LMC WRs had been found accidentally since the Breysacher et al. (1999) catalog. All but one of these were WNs, suggesting that the WC/WN ratio might be biased even in the Magellanic Clouds. The seventh star was found by ourselves, and was a very strong-lined WO-type star, only the second known in the LMC (Neugent et al. 2012b). So, it seemed as if we still had some work to do. We designed a multi-year project, in which we would apply the same successful techniques used in M33 and M31 by Neugent & Massey (2011) and Neugent et al. (2012a), with the imaging done on the Las Campanas Swope, and the followup spectroscopy with Magellan.

We have now finished the second year of the survey; our results are described by Massey et al. (2014) and Massey et al. (2015). With 60% of the survey complete, we have discovered 13 new WRs in the LMC, plus a variety of other previously unknown interesting emission-line objects. However, the most interesting finding is that 8 of these 13 WRs are of a type never before recognized, stars that would naively be classified as WN3+O3 V. These stars are, however, too faint (by several magnitudes) to harbor an O3 V star, and our modeling has shown that we can reproduce both the emission and absorption lines with a single set of physical parameters (Massey et al. 2014). In this conference, Neugent et al. (2015) discuss these stars in detail. Here we would like to comment on a simple question: why haven't we found these stars elsewhere?

Surveys such as ours are not just flux-limited. As emphasized by Massey & Johnson (1998), what matters is the magnitude *difference* Δm between the on-band filter and the off-band filter. Thus, even though an Of-type star has a great deal of flux in the He II λ4686 emission line, they are relatively difficult to detect because they are also bright in the continuum. In other words, the detection limit is sensitive to the equivalent width of the line as a function of continuum flux. In Fig. 4 (left) we see the WRs and Of-stars we successfully detected in our survey, along with our 3σ and 5σ detection limits.

Fig. 4 (left) shows that our survey goes several magnitudes deeper than the faintest WN3/O3s we find, and so there aren't even fainter ones that we are missing. Note too that one or two of the SMC WNs are in a similar region of the diagram. All but one of the SMC WRs show absorption lines, and for many years there has been speculation that all of these stars are binaries, yet only four have orbit solutions. Hainich et al. (2015) has now shown that the absorption and emission can be modeled with a single set of physical parameters. The SMC WNs are more luminous visually than our WN3/O3s, and thus are not the same thing, but likely are related.

Why haven't WN3/O3s been found elsewhere in the Local Group? They probably don't form at high metallicities as no Milky Way ones are known, so it's not surprising that we haven't found them in M31. But what about M33? Earlier we've said that surveys need to be "sensitive enough to detect the weakest-lined WRs at the faintest magnitude limits one expects to find them." But what if we don't know how faint that is? The LMC WN3/O3s are quite faint, with $M_V \sim -2.5$ to -3.0. Do we go sufficiently deep in the M33 survey to find them? As Fig. 4 (right) shows, the answer is "no." We should have found most of the other M33 WRs, but to find WN3/O3s will require a bit more work, and we are planning deeper imaging to find such stars.

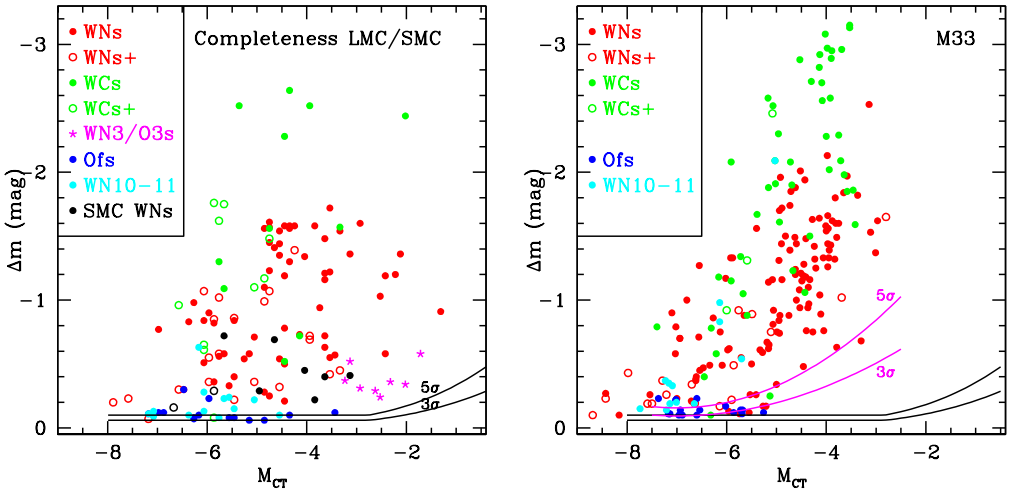

Fig. 4: The magnitude difference Δ m is plotted against the absolute magnitude $M_{\rm CT}$ for WRs in the LMC/SMC (left) and in M33 (right). The 5σ and 3σ detection limits are shown.

We gratefully acknowledge support of this project by Lowell Observatory and the National Science Foundation through AST-1008020.

References

Armandroff, T. E. & Massey, P. 1985, ApJ, 291, 685
Armandroff, T. E. & Massey, P. 1991, AJ, 102, 927
Azzopardi, M. & Breysacher, J. 1979a, A&A, 75, 120
Azzopardi, M. & Breysacher, J. 1979b, A&A, 75, 243
Azzopardi, M. & Breysacher, J. 1980, A&AS, 39, 19
Azzopardi, M., Vigneau, J., & Macquet, M. 1975, A&AS, 22, 285
Breysacher, J., Azzopardi, M., & Testor, G. 1999, A&AS, 137, 117
Conti, P. S. 1975, Memoires of the Societe Royale des Sciences de Liege, 9, 193
Conti, P. S. & Massey, P. 1989, ApJ, 337, 251
Crowther, P. A., Dessart, L., Hillier, D. J., Abbott, J. B., & Fullerton, A. W. 2002, A&A, 392, 653
Crowther, P. A., Drissen, L., Abbott, J. B., Royer, P., & Smartt, S. J. 2003, A&A, 404, 483
Hainich, R., Pasemann, D., Todt, H., et al. 2015, A&A, in press
Jacoby, G. H., Hunter, D. A., & Christian, C. A. 1984, ApJS, 56, 257
Maeder, A., Lequeux, J., & Azzopardi, M. 1980, A&A, 90, L17
Massey, P. 1984, ApJ, 281, 789
Massey, P. 2003, ARA&A, 41, 15
Massey, P. & Armandroff, T. E. 1995, AJ, 109, 2470
Massey, P., Armandroff, T. E., & Conti, P. S. 1986, AJ, 92, 1303
Massey, P., Armandroff, T. E., & Conti, P. S. 1992, AJ, 103, 1159
Massey, P. & Conti, P. S. 1983a, ApJ, 273, 576
Massey, P. & Conti, P. S. 1983b, ApJ, 264, 126
Massey, P., Conti, P. S., & Armandroff, T. E. 1987, AJ, 94, 1538
Massey, P. & Holmes, S. 2002, ApJ, 580, L35
Massey, P. & Johnson, O. 1998, ApJ, 505, 793
Massey, P., Neugent, K. F., & Morrell, N. 2015, ApJ, 807, 81
Massey, P., Neugent, K. F., Morrell, N., & Hillier, D. J. 2014, ApJ, 788, 83
Meynet, G. & Maeder, A. 2005, A&A, 429, 581
Moffat, A. F. J. & Shara, M. M. 1983, ApJ, 273, 544
Moffat, A. F. J. & Shara, M. M. 1987, ApJ, 320, 266
Neugent, K. F. & Massey, P. 2011, ApJ, 733, 123
Neugent, K. F., Massey, P., & Georgy, C. 2012a, ApJ, 759, 11
Neugent, K. F., Massey, P., Hillier, D. J., & Morrell, N. 2015, in Wolf-Rayet Star Workshop, ed. W. Hamann, A. Sander, & H. Todt
Neugent, K. F., Massey, P., & Morrell, N. 2012b, AJ, 144, 162
Royer, P., Smartt, S. J., Manfroid, J., & Vreux, J.-M. 2001, A&A, 366, L1
Royer, P., Vreux, J.-M., & Manfroid, J. 1998, A&AS, 130, 407
Sanduleak, N. 1970, Contributions from the Cerro Tololo Inter-American Observatory, 89
Smith, N. & Owocki, S. P. 2006, ApJ, 645, L45
Vanbeveren, D. & Conti, P. S. 1980, A&A, 88, 230
Westerlund, B. E., Azzopardi, M., Breysacher, J., & Lequeux, J. 1983, A&A, 123, 159
Wray, J. D. & Corso, G. J. 1972, ApJ, 172, 577
Zaritsky, D., Kennicutt, Jr., R. C., & Huchra, J. P. 1994, ApJ, 420, 87

Anthony (Tony) Moffat: (1) The absorption lines you refer to in these weak-line WN stars are not truly photospheric; they have negative RVs relative to the star and are formed in the wind (albeit near the base), not in the stellar photosphere.

(2) In Foellmi et al. (2003) we assigned spectral types of WNha or WNh to many SMC and some LMC WNE stars, which is an alternative that precedes your designation as WN + O or WN/O. As Paul Crowther stated the next day of this meeting to K. Neugent, "You don't need to invent yet another designation".

Philip Massey: (1) Actually according to our CMFGEN modeling, these absorption lines ARE photospheric: the winds are thin enough that we would call the formation region for the absorption photospheric. (2) There are a number of problem with your nomenclature (see Conti 1999, New Astronomy, 4, 489) but one of the most obvious ones in this case is that the "WNa" doesn't really give any description of what the absorption spectrum is like. Does it contain He I and He II? Does it show hydrogen absorption? Is it purely He II? So, that is why we have been using our current designation. The absorption we see is both stronger and of earlier type than that found in the "WN3+O3-4" stars that Massey & Duffy (2001, ApJ, 550, 713) Massey et al (2003, PASP, 115, 1265) discovered in the SMC plus the ones that were already known, as as SMC WR-1. Our LMC WN3/O3s are nothing like HD 9974 (aka WR3) and spectrally not like the SMC WNs, other than in the sense of being "WN3+abs".

Wolf-Rainer Hamann: In some of your statistics you were distinguishing between WNE and WNL stars. I am not sure if this categories do tell the same about their evolutionary stage when considering different metallicity environments. In the Galaxy, the early and late types generally coincide with the absence and presence of hydrogen, respectively. In contrast, the WNE stars in the SMC use to display hydrogen in their spectra (see talk by Rainer Hainich).

Philip Massey: Conti, Garmany, & Massey (1989, ApJ, 341, 113) discussed this, and we suggested that because the wind density might be lower in the SMC WNs that one way of looking at the situation was that the low metallicity resulted in "animals spectral classifications": if the SMC WNs were WNLs rather than WNEs, then their weak lines and the presence of hydrogen would be expected.

Wolf-Rainer Hamann: Comparing the relative number of WNE to WNL stars as a function of metallicity may not be relevant.

Philip Massey: I agree that the comparison of the number of early- and late-WN stars is hiding a lot of the physics. Still, this is the sort of thing that it would be great we could reproduce well with evolutionary models.

Richard Ignace: It appears that there may be a relatively high ratio of WO/WR [in the LMC]. Could you comment?

Philip Massey: We've found two new WOs in the LMC, bringing the total number of WOs known to 3, out of 152. Is that a lot? I don't know; its 2%. In IC 1613, one out of 1 WRs is a WO, so that's a much higher ratio (100%). In the SMC, 1 out of 12 WRs is a WO (8%). So, I don't know how to separate small number statistics from metallicity effects. In the MW, there are four (?) WOs know, out of nominally 600 WRs according to Paul. Is that a metallicity effect, or does it say how poorly we understand the WRs content of the MW?

Christopher Rosslowe: I agree that there are problems with the distances to Galactic WR stars, but I think we're improving things gradually. An advantage of the Galaxy is we can spatially resolve nearby WR stars in clusters – closely spaced WR stars of similar spectral types would presumably appear as single WRs at extra-galactic distances. How much of a problem do you think this is in your surveys?

Philip Massey: This is a potential problem, but it's rare to have two WRs that close to each other. This sort of question always arises in studying stars in nearby galaxies; Rolf Kudritzki notes though that usually there are spectral anomalies that show if one is dealing with one star or two. So, to me if you can fit the spectrum of a star with a single set of physical properties, you are likely (but not certain) to be dealing with a single object. The Potsdam group has done such a nice job fitting the WNs in the LMC with PoWR models (Hainich et al. 2014, A&A, 565, 27), and I think we know which ones have companions.

Dominik Bomans: Going to low metallicity implies lower absolute numbers. Do you see a limit for you WC/WN analysis. I notice you did not mention IC 10 and IC 1613.

Philip Massey: Well, of course it's not just the metallicity; it's also the star formation rates that affect the absolute numbers. For instance, Massey & Holmes (2002, ApJ, 580, L35) claims that IC 10 may have as many as 100 WRs, despite its low metallicity ($\log \mathrm{O/H} + 12 = 8.25$, intermediate between that of the SMC and LMC). I didn't use IC 10 because we are still working on confirming candidates spectroscopically. IC 1613 has a much lower metallicity but it only has one WR star, a WO. Dany has been preaching the importance of binaries in massive star evolution for decades, and I think that IC 1613 WR is an example of where binary evolution really does actually matter.

Anthony (Tony) Moffat: An afterthought (submitted after the conference) to the answer of Phil Massey on my first question:

(1) HD 193077 = WR138 was found to be a long-period binary by Annuk (1990), albeit with fairly noisy RVs especially for the O component. More recently in 2014 (N. Richardson et al., in prep.) we have obtained CHARA snapshot data for this system and find that it is indeed a wide binary (separation 3 milli-arcsec) with NIR magnitudes for both stars that correspond quite well with the spectral types. Parallel CHARA observations show that the other Cygnus long-period binary WR137 = HD 192641 (Lefevre et al. 2005) also has two components separated by 4 milli-arcsec.

(2) Smith et al. (2000, New Astronomy, 5, 423) have dispensed with Conti's (1999) critiques of the otherwise generally well-received Smith et al. (1996) 3D classification system for WN stars. In particular the WN3ha type fits very well for the Galactic WR star WR3, as well as similar types for many weak-line WN stars in both Magellanic Clouds. "h" refers to the presence of hydrogen from the alternating Pickering decrement, while the "a" refers to the presence of hydrogen and other absorption lines intrinsic to the WR star.

Philip Massey: (1) It's funny how two of my thesis stars, HD 193077 and HD 9974, keep being mentioned at this conference! As far as HD 193077 is concerned, I think the jury is still out. Massey obtained many high dispersion spectra of reasonable S/N over three years, finding no evidence of radial velocity variations. We demonstrated that using the centroid of the intensity cubed produced much smaller scatter in the radial velocities than using the simple centroid. Annuk took much poorer quality data, and then tried to combine this with the lower accuracy measurements to decide this star had a 1500 day period. I suspect his result had more to do with the sampling of the measurements than with any actual velocity measurements. The result of the 3mas separation is quite interesting, and I look forward to seeing this as a published result rather than simply reported as "in prep." But, I have to ask then, that companion must be quite an unusual object—our fourier analysis showed that the absorption component was broadened *by rotation* by 500 km/s, higher than that of any known O star. I guess we just did something fundamentally wrong? Still, I'm curious how you can have it both way: a 1500 day period of a $30\,M_\odot$+$30\,M_\odot$ star would have an orbital separation of about 10 AU by Kepler's 3rd law, wouldn't it? If HD 193077 is a member of Cyg OB1, its distance is about 2 kpc. So, that would imply a separation of about 5 mas. I suppose it could be the same punitive companion, but if not, it's a very crowded system. I do think it will be interesting to see if we can reproduce the spectrum of HD 193077 with a single set of physical parameters; I'll send you a preprint once we have this sorted out.

(2) The Smith et al classification scheme has never really caught on, and I think for good reasons. Other than you and your co-authors, and Paul Crowther's group, this system is seldom used. One of my principle objections is that it buries the nature of the absorption spectrum: if you see a WNE+abs spectrum with the "abs" containing lots of He I, well, it's pretty unlikely that the absorption comes is intrinsic. On the other hand, if it's "WNE+abs" with the "abs" dominated by He II with little or no He I, you have to work at it to figure out if the "abs" is intrinsic or from a early-type companion. Despite a few advantages to this scheme, it was not adopted by van der Hucht in his VIIth catalog, by BAT99 in their catalog of LMC WRs, or by Neugent in their classification of hundreds of WRs in M31 and M33. So, I guess you haven't really convinced the rest of us of the usefulness of the third parameter. Besides, the notation is, frankly, awkward.

Anthony (Tony) Moffat (Email, still continuing the after-workshop discussion): (1) Regardless of which spectroscopic data set one believes for WR 138 (HD 193077), the newly discovered, clear presence from CHARA of a resolved companion with appropriate brightness and separation says it all, subject to being published of course. Our observed snapshot projected separation of 3 mas would seem entirely compatible with your estimate of $a = 5$ mas. Also, at this meeting Dany Vanbeveren stressed that O stars in WR+O binaries could have spun-up rotations after RLOF ranging up to some 700 km/s, entirely compatible with the width of 500 km/s for the O star in WR 138.

(2) Actually the Smith et al. (1996) 3D classification system (ionization, hydrogen and line width being the 3 prime dimensions, as had been suspected for some time before this, but never before systematically incorporated into a unique classification system like this one) enjoys a lot of use beyond the world of Peter Conti, yourself and collaborators. In particular, the well-used on-line Galactic WR Catalogue of P. Crowther now numbers over 640 entries and uses the Smith et al. system, along with a variety of references for it. The Smith et al. classification system is clearly laid out and summarized in Table 4 on page 169 of Smith et al. (1996). As a result, the designations are quite simple and straightforward to apply, not to mention their obvious utility. For example, the absorption-line criterion "+abs" means that the absorption lines are of unknown origin. However, if one knows from other evidence that the absorption lines come from the WR star (e.g. from orbital motion or convincing lack thereof) and there is H present in emission, then one simply adds the suffix "ha" to mean that the absorption lines are indeed intrinsic to the WR star. If on the other hand, the star is an SB2 or there are H-absorption line without evidence of H emission, then one can convert "+abs" to "+OB", with "OB" assigned to a more specific subtype as appropriate. There are plenty of WNE+abs stars which

have now been converted to WNEha, especially in the Magellanic Clouds (Foellmi et al. 2003a,b), but also among Galactic stars such as WR3 = HD 9974, WN3ha, which Marchenko et al. (2004) showed convincingly that it is indeed single.

Wolf-Rayet Stars
W.-R. Hamann, A. Sander, H. Todt, eds.
Potsdam: Univ.-Verlag, 2015
URL: http://nbn-resolving.de/urn:nbn:de:kobv:517-opus4-84268

Detection and Characterization of Wolf-Rayet stars in M81 with GTC/OSIRIS spectra and HST images

V. M. A. Gómez-González, Y. D. Mayya & D. Rosa-González
Instituto Nacional de Astrifísica, Óptica y Electrónica, Mexico

Here we investigate a sample of young star clusters (YSCs) and other regions of recent star formation with Wolf-Rayet (W-R) features detected in the relatively nearby spiral galaxy M81 by analysing long-slit (LS) and Multi-Object Spectroscopy (MOS) spectra obtained with the OSIRIS instrument at the 10.4-m Gran Telescopio Canarias (GTC). We take advantage of the synergy between GTC spectra and Hubble Space Telescope (HST) images to also reveal their spatial localization and the environments hosting these stars. We finally discuss and comment on the next steps of our study.

1 Introduction

W-R stars, the short-lived descendants of massive O-type stars at their last stages of evolution, are expected to have an important influence on the energetics, dynamics and chemical evolution of the interstellar medium over the lifetime of galaxies (Hillier 2000). Hence the importance of their study in different galaxies and environments. Even though their mere detection reveals recent burst of high-mass star formation in galaxies (Schaerer & Vacca 1998).

Here we report and characterize an initial sample of YSCs and other regions where we detected W-R features in their spectra: like the strong and broad emission lines of He II, N and C. These were discovered in the disk of the relatively nearby spiral galaxy M81 (3.63 Mpc, m-M = 27.8; Freedman et al. (1994)). W-R features were found by analysing LS and MOS spectra obtained by using the OSIRIS instrument at the 10.4-m GTC in three different seasons of observation. We performed a very detailed multiple Gaussian fitting of the nebular and broad emission lines within the so called W-R bumps to classify these objects into the Nitrogen (WN) or Carbon (WC) sequence, and early (E) or late (L) subtypes, and also to obtain some of their most important parameters: like their typical luminosities, EWs and magnitudes (paper in prep.). Additionally, the use of HST images reveals their spatial localization as well as their environments. The detection of W-R features immediately places strong constraints on several parameters, like the age of the most recent starburst episodes.

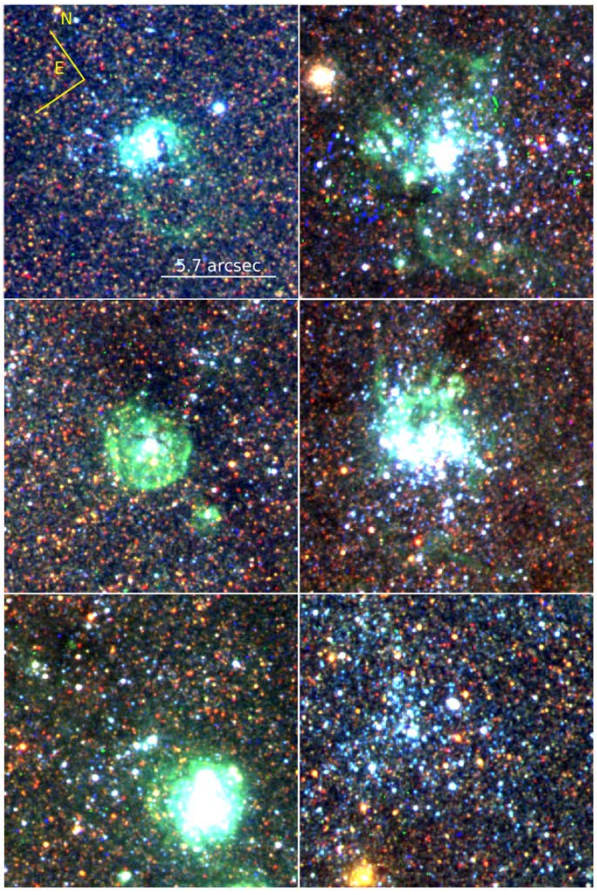

Fig. 1: A representative sample of 6 of the 14 YSCs and other regions hosting the W-R features in M81. The color stamps were formed by combining: B, V and I HST filters. W-R stars are located at the center of each image which it is not necessarily the center of the cluster. Note the ionized gas in form of bubbles and shells extending at least tens to hundreds of pc surrounding some of these objects and presenting a rich diversity of morphologies but also "isolated" with absence of ionized gas around. The orientation and a scale of 5.7 arcsec (100 pc) are also shown for reference.

2 Observations

GTC/OSIRIS observations on M81 W-R stars as well as the HST images used in our study, are briefly presented in this section.

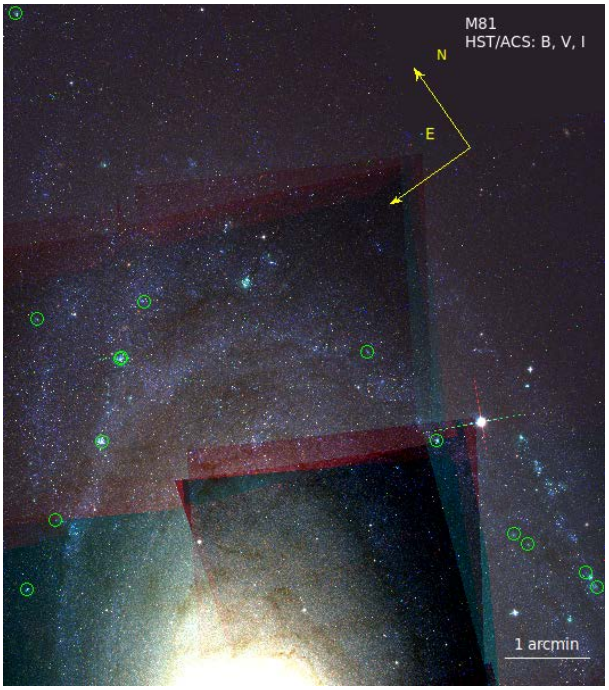

Fig. 2: An image of a section of M81 formed by combining: B, V and I HST filters, showing the spatial locations of the W-R stars detected (green circles). It can be seen that these were discovered in the disk, mostly in the spiral arms of the galaxy. The orientation and a scale of 1 arcmin are also shown for reference.

2.1 Spectroscopy: GTC/OSIRIS

Spectroscopic observations were carried out with the OSIRIS instrument at the 10.4-m GTC in three different seasons of observation with both the LS and MOS. Observations included bias, flat fields, calibration lamps and standard stars. Slits of width 1.2 arcsec, a spatial scale of 0.254 arcsec/pix, the spectra cover a range from 3700 to 7500 Å, with a spectral resolution around 7 Å, and a seeing of around 0.7-1 arcsec. Data reduction were carried out in the standard manner by using the tasks available in the IRAF software package. Fig. 3. shows an example for WR1.

2.2 HST images

We use HST images of M81 publicly available in three different filters: B (F435W), V (F606W) and I (F814W) (PI: Andreas Zesas). With a sampling of 0.05 arcsec/pix which at the distance to M81 it corresponds to 0.88 pc/pix. The spatial resolution in these images, measured as the Full Width at Half Maximum (FWHM) of the Point Spread Function (PSF) is 2.1 pixel (1.8 pc).

The use of HST images reveals the spatial localization of the YSCs, associations and other regions hosting the W-R stars as well as their environments, located in the disk, mostly in the spiral arms of the M81 (see Fig. 2). Shells and ring nebulae have been observed for a subset of W-R stars in M81 exhibiting a variety of morphologies and sizes. These are believed to represent material ejected during the red supergiant (RSG) or luminous blue variable (LBV) phases that is photo-ionized by the W-R stars (Crowther 2007).

3 Analysis and Discussion

Because of the quality of our spectra, we have adopted the approach of Brinchmann et al. (2008) to estimate the bump luminosity of the W-R stars. We calculate the excess flux above the best-continuum in regions around the main W-R features, for each feature we fit the relevant nebular emission lines jointly with multiple Gaussian for each bump which can be expected to be present. Fig. 4. shows an example for WR1. Visual spectral classification of W-R stars is based on emission line strengths and line rations following Smith (1968). WN spectral subtypes follow a scheme involving line ratios of N III-V and He I-II, ranging from WNE to WNL. WC spectral subtypes depend on the line ratios of C III and C IV lines ranging from WCE to WCL (Crowther 2007).

We detected 14 W-R stars in M81 by combining GTC spectra with HST images. All objects present WN features, mostly late type (WNL), 6 of these present additional WC features, early type (WCE). Observed luminosities of He II λ 4686, C IV λ 5808 broad lines are more in agreement with those found in the Milky Way for single WR stars than in the LMC. This is consistent with the near to solar metallicity of M81. The obtained important parameters: like their typical luminosities, EWs and magnitudes will be reported in a coming paper (in prep.)

This work was supported by CONACyT (Mexico) research grant.

References

Brinchmann, J., Kunth, D., & Durret, F. 2008, Astronomy and Astrophysics, 485, 657

Crowther, P. A. 2007, Annual Review of Astronomy & Astrophysics, 45, 177

Freedman, W. L., Hughes, S. M., Madore, B. F., et al. 1994, Astrophysical Journal, 427, 628

Hillier, D. 2000, Encyclopedia of Astronomy and Astrophysics

Santiago-Cortés, M., Mayya, Y. D., & Rosa-González, D. 2010, Monthly Notices of the Royal Astronomical Society, 405, 1293

Schaerer, D. & Vacca, W. D. 1998, The Astrophysical Journal, 497, 618

Smith, L. F. 1968, Monthly Notices of the Royal Astronomical Society, 138, 109

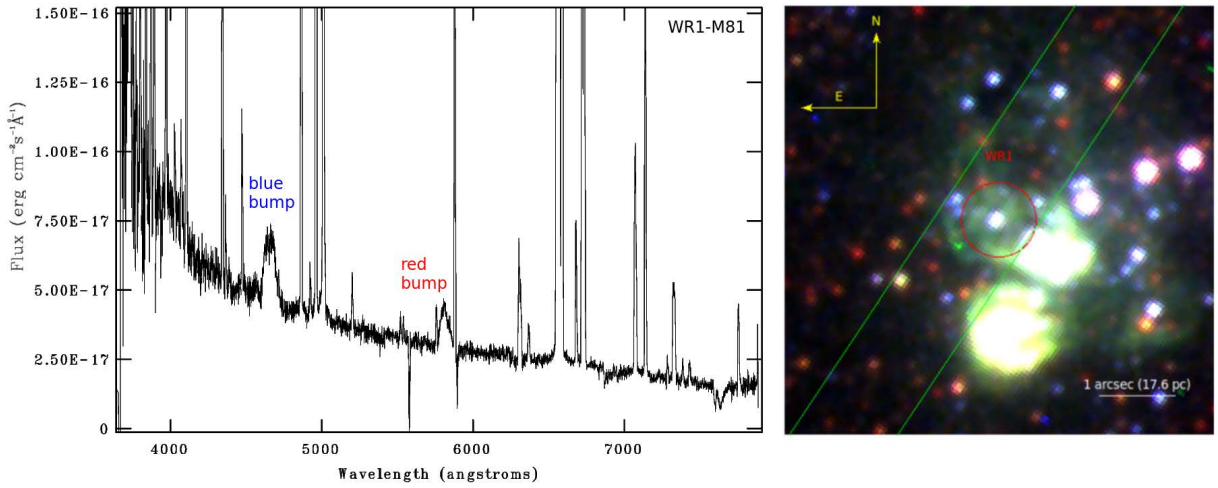

Fig. 3: (Left) An extracted spectrum of WR1, discovered with GTC/OSIRIS long-slit data. As can be seen, it presents strong and broad emission lines, due to their powerful stellar winds, instead of the narrow absorption lines that are typical of normal stellar populations (Crowther 2007); (Right) Thanks to the great spatial resolution of the HST images we can appreciate the environment surrounding the W-R stars in great detail: WR1 (red circle) is located in a rich star cluster complex, not in the center of it, and presenting several bubbles of ionized gas, whose spectra are also separately detected in the ccd. At 1 arcsec to the West there is F04B16353, this is a blue stellar cluster previously reported in the catalogue of Santiago-Cortés et al. (2010). WR1 was has the highest galactocentric radius of the sample. The slit-width (green rectangle) is 1.2 arcsec. A scale of 1 arcsec (17.6 pc) is also shown for reference. North is up, East to the left.

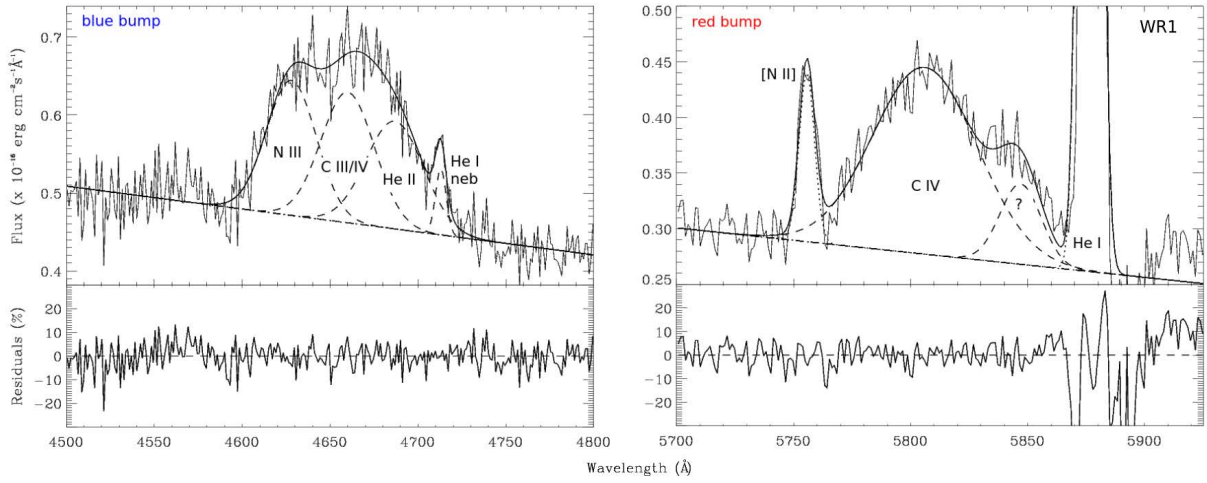

Fig. 4: An illustration of the method followed to classify the W-R stars and to determine some of their most important parameters. We applied a very detailed multiple Gaussian fitting of the nebular and broad emission lines within the so called W-R bumps. Detected emission lines for WR1 were: He II λ 4686, N III λ 4640, CIV λ 5803-08. Nebular emission lines: [He I/Ar IV] λ 4711-13, [N II] λ 5755, He I λ 5676. Detection of He II and N III λ 4640 indicates WNL, there is not detection of N IV neither N V which would indicate WNE. Detection of CIV indicates WCE, there is not detection of C III 5696 which would indicate WCL. The total of the fitted lines are shown by the continuous line, the residuals are also shown.

Paul Crowther: 1) I would recommend using template spectra of WR stars (e.g. Crowther & Hadfield) rather than simple gaussian fittings. 2) Future progress with searches beyond the local group requires large format IFUs (e.g. MUSE).

Víctor Gómez-González: Thank you for your comments. Yes, we will try the WR templates that you recommend and then we can compare with the results obtained by applying the multiple gaussians fittings approach.

Jose Groh: There is an interesting core-collapse SN in M81 (SN 1993 J, IIb). Since the progenitor of this SN seems to have an initial mass similar to the WRs you have detected, it may be interesting to compare the location of this SN with the WR star forming regions that you have detected. This comparison may provide constraints on the massive star population around these WRs.

Claus Leitherer: Some of the stars/clusters are surrounded by gas. Do you see any evidence of narrow, nebular He II 4686 emission?

Víctor Gómez-González: Yes, the majority of our objects with WR features are surrounded by gas and we do see the narrow nebular He II 4686 emission line in some of them, even in some other regions without WR features.

Wolf-Rayet Stars
W.-R. Hamann, A. Sander, H. Todt, eds.
Potsdam: Univ.-Verlag, 2015
URL: http://nbn-resolving.de/urn:nbn:de:kobv:517-opus4-84268

Finding new Wolf-Rayet stars in the Magellanic Clouds

A. Becker[1], D. J. Bomans[1,2], K. Weis[1]
[1] *Astronomical Institute of the Ruhr-University Bochum, Germany*
[2] *Research Department Plasmas with Complex Interactions*

Obtaining a complete census of massive, evolved stars in a galaxy would be a key ingredient for testing stellar evolution models. However, as the evolution of stars is also strongly dependent on their metallicity, it is inevitable to have this kind of data for a variety of galaxies with different metallicities. Between 2009 and 2011, we conducted the Magellanic Clouds Massive Stars and Feedback Survey (MSCF); a spatially complete, multi-epoch, broad- and narrow-band optical imaging survey of the Large and Small Magellanic Clouds. With the inclusion of shallow images, we are able to give a complete photometric catalog of stars between B $\approx$ 18 and B $\approx$ 19 mag.

These observations were augmented with additional photometric data of similar spatial resolution from UV to IR (e.g. from GALEX, 2MASS and Spitzer) in order to sample a large portion of the spectral energy distribution of the brightest stars (B $<$ 16 mag) in the Magellanic Clouds. Using these data, were are able to train a machine learning algorithm that gives us a good estimate of the spectral type of tens of thousands of stars.

This method can be applied to the search for Wolf-Rayet-Stars to obtain a sample of candidates for follow-up observations. As this approach can, in principle, be adopted for any resolved galaxy as long as sufficient photometric data is available, it can form an effective alternative method to the classical strategies (e.g. He II filter imaging).

1 Introduction

The Wolf-Rayet star population is of particular interest for stellar evolution modeling. This applies not only to the pure number count and the WC/WN-ratio but also to the specific locus of the Wolf-Rayet stars in the Hertzsprung-Russell-Diagram. Unfortunately the Wolf-Rayet population in most galaxies is barely known. The census of WR stars in the Magellanic Clouds was long considered to be nearly complete, but new Wolf-Rayet surveys of the Magellanic Clouds, e.g. by Massey et al. (2014, 2015), revealed a new subtype of WR stars and increased the number of known WR stars in the LMC by 9.3 % (139 to 152).

The standard technique to find Wolf-Rayet stars in the optical is based on the use of a He II λ4686 filter and a C III λ4650 filter in combination with the matching continuum filter. This image differencing technique is quite expensive as it requires a large amount of observational time; e.g. $\approx$30 hours HST observations to image large parts of M101 in the F469N filter, see Shara et al. (2013). Another promising method is the selection of candidates via their infrared colors as free-free scattering in the dense ionizing wind of WR stars lead to an excess in the infrared (Mauerhan et al. 2011). This however, requires a set of MIR data.

Here we present a new and more general approach to estimate the spectral type of stars that is also capable of finding Wolf-Rayet candidates. It works for all external galaxies where the stellar population can be resolved. Our method relies only on photometric data and has therefore the potential to make use of the already available and upcoming photometric surveys.

2 The method

Between 2009 and 2011 we conducted the Magellanic Clouds Massive Stars and Feedback Survey (Bomans et al. 2015). Using two 6 inch telescopes at the Universitätssternwarte Bochum on Cerro Armazones in Chile we gathered spatial complete high quality images in a large set of photometric filters (u, B, V, R, I, Hα, [OIII] and [SII]). By including shallow exposures (10 to 30 seconds) we were able to measure even the brightest stars in the Magellanic Clouds. To cover a larger wavelength range the dataset was supplemented with photometric data from the UV (GALEX, Swift) to the IR (2MASS, Spitzer, WISE). By doing so we obtained spectral energy distributions (SED) for $\approx$ 80000 stars. Based on these SEDs we estimate the spectral class of each star.

For the classification we used a supervised learning approach. These stars with an already known spectral classification found in the catalog of Skiff (2013) were used as a so-called training sample. Based on this subset an algorithm is trained to recognize the spectral type only based on the multi-wavelength photometry. Once trained, the algorithm can be applied to the rest of the data to estimate the spectral types of all of the other stars. It turned out that

a decision forest build up by several decision trees that determine the classification by majority vote led to the best result and could reproduce 98% of the training data. The Large and Small Magellanic Cloud were treated separately to avoid confusion due to different metallicities and differences in the set of filters.

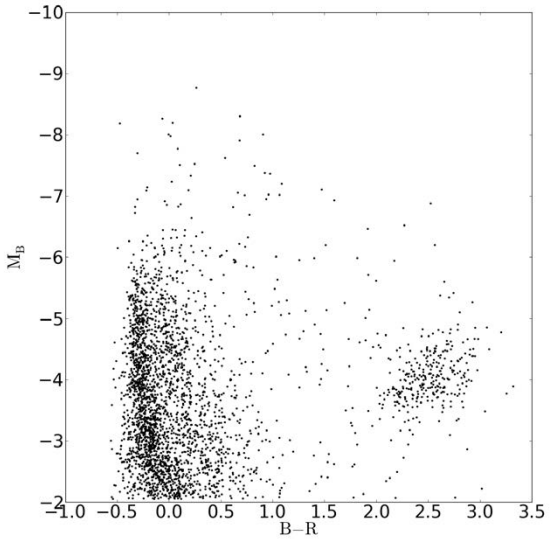

Fig. 1: Distribution of the training sample for the SMC in the color-magnitude-diagram. The region of the foreground stars and the region below the red supergiants are sparsely sampled and will therefore give no reliable classifications.

2.1 Evaluation of the method

To evaluate the results we repeated the training procedure while retaining about 900 objects from the full training sample as a test sample. On this test sample the classification was compared with their true spectral classification as given by Skiff et al. (2013). The result of this test is shown as a histogram in Figure 2. The deviation is measured as the difference between the true spectral class and the estimated spectral class. The value represents the deviation in subtypes (e.g.: An O7 star estimated as O9 deviates by -2; An B2 star estimated as B1 deviates by +1). If we look at all stars we see a deviation of up to 2-3 subtypes with just a few catastrophic outliers and with more than 40% without noticeable deviation. Considering only the O-stars a somewhat larger deviation of about 4 subtypes becomes apparent with a systematic trend to classify them as later types than their actual spectral type.

Systematic errors also occur as a consequence of the training sample. Not all types of stars are equally represented and regions in the color-magnitude-diagram that are sparsely populated with training data will not yield reliable results (see table 1). The smaller sample used in the evaluation might therefore lead to a lower precision compared to the final classification.

2.2 Finding Wolf-Rayet stars

The training sample included 78 of the 139 known Wolf-Rayet stars. Of those the algorithm was able to reproduce all but one. This further proved the reliability of our method and encouraged us to use this method as a new approach to search for Wolf-Rayet candidates. To obtain even better results we fine tuned the method for the identification of Wolf-Rayet stars with a second supervised learning algorithm (multilayer perceptron). This algorithm was just trained on the decision Wolf-Rayet star or no Wolf-Rayet star and applied to the results of the first classification. As an additional cross-check we can compare the results with the observations by Massey et al. (2014, 2015) (see table 1). Unfortunately we do not have an overlap with their newly discovered WN3/O3-type stars as they have a typical brightness that is below the magnitude-cut applied to the algorithm (B $\leq$ 16 (17) for the LMC (SMC)). The classification for the OB-stars is generally in good agreement and within the typical errors of 2-3 subtypes, as discussed before. We were also able to predict the new found WR star LMC143-1. The apparent discrepancy for two stars that were predicted as A-supergiants is still under investigation and subject of the current improvement of the method.

Tab. 1: Comparison between the spectral classifications from Massey et al. (2014, 2015) with the results from our method.

ID	Massey	this work
LMC143-1	WN3+O8-9III	WR
LMC173-1	WN3+O7.5	WR
SMC159-2	O9f?p	B1/5III
LMC156-1	O6If	O4V((f))
LMC164-2	O8f?p	WN4.5
LMC173-2	O7.5Iaf	O9.7Ia
LMC174-4	O4Ifc	A1Iab
LMC174-5	B[e]+WN?	Be
LMCe063-1	WN11	A2Ia
LMC143-1	Onfp	O7n(f)

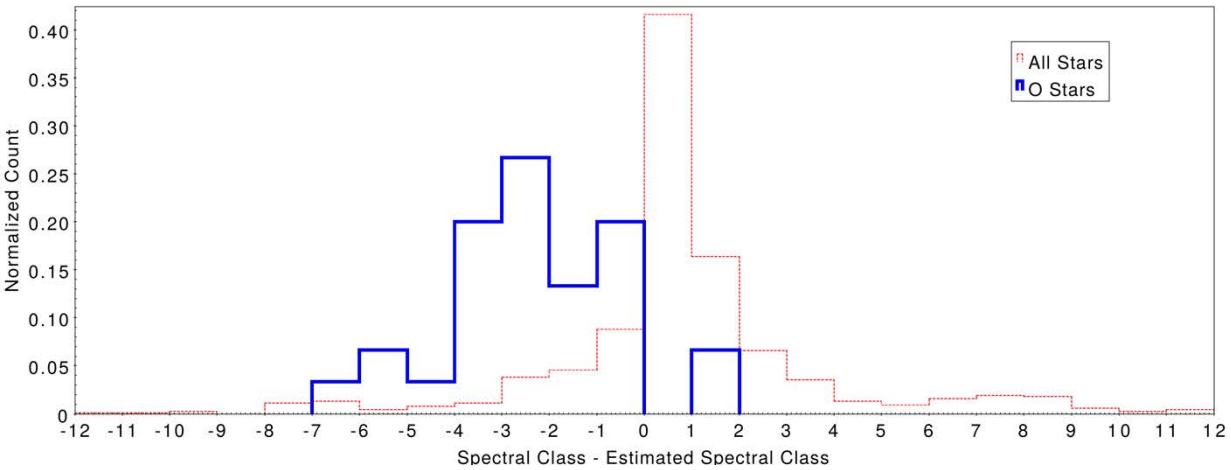

Fig. 2: Deviation of the estimated spectral classification from the true spectral class measured in subtypes. The red dotted line represents all stars and show a deviation of 2-3 subtypes. The blue solid line represents only the O-stars and shows a systematic trend to later spectral types with a deviation of about 4 subtypes.

3 Future prospects

As a next step we will transfer the algorithm to work for other galaxies. M33 would be an obvious target. With its metallicity gradient and a metallicity that is, for some parts of the galaxy, comparable to the LMC it is an ideal object to test the influence of the metallicity on the precision of the estimates. This will help us determine the feasibility of transferring e.g. the SMC training sample to galaxies with lower metallicity where no or few spectral classifications are available (see Bomans et al., this conference). Currently we are still solving some challenges in the preprocessing of the data such as the relative distance between the LMC and M33. This is because we have to match the magnitudes of the LMC photometry to those of M33. And even a small offset, of e.g. 0.2 mag, will result in a complete mismatch in the classification.

4 Summary & Conclusions

With the use of data mining techniques we were able to estimate the spectral type of about 80000 bright stars in the Magellanic Clouds. For that, a training sample, consisting of stars with known spectral classification, was used to train a decision forest that is capable of distinguishing the spectral types by photometric measurements only. The typical precision of our method is currently in the order of 2-3 subtypes. For the O-stars we have a systematic trend to later types with a typical deviation of up to 4 subtypes. This technique was extended to the search for Wolf-Rayet stars in the Magellanic Clouds. The work done so far serves as a proof of concept. By transferring this technique to other local galaxies and photometric datasets we plan to apply the method to upcoming large surveys such as GAIA, LSST and VISTA.

References

Bomans, D. J., Becker, A., & Weis, K. 2015, in IAU Symposium, Vol. 307, IAU Symposium, 414–419

Massey, P., Neugent, K. F., & Morrell, N. 2015, ArXiv e-prints

Massey, P., Neugent, K. F., Morrell, N., & Hillier, D. J. 2014, ApJ, 788, 83

Mauerhan, J. C., Van Dyk, S. D., & Morris, P. W. 2011, AJ, 142, 40

Shara, M. M., Bibby, J. L., Zurek, D., et al. 2013, AJ, 146, 162

Skiff, B. A. 2013, VizieR Online Data Catalog, 1, 2023

John Eldridge: Have you thought about using theoretical spectra as a training set?

Alexander Becker: Yes, and there is an interesting poster, but a problem of putting the distance of the LMC and making it like the observations.

Phil Massey: Neugent and I have new spectral types for $\sim$ 1700 stars in M31 and M33. We're on the verge of publishing them, and they may be usefull in your very interesting work.

Claus Leitherer: Is there anything special with your outliers? E.g., are they in a crowded region, or are they at the faint limit, or is there contamination by nebular lines?

Alexander Becker: No, they are not in problematic regions like 30 Dor or at the faint limit.

Wolf-Rayet Stars
W.-R. Hamann, A. Sander, H. Todt, eds.
Potsdam: Univ.-Verlag, 2015
URL: http://nbn-resolving.de/urn:nbn:de:kobv:517-opus4-84268

Luminous Wolf-Rayet stars at low metallicity

D. J. Bomans[1,2], A. Becker[1], B. Kleemann[1], K. Weis[1], & A. Pasquali[3]
[1] *Astronomical Institute of the Ruhr-Universität Bochum, Germany*
[2] *RUB Research Department Plasmas with Complex Interactions*
[3] *ARI/ZAH, Ruprecht-Karls Universität Heidelberg, Germany*

The evolution of massive stars in very low metallicity galaxies is less well observationally constrained than in environments more similar to the Milky Way, M33, or the LMC. We discuss in this contribution the current state of our program to search for and characterize Wolf-Rayet stars (and other massive emission line stars) in low metallicity galaxies in the Local Volume.

1 Resolved stellar populations

The evolution of massive stars is one of the key input parameters for understanding the formation and evolution of galaxies. The stars provide the ionizing and mechanical feedback into the ISM of their host galaxy and its circumgalactic environment. While these processes are hard to study directly during the epoch of galaxy formation and early evolution, we can use proxies at low redshift, which resemble in many ways the early universe objects. The proxies are the strongly starforming dwarf galaxies with very low metallicity. Using HST and high resolution ground-based imaging it is possible to study the resolved massive star content in such nearby galaxies (e.g. Dalcanton et al. 2009).

Recent progress in stellar evolution models of rotating massive single stars, (e.g. Meynet & Maeder 2005; Brott et al. 2011; Georgy et al. 2012) and binary stars (e.g. Vanbeveren et al. 2007; Eldridge et al. 2008) lead to a bewildering zoo of different evolutionary paths for massive stars and their end products. Testing these scenarios requires detailed observational tests, especially at very low metallicity, which hampers the measurements by, for example, decreasing the intensity of emission lines in the spectra of Wolf-Rayet stars (Crowther & Hadfield 2006). Another basic problem for observational tests is to find suitable, metal-poor galaxies with a significant number of massive stars, since these galaxies are low mass systems in virtue of the galaxy mass-metallicity relation (e.g. Skillman et al. 1989). Additionally, in the Local Volume the number of galaxies with metallicities of 1/10 solar and significantly below this is small, but fortunately far from zero (Bomans & Weis 2011).

2 Wolf-Rayet star searches

Wolf-Rayet stars have a clear signature, the blue and red Wolf-Rayet emission line blends (the WR bumps) (e.g. Brinchmann et al. 2008). The classical method to search for Wolf-Rayet stars uses narrow band filters centered on the optical blue Wolf-Rayet bump, the He II λ468.6 nm line, and/or the red Wolf-Rayet bump, or in the near IR on He I, He II, C IV and Br γ emission lines (Shara et al. 2009). Several recent and ongoing searches for Wolf-Rayet stars in massive galaxies use this method, e.g. the Milky Way using NIR filters with ground based telescopes (Shara et al. 2009, 2012), and M101 (Shara et al. 2013) using HST imaging in the optical. The LMC is target of a recent search also using the optical narrow band filter method (Massey et al. 2014, 2015), see also the contributions by Massey and Neugent et al., and for an alternative method by Becker et al. in this conference. The SMC was surveyed as well (Massey & Duffy 2001; Massey et al. 2003).

The Wolf-Rayet star content of low mass galaxies in the Local Volume was explored so far only for a relative small number of objects: IC 1613 and NGC 6822 (Armandroff & Massey 1985), IC 10 (Massey et al. 1992; Massey & Holmes 2002; Crowther et al. 2003), Gr 8, IC 2574, NGC 1569, and NGC 2366 (Drissen et al. 1993), IC 4662 (Crowther & Bibby 2009), and NGC 3125 (Hadfield & Crowther 2006). HST based analyses were carried out for NGC 1569 (Buckalew et al. 2000) and NGC 2366 (Drissen et al. 2000).

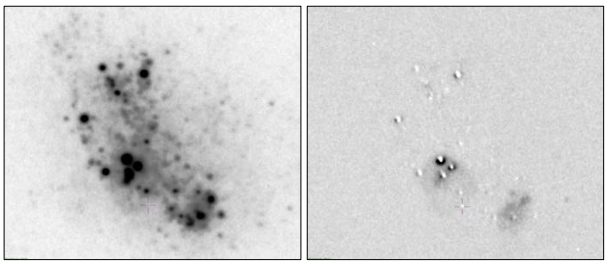

Fig. 1: Left: Broad band g image of the low metallicity dwarf galaxy Gr 8. Right: g band continuum subtracted He II image of the same field of view. The highest probability He II emitter candidate is located about halfway down below the center of the images and is marked with a crosshair. Note the dark (oversubtracted) nebular emission.

Of these galaxies only the SMC, Gr 8, IC 1613, and NGC 2366 have metallicities of 1/10 solar and below. The very low metallicity galaxy Mrk 178 was analyzed by use of IFU spectroscopy (Kehrig et al. 2013), a method we will discuss below in some more detail. With its large distance ($\sim$ 18 Mpc) I Zw 18

is a special case, where individual Wolf-Rayet stars could only be identified individually with HST imaging (de Mello et al. 1998). The presence of Wolf-Rayet stars at the extremely low metal abundance of I Zw 18 together with recent hints for the presence of massive stars similar to Pop III objects (Heap et al. 2015; Kehrig et al. 2015) supports the idea of using nearby low metallicity dwarfs as proxies for galaxies in the early universe.

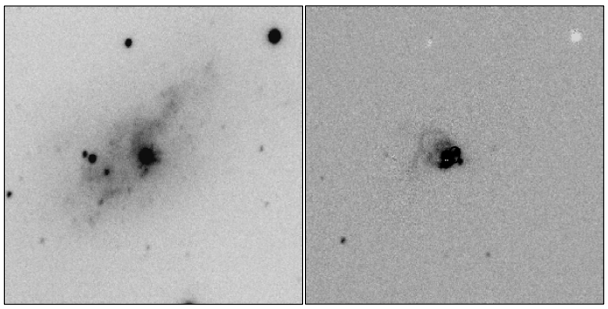

Fig. 2: Left: Broad band image (approximately Stömgren y band) of IC 4870 reconstructed from the data cube, right: continuum corrected He II image generated from the same data cube. Note the several He II point sources and the bright emission of the central cluster and the large diffuse He II emitting shell around the cluster.

3 Searching at low metallicity

IR color-color diagrams

This method is especially successful in highly reddened regions like the Milky Way disk, using the NIR and MIR excess created by the winds of the Wolf-Rayet stars (Hadfield et al. 2007). Since we discuss astro-informatics below, which shares the use of wide-band multi-color data, we did not try this method on low metallicity objects.

Astro-Informatics method

The starting point of the project was the successful application of new search methods for Wolf-Rayet stars in the LMC and SMC, described in more detail by Becker et al., this conference. In short, it uses the SED of known Wolf-Rayet stars and astro-informatics methods to identify candidates. As a test case we applied the method to HST data of Gr 8 and Sextans A. Unfortunately, the effect of the more uncertain distances to galaxies beyond the Magellanic Clouds turned out to have a unexpectedly significant effect on the precision of the candidates selection. We are currently refining the relative distances, adding more filter bands, especially in UV and NIR, and further improve our astro-informatics algorithms.

Narrow-band imaging applied to Gr 8

A proven, efficient method to search for Wolf-Rayet stars is imaging with a narrow band filter centered on the He II line at $\lambda 468.6nm$ and an adjacent (or broad) continuum filter. As discussed above, both ground-based and space-based telescopes can be used. We re-reduced data from the ING archive to search for He II emission objects in the very low luminosity ($M_B = -13.3$) dwarf galaxy Gr 8. At at metallicity of log (O/H) = 7.65 (van Zee et al. 2006) it is one of the most metal-poor starforming galaxy within 5 Mpc. A previous search by Drissen et al. (1993) yielded no He II emitter in this galaxy. In Fig.1 we show the g band image and the He II-continuum image. In the image 3 candidates are visible. The highest confidence candidate marked by a crosshair symbol. This object has no (or only a very weak) counterpart in the g band image and therefore a high flux excess in the He II filter. Several apparent He II peaks are subtraction artifacts of bright stars. The continuum corrected He II shows oversubtracted regions where nebular Hβ and [OIII] emission lines (inside the g filter band) are strong. Clearly, a careful PSF analysis has still to be performed to exclude residual images, filter ghosts, and false positives due to slight geometric mismatches.

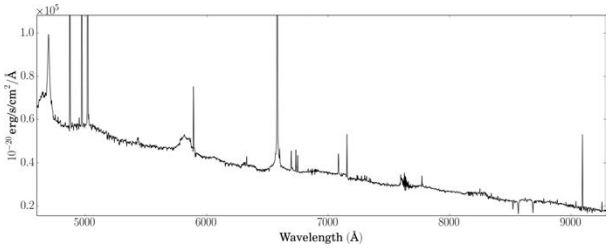

Fig. 3: Extracted spectrum of the central cluster of IC 4870.

IFU based search applied to IC 4870

Searches using IFU spectrographs have significant advantages over narrow band imaging. For each resolution element a full spectrum is available, allowing an improved continuum subtraction and better PSF and astrometric control. Most importantly, it immediately provides at least a classification spectrum of the detected stars. Up to now, this method was strongly hampered by either large spaxels or very small field of view, or both. The new ESO/VLT instrument MUSE delivers a significant progress with a $0.2''$ sampled field of view of $1' \times 1'$.

We present here a first look at the resolved stellar content of the irregular galaxy IC 4870 with about SMC metallicity and a distance of $\sim$ 7 Mpc based on MUSE and HST data. As shown in Fig.2, the data cube allows the efficient detection of several sources in an image isolating the blue Wolf-Rayet bump. The line fluxes imply single stars (2 cases, see Fig.2 for one example) and compact groups of 2-3 Wolf-Rayet stars (2 other cases) as inferred from

the strength of the Wolf-Rayet bump (Kleemann et al., in prep.). As with the narrow band filter method, Malmquist bias leads to the detection of only the intrinsically most luminous Wolf-Rayet stars or unresolved compact groups containing Wolf-Rayet stars.

The central star cluster shows extremely bright Wolf-Rayet features and therefore contains several 100 WN and WC stars (see Fig.3), shadowing even the huge Wolf-Rayet cluster in NGC 3125. Also interesting is the presence of the Ca II indicating the presence of red supergiants, which hints at a significant age spread (or 2 separated bursts of starformation) in the cluster.

4 Conclusions and outlook

Apparently, all presented search methods are capable of finding Wolf-Rayet stars in low metallicity systems. The narrow-band and the IFU methods share the problem of using the same PSF for the narrow and broad band images to achieve an as good as possible continuum subtraction. Obviously space based imaging is superior to ground-based (even with AO support) for more distant galaxies due to a more well behaved and stable PSF. Still, the classical ground based technique can efficiently expand the sample of low metallicity Wolf-Rayet star candidates for nearby objects. Clearly MUSE can be extremely promising as search engine even at a distance of 7 Mpc (and beyond), and immediately provides spectra suitable for further analysis.

Our astro-informatics method shows potential, but needs some fine-tuning still. The necessary accuracy of the relative distances of target galaxy and training sample galaxies can be reached e.g. with TRGB distances or Cepheids. The limiting factor is probably the intercalibration of the methods. Since Wolf-Rayet and other hot stars have significant structure in the SEDs in the UV and NIR/MIR, the use of the widest possible wavelength range and more that 5 filters will also help, as experience from the LMC data taught us already, see Bomans et al. (2015) and Becker et al., this conference. With the availability of the space mission archives (especially HST and SPITZER) and the ongoing and planned deep widefield surveys, there is already a rich data set available for using astro-informatics methods for us to investigate the hot and cool star content of a good number of low metallicity galaxies in the Local Volume.

References

Armandroff, T. E. & Massey, P. 1985, ApJ, 291, 685

Bomans, D. J., Becker, A., & Weis, K. 2015, in IAU Symposium, Vol. 307, IAU Symposium, ed. G. Meynet, C. Georgy, J. Groh, & P. Stee, 414–419

Bomans, D. J. & Weis, K. 2011, in IAU Symposium, Vol. 272, IAU Symposium, ed. C. Neiner, G. Wade, G. Meynet, & G. Peters, 265–270

Brinchmann, J., Kunth, D., & Durret, F. 2008, A&A, 485, 657

Brott, I., de Mink, S. E., Cantiello, M., et al. 2011, A&A, 530, A115

Buckalew, B. A., Dufour, R. J., Shopbell, P. L., & Walter, D. K. 2000, AJ, 120, 2402

Crowther, P. A. & Bibby, J. L. 2009, A&A, 499, 455

Crowther, P. A., Drissen, L., Abbott, J. B., Royer, P., & Smartt, S. J. 2003, A&A, 404, 483

Crowther, P. A. & Hadfield, L. J. 2006, A&A, 449, 711

Dalcanton, J. J., Williams, B. F., Seth, A. C., et al. 2009, ApJS, 183, 67

de Mello, D. F., Schaerer, D., Heldmann, J., & Leitherer, C. 1998, ApJ, 507, 199

Drissen, L., Moffat, A. F. J., & Shara, M. M. 1993, AJ, 105, 1400

Drissen, L., Roy, J.-R., Robert, C., Devost, D., & Doyon, R. 2000, AJ, 119, 688

Eldridge, J. J., Izzard, R. G., & Tout, C. A. 2008, MNRAS, 384, 1109

Georgy, C., Ekström, S., Meynet, G., et al. 2012, A&A, 542, A29

Hadfield, L. J. & Crowther, P. A. 2006, MNRAS, 368, 1822

Hadfield, L. J., van Dyk, S. D., Morris, P. W., et al. 2007, MNRAS, 376, 248

Heap, S., Bouret, J.-C., & Hubeny, I. 2015, ArXiv e-prints, 1504.0274

Kehrig, C., Pérez-Montero, E., Vílchez, J. M., et al. 2013, MNRAS, 432, 2731

Kehrig, C., Vílchez, J. M., Pérez-Montero, E., et al. 2015, ApJ, 801, L28

Massey, P., Armandroff, T. E., & Conti, P. S. 1992, AJ, 103, 1159

Massey, P. & Duffy, A. S. 2001, ApJ, 550, 713

Massey, P. & Holmes, S. 2002, ApJ, 580, L35

Massey, P., Neugent, K. F., & Morrell, N. 2015, ApJ, 807, 81

Massey, P., Neugent, K. F., Morrell, N., & Hillier, D. J. 2014, ApJ, 788, 83

Massey, P., Olsen, K. A. G., & Parker, J. W. 2003, PASP, 115, 1265

Meynet, G. & Maeder, A. 2005, A&A, 429, 581

Shara, M. M., Bibby, J. L., Zurek, D., et al. 2013, AJ, 146, 162

Shara, M. M., Faherty, J. K., Zurek, D., et al. 2012, AJ, 143, 149

Shara, M. M., Moffat, A. F. J., Gerke, J., et al. 2009, AJ, 138, 402

Skillman, E. D., Kennicutt, R. C., & Hodge, P. W. 1989, ApJ, 347, 875

van Zee, L., Skillman, E. D., & Haynes, M. P. 2006, ApJ, 637, 269

Vanbeveren, D., Van Bever, J., & Belkus, H. 2007, ApJ, 662, L107

Jesús Toalá: How can you explain ~ 500 WR stars at the center of your galaxy?

Dominik Bomans: The cluster in the center of the galaxy is indeed extreme, but not unique. A similar object is the somewhat more distant irregular galaxy NGC 3125, which was discussed e.g. by Hadfield & Crowther (2006) and Wofford et al. (2014).

Wolf-Rayet Stars
W.-R. Hamann, A. Sander, H. Todt, eds.
Potsdam: Univ.-Verlag, 2015
URL: http://nbn-resolving.de/urn:nbn:de:kobv:517-opus4-84268

PopIII-star siblings in IZw18 and metal-poor WR galaxies unveiled from integral field spectroscopy

C. Kehrig[1], J. M. Vílchez[1], E. Pérez-Montero[1], J. Iglesias-Páramo[1,2], J. Brinchmann[3], P. A. Crowther[4], F. Durret[5], D. Kunth[5]
[1] *Instituto de Astrofísica de Andalucía (IAA-CSIC), Spain*
[2] *Estación Experimental de Zonas Aridas (CSIC), Spain*
[3] *Leiden University, The Netherlands*
[4] *University of Sheffield, United Kingdom*
[5] *Institut d'Astrophysique de Paris, France*

Here, we highlight our recent results from the IFS study of Mrk178, *the closest metal-poor WR galaxy*, and of IZw18, *the most metal-poor star-forming galaxy known in the local Universe*. The IFS data of Mrk178 show the importance of aperture effects on the search for WR features, and the extent to which physical variations in the ISM properties can be detected. Our IFS data of IZw18 reveal its entire nebular HeIIλ4686-emitting region, and indicate for the very first time that peculiar, hot (nearly) metal-free ionizing stars (called here *PopIII-star siblings*) might hold the key to the HeII-ionization in IZw18.

1 Introduction

Studying the WR content and radiative feedback from WRs in metal-poor star-forming (SF) galaxies is crucial to test evolutionary models for massive stars at low metallicity (Z), where the disagreement between observations and such models is stronger (e.g., Leitherer et al. 2014). In this context, we have initiated a program to investigate nearby low-Z WR galaxies using integral field spectroscopy (IFS). IFS has many advantages in a study of this kind, in comparison with long-slit spectroscopy (e.g., Kehrig et al. 2008, 2012; Pérez-Montero et al. 2011, 2013). By means of IFS one can locate and find WRs where they were not detected before. Also, IFS is a powerful technique to probe issues related with aperture effects, and allows a more precise spatial correlation between massive stars and nebular properties (e.g., Kehrig et al. 2008, 2013, hereafter K13). As a part of this program, we have obtained new integral field unit (IFU) data of the low-Z galaxies Mrk178 and IZw18, published in K13 and Kehrig et al. (2015, hereafter K15), respectively. Below we summarize the main results from these two articles.

2 IZw18: PopIII-star siblings as the source of HeII-ionization

We performed new IFS observations of IZw18 using the PMAS IFU (Roth et al. 2005) on the 3.5m telescope at CAHA (fig.1; K15). IZw18 is a nearby SF galaxy, well known for its extremely low Z $\sim$ 1/32 $Z_\odot$ (e.g., Vílchez & Iglesias-Páramo 1998), and it is considered an excellent local analog of primeval systems. Our IFS data reveal for the first time the entire nebular HeIIλ4686-emitting region (fig.2) and corresponding total HeII-ionizing photon flux [Q(HeII)$_{obs}$] in IZw18. Narrow HeII emission in SF galaxies has been suggested to be mainly associated with photoionization from WRs, but WRs cannot satisfactorily explain the HeII-ionization in all cases, particularly at lowest metallicities where HeII emission is observed to be stronger (e.g., Guseva et al. 2000; Kehrig et al. 2004; Shirazi & Brinchmann 2012). Why is studying the formation of HeII emission relevant ? HeII emission indicates the presence of high energy photons (E $\geq$ 54 eV), and HeII-emitters are apparently more frequent among high-redshift (z) galaxies than for local objects (e.g., Kehrig et al. 2011; Cassata et al. 2013). Narrow HeII emission has been suggested as a good tracer of PopIII-stars (the first very hot metal-free stars) in high-z galaxies (e.g., Schaerer 2003; Pallottini et al. 2015); these stars are believed to have contributed significantly to the reionization of the Universe, a challenging subject in contemporary cosmology. However, the origin of narrow HeII lines remains difficult to understand in many nearby SF galaxies/regions (e.g., Kehrig et al. 2011; Shirazi & Brinchmann 2012). So before interpreting high-z HeII-emitters, it is crucial first to understand the formation of HeII emission at low redshift. IZw18, as the most metal-poor HeII-emitter in the local Universe, is an ideal object to perform this study.

Our observations combined with stellar model predictions point out that conventional excitation sources (e.g. single WRs, shocks, X-ray binaries) cannot convincingly explain the total Q(HeII)$_{obs}$ derived for IZw18 (e.g., Meynet & Maeder 2005; Crowther & Hadfield 2006; Leitherer et al. 2014). Other mechanisms are probably also at work. If the HeII-ionization in IZw18 is due to stellar sources, these might be peculiar very hot stars. Based on wind models of very massive O stars (Kudritzki 2002), $\sim$ 10–20 stars with 300 $M_\odot$ at Z_{IZw18} (or lower, down to Z$\sim$1/100 $Z_\odot$) can reproduce our total Q(HeII)$_{obs}$ (see also Szécsi et al. 2015). However, the super-massive star scenario requires a cluster mass much higher than the mass of the IZw18 NW knot

(where the HeII region is located), and it is not hard enough to explain the highest HeII/Hβ values observed. Also, stellar sources with 300 $M_\odot$ are not observed in IZw18 to date. Next, as an approximation of (nearly) metal-free stars in IZw18 – the so-called *PopIII-star siblings* – we compared our observations with models for rotating Z=0 stars (Yoon et al. 2012), which reproduce our data better: ∼8–10 of such stars with M_{ini}=150 $M_\odot$ can explain the total $Q(HeII)_{obs}$ and the highest HeII/Hβ values observed. The PopIII-star sibling scenario, invoked for the first time in IZw18 by K15, goes in line with the reported metal-free gas pockets in the HI envelope near the IZw18 NW knot (Lebouteiller et al. 2013). These gas pockets could provide the raw material for making such *PopIII-star siblings*.

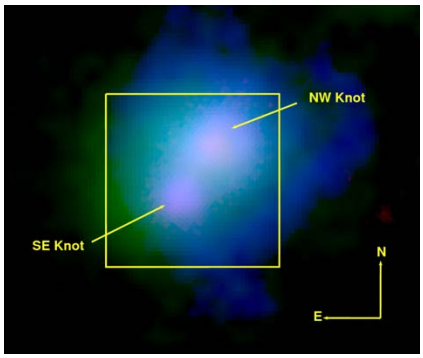

Fig. 1: Color-composite image of IZw18. The box represents the FOV (16"×16") of the PMAS IFU over the galaxy main body which hosts the NW and SE knots (K15).

3 Mrk178

In K13 we present the first optical IFS study of Mrk178, the closest metal-poor WR HII galaxy. IFS data of Mrk 178 were obtained with the INTEGRAL IFU at the 4.2m WHT. In this work we examine the spatial correlation between its WRs and the neighbouring ionized ISM. The strength of the broad WR features and its low metallicity (∼ 1/10 $Z_\odot$) make Mrk178 an intriguing object. We have detected the blue and red WR bumps in different locations across the FOV (∼ 300 pc×230 pc) in Mrk178 (fig.3). The study of the WR content has been extended, for the first time, beyond its brightest SF knot (knot B in fig.3) uncovering new WR star clusters (knots A and C in fig.3). Using SMC/LMC template WRs (Crowther & Hadfield 2006), we empirically estimate a minimum of ∼ 20 WRs in our Mrk178 FOV, which is already higher than that currently found in the literature. Regarding the ISM abundances, localized N and He enrichment, spatially correlated with WRs from knot B, is suggested by our analysis. Nebular HeIIλ4686 emission is shown to be spatially extended reaching well beyond the location of the WRs (fig.4). Shock ionization and X-ray binaries are unlikely to be significant ionizing mechanisms since Mrk178 is not detected in X-rays. The main excitation source of HeII in Mrk178 is still unknown.

From SDSS spectra of metal-poor WR galaxies, we found a too high EW(WR bump)/EW(Hβ) value for Mrk178, which is the most deviant point in the sample (fig.4). Using our IFU data, we showed that this curious behaviour is caused by aperture effects, which actually affect, to some degree, the EW(WR bump) measurements for all galaxies in Fig.4. Also, we demonstrated that using too large an aperture, the chance of detecting WR features decreases, and that WR signatures can escape detection depending on the distance of the object and on the aperture size. Thus, WR galaxy samples constructed on single fiber/long-slit spectrum basis may be biased.

References

Cassata, P., Le Fèvre, O., Charlot, S., et al. 2013, A&A, 556, A68
Crowther, P. A. & Hadfield, L. J. 2006, A&A, 449, 711
Guseva, N. G., Izotov, Y. I., & Thuan, T. X. 2000, ApJ, 531, 776
Kehrig, C., Monreal-Ibero, A., Papaderos, P., et al. 2012, A&A, 540, A11
Kehrig, C., Oey, M. S., Crowther, P. A., et al. 2011, A&A, 526, A128
Kehrig, C., Pérez-Montero, E., Vílchez, J. M., et al. 2013, MNRAS, 432, 2731
Kehrig, C., Telles, E., & Cuisinier, F. 2004, AJ, 128, 1141
Kehrig, C., Vílchez, J. M., Pérez-Montero, E., et al. 2015, ApJ, 801, L28
Kehrig, C., Vílchez, J. M., Sánchez, S. F., et al. 2008, A&A, 477, 813
Kudritzki, R. P. 2002, ApJ, 577, 389
Lebouteiller, V., Heap, S., Hubeny, I., & Kunth, D. 2013, A&A, 553, A16
Leitherer, C., Ekström, S., Meynet, G., et al. 2014, ApJS, 212, 14
Meynet, G. & Maeder, A. 2005, A&A, 429, 581
Pallottini, A., Ferrara, A., Pacucci, F., et al. 2015, ArXiv1506.07173 e-prints
Pérez-Montero, E., Kehrig, C., Brinchmann, J., et al. 2013, Advances in Astronomy, 2013, 18
Pérez-Montero, E., Vílchez, J. M., Cedrés, B., et al. 2011, A&A, 532, A141
Roth, M. M., Kelz, A., Fechner, T., et al. 2005, PASP, 117, 620
Schaerer, D. 2003, A&A, 397, 527
Shirazi, M. & Brinchmann, J. 2012, MNRAS, 421, 1043

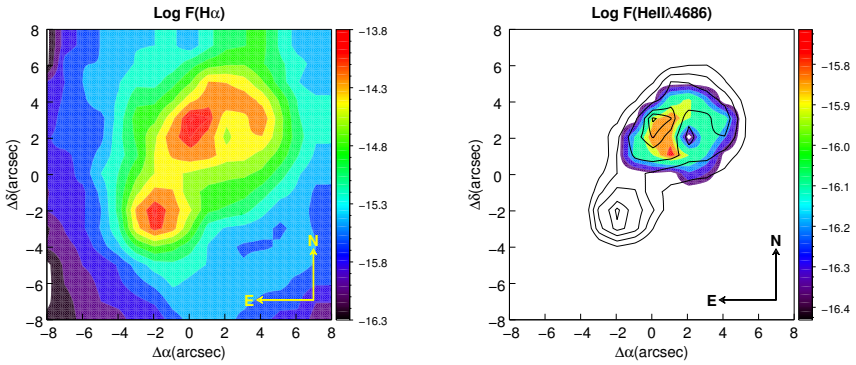

Fig. 2: IZw18: intensity maps of Hα (*left panel*) and nebular HeIIλ4686 (*right panel*) in logarithmic scale; fluxes are in units of erg s^{-1} cm^{-2}. The maps are presented as color-filled contour plots (K15).

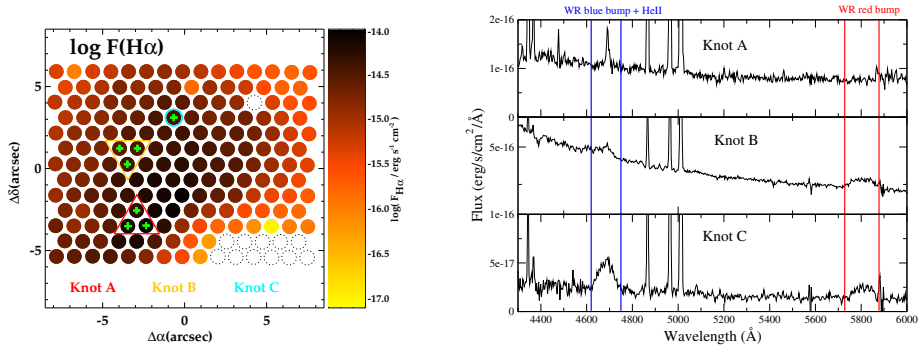

Fig. 3: Mrk178: intensity map of Hα emission line (*left panel*) and integrated spectrum for the 3 knots in which WR features are detected (*right panel*). The spectral range for both blue and red WR bumps are marked (K13).

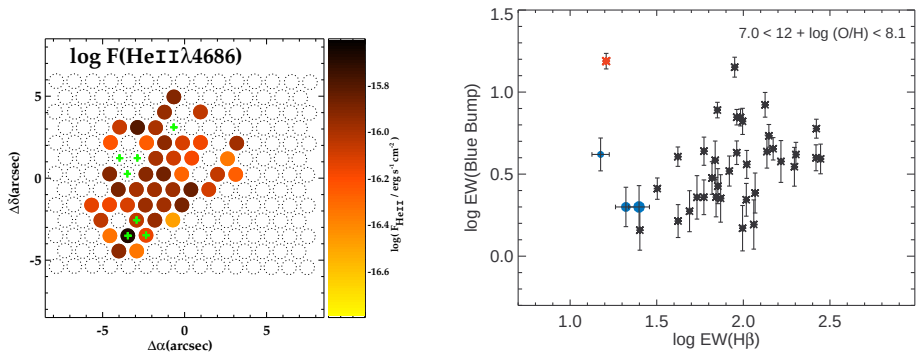

Fig. 4: *Left panel*: map of nebular HeIIλ4686 line; spaxels where we detect WR features are marked with green crosses. *Right panel*: EW(WR blue bump) vs EW(Hβ). Asterisks show values from SDSS DR7 for metal-poor WR galaxies; the red one represents Mrk178. The three blue circles, from the smallest to the biggest one, represent the 5", 7" and 10" diameter apertures from our IFU data centered at the SDSS fiber of Mrk178 (K13).

Szécsi, D., Langer, N., Yoon, S.-C., et al. 2015, ArXiv1506.09132 e-prints
Vílchez, J. M. & Iglesias-Páramo, J. 1998, ApJ, 508, 248
Yoon, S.-C., Dierks, A., & Langer, N. 2012, A&A, 542, A113

Dany Vanbeveren: I suggest that you have a close look at the papers Van Bever and Vanbeveren (2003) or Eldridge et al. (2008). Both papers are cited by Brinchmann et al. (2008)

Carolina Kehrig: IZw18, the galaxy presented in Kehrig et al. (2015), has a metallicity of about 1/10 SMC-metallicity. The papers that you mention do not show model predictions at the metallicity of IZw18.

Wolf-Rainer Hamann: You told that more than 100 WRs would be needed to provide the He-ionizing photons. This might depend a lot on the models and their parameters. Which one did you use?

Carolina Kehrig: We compared the observations of IZw18 with the HeII-ionizing flux expected from WR stellar models which mimic single WR stars close to the conditions in IZw18. These model predictions are given by Crowther & Hadfield (2006).

Norbert Langer: It seems unlikely that we have metal-free gas pockets at low redshift. Perhaps, very metal-poor stars could also explain the HeII photons of IZw18 ?

Carolina Kehrig: Yes, I agree that it is hard to imagine metal-free gas at low redshift. But first it is important to remember that there are still many uncertainties regarding the fate of metals released by massive star winds and SNRs in H II regions. Additionally, the processes of metal dispersal and mixing are still very difficult to model. Please, let me clarify something else here. We are not saying that metal-free ionizing stars are present in IZw18. In fact, the existence of metal-free ionizing stars is not observationally confirmed in any galaxy yet. What we did was to demonstrate that standard models for metal-poor massive/WR stars cannot reproduce the observations of IZw18. Based on current stellar models, the only way to explain the He II ionization budget observed in IZw18 using hot stars with 1/50th (or lower) $Z_{\odot}$ requires super-massive stars ($\sim$ 300 $M_{\odot}$). However, such very massive stars are not observed in IZw18 to date. Also the super-massive star scenario would imply a cluster mass much higher than the mass of the IZw18 NW knot (where the He II region is located), and this scenario does not explain the highest He II/Hβ values observed. In other words, our data challenge current models for metal-poor massive stars. We find that the models for rotating Z=0 stars do a better job in reproducing the data, and the presence of (nearly) metal-free gas pockets in IZw18 is empirically confirmed. So, the raw material for making such stars is there. In order to say anything else about the popIII-like stars scenario (e.g, how these stars have formed, how they reach the NW cluster), one needs to compute photoionization models and simulations which must take into account the detailed geometry of the He II region, the mass of the metal-free gas pockets, etc.

Wolf-Rayet Stars
W.-R. Hamann, A. Sander, H. Todt, eds.
Potsdam: Univ.-Verlag, 2015
URL: http://nbn-resolving.de/urn:nbn:de:kobv:517-opus4-84268

A 2D view of Wolf-Rayet Galaxies

S. Srivastava[1], C. Kehrig[2], N. G. Kantharia[3], E. Pérez-Montero[2], J. M. Vílchez[2], J. Iglesias-Páramo[2], P. Janardhan[1]
[1]*Astronomy & Astrophysics Division, Physical Research Laboratory, Ahmedebad*
[2]*Instituto de Astrofisica de Andalucia, Granada, Spain*
[3]*National Centre for Radio Astrophysics, TIFR, Pune*

The main objective of this work is to investigate the evolution of massive stars, and the interplay between them and the ionized gas for a sample of local metal-poor Wolf-Rayet galaxies. Optical integral field spectrocopy was used in combination with multi-wavelength radio data. Combining optical and radio data, we locate Wolf-Rayet stars and supernova remnants across the Wolf-Rayet galaxies to study the spatial correlation between them. This study will shed light on the massive star formation and its feedback, and will help us to better understand distant star-forming galaxies.

1 Introduction

The complex physics governing the interplay between massive star formation (SF) and the interstellar medium (ISM) is one of the key issues limiting our knowledge of galaxy formation and evolution. Galaxies whose spectra show broad emission lines attributed to Wolf-Rayet (WR) stars are called WR galaxies (Schaerer et al. 1999). Two main classes of WR stars are defined based on emission-line ratios: nitrogen-type (WN) and carbon-type (WO and WC) stars (e.g. Crowther et al. (1998). The blue and red WR bumps observed in galaxy spectra are centered at $\sim$ 4680 and 5808 Å, respectively. While WN stars are mainly responsible for the formation of the blue bump, the carbon-type WR stars contribute the most for the red bump emission.

The WR phase is an evolutionary stage characterized by the ejection of the outer layers of evolved massive stars by stellar winds which supply mechanical energy to the ISM (Freyer et al. 2003, 2006). These WR stars are incredibly massive and luminous, and have very high rates of mass loss. The winds that they produce can collide with regions of gas and drive rapid star formation. WRs have a fundamental influence on the ISM and galaxy evolution and are responsible for the bulk of the ionization observed in H II regions. WR stars enrich the ISM at short time-scales (i.e. <100 Myr) by returning the processed nuclear material during their lifetime and at their end by going off as Supernovae (SN) (Maeder 1981). These stars are the likely progenitors of (at, least some) core-collapse SN, and of Gamma-Ray Bursts (GRBs; Woosley & Bloom (2006)) which are predicted to be optically dim and radio loud. The remnant will be similar to Cas A or the Supernova Remnant (SNR) in the galaxy NGC 4449 showing weak broad optical emission from [O III], [S II] and [Ne III] but no broad hydrogen lines.

The SN explosion energy of the most massive stars is only $\sim 10^{51}$ erg (Hamuy 2003) so their SNRs follow the σ-D relation (Preite-Martinez & Fusco-Femiano 1986) and account for the bulk of the non-thermal radio emission. Both thermal emission from H II regions and non-thermal radiation from cosmic ray electrons contribute to the total radio flux. By comparing the Far Infra-Red (FIR), thermal radio and non-thermal radio luminosities of the WR galaxies, we can search for an older, less massive stellar population underlying the young WR outburst. The youngest star-burst regions should have relatively flat spectra dominated by thermal emission from H II regions ionized by extremely massive ($M > 30M_{\odot}$) short-lived ($<5\times10^6$ yr) WR stars. Steep-spectrum non-thermal emission from cosmic rays accelerated by SNRs of relatively low mass (M$< 8M_{\odot}$) stars will eventually dominate the radio emission at centimeter wavelengths.

To carry out this project, we used low frequency radio observations, optical field spectroscopy (IFS) and multi-wavelength data. Many nearby galaxies have been surveyed in the radio for SNRs, usually using images obtained at 20 cm and 6 cm to constrain discrete sources spectral indices and separate non-thermal SNRs from H II regions. Some of the most successful searches of this kind have been in M33 (Gordon et al. 1999) and NGC 6946 (Lacey & Duric 1997, 2001). We can also study the radio luminosity function of SNRs by their radio emission. Radio bright SNRs typically have diameters of $\sim$10 - 100 pc (Gordon et al. 1999), corresponding to 0.7 - 7 arcsec at a distance of 3 Mpc. Therefore, for nearby galaxies, they will appear as discrete (point like or slightly resolved) sources when observed with most ground-based observatories.

It is well known that SNRs contribute significantly to the non-thermal radio emission which, owing to its steeper spectral index in comparison to that of the thermal emission, is expected to dominate at low (< 1 GHz) radio frequencies (e.g. Bogdan & Volk 1983; Biermann & Strom 1993; Srivastava et al. 2014).

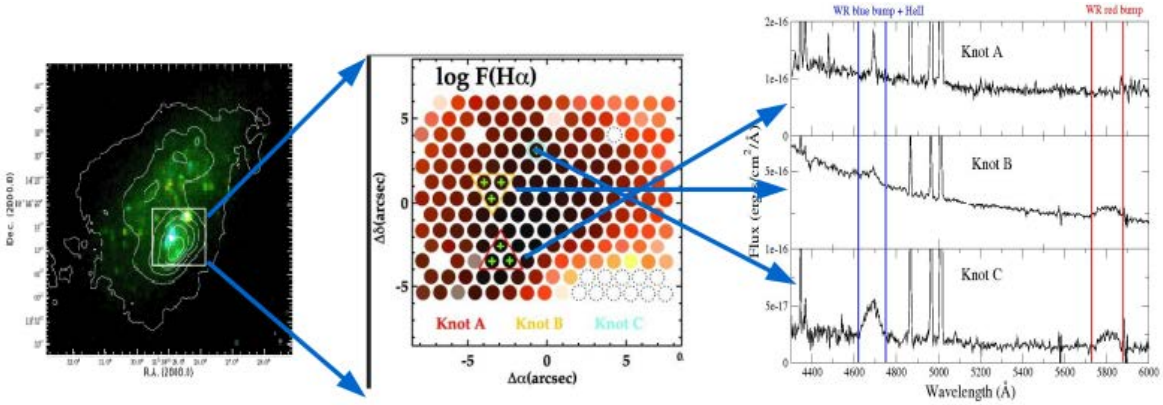

Fig. 1: From left to right:(a) Hα contours (Gil de Paz et al. 2003) drawn on the three-band (z,r,i) SDSS color-composite image of Mrk 178, (b) The three WR knots (A, B and C) are labelled on the Hα flux map, and green crosses mark the spaxels where WR features were detected, (c) Integrated spectrum, in units of erg s^{-1} cm^{-2} Å^{-1}, for the three knots in which the WR features are detected [Image credit: Kehrig et al. (2013)]

Tab. 1: General Properties of the Galaxies

Galaxy	Right Ascension$^{(1)}$ (J2000)	Declination$^{(1)}$ (J2000)	Morphology	Distance (Mpc)
MRK 178	$11^h33^m28.9^s$	$+49°14'14''.0$	Irr+Comp; WR	3.9
NGC 4449	$12^h28^m11.9^s$	$+44°05'40''.0$	IBm; H II	3.7

Source: https://ned.ipac.caltech.edu

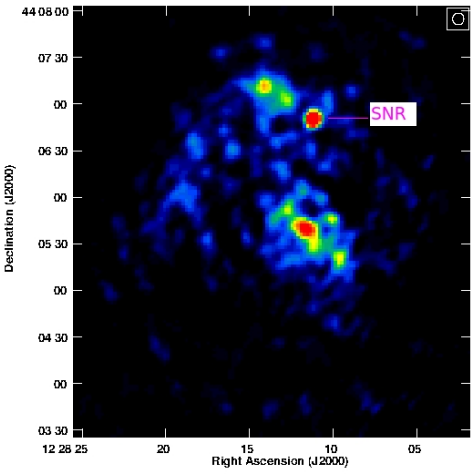

Fig. 2: SNR J1228+441 was detected in the GMRT radio image of NGC 4449 at 610 MHz [Image credit:Srivastava et al. (2014)]

It is worth mentioning that, we have observed NGC 4449 using GMRT (Srivastava et al. 2014). In this context, the main goal of the present project is to perform a comprehensive 2D investigation of the Wolf-Rayet (WR) population, supernovae remnants (SNRs) and the properties of the ionized gas (metallicity, temperature, ionizing sources, etc)for metal poor WR galaxies. In this paper we are presenting optical results of MRK 178 and radio results of NGC 4449. The paper is structured as follows. In §2 we describe the optical and radio observations, and a summary is presented in §3.

2 Observations

2.1 Optical Observation of MRK 178

The integral field spectroscopy (IFS) technique was used to present the optical study of the metal poor galaxy MRK 178 with the INTEGRAL fiber system (Arribas et al. 1998) in combination with the WYFFOS spectrograph (Bingham et al. 1994) at the 4.2 m William Herschel Telescope (WHT), Roque de los Muchachos observatory. This technique is used to collect spectra of many different regions of an extended object. Kehrig et al. (2013) probe the spatial correlation between massive stars and the properties of the surrounding ISM of MRK 178. They were able to locate and resolve star-forming knots hosting a few WR stars and also characterized the WR content.

2.2 Radio Observations of NGC 4449

The radio observations were done using the Giant Metrewave Radio Telescope (GMRT) (Swarup et al. 1991). The GMRT is an interferometric array of 30 antennas, each of 45 m in diameter. NGC 4449 a bright WR galaxy, lying at a distance of about 4 Mpc and has been known as irregular dwarf galaxy which in shape and size is similar to the Large Magellanic Cloud. This galaxy exhibits numerous signs of a recent merger (Annibali et al. 2008, 2011). The SNR J1228+441 was detected (Srivastava et al. 2014) (Fig. 1) in our radio images at 150, 325 and 610 MHz as the most intense feature in NGC 4449. The young SNR is located within a rich cluster of OB stars (along with some WR stars) only a few parsecs in size (Milisavljevic & Fesen 2008). The SNR was first discovered in the radio by (Seaquist & Bignell 1978) as a bright, unresolved non-thermal radio source ($\sim$ 10 mJy at 2.7 GHz) $\sim 1'$ north of the nucleus of the galaxy at a location nearly coincident with an HII region cataloged by Sabbadin & Bianchini (1979). This SNR is five times more luminous than Cas A at 20cm (Chomiuk & Wilcots 2009). It has been extensively monitored (e.g. Lacey et al. (2007) and references therein). Lacey et al. (2007) report steepening of the spectral index from $\alpha = -0.64 \pm 0.02$ in 1994 to $\alpha = -1.01 \pm 0.02$ in 2001–2002, showing rapid evolution. Reines et al. (2008) using high-resolution VLA data at several frequencies find that the SNR had a spectral index of -1.8 between 3.6 and 6 cm and an index of -0.9 between 1.3 and 3.6 cm between 2001 and 2002,indicating a break in the spectrum. From our observations at 325 and 610 MHz in 2008–2009, we estimate flux densities of 35.2 ± 9.1 and 11.2 ± 2.9 mJy, respectively giving radio spectral index to be -1.5.

3 Summary

In summary, by combining optical IFS and radio data we will be able to study the spatial correlation between WRs and SNRs across our sample of WR galaxies. To explore SNRs in MRK 178, observations at 20 and 50 cm using GMRT have been recently taken in the on-going observing cycle. Therefore, this galaxy is one of the best laboratories to study starburst; considered as a template system that helps us to understand distant star-forming galaxies.

References

Annibali, F., Aloisi, A., Mack, J., et al. 2008, AJ, 135, 1900

Annibali, F., Tosi, M., Aloisi, A., & van der Marel, R. P. 2011, AJ, 142, 129

Arribas, S., del Burgo, C., Carter, D., et al. 1998, in Astronomical Society of the Pacific Conference Series, Vol. 152, Fiber Optics in Astronomy III, ed. S. Arribas, E. Mediavilla, & F. Watson, 149

Biermann, P. L. & Strom, R. G. 1993, A&A, 275, 659

Bingham, R. G., Gellatly, D. W., Jenkins, C. R., & Worswick, S. P. 1994, in Society of Photo-Optical Instrumentation Engineers (SPIE) Conference Series, Vol. 2198, Instrumentation in Astronomy VIII, ed. D. L. Crawford & E. R. Craine, 56–64

Bogdan, T. J. & Volk, H. J. 1983, A&A, 122, 129

Chomiuk, L. & Wilcots, E. M. 2009, AJ, 137, 3869

Crowther, P. A., De Marco, O., & Barlow, M. J. 1998, MNRAS, 296, 367

Freyer, T., Hensler, G., & Yorke, H. W. 2003, ApJ, 594, 888

Freyer, T., Hensler, G., & Yorke, H. W. 2006, ApJ, 638, 262

Gil de Paz, A., Madore, B. F., & Pevunova, O. 2003, ApJS, 147, 29

Gordon, S. M., Duric, N., Kirshner, R. P., Goss, W. M., & Viallefond, F. 1999, ApJS, 120, 247

Hamuy, M. 2003, ApJ, 582, 905

Kehrig, C., Pérez-Montero, E., Vílchez, J. M., et al. 2013, MNRAS, 432, 2731

Lacey, C. & Duric, N. 1997, in Bulletin of the American Astronomical Society, Vol. 29, American Astronomical Society Meeting Abstracts #190, 849

Lacey, C. K. & Duric, N. 2001, ApJ, 560, 719

Lacey, C. K., Goss, W. M., & Mizouni, L. K. 2007, AJ, 133, 2156

Maeder, A. 1981, A&A, 99, 97

Milisavljevic, D. & Fesen, R. A. 2008, ApJ, 677, 306

Preite-Martinez, A. & Fusco-Femiano, R. 1986, A&A, 157, 6

Reines, A. E., Johnson, K. E., & Goss, W. M. 2008, AJ, 135, 2222

Sabbadin, F. & Bianchini, A. 1979, PASP, 91, 280

Schaerer, D., Contini, T., & Pindao, M. 1999, A&A, 136, 35

Seaquist, E. R. & Bignell, R. C. 1978, ApJ, 226, L5

Srivastava, S., Kantharia, N. G., Basu, A., Srivastava, D. C., & Ananthakrishnan, S. 2014, MNRAS, 443, 860

Swarup, G., Ananthakrishnan, S., Kapahi, V. K., et al. 1991, Current Science, Vol. 60, NO.2/JAN25, P. 95, 1991, 60, 95

Woosley, S. E. & Bloom, J. S. 2006, ARA&A, 44, 507

Dominik Bomans: Critical for radio spectra is thermal convection. Did you have a deep Hα map of the whole area, and reddening? Do you plan to add higher frequency observations to avoid the thermal estimate?

Shweta Srivastava: We used a Hα map from the NED. I think it covered the full galaxy. We are not planning any high frequency observations for substantiating the thermal estimates.

WR spectroscopy and polarimetry

Wolf-Rayet Stars
W.-R. Hamann, A. Sander, H. Todt, eds.
Potsdam: Univ.-Verlag, 2015
URL: http://nbn-resolving.de/urn:nbn:de:kobv:517-opus4-84268

Spectrum formation in Wolf-Rayet stars

D. J. Hillier
Department of Physics and Astronomy & Pittsburgh Particle Physics, Astrophysics, and Cosmology Center (PITT PACC), University of Pittsburgh

We highlight the basic physics that allows fundamental parameters, such as the effective temperature, luminosity, abundances, and mass-loss rate, of Wolf-Rayet (W-R) stars to be determined. Since the temperature deduced from the spectrum of a W-R star is an ionization temperature, a detailed discussion of the ionization structure of W-R winds, and how it is set, is given. We also provide an overview of line and continuum formation in W-R stars. Mechanisms that contribute to the strength of different emission lines, such as collisional excitation, radiative recombination, dielectronic recombination, and continuum fluorescence, are discussed.

1 Introduction

Wolf-Rayet (W-R) stars exhibit a wide variety of spectra – some show only emission lines in the optical while others can exhibit P Cygni profiles as well as photospheric absorption lines. It is generally accepted that the emission lines are formed in a dense wind with $T(wind) < T_{\rm eff}$. In this review we will discuss some of the key physics behind W-R spectrum formation. Our discussion will be general, and since W-R stars exhibit a wide range of properties, these generalities should be applied carefully.

2 Overview

In brief, the spectrum of a Wolf-Rayet star is determined by:

1. The star's effective temperature.
2. The wind density.
3. Abundances.
4. Atomic physics.

Modeling reveals that similar spectra (i.e., with similar equivalent widths [EWs]) are produced when

$$\frac{\dot{M}}{V_\infty {R_*}^{1.5}\sqrt{f}} \qquad (1)$$

is held constant (Schmutz et al. 1989). f is the volume filling factor – an equivalent quantity is the clumping factor which is related to f by $D = 1/f$. The invariance reflects the importance of density-squared processes in W-R atmospheres.

In their modeling, the Potsdam group utilizes this invariance by constructing a transformed radius (R_t), defined by

$$R_t = R_* \left[\frac{V_\infty}{2500\,{\rm km\,s^{-1}}}\right]^{2/3} \left[\frac{10^{-4}\,M_\odot\,{\rm yr^{-1}}}{\dot{M}\sqrt{D}}\right]^{2/3}$$

(e.g., Sander et al. 2012), to construct model grids for W-R stars. Grids, with $T_{\rm eff}$ and R_t as the independent variable, are constructed and these are used to generate contour diagrams illustrating the functional dependence of the EWs of various lines. The grids have been used with great success to model W-R stars in the Galaxy (e.g., Sander et al. 2012) and the Magellanic Clouds (e.g., Hainich et al. 2014).

As a consequence of the degeneracy, it is not possible to deduce a starÕs distance from its spectrum. When comparing mass-loss rates derived for the same star it is important that the same distance is adopted. The degeneracy implies that $\dot{M}$ scales as $d^{1.5}$ (since R_* scales as d).

Since electron scattering depends on the density, not the density squared, the strength of the electron scattering wings depends on the adopted value of f, and this, in principle, provides a means of determining f. However, while it is easy to show that $f = 1$ produces electron scattering wings that are inconsistent with observation (Hamann & Koesterke 1998; Hillier & Miller 1999), it is difficult to determine f to better than a factor of two, especially since we typically use a very simple radial dependence for f – f is essentially constant in the line formation region.

W-R stars emit much of their flux in the unobservable EUV, shortward of 912Å. Since the observed fluxes represent only a small fraction of the emitted energy, and since it is also affected by the mass-loss rate, velocity law, and interstellar reddening, continuum fluxes cannot be used to constrain the star's $T_{\rm eff}$. Instead, line ratios (such as the strength of He II lines relative to He I lines) are used to constrain the effective temperature.

One has to be careful as to which definition of $T_{\rm eff}$ is being used — $\tau = 2/3$ is often located in the wind implying that the classical $T_{\rm eff}$ is influenced by $\dot{M}$, $V(r)$, and clumping. A common practice is to define the effective temperature using the radius at the base of the stellar wind, and to hope that this can be meaningfully related to evolutionary calculations. However even this is not satisfactory. For stars with a dense wind, the velocity law in the inner wind is not constrained observationally, and the adopted velocity law can substantially influence the derived effective temperature. Fortunately, the derived luminosity is much less sensitive to the adopted velocity law.

Ideally we would calculate $\dot{M}$ and the density structure from first principles, and incorporate them self-consistently into evolutionary calculations. Recent work by Groh et al. (2014) combining CMFGEN (for the atmospheres) and the Geneva evolutionary code have made progress towards calculating more reliable effective temperatures for evolved stars. There has also been work on trying to derive $\dot{M}$ self-consistently (e.g., Gräfener & Hamann 2005, 2008; Gräfener & Vink 2013) which has highlighted the importance of the proximity of W-R stars to the Eddington limit. However there are complications that make this task very difficult. First, we cannot derive the inhomogeneous density structure from first principles. Second, our simple description of clumping using the volume filling factor is likely to be inadequate. Third, opacity bumps (e.g., due to the Fe peak near 200,000 K) can give rise to density inversions and cause the stars to "inflate" in size (by an order of magnitude!) (e.g., Ishii et al. 1999; Petrovic et al. 2006; Sanyal et al. 2015). The amount of inflation is uncertain since it is affected by the treatment of convection, the amount of mass loss (e.g., Sanyal et al. 2015), and the possible existence of radiation instabilities (which occur near the Eddington limit)(Shaviv 2001).

3 Continuum formation

In the radio, the flux is (almost) independent of T (e.g., Wright & Barlow 1975), and we have the simple result that

$$F_\nu \propto \left(\frac{\dot{M}}{V_\infty \sqrt{f}}\right)^{4/3} \frac{1}{d^2} \qquad (2)$$

where we have included the dependence of f using the result of Abbott et al. (1981). A similar result applies to the EW of optically thick recombination lines. Notice how this result is fully consistent with our degeneracy condition, and with our earlier result that $\dot{M}$ scales as $d^{1.5}$. The infrared flux has a similar scaling to the radio, but the shape of the velocity law is also important (e.g., Lamers & Waters 1984). Shallower velocity laws (i.e., with a slower acceleration to terminal velocity) give higher fluxes. The visual flux of W-R stars is also affected by the mass-loss rate. In strong-lined WNE stars the optical continuum flux is directly affected by the mass-loss rate. However in weak-lined W-R stars, those most closely related to O stars, the optical continuum is much less sensitive to the mass-loss rate. While it is difficult to determine accurate mass-loss rates, photometry (particularly K band) allows variations in mass-loss rate of a few percent to be easily detected.

4 Ionization structure

A key property of Wolf-Rayet winds is that the ionization is not constant – the highest ionization stages (e.g., He^{2+}, N^{5+}) are found in the inner wind while low ionization stages (e.g., He^{+}) are found in the outer wind (Fig.1). This property is believed to be crucial for understanding the radiative driving of the stellar wind, since lower ionization stages will have their lines (i.e., the distribution in wavelength) better matched to the flux distribution.

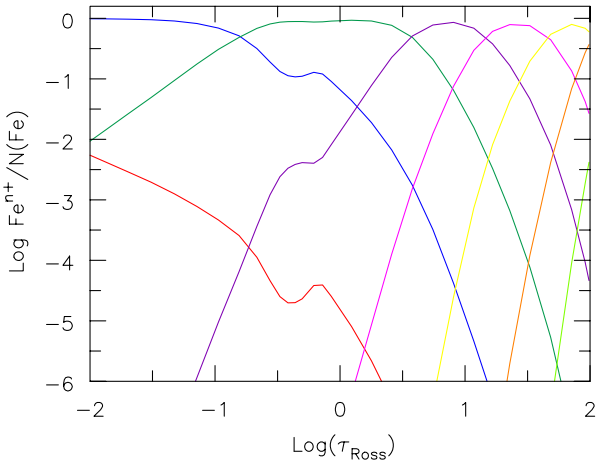

Fig. 1: Example of the ionization structure for a WN7-like model. Shown are the ionization fractions for Fe^{3+} (red) through Fe^{10+}.

Naively, one might have expected constant ionization in the wind. This follows if one assumes that ionizations occur from the ground state, since both the mean intensity and the density scale as $1/r^2$. However, in the dense winds of W-R stars ionization from excited states is important (e.g., Hillier 1987, 1989), and this helps to maintain the ionization. However, the population of the excited states generally falls off faster then $1/r^2$, causing the photoionization rate to decrease more rapidly than the recombination rate, and hence leading to a lowering of the ionization. Of course in the strongest-lined W-R stars the inner wind is optically thick, and changes in ionization occur simply because of changes in temperature.

Consider the case of He in WNE stars. The ionization of He (as He^{2+}) in the wind is maintained by photoionizations out of the $n = 2$ state of He^{+} (Hillier 1987). To first order, the population of the $n = 2$ state is maintained by the radiation field in the He II Lyman resonance transition at 304Å. At larger radii, the population of the $n = 2$ state falls, and He^{+} becomes the dominant ionization stage of He. For stars with a low $T_{\rm eff}$, the transition will occur very close to the star, while for hotter stars the transition may occur (if at all) at 10 (or more)

stellar radii.

For O stars it was found that the inclusion of blanketing in models led to a decrease in $T_{\rm eff}$. This occurred since blanketing led to back warming in the photosphere and hence a higher temperature and ionization (Martins et al. 2002, 2005). In order to maintain a fit to the spectrum, it was thus necessary to reduce $T_{\rm eff}$. In contrast, the inclusion of line blanketing in W-R stars led to an upward revision of their effective temperature (e.g., Hillier & Miller 1999). In this case, blanketing reduces the radiation shortward of 350Å, thereby decreasing the $n = 2$ population and hence reducing the ionization rate. To maintain the ionization at the observed value, as set by the observed ratio of He I to He II line strengths, a higher $T_{\rm eff}$ (and hence luminosity) is required.

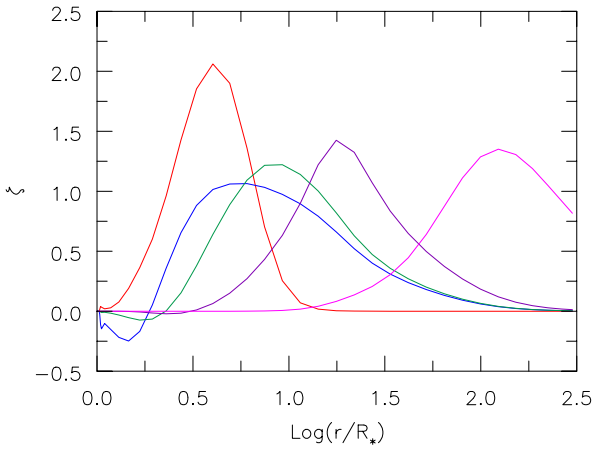

Fig. 2: Illustration of where various lines originate in a WN4-like star. The integral of ζ over $\log r$ gives the EW which has been normalized to unity for illustration purposes (Hillier 1989). Shown (from left to right) are the origin of N V λ 4620, He II 11-4, He II 7-4, He II 5-4 and He I λ10830.

5 Line formation in winds

In general a line can be in emission either because the line source function, S, is larger than in the continuum, or because the emitting surface is larger than in the adjacent continuum. For an optically thick line with constant source function and $V(r) =$ constant it can be shown (using the Sobolev approximation) that

$$\text{Line Flux} \propto R^2_{\tau=1} S \ .$$

For W-R stars, lines are generally in emission because the emitting surface is larger than that of the adjacent continuum. Of course S need not be constant, and will vary with the transition under consideration. In reality, a multitude of processes contribute to line formation in W-R winds. Further, the ionization structure plays a key role in determining line strengths, and not all lines are optically thick (e.g., He I λ5876 in WNE stars). In detailed models each observed line originates over a range of radii, and different lines originate in different regions of the stellar wind (Fig. 2).

It is often assumed that the optically thick stellar core will cause an asymmetry in the observed line profile, since it blocks radiation from the receding hemisphere. However, this asymmetry need not be present since we also 'lose' line emission from material in front of the core. The Eddington-Barbier relation tells us that along a sight line we see the source function at $\tau \sim 1$. If $S(\text{line}) \approx B(\text{continuum})$ we get a symmetric emission profile – there is no (excess) line contribution from directly in front of the star, and no line contribution from directly behind the star. When $S(\text{line}) < B(\text{continuum})$ we get a P Cygni profile while $S(\text{line}) > B(\text{continuum})$ can give rise to blue-shifted emission. In principle, it should be possible to see the influence of core occultation for an optically thin line. However, in practice optically thin lines (such as He I λ5876 in WNE stars) form at larger radii, and the effect of core occultation is small.

Below we consider various mechanisms that contribute to line emission in W-R stars. It is not always possible to identify a single dominant physical mechanism producing a given line – several processes may compete and the dominant process may depend on depth. Further, it does not necessarily make sense to determine the mechanism for a line whose levels are almost in LTE.

5.1 Resonance scattering

This process gives rise, for example, to P Cygni profiles in O stars. If resonant scattering is dominant, the absorption EW should be larger than the emission EW. This is typically observed for the N V and the C IV resonance doublets in O stars.

5.2 Collisional excitation

In dense winds, collisional excitation of low lying levels becomes important. For example, the N IV λ1486 and C III λ1909 intercombination lines are produced by collisional excitation. In W-R stars the UV resonance doublets of C IV and N V also have significant contributions by collisional excitation.

5.3 Recombination

The recombination process is important for H and He emission lines, and for most of the C lines in WC stars. Since the recombination line strength scale (crudely) with the abundance, recombination processes are primarily important for the most abundant species.

5.4 Dielectronic recombination

Low temperature dielectronic recombination (LTDR) refers to recombination via a doubly excited state with an energy just above the ionization limit (Nussbaumer & Storey 1983). For example, the CIII 2p 4d ^{1}F^o state lies just above the C III ionization limit. This state has a very high probability of autoionizing to C^{3+} plus a free electron, and the reverse process also occurs. Since the autoionization probability ($\sim 10^{14}$) is much larger than radiative rates (typically 10^8 to 10^9), the state is in LTE with respect to the ground state of C IV. The state can lead to efficient recombination, and act as a selective excitation mechanism, if one of the two excited electrons has a significant transition probability to a lower state. LTDR autoionizing levels can be treated as bound states, or via resonances in the photoionization cross-sections.

High temperature dielectronic recombination (HTDR) refers to the general dielectronic process, and does not rely on the existence of specific states close to the ionization edge. For C III, HTDR refers to dielectronic recombination through states of the form 2p nl where n is large (e.g., 100). For this process it is the decay of the 2p electron (i.e., 2p nl→2s nl) that provides the recombination route. Limited tests suggest that this process is not crucial in W-R stars.

5.5 Continuum fluorescence

Continuum fluorescence, sometimes called the Swings mechanism, was originally discussed by Swings (1948) to explain the selective excitation of certain lines in various early-type emission-line stars. In this process a UV transition (e.g., C IV 2s ^{2}S 3p ^{2}P^o at 312Å) absorbs continuum radiation. If the transition is optically thick, the radiation will scatter many times in UV transition. However, eventually the upper level (e.g., 3p ^{2}P^o) may decay to an alternative level (i.e., 3s ^{2}S) giving rise to emission at a longer wavelength (e.g., the C IV 5801, 5812Å doublet) (Hillier 1988). For the process to be efficient the UV transition has to be optically thick – for the case discussed above the optically thin transition rate to the 2s ^{2}S state is approximately 150 times the rate to the 3s ^{2}S state.

Continuum fluorescence is important for C IV $\lambda\lambda$5801, 5811 and for some N IV lines in WN stars (e.g., Hillier 1988), as well as for many metal lines (Mg II, Si II, Fe II) in P Cygni-type stars.

5.6 Line interactions

Line transitions may overlap intrinsically (i.e., their intrinsic emission profiles overlap) or they may overlap because of the influence of the velocity field. As a consequence of such overlaps, line strengths can be dramatically changed. Bowen fluorescence is an obvious example of the first case. Such overlap is automatically taken into account in line-blanketing codes, although unfortunately the wavelengths of many EUV lines are unknown, and thus important effects can be missed and/or treated incorrectly (since we include the line transitions but at the wrong wavelength). The use of super levels (see Hillier & Miller 1998) can also cause the effects of line overlap to be treated incorrectly.

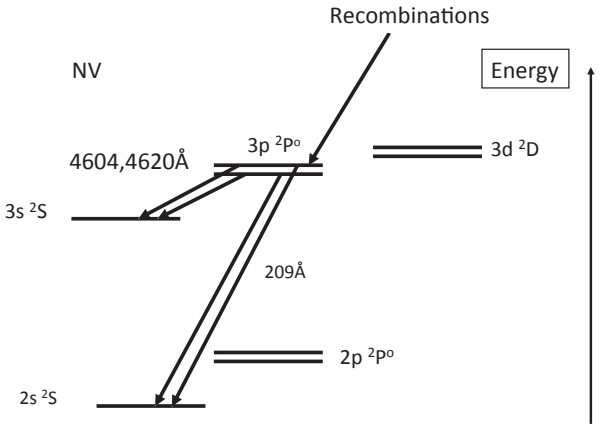

Fig. 4: Grotrian diagram for N V. A similar diagram applies for C IV except for a wavelength shift – the resonance transition is at 312Å, and the optical doublet is at $\lambda\lambda$ 5801, 5812.

5.7 Atomic physics matters

The strengths of emission lines in W-R stars do not always behave in a simple manner. Some lines can be selectively excited (e.g., by continuum fluorescence), while other lines can be unusually weak. For WC stars, the ratio of C III 5696Å to C IV 5805Å is a principal classification ratio. In WC4 stars C III λ5696 is (almost) absent, while its strength increases rapidly toward later spectral types (Torres et al. 1986). Other C III lines do not show the same dramatic variation – lines such as C III λ6740, are still present in WC4 stars (Fig. 3).

The behavior of C III λ5696 can be understood on the basis of the atomic structure of the C III atom (Torres et al. 1986; Hillier 1989). In WC4 stars the 2s 3d ^{1}D state primarily decays to the 2s 2p ^{1}P^o state. Emission in λ5696 (2s 3d ^{1}D to 2s 2p ^{1}P^o) increases in strength as the primary decay route, at 574Å, becomes optically thick. Further, the population in the 2s 3p ^{1}P^o state is efficiently drained by transitions to 2p^2 ^{1}D and 2p^2 ^{1}S. Thus λ5696 can remain optically thin (and hence exhibit a flat-topped profile), even when it is strongly in emission.

Another interesting case occurs with the lithium-like ions C IV and N V (Fig. 4). In HD 50896 (WN5), for example, the C IV $\lambda\lambda$ 5801, 5812 and the N V

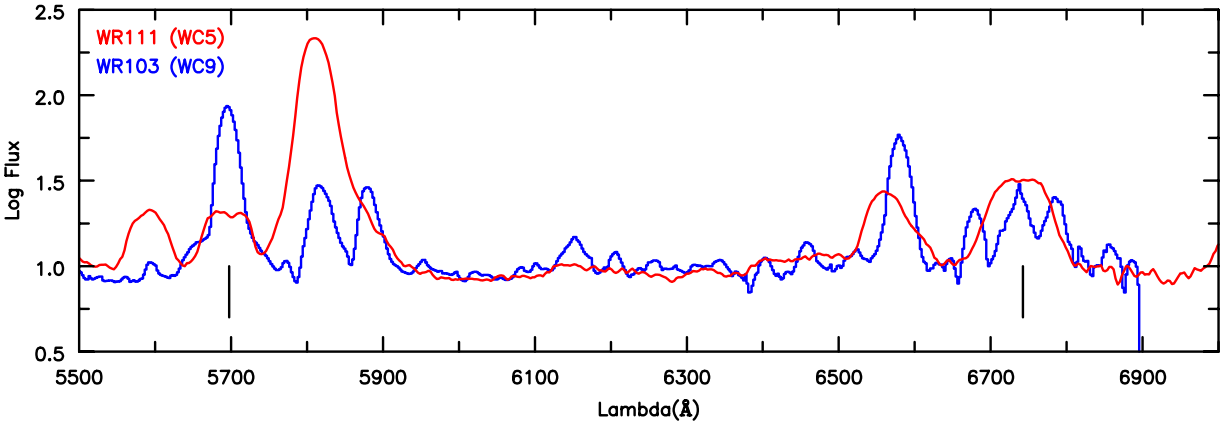

Fig. 3: Spectrum of HD 165763 (WC5, WR111)(red) and HD 164270 (WC9, WR103)(blue)(Torres-Dodgen & Massey 1999). Notice the different relative strengths of the two C III multiplets at λ5696 and λ6742 (indicated by vertical lines). In WC4 stars the λ5696 line is almost absent, while other C III multiplets are still prevalent.

$\lambda\lambda$ 4604, 4620 transitions have "similar" strength (Hillier 1988) despite the fact that the N abundance is roughly 40 times the C abundance (e.g., Maeder & Meynet 1987). While part of this is attributable to a difference in ionization, it also occurs because of the different wavelengths of the respective EUV transitions. The 3p level in C IV is connected to the ground state by a transition at 312Å, and can be pumped efficiently by the EUV radiation field. In contrast, the N V transition lies in the optically thick He II continuum at 208Å where there is little UV flux, and hence it cannot be efficiently pumped. In WN stars the N V doublet primarily arises through recombination.

In the very hottest WN stars the N V $\lambda\lambda$4604, 4620 can actually weaken as $T_{\rm eff}$ increases, even while the strength of other N V (recombination) lines is increasing. This occurs because of the declining optical depth of the 208Å transition – electrons can then decay from the 3p state via this transition rather than via the optical transition.

Understanding line and continuum formation in W-R stars is not simply an academic exercise. With such information one is better able to discern the significance of discrepancies, and to better understand systematic errors associated with the modeling.

Hillier gratefully acknowledges support from HST-GO-13780.002A which was provided by NASA through a grant from the Space Telescope Science Institute, which is operated by the Association of Universities for Research in Astronomy, Incorporated, under NASA contract NAS5-2655.

References

Abbott, D. C., Bieging, J. H., & Churchwell, E. 1981, ApJ, 250, 645
Gräfener, G. & Hamann, W.-R. 2005, A&A, 432, 633
Gräfener, G. & Hamann, W.-R. 2008, A&A, 482, 945
Gräfener, G. & Vink, J. S. 2013, A&A, 560, A6
Groh, J. H., Meynet, G., Ekström, S., & Georgy, C. 2014, A&A, 564, A30
Hainich, R., Rühling, U., Todt, H., et al. 2014, A&A, 565, A27
Hamann, W.-R. & Koesterke, L. 1998, A&A, 335, 1003
Hillier, D. J. 1987, ApJS, 63, 947
Hillier, D. J. 1988, ApJ, 327, 822
Hillier, D. J. 1989, ApJ, 347, 392
Hillier, D. J. & Miller, D. L. 1998, ApJ, 496, 407
Hillier, D. J. & Miller, D. L. 1999, ApJ, 519, 354
Ishii, M., Ueno, M., & Kato, M. 1999, PASJ, 51, 417
Lamers, H. J. G. L. M. & Waters, L. B. F. M. 1984, A&A, 136, 37
Maeder, A. & Meynet, G. 1987, A&A, 182, 243
Martins, F., Schaerer, D., & Hillier, D. J. 2002, A&A, 382, 999
Martins, F., Schaerer, D., & Hillier, D. J. 2005, A&A, 436, 1049
Nussbaumer, H. & Storey, P. J. 1983, A&A, 126, 75
Petrovic, J., Pols, O., & Langer, N. 2006, A&A, 450, 219
Sander, A., Hamann, W.-R., & Todt, H. 2012, A&A, 540, A144
Sanyal, D., Grassitelli, L., Langer, N., & Bestenlehner, J. M. 2015, ArXiv e-prints
Schmutz, W., Hamann, W.-R., & Wessolowski, U. 1989, A&A, 210, 236
Shaviv, N. J. 2001, ApJ, 549, 1093
Swings, P. 1948, Annales d'Astrophysique, 11, 228
Torres, A. V., Conti, P. S., & Massey, P. 1986, ApJ, 300, 379
Torres-Dodgen, A. V. & Massey, P. 1999, VizieR Online Data Catalog, 3143, 0
Wright, A. E. & Barlow, M. J. 1975, MNRAS, 170, 41

Anthony (Tony) Moffat: What do you mean when you say that WR winds are optically thick? As for the continuum, the wind is optically thick only below $\tau_e \sim 2/3$, then thin outside. If optically thick in lines, then does this mean for the whole domain in radius where the line is formed? What about weak vs. strong lines, or lines of different ionization formed at different radii?

D. John Hillier: When I say that W-R winds are optically thick, I mean that $\tau \sim 2/3$ occurs in the wind, above the sonic point. However for W-R stars with "weak winds", this may not be true at all wavelengths. The observed flux will typically arise from regions with tau somewhat above 2/3, and τ below 2/3, but this statement is line/continuum dependent. Because of the extension caused by the wind, much of the flux will/can come from optically thin regions of the wind. In the case of the radio flux, for example, Wright and Barlow (1975) show that the observed radio flux is equivalent to receiving all of the emission coming from optical depths less than 0.244. For many optically thick lines (e.g., He II 4686 in WNE stars), it can be shown that roughly 50% of the flux arises from regions with a Sobolev optical depth > 1. For the case of He I 5876 in WNE stars, the line optical depth in the formation region is less than 1, and this line can be considered to be "optically thin". The strength of such lines is controlled primarily by the location in the wind where the dominant state of He changes from He^{++} to He^{+}.

Gloria Koenigsberger: How does one judge the goodness of the fit of a model to an observed spectrum? What guidance criteria should be used?

D. John Hillier: One needs to run sensitivity tests. That is, one varies the parameter (e.g., mass-loss rate, abundance etc) about the best fit value, and examines how observables changes. In some cases the sensitivity is quite strong (e.g., linear), and in other cases the sensitivity can be weak. When the strength of a feature is bracketed by the models, one can be fairly confident in the results. However, when the model feature is always discrepant with the observations the implications of the discrepancy can be difficult to determine. In other cases the strength of features can be controlled by several model parameters and this requires additional testing. In recent work it is becoming more common to perform systematic studies for a large number of parameters, and then to use, for example, chi squared minimization to deduce the best models. Even then, however, judgement calls are usually made to exclude certain features which cannot be fit.

Wolf-Rayet Stars
W.-R. Hamann, A. Sander, H. Todt, eds.
Potsdam: Univ.-Verlag, 2015
URL: http://nbn-resolving.de/urn:nbn:de:kobv:517-opus4-84268

World-wide amateur observations - A viable future of massive star research

T. Eversberg[1], E. J. Aldoretta[2], J. H. Knapen[3], A. F. J. Moffat[2], T. Morel[4], T. Ramiaramanantsoa[2], G. Rauw[4], N. D. Richardson[2], N. St-Louis[2], M. Teodoro[5]
[1] *Schnörringen Telescope Science Institute, Germany*
[2] *Université de Montréal, Canada* [3] *Instituto de Astrofisica de Canarias, Spain* [4] *Université de Liége, Belgium* [5] *Western Michigan University, USA*

For some years now, spectroscopic measurements of massive stars in the amateur domain have been fulfilling professional requirements. Various groups in the northern and southern hemispheres have been established, running successful professional-amateur (ProAm) collaborative campaigns, e.g., on WR, O and B type stars. Today high quality data (echelle and long-slit) are regularly delivered and corresponding results published. Night-to-night long-term observations over months to years open a new opportunity for massive-star research. We introduce recent and ongoing sample campaigns (e.g. ϵ Aur, WR 134, ζ Pup), show respective results and highlight the vast amount of data collected in various data bases. Ultimately it is in the time-dependent domain where amateurs can shine most.

1 World-wide amateur communities

For some years now spectroscopic observations of massive stars have become well established in the world-wide amateur community. Besides many small teams, this community is still concentrated in the German *VdS Section Spectroscopy* (VdS Spectroscopy) and the French *Astronomical Ring for Access to Spectroscopy* (ARAS). A third presently upcoming group is the *Southern Astrospectroscopy Email Ring* (SASER) in the southern hemisphere (see section 3). Smaller groups and single observers can be found in Canada, China, Denmark, Spain, UK, USA, etc. Websites and internet forums bring these amateurs and professionals together. Data are regularly delivered to respective databases (e.g. the database *Be Star Spectra* (BeSS) presently contains more than 100.000 professional and amateur Be star spectra). Annual conferences with typically 50 participants take place in France and Germany. Observations are performed with standard long-slit spectrographs, as well as Echelles, which can be commercially designed or self-made.

2 Specific amateur domains

Some specific measurements cannot be easily performed with professional telescopes and manpower. These include, e.g., repeated observations for times longer than a month or so. In addition, long-term campaigns of several months can usually not be performed with professional telescopes. Either the necessary small-size instruments do not exist/are not available or observing proposals compete with other programs.

2.1 Monitoring

Long-term monitoring of spectral quantities/indicators is probably an exclusive amateur domain. In contrast to professional observations amateurs can monitor targets for many years delivering solid and uniform information about certain stellar behaviour. Figure 1 shows a 10 year amateur monitoring of the bright Be star δ Scorpii with dramatic changes in EW of the Hα disk emission line.

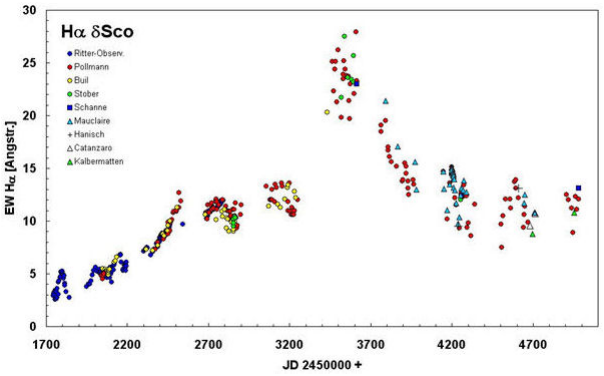

Fig. 1: Amateur Hα observations of the Be star δ Sco for about 10 years. The first observations were performed by professional astronomers, indicating line-strength variability between 3 and 5 Å (blue dots). Amateur observations over 10 years revealed a global long-term variability between 3 and 28 Å (Pollmann et al.).

2.2 Long-term campaigns

Up until now, numerous ProAm long-term campaigns have been performed. Examples are the outburst of the symbiotic star V407 Cyg in 2010, δ Sco periastron passage in 2011, the Algol type eclipsing system AZ Cas in 2012 – 2014 and the erupting Nova

Delphini in 2013. All observations were performed with very small telescopes (∼ 30cm) at private backyard observatories. Two examples:

2.2.1 ϵ Aurigae eclipse campaign 2009–2011

ϵ Aur is the longest-period eclipsing binary known (∼27.1 years). Amateurs and professionals separately measured the 18 month eclipse of the primary F0 star by a dust disk around a B type secondary. Professional observations with the CHARA interferometer (Fig. 2, top) delivered direct imaging of this event. However, no information about the disk structure could be obtained. Amateur equivalent width measurements of neutral Potassium at 7699 Å, however, revealed a line-strength variability which suggests a structured disk (Fig. 2, bottom).

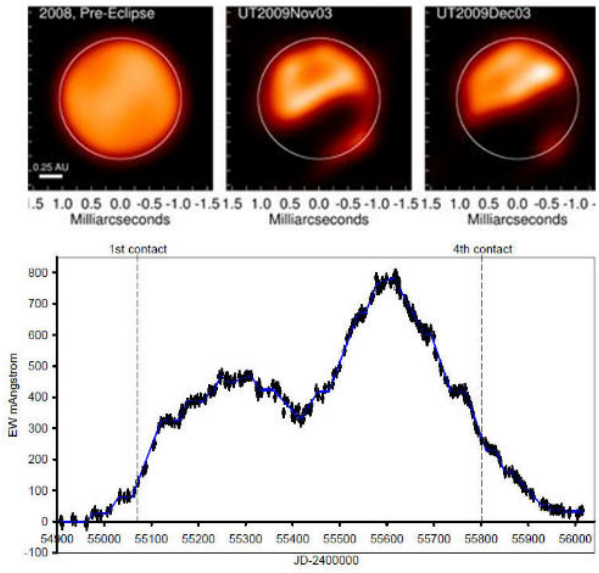

Fig. 2: Observations of the eclipse of ϵ Aur. Top: Observation with the CHARA interferometer. A dust disk obscures the F0 primary (Kloppenborg et al. 2010). Bottom: Excess K I 7699 absorption observed with a 20cm telescope and an off-the-shelf spectrograph (Leadbeater et al. 2012).

2.2.2 Teide WR campaigns

Because IAC-Tenerife generously offers specific amateur access, the professional Teide Observatory is a logical choice for ProAm campaigns together with European amateurs. Besides a ProAm campaign on the Be star δ Sco in 2011 (Miroshnichenko et al. 2013) two campaigns have been performed on WR stars, both in a joint international campaign at world-wide telescopes. These two campaigns also included ground- and space-based X-ray, optical and IR facilities. They monitored the periastron passage of WR 140 and tried to detect periodicities in the winds of WR 134, WR 135 and WR 137. The former delivered accurate ephemerides for the orbit as well as the stellar parameters for the WR star, its O companion and the wind shock-cone (Fahed et al. 2011). The latter confirmed Corotating Interaction Regions (CIR) in the wind of WR 134 including estimation of a typical half-life for the CIR pattern of about 18 stellar rotation periods (Aldoretta et al. 2015). Such long campaigns deliver additional target opportunities. In our case we filled respective time-windows with observations of some B (Morel et al. 2011) and Oe type stars (Rauw et al. 2015).

3 Amateur data quality

It is often believed that amateur spectroscopists deliver data of inferior quality. However, the corresponding instrumentation is only a scaled-down version of that used at larger telescopes. Professional and amateur data (exposure times, signal-to-noise-ratio, spectral resolving power) differ only because of smaller telescopes. Considering 30 cm amateur telescopes, the typical performance for a 7mag star observed at R ∼10.000 is S/N ∼100 for an integration time of ∼30 min.

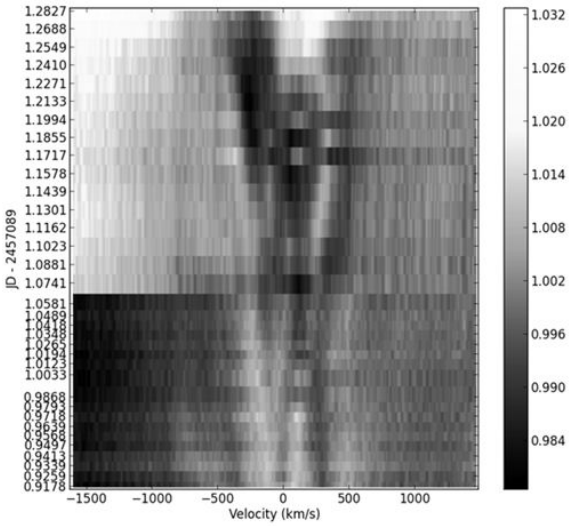

Fig. 3: Amateur He II 4686 observations of ζ Pup from central Melbourne (lower part) and central Perth (upper part). Greyscales of nightly residuals from the mean rectified spectrum are plotted in time vs. radial velocity. Both observations have been performed with 28cm telescopes and off-the-shelf spectrographs.

As an example, during a campaign investigating the long-term behavior of the He II 4686 central reversal of ζ Pup in late 2014 through 2015 May about

700 high-resolution spectra have been obtained by SASER amateurs alone (beside hundreds of other spectra of γ Vel and η Car). For comparison with professional work grey-scale plots of the low-contrast wind clumping residuals in the He II line have been computed. Figure 3 shows two consecutive plots from data obtained in central Melbourne and central Perth. For comparison with professional results we refer to figs. 2 and 3 in (Eversberg et al. 1998) obtained with a 3.6m telescope at Mauna Kea.

4 A Pro-Am campaign recipe

Compared to professional observation campaigns ProAm collaborations require additional care. Amateur spectroscopists often have a relatively high level of expertise, sometimes even holding a scientific degree. They are normally familiar with the basic data reduction procedures (e.g., bias subtraction, flat-fielding, continuum rectification). However, the majority are not familiar with target physics and the details of spectroscopic analysis. Hence, according to our experience a basic guideline for building up a ProAm campaign is required.

→ Besides an announcement among the respective communities a dedicated campaign webpage with background information ensures continuously updated information about the goals, physics and campaign management.
→ It is mandatory to talk to the amateurs, since they may not have the necessary knowledge. Amateurs in both hemispheres have already established discussion forums. Scientists in charge should also use them.

For amateur observations at professional sites additional action is required:

→ The professional prime investigator (PI) should be responsible for the science case including professional support observations. The amateur campaign management should be responsible for organizing all issues with respect to the core observation site.
→ The PI should write the telescope proposal.
→ It is mandatory that all involved professionals offer permanent support.

A specific issue concerns financial resources. Amateurs are willing to contribute their time and money to such a campaign (transportation, accommodation and other resources). But from experience, additional financial resources are often necessary. For the two 4-month WR campaigns on Tenerife we needed about 4000 Euro to cover unexpected costs (e.g., Echelle guiding unit, unexpectedly higher equipment transportation costs, other unforeseen events). One should also take care of the corresponding spectrograph equipment. Normally such instruments can be contributed from the amateur side. But it is highly recommended to organize this central part maybe even before setting the campaign kick-off. Specific care should be invested in explaining the different campaign roles so that every team member remains informed. Especially for volunteer observers the responsibilities during the campaign and the general framework at the observatory (e.g., what is possible and what is not) should be well discussed.

5 Summary and prospects

Amateur spectroscopic observations of massive stars have reached the professional domain. This is clearly the result of modern engineering and corresponding low prices in the "Golden Age of Astronomy". Considering the present situation in astronomy it seems obvious that skilled amateurs equipped with modern instrumentation, can successfully contribute with their knowledge and enthusiasm to professional spectroscopic campaigns, either at their home observatories or at professional sites. Apart from the size, self-designed and off-the-shelf amateur instrumentation fullfils all professional requirements (today, off-the-shelf spectrographs are often in operation at small professional telescopes). For specific goals where long-term observations or quick reaction are required (e.g., binary interactions, long period phenomena, novae) amateurs can often deliver better conditions than professional facilities. The only obstacle for performing continuous observations like those at professional sites is the local weather and the fact that amateur astronomer usually have to work in their daily job. This however can be circumnavigated by joint campaigns, as shown above. It is up to the professional community to uncover this valuable treasure.

References

Aldoretta et al. 2015, these proceedings
ARAS, http://www.astrosurf.com/aras/
BESS, http://arasbeam.free.fr/?lang=en
Eversberg, T., Lépine, S., & Moffat, A. F. J. 1998, ApJ, 288, 679
Fahed et al. 2011, MNRAS, 418, 2
Kloppenborg et al. 2010, Nature, 464, 870
Leadbeater et al. 2012, J. Amer. Assoc. Var. Star Obs., 40, 729
Miroshnichenko et al. 2013, ApJ, 766, 119
Morel et al. 2011, Bull. Soc. Roy. Sci. Liége, Vol. 80, p. 170
Pollmann et al., unpublished
Rauw et al. 2015, A&A, 575, 99
SASER, http://saser.wholemeal.co.nz/
VdS, http://spektroskopie.fg-vds.de/index_e.htm

Michael Corcoran: Can you address the issue of quality control?

Thomas Eversberg: A very important point! I normally recommend to reduce the data by one single person for consistent reduction. BUT: Some amateurs are very skilled in reduction. When working with a new group you will quickly realize their capabilities and skills. Maybe you then can leave this work in their hand just taking the reduced material. In any case, if the data are taken for a thesis, reduction should be performed by the student, anyway. In general: Data quality can certainly be imprived by respective advise and discussions. You need to talk!

Wolf-Rayet Stars
W.-R. Hamann, A. Sander, H. Todt, eds.
Potsdam: Univ.-Verlag, 2015
URL: http://nbn-resolving.de/urn:nbn:de:kobv:517-opus4-84268

The Results of the 2013 Pro-Am Wolf-Rayet Campaign

E. J. Aldoretta[1], N. St-Louis[1], N. D. Richardson[1], A. F. J. Moffat[1], T. Eversberg[2], G. M. Hill[3] and the World-Wide WR Pro-Am Campaign Team[4,5]
[1] *Université de Montréal, Canada*
[2] *Schnörringen Telescope Science Institute, Germany* [3] *W. M. Keck Observatory, United States* [4] *VdS Section Spectroscopy, Germany* [5] *Astronomical Ring for Access to Spectroscopy (ARAS), France*

Professional and amateur astronomers around the world contributed to a 4-month long campaign in 2013, mainly in spectroscopy but also in photometry, interferometry and polarimetry, to observe the first 3 Wolf-Rayet stars discovered: WR 134 (WN6b), WR 135 (WC8) and WR 137 (WC7pd+O9). Each of these stars are interesting in their own way, showing a variety of stellar wind structures. The spectroscopic data from this campaign were reduced and analyzed for WR 134 in order to better understand its behavior and long-term periodicity in the context of CIRs in the wind. We will be presenting the results of these spectroscopic data, which include the confirmation of the CIR variability and a time-coherency of $\sim$ 40 days (half-life of $\sim$ 20 days).

1 Motivation and Campaign Overview

Co-rotating interaction regions (CIRs) form in the winds of hot stars where fast material is colliding with slower material (or vise-versa) as the star rotates (Cranmer & Owocki 1996). This phenomenon was first discovered within the solar wind (Mullan 1984) and has since been seen in massive stars using several different observational methods. The exact cause of these structures could be attributed to phenomena at the base of the wind, such as magnetic fields or nonradial pulsations. While most O-type stars show DACs and NACs within their UV P Cygni lines, only a few WR stars have shown CIRs due to their saturated absorption components, some of which are WR 1, WR 6 and WR 134 (St-Louis (2013), Ignace et al. (2013) and Morel et al. (1999)). Using photometry, spectroscopy and polarimetry it is possible to learn more about these features and how they are formed.

Morel et al. (1999) studied the strong spectral variations of WR 134. An intensive campaign of spectroscopic and photometric monitoring of this star took place in order to reveal the nature of these variations. A coherent 2.25 $\pm$ 0.05 day periodicity in changes of the He II λ4686 emission line was confirmed. The global pattern of variability, however, changed with each epoch. While this period was strongly detected within the spectroscopic data, it was only marginally detected in the photometric data. In an attempt to better understand this period found in the spectroscopic data, we organized a collaboration between amateur and professional astronomers.

During the summer of 2013, a 4-month Wolf-Rayet (WR) campaign began on WR 134, WR 135 and WR 137. Each of these targets were chosen in order to observe different features: WR 134 is known to show co-rotating interaction regions (CIRs) in the spectral lines (Morel et al. 1999), WR 135 is known to show large clumpy structures in its wind (Lepine et al. 1996) and WR 137 is a long-period WR+O binary system with possible CIRs (Lefèvre et al. 2005). All three of these stars could benefit from long-term observations and are relatively easy for amateurs to observe due to their visual magnitudes ($V \sim 8.1$, $V \sim 8.1$ and $V \sim 7.9$, respectively). Several types of data were collected, including interferometry from the CHARA Array, photometry, broad-band polarimetry and spectroscopy. A total of 10 sources have contributed to the spectroscopic data of the campaign, the majority of which was collected on the island of Tenerife. For the object WR 134, the spectroscopic data have been analyzed and the results are presented.

Tab. 1: List of spectroscopic data sources, along with corresponding resolving powers and wavelength coverages.

Observatory	$R(\lambda/\Delta\lambda)$	λ coverage (Å)
Professional Facilities		
Teide	10,000	4500 - 7400
Keck	13,000	4000 - 10000
OMM	4,000	4700 - 6000
DAO	5,500	5100 - 6000
Ondřejov	10,500	5200 - 5750
NOT	11,800	3500 - 6800
Amateur Contributors		
Potter	7,500	5300 - 5850
Li	5,300	5250 - 5600
Strachan	5,300	5300 - 5700
Leadbeater	5,350	5200 - 5600

The spectrosocpic data collected for this project

were taken with a large group of astronomers from 25 May 2013 to 06 October 2013. Ten different observatories contributed to the spectroscopic data for these WR stars, five of which are professional facilities (outlined in Table 1). All observers participating in the campaign observed at least the He II λ5411 emission line, where the CIR perturbations can be easily detected due to the strength of line along with its relative isolation. All data were reduced using standard techniques.

2 Data Analysis

Several calculations were made in order to determine if the 2.25-day period that was found by Morel et al. (1999) would be present within these spectroscopic data. Our first method was to first create an average spectrum in velocity space. Then, a Scargle (1982) periodogram was created over each velocity. Figure 1 shows the results of these calculations. It can be seen that the frequency ~ 0.443 ($P = 2.25$ days) is strong over the majority of the He II λ5411 emission line. The first harmonic of this frequency ($2f$), along with both of their one-day sampling aliases (1 - f and 1 - $2f$) are also detected

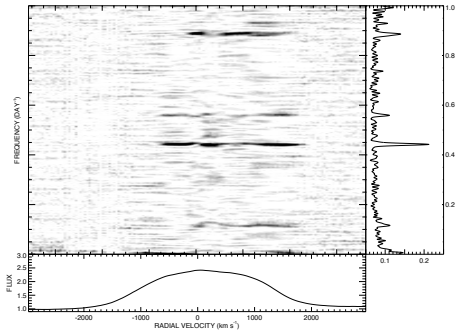

Fig. 1: 2-D Scargle periodogram (Scargle 1982) for the velocity space around the He II λ5411 line. The bottom panel shows the average spectrum of the entire data set. The right panel shows the Scargle periodogram. The middle panel shows the grey-scale of the Scargle analysis for each velocity. It can be seen that the frequency of ~ 0.0443 d^{-1} is the strongest peak.

Moments of the He II line were also calculated over the entire data set. The central n^{th} moment is given by:

$$\mu_n = \Sigma_j(\lambda_j - \bar{\lambda})^n I_j / \Sigma_j I_j$$
$$\bar{\lambda} = \Sigma_j \lambda_j I_j / \Sigma_j I_j, \quad (1)$$

where I_j is the intensity of the line and λ_j is the wavelength. Two dimensionless quantities can be calculated from these moments: the skewness by $\mu_3/\mu_2^{3/2}$ and the kurtosis by μ_4/μ_2^2. A time-dependent Scargle analysis was then conducted on these moments, resulting in a mean period of $\sim 2.255 \pm 0.007$ days.

Once this period was calculated and confirmed, phased difference images from the mean were created in five-day ($\approx$ 2 cycles) segments with a total of 23 images for the entire run. An arbitrary image was chosen from these from which a normalized 2-D cross-correlation was made from the images before and after the fixed image. This was repeated with two other images based on their good time-coverage of data, all showing similar results. The cross-correlations were calculated by:

$$Xc_{ij} = \frac{\Sigma_{jk} I_{1jk} \times I_{ijk}}{\Sigma_{jk} I_{1jk}^2}, \quad (2)$$

with $i = 1$ being the fixed image and j and k referencing the location of the pixels. Then a Gaussian function plus constant background was arbitrarily fit to every data point of the cross-correlation, with the peak coinciding with the maximum correlation. The artificial correlation of 1.0 of the image with itself was ignored.

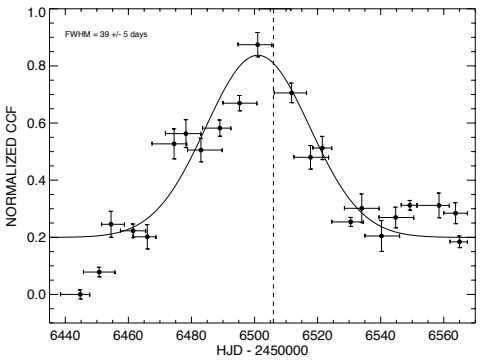

Fig. 2: Cross-correlation of phased gray-scale difference images. Time frame for each image is displayed as x-axis error bars. The reference image is shown along dotted line and was ignored for the Gaussian fit.

Figure 2 shows the time-coherency for the CIR of $\sim$ 40 days (18 cycles) that was found. This was determined by fitting a Gaussian to both (a) the entire data set and (b) both sets of non-overlapping data points in time and calculating the mean FWHM of the three results. This 40-day time-coherency was also present in a time-dependent Scargle periodogram created for the skewness and kurtosis of

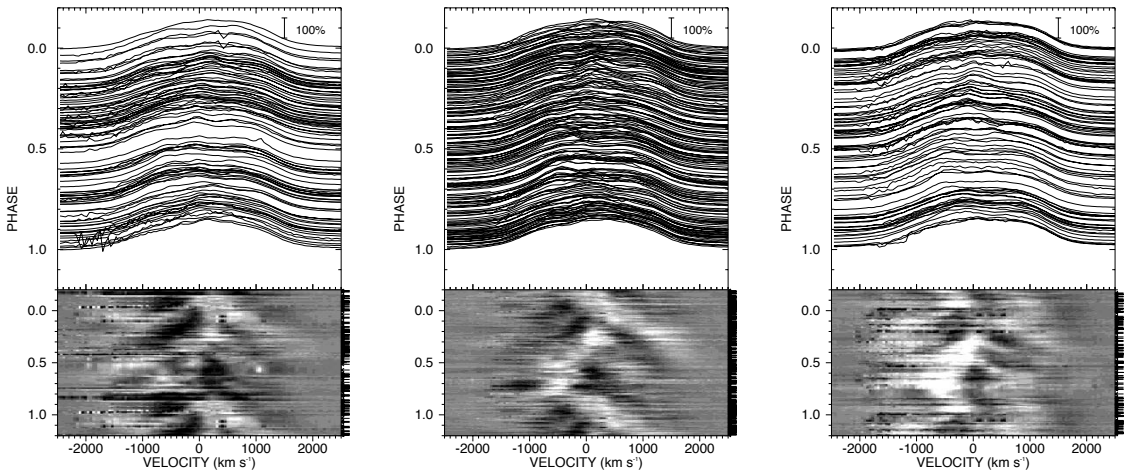

Fig. 3: : Difference gray-scale images of the spectra are shown. The images are increasing with time from left to right and are grouped in 40-day (18 cycle) segments.

this line as well. Between HJD-2456467 and HJD-2456517, the 2.255-day period is the strongest in both of these moments, which corresponds with the time-coherency found in the cross-correlation. This cross-correlation also shows that this CIR displays a half-life time (or decay time) equivalent to the HWHM of the Gaussian, or $\sim$ 20 days.

Once the time-coherency was determined for WR 134, new difference images were created in order to see how the CIRs change every 40 days (see Figure 3). These images show the main CIR rotating within the wind, but also shows weaker CIRs with other separation angles relative to the rotating star underneath. Dessart & Chesneau (2002) created models of CIRs in WR star winds, which showed a similar brightness pattern consistent with multiple CIRs.

3 Summary and Future Work

We were able to determine a CIR period of 2.255 $\pm$ 0.007 days, which agrees with the results by Morel et al. (1999). Once the period was determined, the spectra were then organized by phase in order to create difference grey-scale plots for 5-cycle segments. These grey-scale plots were cross-correlated with each other, showing either a coherence timescale of $\sim$ 40 days (18 cycles) or a half-life time of $\sim$ 20 days for the CIRs. Gray-scale difference plots for 40-day segments were created and show how the CIR changes with the coherence timescale. When compared to the model by Dessart & Chesneau (2002) it can be determined that more than one CIR is likely present in the wind. Future modeling and kinematics could reveal information on the physics causing large-scale structures in WR winds.

References

Cranmer, S. R. & Owocki, S. P. 1996, ApJ, 462, 469
Dessart, L. & Chesneau, O. 2002, A&A, 395, 209
Ignace, R., Gayley, K. G., Hamann, W.-R., et al. 2013, ApJ, 775, 29
Lefèvre, L., Marchenko, S. V., Lépine, S., et al. 2005, MNRAS, 360, 141
Lepine, S., Moffat, A. F. J., & Henriksen, R. N. 1996, ApJ, 466, 392
Morel, T., Marchenko, S. V., Eenens, P. R. J., et al. 1999, ApJ, 518, 428
Mullan, D. J. 1984, ApJ, 283, 303
Scargle, J. D. 1982, ApJ, 263, 835
St-Louis, N. 2013, ApJ, 777, 9

Michael Corcoran: Do new CIRs re-appear at the same phase after each 40-day CIR cycle?

Emily Aldoretta: No, we do not see the same configuration of CIRs re-appear because we do not see the correlation function more than once within our data set, possibly in part due to the finite length of the data stream.

John Eldridge: Could the signal of multiple CIRs actually be because the star is precessing/wobbling as it rotates?

Emily Aldoretta: Possibly, but not on a timescale shorter than our observations. We should perhaps watch for signs of this in the future.

Andy Pollock: Could you tell more about the long-term coherence of the 2.25-day and 40-day periods?

Emily Aldoretta: According to the cross-correlation analysis, the 2.25-day period is seen to be relatively coherent for 40 days for any given reference point in time. Other than the 2.25-day period, there is no evidence for another period in our data.

Peredur Williams: Is the 2.25-day period variation coherent, as if the CIRs originated on the same points on the star?

Emily Aldoretta: This is an interesting point, and our best guess is that we see multiple CIRs coming and going on various time scales on a stellar rotation period of 2.25 days. Whether each CIR originates at the same rotating point on the star remains to be demonstrated.

Thomas Eversberg: Repeating CIR features after 18 cycles smells like a resonance effect. That would be in conflict to the idea of hot spots as the origin of CIRs. What is your impression about that?

Emily Aldoretta: The 18-cycle time-coherency does not represent a periodic repetition, but a time-coherency for which the cross-correlation function fades away.

Wolf-Rayet Stars
W.-R. Hamann, A. Sander, H. Todt, eds.
Potsdam: Univ.-Verlag, 2015
URL: http://nbn-resolving.de/urn:nbn:de:kobv:517-opus4-84268

Studying Large and Small Scale Wind Asymmetries with Spectroscopy and Polarimetry

N. St-Louis[1]
[1] *Département de physique, Université de Montréal*
C.P. 6128, Succ. Centre-Ville, Montréal (Qc), H3C 3J7, Canada

In this paper, I review observational evidence from spectroscopy and polarimetry for the presence of small and large scale structure in the winds of Wolf-Rayet (WR) stars. Clumping is known to be ubiquitous in the winds of these stars and many of its characteristics can be deduced from spectroscopic time-series and polarisation lightcurves. Conversely, a much smaller fraction of WR stars have been shown to harbour larger scale structures in their wind ($\sim 1/5$) while they are thought to be present is the winds of most of their O-star ancestors. The reason for this difference is still unknown.

1 Introduction

Wolf-Rayet (WR) stars, which amongst hot, massive stars, have the strongest, sustained radiatively-driven outflows, were initially assumed to have smooth, spherically symmetric winds. We have since learned that these outflows are highly structured and several have been shown to harbour large-scale structures. Understanding the physical cause of these large-scale asymmetries can enlighten us about processes occurring near or on the, often hidden, stellar surface and allow us to assess how the angular momentum of the star is lost via the wind. In this paper, I review the evidence from spectroscopic and polarimetric observations of the existence of these structures in WR winds.

2 Small-Scale Variability

2.1 Spectroscopy

The earliest report of spectroscopic evidence of fast moving clumps in WR winds is from Moffat et al. (1988) in which narrow emission bumps were identified superposed on the broad HeIIλ5411 emission lines of WR134 and WR136 and found to accelerate outwards with the general wind on a timescale of hours. Since then, several more WR stars have been monitored and if the quality of the data is sufficiently high, accelerating narrow emission peaks are always found. Therefore, clumping is now thought to be universal in WR outflows and probably in all radiatively driven winds. A striking example is shown in Figure 1 where Figure 10 of Chené et al. (2015, submitted) is reproduced and where clump movement in WR2 is shown. Un upper limit of 0.8% of the line flux was previously set for the line variability of this star by Chené & St-Louis (2011). The variability level is in fact $\sim$0.5% and the features rapidly migrate toward line edges in about $\sim$2.6 hours.

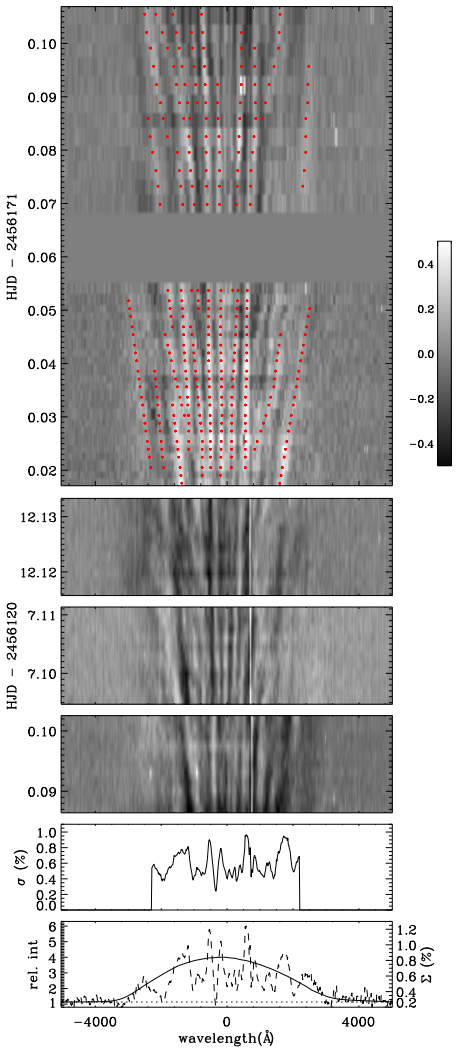

Fig. 1: Clump variability in the HeIIλ4686 line of WR2, reproduced from Chené et al. (2015). The top four panels show differences from the mean as a function of time with the emission sub-peak movement indicated by red doted lines. The bottom two panels show the level of variability of the line flux (σ) and the Temporal Variance Spectrum (Σ) superposed on the mean line profile.

More quantitative analysis of this small-scale spectroscopic variability was carried out by Lépine et al. (1996) in which a wavelet power spectrum was used to characterize the variable component of optical emission lines of WR stars. A dominant scale of $\sim$100 km s^{-1} was identified for all but one star in their sample to characterize the size of the sub-peaks. Later Lépine & Moffat (1999) envisioned the wind as consisting of a large number of randomly distributed Discrete Wind Emission Elements (DWEEs) of various widths and amplitudes propagating radially in the wind. They found that more than 10000 of these DWEEs must be used to account for the line variability and that the velocity dispersion within them must be four times larger in the radial than in the azimuthal direction. From the kinematics of the moving sub-peaks, Lépine & Moffat concluded that the value of the product of the β exponent of the wind velocity law and the stellar radius, $\beta \mathrm{R}_*(R_\odot)$ was between 20–80, hinting to a lower wind acceleration at least in the region of the outflow where the clumps are accelerating.

These observational results stimulated theorist to seek a more physical understanding of the origin of this type of line-profile variability. Dessart & Owocki (2002a) explored the assumption that these small-scale wind structures were caused by the line-driving instability (Owocki & Rybicki 1984, 1985). To do so, they implemented a Smooth Source function Formalism for line driving in the *Zeus*-2D hydrodynamics code, which they used in one dimension (1D) to perform hydrodynamical simulations. The 1D restriction, warranted by computational costs, produced a much higher level of variability at line edges compared to line center than was observed. To alleviate this problem, they introduced a *patch* model in which random wind velocity and density profiles which incorporate the radiative instability are used along a given radial ray and extend over a certain patch size on the surface of the star. The results were that a patch of around 3 degrees qualitatively reproduces the observed properties of the small-scale line-profile variability. Dessart & Owocki (2002b) then carried out a wavelet analysis of synthetic profiles from those models which led them to propose that there are two distinct line broadening mechanisms: (a) the lateral extension of the clumps as detected at line-centre and (b) an intrinsic radial velocity dispersion within the clump, which dominates towards line-edge. They found that their model was not capable of reproducing the observed sub-peak width at line edges, which led them to conclude that the radiative instability did not produce enough velocity dispersion in the gas. Finally, Dessart & Owocki (2003) present a two-dimensional model in which the smooth source function formalism for the line-driving is implemented independently in isolated azimuthal grid zones. The main result was that Rayleigh-Taylor instabilities break-up compressed shells, down to the adopted grid size as they are accelerated outward. An increase in the radial velocity dispersion is found, which agrees more with the observations, and the associated clumping correction factor are reduced and are now closer to the ones inferred from WR emission-line fitting using the radiative transfer code, CMFGEN. However, this breakup of the structures to very small scales does not agree with the 3-degree patches that are required to reproduce the wavelet spectrum.

2.2 Polarimetry

In the highly ionized winds of WR stars, there are copious amounts of free electrons that polarize the light from the star through Thomson scattering. If the wind is smooth and spherically symmetric, all polarized vectors cancel out an no net polarisation is observed. Conversely, any large or small asymmetry in the density distribution or in the light source will create a non-zero value of the linear polarisation. Consequently, polarimetry is a very powerful tool to study stellar wind asymmetries. Furthermore, if the phenomenon creating the asymmetry is time-dependent, secular variations will be produced in the polarisation.

St-Louis et al. (1987) first proposed that the random nature of the stochastic broadband polarimetric variability in the single-line WR star WR103 is compatible with the ejection of blobs of material in the wind on intervals of days. This can be seen in the polarized lightcurve as a sudden rise in the polarisation followed by a gradual decrease back to the initial value.

Based on data on 11 WR stars of WN and WC subtype, Drissen et al. (1987) found a correlation between the standard deviation from the mean of the randomly varying linear polarisation, σ (P), and the wind terminal velocity. This was confirmed later with observations of 26 stars by Robert et al. (1989) who noted that the correlation is fairly tight, although some scatter remains. In Figure 2 we reproduce Figure 11 of Robert et al. (1989) showing this correlation. These authors concluded that the fast-wind stars show less scatter in polarisation than the slow-wind stars, implying that the winds of earlier WC stars are more stable and those of the late WN and WC stars more subject to instabilities. A similar trend was also observed in photometry byLamontagne & Moffat (1987). The polarimetric and photometric variability was interpreted as originating from blobs of dense plasma forming as a result of some perturbation on the surface of the star (non-radial pulsations, line-driving instability, etc.) and being ejected in random directions into the wind. Somehow these blobs would be more stable in slow-moving winds with high-speed wind acting as an efficient homogenizing agent. Robert et al. also mention a possible correlation between σ (P) and log $\dot{M}$ for stars for which $\dot{M}$ can be mea-

sured from polarimetry, i.e. in binaries (which are unaffected by clumping) (see St-Louis et al. 1988) but that this correlation disappears if the $\dot{M}$ values from radio free-free emission are used instead (it was unknown at the time that those measurements were affected by clumping as this diagnostic depends on the density squared).

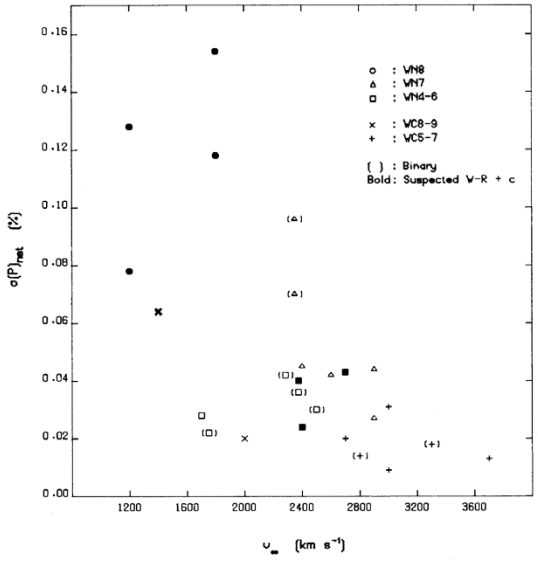

Fig. 2: Standard deviation of the linear polarisation from the mean value as a function of wind terminal velocity for 26 WN and WC stars. Reproduced from Robert et al. (1989).

Almost 20 years later, Davies et al. (2007) explored models of linear polarisation induced by light scattering off clumps in hot-star winds. They present a description of how the polarisation from clumps evolves as a function of their position in the wind and by using a standard beta velocity law as a function of time for different values of the β exponent. In their model, they used the results of Rodrigues & Magalhães (2000) who found that the polarisation increases linearly with the optical depth of the clump but then remains constant for values of τ higher than unity. The main conclusion of the work of Davies et al. was that the observed levels of random polarimetric variability is compatible with two regimes: either a small number of massive, optically-thick clumps or a large number of low-mass clumps. They favoured the regime with a high number of clumps, based mainly on arguments related to the timescale of the observed polarimetric variability. This conclusion is consistent with the observed levels of X-ray fluxes from hot-star winds which, as first suggested by Lucy & White (1980), likely arise from shocks caused by the movement of $\sim 10^9$ blobs in the wind.

Another interesting result these authors found is that the resulting level of polarisation from a population of clumps is proportional to the mass-loss rate; stars with higher $\dot{M}$s have higher levels of polarisation. The fact that the *large number of blobs* regime implies that the inner wind consists of thousands of low mass clumps means that the observed polarisation results in the random statistical deviation from spherical symmetry of a fragmented wind. This leads to night-to-night variations, as observed, and to the result that stars with higher mass-loss rates such as Luminous Blue Variables (LBVs) are more likely to show high levels of polarimetric variability, as hinted by Robert et al. (1989). This is consistent with the data of Davies et al. (2005) who find that polarisation levels and variability is higher in LBVs with stronger Hα lines, i.e. higher $\dot{M}$.

3 Large-Scale Structure

WR stars have also been shown to display variability that has different characteristics and seems to originate in larger scale structures in the wind. Cranmer & Owocki (1996) presented two-dimensional hydrodynamical simulations of the reaction of an optically thin stellar outflow to the presence on the surface of the star of bright or dark spots. They found that Corotating Interaction Regions (CIRs) form when fast-moving material collides with slow-moving material in the wind of a rotating star. Bright spots produce high-density, low-velocity material while dark spots produce low density, high-speed gaz. The presence of large-scale structure in the winds of WR stars has been demonstrated using spectroscopy and polarimetry. This will be discussed in the following sections.

3.1 Spectroscopy

The ubiquitous presence of Narrow Absorption Components (NACs) in the ultraviolet (UV) P Cygni absorption components was demonstrated by Howarth & Prinja (1989) in their study, using the IUE satellite, of 203 galactic O stars. These components are thought to be snapshots of Discrete Absorption Components (DACs), which are broad low-velocity absorptions that evolve into narrow high-velocity absorptions and which are found in time series of UV spectra of selected O stars (e.g. Prinja & Howarth 1988). Cranmer & Owocki (1996) showed that CIRs would have a kinematic signature in P Cygni absorption components in agreement with that observed for DACs. A related observational signature of CIRs is blue-edge variability, which are changes occurring in the P Cygni absorption components at velocities above the terminal velocity of the wind. Such variations are observed in O stars but also in WR stars for which it is impossible

to observe DACs, as in most cases (except for WR24 – see Prinja & Smith 1992), the P Cygni absorption components of strong UV lines are saturated. The presence of blue-edge variability in WR stars therefore constitutes indirect evidence of the presence of CIRs in the winds of these stars. Dessart & Chesneau (2002) used the hydrodynamical simulation of Cranmer & Owocki (1996) to carry out a theoretical study of optical and near-infrared theoretical line variability caused by CIRs in a radiatively driven wind. They simulated changes produced by two diametrically opposed CIRs for different inclination angles with respect to the line-of-sight and for different line formation regions (distance and width). They predict an unambiguous S-shape pattern in the frequency-time space which are extremely reminiscent of those observed for 3 WR stars by Morel et al. (1997, 1999) and Chené & St-Louis (2010) for WR6, WR134 and WR1 respectively. Figure 3 shows an example of such observations for the WN4b star, WR6. St-Louis et al. (2009) and Chené & St-Louis (2011) carried out a survey to identify new candidates for CIR-type spectroscopic variability and concluded that only $\sim 20\%$ of WR stars potentially harbour such structures in their winds. These, however, need to be confirmed by intense and uninterrupted time series of spectra. The reason for the striking contrast between the fraction of O stars showing DACs (most likely 100%) and the number of WR stars showing spectroscopic evidence of CIRs is not known. Possibilities include a rotation rate of WR stars that is too low for a CIR to develop, a CIR lifetime in some WR winds that is too small to make it possible to observed them and the absence of perturbations at the base of the wind.

3.2 Polarimetry

In the literature, one can find some periodic broadband polarisation lightcurves for WR stars that are presumed single. See for example Drissen et al. (1989) or Robert et al. (1992) for WR6. Most of these stars have been shown through spectroscopic observations to have CIRs in their wind. The presence of such large-scale structures within a radiatively driven wind certainly constitutes an asymmetry and should therefore produce a net level of polarisation. Furthermore, as the star rotates, our viewing angle of the asymmetry will change and in consequence the observed polarisation will vary with time. Rotation will render the changes periodic although perhaps not *strictly* periodic as if the CIR dissipates and reforms due to a changing perturbation at the base of the wind, the characteristic of the variability might change, either in phase, amplitude or shape of the curve.

Modelling these polarisation light curves should allow us to determine the physical characteristics of the density asymmetries such as their density contrast with the unperturbed wind, their location in the wind and their originating position on the star, their opening angle, their winding radius, etc. Ignace et al. (2009) published a first model of a spiral-shape asymmetry in the equatorial plane of a hot-star wind. An improved model was presented by Ignace et al. (2015). Although still considering the optically thin case, the latter authors studied the effects of varying the curvature, latitude of the CIR but also the number of CIRs present in the wind. An important conclusion is that the net polarisation produced by these structures is weighted more towards the inner radius of the wind. In consequence, as the outflows have quite high velocities, the CIRs can be considered as mostly conical in shape when modelling the polarisation. It is only after a few stellar radii that the CIR transition towards a more spiral shape. As expected, one CIR or two diametrically located CIRs produce symmetrical polarisation lightcurves with two peaks separated by 0.5 in phase. Changing the winding radius has the effect of changing the amplitude of the curve; a smaller winding radius produces lower polarisation levels and amplitudes of variability due to cancelling effects. Two CIRs that are not diametrically located still produce a lightcurve with two peaks per cycle but the separation between the peaks is no longer 0.5 in phase. The smallest distance between peaks is reached when the two structures are perpendicular to each other. The amplitude of the curve is then smaller as well when all the other parameters are kept the same. Another important result is obtained when considering CIRs at different latitudes. Changing the latitude, all else being equal, has consequences for whether the light curve is single or double peaked. As the polarisation is sensitive to the full 3D structure of the asymmetric distribution of density, a far more diverse range of polarimetric lightcurves is produced. Finally, including more that two CIRs renders the behaviour of the lightcurves even more diverse. In the latter two cases, the potential-added complexity could become a strength when used in conjunction with other diagnostics, such as spectroscopic variability. The optically thick case as well as the modelling of particular lightcurves will be presented in an upcoming publication (St-Louis et al. in prep.).

4 Conclusion

Much has been revealed in the past 25 years about large and small scale structures in WR-star winds using spectroscopy and polarimetry. Stellar wind models now include somewhat arbitrary correction factors to take clumping into account and work is ongoing to incorporate the small-scale asymmetries in a more self-consistent way and to understand all their observational signatures. For large-scale structure, much remains to be understood, as the source of the

perturbation at the base of the wind has not yet been clearly identified. Whatever it might be (small or large scale magnetic field, non-radial pulsations, etc), we are sure to learn more, by studying their observational signature, about physical processes taking place below the dense stellar wind and for which we presently know very little.

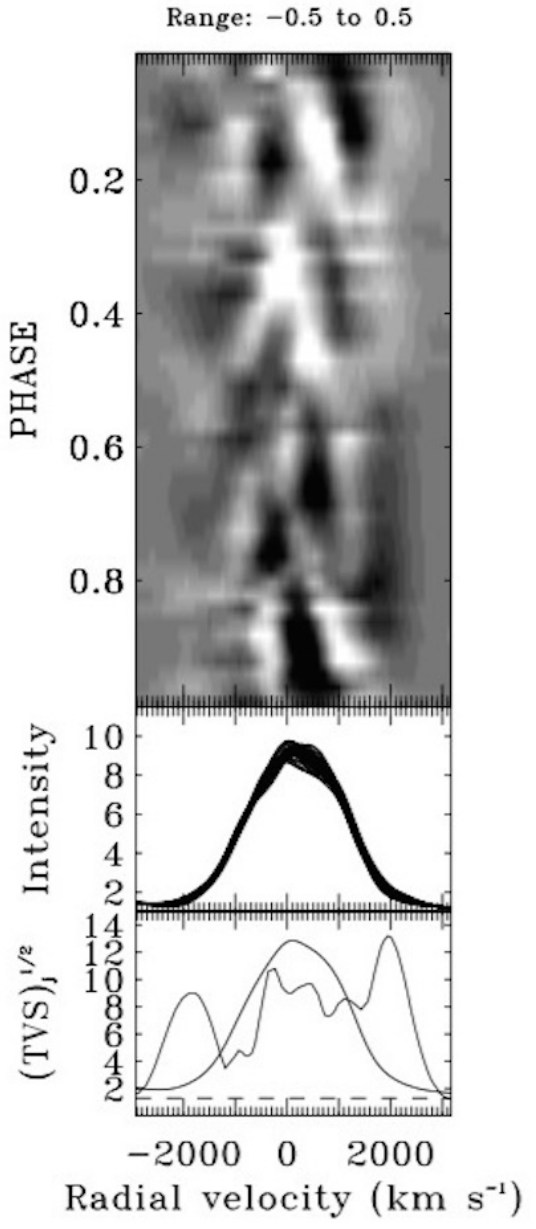

Fig. 3: Top: Differences from the mean as a function of phase using a period of 3.766 days for WR6 reproduced (from Morel et al. 1997). The HeII λ4686 emission line is shown. All superposed spectra are displayed in the middle panel while the mean and TVS spectra are presented in the bottom panel.

References

Chené, A.-N. & St-Louis, N. 2010, ApJ, 716, 929
Chené, A.-N. & St-Louis, N. 2011, ApJ, 736, 140
Cranmer, S. R. & Owocki, S. P. 1996, ApJ, 462, 469
Davies, B., Oudmaijer, R. D., & Vink, J. S. 2005, A&A, 439, 1107
Davies, B., Vink, J. S., & Oudmaijer, R. D. 2007, A&A, 469, 1045
Dessart, L. & Chesneau, O. 2002, A&A, 395, 209
Dessart, L. & Owocki, S. P. 2002a, A&A, 383, 1113
Dessart, L. & Owocki, S. P. 2002b, A&A, 393, 991
Dessart, L. & Owocki, S. P. 2003, A&A, 406, L1
Drissen, L., Robert, C., Lamontagne, R., et al. 1989, ApJ, 343, 426
Drissen, L., St.-Louis, N., Moffat, A. F. J., & Bastien, P. 1987, ApJ, 322, 888
Howarth, I. D. & Prinja, R. K. 1989, ApJS, 69, 527
Ignace, R., Hubrig, S., & Schöller, M. 2009, AJ, 137, 3339
Ignace, R., St-Louis, N., & Proulx-Giraldeau, F. 2015, A&A, 575, A129
Lamontagne, R. & Moffat, A. F. J. 1987, AJ, 94, 1008
Lépine, S. & Moffat, A. F. J. 1999, ApJ, 514, 909
Lépine, S., Moffat, A. F. J., & Henriksen, R. N. 1996, ApJ, 466, 392
Lucy, L. B. & White, R. L. 1980, ApJ, 241, 300
Moffat, A. F. J., Drissen, L., Lamontagne, R., & Robert, C. 1988, ApJ, 334, 1038
Morel, T., Marchenko, S. V., Eenens, P. R. J., et al. 1999, ApJ, 518, 428
Morel, T., St-Louis, N., & Marchenko, S. V. 1997, ApJ, 482, 470
Owocki, S. P. & Rybicki, G. B. 1984, ApJ, 284, 337
Owocki, S. P. & Rybicki, G. B. 1985, ApJ, 299, 265
Prinja, R. K. & Howarth, I. D. 1988, MNRAS, 233, 123
Prinja, R. K. & Smith, L. J. 1992, A&A, 266, 377
Robert, C., Moffat, A. F. J., Bastien, P., Drissen, L., & St.-Louis, N. 1989, ApJ, 347, 1034
Robert, C., Moffat, A. F. J., Drissen, L., et al. 1992, ApJ, 397, 277
Rodrigues, C. V. & Magalhães, A. M. 2000, ApJ, 540, 412
St-Louis, N., Chené, A.-N., Schnurr, O., & Nicol, M.-H. 2009, ApJ, 698, 1951
St-Louis, N., Drissen, L., Moffat, A. F. J., Bastien, P., & Tapia, S. 1987, ApJ, 322, 870
St-Louis, N., Moffat, A. F. J., Drissen, L., Bastien, P., & Robert, C. 1988, ApJ, 330, 286

Tomer Shenar: Are there any observational constraints on the "evolution" of clumping with radius ($D(r)$ or $f_{\rm V}(r)$)?

Nicole St-Louis: To answer your question we need to analyse blob numbers/density and their movement in spectral lines formed at sufficiently different radial distances in the wind. To my knowledge, this has not been done properly yet. Most of the strong emission lines in the optical that have been looked at are formed in similar regions of the wind and the lines that are formed closer to the surface are of low flux and we would need higher S/N data to detect the clumps.

Jesús A. Toalá: Can you tell the difference in the velocity between the CIR and the terminal wind velocity in WR 6?

Nicole St-Louis: In the ultraviolet P Cygni absorption components, we see variations in the edge velocity ($v_{\rm max}$) from -1900 km/s to -2900 km/s. However, it is not totally clear how this is related to the velocity structure of the CIR.

Peredur Williams: What is the density ratio to ambient wind in CIRs?

Nicole St-Louis: In our (Ignace et al. 2014) model of the broadband polarization light-curve of WR 6, we obtained a density contrast of about 2. However, this model is preliminary for a Wolf-Rayet star because it does not include multiple scattering in the inner regions of the wind, which will decrease the overall value of the net polarization.

Gloria Koenigsberger: Do clumps and CIRs coexist and/or interact?

Nicole St-Louis: Yes. CIRs and clumps do coexists. However, so far there has not been a dataset sufficiently long and/or dense enough in sampling to be able to show how exactly this happens and if there is a link between both phenomena.

Andy Pollock: Do clumps flow across CIR boundaries?

Nicole St-Louis: I presume they do but I would not be able to tell what the effect is.

Andy Pollock: Does the small amplitude of variability in the weirdo star WR 2 tell you anything about the global structure of the wind?

Nicole St-Louis: Well, first it shows that the wind of WR 2 is clumped albeit at a very small level of 0.5% of the line flux that is variable. Also, as you can read in Chené et al. (2015), if you believe the acceleration versus projected velocity plots, the product of the beta of the wind's velocity law and radius of the star is 6.2 $R_\odot$ km s^{-1}. If you adopt a radius for WR 2 of 0.89 (Shenar et al. 2014), you obtain a beta value of 7 in the line formation region of He II λ4686.

Wolf-Rayet Stars
W.-R. Hamann, A. Sander, H. Todt, eds.
Potsdam: Univ.-Verlag, 2015
URL: http://nbn-resolving.de/urn:nbn:de:kobv:517-opus4-84268

Structure and fate of binary WR stars: Clues from spectropolarimetry

J. L. Hoffman[1] **& J. R. Lomax**[2]
[1]*Dept. of Physics & Astronomy, University of Denver, USA*
[2]*Homer L. Dodge Dept. of Physics & Astronomy, University of Oklahoma, USA*

Because most massive stars have been or will be affected by a companion during the course of their evolution, we cannot afford to neglect binaries when discussing the progenitors of supernovae and GRBs. Analyzing linear polarization in the emission lines of close binary systems allows us to probe the structures of these systems' winds and mass flows, making it possible to map the complex morphologies of the mass loss and mass transfer structures that shape their subsequent evolution. In Wolf-Rayet (WR) binaries, line polarization variations with orbital phase distinguish polarimetric signatures arising from lines that scatter near the stars from those that scatter far from the orbital plane. These far-scattering lines may form the basis for a "binary line-effect method" of identifying rapidly rotating WR stars (and hence GRB progenitor candidates) in binary systems.

1 Introduction

In recent years, it has become clear that most massive stars evolve in close binary systems (at least 75%; Kiminki & Kobulnicky 2012; Sana et al. 2012; Smith 2014). Meanwhile, a growing number of core-collapse supernovae (SNe) show evidence for binary-induced asphericities in their ejecta and surroundings (e.g., Maund et al. 2009; Chornock et al. 2011; Mauerhan et al. 2014). Similarly, the necessity of rapid rotation to the formation of gamma-ray bursts (GRBs) via stripped-envelope SNe strongly suggests a binary origin as well (de Mink et al. 2013). In short, "it is no longer true that single WR stars are the preferred progenitors of most stripped-envelope SNe" (Smith 2014).

No progenitor (single or binary) of a stripped-envelope SN has yet been detected in pre-explosion images (Smartt 2009). Many theoretical and statistical studies have considered binary channels for SN/GRB production (e.g., Podsiadlowski et al. 1992; Lyman et al. 2014), but observational corroboration relies primarily on nondetections and upper limits to progenitor masses (e.g., Eldridge et al. 2013; Kuncarayakti et al. 2015). By contrast, the "line-effect method" devised by Vink (2007) *directly* identifies rapidly rotating Wolf-Rayet stars, which are the leading candidates for GRB progenitors under the collapsar model (Woosley 1993, 2013). 15 to 20% of single Milky Way WR stars show a line effect (Vink 2007; Vink et al. 2011; Gräfener et al. 2012). However, because polarization arising from scattering in intra-binary circumstellar material (CSM) complicates the diagnostic potential of the line-effect method, this method has not been applied to WR binary systems. Given that most massive stars occur in binaries and that binary interactions dominate massive stellar evolution, the current statistics likely do not represent the full GRB progenitor population.

2 Polarization and the (Binary) Line-Effect Method

Polarimetry provides direct information about an unresolved object's geometrical characteristics. Light from an unresolved spherical electron-scattering envelope is unpolarized due to cancellation of the electric vectors; however, in an aspherical envelope, incomplete cancellation produces a net linear polarization. Nonzero continuum polarization thus implies that the scattering region possesses a global asphericity.

Polarization in spectral lines probes more complex scenarios. Line polarization signatures contain information about the geometries of individual elements in a stellar wind. In a rapidly rotating WR star, continuum photons form near the stellar surface and become polarized in the dense aspherical inner wind, while line photons form farther out in the wind and escape with little net polarization. This causes a depolarization across strong emission lines known as the "line effect" (Vink 2007). The asphericity revealed by this effect implies that the star meets the conditions necessary for GRB formation in the collapsar model.

Despite its diagnostic power, the line effect can be complicated by the effects of binarity. Mass exchange between stars in a binary system gives rise to complex CSM distributions that scatter starlight, producing time-variable continuum polarization signatures. Line photons may also scatter in this CSM and acquire intrinsic line polarization that confuses the line-effect diagnostic. For these reasons, studies of the line effect in WR stars have so far excluded binaries. However, because CSM scattering effects tend to depend on orbital phase, long-term monitoring can disentangle their contributions to WR emission-line polarization, allowing us to add WR binaries to the still-small sample of WR stars examined for the line effect.

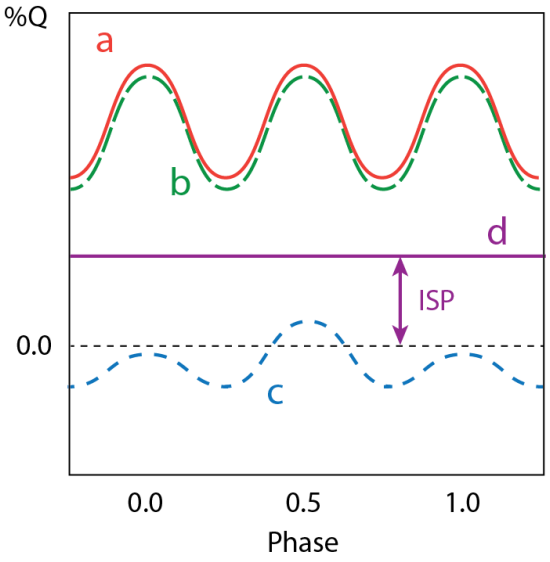

Fig. 1: Schematic polarimetric variation with binary phase of *a)* the continuum; *b)* an emission line arising and scattering like the continuum; *c)* an example emission line arising and scattering differently from the continuum; and *d)* an emission line arising and scattering far from the orbital plane. The dotted horizontal line marks the zero of Stokes Q.

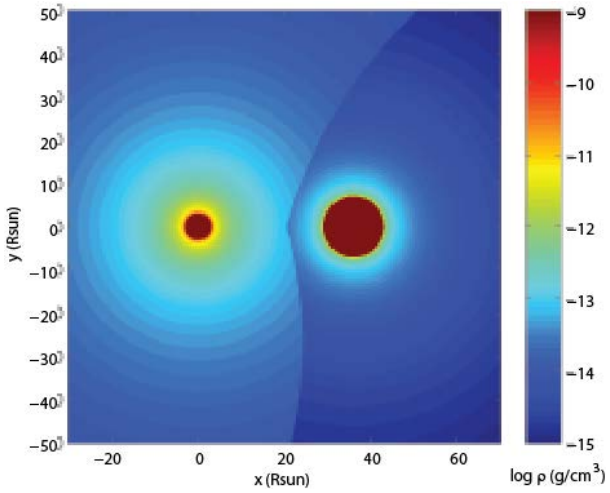

Fig. 2: Density in the orbital plane produced by the two-wind plus shock-cone model fitting the X-ray light curve of V444 Cyg (Lomax et al. 2015). The WN star is on the left and the O star is on the right. The wide opening angle of the shock cone is evidence for radiative braking/inhibition in the system.

Figure 1 depicts the expected phase-dependent polarization behavior of different possible emission lines in a WR binary system. We show here the polarization of the line alone, without continuum contributions. We also display the $\%Q$ Stokes parameter only, taking a coordinate system aligned with the binary orbit. The continuum polarization (a) varies sinusoidally with phase (Brown et al. 1978; St.-Louis et al. 1993). Polarization in an emission line whose photons formed near the stars and scattered near the orbital plane in the same way as the continuum photons (an unlikely scenario) would mirror that of the continuum (b). More commonly, an emission line will both form and scatter differently from the continuum. If the scattering occurs near the orbital plane, it will still show a phase-locked variation, but the shape and magnitude of the polarization curve will be different from that of the continuum (c, for example, as in the He II λ5876 line of β Lyr; Lomax et al. 2012). Finally, an intrinsically unpolarized line forming and scattering far from the orbital plane should show a constant behavior with orbital phase (d); its offset from zero polarization then provides a measure of the interstellar polarization (ISP). Such far-scattering lines have the potential to serve as line-effect diagnostics in binary WR systems. Of course, any given line may contain contributions from multiple, differently scattered components, but because of the vector nature of polarization, good phase coverage should allow the constant and variable components to be separated.

3 Test Case: V444 Cygni (WR 139)

V444 Cygni is a well studied, bright, eclipsing, close WN5+O6 binary system whose colliding winds produce bright and variable X-ray emission. Lomax et al. (2015) reproduced the major features of the X-ray light curves with a model including weaker absorption at phases 0.3–0.75, when the cavity carved out by the O-star wind in the denser WR wind opens along the line of sight (Figure 2). This large phase range suggests that the shock cone has a wide opening angle, providing direct evidence for radiative braking and radiative inhibition effects within the system.

We observed V444 Cyg with the HPOL spectropolarimeter at Pine Bluff and Ritter Observatories (Davidson et al. 2014) and constructed line polarization phase curves for several emission lines (Lomax et al. 2015). Figure 3 shows the phase-dependent polarization behavior of these lines, each with continuum removed and rotated to its own average position angle. All lines show similar phase variations that are unlike those of the continuum (St.-Louis et al. 1993), implying that all contain intrinsic line polarization due to intra-binary scattering. All lines show a distinct difference in polarization between the phases "in" and "out" of the shock cone defined by X-ray modeling (Lomax et al. 2015). None of the lines appears to form far from the stars, though further work is needed to determine whether constant components exist. Additional analysis and modeling

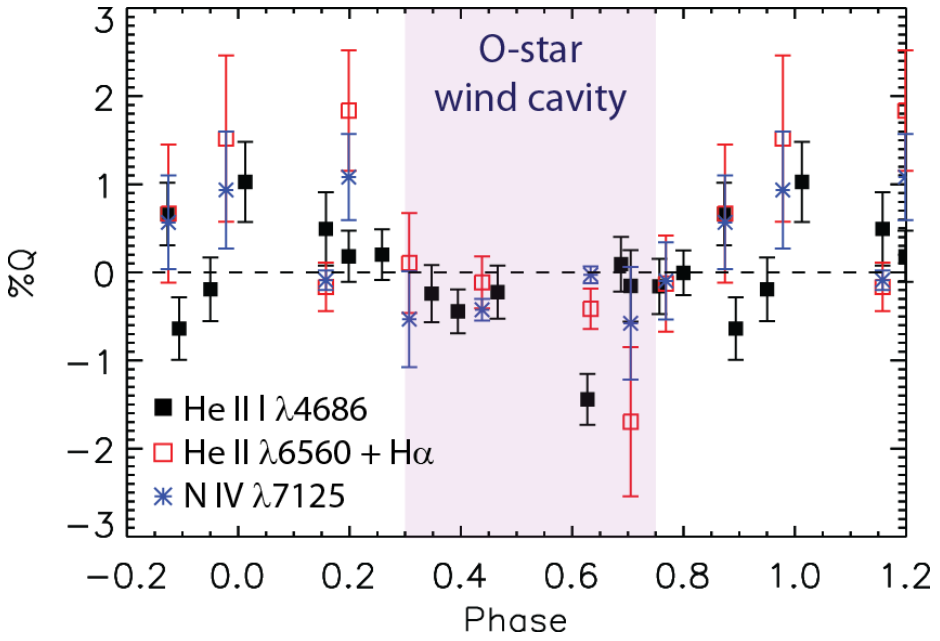

Fig. 3: Intrinsic line polarization for V444 Cyg, measured with HPOL. Data for each line have been rotated to their average PA to align the zero points of polarization. The shaded region denotes the interior of the shock cone produced by the colliding winds in the system, determined from modeling of the X-ray light curve (Lomax et al. 2015). Comparison with Fig. 1 suggests these lines all possess intrinsic polarization.

of these data will provide constraints on the stratified wind structure in V444 Cyg.

Continued spectropolarimetric monitoring of this and other WR binaries, supported by radiative transfer modeling (currently underway in Hoffman's group), will further test the utility of the binary line-effect method. We thank M. Corcoran, J. Davidson, M. de Becker, Y. Nazé, H. Neilson, S. Owocki, J. Pittard, A. Pollock, C. Russell, and the HPOL team for their contributions. This work has been supported by NSF award AST-1210372 and NASA ADAP award NNH12ZDA001N.

References

Brown, J. C., McLean, I. S., & Emslie, A. G. 1978, A&A, 68, 415

Chornock, R., Filippenko, A. V., Li, W., et al. 2011, ApJ, 739, 41

Davidson, J. W., Bjorkman, K. S., Hoffman, J. L., et al. 2014, Journal of Astronomical Instrumentation, 3, 50009

de Mink, S. E., Langer, N., Izzard, R. G., Sana, H., & de Koter, A. 2013, ApJ, 764, 166

Eldridge, J. J., Fraser, M., Smartt, S. J., Maund, J. R., & Crockett, R. M. 2013, MNRAS, 436, 774

Gräfener, G., Vink, J. S., Harries, T. J., & Langer, N. 2012, A&A, 547, 83

Kiminki, D. C. & Kobulnicky, H. A. 2012, ApJ, 751, 4

Kuncarayakti, H., Maeda, K., Bersten, M. C., et al. 2015, A&A, 579, A95

Lomax, J. R., Hoffman, J. L., Elias, II, N. M., Bastien, F. A., & Holenstein, B. D. 2012, ApJ, 750, 59

Lomax, J. R., Nazé, Y., Hoffman, J. L., et al. 2015, A&A, 573, A43

Lyman, J., Bersier, D., James, P., et al. 2014, ArXiv e-prints

Mauerhan, J., Williams, G. G., Smith, N., et al. 2014, MNRAS, 442, 1166

Maund, J. R., Wheeler, J. C., Baade, D., et al. 2009, ApJ, 705, 1139

Podsiadlowski, P., Joss, P. C., & Hsu, J. J. L. 1992, ApJ, 391, 246

Sana, H., de Mink, S. E., de Koter, A., et al. 2012, Sci, 337, 444

Smartt, S. J. 2009, ARA&A, 47, 63

Smith, N. 2014, ARA&A, 52, 487

St.-Louis, N., Moffat, A. F. J., Lapointe, L., et al. 1993, ApJ, 410, 342

Vink, J. S. 2007, A&A, 469, 707

Vink, J. S., Gräfener, G., & Harries, T. J. 2011, A&A, 536, L10

Woosley, S. E. 1993, ApJ, 405, 273

Woosley, S. E. 2013, Models for Gamma-Ray Burst Progenitors and Central Engines, ed. C. Kouveliotou, R. A. M. J. Wijers, & S. E. Woosley (Cambridge, UK: Cambridge University Press)

Gloria Koenigsberger: Isn't the WR component in V444 Cyg an H-free WN? Is Hα from the O-star?

Jennifer Hoffmann: I should not have referred to it so simplistically as "Hα" alone. This line is a blend of Hα and He II λ6563; Khaliullin & Cherepashchuk (1975) showed that it behaves peculiarly with phase in a way that suggests hydrogen contributes significantly to the line. I envision the hydrogen as being located quite far from the stars, perhaps left over from early mass-loss episods, and being ionized by the X-rays from the colliding wind shock. The fact that this line blend varies polarimetrically in a similar way to He II λ4686 may imply that the He II λ6563 to the blend is polarized but the Hα contribution is not. Disendtangling the two would provide us with a more detailed view of the geometrical complexities of the system.

Andy Pollock: Did you see the the change of the hottest plasma temperature of V444 Cyg when the radiative braking is supposed to work? The X-ray spectra can be fit by a two-temperature model. The flux ratio of these two components changed, but their temperature did not need to be changed.

Jennifer Hoffmann: We fit the X-ray spectra with a two-component model and found the same temperatures (0.6 keV and 2 keV) at all phases. The normalization and absorption factors did change, however. We see the effects of radiative braking in the fact that for the hard component especially, these factors behave differently at phases near secondary eclipse (O star in front) than over the rest of the cycle. The length of this eclipse interval implies a large opening angle for the shock cone, a consequence of radiative braking (Lomax et al. 2015; Gayley et al. 1997).

WR spectral analysis, parameters, and wind theory

Wolf-Rayet Stars
W.-R. Hamann, A. Sander, H. Todt, eds.
Potsdam: Univ.-Verlag, 2015
URL: http://nbn-resolving.de/urn:nbn:de:kobv:517-opus4-84268

Wind models and spectral analyses

W.-R. Hamann[1] and the Potsdam group
[1] *Universität Potsdam, Germany*

The emission-line dominated spectra of Wolf-Rayet stars are formed in expanding layers of their atmosphere, i.e. in their strong stellar wind. Adequate modeling of such spectra has to face a couple of difficulties. Because of the supersonic motion, the radiative transfer is preferably formulated in the co-moving frame. The strong deviations from local thermodynamical equilibrium (LTE) require to solve the equations of statistical equilibrium for the population numbers, accounting for many hundred atomic energy levels and thousands of line transitions. Moreover, millions of lines from iron-group elements must be taken into account for their blanketing effect. Model atmospheres of the described kind can reproduce the observed WR spectra satisfyingly, and have been widely applied for corresponding spectral analyses.

1 Expanding atmospheres

The spectra of Wolf-Rayet stars are characterized by bright and broad emission lines, which are formed in their rapidly expanding atmosphere (Beals 1929). These emission lines are mainly powered by recombination cascades. The line width reflects the range of Doppler shifts which the lines-of-sight can encounter (Fig. 1).

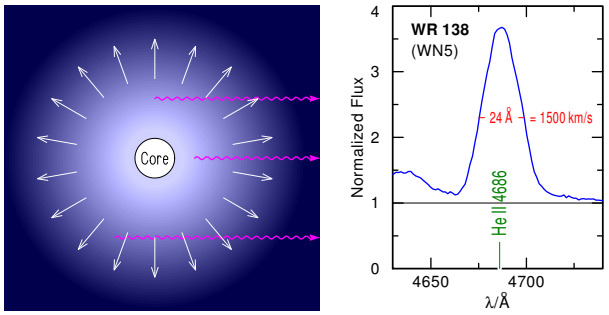

Fig. 1: Sketch of a spherical stellar wind *(left)*, which leads to the formation of broad emission lines *(right)*.

In order to analyze such spectra quantitatively, adequate models are prerequisite. Two major complications make this a non-trivial task: the strong deviations from local thermodynamical equilibrium (non-LTE), and the supersonic expansion.

In non-LTE, the population numbers of the various atomic energy levels must be calculated from the *rate equations*, i.e. from balancing all collisional and radiative transitions that are relevant. Each radiative rate has to be calculated from the local radiation field at the frequencies of the corresponding transition, as seen in the co-moving frame of reference (CMF) of the considered volume element.

Thus, the other part of the task is to calculate the radiation field. In the CMF, a propagating ray of light is continuously changing its CMF frequency due to the differential motion of the medium (cf. Fig. 2). Therefore the radiative transfer in the CMF is described by a set of *partial* differential equations which contain also frequency derivatives,

$$\frac{\partial I_\nu}{\partial z} - \frac{\nu}{c}\frac{\mathrm{d}(\vec{v}\cdot\vec{n})}{\mathrm{d}z}\,\frac{\partial I_\nu}{\partial \nu} = \varkappa\,(I_\nu - S_\nu) \quad . \qquad (1)$$

Here, I_ν denotes the specific intensity, z the spatial coordinate along the ray, and $\vec{v}\cdot\vec{n}$ the velocity projected on the ray's direction $\vec{n}$. The opacity $\varkappa$ and the source function S_ν have to be calculated at each point along the ray from the local non-LTE population numbers.

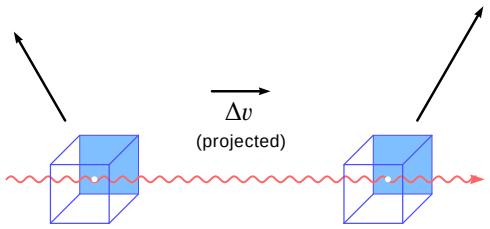

Fig. 2: Radiation transfer in the co-moving frame (CMF) for a differentially expanding atmosphere

The radiative transport couples in space, and the rate equations in frequency. For spherical symmetry, the discretization of these equations was developed in a series of papers more than 40 years ago (e.g. Mihalas et al. 1976). With the need to account for $\sim 10^3$ levels, $\sim 10^5$ frequencies, $\sim 10^2$ radial grid points and the same number of ray directions, the total problem is of high dimension. The numerical solution became only possible when the method of *approximate lambda operators* was developed (Hamann 1986).

Even with sophisticated algorithms, the number of non-LTE levels that can be treated explicitely is limited to $\sim 10^3$, mainly for reasons of numerical stability. On the other hand, iron with its many electrons provides millions of spectral lines which have a significant influence on the temperature and ionization stratification of hot-star atmospheres (so-called *iron line blanketing*). In order to take this into account, the concept of *superlevels* can be adapted (Gräfener et al. 2002), which was proposed originally by Anderson (1989).

In this approximation, the large number of atomic energy levels (termed "sublevels" in the following) is represented by a small number of "superlevels" (cf. Fig. 3). Relative populations within a superlevel are assumed to be in LTE. Each transition between two superlevels comprises a large number of atomic line transitions ("sublines"). In the radiation transport, all sublines must be treated at their proper frequency because of the frequency coupling in expanding atmospheres. Hence, in contrast to static atmospheres, no sampling or re-ordering techniques can be applied. Instead, each superline has a complicated opacity profile function which is a superposition of all sublines involved (Fig. 4).

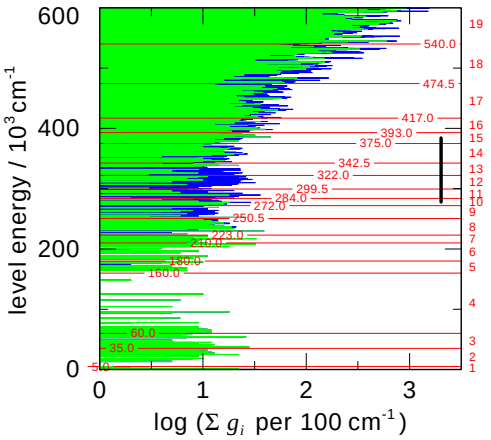

Fig. 3: Superlevel definition for Fe V (plus further iron-group elements). The horizontal stripes indicate the total statistical weight of all lines within energy bins of 100 cm^{-1} (parity coded by green and blue color, respectively). The red lines show a possible division into 19 energy bands.

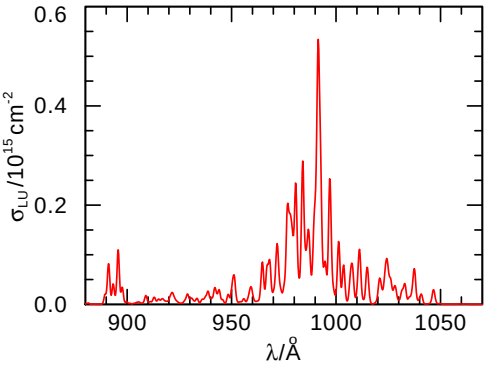

Fig. 4: Superline photo cross section for the transition between superlevels 10 and 15 in Fe V shown in Fig. 3

There is plenty of evidence that stellar winds are not homogeneous. Especially in WR spectra, such evidence is found from the electron-scattering (e.s.) wings of strong emission lines. Due to their low mass, electrons have a high thermal velocity. Radiation transfer theory therefore predicts that electron scattering causes a broad frequency redistribution of line photons (Hummer 1962; Hillier 1984). Assuming a smooth wind, however, models predict much stronger e.s. wings than observed (cf. Fig. 5).

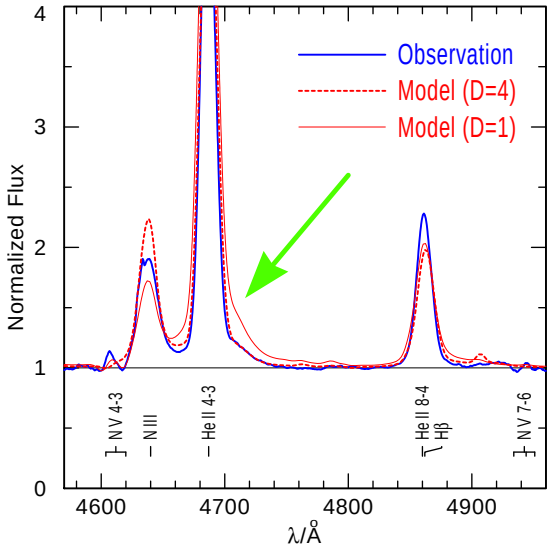

Fig. 5: Effect of electron scattering on the red wing of the strong emission line He II 4686 for the WN7 star Brey 24 in the LMC. The smooth wind model (thin red line) predicts a much stronger e.s. red wing (green arrow) than observed (blue line). With a clumping factor of D=4 and the mass-loss rate reduced by the factor $\sqrt{D}$, this wing fits the observation, while the strength of the emission lines generally remains unchanged (thick dashed red curve).

The effect of wind inhomogeneities can be taken into account in the *microclumping* approximation under the simplifying assumption that the clumps have a small size, compared to the mean free path of the photons at any frequency. In this limit, the radiation field stays smooth and can be calculated with the averaged opacities and emissivities. The rate equations, however, have to be solved for the local density. In the simplest form, we assume that wind consists of clumps with a density that is enhanced by a factor of D compared to the smooth model with same mass-loss rate, while the interclump space is void (e.g. Hamann & Koesterke 1998). Since the emission lines are powered by the recombination cascades and the recombination rate scales with the square of the density, the mass-loss rate has to be reduced by the factor $\sqrt{D}$ compared to the smooth model in order to keep the total line emission unchanged. The electron scattering, however, scales only linear with density and the corresponding line wings are therefore reduced in the clumped

model. Agreement with observations is achieved with clumping factors between 4 and 10 for typical WR stars (cf. Fig. 5). In the next step of approximation, one can account additionally for a non-void interclump medium (Zsargó et al. 2008).

Oskinova et al. (2007) pointed out that the basic assumption for the microclumping approximation is not fulfilled for strong stellar winds: clumps of plausible size are not always optically thin, neither in strong lines, nor at the strong K-shell edges in the X-ray regime. In a statistical approach, they developed a generalized formalism for such *macroclumping*. Opacities are effectively reduced by the porosity. Line transfer is especially affected, since the interaction of a photon with a line transition is anyhow restricted to those small parts of the differentially moving medium where the Doppler shift is suitable. Macroclumping can also induce inhomogeneities in the source function and temperature structure, which had to be neglected in the approximation by Oskinova et al. (2007). Nevertheless, this approach can reconcile the discrepancies between different mass-loss diagnostics (UV resonance lines versus Hα emission) found for O stars: for a given $\dot{M}$ the unsaturated P Cygni profiles become weaker.

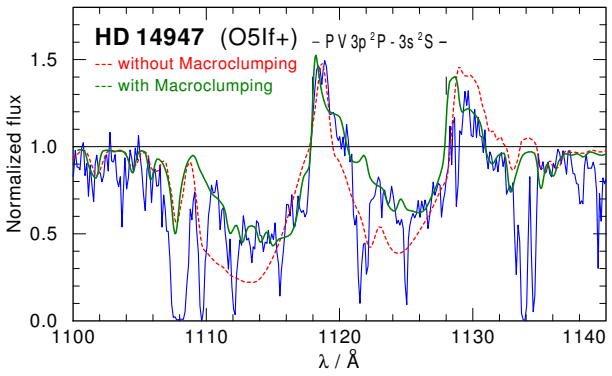

Fig. 6: The effect of macroclumping on the unsaturated P V resonance doublet in HD 14947. The FUSE observation (blue ragged line) is compared to the prediction of the standard PoWR model without macroclumping (red dashed line), and to the result from a Monte-Carlo simulation for macroclumping (green line). The mass loss rate is chosen such that Hα is fitted simultaneously with a clumping factor of D=10. Adapted from Šurlan et al. (2013)

Especially for the scattering in resonance doublets, the radiative transfer in a 3-dimensional clumped wind has been simulated with Monte-Carlo techniques (Šurlan et al. 2012, 2013) for a couple of O stars. As predicted from the statistical approach by Oskinova et al. (2007), the unsaturated P Cygni profiles become weaker by macroclumping (see Fig. 6). A similar result has now been obtained also for WR stars (Kubátova et al., these proc.).

2 Models

A "standard" WR atmosphere is assumed to be expanding in a spherically-symmetric, homogeneous and stationary flow. With a given mass-loss rate $\dot{M}$, the density stratification and the velocity field $v(r)$ are related via the equation of continuity. The velocity field in the supersonic wind is pre-specified in form of the so-called *beta law*,

$$v(r) = v_\infty \left(1 - \frac{r_0}{r}\right)^\beta \qquad (2)$$

where β is usually set to unity for WR winds. r_0 is close to the stellar radius, but its precise value must guarantee a suitable transition to the subsonic part of the atmosphere. The terminal wind velocity v_∞ is a free parameter of these models.

The "stellar radius" R_* refers by definition to the inner boundary of the model atmosphere. It became usual to locate this boundary at the Rosseland optical depth of 20. For most of the WR stars, the expansion velocity at R_* is still subsonic. Nevertheless, R_* might not be identical to the hydrostatic core radius from stellar evolution models because of the recently discovered effect of *envelope inflation* (Gräfener et al. 2012). Moreover, there is a parameter range of very thick winds where the low-velocity parts of the wind are totally hidden beyond large optical depths (see below).

The "stellar temperature" T_* is defined by the luminosity L and the stellar radius R_* via the Stefan-Boltzmann law, i.e. T_* denotes the effective temperature referring to the radius R_*. Only Doppler line broadening must be taken into account in stellar winds. The broadening velocity v_D includes the microturbulence, which turns out to be of the order of 100 km/s in WR winds.

Adopting the described "standard model" assumptions, any particular WR atmosphere is specified by its chemical composition and the basic parameters L, T_*, $\dot{M}$, v_∞. Note that such semi-empirical models are not hydrodynamically consistent. HD models for WR stars which predict $\dot{M}$ and v_∞ consistently are still in their infancy (e.g. Gräfener & Hamann 2008, Sander et al., these proceedings).

Major codes for calculating the described kind of models are CMFGEN (Hillier 2012), which is publicly available[1], and the Potsdam Wolf-Rayet (PoWR) code, from which many models are available via a web interface[2]. The more approximate code FASTWIND (e.g. Puls et al. 2005) has been applied mainly to O stars yet.

[1] kookaburra.phyast.pitt.edu/hillier
[2] www.astro.physik.uni-potsdam.de/PoWR

3 Spectral analyses

With models as described in the previous section, one can usually achieve a satisfactory fit to the observations, regarding the spectral energy distribution as well as the line spectrum. An example is shown in Figs. 7+8 for the Galactic WR star WR 24 (WN6ha) (adapted from Hamann et al. 2006). As result of such an iterative fit procedure, the stellar and wind parameters are empirically determined.

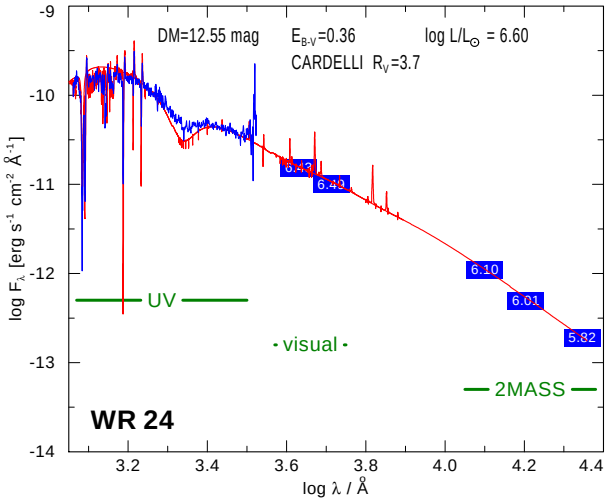

Fig. 7: Fit of a PoWR model to the spectral energy distribution (SED) of the WN6 star WR24. The luminosity and the reddening parameter are adjusted such that the observation (blue) is matched.

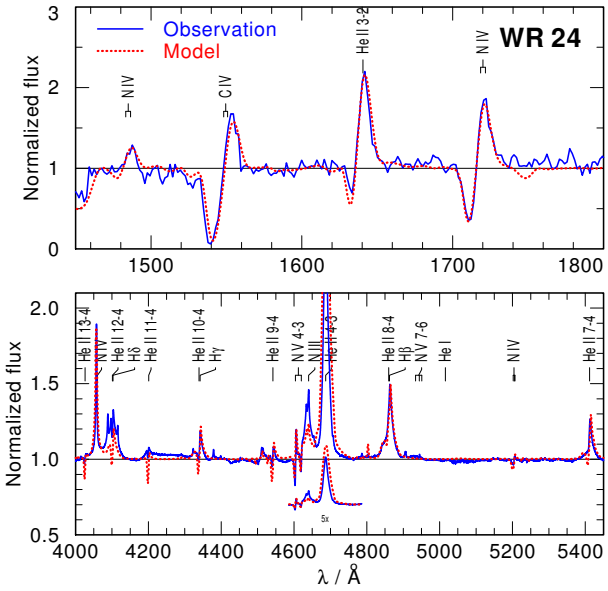

Fig. 8: Fit to the observed line spectrum of WR 24 in the UV and optical

Such analyses are facilitated by the fact that the emission line spectra of WR stars depend mainly on two parameters only, the stellar temperature T_* and a combination of radius, mass-loss rate, and wind velocity. For the latter combination, Schmutz et al. (1989) defined

$$R_t = R_* \left[\frac{v_\infty}{2500\,\mathrm{km\,s^{-1}}} \Big/ \frac{\dot{M}\sqrt{D}}{10^{-4}\,M_\odot\,\mathrm{yr}^{-1}} \right]^{2/3} \qquad (3)$$

and termed this quantity (misleadingly) the "transformed radius". Only later it was realized that R_t is related to the emission measure, normalized to the area of the stellar surface. Anyhow, models with the same R_t show approximately the same normalized line spectrum, while the absolute model flux just scales with the luminosity. Therefore, analyses of WR spectra can be based on a model grid in the $T_* - R_t$ plane which is calculated for only one typical luminosity and v_∞. As an example, Fig. 9 shows the contours of constant equivalent width for a grid of WC models in this parameter plane.

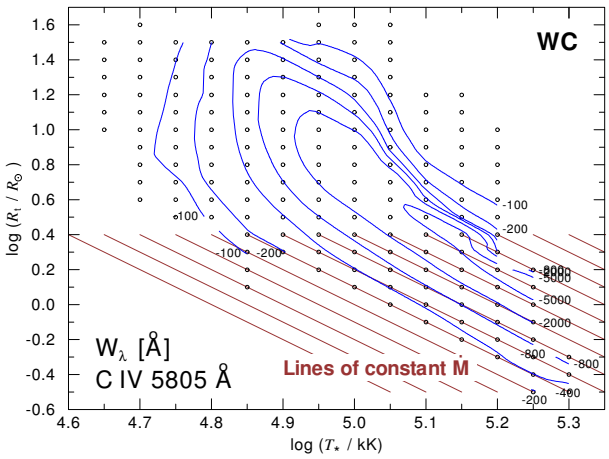

Fig. 9: Contours of constant equivalent width of the C IV line at 5805 Å, labeled with W_λ in Å for the PoWR grid of Galactic WC star models

Fig. 9 illustrates a further parameter degeneracy, which is encountered for the densest WR winds ($\log(R_t/R_\odot) \lesssim 0.4$). In this part of the $\log T_* - \log R_t$ plane, all contour lines become approximately parallel to lines of constant mass-loss rate (brown parallel lines). The spectra then depend only on the ratio $L/\dot{M}^{3/4}$, while neither T_* nor R_* play any role. One can easily understand this when imagining a wind that is so dense that all visible layers expand already with the terminal velocity. Such model is completely determined by this velocity, the luminosity, and the mass-loss rate. The $R_t - T_*$ diagram for the Galactic WN stars (Fig. 10) shows that a couple of stars with earliest subtypes and strong lines (mainly WN4-6s) fall into the domain of this degeneracy where only lower limits for T_* can be derived spectroscopically.

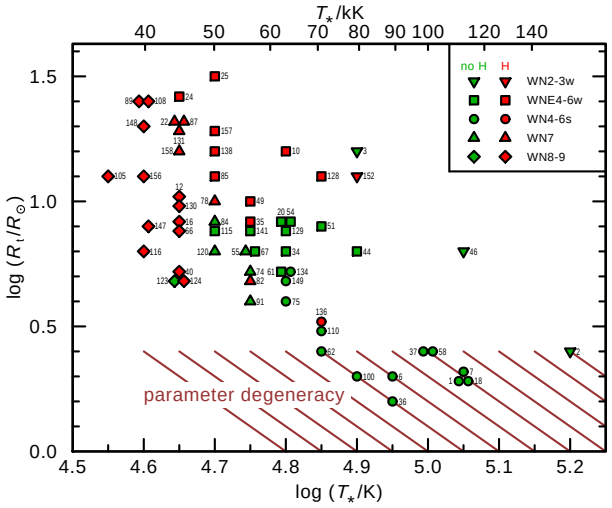

Fig. 10: Location of the Galactic WN stars in the $R_t - T_*$ plane. Red and green symbols indicate whether hydrogen is detectable or absent in their atmosphere, respectively. The shape of the symbol codes the spectral subtype (see inlet). Adapted from Hamann et al. (2006)

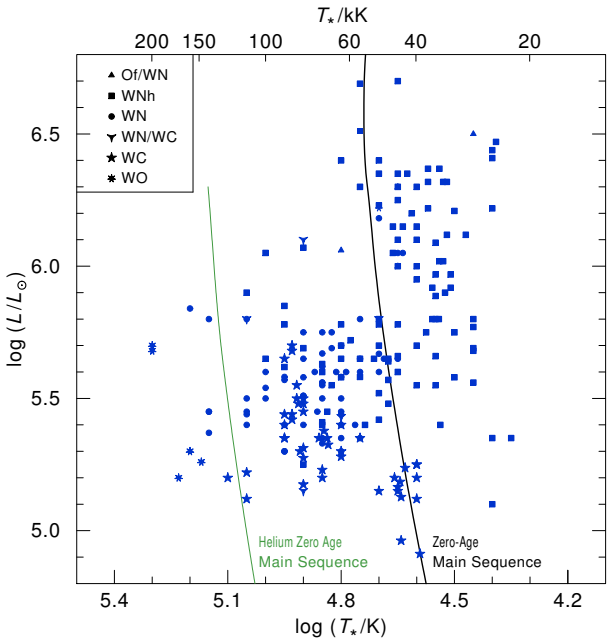

Fig. 11: HRD with the locations of WR stars as obtained from spectral analyses with atmosphere models, compiled from various sources (Crowther et al. 2002; Hamann et al. 2006; Barniske et al. 2008; Martins et al. 2008; Liermann et al. 2010; Sander et al. 2012, 2014; Hainich et al. 2014, 2015; Tramper et al. 2013, 2015)

Up to now, more than 250 WR stars have been analyzed by means of elaborate model atmospheres (cf. Fig. 11), comprising stars in the Milky way, the LMC, the SMC, M33 and a few more nearby galaxies, and thus environments of different metalicities. The obtained stellar and wind parameters provide the empirical basis for understanding the evolution of massive stars, their feedback, and the important role of their population for the ecology of stellar clusters, galaxies, and the whole Universe.

References

Anderson, L. S. 1989, ApJ, 339, 558

Barniske, A., Oskinova, L. M., & Hamann, W.-R. 2008, A&A, 486, 971

Beals, C. S. 1929, MNRAS, 90, 202

Crowther, P. A., Dessart, L., Hillier, D. J., Abbott, J. B., & Fullerton, A. W. 2002, A&A, 392, 653

Gräfener, G. & Hamann, W.-R. 2008, A&A, 482, 945

Gräfener, G., Koesterke, L., & Hamann, W.-R. 2002, A&A, 387, 244

Gräfener, G., Owocki, S. P., & Vink, J. S. 2012, A&A, 538, A40

Hainich, R., Pasemann, D., Todt, H., et al. 2015, A&A, 581, A21

Hainich, R., Rühling, U., Todt, H., et al. 2014, A&A, 565, A27

Hamann, W.-R. 1986, A&A, 160, 347

Hamann, W.-R., Gräfener, G., & Liermann, A. 2006, A&A, 457, 1015

Hamann, W.-R. & Koesterke, L. 1998, A&A, 335, 1003

Hillier, D. J. 1984, ApJ, 280, 744

Hillier, D. J. 2012, in IAU Symposium, Vol. 282, IAU Symposium, ed. M. T. Richards & I. Hubeny, 229

Hummer, D. G. 1962, MNRAS, 125, 21

Liermann, A., Hamann, W.-R., Oskinova, L. M., Todt, H., & Butler, K. 2010, A&A, 524, A82

Martins, F., Hillier, D. J., Paumard, T., et al. 2008, A&A, 478, 219

Mihalas, D., Kunasz, P. B., & Hummer, D. G. 1976, ApJ, 210, 419

Oskinova, L. M., Hamann, W.-R., & Feldmeier, A. 2007, A&A, 476, 1331

Puls, J., Urbaneja, M. A., Venero, R., et al. 2005, A&A, 435, 669

Sander, A., Hamann, W.-R., & Todt, H. 2012, A&A, 540, A144

Sander, A., Todt, H., Hainich, R., & Hamann, W.-R. 2014, A&A, 563, A89

Schmutz, W., Hamann, W.-R., & Wessolowski, U. 1989, A&A, 210, 236

Tramper, F., Gräfener, G., Hartoog, O. E., et al. 2013, A&A, 559, A72

Tramper, F., Straal, S. M., Sanyal, D., et al. 2015, A&A, 581, A110

Šurlan, B., Hamann, W.-R., Aret, A., et al. 2013, A&A, 559, A130

Šurlan, B., Hamann, W.-R., Kubát, J., Oskinova, L. M., & Feldmeier, A. 2012, A&A, 541, A37

Zsargó, J., Hillier, D. J., Bouret, J.-C., et al. 2008, ApJ, 685, L149

Kathryn Neugent: Is there any fundamental difference between CMFGEN and PoWR, and do the results obtained by the two codes generally agree?

Wolf-Rainer Hamann: CMFGEN and PoWR contain the same basic assumptions and physics. However, since the codes have been developed independently, they differ in all possible ways in the numerical details. Since the codes are really complex, it is very valuable to have two codes to compare the results, what we do from time to time. We are not aware of any significant differences so far.

Gloria Koenigsberger: When we look at the temporal sequences of observed lines, such as He II 4686, with a lot of structure attributed to "blobs", is the structure due to emission by the "blobs", absorption, or a combination of both?

Wolf-Rainer Hamann: Both, depending on the line. Those little features drifting on the flat top of, e.g., a C III emission line are pure emission. Drifting features in the P Cygni absorption part of UV resonance lines are pure absorption. And He II 4686 is an emission line which is often optically thick, i.e. here we can have a combination of both, emission and absorption.

Anthony (Tony) Moffat: Is the $\beta = 1$ value determined by fitting or is it adopted? If the latter, then what is the justification, given the observed values of beta from moving clumps in the line-forming regions of many WR stars (Lepine & Moffat 1999) that reveal values $\beta \approx 10$, typically?

Wolf-Rainer Hamann: A velocity law in form of the beta law with exponent $\beta = 1$ is consistent with the observed spectra. However, the model spectra are not very sensitive to the adopted value of β. On one side, this is good news since it means that the derived stellar parameters do not depend much on this assumption. But is also means that we have no handle to determine the velocity law empirically with precision. The hydrodynamical models, as far as available yet, indicate that the beta=1 law is a reasonable approximation for O stars and WNL stars, while for the thick winds from WC stars th elocity law has quite a different shape.

Wolf-Rayet Stars
W.-R. Hamann, A. Sander, H. Todt, eds.
Potsdam: Univ.-Verlag, 2015
URL: http://nbn-resolving.de/urn:nbn:de:kobv:517-opus4-84268

Improving distances to Galactic Wolf-Rayet stars

A.-N. Chené[1], D. Wyrick[1], J. Borissova[2,3], M. Kuhn[2,3], A. Hervé[4], S. Ramírez Alegría[2,3], C. Bonatto[5], J.-C. Bouret[6] & R. Kurtev[2,3]
[1] *Gemini Observatory, U.S.A.*
[2] *Universidad de Valparaíso, Chile*
[3] *Universidad de Valparaíso, Chile*
[4] *Astronomical Institute, Academy of Sciences of the Czech Republic*
[5] *Universidade Federal do Rio Grande do Sul*
[6] *Laboratoire d'Astrophysique de Marseille, France*

Before GAIA improves the HIPPARCOS survey, direct determination of the distance via parallax is only possible for γ Vel, but the analysis of the cluster or association to which WR stars are associated can give distances with a 50% to a 10% accuracy. The list of Galactic clusters, associations and clusters/association candidates has grown significantly in the last decade with the numerous deep, high resolution surveys of the Milky Way. In this work, we revisit the fundamental parameters of known clusters with WR stars, and we present the search for new ones. All our work is based on the catalogs from the VVV (from the VISTA telescope) and the UKIDS (from the UKIRT telescope) near infrared surveys. Finally, the relations between the fundamental parameters of clusters with WR stars are explored.

1 The distance to WR stars

The absolute magnitude of Wolf-Rayet (WR) stars can be estimated to be between $M_v = -3$ mag for earlier subtypes and $M_v = -6$ mag for late ones, or $M_v = -7$ mag for WNH stars. But for accurate determination of the luminosity (and the mass) of WR stars, a precise determination to their distance and extinction is necessary. To this date, the distance to 204 WR stars is fairly well known (Rosslowe & Crowther 2015). A total of 160 of these distances were deduced from the membership of the star to a cluster or an association (the rest are estimates from photometry). However, the distance to more than 2/3 of the ∼640 currently known WR stars is still undetermined. In a near future, the GAIA spacecraft will fix that problem for any stars brighter than $V = 15$ mag, but this still covers a small fraction of all WR stars. In the meantime, new public surveys already deliver good quality near-infrared (NIR) photometry allowing detailed study of the Galactic clusters and association. We count as many as ∼6000 clustery objects (confirmed and candidates combined) in our Galaxy (e.g. Dutra et al. 2002; Dias et al. 2002; Bica et al. 2004; Borissova et al. 2011, 2014), and many of them hang close to the coordinates of known WR stars.

2 WR stars in the public surveys UKIDSS and VVV

The UKIRT Infrared Deed Sky Survey (UKIDSS) was performed by the instrument WFCAM on the UK Infrared Telescope (UKIRT) in Hawai'i. It covers both high and low Galactic latitudes in JHK to $K = 18.3$ mag (Lawrence et al. 2007; Lucas et al. 2008). The Vista Variable in the Vía Láctea (VVV) survey is done with the NIR camera VIRCAM on the ESO 4-m Visible and Infrared Survey Telescope for Astronomy (VISTA) in Chile. It is scanning the bulge and the adjacent section of the disk (Minniti et al. 2010; Saito et al. 2012; Hempel et al. 2014). Both surveys have already observed the area around 95% of the currently known WR stars (see Figure 1). They therefore allow the deepest and the best resolved NIR photometric analysis of the regions near young star forming regions were WR stars are found.

2.1 Study of known clusters with WR stars

The first step is to verify our method on previously studied clusters with WR stars (see Figure 2). We have based this analysis on the aperture photometry delivered by the Cambridge Astronomy Survey Unit (CASU), or on point spread function fitting photometry performed by the SkZ pipeline (Mauro et al. 2013) in the most crowded regions. To determine the clusters fundamental parameters, we follow the methodology described in Chené et al. (2012). We obtain results comparable to what is present in the literature. Also, we can confirm that Hogg 15, debated birth place of the star WR 47 (Piatti et al. 2002; Kook et al. 2010), has an age of ∼10 Myr. However, we cannot add more on the possible membership of WR 47 to the cluster. Finally, we take advantage of this uniform set of data to compare the clusters' parameters and search for possible correlations. Using the Kendall's τrank method, we find the following correlations:

- *Number of WR stars and reddening*: This correlation could be biased by the large number of WR stars in the clusters near the Galactic center, such as the Galactic Center cluster, Arches and the Quintuplet.

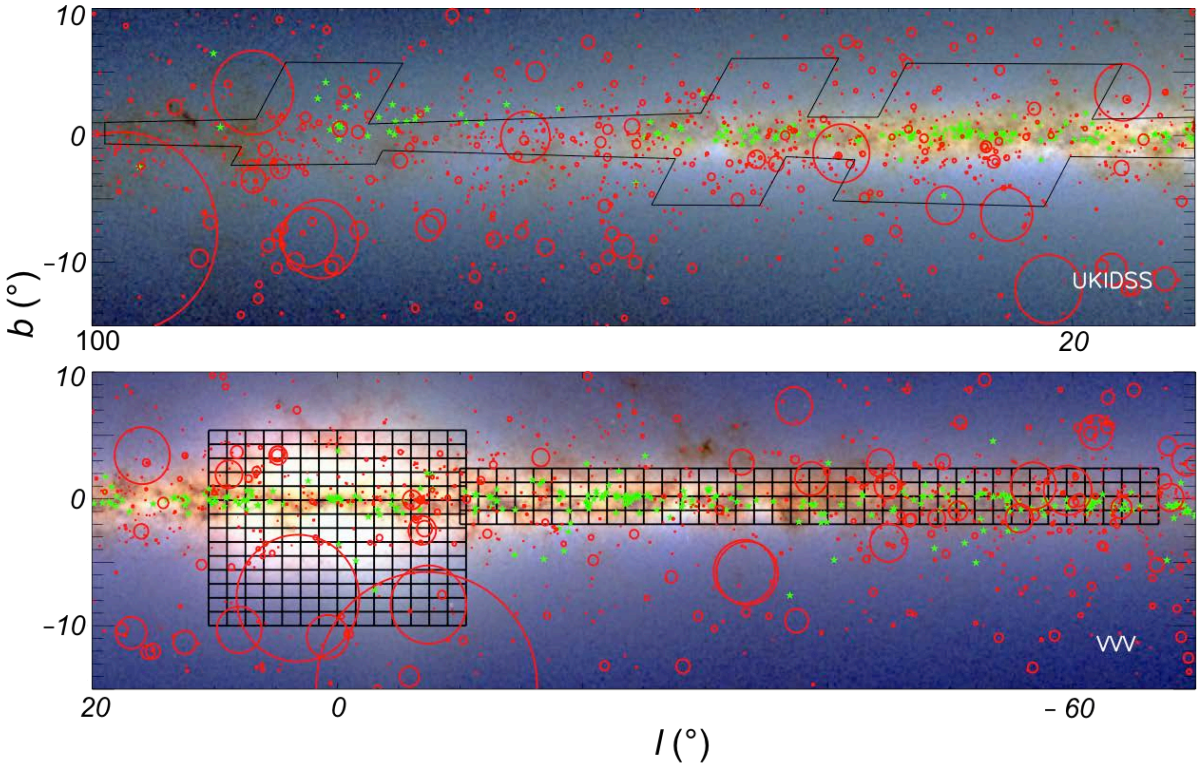

Fig. 1: Area covered by both the UKIDSS and VVV surveys in the Milky Way. The green stars mark the position of known WR stars, and the red circles are cluster and association candidates. The size of the circles correspond to the radii of the clusters/associations.

- *Number of WR stars and the mass of the most massive star in the cluster*: This could be an interesting correlation, but we would prefer to get more clusters for this analysis before making any statement.

- *Total cluster mass and the mass of the most massive star in the cluster*: This is essentially what Weidner et al. (2010, 2014) have already presented.

- *Age and the mass of the most massive star in the cluster*: This could be a simple effect of stellar evolution, causing the older clusters to show less massive stars. An inflexion point in the correlation is seen at around 4 Myr.

- *Total cluster mass and the number of WR stars*: Could be a selection effect, since traditionally, the search for WR stars was done in the most massive clusters. Also, not all the WR stars in the clusters might have been found.

- *Age and total cluster mass*: Could we see here the effect of clusters' evolution? With the data in hand, we would see the mass of the clusters decreasing passed 4 Myr.

2.2 Finding new clusters with WR stars

We take three approaches to find new clusters with WR stars. The first is to **analyse clusters and cluster candidates near known WR stars** (see again Figure 1). We have found nearly a dozen clusters candidates filling this condition and that are not known to have WR stars, but none of them seem to be young enough (some are as old as 100 Myr) and/or to show clear signs of association (older/lower mass population or small radius). The second is to **search for WR stars in young clusters**. We have currently found 7 new clusters with WR stars (Chené et al. 2013, 2015). Interestingly, none of them have a total mass higher than a couple $1000\,M_{\odot}$. These clusters are currently studied in depth to determine the evolution of massive stars (Hervé in prep.), similarly to what was already presented in Martins et al. (2007, 2008, 2012); Crowther & Bohannan (1997); Crowther & Walborn (2011) for other clusters. Finally, we **search for clusters and associations near WR stars**. But this task is the

most challenging and time consuming. Also, we always run the risk that the WR star is the brightest star in the cluster, and the second brightest is fainter by many magnitudes, rending the analysis of the cluster impossible, even with photometry going as deep as $K = 18$ mag.

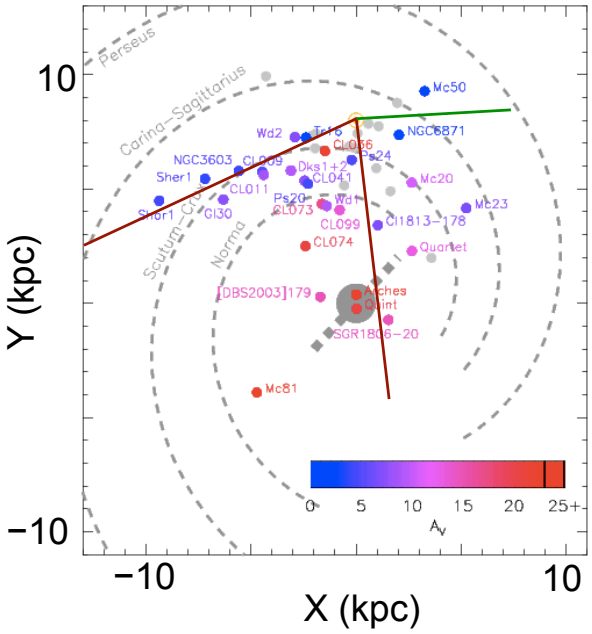

Fig. 2: Positions of the clusters with WR stars in the Milky Way. The model of the Milky Way spiral arms is from Vallée (2008, 2015). The color of the points represents the extinction in the line of sight of the cluster (from blue to red to represent 0 to 25+ mag of extinction). The UKIDSS and VVV surveys cover the area between the left red line and the green line (to the right). The red line in between marks the end of VVV, but UKIDSS overlaps about 20° in the inner part.

3 Conclusions

This is a brief presentation of the past, current and future efforts on the study of clusters and associations with WR stars. We aim to improve our preliminary studies of the correlation between the different fundamental parameters of the clusters in a forthcoming paper. Please, stay tuned for more ...

References

Bica, E., Ortolani, S., Momany, Y., Dutra, C. M., & Barbuy, B. 2004, MNRAS, 352, 226

Borissova, J., Bonatto, C., Kurtev, R., et al. 2011, A&A, 532, A131

Borissova, J., Chené, A.-N., Ramírez Alegría, S., et al. 2014, A&A, 569, A24

Chené, A.-N., Borissova, J., Bonatto, C., et al. 2013, A&A, 549, A98

Chené, A.-N., Borissova, J., Clarke, J. R. A., et al. 2012, A&A, 545, A54

Crowther, P. A. & Bohannan, B. 1997, A&A, 317, 532

Crowther, P. A. & Walborn, N. R. 2011, MNRAS, 416, 1311

Dias, W. S., Alessi, B. S., Moitinho, A., & Lépine, J. R. D. 2002, A&A, 389, 871

Dutra, C. M., Santiago, B. X., & Bica, E. 2002, A&A, 381, 219

Hempel, M., Minniti, D., Dékány, I., et al. 2014, The Messenger, 155, 29

Kook, S.-H., Sung, H., & Bessell, M. S. 2010, Journal of Korean Astronomical Society, 43, 141

Lawrence, A., Warren, S. J., Almaini, O., et al. 2007, MNRAS, 379, 1599

Lucas, P. W., Hoare, M. G., Longmore, A., et al. 2008, MNRAS, 391, 136

Martins, F., Genzel, R., Hillier, D. J., et al. 2007, A&A, 468, 233

Martins, F., Hillier, D. J., Paumard, T., et al. 2008, A&A, 478, 219

Martins, F., Mahy, L., Hillier, D. J., & Rauw, G. 2012, A&A, 538, A39

Mauro, F., Moni Bidin, C., Chené, A.-N., et al. 2013, Rev. Mexicana Astron. Astrofis., 49, 189

Minniti, D., Lucas, P. W., Emerson, J. P., et al. 2010, New A, 15, 433

Piatti, A. E., Bica, E., Santos, Jr., J. F. C., & Clariá, J. J. 2002, A&A, 387, 108

Rosslowe, C. K. & Crowther, P. A. 2015, MNRAS, 447, 2322

Saito, R. K., Hempel, M., Minniti, D., et al. 2012, A&A, 537, A107

Vallée, J. P. 2008, AJ, 135, 1301

Vallée, J. P. 2015, MNRAS, 450, 4277

Weidner, C., Kroupa, P., & Bonnell, I. A. D. 2010, MNRAS, 401, 275

Weidner, C., Kroupa, P., & Pflamm-Altenburg, J. 2014, MNRAS, 441, 3348

John Eldridge: Have you thought of comparing your cluster & WR stars to the Galactic supernova remnant cataloque?

André-Nicolas Chené: Not yet, but it is a good idea. It is a work in progress, and we can always increase the list of areas to study. If someone wants to help, they are welcome.

Phil Massey: I gave the example yesterday of the uncertain distance to NGC 3603. I think we improved on that but we had to get a lot of spectra to do so. How accurate do you expect the distances to be to your clusters?

André-Nicolas Chené: This depends on at what stage our analysis of a given cluster is. When we only have photometry (from the public surveys), the uncertainty can be quite high. But with 2–3 spectra from member stars we can get to ± 1 kpc. Obviously, if we get the chance to observe 10s of members with spectroscopy, it would bring the uncertainty down quite a bit.

Alexandre Roman-Lopez: Have you found any correlation between the cluster candidate morphology and the WR content?

André-Nicolas Chené: I could not find time to look for that yet. We have limited our work to single, simple values for now, but we should move on eventually and try more complex analyses, including morphology.

Wolf-Rayet Stars
W.-R. Hamann, A. Sander, H. Todt, eds.
Potsdam: Univ.-Verlag, 2015
URL: http://nbn-resolving.de/urn:nbn:de:kobv:517-opus4-84268

The Discovery and Physical Parameterization of a New Type of Wolf-Rayet Star

K. F. Neugent[1], P. Massey[1], D. J. Hillier[2], N. I. Morrell[3]
[1]*Lowell Observatory, U.S.A.*
[2]*University of Pittsburgh, U.S.A.*
[3]*Las Campanas Observatory, Chile*

As part of our ongoing Wolf-Rayet (WR) Magellanic Cloud survey, we have discovered 13 new WRs. However, the most exciting outcome of our survey is not the number of new WRs, but their unique characteristics. Eight of our discoveries appear to belong to an entirely new class of WRs. While one might naively classify these stars as WN3+O3V binaries, such a pairing is unlikely. Preliminary CMFGEN modeling suggests physical parameters similar to early-type WNs in the Large Magellanic Cloud except with mass-loss rates three to five times lower and slightly higher temperatures. The evolution status of these stars remains an open question.

1 Discovery

We recently began a multi-year project surveying the Magellanic Clouds for Wolf-Rayet (WR) stars. Using the Swope 1-m at Las Campanas, we took images using on- and off-band interference filters and then used an image subtraction program to identify WR candidates. The candidates were then spectroscopically confirmed using MagE on Magellan. So far we have covered ∼60% of the Magellanic Clouds and discovered 13 new WRs (Massey et al. 2014, 2015). But, it isn't the *number* of newly discovered WRs that makes our survey so successful, but the *types* of these stars. Eight of them appear to belong to an entirely new class of WRs.

Based on the spectrum shown in Figure 1, one might naively classify these stars as WN3+O3V binaries. The WN3 classification comes from the star's N V emission ($\lambda\lambda$4603,19 and λ4945), but lack of N IV. The O3V classification comes from the strong He II absorption lines but lack of He I. However, such a pairing of an WN3+O3V is highly unlikely. First, O3Vs are quite rare since they are the hottest and most luminous of the dwarfs (Ekström et al. 2012). In the Large Magellanic Cloud (LMC), only around a dozen are known outside of the 30 Dor region (Skiff 2014). Second, assuming single star evolution, the lifetimes of these stars preclude such a pairing: WN3s take ∼3–5 million years to form whereas a massive star evolves out of the O3V stage after only a million years. Third, we have yet to see any radial velocity variations as you would expect in a binary system, though we are still gathering data for confirmation. Fourth, our UV data (discussed later) shows no C IV λ1550, the most prominent UV line in O-stars. However, the most convincing evidence deals with the stars' absolute magnitudes. The WN3/O3Vs we have observed are faint with $M_V \sim -2.5$. O3Vs, on the other hand, have much brighter absolute magnitudes with $M_V \sim -5.5$ (Conti 1988). Thus, we conclude these stars are not WN3+O3V binaries and adopt the naming convention of WN3/O3V.

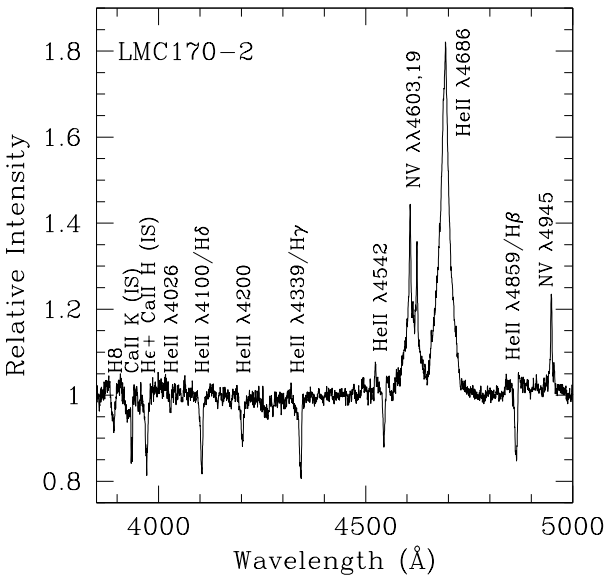

Fig. 1: Spectrum of LMC170-2, one of our newly discovered WN3/O3V stars (Massey et al. 2015).

In addition to the MagE spectra (resolving power, R, of 4100) obtained for all eight newly discovered stars, we observed three stars in the UV using COS on *HST*. We also observed one star using both FIRE and MIKE on Magellan, giving us the NIR and an optical spectrum with $R = 11000 - 14000$. Next we attempted to model our spectra using a single set of physical parameters.

2 Physical Parameterization

To model the WN3/O3s, we turned to CMFGEN (Hillier & Miller 1998), a stellar atmosphere code designed for hot stars with stellar winds where the usual assumptions of plane-parallel geometry and LTE no longer hold. Using only the MagE optical

data, we produced a good fit to both the emission and absorption lines in the spectra, as shown in Figure 2. Table 1 lists the physical parameters used.

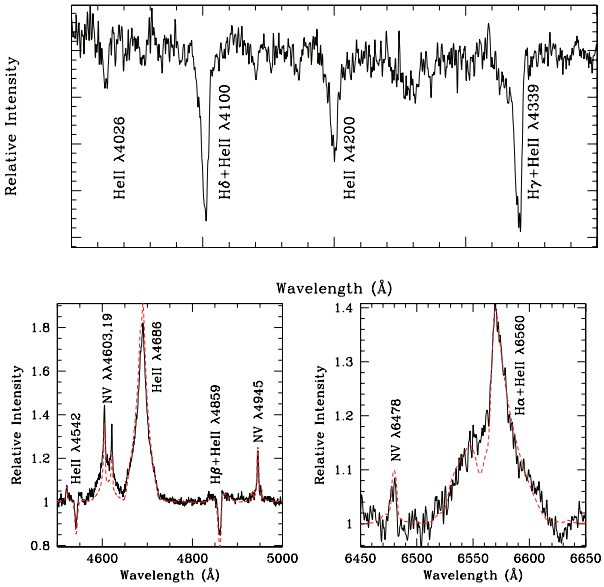

Fig. 2: Best CMFGEN fit to the optical spectrum of LMC170-2 from Massey et al. (2014).

Tab. 1: CMFGEN model parameters for LMC170-2

Parameter	Best Fit
$T_{\rm eff}$ (K)	100,000
$L/L_{\odot}$	4×10^5
$\dot{M}^*$ ($M_{\odot}$/yr)	1.2×10^{-6}
He/H (by #)	1.0
N	10.0× solar
C, O	0.05× solar

Note: Assumes a clumping filling factor of 0.1, v_{∞}=2400 km s^{-1}, β=0.8, and $v \sin i$ = 150 km s^{-1}.

The majority of these parameter values are comparable to those found for early-type LMC WNs (Hainich et al. 2014). Despite the stars' faint visual magnitudes, their bolometric luminosities are normal. These stars appear to be evolved, with significantly enriched N and He. While their effective temperatures are a bit on the high side, they are still within the range found for other WN3s. The most unusual value is their mass-loss rate. As Figure 3 shows, our WN3/O3 star LMC170-2 has a mass-loss rate that is three to five times lower than those found for other early-type LMC WNs as analyzed by Hainich et al. (2014). As discussed later, this low mass-loss rate appears to hold true for all eight WN3/O3s currently known.

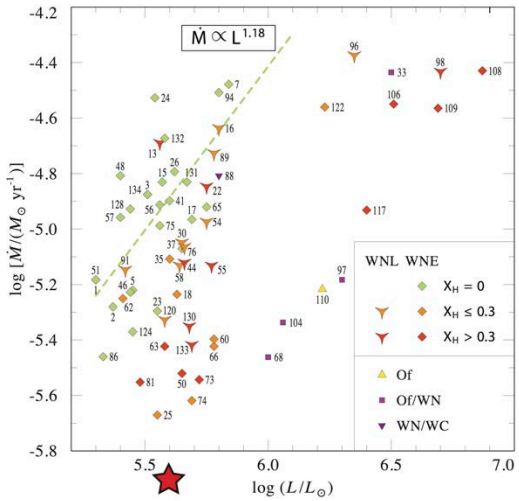

Fig. 3: Luminosity vs. mass-loss rate for LMC170-2 (large red star) compared to those of other early-type LMC WNs analyzed by Hainich et al. (2014). Adapted from Fig. 6 of Hainich et al. (2014) and used with permission.

Since the physical parameters for this model were determined using only the optical data, we were curious to see how well the model would match our newly obtained UV and NIR spectra. As is shown in Figure 4, the agreement between the model and our UV and NIR spectra is practically perfect. Due to space constraints we have only shown the model fit for He IIλ1640 in the UV, but it should be noted that all of our diagnostic lines such as the O IVλ1038 resonance doublet, N Vλ1240, and the lack of C IVλ1550 are similarly well fit. As an added bonus, the spectral energy distribution of the model almost perfectly matches our UV, optical and NIR spectra. This confirms that the reddening is well determined. However, it should be noted that for stars with $T_{\rm eff}$ > 30,000 K, the spectral energy distributions will all look similar longwards of 1000Å as this is the Rayleigh-Jeans tail of the black body distribution.

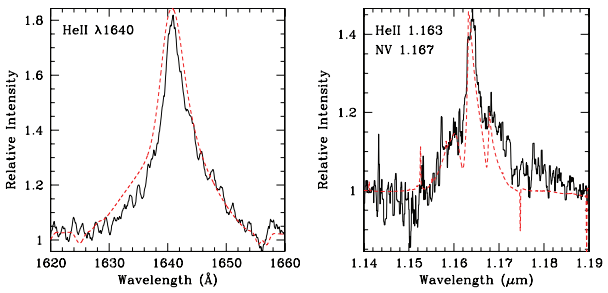

Fig. 4: Best CMFGEN fit to the UV and NIR spectrum of LMC170-2.

With our exemplary model in hand, we began a sensitivity analysis of the model's input parameters. We first attempted to slightly raise and lower the value of each parameter (e.g., increase by 10%, then decrease by 10%). As co-author John Hillier wrote, we soon discovered that, "it's an interesting regime – $\dot{M}$, H/He, $T_{\rm eff}$, and log g all seem to interact in complex ways." For example, decreasing $T_{\rm eff}$ from 100,000 K to 90,000 K yielded a clearly inferior fit to the He and H lines. However, increasing $T_{\rm eff}$ to 110,000 K brought the model too close to the Eddington limit. This could be avoided by changing the surface gravity in parallel with $T_{\rm eff}$. So, doing a clear-cut sensitivity analysis proved to be more difficult than originally expected. Still, we were able to get reasonable uncertainty estimates for the majority of the parameters. However, we hope to refine these once we have separately modeled all eight of the spectra.

Figure 5 shows the striking similarities between the spectra of our WN3/O3s, suggesting that a good model fit to one star will also fit the remaining seven stars quite nicely. And indeed, this is what we found. While there are slight differences, we expect that the physical parameters will only change by small amounts for each star. Certainly none of the spectra suggest a drastically different temperature or mass-loss rate (for example).

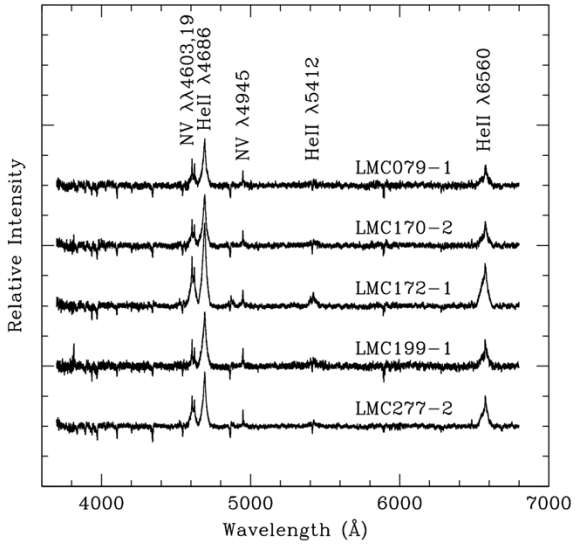

Fig. 5: Spectra of five of our newly discovered WN3/O3s from Massey et al. (2014).

3 Next Up

We still have a lot to learn about these objects and certainly there are many questions left to be answered. We are currently working on constraining the model parameters and determining whether the "best fit" model presented above is unique or if a similarly good model can be obtained using a different set of parameters. Once this has been determined, we will continue modeling all eight stars to get a more global view of the range of expected parameter values within this WR subtype. At that point we can begin working with our stellar evolutionary colleagues to determine whether current models predict the existence of these stars.

We additionally hope to get a better handle on where these stars come from. If they were spatially separated, or more isolated, from the "normal" LMC WRs, one might infer that the WN3/O3s were formed from different (lower metallicity?) progenitors. However their spatial distribution suggests that this is not the case. We also haven't ruled out an explanation dealing with binary evolution. While they don't appear to be binaries now, it is possible that they were in the past. As we continue with our WR survey in the Magellanic Clouds, we hope to find even more of these exciting new stars. Within the next year we should have a much better grasp of their numbers, physical parameters and possibly even their origins.

This work has been supported by the National Science Foundation under AST-1008020. Support for program number HST-GO-13780 was provided by NASA through a grant from the Space Telescope Science Institute, which is operated by the Association of Universities for Research in Astronomy, Incorporated, under NASA contract NAS5-2655. K.F.N. received a National Science Foundation travel grant from the American Astronomical Society that funded her airline travel to and from the meeting in Potsdam. D.J.H. also acknowledges support from STScI theory grant HST-AR-12640.01.

References

Conti, P. S. 1988, NASA Special Publication, 497, 119

Ekström, S., Georgy, C., Eggenberger, P., et al. 2012, A&A, 537, A146

Hainich, R., Rühling, U., Todt, H., et al. 2014, A&A, 565, A27

Hillier, D. J. & Miller, D. L. 1998, ApJ, 496, 407

Massey, P., Neugent, K. F., & Morrell, N. 2015, ApJ, 807, 81

Massey, P., Neugent, K. F., Morrell, N., & Hillier, D. J. 2014, ApJ, 788, 83

Skiff, B. A. 2014, VizieR Online Data Catalog, 1, 2023

Norbert Langer: From the absorption lines, which limit on $v \sin i$ and on radial velocity variations do you derive?

Kathryn Neugent: A $v \sin i$ of 150 km/s fits our high dispersion spectra well. As for radial velocity variations, so far we haven't found any variations but we are still monitoring these stars.

Francisco Najarro: Being so faint, which part of your NIR observation is suitable for modeling? Is it only the J band?

Kathryn Neugent: We primarily relied on the J band. The spectrum was taken using FIRE on Magellan at Las Campanas, but due to the observation being taken under non-optimal conditions, only the J band was usable.

Paul Crowther: The weak lined WN3 stars in the LMC are not so different from WR3 (WN3+abs) in the Milky Way and SMC WN3 stars. Also, the '/O3' classification is misleading (since it is not intermediate between WN3 and O3 stars).

Kathryn Neugent: The spectra of these stars are actually quite a bit different from WR3 in the Milky Way – the absorption lines in our stars are much stronger. Additionally, our stars are hotter (100 K vs. 75 K) as well as fainter. We are currently investigating a correlation between the SMC WN3 stars and our LMC stars.

In terms of the naming convention, we were trying to avoid using a "+" (WN3+O3) that would suggest these stars are WN3 and O3 binaries. We additionally wanted to provide more information than a simple "WN3+abs" classification would provide.

Dany Vanbeveren: Your second argument, why it is probably not a WN3+O3V binary, may be wrong. Binary evolution = RLOF + mass transfer, and mass transfer implies rejuvenation of the mass gainer (similar to the formation of blue stragglers in clusters). So a WN3+O3V is perfectly possible within a binary evolutionary scenario.

Jose Groh: Are the absorption lines formed in the wind or in the photosphere? In case they are photospheric, what would be the value of $\log g$?

Kathryn Neugent: CMFGEN modeling indicates the absorption lines are photospheric. We have found that a model with $\log g$ of ≈ 5 fits our spectra well.

Andy Pollock: WR 2 is a WR star in the Galaxy of type WN3. What features make your stars cooler than WR 2 ?

Kathryn Neugent: WN3 stars have N V emission unlike WN2 stars. We are unaware of any WN2 modeling studies so we can't comment on the temperature difference.

Wolf-Rayet Stars
W.-R. Hamann, A. Sander, H. Todt, eds.
Potsdam: Univ.-Verlag, 2015
URL: http://nbn-resolving.de/urn:nbn:de:kobv:517-opus4-84268

Physical properties of the WR stars in Westerlund 1

C. K. Rosslowe[1], P. A. Crowther[1], J. S. Clark[2] & I. Negueruela[3]
[1] *University of Sheffield, UK*
[2] *The Open University, UK*
[3] *Universidad de Alicante, Spain*

The Westerlund 1 (Wd1) cluster hosts a rich and varied collection of massive stars. Its dynamical youth and the absence of ongoing star formation indicate a coeval population. As such, the simultaneous presence of both late-type supergiants and Wolf-Rayet stars has defied explanation in the context of single-star evolution. Observational evidence points to a high binary fraction, hence this stellar population offers a robust test for stellar models accounting for both single-star and binary evolution. We present an optical to near-IR (VLT & NTT) spectroscopic analysis of 22 WR stars in Wd 1, delivering physical properties for the WR stars. We discuss how these differ from the Galactic field population, and how they may be reconciled with the predictions of single and binary evolutionary models.

1 Introduction

Westerlund 1 (Wd1) is amongst the most massive young clusters in the Galaxy ($>10^5 M_\odot$ Clark et al. 2005, C05) and contains a plethora of massive stars. The pre-Main Sequence (MS) population in Wd1 indicates a very narrow age spread (Kudryavtseva et al. 2012), implying a narrow range in initial mass for the current post-MS. Wd1 therefore provides an excellent opportunity to constrain the initial mass ranges and evolutionary connections of post-MS phases.

Evidence for binarity is prevalent amongst the Wolf-Rayet (WR) stars, including dust production in WC stars and coincidental hard X-ray sources – both signposts of colliding stellar winds. The contribution of a binary evolution channel to the WR population at large is still debated, but evidence is growing. The present-day orbits and mass configurations of many field WR binaries can only be explained by previous interactions (Petrovic et al. 2005). Furthermore, the observed rate of H-free core-collapse supernovae and long-gamma ray bursts are better reproduced with a binary channel producing H-free massive stars (Smith et al. 2011; Trenti et al. 2015).

1.1 The Westerlund 1 cluster

The simultaneous presence of WR and RSG stars is consistent with narrow age spread (Vanbeveren et al. 1998). Population synthesis models (Eldridge & Tout 2004) best reproduce the observed WR/BSG fraction at an age of 4.5–5.0 Myr, and OB supergiants give 5–6 Myr (Negueruela et al. 2010). Brandner et al. (2008) fit pre-MS and MS isochrones to deep near-IR photometry to derive 3.6 ± 0.7 Myr, and Kudryavtseva et al. (2012) perform similar fits to MS stars deriving 5.0 Myr (with a spread <0.5 Myr). We assume an age of 5.0±1.0 Myr for Wd1, with an age spread smaller than this uncertainty. Kothes & Dougherty (2007) present the most direct (kinematic) distance measurement to Wd1 of 3.9 ± 0.7 kpc. Koumpia & Bonanos (2012) use the eclipsing binary W13 to measure 3.7 ± 0.6 kpc. We assume a distance of 4.0 ± 0.5 kpc.

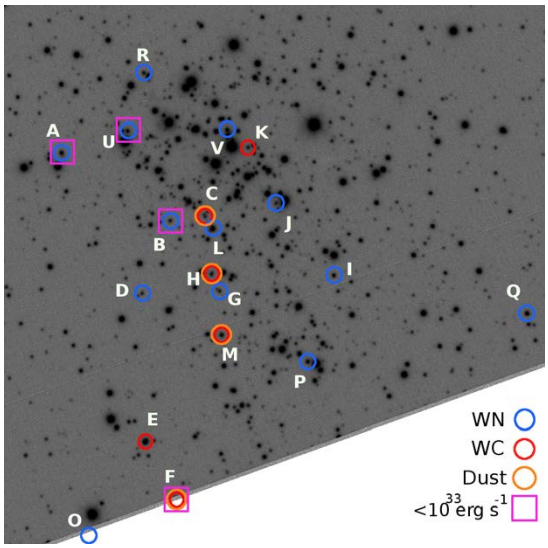

Fig. 1: Archival VLT R-band image of the central $2.5' \times 2.5'$ (2.9×2.9 pc at 4 kpc) of Wd1, with known WR stars indicated.

The first 11 WR stars in Wd1 were reported by Clark & Negueruela (2002). Crowther et al. (2006) completed a near-IR census of the cluster, bringing the total to 23 (8 WC + 15 WN) and finding strong evidence of circumstellar dust in the majority of WC stars.

The only bona-fide spectroscopic binary WR in Wd1 is Wd1–B (Koumpia & Bonanos 2012). However, Bonanos (2007) detected optical variability in half of the WR stars, including smooth periodic (7.63 d) variations in Wd1–A. Three WN (A, B, U) and 1 WC (F) are >0.1 dex above the median $L_X = 10^{32.2}$ergs^{-1} for WN stars in Wd1 (Clark et al. 2008), and are typical of colliding-wind binaries. Of the 12 WRs detected in X-rays, 9/9 WN and 2/3 WC

display hard spectra, indicative of colliding winds. Moreover, these two WC stars are also amongst the 6/8 showing warm circumstellar dust.

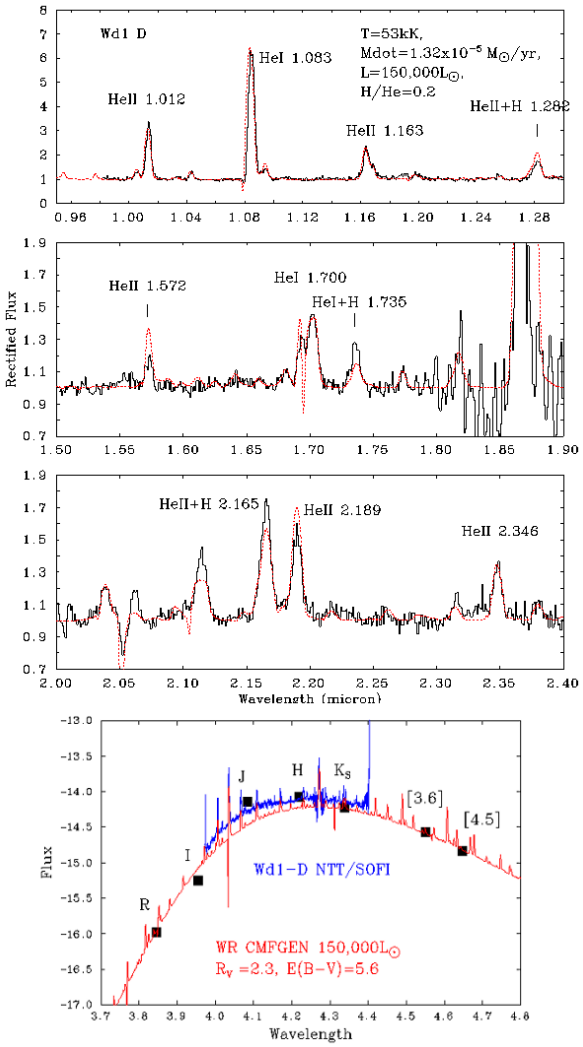

Fig. 2: Example model fit to the spectrum and SED of Wd1-D (WN7o). Key diagnostic lines are labelled. The models is shown in red, spectra in black/blue, and photometric points as black squares.

2 Data

We retrieved archival VLT/FORS2 and NTT/EMMI optical spectra (∼5500–8000 Å) for 3 WN and 7 WC stars. Additionally, we utilised a uniform set of flux-calibrated NTT/SOFI spectra, with R∼1000 covering 0.9–2.5μm for every WR star in Wd1 (Crowther et al. 2006).

We toook BVRI photometry for 7 of the WR stars from C05. Due to the importance of R and I photometry in constraining the reddening to individual stars, we re-derived a consistent set of photometry in these bands by performing PSF fitting (DAOPHOT) photometry on archival VLT/FORS2 (R_SPECIAL, shown in Fig 1) and WFI MPG/ESO 2.2m (I_c) images.

We suplemented these with IR photometry from the 2MASS and *Spitzer* GLIMPSE catalogues for isolated stars.

3 Spectral modelling

Initial parameter estimates for each star were obtained by comparison of their spectra to published grids models generated by the non-LTE `PoWR` code (Gräfener et al. 2002). We then calculated tailored models using the `CMFGEN` code (Hillier & Miller 1998) ($\beta = 1.0$, $f = 0.1$). An example model fit is shown in Fig 2.

For WN stars, we derive temperatures ($T_\star$) using the relative strengths of HeII/HeI lines, giving an estimated uncertainty of 2.5kK. We measured surface H abundances by comparing Paβ+HeII 1.282μm and Brγ+HeI+II 2.164–2.166μm to the nearby pure HeII lines. The overall strength of the recombination line spectrum was used to determine $\dot{M}$, particularly HeI 1.083μm.

For WC stars, we derive temperatures using the relative strengths of CII/CIII lines, with less weight given to CIV. We used the general strength of the carbon spectrum with respect to helium to derive a surface carbon abundance (C/He). It was essential to derive $\dot{M}$ and $T_\star$ in unison, as changes in ionisation structure resulting from changes in wind density have a more profound effect on the ionisation structure of carbon.

We determined the luminosity (L) of each star by matching the observed K-band flux, and used the SED shape shortward of this to determine reddening to each star individually. The flux contributions of a binary companion or circumstellar dust, represented by a scaled Kurucz model O7V stars or black body with T=1000–1400K respectively (where included), were gauged by spectral line-dilution and the SED shape.

4 Results

In Figure 3 we present a H-R diagram showing $T_\star$ and L for all analysed WR stars. The WN stars in Wd1 have median $X_H = 0.02$, significantly below that for Galactic WN6–8 stars (0.1, Hamann et al. 2006), but are similar in luminosity to the H-free field population.

For four of the WC9 stars in Wd1, we measure similar L and $T_\star$ to the field and GC cluster populations (Sander et al. 2012; Martins et al. 2007)

but three (Wd1–E, H, N) have a somewhat higher L, and lower $T_\star$, indicating unusually large radii for WC stars.

Mass-loss rates derived for the WC and WN stars are largely consistent with the Nugis & Lamers (2000) $\dot{M}$–L relation, with the exception of the strong-line Wd1–A.

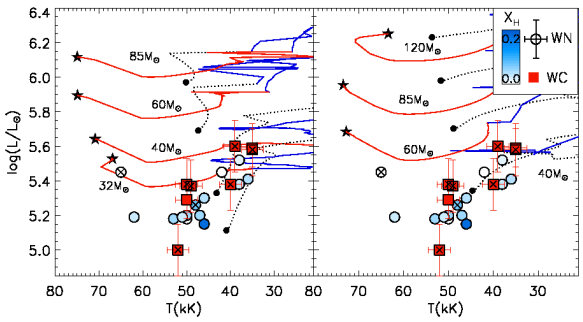

Fig. 3: H-R diagram showing the WR stars in Wd1 (WN circles, WC squares), with non-rotating (left) and fast rotating (right) stellar models (Ekström et al. 2012).

5 Discussion

In Figure 3 I show single-star models with initial masses from 32 $M_\odot$ to 120 $M_\odot$ at solar metallicity ($Z = 0.014$), with (left) and without (right) stellar rotation (Ekström et al. 2012). However, it should be noted that $\geq$40 $M_\odot$/$\geq$60 $M_\odot$ non-rotating/rotating models terminate at an age $<$5 Myr. The moderately super-solar metallicity of Wd1 – exceeding that of the Orion nebula by $\sim$40% – has little effect on $\leq$40 $M_\odot$ models shown ($<$0.1 dex in L). The majority of WN stars are sub-luminous compared to single-star models. All WC stars but Wd1-F are consistent in L with rotating 40 $M_\odot$ and 32 $M_\odot$ tracks. However, the carbon abundances we measure ($X_C \geq 0.17$) are much higher than at the WN$\rightarrow$WC transition in the stellar models models ($X_C \sim 1\%$).

Regarding the progenitors fo the WR stars, the youth of Wd1 prohibits $\lesssim$25 $M_\odot$, and the presence of RSGs – assuming coevality – suggest an upper limit 40–50 $M_\odot$. Therefore, any single-star origin would require additional mass-loss in 25–50 $M_\odot$ stars. Such stars are not expected to obtain Eddington factors close to one, and so are not candidates for enhanced mass-loss in the upper H-R diagram (Gräfener et al. 2011), leaving episodic mass-loss via an LBV phase as the leading single-star scenario.

Alternatively, the evidence for a high binary fraction appeals to a binary origin for these low-L H-free WR stars. A 40 $M_\odot$ primary star, which expands to fill its Roche-lobe, will be H-free at an age of 5 Myr (Eldridge et al. 2008). However, despite uncertainties in mass transfer efficiency, most close binary interactions are thought to result in a *more* luminous secondary (Langer 2012). Adequate spectral fits using single-star models provide an approximate flux limit of $F_O/F_{WR} < 1.0$. The formation of such faint secondary stars requires highly non-conservative mass-transfer, which may occur if initial mass ratios are low (Petrovic et al. 2005).

References

Bonanos, A. Z. 2007, AJ, 133, 2696

Brandner, W., Clark, J. S., Stolte, A., et al. 2008, A&A, 478, 137

Clark, J. S., Muno, M. P., Negueruela, I., et al. 2008, A&A, 477, 147

Clark, J. S. & Negueruela, I. 2002, A&A, 396, L25

Clark, J. S., Negueruela, I., Crowther, P. A., & Goodwin, S. P. 2005, A&A, 434, 949

Crowther, P. A., Hadfield, L. J., Clark, J. S., Negueruela, I., & Vacca, W. D. 2006, MNRAS, 372, 1407

Ekström, S., Georgy, C., Eggenberger, P., et al. 2012, A&A, 537, A146

Eldridge, J. J., Izzard, R. G., & Tout, C. A. 2008, MNRAS, 384, 1109

Eldridge, J. J. & Tout, C. A. 2004, MNRAS, 353, 87

Gräfener, G., Koesterke, L., & Hamann, W.-R. 2002, A&A, 387, 244

Gräfener, G., Vink, J. S., de Koter, A., & Langer, N. 2011, A&A, 535, A56

Hamann, W.-R., Gräfener, G., & Liermann, A. 2006, A&A, 457, 1015

Hillier, D. J. & Miller, D. L. 1998, ApJ, 496, 407

Kothes, R. & Dougherty, S. M. 2007, A&A, 468, 993

Koumpia, E. & Bonanos, A. Z. 2012, A&A, 547, A30

Kudryavtseva, N., Brandner, W., Gennaro, M., et al. 2012, ApJ, 750, L44

Langer, N. 2012, ARA&A, 50, 107

Martins, F., Genzel, R., Hillier, D. J., et al. 2007, A&A, 468, 233

Negueruela, I., Clark, J. S., & Ritchie, B. W. 2010, A&A, 516, A78

Nugis, T. & Lamers, H. J. G. L. M. 2000, A&A, 360, 227

Petrovic, J., Langer, N., & van der Hucht, K. A. 2005, A&A, 435, 1013

Sander, A., Hamann, W.-R., & Todt, H. 2012, A&A, 540, A144

Smith, N., Li, W., Filippenko, A. V., & Chornock, R. 2011, MNRAS, 412, 1522

Trenti, M., Perna, R., & Jimenez, R. 2015, ApJ, 802, 103

Vanbeveren, D., De Donder, E., Van Bever, J., Van Rensbergen, W., & De Loore, C. 1998, New A, 3, 443

Andreas Sander: You just mentioned that you do not see the O-star in your combined fit. How did you constrain the models you are using in your analyses?

Christopher Rosslowe: At ∼6000 Å the flux is mostly WR+O, at ∼2 μm it's mostly WR+dust – so we use the variation in the flux ratios and emission line dikution to constrain the relative contributions.

Anthony (Tony) Moffat: Given the high number of evolved stars in Wd1, there should be many more (hundreds!) of upper main-sequence stars. Have you looked for such stars? This would be very important to constrain the cluster age and check for a normal IMF.

Also: what is the latest news on the putatively associated magnetar in Wd1? What kind of star could have been its progenitor, assuming it is a cluster member?

Christopher Rosslowe: Such stars are difficult to confirm spectroscopically. Due to the high cluster reddening, an O7V would have V 20 – this is about the depth of the published spectroscopic follow-up (Clark et al. 2005, A&A 434, 939).

The peculiar B hypergiant Wd1-5 has been identified as a high-velocity runaway, and has been shown to have a CNO abundance pattern incompatible with single-star evolution (Clark et al. 2014, A&A 565, A90) – this has lead Clark et al. to propose Wd1-5 as the pre-SN companion to the magnetar.

Wolf-Rayet Stars
W.-R. Hamann, A. Sander, H. Todt, eds.
Potsdam: Univ.-Verlag, 2015
URL: http://nbn-resolving.de/urn:nbn:de:kobv:517-opus4-84268

Massive Wolf-Rayet stars on the verge to explode: the properties of the WO stars

F. Tramper[1], S. M. Straal[1,2], D. Sanyal[3], H. Sana[4], A. de Koter[1,5], G. Gräfener[6], N. Langer[3], J. S. Vink[6], S. E. de Mink[1], & L. Kaper[1]

[1]*Anton Pannekoek Institute for Astronomy, University of Amsterdam, The Netherlands*
[2]*ASTRON, Dwingeloo, The Netherlands*
[3]*Argelander Institut für Astronomie, University of Bonn, Germany*
[4]*ESA/STScI, Baltimore, USA*
[5]*Instituut voor Sterrenkunde, KU Leuven, Belgium*
[6]*Armagh Observatory, UK*

The enigmatic oxygen-sequence Wolf-Rayet stars represent a rare stage in the evolution of massive stars. Their properties can provide unique constraints on the pre-supernova evolution of massive stars. This work presents the results of a quantitative spectroscopic analysis of the known single WO stars, with the aim to obtain the key stellar parameters and deduce their evolutionary state.

X-Shooter spectra of the WO stars are modeled using the line-blanketed non-local thermal equilibrium atmosphere code CMFGEN. The obtained stellar parameters show that the WO stars are very hot, with temperatures ranging from 150 kK to 210 kK. Their chemical composition is dominated by carbon (>50%), while the helium mass fraction is very low (down to 14%). Oxygen mass fractions reach as high as 25%. These properties can be reproduced with dedicated evolutionary models for helium stars, which show that the stars are post core-helium burning and very close to their eventual supernova explosion. The helium-star masses indicate initial masses or approximately $40 - 60 M_{\odot}$.

Thus, WO stars represent the final evolutionary stage of stars with estimated initial masses of $40 - 60 M_{\odot}$. They are post core-helium burning and may explode as type Ic supernovae within a few thousand years.

1 Introduction

The enigmatic oxygen sequence Wolf-Rayet (WO) stars are the rarest kind of Wolf-Rayet (WR) stars, with currently only nine members of the class known. Their spectra are characterized by strong emission of O VI, in particular the doublet at 3811-34 Å.

Since their discovery, the WO stars have typically been interpreted as being in a short evolutionary stage following the more common WC stage. In this case the oxygen emission results from an enhanced abundance as the deep layers of the star are revealed by the stripping through the stellar wind (e.g., Langer 2012). An alternative scenario is that the stars originate from higher mass progenitors than the WC stars, and the O VI emission is purely an excitation effect due to the higher stellar temperature and not necessarily reflects a higher oxygen abundance (Hillier & Miller 1999).

To investigate the nature of the WO stars, we have performed a quantitative spectroscopic analysis of the known single WO stars using CMFGEN (Hillier & Miller 1998). We use dedicated evolutionary models to reproduce the obtained stellar parameters and determine the evolutionary state of the WO stars.

2 Observations & Analysis

The spectra of six single WO stars were obtained using the X-Shooter spectrograph on ESO's Very Large Telescope. Only the recently discovered WO star LMC195-1 (Massey et al. 2014) is not included in our sample. Table 1 gives an overview of the observed WO stars. Data reduction has been done using the X-Shooter pipeline v2.2.0. The flux-calibrated spectra were dereddened using the CCM extinction laws (Cardelli et al. 1989; O'Donnell 1994), using a CMFGEN WO star model as a template for the slope of the continuum.

The modeling of the spectra is described in detail in Tramper et al. (2013) and Tramper et al. (2015). The observed magnitudes of the stars were used to correct for errors in the flux calibration in order to derive proper luminosities. The obtained stellar parameters are given in Table 2. The given mass-loss rates assume a clumping factor of 10. The location of the stars in the Hertzsprung-Russell diagram (HRD) is shown in Figure 1.

Tab. 1: List of the observed WO stars.

ID	R.A. (J2000)	Dec. (J2000)	Spectral Type	Galaxy	$\frac{Z}{Z_\odot}$	Other IDs
WR102	17:45:47.56	−26:10:26.9	WO2	MW	1	Sand 4
WR142	20:21:44.35	+37:22:30.6	WO2	MW	1	Sand 5
WR93b	17:32:03.31	−35:04:32.4	WO3	MW	1	
BAT99-123	05:39:34.31	−68:44:09.1	WO3	LMC	0.5	Sand 2, Brey 93
LH41-1042	05:18:11.01	−69:13:11.3	WO4	LMC	0.5	
DR1	01:05:01.61	+02:04:20.6	WO3	IC1613	0.15	B17

Tab. 2: Derived properties of the single WO stars.

ID	$\log L/L_\odot$	T_* (kK)	R_* ($R_\odot$)	$\dot{M}$ (km s^{-1})	v_∞	$\frac{N_C}{N_{He}}$	$\frac{N_O}{N_{He}}$	X_{He}	X_C	X_O
WR102	5.45	210	0.39	-4.92	5000	1.50	0.45	0.14	0.62	0.24
WR142	5.39	200	0.40	-4.94	4900	1.00	0.16	0.26	0.54	0.21
WR93b	5.30	160	0.58	-5.00	5000	0.60	0.15	0.29	0.53	0.18
BAT99-123	5.20	170	0.47	-5.14	3300	0.63	0.13	0.30	0.55	0.15
LH41-1042	5.26	150	0.62	-5.05	3500	0.90	0.20	0.22	0.60	0.18
DR1	5.68	150	1.06	-4.76	2750	0.35	0.06	0.44	0.46	0.10

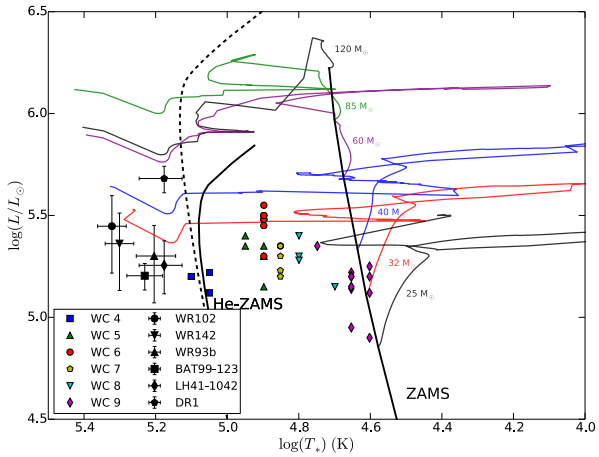

Fig. 1: Location of the single WO stars in the HRD. Also indicated are the WC stars analyzed by Sander et al. (2012) and evolutionary tracks from Ekström et al. (2012).

3 WO star properties and lifetimes

In Figure 1 the WO stars are located left of the helium terminal-age main sequence, a first indication that they are likely post core-helium burning. To further investigate their evolutionary state, we use the *Binary Evolution Code* (BEC, Yoon et al. 2006, 2010; Brott et al. 2011) to model the WO stars starting from the helium zero-age main sequence. The aim is to reproduce their observed luminosity, temperature, and surface helium abundance. The derived mass-loss rates in Table 2 are much higher than the rates from Nugis & Lamers (2000) that are normally used in BEC. We therefore calculate new models assuming a fixed mass-loss rate throughout the core-helium burning evolution and beyond. The observed non-clumped mass-loss rates set an upper limit to the modeled mass loss, while the need to reveal the layers with the observed helium abundances provides a lower limit, as well as a tentative constraint on the clumping factor.

With this approach the observed stellar properties can be well reproduced by the models. In Figure 2 we show an example of the modeling of WR102. We find that all WO stars are indeed in a post core-helium burning phase. With the exception of DR1, they may all explode within 10 000 years. Table 3 shows the helium star masses, final masses, and estimated time to supernova explosions for each of the WO stars. The mass-loss rate that is needed to model the star is also given, as well as the clumping factor this implies.

Tab. 3: Derived masses and lifetimes for the WO stars.

ID	$M_{\rm He,ini}$ ($M_\odot$)	$M_{\rm final}$ ($M_\odot$)	$t_{\rm SN}$ (yr)	$\dot{M}_{\rm evol}$ ($10^5 M_\odot$ yr^{-1})	f_c
WR102	22	9.8	1500	2.8	> 0.4
WR142	17	8.8	2000	1.7	> 0.4
WR93b	17	8.8	8000	1.7	> 0.3
BAT99-123	15	7.7	7000	1.4	> 0.3
LH41-1042	17	8.4	9000	1.8	> 0.4
DR1	23	15.4	17000	1.8	0.1

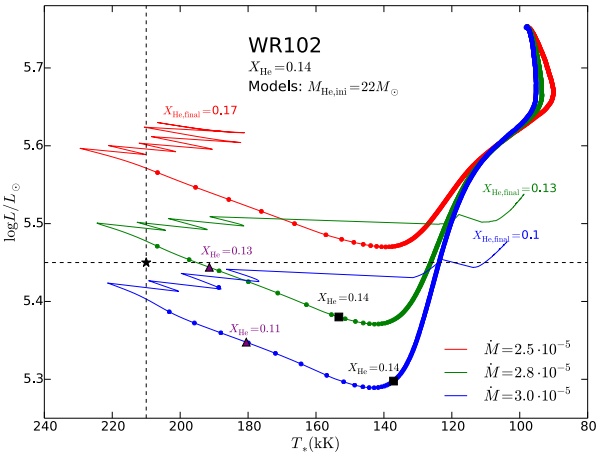

Fig. 2: HRD with evolutionary models for WR102. The best-fit parameters are indicated, as well as some of the surface helium abundances of the models. the dots indicate 1000 year time intervals.

4 Conclusions

The WO stars represent a final stage in massive star evolution. The stars are post core-helium burning and will explode as type Ic supernovae within a few thousand years. If the evolutionary models are representative for the WO stars, they have evolved from early-type WC stars with similar surface abundances, as these do not change appreciatively during their bluewards evolution. The derived helium-star masses indicate that the WO stars originate from massive stars with initial masses around $40-60 M_\odot$.

References

Brott, I., de Mink, S. E., Cantiello, M., et al. 2011, A&A, 530, A115

Cardelli, J. A., Clayton, G. C., & Mathis, J. S. 1989, ApJ, 345, 245

Ekström, S., Georgy, C., Eggenberger, P., et al. 2012, A&A, 537, A146

Hillier, D. J. & Miller, D. L. 1998, ApJ, 496, 407

Hillier, D. J. & Miller, D. L. 1999, ApJ, 519, 354

Langer, N. 2012, ARA&A, 50, 107

Massey, P., Neugent, K. F., Morrell, N., & Hillier, D. J. 2014, ApJ, 788, 83

Nugis, T. & Lamers, H. J. G. L. M. 2000, A&A, 360, 227

O'Donnell, J. E. 1994, ApJ, 422, 158

Sander, A., Hamann, W.-R., & Todt, H. 2012, A&A, 540, A144

Tramper, F., Gräfener, G., Hartoog, O. E., et al. 2013, A&A, 559, A72

Tramper, F., Straal, S. M., Sanyal, D., et al. 2015, ArXiv e-prints

Yoon, S.-C., Langer, N., & Norman, C. 2006, A&A, 460, 199

Yoon, S.-C., Woosley, S. E., & Langer, N. 2010, ApJ, 725, 940

Andy Pollock: If you sacrificed the rest of the spectrum and fit O VI, what would the temperature then be?

Frank Tramper: The temperature would not be greatly affected; instead, a much lower $\dot{M}$ is needed to fit O VI 3811–34 Å.

Anthony (Tony) Moffat: So you are saying that WO stars are not merely an extension of the WC sequence to higher T_*, right? This makes them a different animal. This raises the question if there is intra-subtype evolution, e.g. WO4 → WO3 → WO2 → WO1, as peeling off occurs and the O/C abundance increases, while He decreases.

Frank Tramper: From our models it seems that the WO stars do evolve from WC stars. Since the surface abundances do not change very much when the evolutionary tracks migrate to the very hot temperatures, early-type WC stars with similar low helium abundances would be expected. The WO subtype of the star is dependent on the initial mass of the helium star and the amount of mass that is lost during helium burning. However, it is indeed possible that there is sub-type evolution as the star migrates to the hot temperature regime after core-helium exhaustion. This would be purely a temperature effect and the abundances would not change significantly considering the short timescales involved (see e.g. the very similar helium abundances of the WO2, WO3 and WO4 stars which are mostly between 20 and 30% by mass, with exception of WR102 and DR1). Mass loss also determines if a star undergoes a WO phase at all; for low mass-loss rates (e.g. Nugis & Lamers) the models do not migrate to the hot region of the HRD after helium exhaustion.

Helge Todt: Do you include sodium in your models? The O VI 3811/34 doublet is sensitive to metallicity effects, and Keller et al. (2011) report that a consistent modeling of the O V and O VI lines needs the inclusion of sodium in the model.

Frank Tramper: Sodium is currently not included in our models. Thanks for the suggestion.

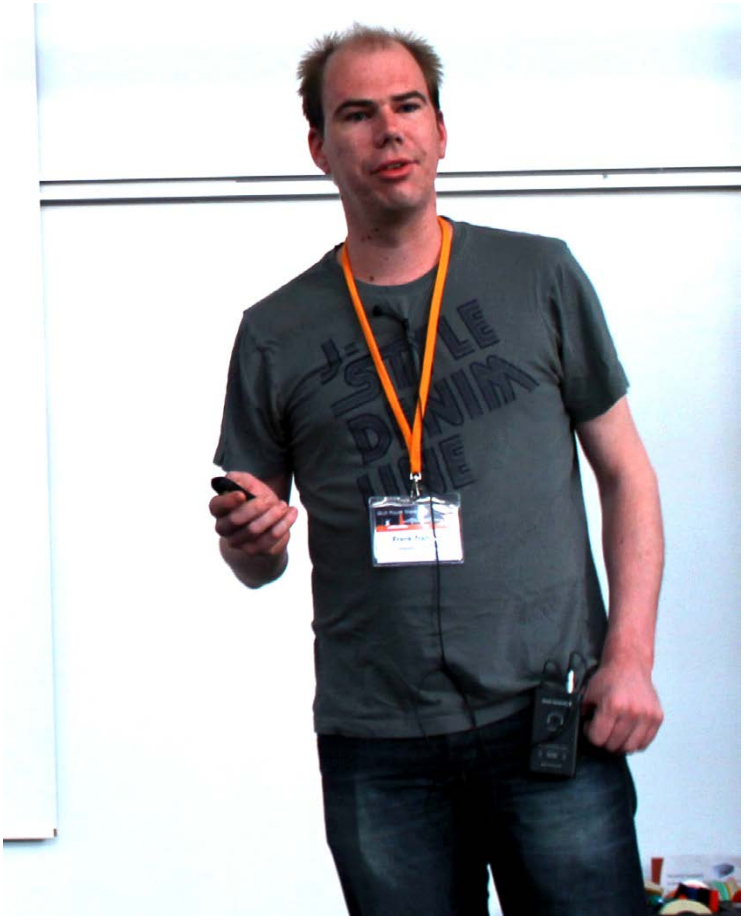

Wolf-Rayet Stars
W.-R. Hamann, A. Sander, H. Todt, eds.
Potsdam: Univ.-Verlag, 2015
URL: http://nbn-resolving.de/urn:nbn:de:kobv:517-opus4-84268

The WR population in the Galactic Center

F. Najarro[1], D. de la Fuente[1], T. R. Geballe[2], D. F. Figer[3], D. J. Hillier[4]
[1] *Centro de Astrobiología (CSIC/INTA), ctra. de Ajalvir km. 4, 28850 Torrejón de Ardoz, Madrid, Spain*
[2] *Gemini Observatory, 670 N. A'ohoku Place, Hilo, HI 96720, USA*
[3] *Center for Detectors, Rochester Institute of Technology, 54 Lomb Memorial Drive, Rochester, NY 14623, USA*
[4] *Department of Physics and Astronomy, University of Pittsburgh, 3941 O'Hara Street, Pittsburgh, PA 15260*

The Galactic Center (GC) hosts three of the most massive WR rich, resolved young clusters in the Local Group as well as a large number of apparently isolated massive stars. Therefore, it constitutes a test bed to study the star formation history of the region, to probe a possible top-heavy scenario and to address massive star formation (clusters vs isolation) in such a dense and harsh environment. We present results from our ongoing infrared spectroscopic studies of WRs and other massive stars at the Center of the Milky Way.

1 Massive stars in the GC: Clusters vs isolation

Recent studies have revealed the presence of a large number of isolated massive stars (Mauerhan et al. 2010a,b) at the GC which is comparable to the massive star population of each of the clusters (Figer et al. 1999, 2002). Such detection of apparently isolated massive stars in this region has raised a further fundamental issue – whether these "massive field stars" are results of tidal interactions among clusters, are escapees from a disrupted cluster, or represent a new mode of massive star formation in isolation (Dong et al. 2014). Following the numerical dynamical simulations from Harfst et al. (2010), and including the effects of stellar evolution and the orbit of the Arches cluster in the Galactic Center potential, Habibi et al. (2014) investigated the first option and found that models were able to account for ∼60% of the isolated sources within the central 100pc as sources drifted away from the center of the clusters. On the other hand radial velocity measurements of a sample of eight objects in the vicinity of the Arches cluster (Dong et al. 2014) suggest that two of them could have been associated with the cluster while two others likely formed in isolation. The latter option was also derived for WR102ka from radial velocity studies and a deep integral-field spectroscopy survey of its surroundings by Oskinova et al. (2013). However, we note that radial velocity estimates of these objects (mainly OIf+ and WNh) may be subject to high uncertainties, as the spectral lines utilized in these studies are severely contaminated by the stellar winds (see below). Thus, further detailed evidence for or against these scenarios is still lacking and awaits precise proper motion measurements (currently underway) providing 3-D velocities of the sources relative to the clusters.

A major step to differentiate among the above scenarios can be achieved through spectroscopic studies of the isolated sources, yielding stellar properties, ages and abundances. Comparison of the results of the quantitative model-atmosphere analysis to theoretical isochrones will allow us to determine if these stars were born in single co-eval cold molecular cloud event or formed over an extended (e.g. 1–10 Myr) period. Obtaining metal abundances from these "field" objects is crucial to understand the metal enrichment history of the GC and to test whether these isolated stars have followed a metal-enrichment scenario different than those in the GC clusters.

The Quintuplet and Arches clusters provide the stellar reference sources to perform such studies. At its current evolutionary phase (age ∼4 Myr, Figer et al. 1999), the massive members of the Quintuplet Cluster are currently WN9-10h (plus a WN6), weak lined WC9, OIf+ stars and LBVs (Figer et al. 1999; Liermann et al. 2009), while the massive population of the younger Arches cluster is dominated by WN8-9h and OIf+ stars (Figer et al. 2002; Najarro et al. 2004; Martins et al. 2008). These spectral types basically encompass all the isolated evolved massive stars identified from recent follow-up spectroscopic observations of Paα emission objects in the GC (Mauerhan et al. 2010a,b) which show quite similar spectral morphology to those present in the Quintuplet and some of the brightest Arches members.

Another current hot-topic is whether the IMFs of massive star clusters are top-heavy. In such occurrences the larger number of type II supernovae produce enhanced yields of α-elements, resulting in an increase of α-element vs Fe (the main suppliers of iron are type Ia SNe). Najarro et al. (2004, 2009) have shown that quantitative NIR spectroscopy of high-mass stars may provide estimates of both absolute abundances and abundance ratios, telling us about the global integrated enrichment history up to the present, placing constraints on models of galactic chemical evolution, and acting as clocks by which chemical evolution can be measured. Abundance analyses may thus help to distinguish between top-heavy and standard star formation in the region.

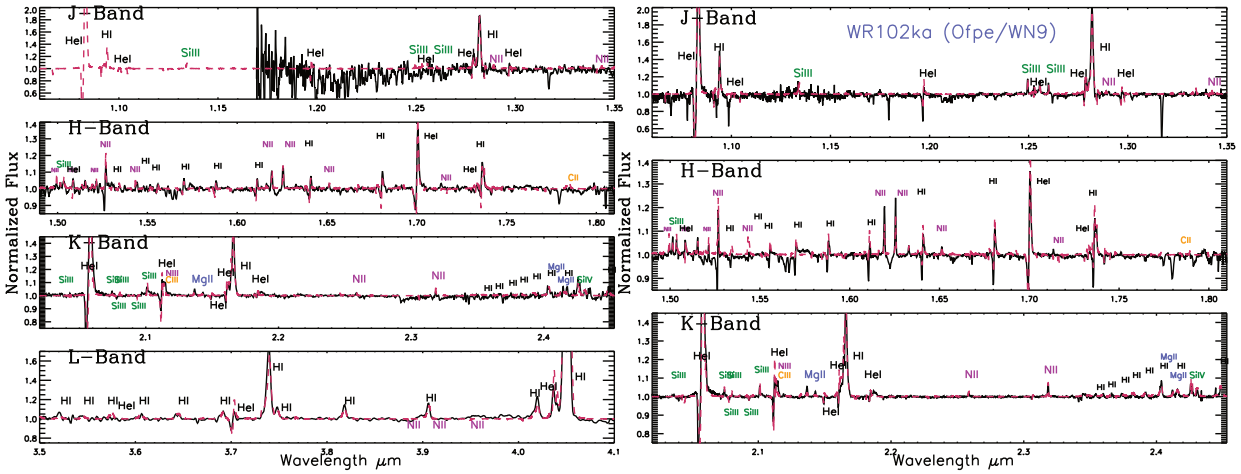

Fig. 1: Breaking the $T_{\rm eff}$ degeneracy in OIfpe/WN9 stars. Previous uncertainties in $T_{\rm eff}$ (±6000 K) due to the lack of He II lines in the spectra, are drastically reduced (±1000 K) by making use of the N II/N III and Si III/Si IV ionization equilibria. **Left)** Q8 in the Quintuplet Cluster. **Right)** The isolated WR102ka star.

2 Observations and preliminary results

We started in 2010 an observing program at GEMINI North (currently ongoing) which has been obtaining high S/N, medium-resolution spectra of the most massive stars in the Quintuplet (including the dusty WCL proper members) as well as isolated massive stars in the inner GC. So far, around 20 massive stars in the Quintuplet cluster and GC inner region have been observed since 2011 with GEMINI NIFS and GNIRS near infrared spectrographs in the H and K bands at medium-resolution (R ∼5000). The brightest targets were also secured at the shorter X and J Bands. We expect to complete our sample by Aug–Sep 2016.

We are currently in the process of modeling the early-type spectra with the CMFGEN code (Hillier & Miller 1998), to obtain physical and chemical properties and present below some results from our ongoing analysis:

We obtain a clear α-element enrichment from the analysis of the Quintuplet WNh stars, consistent with the results derived for the LBVs (Najarro et al. 2009) which denoted a clearly enhanced α/Fe=2 ratio with respect to solar.

Stellar abundances of the isolated objects seem to show a similar trend on average, with the presence of even higher α-element enrichment in some cases.

Our new high S/H spectroscopic J, H and K data provide important diagnostic lines (N II-III, SiII-IV, CII-IV, etc), which are crucial not only for abundance determinations but also to constrain stellar properties. As an example, previously found uncertainties in $T_{\rm eff}$ (±6000 K) for the Ofpe/WN9 objects at the GC (Najarro et al. 1997; Martins et al. 2007) due to the lack of He II lines in the spectra, are drastically reduced (±1000 K)by making use of the N II/N III and Si III/Si IV ionization equilibria. This is shown in Fig. 1, where preliminary fits are displayed for two OIfpe/WN9 stars in our sample (Q8 in the Quintuplet cluster and WR102ka, an object relatively far from the three clusters).

When available the HI and He lines at Pβ, provide an excellent He/H ratio diagnostic, allowing much more accurate He abundance determinations than those performed by means of K-Band spectra. Simple blue (He I) to red (H I) peak ratios may be used (see Q8 and WR102ka Pβ complex in Fig. 1)

Radial velocity estimates, if obtained for OIf+ and WNh stars, require detailed modeling of the observed spectra (Figer et al. 2004). For the OIf+ stars, the He II absorption lines, which are decent diagnostics for OV and for some OI stars with weak-to-moderate stellar winds start to be filled by the stellar wind, producing an effective blue-shift as high as 80–90 km s^{-1}. This may have important consequences when associating the radial velocities of these objects with the nearby gas and clusters. Further, even quantitative modeling may suffer from high uncertainties. Our preliminary fits to WR102ka making use of the full J, H and K band spectra reveal a radial velocity of ∼100 km s^{-1}. This value differs significantly from the 60 km s^{-1} obtained by Oskinova et al. (2013) by means of only K-band spectra and with a slightly (25%) lower spectral resolution.

We detect, for the first time, the WR stellar lines in the NIR SEDs of the dusty WCL proper members in the Quintuplet Cluster (see Fig.2). The deep J band spectra, where the dust contribution weakens, clearly display the presence of the He I-II and

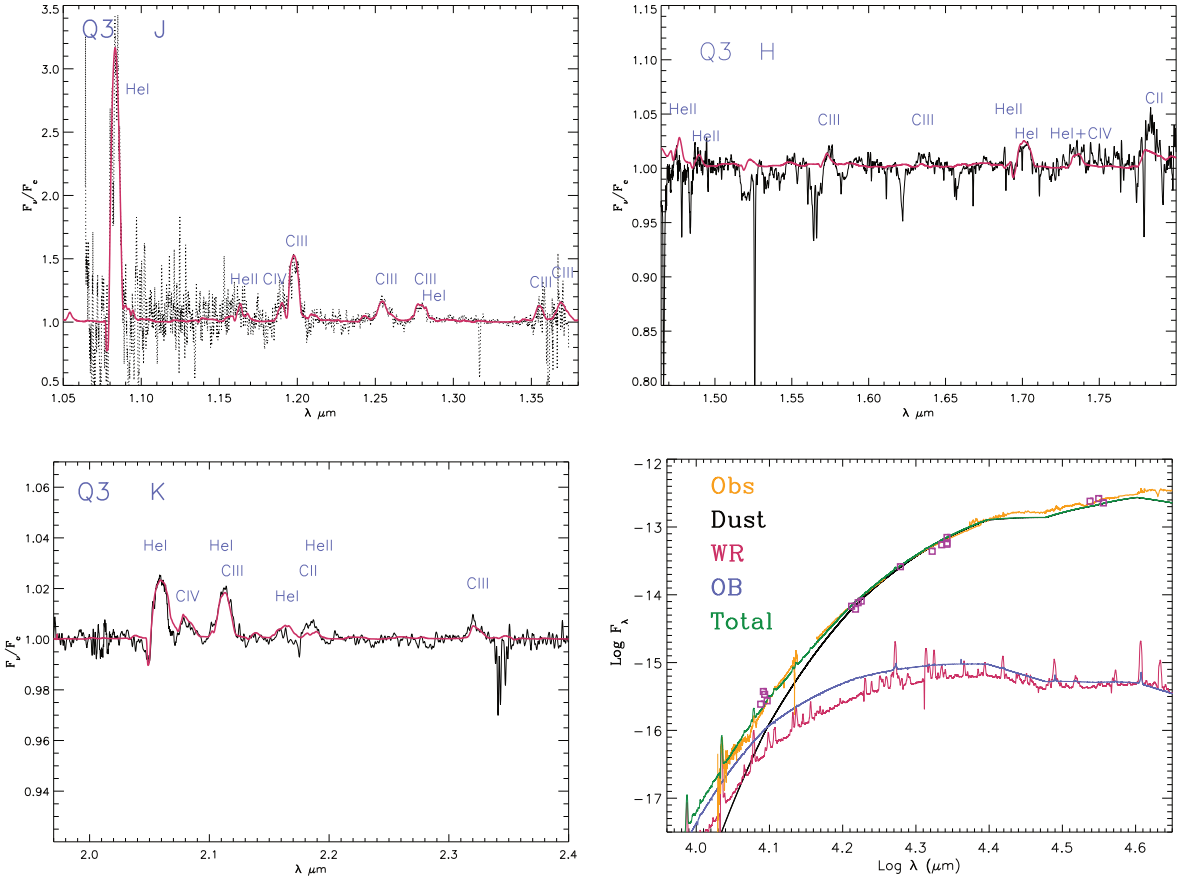

Fig. 2: First detection of stellar lines in the NIR spectra of the dusty WCL proper members of the Quintuplet Cluster. J, H and K band observations and model fits for GCS4 (Q3). Fit to the observed SED (orange) assuming that the total flux (green) is due to the contribution by dust (black), the WR (red) and an OB star (blue).

C III-IV lines of the WC9 component. Further, the huge S/N achieved in the H and K band allows to clearly identify and model the stellar lines which are severely diluted by the dust continuum. Thus, we confirm spectroscopically the WR+OB binary nature of these systems and, fitting spectrophotometric data, derive the individual contributions of the dust, WR and OB components to the total SED of the system (see Fig.2).

F.N. and D.dF. acknowledge grants AYA2010-21697-C05-01 and FIS2012-39162-C06-01 and ESP2013-47809-C3-1-R.

References

Dong, H., Mauerhan, J., Morris, M. R., Wang, Q. D., & Cotera, A. 2014, in IAU Symposium, Vol. 303, IAU Symposium, ed. L. O. Sjouwerman, C. C. Lang, & J. Ott, 230–234

Figer, D. F., McLean, I. S., & Morris, M. 1999, ApJ, 514, 202

Figer, D. F., Najarro, F., Gilmore, D., et al. 2002, ApJ, 581, 258

Figer, D. F., Najarro, F., & Kudritzki, R. P. 2004, ApJ, 610, L109

Habibi, M., Stolte, A., & Harfst, S. 2014, A&A, 566, A6

Harfst, S., Portegies Zwart, S., & Stolte, A. 2010, MNRAS, 409, 628

Hillier, D. J. & Miller, D. L. 1998, ApJ, 496, 407

Liermann, A., Hamann, W.-R., & Oskinova, L. M. 2009, A&A, 494, 1137

Martins, F., Genzel, R., Hillier, D. J., et al. 2007, A&A, 468, 233

Martins, F., Hillier, D. J., Paumard, T., et al. 2008, A&A, 478, 219

Mauerhan, J. C., Cotera, A., Dong, H., et al. 2010a, ApJ, 725, 188

Mauerhan, J. C., Muno, M. P., Morris, M. R., Stolovy, S. R., & Cotera, A. 2010b, ApJ, 710, 706

Najarro, F., Figer, D. F., Hillier, D. J., Geballe, T. R., & Kudritzki, R. P. 2009, ApJ, 691, 1816

Najarro, F., Figer, D. F., Hillier, D. J., & Kudritzki, R. P. 2004, ApJ, 611, L105

Najarro, F., Krabbe, A., Genzel, R., et al. 1997, A&A, 325, 700

Oskinova, L. M., Steinke, M., Hamann, W.-R., et al. 2013, MNRAS, 436, 3357

Paul Crowther: Can you say anything about the binary fraction of Galactic center WR stars (beyond dusty WCs)?

Paco Najarro: We lack different spectroscopic epochs for most of the objects. We know that some of the OIfpe/WN9 stars at the GC (16NE and 16SW) are binaries. In the Arches there is an ongoing monitoring campaign looking for binaries led by Simon Clark. For some stars (Pistol, #362, LBV3) we see variability but no traces of binarity.

Gloria Koenigsberger: Are wind velocities and mass-loss rates typical for these types of stars?

Paco Najarro: Yes, the terminal velocities and mass-loss rates we obtain are consistent with those derived for other massive objects with similar spectral types.

Alexandre Roman-Lopes: Have you considered to use the VVV K-band survey in your study of isolated massive stars in the GC region?

Paco Najarro: For those objects which are isolated enough (not contaminated by nearby sources) we certainly could make use of VVV as well.

Wolf-Rayet Stars
W.-R. Hamann, A. Sander, H. Todt, eds.
Potsdam: Univ.-Verlag, 2015
URL: http://nbn-resolving.de/urn:nbn:de:kobv:517-opus4-84268

The WN population in the Magellanic Clouds

R. Hainich[1], U. Rühling[1], D. Pasemann[1] & W.-R. Hamann[1]
[1] *Institut für Physik und Astronomie, Universität Potsdam, Germany*

A detailed and comprehensive study of the Wolf-Rayet stars of the nitrogen sequence (WN stars) in the Small Magellanic Cloud (SMC) and the Large Magellanic Cloud (LMC) is presented. We derived the fundamental stellar and wind parameters for more than 100 massive stars, encompassing almost the whole WN population in the Magellanic Clouds (MCs). The observations are fitted with synthetic spectra, using the Potsdam Wolf-Rayet model atmosphere code (PoWR). For this purpose, large grids of line-blanket models for different metallicities have been calculated, covering a wide range of stellar temperatures, mass-loss rates, and hydrogen abundances. Our comprehensive sample facilitates statistical studies of the WN properties in the MCs without selection bias. To investigate the impact of the low LMC metallicity and the even lower SMC metallicity, we compare our new results to previous analyses of the Galactic WN population and the late type WN stars from M 31. Based on these studies we derived an empirical relation between the WN mass-loss rates and the metallicity. Current stellar evolution tracks, even when accounting for rotationally induced mixing, partly fail to reproduce the observed ranges of luminosities and initial masses.

1 Introduction

The Magellanic Clouds (MCs) offer the almost unique possibility to study massive stars on all scales, from putatively single stars to massive binary systems, to fairly complete stellar populations. Due to the low interstellar extinction in the direction of the MCs and within the MCs, most of their WR population is known, although some objects escaped detection so far (see e.g. Massey et al., these proceedings). Moreover, because of the known distance to the MCs, the results obtained from the spectral analysis of their massive star population are free from uncertainties inferred from unsure distances, which is in strong contrast to the Milky Way (MW).

Although the WN phase is an important stage in the life of massive stars, the evolution of these objects is not yet completely understood. One essential factor that affects the evolution of massive stars is the mass loss due to their stellar winds. Especially, the dependence of the mass-loss rates of WR stars on the initial metallicity is so far only poorly studied. Due to the sizable number of WN stars in the MCs and the significant sub-solar metallicities that characterize these extraordinary galaxies, the MCs provide an ideal opportunity to address this issue.

2 PoWR model atmospheres

The spectral analysis was performed with synthetic spectra calculated with the Potsdam Wolf-Rayet (PoWR) model atmosphere code. PoWR is a state-of-the-art code for expanding atmospheres, which accounts for both a quasi hydrostatic domain and an rapidly expanding stellar wind. The code assumes a stationary, spherically symmetric outflow. The equations of statistical equilibrium are solved iteratively with the radiative transfer that is calculated in the co-moving frame, while energy conservation is ensured. For further details to the applied methods and the implemented physics we refer to Hamann & Koesterke (1998), Gräfener et al. (2002), and Sander et al. (these proceedings).

2.1 Model grids

For the analysis of the WN stars in the MCs, we calculated three model grids with LMC metallicities and four grids with SMC metallicities. The main parameters of these grids are the stellar temperature T_* and the so-called transformed radius

$$R_\mathrm{t} = R_* \left(\frac{v_\infty}{2500\,\mathrm{km\,s^{-1}}} \Big/ \frac{\dot{M}\sqrt{D}}{10^{-4}\,M_\odot\,\mathrm{yr^{-1}}} \right)^{2/3}, \quad (1)$$

which is related to the emission measure of the wind (e.g. Hamann, these proceedings). For more details on the model grids we refer to Hainich et al. (2014), Hainich et al. (2015), and Todt et al. (2015). These grids are available online on the PoWR website[1].

3 Mass-loss rates

On average, the winds of the WN stars in the MCs are weaker and the mass-loss rates are lower than what is observed for their counterparts in the Galaxy. Figure 1 shows the averaged mass-loss rates of the WN stars in the Milky Way (Hamann et al. 2006; Martins et al. 2008; Liermann et al. 2010; Oskinova et al. 2013), M 31 (Sander et al. 2014), the LMC (Hainich et al. 2014), and the SMC (Hainich et al. 2015) as a function of their initial metallicities,

[1] www.astro.physik.uni-potsdam.de/PoWR.html

which are assumed to be the metallicity of the corresponding host galaxies. From this figure, it is obvious that the mass-loss rates of the WN stars clearly decline with a decreasing content of heavy elements. A linear regression to the averaged mass-loss rates of the WN stars in the MCs, the Galaxy, and M 31 results in a power law with an exponent of 1.2 ± 0.1, which is significantly higher than the ≈ 0.7 predicted and observed for OB-type stars (Vink et al. 2000, 2001; Mokiem et al. 2007). It also is larger than the 0.8 predicted by Vink & de Koter (2005) for late-type WN stars.

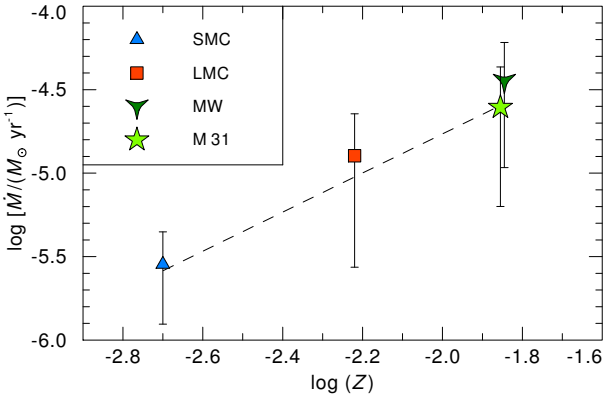

Fig. 1: Averaged mass-loss rate of the WN population in the SMC, LMC, M 31, and the Galaxy plotted versus the metallicity of the corresponding host galaxy. The error bars are the standard deviation within each sample. The dashed line is a linear regression to these data points.

For the determination of the $\dot{M}$-Z-relation, we also utilized the modified wind-momentum luminosity relation (WLR, Kudritzki et al. 1999). The modified wind-momentum

$$D_{\rm mom} = \dot{M} v_\infty R_*^{1/2} \qquad (2)$$

shows the same dependence on the metallicity as the mass-loss rate, since the terminal wind velocity v_∞ and the stellar radius R_* are not metallicity dependent in a first-order approximation. Because of the deviations in the exponents of the individual WLRs, these relations need to be evaluated at a specific luminosity. We choose a value of $\log L/L_\odot = 5.8$, since it is right in the middle of the luminosities where these relations overlap. This method results in an exponent for the $\dot{M}$-Z-relation of 1.3 ± 0.1, confirming the value that is obtained from the rather simplistic approach described above.

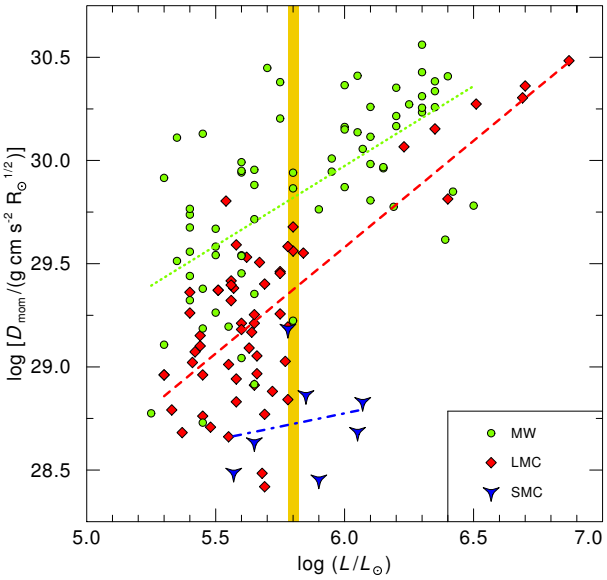

Fig. 2: Modified wind-momentum of the WN stars in the SMC, LMC, and the Galaxy vs. the corresponding luminosity. The straight lines denote the WLRs for the SMC (blue dashed dotted line), the LMC (red dashed line), and the MW (green dotted line). The vertical orange bar refers to the luminosity that we chose to evaluate the different WLRs.

4 Stellar evolution

Our comprehensive spectral analysis of the WN stars in the MCs allows to test the predictions of stellar evolution calculation at low metallicities. The comparison between empirical HRD positions with stellar evolution models reveals that the corresponding tracks partly fail to reproduce the observed WN parameter range.

Figure 3 shows the Hertzsprung-Russell diagram (HRD) of the putatively single WN stars from the LMC (left panel) and the SMC (right panel). For comparison, we also plot stellar evolution tracks computed by Meynet & Maeder (2005) and Eldridge & Vink (2006) for LMC and SMC metallicities, respectively. In both cases the evolution models are not able to reproduce the HRD positions of those objects with the lowest luminosity. Thus, these models overpredict the initial mass necessary to reach the WR phase. Therefore, population synthesis calculations that rely on these models will potentially underestimate the total number of WR stars. Moreover, stellar evolution tracks predict surface hydrogen abundances at the empirical HRD positions of most SMC WN stars that are significantly lower than observed.

We note that the stellar evolution tracks plotted in Fig. 3 are just exemplary and that similar conclusions are obtained with other evolution tracks that

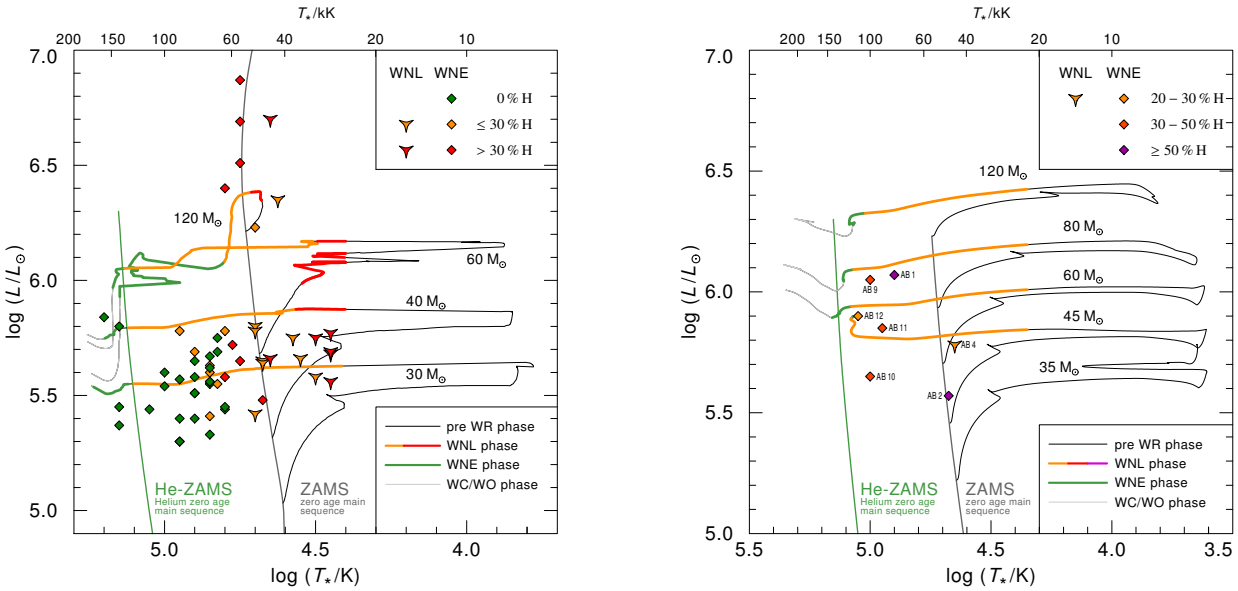

Fig. 3: Hertzsprung-Russell diagram of the single WN stars from the LMC (left panel) and form the SMC (right panel) compared to stellar evolution tracks calculated by Meynet & Maeder (2005) and Eldridge & Vink (2006), respectively. The labels at the tracks give the initial mass of the corresponding models. The filling color of the symbols and the color coding of the tracks refer to the surface hydrogen abundance.

are available. The only exception are such models that predict quasi-homogeneous evolution, owing to very fast initial rotation. These models (Brott et al. 2011) are able to reproduce the HRD positions of all SMC WN stars. However, the corresponding tracks also underestimate the surface hydrogen abundances. In the context of the results presented in Sect. 3, stellar evolution models that evolve quasi homogeneously and account for mass-loss rates lower than currently assumed might be able to reproduce the results obtained from our spectral analysis of the SMC WN stars.

5 Summary

We investigated nearly the complete WN population in the MCs, providing the first comprehensive analysis of this class of massive stars at low metallicities. Based on this work, we derived a clear relation between the initial metallicity and the mass-loss rates that is significantly steeper compared to what is known for OB-type stars. Moreover, we showed that the current generation of stellar evolution models are not able to completely reproduce the observed WN parameter range.

References

Brott, I., de Mink, S. E., Cantiello, M., et al. 2011, A&A, 530, A115
Eldridge, J. J. & Vink, J. S. 2006, A&A, 452, 295
Gräfener, G., Koesterke, L., & Hamann, W.-R. 2002, A&A, 387, 244
Hainich, R., Pasemann, D., Todt, H., et al. 2015, A&A, 581, A21
Hainich, R., Rühling, U., Todt, H., et al. 2014, A&A, 565, A27
Hamann, W.-R., Gräfener, G., & Liermann, A. 2006, A&A, 457, 1015
Hamann, W.-R. & Koesterke, L. 1998, A&A, 335, 1003
Kudritzki, R. P., Puls, J., Lennon, D. J., et al. 1999, A&A, 350, 970
Liermann, A., Hamann, W.-R., Oskinova, L. M., Todt, H., & Butler, K. 2010, A&A, 524, A82
Martins, F., Hillier, D. J., Paumard, T., et al. 2008, A&A, 478, 219
Meynet, G. & Maeder, A. 2005, A&A, 429, 581
Mokiem, M. R., de Koter, A., Vink, J. S., et al. 2007, A&A, 473, 603
Oskinova, L. M., Steinke, M., Hamann, W.-R., et al. 2013, MNRAS, 436, 3357
Sander, A., Todt, H., Hainich, R., & Hamann, W.-R. 2014, A&A, 563, A89
Todt, H., Sander, A., Hainich, R., et al. 2015, A&A, 579, A75
Vink, J. S. & de Koter, A. 2005, A&A, 442, 587
Vink, J. S., de Koter, A., & Lamers, H. J. G. L. M. 2000, A&A, 362, 295
Vink, J. S., de Koter, A., & Lamers, H. J. G. L. M. 2001, A&A, 369, 574

Kathryn Neugent: We've hypothesized that the SMC WRs with absorption might somehow be related to the WN3/O3 stars found in the LMC. I see that you've fit all 7 of these SMC WRs. Did you find that their physical parameters (effective temperature, luminosity) were similar to the WN3/O3s? Additionally, it seems that the mass loss rates you find are quite low, which is to be expected in such a low metallicity galaxy as the SMC. However, do you think the low mass loss rates could be even lower than expected in a similar way as the WN3/O3s?

Rainer Hainich: By comparing our results with the parameters published by Massey et al. (2015) for one of the recently discovered WN3/O3 stars in the LMC, we find that the hydrogen abundances and the stellar temperatures are similar. However, the luminosity of the SMC WN stars are on average significantly higher compared to the LMC WN3/O3 stars. Moreover, the mass-loss rates derived for the SMC WN stars are higher than what is obtained by Massey et al. (2015), which is quite astonishing. It definitely raises some interesting questions regarding the evolutionary status of these objects.

Paul Crowther: Use of solely single WN stars in the SMC excludes the very strong lined WN binaries HD 5980.

Rainer Hainich: That is true. We are right now analyzing the WN binaries in the SMC, investigating whether these objects exhibit systematic differences compared to the single SMC WN stars (Shenar et al. in prep.).

Paul Crowther: The small numbers of low metallicity WN stars can be enhanced by addition of IC10, which hosts many more WN stars and has 1/3 solar composition.

Rainer Hainich: I completely agree. We should investigate more WN stars at low and intermediate metallicities and, IC10 is an ideal candidate for further studies.

Norbert Langer: Can you comment on the scatter of the mass-loss parameters for WN stars of a fixed luminosity, which is about a factor of 30?

Rainer Hainich: This scatter is seen in all WN populations analyzed so far, covering a wide range of metallities form solar-like values in the Galaxy and M 31 to low metallicity environments like the MCs. A certain fraction of this scatter might be attributable to assumptions made in the context of the spectral analyses of these objects, like a single clumping factor for a whole WN population. However, the major fraction of the scatter in the mass-loss rates of WN stars appears to be intrinsic to these kind of stars and probably reflects the different evolution stages and evolution histories of these objects. This also finds expression in other parameters like the stellar temperature and the hydrogen surface abundance, which could be very different for WNL and WNE stars.

Wolf-Rayet Stars
W.-R. Hamann, A. Sander, H. Todt, eds.
Potsdam: Univ.-Verlag, 2015
URL: http://nbn-resolving.de/urn:nbn:de:kobv:517-opus4-84268

Accurate parameters of massive binaries in the Danks clusters

M. Kourniotis[1], A. Bonanos[1] & F. Najarro[2]
[1]*IAASARS, National Observatory of Athens, GR-15236 Penteli, Greece*
[2]*Centro de Astrobiologia (CSIC/INTA), 28850 Torrejon de Ardoz, Madrid, Spain*

We present results from our near-infrared spectroscopy with VLT/ISAAC of four, massive eclipsing binary systems in the young, heavily reddened, massive Danks clusters. We derive accurate fundamental parameters and the distance to these massive systems, which comprise of OIf+, WR and O-type stars. Our goal is to increase the sample of well-studied WR stars and constrain their physics by comparison with evolutionary models.

1 Introduction

Eclipsing binaries (EBs) observed as double-lined spectroscopic binaries stand as unique tools to accurately derive fundamental parameters of stars (Andersen 1991). The majority of hot massive stars are known to form close binary systems (Sana et al. 2012) and hence, such systems constitute ideal tracers for the properties of young Galactic clusters (e.g. Koumpia & Bonanos 2012). In addition, they serve as anchors for the calibration of the extragalactic distance scale (e.g. Hilditch et al. 2005; Bonanos et al. 2006, 2011; Pietrzyński et al. 2013). We aim to explore the properties of massive stars located at the optically faint young, Danks clusters by studying three luminous EBs which are found to contain OIf+, WR and O-type stars.

2 Methodology

An optical variability survey of the Danks clusters was taken by Bonanos et al. (in prep), yielding a total of 21 EBs. Of these, five were observed with VLT/ISAAC in medium resolution ($R \sim 7500$) yielding K-band spectroscopy of S/N$\sim$ 150. Radial velocities were measured employing the near-infrared atlas of hot stars by Hanson et al. (2005) (for D2-EB) and the synthetic non-LTE stellar atmosphere codes FASTWIND (for D2-EB) and CMFGEN (for D1-EB1,2). The binary modeling was achieved proceeding simultaneously with the light curves and radial velocity curves using PHOEBE (Prša & Zwitter 2005) that implements the Wilson-Devinney code (Wilson & Devinney 1971). The genetic optimizer of ELC (Orosz & Hauschildt 2000) was also used, to assist the determination of the uncertainties for the parameters of D2-EB.

3 Results

3.1 D2-EB

D2-EB is a detached, double-lined system with a period of $\sim$ 3.37 days and a circular orbit. We generated a grid of FASTWIND templates assuming Galactic metallicity, at the temperature range $35 - 40$ kK, adopting surface gravity $\log g \sim 3.9$ resulting from the binary modeling. We fit the Brγ (2.166 μm)/ He I (2.162 μm) blend and the He II (2.189 μm) feature, providing temperatures of 38 and 37 kK for the primary and the secondary component, respectively. In addition, the spectrum was also compared against the atlas by Hanson et al. (2005), providing an O6.5 spectral type for both components.

Radial velocities were measured selecting different K-band diagnostic lines such as the CIV at 2.08 μm, the blend of the CNO complex at 2.115 μm with He I at 2.112 μm and the He II line at 2.18852 μm. We found that the best-fit model is obtained with the use of the HeI/CNO blend, being the best tracer of the motion of the components. We derived masses and radii of $24.5 \pm 0.9 M_{\odot}$ and $9.2 \pm 0.1 R_{\odot}$ for the primary and $21.7 \pm 0.8 M_{\odot}$ and $8.7 \pm 0.1 R_{\odot}$ for the secondary component with an accuracy $\sim$3.8% for the masses and $\sim$1% for the radii. This best-fit model is displayed in Fig. 1.

We employed spectral energy distributions generated by FASTWIND using the modeled parameters and fit the available BVI_c photometry by Baume et al. (2009) and near-infrared photometry from 2MASS, as shown in Fig. 2. We derived a distance $d = 3.52 \pm 0.08$ kpc, with a precision of 2% and a visual extinction of $A_{5495} = 11.9 \pm 0.1$ mag. Based on the position of D2-EB on the mass-radius diagram, the system is found coeval to the Danks 2 cluster with an age of $\sim$5 Myr. The measured systemic velocity is inconsistent to that of the cluster, indicating that D2-EB was likely ejected from the cluster as a runaway binary in the recent past. A detailed analysis of the system is presented in Kourniotis et al. (2015).

3.2 D1-EB1 and D1-EB2

D1-EB1 is an eccentric ($e = 0.14$), detached system with a period of $\sim$ 5.97 days. The spectrum of D1-EB1 displays emission of the CIV/CNO/Brγ features while the 2.18852 μm HeII line shows a P-Cygni profile for the primary and absorption for the

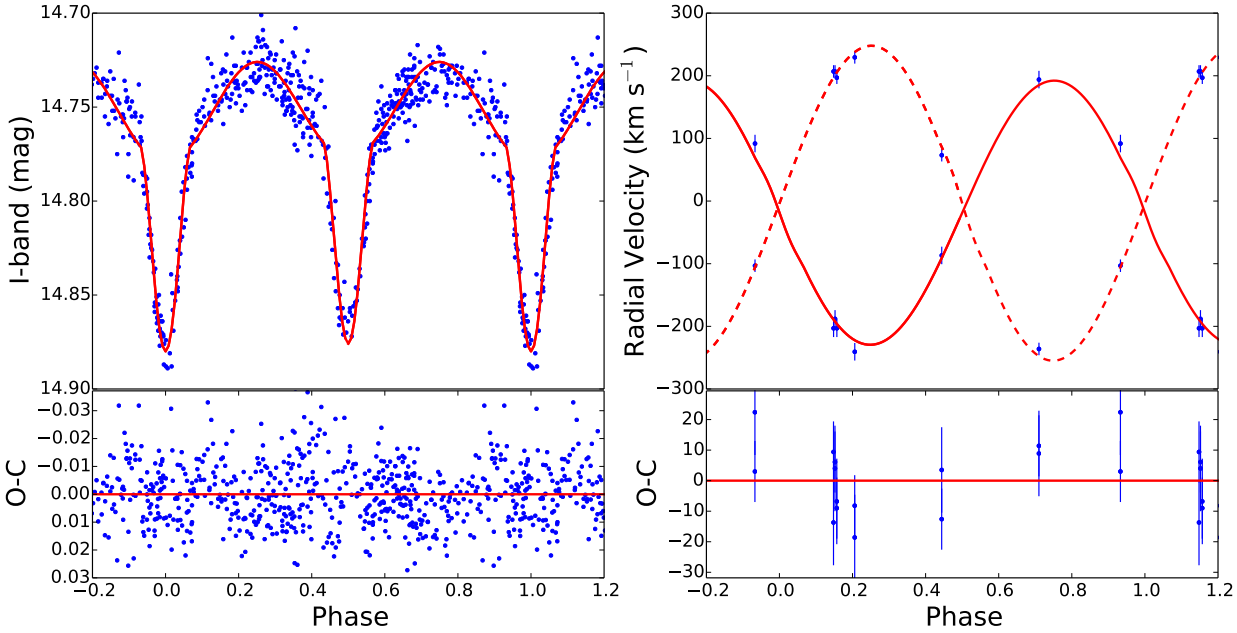

Fig. 1: The *left* panel shows the modeled light curve (red) and the I-band observations of Bonanos et al. (in prep). The *right* panel displays the radial velocities measurements from the ISAAC/VLT K-band spectra, and the overplotted modeled curves. Residuals of the fits are shown in the lower panels.

secondary. The system was modeled with the non-LTE atmosphere code CMFGEN and the best fit was achieved using an O5.5 − 6 If+ spectral type of $T_{\rm eff1} = 34.5$ kK for the primary component and an O5 − 5.5 If spectral type of $T_{\rm eff2} = 36.5$ kK for the secondary component. Radial velocities were measured using the HeI/CNO blend, which provided the best-fit curve, as in D2-EB. Our preliminary analysis has yielded masses of $\sim 75 M_{\odot}$ and $\sim 69 M_{\odot}$ for the primary and the secondary component, respectively.

The single-lined spectrum of D1-EB2 was classified by Davies et al. (2012) as a WNLh-type star which, based on its position on a near-infrared colour-magnitude diagram, is assigned an initial mass of $\sim 120 M_{\odot}$. We are the first to report D1-EB2 as an eclipsing system with a period of ~ 3.29 days. The light curve indicates overflow for the Roche lobe of the primary and/or the secondary component. The spectrum displays HeI/CNO/Brγ in emission and HeII in a P-Cygni profile. We employed the CMFGEN code to provide the best-fit model which corresponds to a hydrogen-rich WN star with $T_{\rm eff} = 34.5$ kK. Further analysis of the second quadrature of D1-EB2 may reveal the presence of the companion. Preliminary results based on the single radial velocity curve and an assumption for the mass of the primary from the range $60 - 120 M_{\odot}$ typical for hydrogen-rich WN stars, give rise to a double contact scenario and indicate an early O-type giant companion.

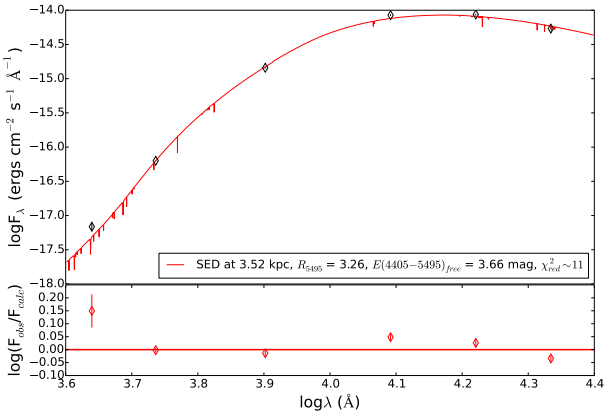

Fig. 2: Fit of the reddened, composite spectral energy distribution of D2-EB to the available BVI_cJHK_s photometry (points). We find a distance of 3.52 kpc, with a visual extinction of $A_{5495} = 11.9$ mag.

We searched the 3XMM-Newton source catalogue for evidence of X-ray emission, reporting a bright source within 5" from D1-EB2, and a fainter source associated with D1-EB1 which, however, could be likely affected by the bright, nearby X-ray counterpart of WR48a. The X-ray spectrum of the single-lined D1-EB2 was fit with a soft component with $kT = 0.78$ keV and a hard component with $kT = 3.33$ keV. Column density is found to be $n_{\rm H} = 2.30 \times 10^{22} {\rm cm}^{-2}$ and we derived the 0.5 − 8

keV X-ray luminosity of $\log L_{\rm X} \sim 33.72$. Comparing to the X-ray survey of colliding wind binaries by Gagné et al. (2012), the inferred X-ray luminosity that emerges from shocks in the wind collizion zone of D1-EB2, is typical for WR+O type systems. Nevertheless, the short period of D1-EB2 is unusual compared to the long periods that wide, X-ray bright systems typically have.

4 Acknowledgements

MK and AZB acknowledge funding by the European Union (European Social Fund), National Resources under the "ARISTEIA" action of the Operational Programme "Education and Lifelong Learning" in Greece, and research and travel support from the European Commission Framework Program Seven under the Marie Curie International Reintegration Grant PIRG04-GA-2008-239335.

References

Andersen, J. 1991, A&A Rev., 3, 91

Baume, G., Carraro, G., & Momany, Y. 2009, MNRAS, 398, 221

Bonanos, A. Z., Castro, N., Macri, L. M., & Kudritzki, R.-P. 2011, ApJ, 729, L9

Bonanos, A. Z., Stanek, K. Z., Kudritzki, R. P., et al. 2006, ApJ, 652, 313

Davies, B., Clark, J. S., Trombley, C., et al. 2012, MNRAS, 419, 1871

Gagné, M., Fehon, G., Savoy, M. R., et al. 2012, in Astronomical Society of the Pacific Conference Series, Vol. 465, Proceedings of a Scientific Meeting in Honor of Anthony F. J. Moffat, ed. L. Drissen, C. Robert, N. St-Louis, & A. F. J. Moffat, 301

Hanson, M. M., Kudritzki, R.-P., Kenworthy, M. A., Puls, J., & Tokunaga, A. T. 2005, ApJS, 161, 154

Hilditch, R. W., Howarth, I. D., & Harries, T. J. 2005, MNRAS, 357, 304

Koumpia, E. & Bonanos, A. Z. 2012, A&A, 547, A30

Kourniotis, M., Bonanos, A. Z., Williams, S., et al. 2015, A&A, submitted

Orosz, J. A. & Hauschildt, P. H. 2000, A&A, 364, 265

Pietrzyński, G., Gieren, W., Graczyk, D., et al. 2013, in IAU Symposium, Vol. 289, IAU Symposium, ed. R. de Grijs, 169–172

Prša, A. & Zwitter, T. 2005, ApJ, 628, 426

Sana, H., de Mink, S. E., de Koter, A., et al. 2012, Science, 337, 444

Wilson, R. E. & Devinney, E. J. 1971, ApJ, 166, 605

Philip Massey: Back in the olden days, Peter Conti and I did orbit solutions for a number of Of+Of systems, and often found that the gamma-velocities didn't agree. The reasons behind this make sense; the lines are formed in a region that is already part of the wind. Did you allow for this in your orbit solutions?

Michalis Kourniotis: I indeed report a discrepancy between systemic velocities modeled with different features. For instance, modeling the eccentric D1-EB1 using just the CNO complex, I got $\gamma \approx -110\,\mathrm{km/s}$ but using the He II instead, I got $\gamma \approx 0\,\mathrm{km/s}$. Taking this discrepancy into account, I proceeded into working with either feature separately. I found that the best-fit radial velocity curve was achieved with the use of the CNO/He I blend rather than the He II line. In general, I suggest that for such systems it is hard to claim membership to the cluster based on systemic velocities that are derived from K-band features.

Mike Corcoran: The high X-ray luminosity of the contact binary D1-EB2 is surprising, since in a contact system the winds near the line of centers do not collide at terminal velocities. Have you tried to fit the X-ray spectrum with colliding wind models of the emission?

Michalis Kourniotis: For the X-ray modelling, two-temperature models (apec) of thermal emission from collisionally ionized plasma were applied. The integrated flux corresponds to the range $0.5 - 8\,\mathrm{keV}$. To convert flux to luminosity, a distance of $3.8\,\mathrm{kpc}$ was employed, typical of the distance to the Danks 1 cluster.

Wolf-Rayet Stars
W.-R. Hamann, A. Sander, H. Todt, eds.
Potsdam: Univ.-Verlag, 2015
URL: http://nbn-resolving.de/urn:nbn:de:kobv:517-opus4-84268

Macroclumping in WR 136

B. Kubátová[1,3], W.-R. Hamann[2], H. Todt[2], A. Sander[2], M. Steinke[2], R. Hainich[2], & T. Shenar[2]

[1] *Astronomický ústav AV ČR, Fričova 298, 251 65 Ondřejov, Czech Republic*
[2] *Institut für Physik und Astronomie, Universität Potsdam, Karl-Liebknecht-Straße 24/25, 14476 Potsdam-Golm, Germany*
[3] *Matematički institut SANU, Kneza Mikhaila 36, 110 01 Beograd, Serbia*

Macroclumping proved to resolve the discordance between different mass-loss rate diagnostics for O-type stars, in particular between Hα and the P V resonance lines. In this paper, we report first results from a corresponding investigation for WR stars. We apply our detailed 3-D Monte Carlo (MC) line formation code to the P V resonance doublet and show, for the Galactic WNL star WR 136, that macroclumping is require to bring this line in accordance with the mass-loss rate derived from the emission-line spectrum.

1 Introduction

State-of-the-art model-atmosphere codes which are commonly used for analyses of WR star spectra usually treat inhomogeneities in the wind in a simplified manner. It is assumed that clumps are optically thin at all frequencies. Density inside clumps is described using a clumping factor D, which relates it to the smooth wind density with the same mass-loss rate. The interclump space is assumed to be void while the velocity of clumps corresponds to the adopted velocity law of the wind. The main consequence of this formulation (the so-called "microclumping" approach) is that mass-loss rates derived from recombination lines are overestimated by a factor $\sqrt{D}$ when microclumping is neglected, and have to be reduced. The resonance lines, which depend only linearly on density, are not sensitive to microclumping.

As a possible solution for this problem, Oskinova et al. (2007) suggested a *macroclumping* approach, in which the clumps are not restricted to be optically thin at all frequencies. For ζ Pup they showed that resonance lines are sensitive to macroclumping and, consequently, macroclumping can reconcile the discrepancy between mass-loss rates derived from the recombination Hα line and the P V resonance doublet ($\lambda\lambda$ 1118, 1128 Å). Therefore, in order to get these mass-loss rate diagnostics in agreement there is no need for reduction of the mass-loss rate and for the use of stronger clumping in the wind. This result was confirmed by Šurlan et al. (2013) by analysing a sample of O-type stars using a 3-D Monte Carlo Radiative Transfer (MCRT) code for inhomogenuous winds.

While the discordance between different mass-loss rate diagnostics was explained this way for O-type stars, it is not yet known to which extent macroclumping affects the winds of WR stars. Here we present preliminary results obtained for the Galactic WNL star WR 136.

2 Observational data, models and fitting procedure

Observational data. Optical and low-resolution IUE spectra are the same as used in the paper by Hamann et al. (2006), where also the procedure of spectra normalization is described. High-resolution FUSE spectra in the range of the P V resonance doublet where retrieved from the MAST (http://archive.stsci.edu) archive. These UV spectra have been divided by the reddened model continuum for normalization.

1-D spherically symmetric wind models. Models for WR 136 are calculated with the Potsdam Wolf-Rayet (PoWR) 1-D code (for more details see Hamann & Gräfener 2004). Detailed model atoms of the most relevant elements and line blanketing with the iron-group elements treated in the super-level approach were taken into account. The clumping parameter is set to $D = 4$. The Doppler velocity $v_{\rm D}$, which reflects random motions on small scales ("microturbulence"), is set to 100 km s^{-1}. The supersonic part of the wind is described with the β-law. with exponent $\beta = 1$. Mass-loss rate and wind velocity are among the free parameters of the models.

WR 136 has been analyzed already with PoWR models by Hamann et al. (2006). We adopt the stellar and wind parameters from this paper, but calculate a new PoWR model that now accounts additionally for the elements Si and P. Only H, He, C, N, and a generic iron-group atom were included in the previous model. The mass fractions of all elements used in the model now are: 0.78, 0.2, 1.0×10^{-4}, 0,015, 6.6×10^{-4}, 5.8×10^{-6}, and 1.4×10^{-3} for H, He, C, N, Si, P, and the Fe-group element, respectively.

3-D Monte Carlo Radiative Transfer clumped wind model. To model the P V resonance line profile, we use our 3-D MCRT code for clumped winds. The code is adequate to simulate the effects of clumping on resonance line formation (of both singlets

and doublets). For more details about this code see Šurlan et al. (2012).

In the wind, a random distribution of spherical clumps is created. These clumps move with the velocity v_β according to the β-law, but they also may have an additional internal velocity gradient described with the velocity deviation parameter $m = v_{\rm dis}/v_\beta$, where $v_{\rm dis}$ is the velocity dispersion inside the clump. The number density of clumps obeys the continuity equation. The density in the clumps and in the interclump medium is specified from the mass-loss rate and the clumping parameters.

Clumps are described with following parameters (see Šurlan et al. 2012): clump separation parameter (L_0), clumping factor (D), interclump density factor (d), on-set radius of clumping ($r_{\rm cl}$), and velocity deviation parameter (m).

The line scattering is assumed to be isotropic in the comoving frame of reference, while the frequencies are completely redistributed over the Doppler-broadened opacity profile. The line opacity is computed according to the mass-loss rate, element abundance, and ionization fraction.

Fitting procedure. The PoWR model, which gave a reasonable fit to the observed spectral energy distribution and the line spectrum of WR 136, yields the stratification of the the P V ionization fraction which is now used as input for the MCRT calculation. Moreover, the "photospheric" spectrum underlying the P V resonance doublet is simulated with a model where P and Si lines are suppressed, and then used as incident radiation at the inner boundary for the 3-D MCRT code. The clumping parameters are then determined by optimizing the fit to the P V resonance doublet.

3 Results of models fitting

The final result of the modelling is given in Fig. 1, model parameters are in the figure caption. As it can be seen in Fig. 1, the obtained P V line profile with the PoWR code is much stronger than the observed one. Much better agreement with observations is achieved with the 3-D MCRT code which includes macroclumping. The P V doublet is severely blended by a doublet (not resonance!) of Si IV at $\lambda\lambda$ 1122.49, 1128.34 Å. In the O stars, these subordinate lines appear only as small absorptions, but in the WR 136 spectrum these lines form large emissions, which are seen in the observations and also modeled in the PoWR model of Fig. 1. To get a better insight into the importance of particular clumping parameters, we did several additional calculations.

Number of clumps. The total number of clumps ($N_{\rm cl}$) in the 3-D MCRT code is controlled by the parameter L_0. The smaller L_0 is, the more clumps are generated.

First, we calculate the P V line profile assuming a smooth wind which shows deeper absorption and higher emission compared to the observation (see the dotted orange line in Fig. 2). To test the macroclumping effect, we then calculate a clumped wind model by setting $L_0 = 2.3$, which implies only 115 clumps within $100\,R_*$ (cf. Eq. 24 in Šurlan et al. 2012) and hence corresponds to an extremely porous wind. The other clump parameters are set to $d = 0$, $r_{\rm cl} = 1$, and $m = 0$. As a result, the calculated P V line profile is drastically reduced (green line with crosses in Fig. 2) and now weaker than observed. A satisfactory fit is obtained by setting $L_0 = 1.8$, which implies 237 clumps. Now, the strength of the emissions and the depth of the absorptions are better reproduced (see the black line with asterisks in Fig. 2). If we increase the number of clumps further by setting $L_0 = 0.9$, which implies 1763 clumps, the obtained line profile shows a deeper absorption and slightly higher emission than observed (see the purple line with triangles in Fig. 2.

From these tests we can conclude that a reasonable fit of the P V resonance doublet requires a wind that is extremely porous (only ≈200 clumps within $100\,R_*$). For O star winds we estimated a smaller average clump separation (see Šurlan et al. 2013).

Inter-clump medium. The density between clumps is described with the interclump medium density parameter d (see Sect. 2.1.2. in Šurlan et al. 2012). Using this parameter, a two-component wind is created with dense clumps and non-void interclump medium. We set $L_0 = 2.3$, $r_{\rm cl} = 1$, and $m = 0$, and then increase d until satisfactory agreement is reached. As the parameter d increases, the depth of absorptions becomes deeper while the emission changes only slightly. We find that for $d = 0.003$ a reasonable fit to the observation can be achieved. However, different combinations of L_0 and d may give equally good agreement with observations. Therefore, it is not possible to say with confidence which combination of L_0 and d corresponds to reality. A completely void interclump space is certainly unrealistic, as we had also found for O-type stars (Šurlan et al. 2013).

Velocity dispersion – "vorosity". For line formation in an expanding atmosphere, the porosity effect is enhanced. Since the clumps move with different velocities, gaps in the coverage of Doppler shifts may occur. This "vorosity" effect depends on the range of Doppler shifts which is covered by one individual clump. This range is characterized in our formalism by the velocity deviation parameter m (see Eq. 20 and Fig. 3 in Šurlan et al. 2012). Guided by hydrodynamical simulations, we assume a negative velocity gradient inside the clumps. The clump center and the ambient interclump medium is set to

move monotonically according to the β-law. We set $L_0 = 2.3$, $r_{\rm cl} = 1$, and $d = 0.003$ while m is varied. Increasing the value of m leads to an extension of the absorption beyond v_∞, thus softening the blue edge of the P V line profile (see the difference between the blue edge of the black dotted line profile in Fig. 1 and the profiles in Fig. 2). Similar results were obtained for O-type stars (see the upper panel of Fig. 8 in Šurlan et al. 2013). We find here that "vorosity" does not influence the overall line strength significantly.

Onset of clumping. In Fig. 2 it can be seen that the part of the P V line profile which corresponds to the inner wind cannot be reproduced with the clumped wind model where clumping develops at the wind base (i.e. photosphere). Even if matter is added between clumps, the calculated profiles show stronger emissions. To improve the fit of this part of the P V line profile we vary the parameter $r_{\rm cl}$ which controls the radius where clumping sets in. When we increase $r_{\rm cl}$, more absorption is added to the inner wind. For $r_{\rm cl} = 2.8$ the level of absorption in the inner wind is reproduced (see black dotted line in Fig. 1). It seems that for the case of clumped wind and non-void interclump medium, clumps should start to develop a bit farther from the photosphere. This result is different from the case of O-type stars, where clumps seem to start at the photosphere (see Sect. 6.3 in Šurlan et al. 2013).

4 Summary

From analyzing the spectrum of WR 136 with the PoWR and 3-D MCRT codes, we demonstrate that macroclumping has impact on the formation of resonance lines.

a) A smooth wind cannot reproduce the observed P V line profile, when the mass-loss rate is adopted according to the emission-line spectrum. The porosity seems to be pronounced (only ≈200 clumps within 100 R_*).

b) Different combinations of the clump-separation parameter L_0 and the interclump density factor d can reproduce the observation equally good, i.e. the interclump density remains unconstrained.

c) The results are not sensitive to the velocity dispersion within each clump ("vorosity"), except of an additional blue-shift of the P-Cygni absorption edge.

We intend to study a larger sample of WR stars in order to better understand the inhomogeneous structures of their winds.

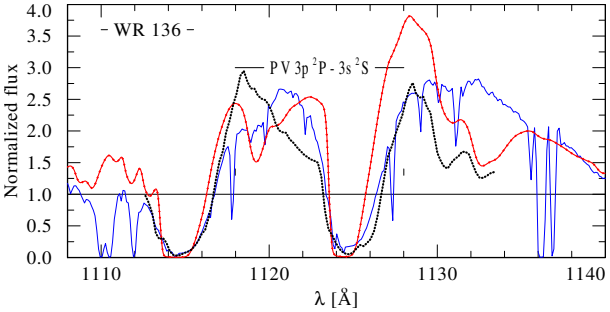

Fig. 1: Comparison between observed (thin solid blue line) and synthetic spectra of the P V line of WR 136 obtained with the PoWR code without macroclumping (red line with croses), and 3-D MCRT codes (dotted black line) with $L_0 = 2.3\,(N_{\rm cl} = 115)$, $d = 0.003$, $m = 0.1$, and $r_{\rm cl} = 2.8$.

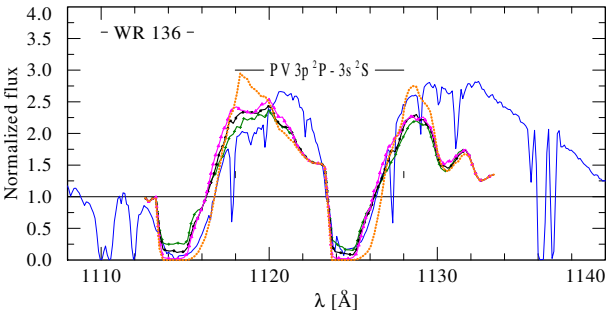

Fig. 2: Comparison between observed (thin solid-blue line) and calculated P V line profiles of WR 136 calculated with 3-D MCRT code for different numbers of clumps. The green line with crosses is calculated with $d = 0$, $r_{\rm cl} = 1$, $m = 0$, and $L_0 = 2.3\,(N_{\rm cl} = 115)$. The black line with asterisks and the purple line with triangles differ only by $L_0 = 1.8\,(N_{\rm cl} = 237)$ and $L_0 = 0.9\,(N_{\rm cl} = 1763)$, respectively. The dotted orange line corresponds to the smooth wind. The blending Si IV emission lines at 1122.49, 1128.34 Å are omitted in these models for consistency.

Acknowledgements. This work was supported by grant GA ČR 13-10589S. BK thanks to Ministry of Education and Science of Republic of Serbia who supported this work through the project 176002 "Influence of collisions on astrophysical plasma spectra".

References

Hamann, W. R. & Gräfener, G. 2004, A&A, 427, 697
Hamann, W. R., Gräfener, G., & Liermann, A. 2006, A&A, 457, 1015
Oskinova, L. M., Hamann, W. R., & Feldmeier, A. 2007, A&A, 476, 1331
Šurlan, B., Hamann, W. R., Aret, A., et al. 2013, A&A, 559, A130
Šurlan, B., Hamann, W. R., Kubát, J., Oskinova, L. M., & Feldmeier, A. 2012, A&A, 541, A37

Richard Ignace: 1) Comment: Expressing onset of clumping in speed may be more interesting than in radius. 2) Do the clump and inter-clump components follow the same velocity law?

Brankica Kubátová: 1) Yes, I agree. Good suggestion. I'll prepare the plot for the Proceedings.

2) We assume that the inter-clump velocity follows the smooth-wind velocity law, while velocities within clumps have an additional contribution defined by the velocity deviation parameter m, where $m = V_{\rm dis}(r)/V_{\rm smooth}(r)$. The velocity inside each clump has a negative velocity gradient.

Andy Pollock: With such a small number of clumps as about 100, would you expect to see line profile variability in the P v profile?

Brankica Kubátová: I would expect to see line profile variability in the P v profile with such a small number of clumps. But more details how line profile variability would look like depending on different numbers of clumps we can confirm after we have obtained results from our new version of 3D MCRT code with time evolution of clumps. I hope it will be soon.

Wolf-Rayet Stars
W.-R. Hamann, A. Sander, H. Todt, eds.
Potsdam: Univ.-Verlag, 2015
URL: http://nbn-resolving.de/urn:nbn:de:kobv:517-opus4-84268

Evolution of Wolf-Rayet spectra

A. Liermann[1]
[1] *Leibniz-Institut für Astrophysik Potsdam (AIP), Germany*

Wolf-Rayet stars are important sources for the enrichment of the ISM with nuclear processed elements, UV photons and momentum. They are descendants of high-mass stars for which short lifetimes and transition times can hamper the spectral classification of the stars in their different evolutionary phases. The expanded stellar atmospheres of Wolf-Rayet stars can show spectra which seem inconsistent with the anticipated underlying evolution phase, for example in late hydrogen-burning WN stars and Of/WN transition stars. We present a sequence of synthetic spectra of the Potsdam Wolf-Rayet models based on the latest Geneva stellar evolution models. This will visualize the changes in stellar spectra over a full stellar lifetime. Direct comparison with observed stellar spectra, as well as the evolution of diagnostic line ratios will improve the connection of spectral classification and evolution phase.

1 Motivation

The spectral classification of high-mass stars can be hampered by many factors, for example, the observed wavelength range with limited numbers of characteristic lines, diluted lines due to a high flux contribution from a binary companion, a short lived stellar evolution phase with the lack of templates for comparison, and so on.

Also, radiative-driven stellar winds like in Wolf-Rayet (WR) stars mask direct observations of the photosphere. For proper spectral classification and to determine stellar and wind parameters we rely on observed characteristic (wind) lines and the comparison to adequate models of expanding stellar atmospheres. The evaluation of observations and derived stellar parameters in the context of stellar evolution is still a challenge, for example to estimate the age and initial mass range of a star by comparison with stellar evolution tracks.

Stellar evolution models provide such tracks with well defined observable stellar parameters like temperature, magnitude, and surface abundance in connection with the underlying physical processes like rotational mixing or central burning processes. Groh et al. (2014) used the Geneva evolution tracks to compute CMFGEN models for a 60 $M_\odot$ star (Hillier & Miller 1998) and analyze the synthetic spectra in terms of spectral subtype assignment and stellar evolution.

In this work, we explore the use of stellar evolution models to create normalized synthetic spectra and flux-calibrated spectral energy distributions (SEDs) with model atmospheres further to support the spectral classification and thus understanding of various stellar evolution phases. We construct a grid of Potsdam Wolf-Rayet (PoWR) model atmospheres (e.g., Gräfener et al. 2002; Hamann & Gräfener 2004) for stellar evolution tracks of different initial stellar masses. This will enable us to study in detail the line profile variation, spectral transition phases, and evolution of quantities such as wind momentum, ionizing flux, etc. In addition, the available synthetic spectra can serve as templates for spectral classification throughout the high-mass regime in the Hertzsprung-Russell diagram.

2 Model grid

2.1 Potsdam Wolf-Rayet model atmospheres

We used the PoWR models to calculate normalized synthetic (emission) line spectra and spectral energy distributions.

The models assume spherically symmetric, stationary mass-loss with a prescribed velocity field; a β-law is adopted for the supersonic part of the stellar atmosphere, with the terminal velocity v_∞ as a free parameter and $\beta = 1$ in this work. The velocity field in the subsonic region is defined so that a hydrostatic density stratification is approached.

The inner boundary of the model atmosphere, the "stellar radius" R_*, corresponds to a Rosseland optical depth of 20. And the "stellar temperature" T_* is linked to the luminosity L and the stellar radius R_* via the Stefan-Boltzmann law.

The PoWR models account for wind inhomogeneities ("clumping") in a first-order approximation, assuming that optically thin clumps fill a volume fraction f_V and the inter-clump space is void. We specify a clumping factor $D = f_\mathrm{V}^{-1} = 4$ in this work. The Doppler velocity v_dop, which reflects random motions on small scales ("microturbulence"), is approximated as one tenth of the terminal velocity and thus might vary from model to model along the evolution track (see below).

2.2 Model input

Calculated PoWR models are based on the stellar evolution tracks provided by the Geneva group (Ekström et al. 2012) for solar metallicities, with and without the effects of rotation. As model input, the evolution tracks provide per time step the parameters temperature, luminosity, mass-loss rate and

chemical surface abundances as listed in Table 1. For stars on the main sequence up to turn-off we used the effective temperature $T_{\rm eff}$ rather then the one not corrected for thickness of the stellar wind T_*.

Tab. 1: PoWR model input parameters from (1) Ekström et al. (2012), (2) Kudritzki & Puls (2000), (3) Hamann et al. (2006), (4) Sander et al. (2012).

Parameter		Reference
$T_{\rm eff}$, T_*, $\log(L/L_\odot)$		(1)
$\dot{M}$, X, Y, $X_{\rm CNO,surf}$		(1)
$v_\infty \cong$		
$f \cdot v_{\rm esc}$	O stars	(2)
1000 km/s	WN with hydrogen	(3)
1600 km/s	WN without hydrogen	(3)
2000 km/s	WC/WO	(4)

The terminal velocity v_∞ during the main-sequence up to turn-off time is derived via the escape velocity following Kudritzki & Puls (2000) with a factor f depending on the effective temperature of the star. For the later evolution phases we list the fixed values and references in Table 1.

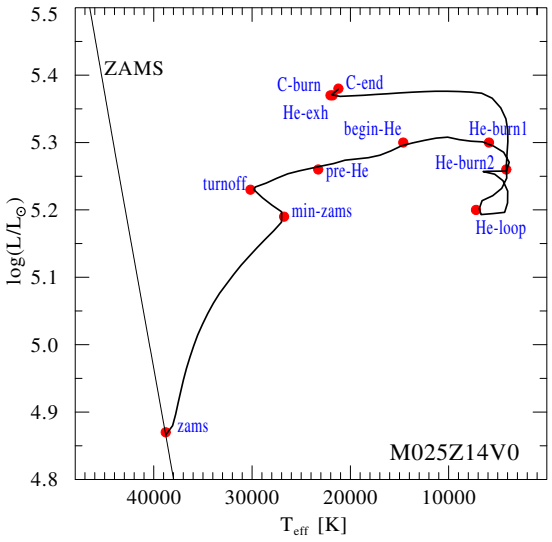

Fig. 1: Sampling of time steps for calculating PoWR models along the evolution model for a star with 25 $M_\odot$ initial mass without effects of rotation.

2.3 Sampling the evolution track

The Geneva evolution tracks comprise 400 time steps for a given initial mass. Computation-wise, it is infeasible to compute 400 PoWR models for each evolution track. Thus, input parameters are taken from selected time steps sampling the most significant phases in stellar evolution. This sampling follows the normalization scheme given by Ekström et al. (2012) and covers the main sequence towards turn-off, helium burning phases including a loop in the HR diagram, and carbon burning phases as shown in Fig. 1. Sub-grid sampling to cover transition phases in stellar evolution such as turn-off to possible luminous blue variable (LBV) phase can be calculated in a future project.

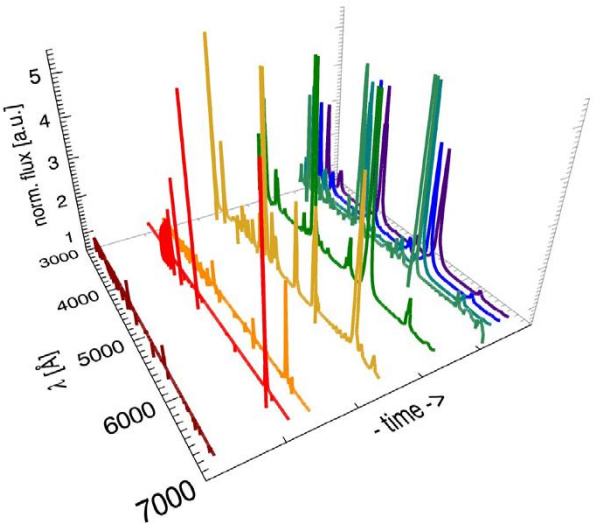

Fig. 2: Time sequence of PoWR spectra for an initial 60 $M_\odot$ star without effects of rotation.

3 Results

The grid of calculated PoWR models covers the evolution tracks of 25, 40, and 60 $M_\odot$ initial mass so far, each with $v_{\rm rot} = 0.4\, v_{\rm crit}$ and without the effects of rotation. Extension of this grid to other initial masses is considered for future work. In the following we focus on the track for 60 $M_\odot$ without rotation.

The output of the PoWR models summarizes the stellar parameters, including the input parameters, absolute magnitudes in different filter systems, and emergent astrophysical flux at each time step. More importantly the PoWR models provide synthetic (emission) line spectra and spectral energy distributions. The wavelength range of those covers the UV and Optical (1200–7800 Å), Helium I (9500–12000 Å) in detail, and near-infrared JHK (1–2.5 μm) regime for this work. The sequence of optical spectra across time following the evolution track is shown in Fig. 2.

Depending on the specific interest, the available grid allows for different aspects to be analyzed both individually per time step and in total in the framework of stellar evolution:

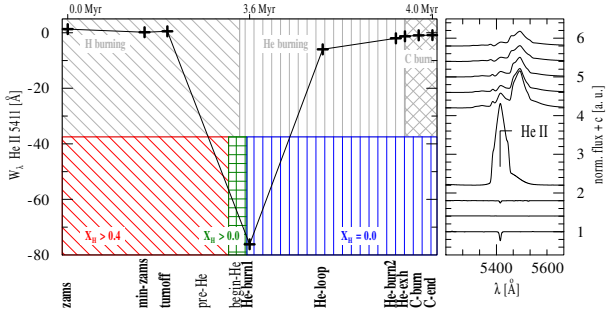

Fig. 3: Evolution of W_λ of a He II line. The background (left panel) represent the ongoing central burning process and hydrogen surface abundances of the according evolution track. Normalized emission line spectrum (right panel) flux plus constant shift over time.

(i) direct comparison to observed spectra for line identification and spectral classification,

(ii) correlation of properties of diagnostic lines in different wavelength regimes,

(iii) SED fitting to obtain reddening and distance/luminosity estimates,

(iv) spectral line profile fitting to derive stellar and wind parameters,

(v) evolution of line properties, like equivalent width, FWHM, and line ratios, and

(vi) energy and momentum output over stellar lifetime.

As an example, we present the evolution of the equivalent width W_λ of the He II line at $\lambda 5411$ Å in Fig. 3. It can be clearly seen that during main-sequence evolution, associated with the hydrogen burning phase, the line is hardly present in the spectrum but becomes a prominent emission line for the Wolf-Rayet phases. The pattern and color coding of the background helps to distinguish between hydrogen-depleted or hydrogen-free atmospheres for these later phases. Also the underlying central burning process of the evolution model might help to classify transition phases, for example, between O stars leaving the main sequence and very late WN stars.

In Fig. 4, we present the evolution of absolute Johnson magnitudes over time (top panel) as well as the number of ionizing photons for hydrogen and helium (bottom panel). The biggest changes in the number of ionizing photons are found towards the end of the main-sequence life with a decrease of the order of a magnitude. Over the remaining stellar lifetime the numbers remain at an about constant level.

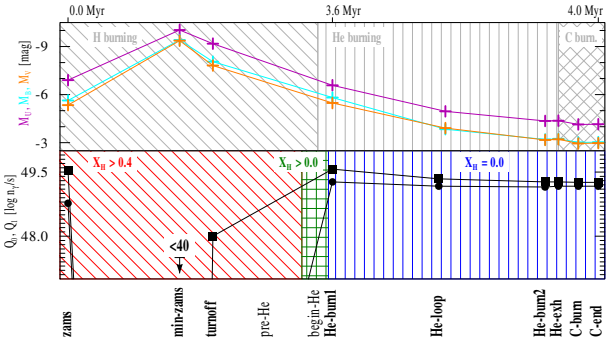

Fig. 4: Evolution of absolute magnitudes (top panel) and ionizing photons for H (Q_0, crosses) and He I (Q_1, circles), respectively (bottom panel). See Fig. 3 for explanation of the background pattern.

In the ongoing analysis, we will relate spectral subtypes to the evolution phases. This will allow also a better understanding of findings like line-profile or emergent-flux changes in the context of stellar evolution to be established.

The grid of models will be available upon request.

Acknowledgments

I am thankful to the present PoWR team (Wolf-Rainer Hamann, Helge Todt, Andreas Sander, Rainer Hainich, Tomer Shenar) for providing and maintaining the model atmosphere code and helpful discussion during this project.

References

Ekström, S., Georgy, C., Eggenberger, P., et al. 2012, A&A, 537, A146

Gräfener, G., Koesterke, L., & Hamann, W.-R. 2002, A&A, 387, 244

Groh, J. H., Meynet, G., Ekström, S., & Georgy, C. 2014, A&A, 564, A30

Hamann, W.-R. & Gräfener, G. 2004, A&A, 427, 697

Hamann, W.-R., Gräfener, G., & Liermann, A. 2006, A&A, 457, 1015

Hillier, D. J. & Miller, D. L. 1998, ApJ, 496, 407

Kudritzki, R.-P. & Puls, J. 2000, ARA&A, 38, 613

Sander, A., Hamann, W.-R., & Todt, H. 2012, A&A, 540, A144

Anthony (Tony) Moffat: Can you convert your predicted spectral variations into variations in spectral subtype? This would be very useful for observers. Do you see evidence for the peeling-off scenario?

Adriane Liermann: This is work in progress, and we plan to do the spectral classification and assign subtypes for the evolution phases. On the second part of your comment I'd like to pass on to José for an answer.

José Groh: We do see an evolution of spectral types during the WN phase as the hydrogen envelope is peeled off. However, during the WC phase we see a quite constant spectral type.

Wolf-Rayet Stars
W.-R. Hamann, A. Sander, H. Todt, eds.
Potsdam: Univ.-Verlag, 2015
URL: http://nbn-resolving.de/urn:nbn:de:kobv:517-opus4-84268

The True origin of Wolf-Rayet stars

J. S. Vink[1]
[1] *Armagh Observatory, College Hill, BT61 9DG Armagh, Northern Ireland, UK*

The Wolf-Rayet (WR) phenomenon is widespread in astronomy. It involves classical WRs, very massive stars (VMS), WR central stars of planetary nebula CSPN [WRs], and supernovae (SNe). But what is the root cause for a certain type of object to turn into an emission-line star? In this contribution, I discuss the basic aspects of radiation-driven winds that might reveal the ultimate difference between WR stars and canonical O-type stars. I discuss the aspects of (i) self-enrichment via CNO elements, (ii) high effective temperatures ($T_{\rm eff}$), (iii) an increase in the helium abundance (Y), and finally (iv) the Eddington factor $\Gamma_{\rm e}$. Over the last couple of years, we have made a breakthrough in our understanding of $\Gamma_{\rm e}$-dependent mass loss, which will have far-reaching consequences for the evolution and fate of the most massive stars in the Universe. Finally, I discuss the prospects for studies of the WR phenomenon in the highest redshift Lyα and He II emitting galaxies.

1 Introduction

Before being able to address the question regarding the true origin of Wolf-Rayet (WR) stars, we need to ask ourselves what exactly do we mean with the term "origin", as it could potentially refer to an evolutionary origin, as classical WR stars are thought to be evolved massive stars. It is thus important to emphasize that evolutionary status is not the only factor that decides whether a given object is expected to give rise to the WR phenomenon. Instead, what I am interested in here is which physical mechanism is responsible for the WR phenomenon? In other words, what is the root cause for a certain type of object to reveal the strong emission lines caused by recombination cascades?

There are basically *four* types of objects which we would wish to explain by the same mechanism. These four groups are: (i) the evolved WR stars of type WN/WC/WO (nitrogen, carbon, oxygen-rich respectively), (ii) WNh stars, which are very massive stars (VMS) with $M > 100 M_{\odot}$ (Vink 2015a), (iii) WR central stars of planetary nebula CSPN [WRs], and since very recently also (iv) young supernovae (SNe) such as SN 2013cu, which reveal WR-like spectra, as depicted in Fig. 1.

Because of the WR phenomenology in the latter case of SN 2013cu, Gal-Yam et al. (2014) proposed a WR progenitor system, however, whilst the Type IIb SN 2013cu indeed shows a WR-like emission-line spectrum, the narrow lines are more consistent with the slow winds of Luminous Blue Variables (LBVs), as has been discussed by Groh (2014) and Gräfener & Vink (2015b). This is also more consistent with the fact that LBVs were first suggested to be the variable-wind progenitors of Type IIb SNe with the additional evidence of their much slower winds than WR stars (Kotak & Vink 2006).

In this contribution, I discuss several properties of WR stars that may potentially make them distinct from the more common O-type stars. These involve (i) self-enrichment with large amounts of carbon (in WC stars) and oxygen (in WO stars); (ii) high effective temperatures ($T_{\rm eff}$) ; (iii) an enhanced helium (Y) abundance, and finally, (iv) a high luminosity-to-mass ratio (L/M), as represented by the Eddington factor $\Gamma_{\rm e}$:

$$\Gamma_{\rm e} \; = \; g_{\rm rad}^{\rm elec}/g_{\rm grav} \; = \; \sigma_{\rm elec} L/(4\pi c G M) \qquad (1)$$

where $g_{\rm rad}^{\rm elec}$ is the radiative acceleration on electrons, and the other symbols have their usual meaning. I will be assuming some basic knowledge of radiation-driven wind theory, but if the reader wishes to learn more details, I refer to Puls et al. (2008), Owocki (2015) and Vink (2015b).

2 Self-enrichment (CNO)

Classical WR stars are evolved objects that have lost a significant amount of their initial mass (50–90 %) due to stellar winds or alternative mass-loss (either single star or binary) during earlier evolutionary phases. WC/WO stars are significantly enriched in C and O (e.g. Sander et al. 2012; Tramper et al. 2015; Georgy et al. 2012; Yoon et al. 2012).

For decades it was assumed that the high metal (Z) content in classical WC/WO atmospheres was responsible for the high mass-loss rates due to Z-dependent stellar winds, where Z includes CNO elements. For instance, the oft-used empirical mass-loss formula for classical WR stars by Nugis & Lamers (2000) includes a Z-dependence, where Z primarily refers to the abundant CNO elements. It was not until 2005, that it became clear that classical WR stars do in fact show an iron (Fe) Z-dependence (see Fig. 2) – where Z is now the Fe abundance of the host galaxy – due to the millions of Fe lines that drive the inner winds (Vink & de Koter 2005; Gräfener & Hamann 2008).

This strong dependence on Fe, and implicit weak dependence on CNO elements in the inner wind, is very similar in O-type stars (Vink et al. 1999; Puls et al. 2000), which implies that self-enrichment cannot be the prime reason for the WR phenomenon in

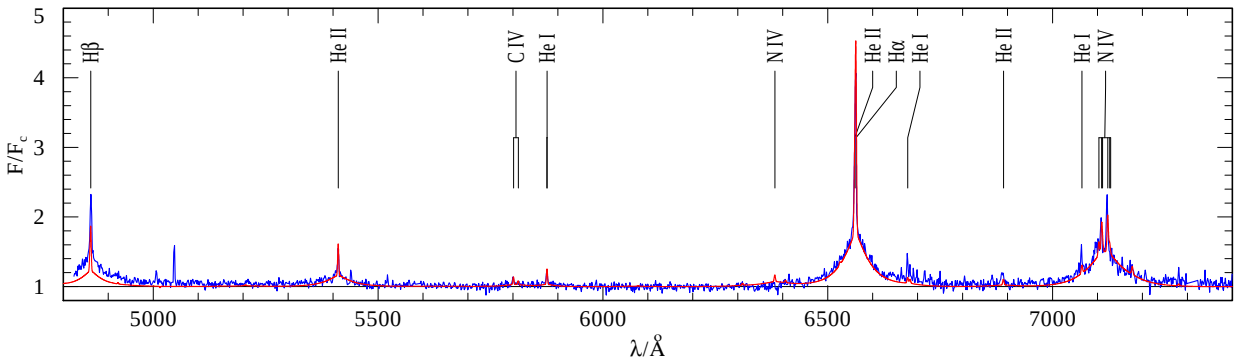

Fig. 1: Model fit to the observed spectrum of the IIb supernova SN 2013cu, 15.5 hours after explosion (Gal-Yam et al. 2014). See Gräfener & Vink (2015b) for more details on the model fit.

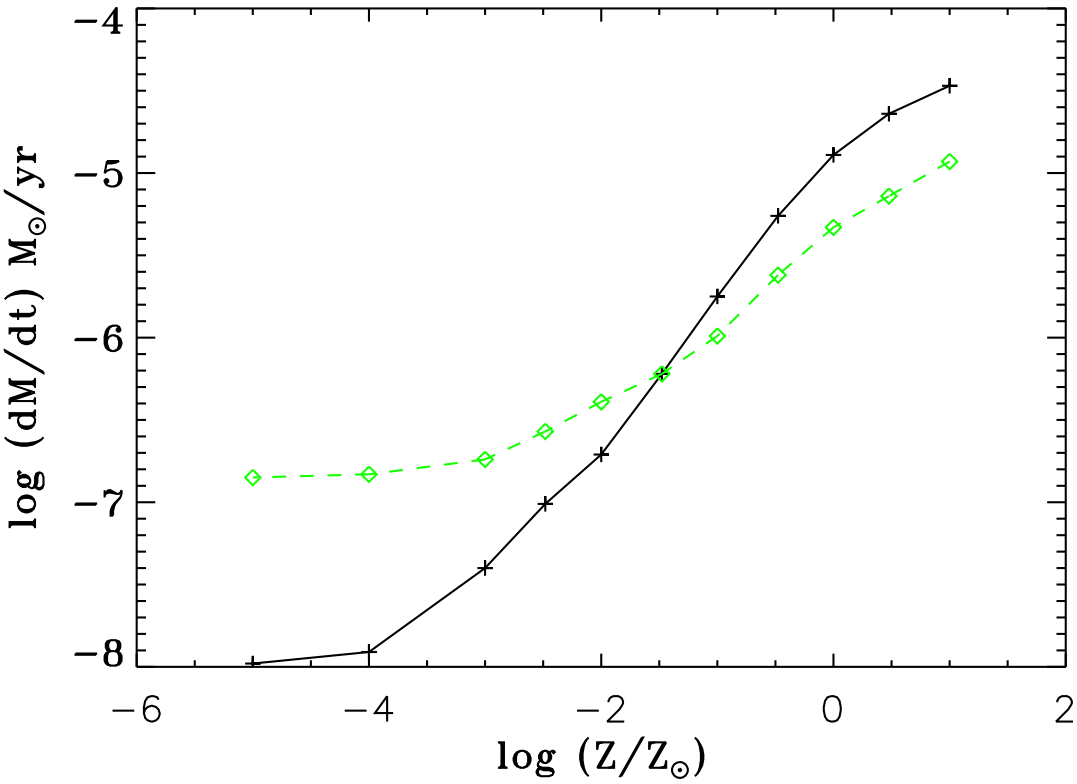

Fig. 2: Monte Carlo WR mass-loss predictions as a function of metallicity Z. The dark line represents the late-type WN stars, whilst the lighter dashed line shows the results for late-type WC stars. The slope for the WN models is similar to the predictions for OB-supergiants, whilst the slope is somewhat shallower for WC stars. At lower Z, the slope becomes smaller, whilst it flattens off entirely at extremely low Z. These computations are from Vink and de Koter (2005).

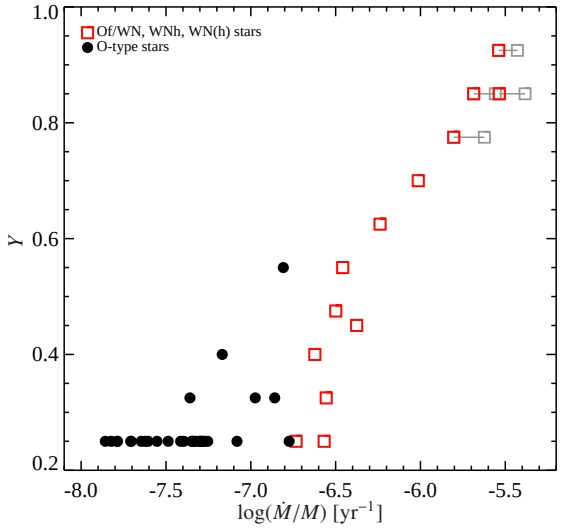

Fig. 3: He surface mass fractions Y vs. relative mass-loss rates $\log(\dot{M}/M)$ for the VMS in VFTS by Bestenlehner et al. (2014) (normal O-type stars are indicated with black circles). Masses have been estimated using the assumption of chemical homogeneity (from Gräfener et al. 2011). I.e. they are upper limits. Potential core He-burning masses are also indicated (in light grey).

the local Universe (this might be different at very low Z where CNO line-driving takes over; Vink & de Koter 2005).

3 High temperatures $T_{\rm eff}$

Classical WR stars are very hot with high core temperatures and high wind densities. These properties result in a well-stratified ionization structure (Lucy & Abbott 1993), with the special properties that gaps in one atmospheric/wind layer become effectively "blocked" by the emergence of a new set of lines from a lower ionization stage. This physical mechanism involving photon trapping (e.g. Owocki 1994) leads to a very efficient momentum transfer via highly efficient multiple scattering and high mass-loss rates. It is thus very tempting to argue that the high temperatures are the main reason for the high mass-loss rates in WR stars. This argument becomes even stronger when one realizes that also [WR] stars of central stars of planetary nebulae (CSPNe) are very hot, with mass-loss rates higher than O-type CSPNe (see Todt, these proceedings).

However, the more recent discovery and modelling of WNh VMS stars in young clusters like the Arches cluster and S Dor (Martins et al. 2008; Bestenlehner et al. 2014) has revealed that their temperatures are not in any way special with respect to those of more common lower-luminosity O-type stars. The only real difference is that they are more luminous, and thus more massive, which explains why they are oftentimes referred to as "O-stars on steroids".

The fact that these moderately-hot WR stars (of order 50 000 K instead of 100 000–200 000 K for classical WRs) can still entertain strong stellar outflows above the single-scattering limit (Vink & Gräfener 2012) indicates that high temperatures alone cannot be the sole reason for the WR phenomenon either.

4 High helium abundance (Y)

Due to its atomic structure, helium has more spectral lines available than hydrogen. This simple fact could thus potentially play a role in providing more efficient wind driving. Furthermore, the underlying spectral energy distribution (SED) of a helium star is different from that of a main-sequence hydrogen burning object, which could potentially also affect the efficiency of radiative driving. Furthermore, the empirical mass-loss formula of Nugis & Lamers (2000) shows a clear dependence on Y. Finally, recent results in the context of the VLT Flames Tarantula survey (VFTS) of the most massive stars in 30 Dor by Bestenlehner et al. (2014) reveal higher mass-loss rates for higher Y abundance (see Fig. 3).

However, I would find it highly unlikely that high Y content is the key to the WR phenomenon. Already in 2002, Monte Carlo predictions for LBVs showed that the differences in radiation driven wind mass loss due to Y enrichment were only subtle (Vink & de Koter 2002). It is therefore far more likely that there is no causal relationship between Y and dM/dt as Fig. 2 might naively suggest, but that helium enrichment is actually the *result* of a high-mass loss rate instead (Bestenlehner et al. 2014).

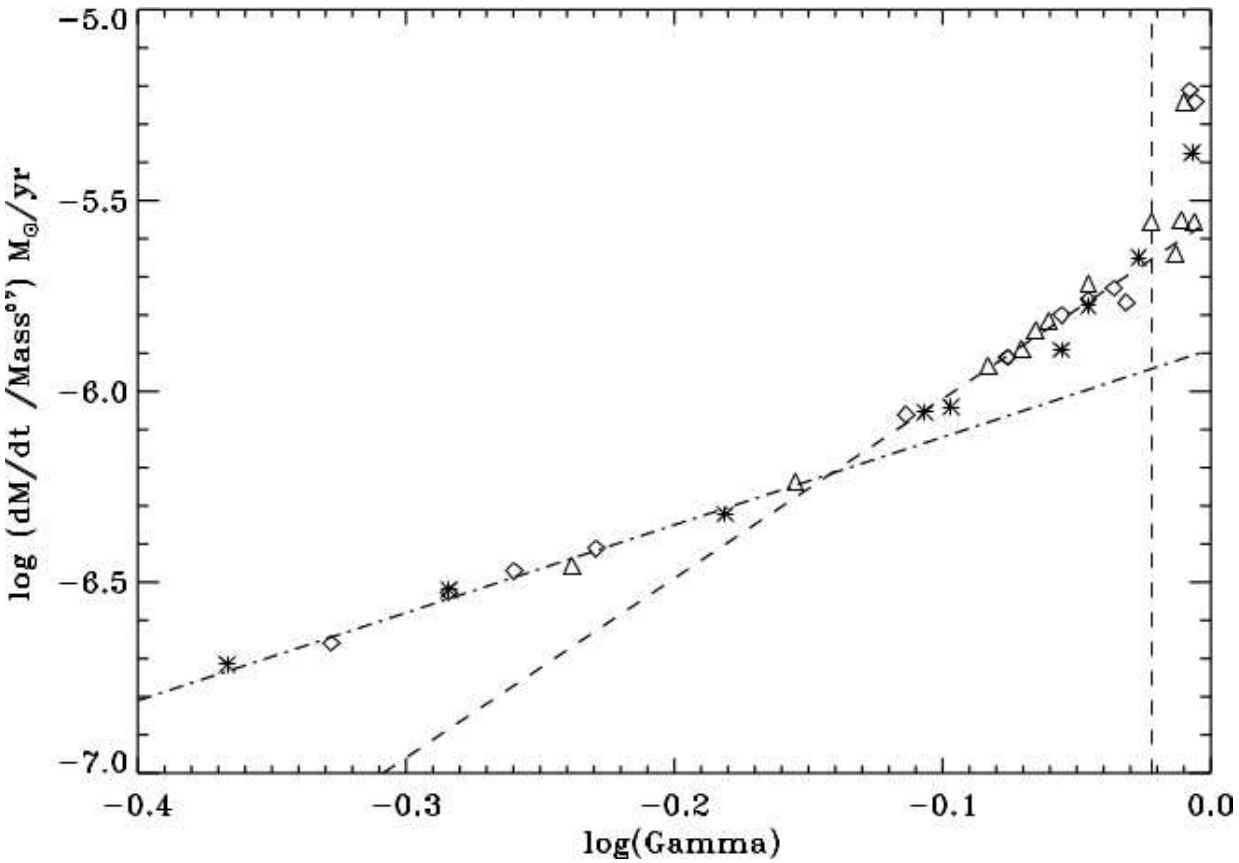

Fig. 4: Monte Carlo mass-loss predictions (divided by$M^{0.7}$) versus Γ_e for models approaching the Eddington limit. The dashed-dotted line represents the best linear fit for the range $0.4 < \Gamma_e < 0.7$. The dashed line represents the higher $0.7 < \Gamma_e < 0.95$ range (from Vink et al. 2011). The *kink* occurs where the winds become optically thick, and where the single-scattering limit is crossed simultaneously.

5 Proximity to Eddington limit

The results in Fig. 3 may easily be explained by the fact that the kink in Fig. 3 is seen at exactly the same position as the kink in Fig. 4. Figure 4 shows Monte Carlo mass-loss predictions for VMS including both optically thin O-type stars as well as optically thick WNh stars.

The slope in the relationship switches abruptly from 2 to 5 when the optical depth crosses unity (Vink & Gräfener 2012). It is noteworthy to emphasize that whilst the shallow slope of the canonical O-type stars is consistent with classical Castor, Abbott & Klein (1995) (hereafter CAK) radiation-driving, the steep slope is clearly inconsistent with classical CAK-type radiation driven winds for optically thin winds. Instead, these optically thick winds are determined by physics beyond CAK (see Bestenlehner et al. 2014 for a more extensive discussion as to whether the kink could alternatively also be reproduced by (modified) CAK theory with variable force multipliers).

I would like to note that the steep slope shown in Fig. 4 is also found in independent calculations by Gräfener & Hamann (2008), as well as empirical results by Gräfener et al. (2011) and Bestenlehner et al. (2014) for VMS in the Arches cluster and 30 Dor, respectively. Given these latest results on VMS stars it seems most likely that it is *the Eddington factor* Γ_e *that is the key to the WR phenomenon*, but only the future will be able to tell if this assertion is correct.

6 Outlook on He II emission

Helium II emission is now routinely detected in the highest redshifts Lyα emitting star-forming galaxies. VMS with WR phenomena likely play a pivotal role in this He II emission, as these hot VMS are now known to dominate the ionizing radiation in local starbursts such as 30 Dor (Doran et al. 2013). Understanding the WR phenomenon in VMS is thus pivotal for understanding high-redshift galaxies, as well as the reionization of the Universe (Vink 2015a).

It may not only be the ionizing radiation of VMS that is relevant for Helium II emission: Cassata et al. (2013) recently published a study of He II emitters between redshifts 2 and 5 including some *narrow* He II emitters. Note that broad He II emission is generally attributed to stellar emission from classical WR stars, whilst narrow He II emission is normally attributed to nebular emission – excited by hot stars.

However, Gräfener & Vink (2015a) recently suggested an alternative scenario for the origin of narrow He II emission, namely the *slow* winds of VMS at low Z, as a result of their proximity to the Eddington limit. This narrow He II emission from very early generations of VMS may become detectable in studies of star-forming galaxies at high redshifts with the James Webb Space Telescope (JWST).

The WR phenomenon may thus still hold a number of future intriguing surprises!

References

Bestenlehner, J. M., Gräfener, G., Vink, J. S., et al. 2014, A&A, 570, A38

Cassata, P., Le Fèvre, O., Charlot, S., et al. 2013, A&A, 556, A68

Castor, J. I., Abbott, D. C., & Klein, R. I. 1975, ApJ, 195, 157

Doran, E. I., Crowther, P. A., de Koter, A., et al. 2013, A&A, 558, A134

Gal-Yam, A., Arcavi, I., Ofek, E. O., et al. 2014, Nature, 509, 471

Georgy, C., Ekström, S., Meynet, G., et al. 2012, A&A, 542, A29

Gräfener, G., & Hamann, W.-R. 2008, A&A, 482, 945

Gräfener, G., & Vink, J. S. 2015a, A&A, 578, L2

räfener, G., & Vink, J. S. 2015, MNRAS, submitted

Gräfener, G., Vink, J. S., de Koter, A., & Langer, N. 2011, A&A, 535, A56

Groh, J. H. 2014, A&A, 572, L11

Kotak, R., & Vink, J. S. 2006, A&A, 460, L5

Lucy, L. B., & Abbott, D. C. 1993, ApJ, 405, 738

Martins, F., Hillier, D. J., Paumard, T., et al. 2008, A&A, 478, 219

Nugis, T., & Lamers, H. J. G. L. M. 2000, A&A, 360, 227

Owocki, S. P. 1994, Ap&SS, 221, 3

Owocki, S. P. 2015, Astrophysics and Space Science Library, 412, 113

Puls, J., Springmann, U., & Lennon, M. 2000, A&AS, 141, 23

Puls, J., Vink, J. S., & Najarro, F. 2008, A&A Rev., 16, 209

Sander, A., Hamann, W.-R., & Todt, H. 2012, A&A, 540, A144

Tramper, F., Straal, S. M., Sanyal, D., et al. 2015, arXiv:1507.00839

Vink, J. S. 2015a, Astrophysics and Space Science Library, 412

Vink, J. S. 2015b, Astrophysics and Space Science Library, 412, 77

Vink, J. S., & de Koter, A. 2002, A&A, 393, 543

Vink, J. S., & de Koter, A. 2005, A&A, 442, 587

Vink, J. S., & Gräfener, G. 2012, ApJ, 751, L34

Vink, J. S., de Koter, A., & Lamers, H. J. G. L. M. 1999, A&A, 350, 181

Vink, J. S., Muijres, L. E., Anthonisse, B., et al. 2011, A&A, 531, A132

Yoon, S.-C., Gräfener, G., Vink, J. S., Kozyreva, A., & Izzard, R. G. 2012, A&A, 544, L11

Tony Moffat: With $\dot{M} = 10^{-4} M_{\odot}$/yr for the most luminous VMS, this means a mass loss of 100 $M_{\odot}$ in a million years or so. This should have observable consequences, right?

Jorick Vink: A million years is a long time for material to be blown out, and dispersed. When comparing VMS to for instance LBVs: the kinematic ages of LBV nebulae are thousands of years, not millions, so I do not think there is a contradiction.

Lidia Oskinova: Including macroclumping in models of massive star spectra results in empirical mass-loss rates that are in good agreement with theoretical expectations.

Vikram Dwarkadas: You showed the spectrum of a SN which exhibits clear WR features. Why don't we see these features in Ib/c supernovae which are supposed to arise from WR stars? What would it take to see them?

Jorick Vink: The SN 2013cu is so far unique, as its progenitor wind was observed (15 hours after explosion). Hopefully, this will one day also become available for SN Ibc. For now there are only photometric pre-explosion images. These progenitors may become very hot just prior to explosion, but are so far undetected (Yoon et al. 2012).

Wolf-Rayet Stars
W.-R. Hamann, A. Sander, H. Todt, eds.
Potsdam: Univ.-Verlag, 2015
URL: http://nbn-resolving.de/urn:nbn:de:kobv:517-opus4-84268

Hydrodynamic modeling of massive star atmospheres

A. Sander[1], W.-R. Hamann[1], R. Hainich[1], T. Shenar[1], & H. Todt[1]
[1] *Universität Potsdam, Institut für Physik und Astronomie, Potsdam, Germany*

In the last decades, stellar atmosphere codes have become a key tool in understanding massive stars, including precise calculations of stellar and wind parameters, such as temperature, mass-loss rate, and terminal wind velocity. Nevertheless, for these models the hydrodynamic equation is not solved in the wind. Motivated by the results of the CAK theory, the models typically use a beta velocity law, which however turns out not to be adequate for stars with very strong winds, and treat the mass-loss rate as a free parameter. In a new branch of the Potsdam Wolf-Rayet model atmosphere (PoWR) code, we solve the hydrodynamic equation consistently throughout the stellar atmosphere. The PoWR code performs the calculation of the radiative force without approximations (e.g. Sobolev). We show the impact of hydrodynamically consistent modelling on OB and WR stars in comparison to conventional models and discuss the obtained velocity fields and their impact on the observed spectral lines.

1 Introduction

Already since mass-loss is known to be common for hot and massive stars, the concept of line-driven winds, i.e. the momentum transfer from photons to metal ions by line absorption, has been suggested as the main mechanism to overcome gravity, backed by early calculations from Lucy & Solomon (1970) for UV resonance lines. A few years later, Castor, Abbott, & Klein (1975, hereafter CAK) developed a theoretical description for the radiative force on many lines using analytical approximations calibrated by fitting numerical calculations. Although their underlying assumptions in terms of which lines are important do not hold in the general case, their basic way of describing the radiative force, especially in the simplified way introduced by Abbott (1980), has been kept through all refinements of the CAK theory (e.g., Friend & Abbott 1986; Pauldrach et al. 1986; Kudritzki et al. 1989; Gayley 1995; Puls et al. 2000).

Backed by empirical mass-loss rates derived from the radio (Wright & Barlow 1975) or infrared (Barlow & Cohen 1977) regime, the modified CAK theory (mCAK) became the standard concept for describing the winds of hot stars, especially OB stars. However, the mCAK description fails for the winds of Wolf-Rayet (WR) stars for which much higher mass-loss rates $\dot{M}$ were deduced than what could be provided by mCAK. Lamers & Leitherer (1993) demonstrated that this shortcoming of the mCAK predictions occurs not only for WR stars, but instead for all hot, massive stars with dense winds.

Since the CAK-like theories use significant approximations, the question pops up whether the failure of the theory for certain objects stems from these approximations or if additional wind driving mechanisms need to be considered. To provide a reliable answer, radiation-driven wind models which do not rely on the CAK approximations are inevitable.

2 Obtaining the radiative acceleration

In order to study the influence of radiative driving, the hydrodynamic equation needs to be considered, since it describes the detailed acceleration balance of inward and outward forces. For a spherically-symmetric star with a stationary outflow, this equation can be written in the form

$$v\left(1-\frac{a^2}{v^2}\right)\frac{\mathrm{d}v}{\mathrm{d}r} = a_{\mathrm{rad}}(r) - g(r) + 2\frac{a^2}{r} - \frac{\mathrm{d}a^2}{\mathrm{d}r}. \quad (1)$$

Hereby the equation of state for an ideal gas $P = \rho a^2$ and the equation of continuity

$$\dot{M} = 4\pi r^2 \rho(r)\, v(r) \quad (2)$$

have been implied. The intricate quantity in Eq. (1) is, of course, the radiative acceleration a_{rad}, which is composed of

$$a_{\mathrm{rad}} = a_{\mathrm{lines}} + a_{\mathrm{thom}} + a_{\mathrm{true\ cont}}, \quad (3)$$

i.e., of line and continuum contributions with the latter being further split into the Thomson term and the so-called "true continuum". In the CAK-like approaches, the very last term is omitted, while the line term is approximated in the form

$$a_{\mathrm{lines,CAK}} \propto \left(\frac{r^2 v}{\dot{M}}\frac{\mathrm{d}v}{\mathrm{d}r}\right)^{\alpha}. \quad (4)$$

While this approach allows a fast calculation based on only a few parameters, its simplifications are not sufficient for more dense winds as mentioned above.

One method to obtain a_{rad} without requiring CAK-like approaches is to use Monte Carlo (MC) simulations (Abbott & Lucy 1985; de Koter et al. 1993, 1997; Vink et al. 1999, e.g.), where the radiative acceleration is calculated by following energy packets throughout the stellar atmosphere, allowing for multiple line transitions. However, such MC models need a prescribed wind velocity law and thus can obtain consistency only on a global scale.

For a more detailed understanding, wind models have to be locally consistent, i.e. the hydrodynamic equation must be fulfilled at every point throughout the stellar atmosphere. This can be obtained by using a comoving frame (CMF) approach for the radiative transfer calculation, which yields the radiative acceleration as a function of radius. The results are then used to derive a consistent velocity field via the hydrodynamic equation. The first attempt in this direction with the PoWR code has been performed by Gräfener & Hamann (2005, 2008), constructing a hydrodynamically consistent models for a WC star and several hydrogen-rich WNL stars. Unfortunately their approach turned out to have certain limitations in terms of applicability and was computationally extremely time-consuming.

Both issues have now been addressed in a new approach which is not only faster, but also applicable to a wide range of hot star atmosphere models, including O and B stars. In contrast to the approach from Gräfener & Hamann (2005), the calculation of a force multiplier parameter is not required. The hydrodynamic equation is integrated inwards and outwards from the sonic point. Furthermore, several code improvements have been performed in order to allow faster and more detailed calculations.

A side product of these developments is the implementation of a hydrodynamically consistent treatment of the quasi-hydrostatic, subsonic layers, which has now become a standard branch in the PoWR code and allows the calculation of models that can be used to precisely analyze O and B star spectra. Details of this improvement are described in Sander et al. (2015). These improvements are also crucial for Wolf-Rayet stars with lower mass-loss rates, as successfully shown in the analysis of the SMC single WR-stars by Hainich et al. (2015).

3 Hydrodynamically consistent models

The integration of the hydrodynamic equation (1) requires the values of $a(r)$ and $a_{\rm rad}(r)$ to be given. Since the latter one requires a CMF radiative transfer calculation, hydrodynamic models cannot be calculated from scratch, but instead a start approximation is necessary. The best models for this task are atmosphere models, which might not be hydrodynamically consistent at each depth point, but at least in terms of the global energy budget. To obtain this budget the hydrodynamic equation is written in the form

$$v\frac{\mathrm{d}v}{\mathrm{d}r} + \frac{GM_*}{r^2} = a_{\rm rad} - \frac{1}{\rho}\frac{\mathrm{d}P}{\mathrm{d}r} \qquad (5)$$

and then integrated and multiplied with $\dot{M}$:

$$\dot{M}\int\left(v\frac{\mathrm{d}v}{\mathrm{d}r} + \frac{GM_*}{r^2}\right)\mathrm{d}r = \dot{M}\int\left(a_{\rm rad} - \frac{1}{\rho}\frac{\mathrm{d}P}{\mathrm{d}r}\right)\mathrm{d}r$$
$$L_{\rm wind} = W_{\rm wind} \qquad (6)$$

This equation describes the balance between the modeled wind luminosity of the model $L_{\rm wind}$ and the provided work $W_{\rm wind}$. Dividing Eq. (6) by $L_{\rm wind}$ yields the so-called *work ratio*

$$Q := \frac{W_{\rm wind}}{L_{\rm wind}}. \qquad (7)$$

While stellar atmosphere models with $Q < 1$ do not provide a radiation field that is sufficient to drive the wind, models with $Q > 1$ possess a radiation field that could actually drive a stronger wind while models with $Q = 1$ exactly provide the energy that is required to drive the wind. Models with $Q \approx 1$ are therefore the best choice to start the hydrodynamic calculations.

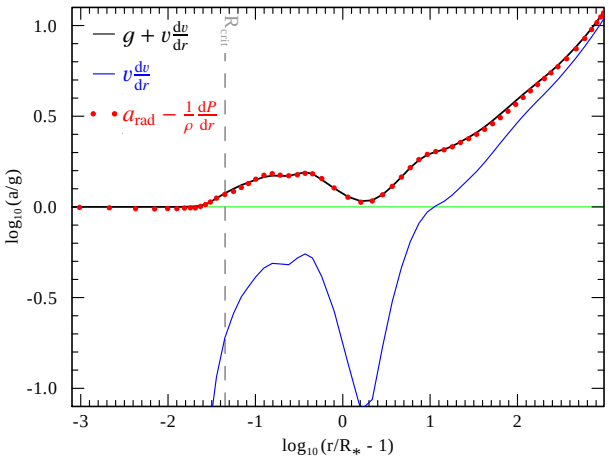

Fig. 1: Detailed acceleration balance for a hydrodynamically consistent WNE model. The black solid curve and the red dotted curve refer to the left and the right hand side of Eq. (5). The blue curve denotes the inertia term.

After a proper starting model is chosen, the velocity field is constantly updated by solving the hydrodynamic equation. Apart from this additional step, the atmosphere models are solved in the same way as models with a prescribed velocity field, i.e. until a consistent solution for the population numbers, the temperature structure, and the radiation field are obtained. Of course the update of the velocity field typically leads to larger corrections, thereby increasing the total calculation time of a hydrodynamically consistent model compared to a "standard" model. In contrast to the hydrostatic equation, the hydrodynamic equation (1) has a critical point, which is located at $v = a$, i.e. the sonic point. In order to have

a finite velocity gradient at the critical point, the right-hand side of Eq. (1) must vanish at the sonic point. The new velocity field is obtained by integrating the hydrodynamic equation inwards and outwards from the current critical point r_c, i.e. where the righthand side of Eq. (1) vanishes, and setting $v(r_c) = a(r_c)$. If necessary, the mass-loss rate $\dot{M}$ is also adjusted, so that $Q \approx 1$ is always maintained during the iteration.

The result of a converged model with a hydrodynamically consistent stratification can be seen in Fig. 1, where the acceleration contributions for a consistent, early-type, hydrogen-free WN star model are shown. The total outward forces, radiation and gas pressure, now balance the total inward forces, gravity and inertia, at each depth point throughout the stellar atmosphere.

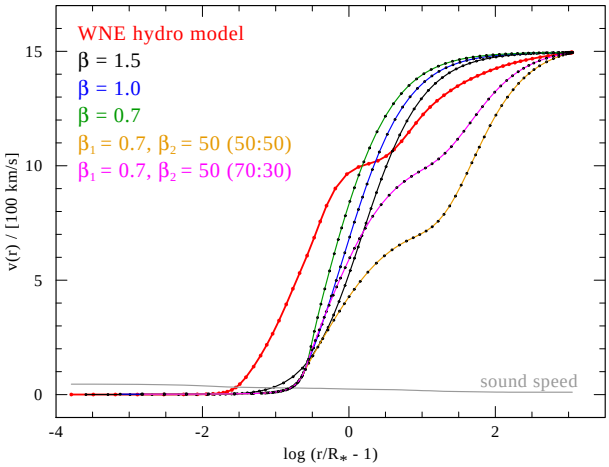

Fig. 2: The velocity field of the hydrodynamically consistent model (red curve) is compared to various prescribed velocity laws.

The velocity field obtained for the hydrodynamically consistent WNE star model is displayed in Fig. 2, where it is compared to several β-laws and two double-β-laws. The drop of the inertia term visible in Fig. 1 corresponds to the plateau in the velocity field seen here. Obviously a β-law is insufficient in describing the obtained velocity field in this example. In principle, the velocity field might be approximated by a double-β-law, but even though very few models have been calculated to far, it does not seem that there is something like a "typical" set of β-values which could be used to describe WR star velocity fields. For hydrogen-rich WR stars, Gräfener & Hamann (2008) showed that the hydrodynamic velocity fields could be approximated by a standard β-law. However, these stars are more like O stars and have less dense winds. Nevertheless, even for dense winds it might be hard to obtain "typical" values as a further model for WO star developed in this work did not show a similar plateau in the velocity field. Instead detailed calculations will likely need to be carried out at least for each spectral WR subtype. Assuming a β-law for dense winds in order to obtain the wind velocity at a certain distance can therefore only be a rough approximation, especially in the inner parts of the wind.

4 HD models as a diagnostic tool

In order to yield proper results for the mass-loss rates, the atmosphere models need to consider all elements which contribute significantly to the radiative acceleration due to their opacities. While this means that a large number of levels has to be accounted for, it also opens the perspective of using hydrodynamically consistent models as diagnostic tools, since detailed information about the depth-dependent contribution of each element is automatically obtained during the calculations of the CMF radiative transfer. These models will therefore allow a detailed study of the wind acceleration around the sonic point, including a check of the CAK approximations.

References

Abbott, D. C. 1980, ApJ, 242, 1183
Abbott, D. C. & Lucy, L. B. 1985, ApJ, 288, 679
Barlow, M. J. & Cohen, M. 1977, ApJ, 213, 737
Castor, J. I., Abbott, D. C., & Klein, R. I. 1975, ApJ, 195, 157
de Koter, A., Heap, S. R., & Hubeny, I. 1997, ApJ, 477, 792
de Koter, A., Schmutz, W., & Lamers, H. J. G. L. M. 1993, A&A, 277, 561
Friend, D. B. & Abbott, D. C. 1986, ApJ, 311, 701
Gayley, K. G. 1995, ApJ, 454, 410
Gräfener, G. & Hamann, W.-R. 2005, A&A, 432, 633
Gräfener, G. & Hamann, W.-R. 2008, A&A, 482, 945
Hainich, R., Pasemann, D., Todt, H., et al. 2015, A&A, 581, A21
Kudritzki, R. P., Pauldrach, A., Puls, J., & Abbott, D. C. 1989, A&A, 219, 205
Lamers, H. J. G. L. M. & Leitherer, C. 1993, ApJ, 412, 771
Lucy, L. B. & Solomon, P. M. 1970, ApJ, 159, 879
Pauldrach, A., Puls, J., & Kudritzki, R. P. 1986, A&A, 164, 86
Puls, J., Springmann, U., & Lennon, M. 2000, A&AS, 141, 23
Sander, A., Shenar, T., Hainich, R., et al. 2015, A&A, 577, A13
Vink, J. S., de Koter, A., & Lamers, H. J. G. L. M. 1999, A&A, 350, 181
Wright, A. E. & Barlow, M. J. 1975, MNRAS, 170, 41

Luca Grassitelli: Is the transition between the two velocity laws corresponding to a specific temperature or physical conditions?

Andreas Sander: In the hydrodynamically-consistent models throughout the atmosphere there is just one velocity law. If you refer to the transition from subsonic to supersonic, this is highly model-dependent and has to do with the opacities, mostly iron. There are just very few models so far, so I cannot really say anything about trends, but I doubt that you can assign a temperature to the transition which would hold for more than a particular model. In the standard models using a hydrodynamically-consistent solution in the quasi-hydrostatic regime and a beta-law outwards, we use the criterion of a constant velocity gradient for finding a connection point between the two laws.

Norbert Langer: Can line driving explain the WR winds even if the radii of WR stars are just $1\,R_\odot$ rather than $3\,R_\odot$?

Andreas Sander: So far, just a handful of models have been calculated, but the WNE and the WNO model shown in the talk both have $R_* < 1\,R_\odot$. More calculations have to be done in order to check if this also holds for a broader range of WR stars,

Jorick Vink: Did you need to adopt a clumping factor to achieve consistent models? And if so, what was the assumed value of D?

Andreas Sander: Yes, the models indeed assume a clumping factor, more precisely a depth-dependend one. The clumping in the test models so far starts around the sonic point and increases outwards with maximum values on the order of $D \approx 10$.

Götz Gräfener: Could you reproduce the observed terminal wind velocities with moderate clumping factors of ≈ 10?

Andreas Sander: The WNE star model is actually not adjusted to fit a particular observation, although its spectral appearance is not so far from a WN4 star. The WNE model uses a depth-dependent clumping with a maximum density contrast of $D = 20$. The WO model is based on the results of Tramper et al. (2015) and requires indeed only a maximum value of $D = 10$ to reproduce the terminal velocity of $\approx 5000\,\mathrm{km/s}$.

Wolf-Rayet Stars
W.-R. Hamann, A. Sander, H. Todt, eds.
Potsdam: Univ.-Verlag, 2015
URL: http://nbn-resolving.de/urn:nbn:de:kobv:517-opus4-84268

Magnetospheres of massive stars

M. Küker[1]
[1] *Leibniz-Institut für Astrophysik Potsdam, Germany*

We study the interaction of line-driven winds from massive stars with the magnetic field rooted in these stars by carrying out numerical simulations using the Nirvana MHD code in 2D in spherical polar coordinates. The code's adaptive mesh refinement feature allows high spatial resolution across the whole simulation box. We study both O and Wolf-Rayet stars for a range of magnetic field strengths from weak to strong as measured by the confinement parameter. For weak fields our simulations show that the initially dipolar field opens up far away from the star and a thin disk-like structure forms in the equatorial plane of the magnetic field. For stronger fields the disk is disrupted close to the stellar surface and closed field lines persist at low latitudes. For very strong fields a pronounced magnetosphere forms where the gas is forced to move along the field lines and eventually falls back to the stellar surface.

1 Introduction

Massive stars lack outer convection zones and are therefore not expected to show magnetic activity as observed on stars on the lower main sequence. Nevertheless, surface magnetic fields have been detected for a number of these stars, often with field strengths of the order 1 kG (Hubrig et al. 2011; Petit et al. 2013). As these objects lose mass through line driven winds, such strong magnetic fields must be expected to have a profound impact on the gas flow in the vicinity of the star. Babel & Montmerle (1997) proposed the Magnetically Confined Wind Shock model to explain the X-ray emission of Bp/Ap stars. In this model the wind is trapped in a dipolar field and channeled towards the equatorial plane where gas flows from both hemispheres collide. For the more massive OB stars with their high mass loss rates the gas can no longer be expected to flow along the field lines far away from the stellar surface. Numerical simulations of θ^1 Ori C by ud-Doula & Owocki (2002) indeed show that the initially dipolar magnetic field opens up except for a region at low latitudes and of limited radial extent, where the field lines remain closed and the gas is trapped and actually falls back towards the star. To characterise the magnetic field strength in terms of the kinetic energy of the gas, ud-Doula & Owocki (2002) define the magnetic confinement parameter,

$$\eta_* = \frac{B_0^2 R_*^2}{4\dot{M} v_\infty} \tag{1}$$

where B_0 is the magnetic field strength at the poles. For small values of η_* no magnetosphere forms. For $\eta_* = 1$ a disk forms in the equatorial plane of the magnetic field where the gas density is enhanced and the flow speed reduced. For θ^1 Ori C a surface field of $\simeq$ 1kG leads to η_*=10 and the formation of a magnetosphere close to the star while at larger distances the flow structure is similar to the η_*=1 case.

Wolf-Rayet stars are the sources of winds with even higher mass loss rates than OB stars. So far little is known about possible magnetic fields. In this paper we present the first results for WR3. Lacking observational constraints, we show numerical simulations for both weak and strong magnetic fields.

2 Model setup

Our model setup is similar to that of ud-Doula & Owocki (2002). We use the Nirvana MHD code Ziegler (2004) in spherical polar coordinates with adaptive mesh refinement in two dimensions. The simulation box is a spherical shell. The inner boundary represents the stellar surface. The outer boundary does not represent a physical boundary. It is chosen far enough from the star to capture the essential physics of the interaction between magnetic field and wind inside the box. Typical choices are five to ten times the stellar radius, R_*. We choose 10 R_* for θ^1 Ori C and 5 R_* for WR3. The basic mesh is equidistant in both the radial and the meridional directions. We use a resolution of 256x128 cells and allow for five refinement levels, which brings the effective mesh size up to 8192x4096.

We start with a dipolar magnetic field that is aligned with the polar axis of the coordinate system. The velocity is purely radial and follows a β law,

$$v_r = v_\infty \left(1 - \frac{R_*}{r}\right)^\beta \tag{2}$$

where v_∞ is the terminal velocity and β a parameter of order unity. The density is then chosen to keep the mass flow constant throughout the box, i.e. $\rho = \dot{M}/4\pi r^2 v_r$. The gas is assumed isothermal, with the temperature the same as the effective temperature of the star. We use the line force as derived by Castor et al. (1975) in the parametrisation of ud-Doula & Owocki (2002).

The boundary conditions at the inner boundary keep the radial component of the magnetic field fixed while the meridional field component can vary. Density and radial velocity component are kept fixed while the meridional velocity component can vary. We apply the Nirvana code's built-in treatment of

the symmetry axis and outflow conditions on the outer boundary.

Tab. 1: Stellar and wind parameters used in this paper. The second column lists the units. The B_0 value is for $\eta_* = 10$.

		θ^1 Ori C	WR3
M	$M_\odot$	50	11
L	$L_\odot$	10^6	3.8×10^5
$T_{\rm eff}$	K	50,000	85,000
R	cm	1.3×10^{12}	2×10^{11}
$\dot{M}$	$M_\odot$/a	2.6×10^{-6}	5×10^{-6}
v_∞	km/s	2,300	2,200
ρ_0	g/cm^3	4.3×10^{-11}	10^{-8}
$\bar{Q}$		500	2000
α		0.6	0.6
B_0	kG	0.95	8.33
β		1	0.8

To verify our setup we reproduce the model of ud-Doula & Owocki (2002) for θ^1 Ori C. We then study the Wolf-Rayet star WR3. The stellar and wind properties of this star have been adopted from Crowther (2007). The model parameters for both cases are summarised in Table 1. We choose the strength of the stellar dipole field such that η_* assumes values of 0.1 (weak field), 1 (intermediate), and 10 (strong field), respectively. For WR 3, this corresponds to polar field strengths of 0.833 kG, 2.6 kG, and 8.33 kG.

3 Results

In the non-magnetic case, it is possible to choose a start configuration that is already close to the steady final solution. The system then evolves through a transient phase before the final solution is reached. After that the system does not change any more. Figure 1 shows these steady solutions for the θ^1 Ori C and WR3 models. They are characterised by a sharp decrease of the density above the stellar surface and a corresponding increase of the gas velocity. At the outer boundary of the simulation box the radial gas velocity is approaching the terminal velocity. The radial velocity profiles are close to β laws as in Eq. 2 except close to the star. Note that despite the similar terminal velocities and mass loss rates the mass density in the θ^1 Ori C model is substantially lower than in the WR3 model because the radius of θ^1 Ori C is larger than that of WR3. The time needed to reach the steady state is essentially the time it takes the wind material to cross the simulation box, about 2×10^5 s for θ^1 Ori C and 2×10^4 s for WR 3. The reason for the shorter time scale is the smaller radius of WR3 and, consequently, the smaller simulation box.

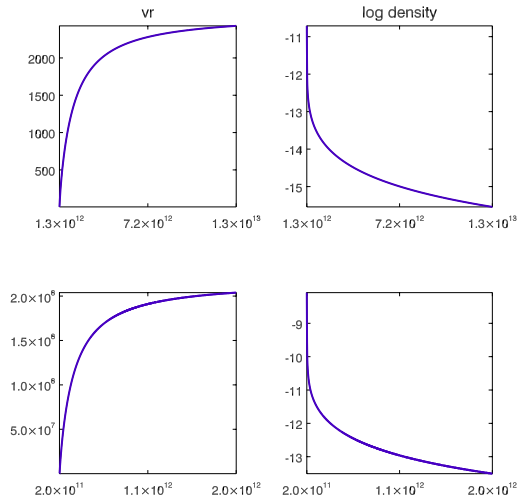

Fig. 1: The non-magnetic solution for θ^1 Ori C (top) and WR3 (bottom). Left: (radial) velocity, right: log(density). Units are km s^{-1} and g cm^{-3}.

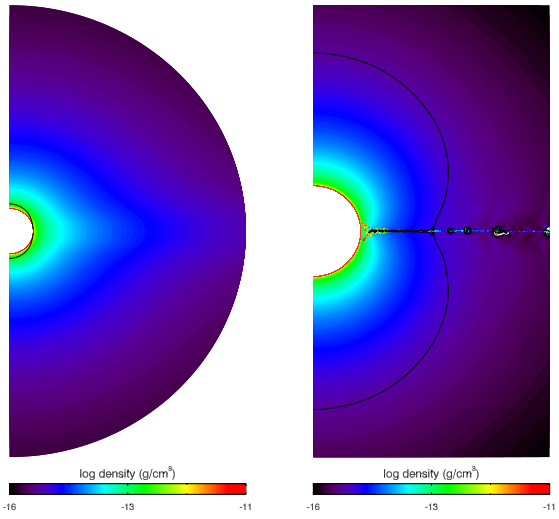

Fig. 2: The density distribution in the inner part of the simulation box for the θ^1 Ori C model with η_*=0.1 (left) and η^*=10 (right). The black line indicates η=1.

For finite field strength there is generally no steady solution. The system settles into a quasi-steady state after about the same time span as in the non-magnetic case but generally remains variable. The amplitude of the variation increases with increasing value of η_*. The variation is very small for η_*=0.1

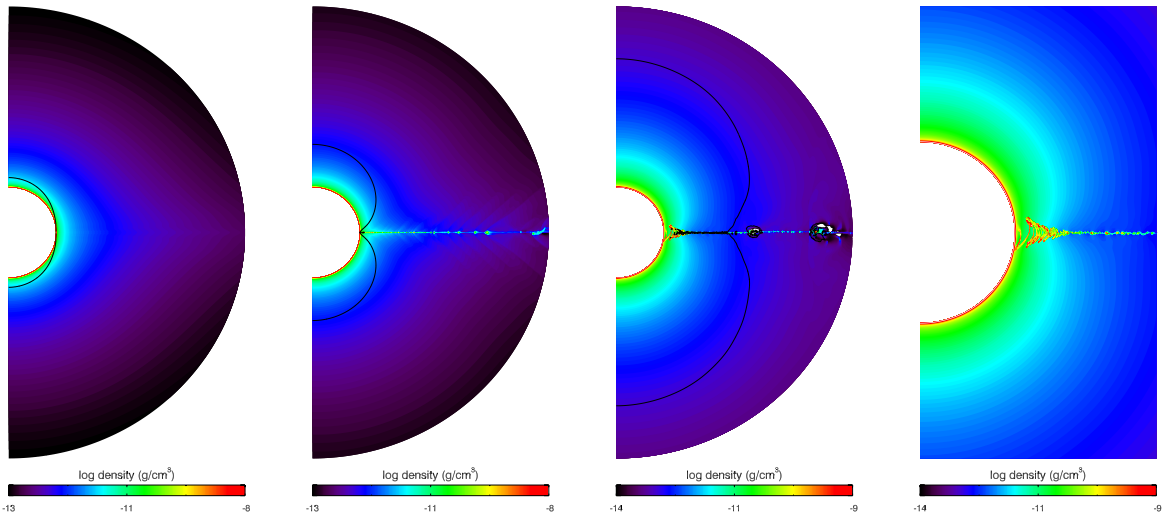

Fig. 3: Density distribution for the WR3 model with η_*= 0.1, 1, and 10 (from left) and a zoom into the inner region for η_*=10 (right panel). The black line indicates η=1.

but substantial for η_*=1 and η_*=10. Total run time is a multiple of the box-crossing time scale, i.e. 10^6 s for θ^1 Ori C and 10^5 s for WR3.

Our model for θ^1 Ori C largely reproduces the results of ud-Doula & Owocki (2002). Figure 2 shows the cases of a weak (η_*=0.1) and strong magnetic field (η_*=10; B_0=0.95 kG). The black line indicates the boundary between the magnetically dominated region and the region dominated by the kinetic energy of the gas, as defined by the ratio of the energy densities,

$$\eta = \frac{B^2/8\pi}{\rho v^2/2}. \quad (3)$$

In the weak field case the magnetically dominated region is limited to a small area right above the stellar surface while in the strong field case the magnetic field is dominant for several stellar radii above the stellar surface.

As in ud Doula & Owocki (2002), the density distribution is oblate for weak magnetic field and prolate for strong magnetic field. For η_*=1 a disk forms in the equatorial plane. The disk is broken up into multiple outwards-moving rings rather than smooth. This is even more pronounced in the strong field case, where we find the same snake-like gas distribution close to the stellar surface at low latitudes as ud-Doula & Owocki (2002).

Figure 3 shows the density distribution for the weak field, intermediate, and strong field cases of the WR3 model. As in case of θ^1 Ori C, the density contours are oblate for weak magnetic field while for intermediate and strong fields the contours are oblate except for the disk in the equatorial plane. Note that the range of density contours in the η_*=10 case is different from the weak field and intermediate cases. The presence of the magnetic field causes a steeper decrease of the density with radius and the formation of cavities behind the gas rings in the disk. The radial gas velocity shows the opposite behaviour to the density. With increasing field strength there is an increasing contrast between the outflow speeds at high and low latitudes, with the outflow being faster at high latitudes. The mass flux largely follows the density, as the latter varies more strongly with latitude than the gas velocity. Mass flux in the disk is strongly enhanced. The overall mass loss rate is slightly enhanced for weak magnetic field but substantially decreased for strong field.

Our findings for WR3 resemble those for θ^1 Ori C for the same values of the confinement parameter. Note though that the polar field strength of 8.33 kG needed for η_*=10 is very large and may not be realistic. As η_*=1 still requires a polar field strength of 2.6 kG, the weak field case may the most realistic. This would mean no notable variation with time but a pronounced flattening of the density distribution, as in the left panel of Fig. 3.

References

Babel, J. & Montmerle, T. 1997, A&A, 323, 121
Castor, J. I., Abbott, D. C., & Klein, R. I. 1975, ApJ, 195, 157
Crowther, P. A. 2007, ARA&A, 45, 177
Hubrig, S., Schöller, M., Kharchenko, N. V., et al. 2011, A&A, 528, A151
Petit, V., Owocki, S. P., Wade, G. A., et al. 2013, MNRAS, 429, 398
ud-Doula, A. & Owocki, S. P. 2002, ApJ, 576, 413
Ziegler, U. 2004, Journal of Computational Physics, 196, 393

Jorick Vink: For the non-magnetic case, was the instability caused by the LDI (line-driven instability)?

Manfred Küker: Yes.

Andy Pollock: What is the ratio of the mass-loss rate through the disk and through the magnetosphere?

Manfred Küker: The local mass flux in the disk can easily exceed that in the magnetosphere by an order of magnitude, but the disk is too thin to dominate the mass loss. The exact value varies between models and with time, but 25 percent of the total mass-loss rate is a typical value for the region within $\pm 5^\circ$ of the equatorial plane (which makes for 8.7% of the total surface area).

Alex Gormaz-Matemala: How many Gauss does the model have? De la Chevrotière et al. have found an upper limit of only 100 G for WR 6.

Manfred Küker: About 1000 Gauss.

Eta Car, LBVs

Wolf-Rayet Stars
W.-R. Hamann, A. Sander, H. Todt, eds.
Potsdam: Univ.-Verlag, 2015
URL: http://nbn-resolving.de/urn:nbn:de:kobv:517-opus4-84268

Eta Carinae: Many Advances .... Even More Puzzles

T. R. Gull[1]
[1] *Code 667, NASA/GSFC, Greenbelt, MD, USA*

Since Augusto Damineli's demonstration in 1996 that Eta Carinae is a binary with a 5.52 year period, many innovative observations and increasingly advanced three-dimensional models have led to considerable insight on this massive system that ejected at least ten, possibly forty, solar masses in the nineteenth century. Here we present a review of our current understanding of this complex system and point out continuing puzzles.

1 The Historical η Car

Eta Argus (η Car in earlier nomenclature) burst upon the astronomical scene in the 1840s when southern observers noted the star brightened to rival Sirius, then faded (Davidson & Humphreys 1997). Late in the nineteenth century, it again brightened to almost naked-eye visibility, then faded. By the 1940s, Gaviola (1950, 1953) noted that the star was again brightening. Gaposchkin (1954) suggested η Car as a galactic nova with a possible period of 16.5 years. Later Zanella et al. (1984) noticed a potential eleven year period. Neugebauer & Westphal (1968) noted that η Car was the brightest ten micron source outside of the solar system. Davidson et al. (1986) noted that spectra, recorded of associated nebular ejecta by the *International Ultraviolet Explorer* and facilities at Cerro Tololo Inter-American Observatory, showed greatly enhanced nitrogen at the expense of carbon and oxygen, signifying that the Great Eruption of the 1840s came from a very massive star. Yet a stellar remnant with $5{\times}10^6$ $L_\odot$, remained. Weigelt & Ebersberger (1986), using ground-based speckle interferometry, noted that four point-like sources, separated by less that 0.3", were present. Even with the uncorrected primary optics of the Hubble Space Telescope, Weigelt et al. (1995) confirmed the four point-like structures using the Faint Object Camera (see Figure 1, Left), but Davidson et al. (1995), with the Faint Object Spectrograph, determined that the brighter component was a point stellar source, but the other three sources, commonly known as Weigelt blobs B, C and D, were very bright nebular clumps rivaling the brightness of the ionizing source.

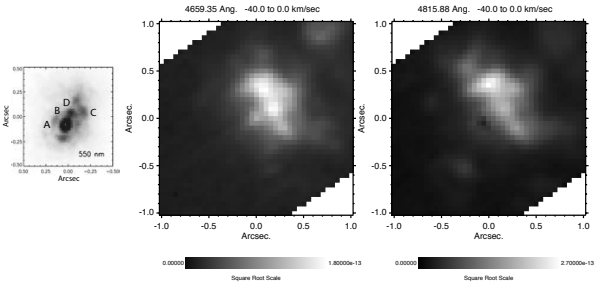

Fig. 1: The central region about η Car as imaged with HST. Left: FOC deconvolved imagery with the 550M filter, recorded in 1992 (Weigelt et al. 1995). Middle: STIS [Fe III] 4659Å and Right: STIS [Fe II] 4815Å. The continuum-subtracted STIS images, recorded in 2012, are 40 km/s wide centered at -20 km/s (Gull et al. in prep). In the two decades between the FOC and STIS observations, the central source brightened at least five-fold and the emission sources expanded and changed. Note that the forbidden emission line structures are exterior to the stellar point source.

2 What we learned since 1996

2.1 η Car has a 5.5-year period!

Interest greatly increased with the discovery by Damineli (1996) that η Car had a 5.52-year period defined by the drop in ionization state associable with the periastron passage, that was traceable back to the 1940s through spectroscopy by Gaviola (1950) and others. Corcoran et al. (1997) demonstrated that variable X-ray emission was associable with the interacting winds of η Car and began monitoring the X-ray flux with the Rossi X-ray Timing Explorer (*RXTE*). Steiner & Damineli (2004) detected He II 4686Å and its strengthening leading up to disappearance across the low (periastron) state. Ground-based spectroscopy and X-ray photometry has continued through early 2015 with focus on the behavior of He II 4686Å and X-ray flux especially across the periastron events (Damineli et al. 2008; Teodoro et al. 2012). The most current period measures are from X-ray photometry: 2023.7+/- 0.7 days (Corcoran et al., submitted; see Corcoran, these proceedings), and from He II 4686Å: 2022.7+/-0.8 days (Teodoro et al., submitted).

Crucial to the studies of η Car over the past two decades has been the *HST* with the Wide Field/Planetary Camera-2 (WFPC2) (Trauger et al. 1994) and the Space Telescope Imaging Spectrograph (STIS) (Kimble et al. 1998), both of which optimally sampled at, or close to, the diffraction limit of the *HST*.

The *HST*/WFPC2 provided sharp imagery of the Homunculus (see Middle of Figure 2) that revealed the dusty structure appeared to be bipolar with an

intervening skirt. Repeated visits revealed expansion over the sixteen year lifetime of WFPC2 in HST and the changing structure in the NUV within the Homunculus to the northwest (Smith et al. 2004). From early 1998 to 2004, a series of observations with the STIS recorded spectra of the star and selected emission structures within the Homunculus from below Lyman α to one micron. Hillier et al. (2001, 2006) using *CMFGEN* (Hillier & Miller 1998) to match the UV spectrum, found no direct evidence for η Car B, the secondary star, largely because of the very dense, extended wind of η Car A. While the spectrum of η Car B should peak in the Far UV, accessible to the Far Ultraviolet Spectrographic Explorer, *FUSE*, signatures of the primary wind and intervening material completely swamps any direct evidence.

Indirect evidence for the secondary star arises from X-ray spectroscopy. Pittard & Corcoran (2002) generated synthetic X-ray spectra that required a secondary mass loss rate, $\dot{M}_{\rm b} \approx 10^{-5}\ M_{\odot}{\rm yr}^{-1}$ with $v_{b,t} \approx 3000\ {\rm km\,s^{-1}}$. More recent models support those values for η Car B with the estimated values of $\dot{M}_{\rm a} \approx\ 8.5{\times}10^{-4}\ {\rm yr}^{-1}$ with $v_{a,t}$ =420 ${\rm km\,s^{-1}}$ (Madura et al. 2013, see also T. Madura, these proceedings).

Ground-based spectroscopy of η Car is greatly contaminated by both emission and scattered star light from associated nebulosities. Indeed approximately half of the visible radiation comes from the Homunculus and structures within. An extreme example is presented in Figure 1 which compares the emission recorded through the FOS 550M filter to low velocity images from the STIS centered on [Fe III] 4659.35Å and [Fe II] 4815.88Å. Within the central 0.15" region centered on η Car no [Fe II] and little [Fe III] emission is present. Teodoro et al (submitted) demonstrated that He II 4686Å originates in this central core and that ground-based measures overestimate core continuum due to starlight scattered by nearby structures. Hence, spatially-resolved spectroscopy with *HST*/STIS is critical for in-depth understanding of the central source AND the surrounding nebular structures.

2.2 The associated nebular structures

η Car is exceptional because 1) it has gone through major ejections within historical times, 2) the 1840s huge mass ejection kinetically rivals a supernova event but a massive binary survived, and 3) the massive binary has such massive interacting winds that many forbidden emission lines, characteristic of relatively high densities ($n_e \approx 10^7\,{\rm cm^{-3}}$) and relatively low ionization (I<40 eV and, for many structures, I<13.6 eV). Much can be learned about the ejecting star, the expanding ejecta – how the massive amounts of material evolve from heated, dense stellar atmospheres to compressed, rapidly cooling shells of gas that rapidly lead to molecular and dust formation – and the ongoing winds that form detectable fossil structures. Even more can be learned about nebular structures as a wide range of photoionization, temperature, density, shocks exists in the interacting winds, their persisting fossil structures, neutral- , ionized metal- and H II-regions, We can examine the multi-tiered structures that are spatially resolved by *HST*, spectrally probed by *Herschel* and many ground-based telescopes, especially instruments on the multiple *VLT* telescopes.

2.2.1 The Homunculus

Gaviola (1950) coined the name, Homunculus, based upon the humanoid-apparent nebulosity he photographed in the 1940s. As shown in Figure 2 (Middle), the *HST* visible wavelength image reveals a dusty, bipolar shell, centered on η Car with an apparent skirt located between the two lobes.

Spatially-resolved long slit spectra from Davidson et al. (2001) used a single *HST*/STIS long slit spectrum across the central axis and the *HST*/WFPC2 imagery to demonstrate the hourglass shape of the Homunculus. Five Gemini long-slit spectra in the near infrared detected a thin shell of H_2 that bounds a thicker interior structure seen in NIR [Fe II] (Smith 2006). A minimum of 10 $M_{\odot}$ of H_2 was estimated based upon an average density of 10^6 ${\rm cm^{-3}}$. However, Gull et al. (2005) derived densities of $n_e \approx 10^7$ ${\rm cm^{-3}}$ in a thin, interior, low-ionization, absorbing shell at a radial velocity of -513 km ${\rm s^{-1}}$.

More recently, *VLT*/XShooter mapping of the H_2 (Steffen et al. 2014, see Figure 2) demonstrated that the bipolar geometry is distorted by (1) holes in the caps near the axis of symmetry, (2) grooves in the caps that are point-symmetrical relative to the central source, (3) two proturbences near the equatorial region that roughly correspond to the 120^o angular separation of the bowshock defined by the interacting binary winds (see Subsection 2.2.5) and (4) significant dust between the fore and back walls, or interior to the H_2 shell.

The *HST*/STIS provided very high-spectral, high-spatial resolution spectroscopy from 1175 to 3160Å at critical orbital phases in the early 2000s from apastron across the 2003.5 periastron event (Gull et al. 2005; Nielsen et al. 2005). At an expansion velocity of -513 km ${\rm s^{-1}}$, nearly a thousand H_2 absorption lines were identified in the FUV as well as a similar number of singly-ionized metals absorption lines, including first time detection of V^+, Sr^+ and Sc^+ in interstellar space. Additionally, absorptions from CH, OH, CH^+ and NH in the NUV were seen originating from the ground state ($T_{\rm e} < 40\,{\rm K}$)(Verner et al. 2005b), but ionic metals at -513 km ${\rm s^{-1}}$ show transitions originating from energy levels consistent with $T_{\rm e} = 760\,{\rm K}$. While the many H_2 absorption lines were present across the broad high state, they

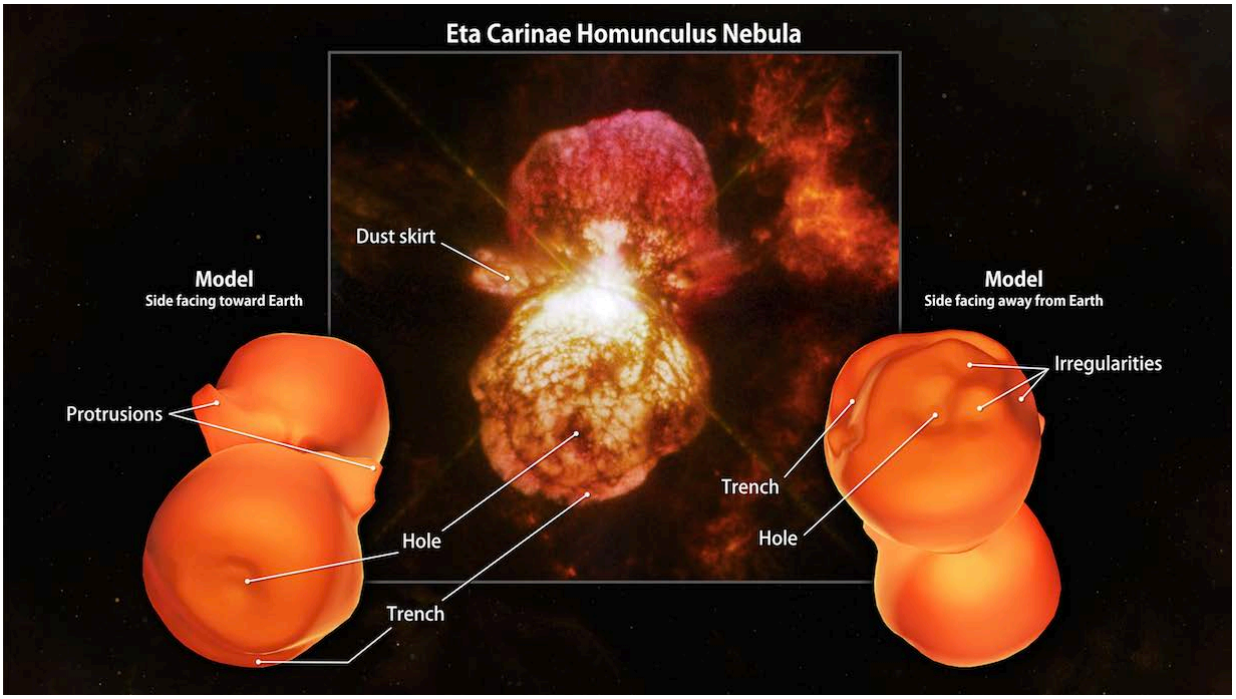

Fig. 2: Comparison of H_2 to the light-scattering dust spatial structures. Left: Projection of H_2 as seen from Earth. Center: *HST/WFPC2* image in near red light. Right: Projection of H_2 as seen from far side. Both the H_2 and dust images show evidence for side trenches and holes near center of the lobe caps, the dusty skirt is not seen in H_2, but two protrusions appear to correlate with obscurations against the far lobe. Likely the H_2 has been destroyed by ultraviolet radiation in the skirt region and interior to the thin H_2 shell.

disappear during the low ionization state as UV radiation short ward of 1700 Å disappears within the Homunculus across periastron. Additionally, absorption systems with velocities ranging between -513 and -384 km s^{-1} are present with with column densities that decrease with decreasing velocities. Is this evidence of changing mass loss properties between the 1840s and 1890s eruptions?

Despite η Car being the brightest ten-micron source (Neugebauer & Westphal 1968), the total amount of material ejected continues to be poorly determined. Chesneau et al. (2005) found the warm dust in the central 3" is corundum (Al_2O_3) and silicates. However, cooler dust and molecules exist in the outer Homunculus and are not easily quantified without additional studies and dust modeling. Consistent with the lower limit placed by Smith (2006), Morris (these proceedings) estimates that the total ejecta could exceed 40 $M_\odot$!

2.2.2 The Little Homunculus

Detailed mapping of the Homunculus with the *HST*/STIS 52" $\times$ 0.1" aperture, led to the detection of an ionized, internal bipolar structure, the Little Homunculus, seen in a number of [Fe II] lines with characteristic critical densities of $N_e = 10^6\,cm^{-3}$. The Little Homunculus has a line of sight at -147 km s^{-1}, but its caps expand at 300 km s^{-1}. Ishibashi et al. (2003) estimated a total mass of 0.1 to 0.5 $M_\odot$. STIS-measured proper motions are consistent with the 1890s mass ejection. While not seen during the high ionization state, saturated Ti^+ (ionization potential 13.58 eV) absorptions appear during the several month long low ionization state, signifying brief disappearance of Lyman continuum photons during periastron passage (Gull et al. 2006).

2.2.3 The Strontium Filament and the Butterfly

A most curious set of emission lines were noticed in the STIS spectra redward of Hα located about 2" north of η Car. Zethson et al. (2001) identified them to be [Sr II], leading to labeling this structure, the Strontium Filament. Hartman et al. (2004) found hundreds of forbidden emissions from singly-ionized metals with most being [Ti II]. These spectra led to greatly improved atomic models of singly-ionized iron-peak elements including Ti^+, Ni^+, Sc^+, Cr^+ and Mn^+ and reinforcement that both carbon and oxygen are so depleted that normal molecular and dust formation involving these elements is greatly reduced i.e. the chemistry leading to dust formed in the ejecta of η Car is very peculiar (Bautista et al.

2006, 2009, 2011).

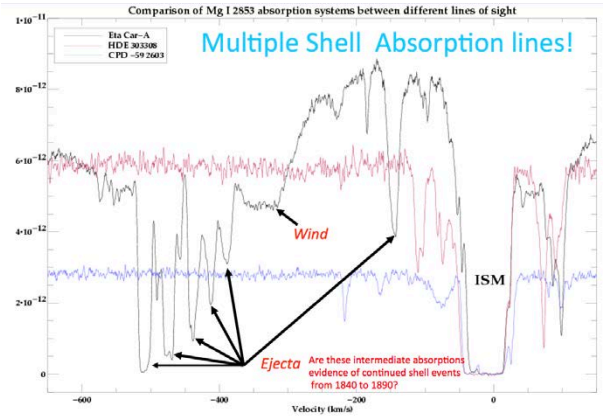

Fig. 3: Intermediate velocities seen in line of sight Multiple absorption components are seen in low ionization systems between -513 and -384 km s^{-1}. Are these evidence of declining wind properties between the 1840s and 1890s ejections?

Chesneau et al. (2005) noted that in the NIR a several arcsecond-sized butterfly-shaped cavity surrounds η Car. A spot inspection of these structures using STIS mapping spectra, discussed in section 2.2.5, indicate the butterfly boundaries are fainter versions of the Strontium Filament.

2.2.4 The Weigelt Blobs

The three very bright point-like emission structures, called Weigelt B, C and D (Weigelt & Ebersberger 1986), provide major clues as to the properties of the η Car binary and its recent history. Zethson et al. (2012) did a complete spectral inventory of Weigelt B and D from 1700 to 10,000Å during the low- and high-ionization states. Differences in nebular photoionization between the low- and high-ionization states led to estimates of the FUV properties of the secondary (Verner et al. 2005a; Mehner et al. 2010). With a temperature range from 32,000 to 39,000 K and $4{\times}10^5$ to 10^6 $L_\odot$, and mass loss rates estimated to be $\dot{M}{\approx}10^{-5}$ $M_\odot$yr^{-1}, the hidden secondary could still be an early WN or O star. Teodoro et al. (submitted) find that the blobs are partially-ionized surfaces of large, slow moving ejecta, possibly thrown out in the 1890s event. More observations and modeling are needed.

2.2.5 The Fossil Winds

The *HST*/STIS long slit observations indicated considerable wind/nebular emission structures in addition to the central binary and the Weigelt blobs and led to systematic mapping of the central 2"×2" region from June 2009 to March 2015, which spans the 5.53-year binary cycle (Gull et al., in prep). Spatially-resolved velocity structures extend out to 0.7" and from -420 to +400 km s^{-1} in multiple permitted and forbidden lines. Two forbidden lines, [Fe III] 4659Å and [Fe II] 4815Å, are well isolated and prove to be very effective tracers of fossil wind structures ranging from those being formed in the current cycle and those formed in previous cycles 5.52, 11.04, 16.08 years previously. To date, η Car uniquely provides these fossil winds because of the very massive interacting winds, highly eccentric orbit and hence variable ionization states. These forbidden emissions have critical densities, $N_e = 10^7$ cm^{-3} that are obtained by the interacting winds and resulting shocks.

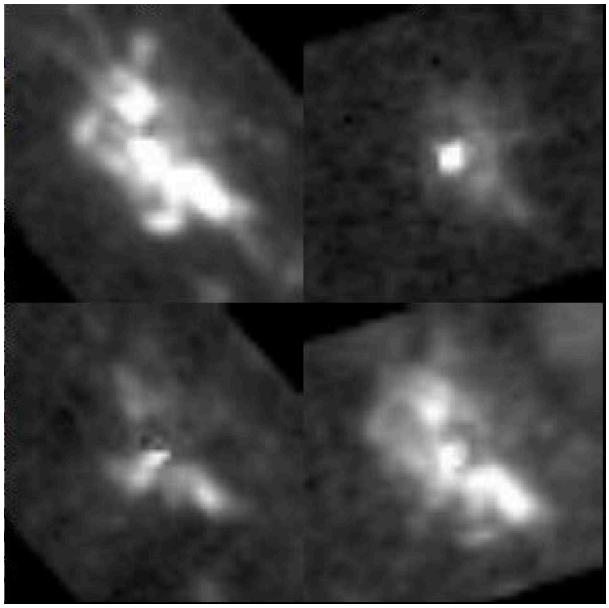

Fig. 4: Changes in photoionization of the fossil winds between the high- and low-ionization states Note the [Fe III] features at periastron (upper left) appear as [Fe II] features at apastron (lower right) correcting for 2.7 years expansion. Maps of continuum-subtracted [Fe III] 4659Å (upper row) and [Fe II] 4815Å (lower row) at apastron (left column) and periastron(right column). Field of view is 2". Velocity interval is -160 to -120 km s^{-1}.

Teodoro et al. (2013), using several sets of maps of [Fe II] and [Ni II] emissions recorded across the broad high state from 2010 to 2013, demonstrated that the red-shifted shells of primary wind were expanding at 470 km s^{-1}, consistent with the modeled primary wind velocity, 420 km s^{-1} as determined by Groh et al. (2012). These studies reinforce the three dimensional modeling of the interacting winds (Gull et al. 2009, 2011; Madura 2011; Madura et al. 2013, and Madura, this volume).

3 Questions that continue to challenge us today:

Our vantage point is such that several stellar magnitudes obscure our view. Yet so much nebular structure is in the vicinity that we can obtain indirect measures of the massive binary and answer some of our questions. However, for each question that is answered, two more questions appear. These include:

What is the current secondary?

Which star ejected during the Great Eruption?

Was the event a merger?

What caused the H_2 protrusions and are they clues to the ejection mechanism?

Are the multiple absorption velocities between -512 and -384 km/s evidence for decreasing primary mass loss properties between the 1840s and the 1890s events?

How and where did (do) molecules and dust form?

What is the total mass ejected in the Great Eruption?

How stable is the current binary system?

When will a supernova occur?

As I move to emeritus status at Goddard, I most sincerely thank the many collaborators with whom I have enjoyed these studies these past two decades.

References

Bautista, M. A., Ballance, C., Gull, T. R., et al. 2009, MNRAS, 393, 1503

Bautista, M. A., Hartman, H., Gull, T. R., Smith, N., & Lodders, K. 2006, MNRAS, 370, 1991

Bautista, M. A., Meléndez, M., Hartman, H., Gull, T. R., & Lodders, K. 2011, MNRAS, 410, 2643

Chesneau, O., Min, M., Herbst, T., et al. 2005, A&A, 435, 1043

Corcoran, M. F., Ishibashi, K., Davidson, K., et al. 1997, Nature, 390, 587

Damineli, A. 1996, ApJ, 460, L49

Damineli, A., Hillier, D. J., Corcoran, M. F., et al. 2008, MNRAS, 384, 1649

Davidson, K., Dufour, R. J., Walborn, N. R., & Gull, T. R. 1986, ApJ, 305, 867

Davidson, K., Ebbets, D., Weigelt, G., et al. 1995, AJ, 109, 1784

Davidson, K. & Humphreys, R. M. 1997, ARA&A, 35, 1

Davidson, K., Smith, N., Gull, T. R., Ishibashi, K., & Hillier, D. J. 2001, AJ, 121, 1569

Gaposchkin, C. P. 1954, Variable Stars & Galactic Structure. (Athlone Press)

Gaviola, E. 1950, ApJ, 111, 408

Gaviola, E. 1953, ApJ, 118, 234

Groh, J. H., Hillier, D. J., Madura, T. I., & Weigelt, G. 2012, MNRAS, 423, 1623

Gull, T. R., Kober, G. V., & Nielsen, K. E. 2006, ApJS, 163, 173

Gull, T. R., Madura, T. I., Groh, J. H., & Corcoran, M. F. 2011, ApJ, 743, L3

Gull, T. R., Nielsen, K. E., Corcoran, M. F., et al. 2009, MNRAS, 396, 1308

Gull, T. R., Vieira, G., Bruhweiler, F., et al. 2005, ApJ, 620, 442

Hartman, H., Gull, T., Johansson, S., Smith, N., & HST Eta Carinae Treasury Project Team. 2004, A&A, 419, 215

Hillier, D. J., Davidson, K., Ishibashi, K., & Gull, T. 2001, ApJ, 553, 837

Hillier, D. J., Gull, T., Nielsen, K., et al. 2006, ApJ, 642, 1098

Hillier, D. J. & Miller, D. L. 1998, ApJ, 496, 407

Ishibashi, K., Gull, T. R., Davidson, K., et al. 2003, AJ, 125, 3222

Kimble, R. A., Woodgate, B. E., Bowers, C. W., et al. 1998, ApJ, 492, L83

Madura, T. I., Gull, T. R., Okazaki, A. T., et al. 2013, MNRAS, 436, 3820

Madura, T. I. e. a. 2011, MNRAS, 125, 102

Mehner, A., Davidson, K., Ferland, G. J., & Humphreys, R. M. 2010, ApJ, 710, 729

Neugebauer, G. & Westphal, J. A. 1968, ApJ, 152, L89

Nielsen, K. E., Gull, T. R., & Vieira Kober, G. 2005, ApJS, 157, 138

Pittard, J. M. & Corcoran, M. F. 2002, A&A, 383, 636

Smith, N. 2006, ApJ, 644, 1151

Smith, N., Morse, J. A., Collins, N. R., & Gull, T. R. 2004, ApJ, 610, L105

Steffen, W., Teodoro, M., Madura, T. I., et al. 2014, MNRAS, 442, 3316

Steiner, J. E. & Damineli, A. 2004, ApJ, 612, L133

Teodoro, M., Damineli, A., Arias, J. I., et al. 2012, ApJ, 746, 73

Teodoro, M., Madura, T. I., Gull, T. R., Corcoran, M. F., & Hamaguchi, K. 2013, ApJ, 773, L16

Trauger, J. T., Ballester, G. E., Burrows, C. J., et al. 1994, ApJ, 435, L3

Verner, E., Bruhweiler, F., & Gull, T. 2005a, ApJ, 624, 973

Verner, E., Bruhweiler, F., Nielsen, K. E., et al. 2005b, ApJ, 629, 1034

Weigelt, G., Albrecht, R., Barbieri, C., et al. 1995, in Revista Mexicana de Astronomia y Astrofisica Conference Series, Vol. 2, Revista Mexicana de Astronomia y Astrofisica Conference Series, ed. V. Niemela, N. Morrell, & A. Feinstein, 11

Weigelt, G. & Ebersberger, J. 1986, A&A, 163, L5

Zanella, R., Wolf, B., & Stahl, O. 1984, A&A, 137, 79

Zethson, T., Gull, T. R., Hartman, H., et al. 2001, AJ, 122, 322

Zethson, T., Johansson, S., Hartman, H., & Gull, T. R. 2012, A&A, 540, A133

André-Nicolas Chené: Is there any remaining argument to support the idea that η Car is *not* a binary?

Ted Gull: The recent periastron event (August 2014) arrived on schedule. Both X-ray and He II 4686Å photometry are consistent with binarity. But there will always be doubters.

Paul Crowther: Although η Car is unique it might resemble the nebula associated with AG Car in 10^4 years and NaSt1 (WR 122) shares some nebular similarities to η Car (high N/O ratio, high density, hot dust).

Ted Gull: The phase – post outburst – of η Car is transient. Likely the ejecta disperses on timescales of 10^4 years. There is no obvious evidence of another post outburst comparable to η Car in the Milky Way. But that does not exclude NaSt1 as being a more evolved analog.

Wolf-Rayet Stars
W.-R. Hamann, A. Sander, H. Todt, eds.
Potsdam: Univ.-Verlag, 2015
URL: http://nbn-resolving.de/urn:nbn:de:kobv:517-opus4-84268

Measuring η Carinae's High Mass Ejecta in the Infrared and Sub-millimeter

P. W. Morris[1]
[1]*IPAC, California Institute of Technology, Pasadena, CA, USA*

I address uncertainties on the spatial distribution and mass of the dust formed in η Carinae's Homunculus nebula with data being combined from several space- and ground-based facilities spanning near-infrared to sub-mm wavelengths, in terms of observational constraints and modeling. Until these aspects are better understood, the mass loss history and mechanisms responsible for η Car's enormous eruption(s) remain poorly constrained.

1 η Car's dusty Homunculus

The LBV and massive binary system η Car is one of the most extensively observed objects in stellar astronomy and has the highest flux density of any object at 25 μm (second only to Jupiter and Mars during opposition), yet the nature of the Homunculus nebula's infrared emission remains poorly understood. Prior to space-borne infrared observations, the total (gas + dust) mass of the nebula was estimated to be around 2.5 $M_\odot$, distributed in the lobes and equatorial skirt in two principle thermal components of 250 and 400 K (e.g. Davidson & Humphreys 1997). Infrared Space Observatory (ISO) spectroscopy covering 2.4–200 μm revealed much higher emission at $\lambda > 20$ μm than expected from 250 K dust, and by fitting blackbody SEDs modified with an emissivity factor suited to silicate grains $F_\nu \sim \nu^{1.22} B_\nu(T_d)$ to the thermal continuum, Morris et al. (1999) (hereafter M99) derived a 3-component model of $T_d = 110$, 190, and 400 K with a total dust mass $M_{dust} \geq 0.17$ $M_\odot$, or $M_{total} \geq 17$ $M_\odot$ for an ISM-like gas to dust ratio $\rho_{gd} = 100$.

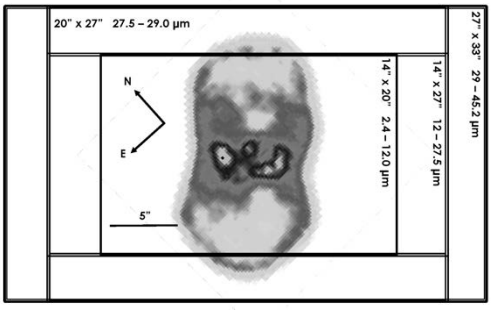

Fig. 1: Schematic layout of the ISO/SWS apertures on η Car during 1996 and 1997 observations. The 17 μm image of the Homunculus is from M99.

The main questions about η Car's dust are its location, especially the cool dust containing the bulk of the mass, and its composition given the uniqueness of nebular C- and O-depletion and N-enhancement (Hillier et al. 2001). The distribution is key to understanding the potential role of continued formation and destruction in the dynamic central region, i.e., in the colliding winds of the erupting OB-type primary star and its putative Wolf-Rayet star companion, versus the expanding lobes where the bulk of the dust would be condensed following the 1843 eruption that formed the nebula. The distribution could not be directly measured with ISO due to the large apertures of the SWS and LWS instruments compared to the $10'' \times 18''$nebula, but have been inferred by means discussed below, aided by recent observations of the sub-mm continuum and molecules such as CO, CH, HCO, and other hydrated N- and O-bearing species with the spectrometers onboard the *Herschel* Space Observatory (P.I. T. Gull; see these proceedings). The molecules can trace physical conditions at different locations in the Homunculus that can support dust formation and survival. An examination of the molecular gas in relation to the dust is a subject of our forthcoming paper.

2 Dust distribution, chemistry, and mass in the Homunculus

As mentioned, the apertures of the ISO spectrometers were large compared to the size of the Homunculus, however they did not completely encompass all nebula emission as assumed by Smith et al. (2003) and Gomez et al. (2006). The rectangular apertures were oriented with their cross-dispersive (spatial) minor axes parallel to the major axis of the Homunculus; see Fig. 1. The progressive increasing size of the apertures in this direction with wavelength, plus the peaked beam profile shapes should create discontinuities in the SED peaking near 25 μm from an extended emitting source in this setup, as observed in many ISO spectra of nebulae such as NGC 7027 and AG Car. The lack of beam-related jumps in the calibrated SED lead M99 to conclude that the emitting region is more compact than extended where the cool emission peaks, originating from within 6–8 arcsec of the core. M99 suggested that the source is unresolved in the mid-IR, perhaps in a torus geometry that is unrelated to previously detected features, but not that it is necessarily 1–2 arcseconds in size (as erroneously attributed by Davidson & Smith 2000). Some cool dust is expected

in the lobes on the basis of resolved H_2 observations (Steffen et al. 2014), however the observational constraints on the *bulk* of this component are inconsistent with primary location in the lobes as claimed by Smith et al. (2003) based on an incorrect supposition about the ISO apertures and ground-based imaging at wavelengths where the cool dust is undetectable.

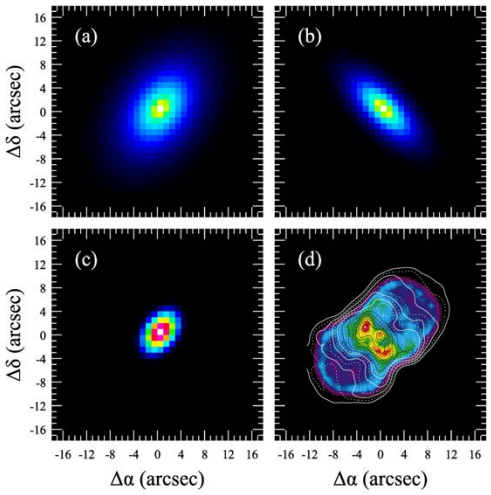

Fig. 2: Profiles from best-fit extended source corrections to the SPIRE spectra for elliptical profiles, scale diameters, and rotation angles of: (a) Sersic, 7.″0, 50°; (b) Sersic, 9.″5, 140°; and (c) Gaussian, 6.″5 (FWHM), 50°. A comparison TIMMI image of 17 μm emission with 10 μm contours is shown in panel (d), from M99.

Our *Herschel* observations sampling numerous molecular lines and the cool thermal emission support the conclusion of a dominant compact source of emission. The SPIRE spectrometer covering 194–601 μm has variable beam sizes with a drastic difference at ∼305 μm where the short and long wavelength modules overlap, causing a discontinuity of the two spectral fragments in the standard pipeline processing using point source calibrations on the one extreme, or fully extended calibrations on the other. This can be corrected interactively with different source profiles and semi-extended sizes (see Fig. 2), and indeed a best fit after removing background emission using off-axis detector elements is found with an elliptical sersic source profile with an effective diameter of 7.″0. This correction "closes the gap" between the SPIRE short and long wavelength spectra, and provides very good continuity (within 10%) with the ISO spectrum. Similar corrections are obtained in observations collected with the high velocity resolution HIFI instrument. Such agreement between ISO and *Herschel* observations is not expected *a priori* due to possible variability in the FIR continuum between the 1996–1997 and 2011–2013 observations. These data provide only indirect indications of the emitting source size. ALMA observations and our Cycle 3 SOFIA imaging program (P.I. P. Morris) over 19–38 μm will provide more direct measurements of the cool dust distribution.

The full SED of η Car comprised of the ISO and *Herschel* data as well as ALMA observations obtained by Abraham et al. (2014) and other ground-based sources, spanning 2 to 7000 μm, is shown in Fig. 3. The ground-based observations are all taken with large beams except for the ALMA data which were obtained with beams 0.″45 to 2.″88 FWHM from short to long wavelengths. With this extended dataset I have updated the 3-component model and obtain revised best-fit dust temperatures T_d = 400, 170, and 95 K, and respective dust masses of $3{\times}10^{-4}$, 0.095, and 0.17 $M_\odot$. The two coolest components have lower T_d than estimated from the original ISO data alone by M99. These values are markedly lower than deduced by Smith et al. (2003) who attempted to re-fit the same ISO observations published by M99, but used photometrically miscalibrated data (the standard archival data they used are uncorrected for high-flux non-linearities and detector hysteresis), and failed to recognize the solid state dust features over the 18–40 μm range, fitting through these instead and thus arriving at faulty temperatures and dust masses.

The method of fitting Planck curves to the SED provides a decent approximation of dust temperatures and masses, but for the dust chemistry and grain properties a full radiative transfer solution that models the observed solid-state features is required. This is the subject of our forthcoming paper, meanwhile I can summarize that fitting has been carried out using laboratory optical constants for a range of amorphous and crystalline silicates, glasses, metal oxides, pure metals, sulfides, and carbon-based dust (e.g. Jäger et al. 2003), and absorption coefficients for metal nitrides (Pitman et al. 2006). By and large the dust chemistry of the Homunculus is not surprising with a mix of Ca-, Fe-, Mg-, and Al-rich silicates (olivines, pyroxenes) and metal oxides (e.g. corundum) as well as a substantial presence of pure Fe grains. Each has a different characteristic T_d, where the coolest dust appears to be dominated by the Fe dust and to a lesser degree corundum which produce broad, smooth emission bands.

The large (≈0.5–10 μm diameter) grains are amorphous and crystalline, indicating condensation conditions of both slow annealing at high gas densities, and rapid cooling at lower densities. Whether there is a preference of either for the central region, skirt, or lobes is unknown, but it would not be unreasonable if the warm ($T_d > 115$ K) crystalline dust which contributes less than 10% to the total mass may be located in the lobes, possibly mixed with amorphous dust in layers exterior to the H_2 shells observed by Steffen et al. (2014). A second remarkable point is indications of nitrides, particularly in the red wing

of the broad 10 μm band which is primarily composed of metal-rich silicates. A full set of optical constants for the nitrides is not available so they cannot be included in the radiative transfer modeling, but indications of a relative contribution, if confirmed, would make η Car's N-rich nebula the only circumstellar environment so far with Si_xN_y dust. Si_3N_4 dust identified as pre-solar grains in meteorites are attributed to Type II supernovae (Nittler et al. 1995), but no characteristic feature in a stellar envelope has been unambiguously identified with nitrides that could not be subsequently linked to an alternative carrier (cf. Pitman et al. 2006).

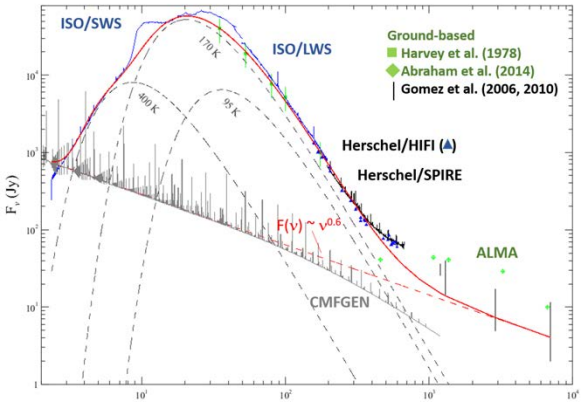

Fig. 3: The IR to sub-mm SED of η Car from combined ISO, *Herschel*, and ground-based data as labeled.

A total mass estimate for the Homunculus is obtained by summing the individual dust contributions scaled by the associated value of ρ_{gd}. A strong contribution of metallic Fe implies that ρ_{gd} is much higher than the ISM value as discussed by Gail et al. (2005). This is because only a fraction of the Fe gas condenses into grains (10–15% into pure Fe or FeS) leaving most Fe in the gas phase which is abundantly evident in η Car's spectrum (e.g. Hillier et al. 2001), and yielding a value of ρ_{gd} much higher than 100. Conversely ρ_{gd} based on the silicate and metal oxide content could be more ISM-like, as free atomic oxygen and carbon are depleted, present in the gas phase as molecules (OH, CH, CO, HCN, etc.).

Summing the contributions of dust at values of ρ_{gd} = 200 for the Fe dust and 100 for the silicates and oxides, a *lower* limit estimate of the total mass of the Homunculus is $M_{\rm tot} \geq 40$ M$_\odot$. This mass refers to the Homunculus, not in surrounding material as proposed by Gomez et al. (2006) who attribute excess sub-mm fluxes (see Fig. 3) observed though large beams to material of a pre-1843 outburst. Abraham et al. (2014) have shown with ALMA that this component (also detected with *Herschel*) is associated with an unresolved source of free-free emission near the core, probably arising from wind-wind interactions of the binary system (T. Gull, priv. comm.).

3 Conclusions

The distribution of dust in η Car's nebula, indicated to be concentrated within 6–7 arcsec around the core, is not certain without observations (e.g. ALMA, SOFIA) that can distinguish thermal components in the central region, skirt, and bi-polar lobes. The total mass $\geq$ 40 M$_\odot$ motivates us to consider the binary merger hypothesis as a potential scenario for the main eruption which formed the Homunculus, involving the release of kinetic energy through mass ejection from the merger of two rotating high mass stars, resulting in an eccentric orbit with a tertiary companion. This scenario has been proposed for Be supergiants and as a general phenomenon in LBVs (Podsiadlowski et al. 2006; Suzuki et al. 2007; Justham et al. 2014). If the bulk of the dust is concentrated in the core region, then continued formation (and destruction) in the colliding stellar winds similar to dusty WC binaries must also be taken into account in the mass budget.

References

Abraham, Z., Falceta-Gonçalves, D., & Beaklini, P. P. B. 2014, ApJ, 791, 95
Davidson, K., & Humphreys, R. M. 1997, ARA&A, 35, 1
Davidson, K., & Smith, N. 2000, Nature, 405, 532
Gail, H.-P., Duschl, W. J., Ferrarotti, A. S., & Weis, K. 2005, Fate of the Most Massive Stars, 332, 317
Gomez (Née Morgan), H. L., Dunne, L., Eales, S. A., & Edmunds, M. G. 2006, MNRAS, 372, 1133
Hillier, D. J., Davidson, K., Ishibashi, K., & Gull, T. 2001, ApJ, 553, 837
Jäger, C., Il'in, V. B., Henning, T., et al. 2003, J. Quant. Spec. Radiat. Transf., 79, 765
Justham, S., Podsiadlowski, P., & Vink, J. S. 2014, ApJ, 796, 121
Loinard, L., Menten, K. M., Güsten, R., Zapata, L. A., & Rodríguez, L. F. 2012, ApJ, 749, L4
Morris, P. W., Waters, L. B. F. M., Barlow, M. J., et al. 1999, Nature, 402, 502 (M99)
Nittler, L. R., Hoppe, P., Alexander, C. M. O., et al. 1995, ApJ, 453, L25
Pitman, K. M., Speck, A. K., & Hofmeister, A. M. 2006, MNRAS, 371, 1744
Podsiadlowski, P., Morris, T. S., & Ivanova, N. 2006, Stars with the B[e] Phenomenon, 355, 259
Smith, N., Gehrz, R. D., Hinz, P. M., et al. 2003, AJ, 125, 1458
Steffen, W., Teodoro, M., Madura, T. I., et al. 2014, MNRAS, 442, 3316
Suzuki, T. K., Nakasato, N., Baumgardt, H., et al. 2007, ApJ, 668, 435

Francisco Najarro: Are the ALMA continuum values consistent with the 1.2 and 2.9 mm observations from Cox et al. 1995?

Patrick Morris: My recollection is that they are different by 20% or more (I'm not sure about that number), but if the interpretation that the flux levels there are actually from wind-wind interaction between the companions (rather than an unresolved free-free shell) then you would expect some variability depending on orbit phase.

Anthony Marston: Does the temperature fit include full SPIRE SED information? Are there no cooler dust components than 110 K?

Patrick Morris: Our full model uses all of the ISO data plus the SPIRE SED, and HIFI continuum points. The SPIRE and HIFI data are converted assuming an emitting source size of 6.6 arcsec (giving a best fit to the ISO and ALMA data).

The full SED, excluding the ALMA points which are non-thermal, gives 95 K for the coolest component (slightly cooler that our ISO-only fit), but no other cool dust indicated.

Jose Groh: Could you remind us of the size of the ISO aperture and how that compares with the Homunculus size? Can you rule out that part of the $40\,M_{\odot}$ resides outside the Homunculus?

Patrick Morris: Going back to the slide which has the ISO apertures overlaid, the cross-dispersed (spatial) axes are oriented almost exactly along the 18" length of the Homunculus, and the apertures sizes vary in that direction from 14" to 40", in several steps. If we had emission from outside the Homunculus (where there may indeed be material from a previous eruption), or even significantly into the lobes, the spectral orders would have shown discontinuities given the ISO beam shapes, which they did not after flux calibration. The Herschel data do have off-source background corrections, and the remaining discontinuity in SPIRE is due to non point-like emission, and are well corrected with a 6 arcsec source size. Corrected this way, the agreement between Herschel and ISO is excellent, so we're confident that the emission is from the Homunculus, and in fact indicated to be dominated by the inner several arcsec. But we hope the answer on location will be settled by upcoming SOFIA observations.

Wolf-Rayet Stars
W.-R. Hamann, A. Sander, H. Todt, eds.
Potsdam: Univ.-Verlag, 2015
URL: http://nbn-resolving.de/urn:nbn:de:kobv:517-opus4-84268

Extremely Hard X-ray Emission from η Car Observed with *XMM-Newton* and *NuSTAR* around Periastron in 2014.6

K. Hamaguchi[1,2], M. F. Corcoran[1,3] and the η Car team
[1] *CRESST NASA Goddard Space Flight Center*
[2] *University of Maryland, Baltimore County*
[3] *Universities Space Research Association*

The super massive binary system, η Car, experienced periastron passage in the summer of 2014. We observed the star twice around the maximum ($\phi_{\rm orb}$ =0.97, 2014 June 6) and just before the minimum ($\phi_{\rm orb}$ =0.99, 2014 July 28) of its wind-wind colliding (WWC) X-ray emission using the *XMM-Newton* and *NuSTAR* observatories, the latter of which is equipped with extremely hard X-ray (>10 keV) focusing mirrors. In both observations, *NuSTAR* detected the thermal X-ray tail up to 40−50 keV. The hard slope is consistent with an electron temperature of ∼6 keV, which is significantly higher than the ionization temperature (kT ∼4 keV) measured from the Fe K emission lines, assuming collisional equilibrium plasma. The spectrum did not show a hard power-law component above this energy range, unlike earlier detections with *INTEGRAL* and *Suzaku*. In the second *NuSTAR* observation, the X-ray flux above 5 keV declined gradually in ∼1 day. This result suggests that the WWC apex was gradually hidden behind the optically thick primary wind around conjunction.

1 Extremely Hard X-ray Emission from η Car

The super massive binary system, η Car, has been known to emit strong thermal X-ray emission below 10 keV from collision of winds from two stars (wind-wind collision: WWC). See the details of the η Car system and its WWC X-ray emission observed in the 2−10 keV band in the reviews by T. R. Gull and M. F. Corcoran et al. in these proceedings.

On the other hand, its X-ray characteristics above 10 keV are not well understood due to the limited imaging capabilities of previous hard X-ray observatories. The *INTEGRAL*'s coded mask instrument, which enables to map extremely hard X-ray emission with angular resolution of 12′ (FWHM), detected a point-like source within 2.′4 of η Car (Leyder et al. 2008, 2010). Without any known high energy sources around, η Car is considered as the best candidate of its counterpart. The flat spectrum, extending up to 100 keV, requires a hard power-law component. The *Suzaku*'s hard X-ray detector (HXD), whose PIN sensor had had the best sensitivity between 15−50 keV before *NuSTAR*, confirmed the presence of hard power-law emission with $\Gamma \approx$1.4, as well as strong WWC thermal emission below ∼25 keV (Sekiguchi et al. 2009).

The *AGILE* and *Fermi* γ-ray observatories discovered a relatively stable γ−ray source to the direction of η Car between 0.1−100 GeV (Tavani et al. 2009; Abdo et al. 2010). Eta Carinae is, again, the only known high energy source within its error circle, but its extremely high energy nature — as energetic as a neutron star — was unexpected from η Car. One promising mechanism that may explain both the extremely hard X-ray emission and the γ-ray emission is the acceleration of particles at the WWC regions to the GeV energy through the 1st-order *Fermi* mechanism; such particles should upscatter stellar UV up to γ-rays by Compton recoil. However, neither of the extremely hard X-rays nor GeV γ-rays looks well correlated with the WWC X-rays (Hamaguchi et al. 2014; Reitberger et al. 2015).

To understand the nature of extremely hard X-ray emission from η Car, we performed two joint broadband X-ray observations of the star with *XMM-Newton* and *NuSTAR* in the key orbital phases around periastron in the summer of 2014.6. *XMM-Newton* can obtain high resolution X-ray spectra below 10 keV covering the detailed profile of the Fe K emission line complex and the absorption structure of the Fe K edge, while *NuSTAR* can obtain high quality spectra in the hard X-ray band extending beyond 10 keV. Because *NuSTAR* is the first focusing X-ray telescope above 10 keV, it also allows us to determine an accurate location of the extremely hard X-ray source.

2 *XMM-Newton* + *NuSTAR* Observations in 2014.6

The first joint observation started on 2014 June 6 near periastron when the X-ray flux had already increased by a factor of 4 from that around apastron. The second observation started on 2014 July 28 when the X-ray emission had almost dropped by two orders of magnitude from the X-ray maximum — it was only several days before entering to the deep X-ray minimum phase when the WWC thermal X-ray emission is suspected to be eclipsed by the thick primary stellar winds.

Fig. 1 shows X-ray images of the η Car field in multiple energy bands during the first observation. Eta Carinae at center dominates emission below 30 keV; the source position does not shift significantly between the energy bands. The emission almost disappears in the 30−79 keV band.

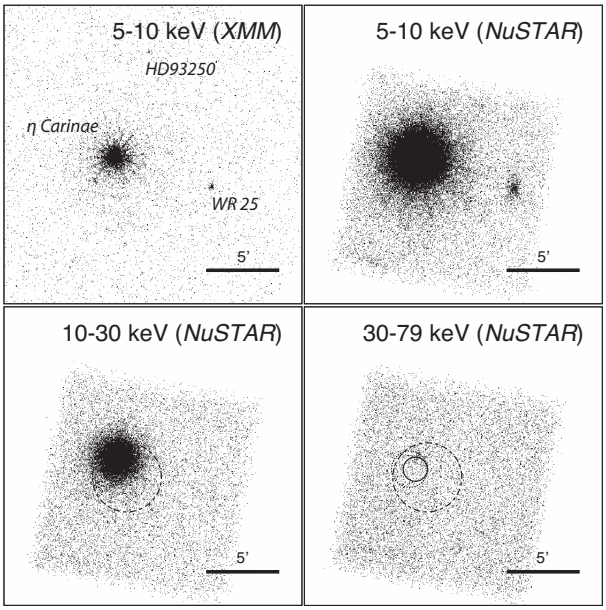

Fig. 1: X-ray images of the η Car field on 2014 June 6. The dotted bar circles show the 90% confidence range of the *INTEGRAL* source (Leyder et al. 2010) and the solid and dotted circles do the 95.4% confidence ranges of the *Fermi* source in the low-energy and high-energy bands, respectively (Reitberger et al. 2015).

2.1 First Observation

The *XMM-Newton* observation started 32 ksec after the start of the *NuSTAR* observation and covered a part of the latter half of the *NuSTAR* observation (top left panel of Figure 2). During these observations, η Car did not show any long-term X-ray variation, though it might exhibit small fluctuations on timescales of ∼1 ksec.

The top right panel of Figure 2 shows the *XMM-Newton* and *NuSTAR* spectra of η Car above 3 keV. The *NuSTAR* spectra clearly extend up to ∼50 keV. The spectral slope above ∼9 keV matches very well with optically-thin thermal emission from kT ∼6 keV plasma.

Both of the *NuSTAR* FPMA/FPMB spectra show marginal excess above 50 keV over the extrapolation of the thermal tail, but this excess is smaller than the raw background count rate. Since the image above 50 keV shows no hint of a point source at the η Car position, the excess is probably caused by uneven background structure.

2.2 Second Observation

The *XMM-Newton* observation started 20 ksec after the *NuSTAR* observation start and covered until the middle of the *NuSTAR* observation (bottom left panel of Figure 2). The short *XMM-Newton* observation for ∼34 ksec did not show a clear time variation, but the long *NuSTAR* observation for ∼102 ksec displayed a gradual flux decrease by ∼40% above ∼5 keV.

The 5−10 keV light curve seems to follow an exponential decay. We fitted this light curve by an exponential plus constant model and found an acceptable fit with an e-folding time of 0.48 (0.34−0.78) day. The 3−5 keV and 10−25 keV light curves also show similar flux declines.

The bottom right panel of Figure 2 shows the *XMM-Newton*/PN, MOS1 and *NuSTAR*/FPMA, FPMB spectra of the second observation. The spectra above ∼10 keV have a similar slope to those of the first observation, suggesting kT ∼6 keV plasma emission. They also showed an apparent small excess above 40 keV, but, again, the image above 30 keV did not show any clear point source at the position of η Car and this excess is lower than the background level.

We split the *NuSTAR* observation into three evenly spaced intervals and extracted spectra from each interval to track the spectral variation. The spectral shape above 5 keV did not apparently change between the intervals; only the spectral normalization decreased.

3 Nature of the Extremely Hard X-ray Emission

The *NuSTAR* spectra clearly showed that the thermal X-ray slope of η Car extended up to the 40−50 keV energy range. This slope is consistent with bremsstrahlung thermal emission with kT ∼6 keV, which was significantly higher than ionization temperature of Fe K shell ions measured from the *XMM-Newton* spectra. This result may suggest that the Fe K emission line has significant contribution of cooler plasma emission, or the hottest plasma does not reach ionization equilibrium.

During the second observation, the X-ray flux above 5 keV gradually declined by ∼40% in a day. This decline can be reproduced with a constant flux plus an exponential decay with τ ∼0.5−1.5 day, which smoothly connects to the deep minimum onset on August 1st. This decline shows no color variation, suggesting that the hottest plasma was gradually hidden from the sight. A spectral fit also suggests extremely strong absorption ($N_{\rm H}$∼7×10^{23} cm^{-2}), which is as high as the absorption measured after the deep minimum. These results support the hy-

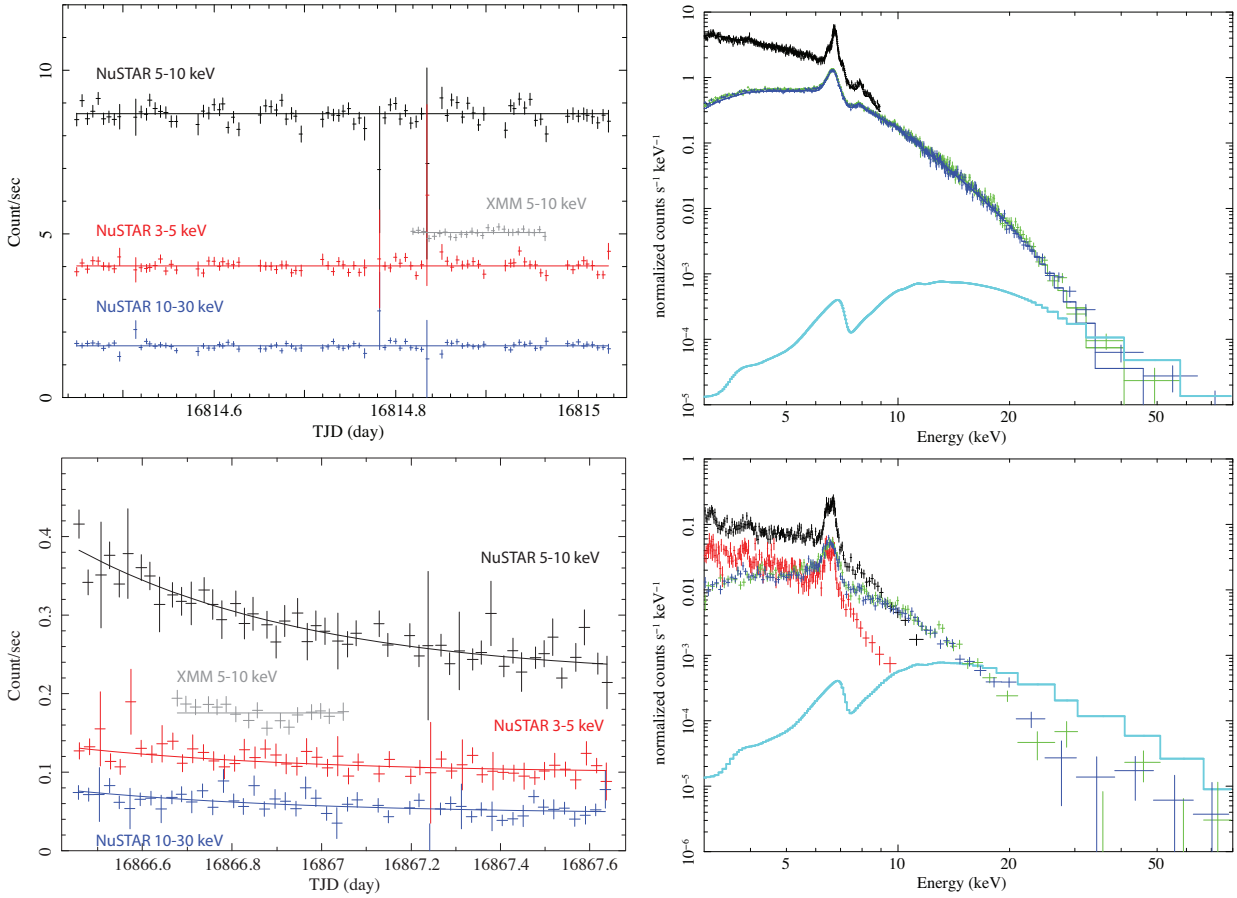

Fig. 2: Light curves (*left*) and spectra (*right*) of the first (*top*) and second (*bottom*) observations. *Left*: *XMM-Newton* EPIC PN (*grey*, 5−10 keV) and *NuSTAR*/FPMA+FPMB (*red*: 3−5 keV, *black*: 5−10 keV, *blue*: 10−30 keV) light curves. *Right*: *XMM-Newton* PN/MOS1 (*black*/*red*) and *NuSTAR* FPMA/FPMB (*green*/*blue*) spectra of η Car. The solid cyan line on each panel shows the power-law component measured from the *Suzaku* observations (Hamaguchi et al. 2014).

pothesis that the deep minimum is produced by an eclipse of the WWC apex by the thick primary wind at conjunction.

The *NuSTAR* data did not show any hint of power-law emission above ∼30 keV within the *INTEGRAL* error circle, giving an upper-limit below the *INTEGRAL* and *Suzaku* detection before 2011. The power-law source should have been faint during the observations in 2014. The GeV γ-ray source was rather stable around this orbital phase, suggesting an increase of the absorption to the power-law source during these observations, or no connection between the extremely hard X-ray and γ-ray power-law sources.

References

Abdo, A. A., Ackermann, M., Ajello, M., et al. 2010, ApJ, 723, 649
Hamaguchi, K., Corcoran, M. F., Takahashi, H., et al. 2014, ApJ, 795, 119
Leyder, J.-C., Walter, R., & Rauw, G. 2008, A&A, 477, L29
Leyder, J.-C., Walter, R., & Rauw, G. 2010, A&A, 524, A59
Reitberger, K., Reimer, A., Reimer, O., & Takahashi, H. 2015, ArXiv e-prints
Sekiguchi, A., Tsujimoto, M., Kitamoto, S., et al. 2009, PASJ, 61, 629
Tavani, M., Sabatini, S., Pian, E., et al. 2009, ApJ, 698, L142

Jesús A. Toalá: Why do you ignore the low energy part of the *XMM-Newton* spectrum ($E \leq 3\,\mathrm{keV}$)? It will help you to better constrain the column density!

Kenji Hamaguchi: The Eta Carinae spectra have multiple temperature components, each of which has individual line of sight absorption. The soft band spectrum mostly originates from cooler components and does not quite help to constrain the absorption to the hottest plasma. We normally use the Fe K edge feature at 7.1 keV for measuring absorption to the hottest plasma emission.

Lidia Oskinova: Very interesting result! Do you see any background source in *NuSTAR* images that could be confused with *Fermi* and *INTEGRAL* sources?

Kenji Hamaguchi: Thank you! No, we have not found any sources within the *Fermi* and *INTEGRAL* error circles in the *NuSTAR* hard band images.

Vikram Dwarkadas: You have assumed a mass-loss rate to carry out the simulations. Is the large column density consistent with the material in the wind + wind collision region, or do you need other absorbers?

Kenji Hamaguchi: The wind-wind colliding simulations using the current best estimate of the mass loss rate and the orbital parameters give the maximum absorption of $\sim 10^{24}\,\mathrm{cm}^{-2}$ or more around conjunction. This is consistent with the observed column density ($8 \times 10^{23}\,\mathrm{cm}^{-2}$) measured right before the bottom flux phase, deep minimum, which is probably produced by an eclipse of the wind-wind colliding plasma. We thus do not require additional absorption components to explain the observation result.

Wolf-Rayet Stars
W.-R. Hamann, A. Sander, H. Todt, eds.
Potsdam: Univ.-Verlag, 2015
URL: http://nbn-resolving.de/urn:nbn:de:kobv:517-opus4-84268

3D hydrodynamical and radiative transfer modeling of η Carinae's colliding winds

T. I. Madura[1], N. Clementel[2], T. R. Gull[3], C. J. H. Kruip[4], J.-P. Paardekooper[5] & V. Icke[4]
[1] *USRA & NASA Goddard Space Flight Center, Greenbelt, MD, USA*
[2] *South African Astronomical Observatory, Cape Town, South Africa*
[3] *NASA Goddard Space Flight Center, Greenbelt, MD, USA*
[4] *Leiden Observatory, Netherlands*
[5] *Universität Heidelberg, Germany*

We present results of full 3D hydrodynamical and radiative transfer simulations of the colliding stellar winds in the massive binary system η Carinae. We accomplish this by applying the SimpleX algorithm for 3D radiative transfer on an unstructured Voronoi-Delaunay grid to recent 3D smoothed particle hydrodynamics (SPH) simulations of the binary colliding winds. We use SimpleX to obtain detailed ionization fractions of hydrogen and helium, in 3D, at the resolution of the original SPH simulations. We investigate several computational domain sizes and Luminous Blue Variable primary star mass-loss rates. We furthermore present new methods of visualizing and interacting with output from complex 3D numerical simulations, including 3D interactive graphics and 3D printing. While we initially focus on η Car, the methods employed can be applied to numerous other colliding wind (WR 140, WR 137, WR 19) and dusty 'pinwheel' (WR 104, WR 98a) binary systems. Coupled with 3D hydrodynamical simulations, SimpleX simulations have the potential to help determine the regions where various observed time-variable emission and absorption lines form in these unique objects.

1 3D SPH Simulations of η Car's Colliding Winds

As already discussed in these proceedings (e.g. Gull, Morris et al., Corcoran et al., Hamaguchi et al.), Eta Carinae (η Car) and its surrounding bipolar Homunculus nebula constitute an ideal astrophysical laboratory for the study of massive binary interactions and evolution, and stellar wind-wind collisions. Recent three-dimensional (3D) simulations set the stage for understanding the complex time-dependent 3D stellar wind outflows in η Car. Spurned by recent suggestions that the mass-loss rate of the Luminous Blue Variable (LBV) primary star might have dropped by a factor of $2-3$ over roughly the past decade (Corcoran et al. 2010; Mehner et al. 2012), Madura et al. (2013) presented results from a series of 3D smoothed particle hydrodynamics (SPH) simulations of η Car's binary colliding winds assuming three different primary star mass-loss rates and using various computational domain sizes.

These SPH simulations reveal that the value of the primary's mass-loss rate greatly affects the time-dependent hydrodynamics of the wind-wind collision at all spatial scales investigated ($\sim$15.5 AU to 1550 AU). The SPH simulations also show that the post-shock wind of the companion star switches from the adiabatic to the radiative-cooling regime during periastron passage ($\phi \approx 0.985 - 1.02$). This switchover starts later and ends earlier the lower the value of the primary's mass-loss rate and is caused by the encroachment of the primary wind into the acceleration zone of the companion's wind, plus radiative inhibition of the companion's wind by the more luminous primary. This cooling switchover has important implications for understanding the peculiar behavior of η Car's X-ray light curve during the past two periastron passages, which showed an inconsistent recovery from the X-ray minimum (Corcoran et al. 2010, Corcoran et al., these proceedings).

Understanding the behavior of the post-shock companion wind in η Car is crucial for understanding the behavior of the X-ray light curve, since it is in the extremely hot (up to $\sim 10^8$ K) post-shock secondary wind that the majority of the hard X-rays observed are generated. As discussed in detail in Madura et al. (2013), the varying duration of η Car's X-ray minimum from cycle-to-cycle likely depends strongly on the length of time the post-shock secondary wind can remain in the radiative cooling regime during periastron passage. For most of η Car's highly eccentric orbit ($e \sim 0.9$), the post-shock companion wind cools adiabatically and thus remains relatively hot, generating hard X-rays. However, the cooling parameter χ that determines whether the post-shock gas is in the adiabatic or radiative cooling regime is proportional to the pre-shock wind speed to the fourth power (Stevens et al. 1992). Thus, even a small change in the pre-shock wind speed of the companion star can have a dramatic effect on the cooling of the post-shock gas.

Normally, we think of the radiatively-driven wind from a massive star as following a so-called β-law, wherein the wind speed at radius r is given by $v(r) = v_\infty(1 - R_\star/r)^\beta$, where v_∞ is the wind terminal speed and $R_\star$ the stellar radius. However, as discussed in Madura et al. (2013), because of the highly elliptical orbit and presence of the incredibly luminous primary star, the pre-shock companion wind speed in the η Car system is a complicated function

of the stellar luminosity ratio and stellar separation. The pre-shock wind speed of the companion star in η Car decreases by roughly a factor of three between apastron (phase 0.5) and phase 0.99 (Madura et al. 2013). Because the cooling parameter χ depends on the wind speed to the fourth power, a factor of three reduction in the companion's wind speed around periastron causes the post-shock gas to switch from being adiabatic to strongly radiative. This reduces greatly the volume of hot X-ray generating gas, and thus the observed X-ray flux. Only after periastron when the stellar separation starts to increase does the pre-shock companion wind speed also increase, and the post-shock gas can switch back to the adiabatic regime, again producing hard X-rays. The duration of the radiative cooling phase of the post-shock companion wind thus very likely affects the duration of the observed X-ray minimum and timing of the X-ray recovery following periastron.

Since the primary star in η Car is a known LBV subject to periods of instability, and because the wind-wind collision region is very chaotic and dynamic due to the various instabilities that arise at the interface between the two colliding winds (Stevens et al. 1992; Madura et al. 2013), it is reasonable to suggest that such instabilities and/or small variations in stellar/wind parameters can lead to changes in the overall pre-shock wind speeds, location of wind momentum balance, and duration of strong radiative cooling in the post-shock companion wind. Thus, changes in the duration of the X-ray minimum and timing of the X-ray recovery following periastron may be natural in a system like η Car.

2 3D Radiative Transfer Models

In addition to the 'current' colliding winds interaction responsible for the X-ray emission, which occurs in the innermost regions of the η Car system (at spatial scales comparable to the orbital semimajor axis length $a = 15.4$ AU), larger scale ($\sim$ 3250 AU diameter) 3D SPH simulations reveal outer wind-wind collision regions (WWCRs) that extend thousands of AU from the central stars (Madura et al. 2012, 2013). Long-slit spectral observations with the Hubble Space Telescope/Space Telescope Imaging Spectrograph (HST/STIS) reveal these spatially-extended WWCRs, seen via emission from multiple low- and high-ionization forbidden lines (Gull et al. 2009, 2011; Teodoro et al. 2013). Observations of the different broad high- and low-ionization forbidden emission lines provide an excellent tool to constrain the orientation of the system, the primary's mass-loss rate, and the ionizing flux of the hot secondary star. In addition to emission from forbidden lines, helium presents several interesting time-variable emission and absorption features that provide important clues on the geometry and physical proprieties of the system and the individual stars.

To set the stage for future efforts aimed at generating synthetic observations for comparison with available and future HST/STIS and ground-based data, we have performed a series of 3D radiative transfer simulations of the interacting winds in η Car. We use the SimpleX algorithm to post-process the 3D SPH simulation output and obtain detailed 3D maps of the ionization fractions of hydrogen and helium. The resultant ionization maps constrain the regions where observed forbidden emission lines can form, and the regions where helium is singly- and doubly-ionized.

Our SimpleX results recently appeared in the series of papers Clementel et al. (2014, 2015a,b). In Clementel et al. (2014), we focus on large-domain ($\sim$3250 AU diameter) simulations at an orbital phase of apastron, investigating the 3D ionization structure of the extended colliding wind structures assuming different primary mass-loss rates. These simulations are comparable in size to the HST/STIS observations of the extended forbidden emission structures (Gull et al. 2009, 2011; Teodoro et al. 2013). We find that at apastron, the dense primary wind confines the photoionization, and hence the forbidden line emission, to the secondary star's (and observer's) side of the system. Changing the primary's mass-loss rate results in quite different ionization volumes, with much more ionized gas present for lower mass-loss rates. The large apparent changes in ionization volume with decreasing primary mass-loss rate imply that any major decrease in primary mass-loss should lead to significant observable changes in the spatial extent, location, and flux (proportional to density squared) of the broad high-ionization forbidden emission lines. Future models based on the SimpleX results may be used to constrain any such potential mass-loss changes.

Clementel et al. (2015a) and Clementel et al. (2015b) investigate the ionization structure of helium in η Car's innermost regions ($\lesssim$310 AU in diameter) at apastron and periastron, respectively, for different primary mass-loss rates. We find that reducing the primary's mass-loss rate increases the volume of He^{+}. Doubly-ionized helium (He^{++}) only exists in the extremely hot post-shock secondary wind. At orbital phases near apastron, lowering the primary mass-loss rate produces large variations in the volume of He^{+} in the pre-shock primary wind located on the periastron side of the system. Our results show that binary orientations in which the secondary star at apastron is on our side of the system are most consistent with the available observations.

At an orbital phase of periastron, our simulations show that generally, He^{0+}-ionizing photons from the companion star are not able to penetrate into the pre-shock primary wind, and that He^{+} due to the companion's ionizing flux is only present in a thin layer along the leading arm of the inner WWCR and in a small region close to the stars. Lowering the primary's mass-loss rate allows the companion's

ionizing photons at periastron to reach the expanding unshocked secondary wind on the apastron side of the system, and create a low fraction of He^+ in the pre-shock primary wind. With the companion at apastron on our side of the system, our results are qualitatively consistent with the observed variations in strength and radial velocity of η Car's helium emission and absorption lines.

3 3D Visualization and Printing

3D hydrodynamical and radiative transfer simulations of η Car show that the complex time-varying WWCR has a major impact on the observed X-ray emission, the optical and ultraviolet light curves and spectra, and the interpretation of various line profiles and interferometric observables (see Madura et al. 2015, and references therein). While 3D simulations have helped to increase substantially our understanding of the present-day η Car binary, historically we have been limited by an inability to adequately visualize the full 3D time-dependent geometry of the WWCR. However, this is crucial if we are to thoroughly understand how and where various forms of observed emission and absorption originate.

In an effort to better understand the 3D structure of η Car's time-dependent WWCRs, Madura et al. (2015) recently published 3D interactive visualizations and 3D prints of η Car's colliding stellar winds at orbital phases of apastron, periastron, and three months after periastron. The figures in the PDF version of Madura et al. (2015), downloadable directly from the NASA ADS service (http://adsabs.harvard.edu/abs/2015MNRAS.449.3780M), are fully 3D interactive when using the standard Adobe Reader (https://get.adobe.com/reader/). The 3D models presented in Madura et al. (2015) also constitute the first 3D printable output from a supercomputer simulation of a complex astrophysical system.

The 3D visualizations and prints in Madura et al. (2015) reveal important, previously unknown 'finger-like' structures at orbital phases shortly after periastron (~ 1.045) that protrude radially outwards from the spiral WWCR. We speculate that these fingers are related to instabilities (e.g. thin-shell, Rayleigh-Taylor) that arise at the interface between the radiatively cooled layer of dense post-shock primary-star wind and the faster (~ 3000 km/s), adiabatic post-shock companion-star wind. The 3D visualizations also reveal that the inability of the companion star's wind to collide with the prmiary's downstream wind produces a large 'hole' in the trailing arm near the WWCR apex at periastron. The size of this hole is directly connected with the wind momentum ratio, and therefore the WWCR opening angle. As expected, higher primary mass-loss rates cause a larger hole than lower primary mass-loss rates. After periastron, this hole expands and propagates downstream along the vanishing WWCR trailing arm.

The success of the work in Madura et al. (2015) and the relatively easy identification of previously unrecognized physical features highlight the important role 3D printing and interactive 3D graphics can play in the visualization and understanding of complex 3D time-dependent numerical simulations of astrophysical phenomena. The 3D printable models of η Car's colliding winds and the η Car Homunculus nebula (Steffen et al. 2014) are freely available online at the NASA 3D Resources website http://nasa3d.arc.nasa.gov/.

References

Clementel, N., Madura, T. I., Kruip, C. J. H., Icke, V., Gull, T. R. 2014, MNRAS, 443, 2475

Clementel, N., Madura, T. I., Kruip, C. J. H., Paardekooper, J.-P., Gull, T. R. 2015a, MNRAS, 447, 2445

Clementel, N., Madura, T. I., Kruip, C. J. H., Paardekooper, J.-P. 2015b, MNRAS, 450, 1388

Corcoran, M. F., Hamaguchi, K., Pittard, J. M., et al. 2010, ApJ, 725, 1528

Gull, T. R., Madura, T. I., Groh, J. H., Corcoran, M. F. 2011, ApJL, 743, L3

Gull, T. R., et al. 2009, MNRAS, 396, 1308

Madura, T. I., Clementel, N., Gull, T. R., Kruip, C. J. H., Paardekooper, J.-P. 2015, MNRAS, 449, 3780

Madura, T. I., Gull, T. R., Okazaki, A. T., et al. 2013, MNRAS, 436, 3820

Madura, T. I., Gull, T. R., Owocki, S. P., Groh, J. H., Okazaki, A. T., Russell, C. M. P. 2012, MNRAS, 420, 2064

Mehner, A., Davidson, K., Humphreys, R. M., et al. 2012, ApJ, 751, 73

Steffen, W., Teodoro, M., Madura, T. I., et al. 2014, MNRAS, 442, 3316

Stevens, I. R., Blondin, J. M., Pollock, A. 1992, ApJ, 386, 265

Teodoro, M., Madura, T. I., Gull, T. R., Corcoran, M., Hamaguchi, K. 2013, ApJL, 773, L16

Thomas Madura (r.) with his η Car model from the 3D printer

Wolf-Rayet Stars
W.-R. Hamann, A. Sander, H. Todt, eds.
Potsdam: Univ.-Verlag, 2015
URL: http://nbn-resolving.de/urn:nbn:de:kobv:517-opus4-84268

Family ties of WR to LBV nebulae yielding clues for stellar evolution

K. Weis[1,2]
[1] *Astronomical Institute, Ruhr-University Bochum, Germany*
[2] *Lise Meitner fellow*

Luminous Blue Variables (LBVs) are stars is a transitional phase massive stars may enter while evolving from main-sequence to Wolf-Rayet stars. The to LBVs intrinsic photometric variability is based on the modulation of the stellar spectrum. Within a few years the spectrum shifts from OB to AF type and back. During their cool phase LBVs are close to the Humphreys-Davidson (equivalent to Eddington/Omega-Gamma) limit. LBVs have a rather high mass loss rate, with stellar winds that are fast in the hot and slower in the cool phase of an LBV. These alternating wind velocities lead to the formation of LBV nebulae by wind-wind interactions. A nebula can also be formed in a spontaneous giant eruption in which larger amounts of mass are ejected. LBV nebulae are generally small ($< 5\,\mathrm{pc}$) mainly gaseous circumstellar nebulae, with a rather large fraction of LBV nebulae being bipolar.

After the LBV phase the star will turn into a Wolf-Rayet star, but note that not all WR stars need to have passed the LBV phase. Some follow from the RSG and the most massive directly from the MS phase. In general WRs have a large mass loss and really fast stellar winds. The WR wind may interact with winds of earlier phases (MS, RSG) to form WR nebulae. As for WR with LBV progenitors the scenario might be different, here no older wind is present but an LBV nebula! The nature of WR nebulae are therefore manifold and in particular the connection (or family ties) of WR to LBV nebulae is important to understand the transition between these two phases, the evolution of massive stars, their winds, wind-wind and wind-nebula interactions. Looking at the similarities and differences of LBV and WR nebula, figuring what is a genuine LBV and WR nebula are the basic question addressed in the analysis presented here.

1 Massive stars, LBVs and WRs

Nearly all massive stars will turn into *Wolf-Rayet (WR)* stars at the end of their life. The WR star population spans an initial mass range of stars as low as $20\,\mathrm{M}_\odot$ to stars above $90\,\mathrm{M}_\odot$. Several evolutionary scenarios are proposed that lead to WR stars. One found and published by Meynet & Maeder (2005) is valid for stars with a rotation of $\mathrm{v_{ini}} \sim 300\,\mathrm{km/s}$ and will be be used here to put WR stars in context to other evolutionary phases.

M>90 $\mathrm{M}_\odot$:
O–Of–WNL–(WNE)–WCL–WCE–SN
M = 60–90 $\mathrm{M}_\odot$:
O–Of/WNL–LBV–WNL(H poor)–WCL-E–SN(SNIIn?)
M = 40–60 $\mathrm{M}_\odot$:
O–BSG–LBV–WNL–(WNE)–WCL-E–SN(SNIb)
alternative way:
O–BSG–LBV–WCL-E–WO–SN(SNIc)
M = 30–40 $\mathrm{M}_\odot$:
O–BSG–RSG–WNE–WCE–SN(SNIb)
alternative way:
O–BSG–OH/IR–LBV–SN(SNIb)

In several cases the WR phase is reached after the star was an *Luminous Blue Variable (LBV)*. The term LBV was introduced by Peter Conti rather ad hoc during a conference, stating that: "... I shall refer to the non W-R or other, hot stars as luminous blue variables, or LBV, in my talk..." (Conti 1984). Obviously not planned as a real definition but rather an easy reference for a diverse group of stars, this comment unified the already known Hubble-Sandage and S Dor variables, with the P Cygni and η Car type stars into one new class: the LBVs. It also explicitly excluded Wolf-Rayet stars from this group.

2 LBVs and LBV nebulae

Since then the LBV group has grown considerably and a clear definition of the term and class has been established. Luminous and blue are qualifications many massive stars possess, but variability is a or rather **the** key to identify LBVs. Two very distinct types of variability are known for LBVs.

The so called *S Dor variability* or S Dor cycle is a combined photometric and spectroscopic variation, see for example van Genderen et al. (1997); van Genderen (2001). During the S Dor cycle the star changes its radius and thereby spectrum. It moves from a hotter (visibly fainter) phase to a cooler (visibly bright) state and finally closes the cycle by returning to the hot (visibly faint) regime. During such a cycle the spectrum changes, as does the brightness in the visual regime of the light curve. This simultaneous change of visual brightness and stellar spectrum is observed in LBVs only. Even more energetic events are the *Giant Eruptions*. Here the visible brightness increases spontaneously by several magnitudes (Humphreys et al. 1999). Best known and well documented is the giant eruption of

η Carinae (in 1843), other giant eruptions are those of P Cygni, SN1961V, SN1954J. While LBVs have multiple S Dor cycles on very various timescales, spanning a few years to decade (van Genderen 2001) it is not clear if an LBV can undergo more than one giant eruption. LBVs can show one or both of these variations, but the detection of one is already sufficient for a star to qualify as LBV.
In the wake of several SN search programs so called SN imposters are found. These are SN-like events that for one or the other reasons (brightness, spectrum, lightcurve) are not clearly a SN. Many of these are good candidates for being an LBV giant eruption. Note however that a giant eruption may look like a SN imposter but not all SN imposters may be giant eruptions.

LBVs have a large mass loss rate and by changing their spectra an alternation of fast and slow wind phases. This gives rise to wind-wind interaction of the older, slow and dense wind during the cool spectral phase with the fast, less dense wind shedded during the hot phase. This interaction and sweeping up of material can lead to the formation of small and dense LBV nebulae. Alternatively a nebula is created as mass and several layers of the stars envelope are be ejected during a giant eruption.

LBV nebulae are small circumstellar structures with sizes of a fractions to a maximum of a few parsec (Weis 2011, 2013). With these sizes so far only galactic and LMC LBV nebulae are resolved (there is no SMC LBV nebula). Galactic LBV nebulae are generally smaller than nebulae around LMC LBVs. All nebulae show a nitrogen enhancement from the CNO processed material they contained. Expansion velocities are generally between 10–100 km/s (Weis 2011), with one major exception — structures in the outer ejecta of η Carinae reach several 1000 km/s (Weis et al. 2004), maybe even above 3000 km/s (Smith & Morse 2004). The expansion velocities are larger for galactic and lower for LMC nebula. As for the morphology, a few are spherical, so far only one, the nebulae around R 143, is rather irregular (Weis 2011). Given the star is situated in the middle of 30 Dor region and therefore subject to larger turbulent motions of the surrounding gas, this shape is not too surprising (Weis 2003). An astonishingly large fraction (77% of the galactic and 24% of the LMC nebulae) are bipolar. Bipolarity is found either in hourglass shapes like the Homunculus around η Car or in attachments often dubbed caps to the main body that kinematically manifest bipolar features by expanding in opposite directions, see the galactic LBV WRA 751 or R 127 in the LMC (Weis 2000, 2003). LMC nebulae are larger, expand slower and have a lower rate for bipolar morphology compared to the galactic LBV nebulae. Several physical mechanism are likely that lead to bipolarity.

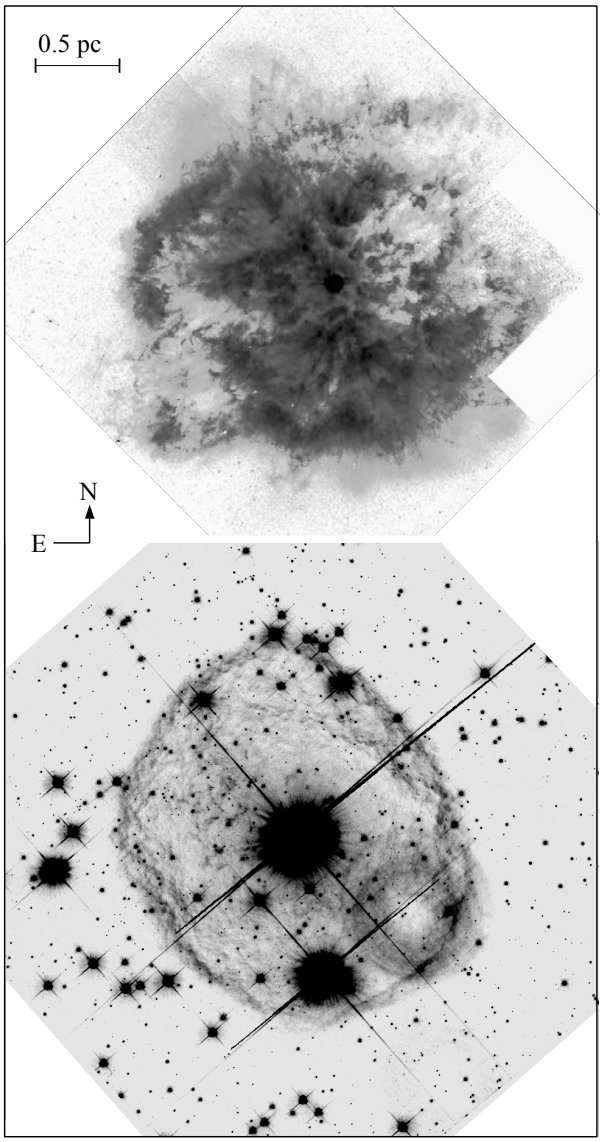

Fig. 1: The LBV nebulae around the Wolf-Rayet star WR 124 (top) and the LBV He 3-519 (bottom). A spherical structure SE of He 3-519 is caused by internal reflection in the instrument.

Promising scenarios are stellar rotation or a density gradient in the stellar wind. The latter might occur if the star passes the bistability limit (in a S Dor cycle) and the wind changes from polar to equatorial. Finally a binary system could do the job. There are two known LBV binaries, HD 5980 (Hoffman et al. 1978) and η Car (Damineli et al. 1997), but only one, η Car with a bipolar nebula, so this seems not the dominant process.

For at least two objects bipolarity can be linked to rotation. Both AG Car (Weis 2013, 2015) and HR Car (Weis et al. 1997) have bipolar nebulae and are fast rotators (Groh et al. 2006, 2009).

Are LBV nebulae formed via wind-wind interaction or eruptions? With the small sample of known giant eruption LBVs and nebulae formed thereby (2 known), it is currently hard to identify any differences in the scenarios. With the large kinematic ages of the known LBV nebulae ranging from 10^{3-4}yrs (Weis 2011) it also is not possible to exclude a giant eruption for all other LBVs since the eruption might have been several 1000 years ago and at that time was not observed or no records exits.

3 WR stars and WR nebulae

At the beginning it was shown that via various evolutionary scenarios nearly all massive stars turn into a WR star. Fast stellar winds (> 1000–2000 km/s) during the WR phase will compress remnant wind material shed during the star's previous phases (MS, LBV or RSG) and eventually for a WR nebula. The sizes WR nebulae are on average around 20–50 pc, the morphology is mostly spherical, elliptical or irregular but rarely if any bipolar. The expansion velocities range between a 10–80 km/s (few above 100 km/s), with an average around 50 km/s. The LMC WR nebulae are smaller and somewhat slower compared to the galactic objects, the same trend as observed for LBV nebulae!

4 LBV and/or WR nebulae

The major, maybe even the only difference between LBV and WR nebula as it turns out, is the lack of bipolar WR nebulae. Indeed only one object, the nebulae M1-67 around WR 124 (Sirianni et al. 1998) has been reported to have a bipolar component!

WR 124 and the M1-67 nebula:
The top panel in Fig. 1 shows the central part of the HST image of the nebula. The size is only 2–3 pc, making it one of the if not the smallest WR nebula. Already Sirianni et al. (1998) noticed and recent work by Fernández-Martín et al. (2013) further supported that the nebula abundances are with a N over and O underabundance atypical. The most straight forward conclusion for these values is simply that the nebula was formed during the LBV phase of the star. M1-67 is therefore a bipolar LBV nebula around a retired LBV, now a Wolf-Rayet star (WN8). So the count for known bipolar WR nebula should be set back to zero!

He 3-519:
The LBV He 3-519 has with about 2 pc one of the largest galactic LBV nebulae. In an ongoing analysis I found from kinematics hints that beside the more spherical or elliptical shape from the images (see Fig. 1) a weak but noticeable bipolar structure is present. The size of the nebula, the weak photometric variability and the spectral type WN11, suggest that He 3-519 is an LBV currently in transition to the WR phase. It is an LBV on the way to retirement.

5 The family ties

The examples of WR 124 and He 3-519 show nicely the transition – or family ties – of LBV to WR stars. The nebulae analysis helped to pinpoint the evolutionary status of the stars, both spectral classification WN, even better. WR 124 is the older retired LBV, He 3-519 is on the way to retirement.

The major difference of LBV and WR nebula is the lack of bipolar WR nebula. With the only bipolar WR nebulae actually being an LBV or ex-LBV nebulae this difference is gone. With other rather good similarities this gives rise to speculate about a new scenario: WR nebulae being aged, inflated LBV nebulae.

References

Conti, P. S. 1984, in IAU Symposium, Vol. 105, Observational Tests of the Stellar Evolution Theory, ed. A. Maeder & A. Renzini, 233

Damineli, A., Conti, P. S., & Lopes, D. F. 1997, New A, 2, 107

Fernández-Martín, A., Vílchez, J. M., Pérez-Montero, E., et al. 2013, A&A, 554, A104

Groh, J. H., Damineli, A., Hillier, D. J., et al. 2009, ApJ, 705, L25

Groh, J. H., Hillier, D. J., & Damineli, A. 2006, ApJ, 638, L33

Hoffman, M., Stift, M. J., & Moffat, A. F. J. 1978, PASP, 90, 101

Humphreys, R. M., Davidson, K., & Smith, N. 1999, PASP, 111, 1124

Meynet, G. & Maeder, A. 2005, A&A, 429, 581

Sirianni, M., Nota, A., Pasquali, A., & Clampin, M. 1998, A&A, 335, 1029

Smith, N. & Morse, J. A. 2004, ApJ, 605, 854

van Genderen, A. M. 2001, A&A, 366, 508

van Genderen, A. M., Sterken, C., & de Groot, M. 1997, A&A, 318, 81

Weis, K. 2000, A&A, 357, 938

Weis, K. 2003, A&A, 408, 205

Weis, K. 2011, in IAU Symposium, ed. C. Neiner, G. Wade, G. Meynet, & G. Peters, Vol. 272, 372–377

Weis, K. 2013, in ASP Conf. Ser., Vol. 470, 370 Years of Astronomy in Utrecht, ed. G. Pugliese, A. de Koter, & M. Wijburg, 129

Weis, K. 2015, A&A, in prep.

Weis, K., Corcoran, M. F., Bomans, D. J., & Davidson, K. 2004, A&A, 415, 595

Weis, K., Duschl, W. J., Bomans, D. J., Chu, Y.-H., & Joner, M. D. 1997, A&A, 320, 568

Jesús A. Toalá: If you take a look at the nebula around WR31a you will easily see that it is a bipolar WR nebula. Another WR nebula result of an LBV phase could be NGC2359 around WR7.

Götz Gräfener: Why is He3-519 classified as an LBV?

Kerstin Weis: While it is only slightly variable now (in van Genderen's classification = dormant) larger variability in the light curve is known from earlier observation. In my LBV definition term: it quaked.

Anthony (Tony) Moffat: Another indicator that WR124 in M1-67 may be at the beginning of its WR phase is that it is WN8h (as opposed to WN8o), implying that with relatively high H-abundance, it has just entered the WR stage.

Kerstin Weis: Thanks for the additional argument that is in well support of my scenario.

Anthony Marston: One note: LBV & WR nebulae basically form from LBV ejecta and should have similar metallicity. But WR stars show only ejecta nebulae in one third of the cases. Why might this be?

Kerstin Weis: In the WR phase, the strong stellar winds will act on the nebula. It will be inflated and the density decreases. So it might/will fall below the detection limit. Furthermore, not all WR stars are post-LBV objects.

Jose Groh: Are there estimates of nebular mass and dynamical age for WR124? In principle, the star would need to lose several $M_\odot$ to support the "retirement" scenario.

Kerstin Weis: The rough estimate I remember of the mass in the nebula as seen in the HST image (= the inner part) is around $1\,M_\odot$. The nebula however is much larger, so this is a lower limit, roughly consistent with what one expects.

Wolf-Rayet Stars
W.-R. Hamann, A. Sander, H. Todt, eds.
Potsdam: Univ.-Verlag, 2015
URL: http://nbn-resolving.de/urn:nbn:de:kobv:517-opus4-84268

HD 5980: wind collisions and binary star evolution

G. Koenigsberger[1]
[1]*Instituto de Ciencias Físicas, Universidad Nacional Autónoma de México, México*

HD 5980 is a multiple system containing at least 3 very massive and luminous stars. Located in the Small Magellanic Cloud, it is an ideal system for studying the massive star structure and evolutionary processes in low-metallicity environments. Intensely observed over the past few decades, HD 5980 is a treasure trove of information on stellar wind structure, on wind-wind collisions and on the formation of wind-blown circumstellar structures. In addition, its characteristics suggest that the eclipsing WR+LBV stars of the system are the product of quasi-homogeneous chemical evolution, thus making them candidate pair production supernovae or GRB progenitors. This paper summarizes some of the outstanding results derived from half a century of observations and recent theoretical studies.

1 Variable wind structure and wind collisions

The most prominent components of the HD 5980 system are the eclipsing binary pair, *Star A* and *Star B* ($P_{\rm orb}$=19.3d, e=0.3), both of which currently have a Wolf-Rayet type spectrum. *Star A* became the dominant component after the 1994 eruption, an event similar to the major eruptions observed in Luminous Blue Variables. A third component that is observed in the spectrum, *Star C*, is an O-type star with photospheric absorption lines indicating a highly eccentric orbit (P=97d, e ∼0.8; Schweickhardt 2000; Koenigsberger et al. 2014). A review of the pre-eruption and eruption properties is given in Koenigsberger (2004) and references therein.

Available spectroscopic observations date back to 1956 in the optical and to 1978 in the UV. An outstanding result concerns v_∞, the terminal wind velocity of *Star A*. Its value declined from ∼3000 km s^{-1} in 1979 to ∼300 km s^{-1} during the 1994 eruption, increasing thereafter. By 2014, it had once again attained speeds similar to those of 1979. These observations provide a unique testing ground for wind theory, specifically:

a) Wind-blown circumstellar structures. The interaction that occurs when a fast wind catches up and collides with a slow wind that was emitted previously is predicted to produce an expanding shell with a particular velocity structure. The very early stage of this phenomenon associated with the 1994 eruption was observed in HD 5980 (González & Koenigsberger 2014). A tantalizing possibility is that this event was not an isolated one, but that it re-occurs on a ∼40 year timescale (Koenigsberger et al. 2010), in which case the circumstellar vicinity of HD 5980 might be highly structured, with concentric high and low density regions.

b) Binary wind-wind interaction. The characteristics of the region where the winds of two stars collide are determined by the orbital separation, wind velocities and mass-loss rates. HD 5980 offers the extraordinary opportunity for studying this phenomenon in a system in which one of the two winds changes in a known manner over time. Thus, the morphology and strength of the interaction region may be predicted, and observable diagnostics compared with the actual observations. For example, the opening angle of the wind collision shock cone must have varied over time due to the changing wind momentum of *Star A*. By tracing spectral features over orbital phase at different epochs, the potential exists for answering the question of how much optical emission is produced in the shock cone region which, in turn, may help constrain the cooling efficiency.

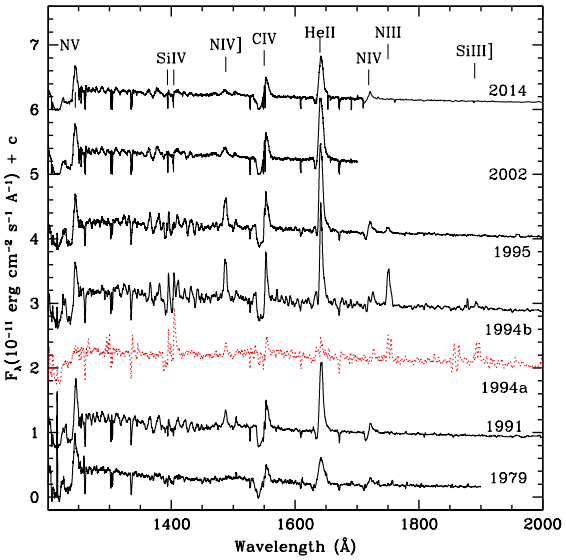

Fig. 1: UV spectra of HD 5980 obtained in 1979–1995 by *IUE* and 2002–2014 by *HST*/*STIS*. The spectrum during the maximum of the 1994 eruption was very similar to that of a B1.5I$^+$ star, but transitioned rapidly through WNL and into WN5-6.

c) Stellar wind structure. Empirical correlations have emerged from the UV observations of HD 5980 that relate wind velocity, continuum intensity and emission-line strengths (Georgiev et al. 2011). Com-

bined with the determination of luminosity (L), radius (R) and mass-loss rate ($\dot{M}$) from wind models for each of the corresponding epochs, the wind driving mechanisms may be directly tested. For example, we have found that the 1994 eruptive process involved an increase in L and $\dot{M}$ and a decrease in v_∞.

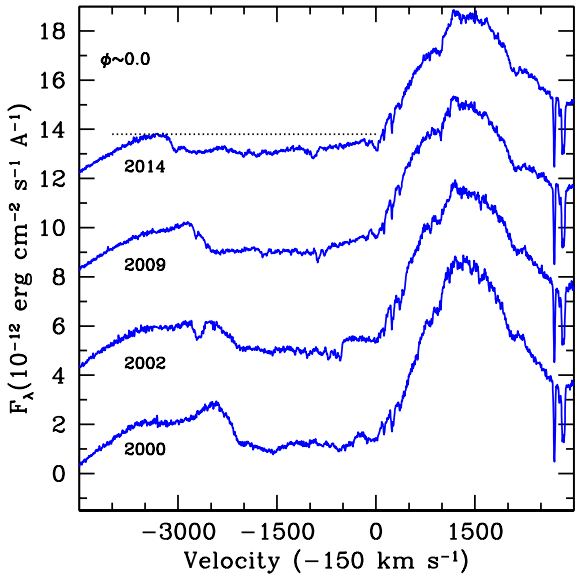

Fig. 2: Montage of the N v 1238/1242 P Cygni profile for the 4 epochs for which *HST*/*STIS* observations were acquired during the eclipse of *Star B* by *Star A* and thus reflect the wind velocity of the latter. The abscissa is given in velocity measured from the laboratory wavelength of the N v 1238 Å line, corrected for the velocity of the SMC in the HD 5980 vicinity. Note the increasing extent of the flat bottom region in the P Cygni absorption, which provides a measure of the maximum wind speed.

2 Evolutionary state

HD 5980 is clearly a system that is in its late stages of evolution, as can be concluded from the enrichment of surface layers with nuclear-processed elements and the LBV-type behavior. The orbital solution for the *Star A* + *Star B* binary was recently refined by Koenigsberger et al. (2014), who also discussed its evolutionary state and concluded that the most likely scenario is one in which *Star A* and *Star B* are following a quasi-homogeneous chemical evolution track.

Yoon et al. (2006) discussed the role of chemically homogeneous evolution in the context of the progenitor formation of slow gamma ray burst (GRB) sources and Langer et al. (2007) discuss it in the context of pair creation supernovae. A requirement for such models is the presence of an efficient mixing mechanism during most of the stellar lifetime which, in single stars, is rapid rotation. For binary stars, the usual hypothesis is that the stellar rotation synchronizes with the orbital angular velocity, thus leading to relatively slow rotation in binaries such as HD 5980. However, the relatively large orbital eccentricity of this system precludes synchronization, in the strict sense of the term.

Non-synchronous binary stars undergo perturbations that, one may speculate, could contribute to internal mixing in a manner as efficient as rapid rotation (Koenigsberger & Moreno 2013). Thus, a plausible argument can be made that *Star A* and *Star B* in HD 5980 are, indeed, following quasi-homogeneous chemical evolutionary tracks.

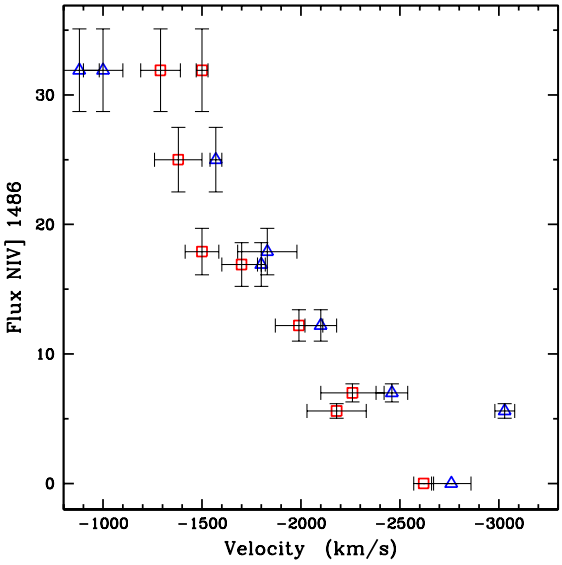

Fig. 3: Correlation of line strength *vs.* wind velocity. The N IV] 1486 Å emission-line flux obtained from *IUE* and *HST* observations is plotted against the wind velocity derived from P Cygni absorption profiles. Plotted are only the data from spectra obtained when *Star A* is in front of *Star B*. Squares correspond to the edge-velocity of He II 1640 Å and triangles correspond to the saturated portion of N v 1238 Å. The abscissa is un-dereddened flux in units of 10^{12} erg cm^{-2} s^{-1}.

Acknowledgements: I thank Norbert Langer for many helpful discussions and Ulises Amaya for computing support. This work was funded by UNAM/PAPIIT grant 105313 and CONACYT grant 129343. Spectra reported in this paper were obtained with the *International Ultraviolet Explorer*, and by the *Hubble Space Telescope*. *HST* is operated by the Space Telescope Science Institute, which is

operated by the Association of Universities for Research in Astronomy, Inc., under NASA contract NAS5-26555.

References

Georgiev, L., Koenigsberger, G., Hillier, D. J., et al. 2011, AJ, 142, 191

González, R. F. & Koenigsberger, G. 2014, A&A, 561, A105

Koenigsberger, G. 2004, Rev. Mexicana Astron. Astrofis., 40, 107

Koenigsberger, G., Georgiev, L., Hillier, D. J., et al. 2010, AJ, 139, 2600

Koenigsberger, G. & Moreno, E. 2013, in EAS Publications Series, Vol. 64, EAS Publications Series, ed. K. Pavlovski, A. Tkachenko, & G. Torres, 339–342

Koenigsberger, G., Morrell, N., Hillier, D. J., et al. 2014, AJ, 148, 62

Langer, N., Norman, C. A., de Koter, A., et al. 2007, A&A, 475, L19

Schweickhardt, J. 2000, PhD thesis, PhD Thesis, Landessternwarte Heidelberg/Königstuhl (2000).

Yoon, S.-C., Langer, N., & Norman, C. 2006, A&A, 460, 199

Structure & Evolution of WR stars

Wolf-Rayet Stars
W.-R. Hamann, A. Sander, H. Todt, eds.
Potsdam: Univ.-Verlag, 2015
URL: http://nbn-resolving.de/urn:nbn:de:kobv:517-opus4-84268

The importance of getting single-star and binary physics correct.

J. J. Eldridge[1], L. A. S. McClelland[1], L. Xiao[1], E. R. Stanway[2] & J. Bray[1]
[1] *Department of Physics, University of Auckland, Private Bag 92019, Auckland, New Zealand*
[2] *Department of Physics, University of Warwick, Gibbet Hill Road, Coventry CV4 7AL, UK*

We discuss the uncertainties that need to be considered when creating numerical models of WR stars. We pay close attention to inflation and duplicity of the stellar models, highlighting several observational tests that show these are key to understanding WR stellar populations.

1 Introduction

There are several groups making stellar evolution models today, with a number of them also represented within these proceedings (e.g. Geneva, Bonn and Brussels). In general the predictions of various groups are consistent. However, there are important differences of approach regarding uncertainties that still affect the results of stellar models.

In this review we outline the major uncertainties that have important effects on the evolution of Wolf-Rayet stars. Then we will discuss how these could be reduced by comparisons between observations and theoretical predictions for single stars and interacting binaries. We highlight the importance of binary interactions that are not normally full appreciated.

Throughout this review we have used our own stellar models to create the relevant figures. These are calculated with the Cambridge STARS code, the version employed here is described in Eldridge et al. (2008). These models of single stars and interacting binaries were used to create our Binary Population and Spectral Synthesis code, BPASS. In the examples below we outline the observational tests that BPASS has confronted. These models are available at `http://bpass.auckland.ac.nz`. Those described below are mostly based on the Version 1.1 results. However, we have now released the highly improved Version 2.0 of BPASS. The improvements include a new faster synthesis code that has been thoroughly debugged, a larger number stellar evolution models and, importantly, new stellar atmosphere spectra. Key to the latter has been the release of a large number of new atmosphere models by the Potsdam Wolf-Rayet group, PoWR. These include calculations at lower metallicities where before we had extrapolated. This has greatly improved the accuracy of the low metallicity predictions of BPASS. The new version will be fully described and compared to many observational tests in the forthcoming instrument paper, Eldridge et al. (in prep.).

2 Stellar uncertainties

There are five key uncertainties of stellar evolution relevant for Wolf-Rayet stars. The evidence that standard single-star evolution models are not sufficient to reproduce the observed Wolf-Rayet population is demonstrated by Figure 1. The primary issue is that WC stars are less luminous and cooler than predicted by single-star evolution models, while WN stars are cooler than stellar evolution predictions. These results were first shown in Hamann et al. (2006) and Sander et al. (2012). Georgy et al. (2012) showed that even the latest stellar evolution models including rotation were unable to remove these issues. Reproducing these observed locations of WR stars in the HR diagram is the key point we use in discussing how the uncertainties can drive a match or mismatch between observation and theory.

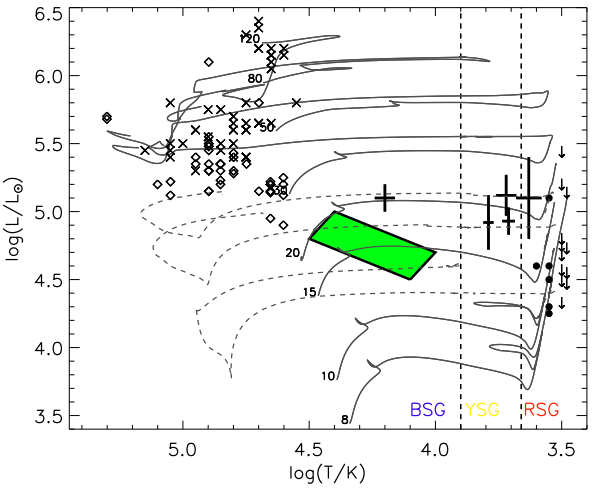

Fig. 1: HR diagram comparing stellar evolution tracks to observed WR stars. The solid lines are for single stars and dashed lines for interacting binary stars. The numbers give the initial masses in $M_{\odot}$. The circles, arrows and points with error bars represent the locations of observed type II, hydrogen rich, supernova progenitors, data taken from Smartt et al. (2009) and Eldridge et al. (2013). The location of the type Ib supernova progenitor for iPTF13bvn is indicated by the green box (Eldridge et al. 2015). The crosses are the locations of Galactic WN stars from Hamann et al. (2006) while the diamonds are the locations of Galactic WC stars from Sander et al. (2012).

2.1 Composition and opacity

In the last century it was thought that the standard Solar mass fraction of metals was about 2% (Grevesse & Sauval 1998). However, in reanalysis of the Solar atmosphere with updated 3D models, a new lower value of the metal content was found. Initially it dropped as low as 1.2% before increasing to somewhere around 1.4% (Asplund et al. 2009; Caffau et al. 2011). The main reason for this large drop was a decrease in the amount of oxygen inferred in the Sun's atmosphere. However, the new composition from looking at the surface did not agree with the composition inferred from the interior by helioseismology, e.g. Basu & Antia (2008), which was more inline with the original old Solar composition. This mismatch has yet to be resolved. Despite this, in the last few years, many groups have switched to the new Solar composition, creating stellar models with the lower oxygen abundance so that the metallicity, $Z = 0.014$.

The question, however, may not be, "what is the correct Solar abundance?", but "should we be using the Sun as our abundance standard at all?". The Sun is around 4.5 billion years old and is unlikely to have been formed in its current location in the Galaxy. The massive stars we observe in the Galaxy formed much more recently and thus we should use those stars as our abundance standard instead. This was suggested by the work of Nieva & Przybilla (2012) who have provided an alternative Galactic abundance standard that lies between the old and new Solar compositions.

The abundance that modellers should be using is still uncertain, and in essence it comes down to how much oxygen we use in our stellar models of the Galaxy. The amount of iron in the different compositions is almost identical and it is this that is key to determine the mass-loss rates in the stars from stellar winds. The key point is that we should not be too keen to use the new Solar composition for modelling anything other than the Sun.

2.2 Mass-loss rates

The main way to form a WR star in the Galaxy and in most other environments is via mass loss. Nuclear fusion creates a helium core at the centre of a star during the main-sequence. The surface hydrogen then needs to be removed to expose this helium core for it to become a WR star. The mass-loss probably happens during the red supergiant (RSG) or luminous-blue variable (LBV) stages of evolution. The mass-loss rates, however, are quite uncertain and there is still the possibility that they could be in error (Smith 2014). An open question is also how should mass-loss rates be scaled with metallicity. We know that mass-loss rates decrease with metallicity but exactly how quickly they vary has yet to be accurately determined.

The only way to remove this uncertainty is to test mass-loss rates by studying the period change in eclipsing binaries as in Shenar et al. (2015). Relevant samples are only now becoming available and these will be the most stringent tests in the future. However, there are few post-main sequence eclipsing binaries so these are difficult to constrain. Work by Georgy (2012) and Georgy et al. (in prep.) determine some of the impacts of varying RSG mass-loss rates within the range of observed values. The problem with this is that it is difficult to disentangle variation in the RSG mass-loss rates with varying the binary evolutionary pathways.

We note, however, once the WR star is formed the mass-loss rates appear to still be approximately consistent with Nugis & Lamers (2000) as shown in the work of the Potsdam WR group, e.g. Hamann et al. (2006) and Sander et al. (2012).

2.3 Convection and inflation

Energy transport by convection is normally parametrised in stellar models by mixing-length. We calibrate the mixing length to the Sun and then recklessly apply it to all other stars in the Universe. However for WR stars simple tests show that adjusting the mixing-length parameters has only a small effect on the surface temperatures and radii. The convective envelopes of WR stars are atypical, being extended and almost constant density, with a small density inversion near the surface. In addition most of the energy transport is by radiation despite stellar models indicating these envelopes are convective. This is why varying the mixing-length parameter has little effect on a model's radius.

Clearly there is something else wrong with our models of convection if we are to move our stellar models closer to the temperatures inferred from the Potsdam WR group's observations. As discussed by others, the convective zones may have typical convective velocities that exceed the sound speed of the stellar interior. Therefore they may be highly turbulent and clumped. Gräfener et al. (2012) suggest that clumping of the convective flows in outer parts of the star could be what seeds the clumping in stellar winds. In stellar models they increase the opacity of the material due to this clumping but shift the average opacity to a higher density. This increase in opacity, inflates the envelope further leading to cooler temperatures, as shown by models in Figure 2 that have had this effect included.

We can conclude from this that we need to include this inflation effect, which is present in most stellar models, but also increase it beyond what is already found from the evolution models. This is work in progress.

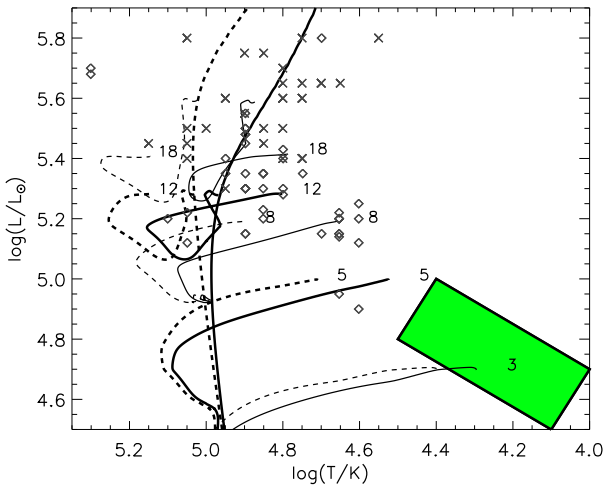

Fig. 2: Similar to Figure 1 but now showing models based on helium star only models (see McClelland this proceedings). The numbers give the initial helium star masses in $M_\odot$ Crosses represent the locations of Galactic WN stars and diamonds the Galactic WC stars. The dashed lines are standard models, the solid lines are stellar models including the clumping factor for stellar opacity in the inflated envelope given by Gräfener et al. (2012).

2.4 Rotation and magnetic fields

Rotation and magnetic fields are both important in stellar evolution, although how important is an open question. It is summarised in these proceedings by Meynet and Georgy. Rotation has two effects. First it will extend the main-sequence lifetimes. Second it will increase mass loss and therefore produce WR stars from lower initial mass stars. However, as shown, in Georgy et al. (2012) such single star models cannot reproduce the bulk of the WC stars.

As suggested by de Mink et al. (2013) the most rapidly rotating stars are produced during binary interactions. The accreting companion in a binary can accrete mass and angular momentum and be left rapidly rotating. However, rapid rotators are relatively rare with the majority of stars rotating too slowly to lead to significantly observable effects. However, including rotation accurately is still important.

2.5 Duplicity

Why duplicity and not binarity? Binarity typically indicates something that can be switched on/off. This does not apply to binary evolution as it encompasses a range of behaviour of different strengths. In the dictionary definition, duplicity is the state of being double. Fortunately the more modern use of implying deceitfulness is also apt as binaries are confusing and make our task of understanding their evolution more difficult.

As described by Vanbeveren in these proceedings, the history of massive stars is an interesting story of research pathways taken by the field. For various reasons the community first considered binary evolution important, then moved away to considering only single stars and rotation and now are returning to taking account of interacting binaries.

An important point to make is that there are several groups worldwide creating binary evolution models and performing population synthesis including interacting binaries; Brussels, Yunnan, Amsterdam, Auckland and many more. All these groups demonstrate that interacting binaries have an important effect on stellar populations that must be taken into account. Their results are broadly consistent. This is an important point as it is normally assumed that with the large number of free-parameters that binary evolution is somehow untrustworthy. However, similar results obtained with different methods lend some confidence to the results of binary evolution codes.

In Figure 1 the tracks where the stars have experienced a binary interaction and lost their hydrogen envelope are able to reproduce the luminosities of the observed Galactic WC stars. While the temperatures are still slightly too hot we have not yet included the inflation effect of effect Gräfener et al. (2012) into these models.

Achieving the correct luminosity is a positive step. Assuming these stars are in binaries is a preferable assumption to having to arbitrarily boost the mass-loss rates of these lower-luminosity RSGs to produce the WR stars. In fact many RSGs with boosted mass-loss rates are likely to be binary systems where the RSG has an unobservable low-mass companion.

The best evidence that we must take account of binaries comes from the work of Sana et al. (2012, 2014) who directly measured the binary fraction of stars and their periods and mass ratios. They find that 70% of O stars are in an orbit where they will have the evolution altered by a binary interaction.

3 Resolved WR populations

Duplicity and inflation then are the key uncertainties to consider in attempting to reproduce the observed WR population in our Galaxy. While we are still currently working on inflation, we now discuss observational tests for synthetic binary populations highlighting their importance. We divide these into those considering resolved stellar populations and those with unresolved populations in more distant galaxies.

The next step beyond matching the location of WR stars on the HR diagram is to model the relative numbers of different WR subtypes and the relative numbers of massive stars in other phases of

evolution such as the main-sequence and red supergiants. For a complete test these must be reproduced in galaxies with various metallicities such as the Magellanic clouds. The problem with such tests is they have been plagued by observational selection effects as discussed by Massey in these proceedings. However, as also discussed by Massey and Neugent, at least for some samples, progress has been made and models face more stringent tests.

The three main population number ratios to test are the ratios of the number of WR to O stars, RSG to WR stars and the WC to WN. In calculating these for a theoretical population a constant star-formation rate and fully sampled initial-mass function are assumed. Populations including single star evolution models only are not able to reproduce the observed ratios, however, binary models are able to, e.g. Eldridge et al. (2008). While the RSG/WR ratio is difficult to reproduce, new observed ratios from Massey in these proceedings indicate the disagreement is not as bad as suggested previously. Both Vanbeveren et al. (2007) and Eldridge et al. (2008) predicted similar WC/WN ratios from binary populations that were lower than the available observed samples at the time the work was done. The newer, lower, ratios as the various metallicities given in these proceedings by Massey are in agreement with these predictions.

We stress, however, that further refined comparisons must be performed, for example the relative rates of early to late WR stars. This will be dependent on the importance of inflation. One detail that is insensitive to inflation will be the luminosity distribution of the WR stars in the HR diagram.

Another test that involves resolved populations is the SN progenitors observed in pre-explosion images (Smartt et al. 2009; Eldridge et al. 2013; Smartt 2015). WR stars were long expected to be the progenitors of type Ib/c SNe (these are supernovae with no hydrogen observed). However, as discussed by Yoon et al. (2012) and Yoon (2015), the brightest and most visible type Ib/c progenitors are in fact helium giant stars that are not WR stars at all. However, such helium giants have still not been observed in our Galaxy so their exact numbers are only theoretically predicted. The one progenitor observed for a type Ib SN is most likely to have been a helium giant, see Bersten et al. (2014); Eldridge et al. (2015) and references therein.

WR stars are likely to still produce some type Ib/c SNe but their observability as SN progenitors is uncertain and model dependent. Inflation will actually make it easier to observe progenitors (if it occurs). Interestingly to explain the relative ratios of type Ib/c to type II SNe some WR stars must explode and give rise to type Ib/c SNe as well as long-Gamma-ray bursts. Also their contribution to the rate may be reduced if most of them form black holes at core-collapse and not give rise to a luminous explosion (Smartt 2015).

4 Unresolved WR population

For more distant galaxies individual WR stars cannot be resolved but their contribution to the integrated light can be estimated. The most easily identifiable features are the Blue and Red WR bumps. A large sample of SDSS galaxies were studied by Brinchmann et al. (2008). In their study they used optical fluxes to infer the ratio of WR to O stars and compared these to theoretical predictions from various models, finding binary models and those including rotation performed best.

In Eldridge & Stanway (2009) we took the alternative approach and attempted to model the observed WR bump fluxes directly using stellar population models linked to atmosphere models. Using the resultant BPASS models we found that a population including interacting binaries could reproduce the observed range of equivalent widths for the WR features of SDSS galaxies versus metallicity. In effect this is equivalent to matching both the observed WR/O and WC/WN ratios in nearby galaxies. Similar studies have been performed by others using the same population models, e.g. Miralles-Caballero et al. (2014).

In Eldridge & Stanway (2012) we took this one step further and attempted to reproduce the ultraviolet O star and WR lines in the observed spectra of galaxies at redshifts greater than 2. Interestingly here we found the binary interactions were not sufficient to produce the WR lines but we also needed to account for the spin-up of the companion stars during the mass-transfer events to reproduce the observed He II 1640Å line.

The population model predictions used in the above studies are summarised in Figure 3. It can be seen that binary populations do not just produce more WR stars and therefore more ionising flux, they do so at a later age than a single star population. As the observed WC stars are from stars of a lower initial mass, these can only appear at a later phase of evolution.

This difference in behaviour means more ionising flux, and significantly harder ionising flux at later ages. This fact was used by Stanway et al. (2014) to explain the surprisingly strong ionisation state of high redshift Lyman-break galaxies as well as their nearby analogues. While single star models could almost reproduce them they are limited to ages less than 10Myrs, binary models can match the observed galaxies over a broader age range of up to 100Myrs. In addition Kehrig, Sokal and Walsh discuss how there are clusters and galaxies observed with strong ionising lines but no WR features. The predictions of binary evolution models may be able to explain these features too.

The evidence that binary stars are important and key to many observational signatures cannot be ignored. As shown in Figure 3 the binary models can

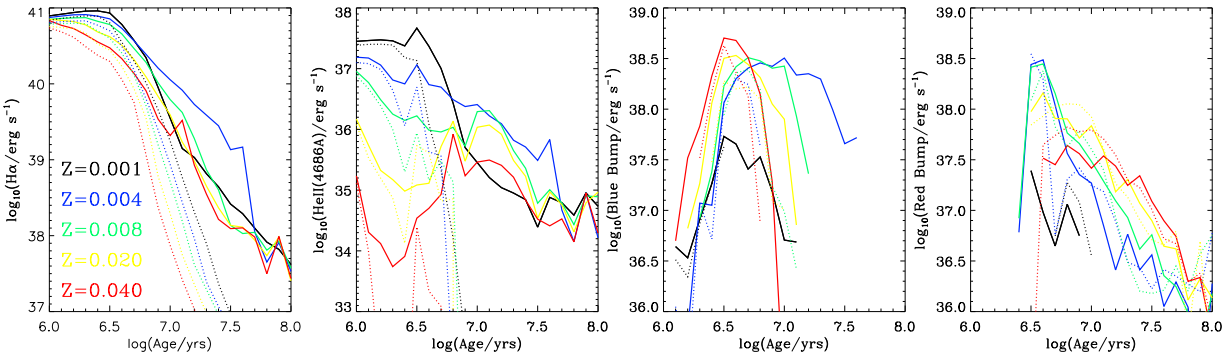

Fig. 3: Predictions for emitted fluxes from stellar populations of single stars (dotted lines) and interacting binaries (solid lines). Left to right the panels are Hα flux, He II flux at 4686Å, the blue WR bump and the red WR bump. The models are for an instantaneous starburst of 10^6 $M_\odot$ at five different metallicities.

produce strong He II ionising fluxes with and without WR emission.

5 Summary

In summary, the modelling of stellar evolution is still subject to many uncertainties. Key amongst these are the role and impact of interacting binary evolution, inflation of WR envelopes and rapid rotation. However, we are now reaching an epoch in which models and observations are tending towards agreement. Refining the uncertainties on both models and the observational data will be essential to future progress.

References

Asplund, M., Grevesse, N., Sauval, A. J., & Scott, P. 2009, ARA&A, 47, 481

Basu, S. & Antia, H. M. 2008, Phys. Rep., 457, 217

Bersten, M. C., Benvenuto, O. G., Folatelli, G., et al. 2014, AJ, 148, 68

Brinchmann, J., Kunth, D., & Durret, F. 2008, A&A, 485, 657

Caffau, E., Ludwig, H.-G., Steffen, M., Freytag, B., & Bonifacio, P. 2011, Sol. Phys., 268, 255

de Mink, S. E., Langer, N., Izzard, R. G., Sana, H., & de Koter, A. 2013, ApJ, 764, 166

Eldridge, J. J., Fraser, M., Maund, J. R., & Smartt, S. J. 2015, MNRAS, 446, 2689

Eldridge, J. J., Fraser, M., Smartt, S. J., Maund, J. R., & Crockett, R. M. 2013, MNRAS, 436, 774

Eldridge, J. J., Izzard, R. G., & Tout, C. A. 2008, MNRAS, 384, 1109

Eldridge, J. J. & Stanway, E. R. 2009, MNRAS, 400, 1019

Eldridge, J. J. & Stanway, E. R. 2012, MNRAS, 419, 479

Georgy, C. 2012, A&A, 538, L8

Georgy, C., Ekström, S., Meynet, G., et al. 2012, A&A, 542, A29

Gräfener, G., Owocki, S. P., & Vink, J. S. 2012, A&A, 538, A40

Grevesse, N. & Sauval, A. J. 1998, Space Sci. Rev., 85, 161

Hamann, W.-R., Gräfener, G., & Liermann, A. 2006, A&A, 457, 1015

Miralles-Caballero, D., Rosales-Ortega, F. F., Díaz, A. I., et al. 2014, MNRAS, 445, 3803

Nieva, M.-F. & Przybilla, N. 2012, A&A, 539, A143

Nugis, T. & Lamers, H. J. G. L. M. 2000, A&A, 360, 227

Sana, H., de Mink, S. E., de Koter, A., et al. 2012, Science, 337, 444

Sana, H., Le Bouquin, J.-B., Lacour, S., et al. 2014, ApJS, 215, 15

Sander, A., Hamann, W.-R., & Todt, H. 2012, A&A, 540, A144

Shenar, T., Oskinova, L., Hamann, W.-R., et al. 2015, ArXiv e-prints

Smartt, S. J. 2015, PASA, 32, 16

Smartt, S. J., Eldridge, J. J., Crockett, R. M., & Maund, J. R. 2009, MNRAS, 395, 1409

Smith, N. 2014, ARA&A, 52, 487

Stanway, E. R., Eldridge, J. J., Greis, S. M. L., et al. 2014, MNRAS, 444, 3466

Vanbeveren, D., Van Bever, J., & Belkus, H. 2007, ApJ, 662, L107

Yoon, S.-C. 2015, PASA, 32, 15

Yoon, S.-C., Gräfener, G., Vink, J. S., Kozyreva, A., & Izzard, R. G. 2012, A&A, 544, L11

Norbert Langer: Can rotation affect the mass transfer efficiency in binaries and what do you assume for that in your models?

J. J. Eldridge: Yes, this is the most uncertain thing in the models. We assume that the accreting star can only accrete at a rate determined by the thermal timescale. The star puffs up if it accretes material too fast. We also assume that a star is spun up to rapid rotation if it accretes 10% of its initial mass.

Paul Crowther: Many more parameters are required for massive binary models, (period distributions, mass ratio, etc. ...) than single ones, which have been revised recently by Sana et al. (2012, 2013). Are your models consistent with these?

J. J. Eldridge: Yes they are consistent with them, although I chose flat mass ratio and log(separation) distributions, but these are similar. The key point is I do not vary any parameters. My models take time so I only have one set that I compare to observations. Which is nice as it appears I don't have to fudge anything to get a better agreement with binaries.

Wolf-Rayet Stars
W.-R. Hamann, A. Sander, H. Todt, eds.
Potsdam: Univ.-Verlag, 2015
URL: http://nbn-resolving.de/urn:nbn:de:kobv:517-opus4-84268

Physics of massive stars relevant for the modeling of Wolf-Rayet populations

G. Meynet[1], C. Georgy[1,2], A. Maeder[1], S. Ekström[1], J. H. Groh[1], F. Barblan[1] & H. F. Song[3] & P. Eggenberger[1]
[1] *Geneva University, Switzerland*
[2] *Keele University, UK*
[3] *Guizhou University, China*

Key physical ingredients governing the evolution of massive stars are mass losses, convection and mixing in radiative zones. These effects are important both in the frame of single and close binary evolution. The present paper addresses two points: 1) the differences between two families of rotating models, *i.e.* the family of models computed with and without an efficient transport of angular momentum in radiative zones; 2) The impact of the mass losses in single and in close binary models.

1 Rotation

Present extended grids of massive star rotating models (see e.g. the review by Maeder & Meynet 2012, and references therein) can be classified into two main families (note that this is true for both single and close binary evolution). The first family consists in models where the transport of the angular momentum is driven by meridional currents and shear instabilities according to the theory proposed by Zahn (1992) (see for instance the grid by Ekström et al. 2012). We shall call these models, the shear models. The shear models allow a small contrast between the angular velocity of the convective core and the angular velocity of the surface to develop during the Main-Sequence phase as shown in Fig. 1. The contrast is more pronounced in models starting with a slow initial rotation. This is due to the fact that when the initial rotation is smaller, the processes transporting the angular momentum are slower. Thus the contrast in rotation between the core and the envelope, that builds up during the Main-Sequence phase when the core contracts and the envelope expands, is less smoothed. In Fig 1, the contrast deduced from asteroseismology for three stars are indicated by horizontal dotted lines. We see that for two stars, the measured values are compatible with those of initially slowly rotating models, while for the third one, the observed result is compatible with solid body rotation or with the models shown in Fig. 1 at a very early stage of the core H-burning phase. It is interesting to note that the good agreement with initially slowly rotating models is consistent with the fact that such asteroseismic estimates are only available for slow rotators.

The second family is composed from models computed with the dynamo mechanism proposed by Spruit (2002). Among grids of massive star models computed with that theory we can mention for instance the grids by Brott et al. (2011). We shall call these models, the magnetic models. This theory has been criticized by Zahn et al. (2007), but we shall not develop here the arguments, we rather point a few similarities/differences when the outputs are compared with those of the shear models.

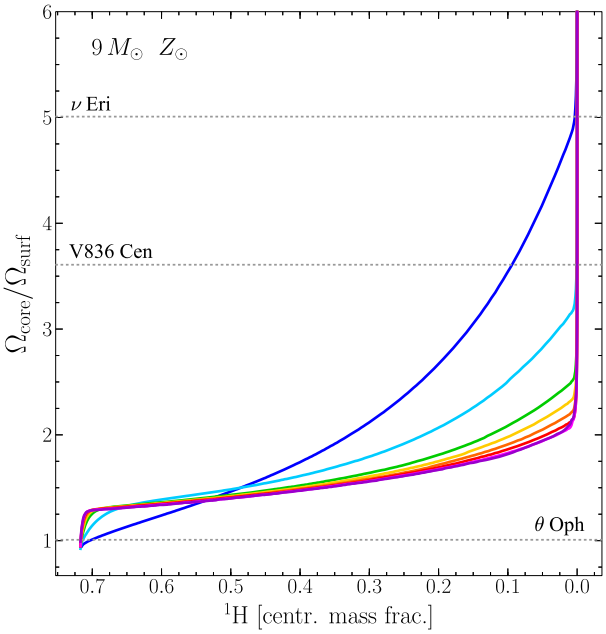

Fig. 1: Variation of the ratio between the angular velocity of the core and the angular velocity at the surface as a function of the remaining mass fraction of hydrogen in the core during the core H-burning phase in 9 $M_\odot$ models for a metallicity Z=0.014. The lines from top to bottom correspond to increasing initial rotation on the ZAMS, they correspond to initial surface angular velocities equal to 0, 10, 30, 50, 60, 70, 80, 90 and 95% the critical angular velocity (the critical angular velocity being the value for which the centrifugal acceleration balances the gravity at the equator). The ratios estimated by asteroseismology are indicated for a few cases as horizontal dotted lines (Aerts 2008, and references therein). The models are those by Georgy et al. (2013).

Among the similarities, we can mention that, in the two families of models, the efficiency of the chem-

ical mixing varies qualitatively in the same way when the initial rotation, mass and metallicity vary. For both families, when the rotation increases, the mixing becomes more efficient, the same occurs when the initial mass increases; when the metallicity increases, the mixing becomes less efficient. These similarities are striking because they are due to different physical reasons in both families (see a more detailed discussion in Song et al. 2015).

Let us now turn to the differences. A main difference is that magnetic models produce nearly solid body rotating models during the Main-Sequence (MS) phase. If plotted in a figure like Fig. 1, they would show quasi horizontal lines fixed at an ordinate equal to 1. Such model could be compatible with the case of θ Oph. A second difference is that the magnetic models, with no magnetic braking at the surface, all other characteristics being kept the same (mass, metallicity, initial rotation, age) are more efficiently mixed than shear models (Maeder & Meynet 2005). This implies that magnetic models will for instance produce a homogeneous evolution (*i.e.* an evolution during which the chemical composition at the centre of the star is quasi the same as the chemical abundance at the surface) with an initial rotation that is smaller than for shear models. Fig. 2 show the time-averaged surface velocity for different magnetic models, single or in wide binaries (see the continuous black lines) and in close binaries (see the colored dashed lines), starting with different initial velocities. For these magnetic models, it suffices that the time-averaged surface velocity be above ∼250 km s^{-1} to follow an homogeneous evolution, while for shear models, much larger velocities are needed (see below). This last point can be illustrated comparing the evolution of the magnetic 39 M$_\odot$ model computed with an initial rotation of 350 km s^{-1} by Szécsi et al. (2015) for the metallicity of IZw18. This model follows a homogeneous evolution. The corresponding shear model (initial mass of 40 M$_\odot$) computed for an initial velocity of 393 km s^{-1} follows a regular, non-homogeneous evolution (Groh et al. in preparation). Thus, the link between a given evolution (here for instance between homogeneous or non homogeneous evolution) and the initial rotation is thus very different depending on the type of models (shear and magnetic) considered. For a given initial distribution of velocities, the predicted outputs for a population of massive stars and in particular the populations of WR stars can therefore be significantly different. This has to be kept in mind when comparisons with observations are done.

At the moment, it is not possible to make strong conclusions about which kind of models would be the most representative of the behavior of the bulk of the real stars. Some indirect arguments as the angular momentum content in white dwarfs and neutron stars support magnetic models (Suijs et al. 2008; Heger et al. 2005). The magnetic models allow to extract more angular momentum from the central

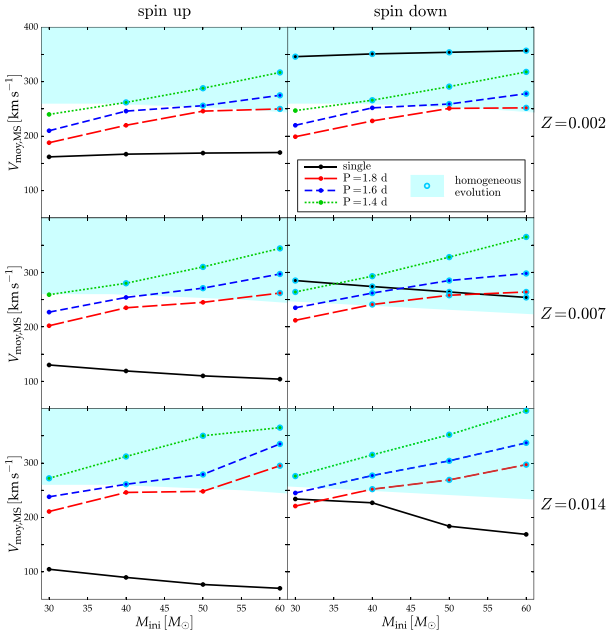

Fig. 2: Time-averaged surface equatorial velocity of single and binary stars as a function of the initial mass for various metallicities. The models have been computed with an internal magnetic field. The (black) continuous line connects the single star models. The (colored) dashed lines connect the binary stellar models. The initial period in days is indicated. The results corresponds to a companion having 2/3 the mass of the primary. The (blue) big dots show the models that follow a homogeneous evolution. The zone of homogeneous models lay is hatched in blue. The panels on the left column correspond to spin-down cases and the panels on the right column to spin-up cases for binaries. The figure is taken from Song et al. (2015, and see the text for more details on spin-up and spin-down cases.).

regions and thus predict final rotations for the compact remnants that are more compatible with the observations than the predictions of the shear models that predict too high rotation for these remnants. On the other hand, as indicated above, magnetic models predict solid body rotation during the MS phase, which is in contradiction with some asteroseismic constraints. Is there any possibility to reconcile the asteroseismic constraints and those coming from the measured rotation rates of young pulsars? Let us make here a few remarks: 1) the rotation of young pulsars might result from processes occurring at the time of the supernova explosion, or during the early phases of the new born neutron stars; 2) recent works have suggested other mechanisms to extract angular momentum from the core, very different from the theory by Spruit (2002). One of them invokes a coupling between the core and the surrounding radiative layers by a fossil magnetic field (Maeder & Meynet 2014). Fuller et al. (2015) sug-

gests another way by demonstrating that internal gravity waves, excited via envelope convection during a red supergiant phase or during vigorous late time burning phases, may substantially spin down the core.

To make progresses, we need to find some additional discriminating observations that would allow to check which kind of models seem the most appropriate. It might be that shear models and magnetic models both occur in nature. In that case it is important to understand what are the causes of these different behaviors and what are their respective frequency. A possible way of differentiating these two kinds of models will be through the observations of stars in close binaries. As can be seen in the upper panel of Fig. 3, shear models in close binaries show larger surface enrichments when the orbital period increases, while we have the reverse behavior in magnetic models (see the lower panel Fig. 3). This comes from the fact that in shear models, the mixing is driven by the gradients of Ω, while in magnetic models, the mixing is driven by Ω. In shear models, a larger orbital period imposes a slower rotation at the surface and thus a stronger contrast with the centre making the gradients of Ω stronger and the mixing stronger. In magnetic models, a larger orbital period imposes a lower value of Ω in the whole star and thus weakens the efficiency of mixing.

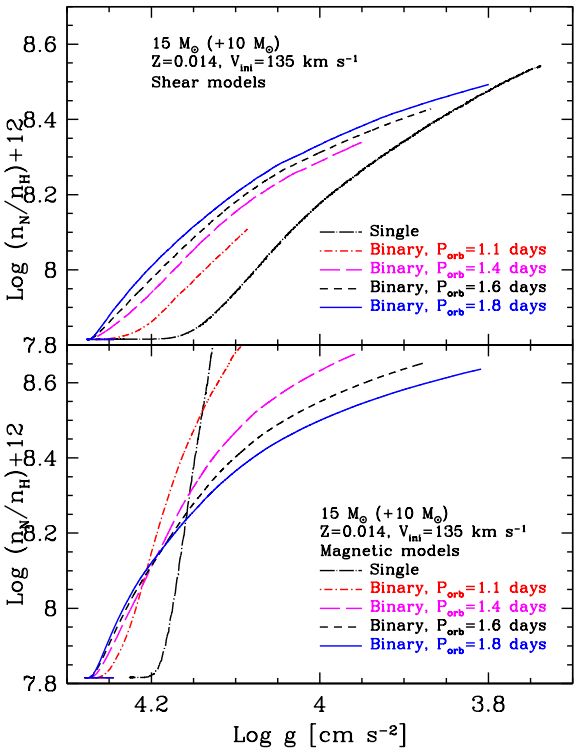

Fig. 3: Evolution of the abundance ratio (in number) of nitrogen to hydrogen at the surface of rotating 15 $M_\odot$ models at solar metallicity as a function of the surface gravity. Single models and models in close binaries are shown. The initial velocity is 135 km s^{-1}. *Upper panel:* the models have been computed according to the rules of the shear models. Figure taken from Song et al. (2013). *Lower panel:* the models have been computed according to the rules of the magnetic models and are discussed in Song et al. (2015).

2 Mass loss rates

Mass loss rates by stellar winds and/or through mechanical winds when the star is rotating near the critical limit are also very important quantities relevant for WR star modeling. Actually the intensity of the winds *prior* the star enters the WR regime has a strong impact on the duration of the WR lifetime and hence on estimating quantities as the number ratio of WR to O-type stars. Higher the mass loss rates, longer will be the WR lifetime. This is illustrated for instance by looking at how, in the frame of single star models, the lifetime of 60 $M_\odot$ models in the WR phase increases when the initial metallicity and therefore the mass loss rates increase (see for instance Fig. 7 in Meynet & Maeder 2005). On the other hand, mass loss rates *during* the WR phases may significantly change the durations of the various WR subphases. For instance, increasing the mass loss rate during the WN phase would reduce the duration of the WN phase and increases the duration of the WC phase, having a strong impact on the number ratios of WC to WN stars.

In order to know whether a given model has to be considered a WN or a WC star, the most precise procedure would be to compute the emergent spectrum compatible with the interior structure and then apply to this synthesized spectrum the same criteria of classifications, based on various line ratios, to assign a spectral WR subtype. At the moment, there is only one complete evolution for which spectra were computed all along the stellar life. This was done for a non-rotating 60 $M_\odot$ model at solar metallicity by Groh et al. (2014). It is interesting to compare the lifetimes obtained for the different evolutionary phases when spectral criteria are used and when more global criteria based on the effective temperature and the surface abundances are used (for a detailed comparison see Table 3 in Groh et al. 2014). Some durations are the same whatever the spectral or the global properties are used. This is for instance the case for the total duration of the WR phase which differs by only half a percent between the two methods. Others are strongly affected. For instance, the spectral classification gives a much shorter WNL phase (the spectral duration corresponds to 8% the duration obtained by the global properties) and a much longer WNE phase (the spectral duration corresponds to about 2 times the duration obtained by

the global properties). This spectral modeling, we see would be here particularly important for predicting number ratios involving WNL and WNE stars and for making comparisons with observed positions of this two types of stars in the HR diagram. Let us note that the mass loss rates used have an impact on the output spectra. More consistent models would be obtained if the mass loss rates would result from the model physics rather than from some empirical recipes.

Mass loss can also be triggered by mass transfer in a close binary system. This channel may be important to produce WR stars from lower initial masses or from lower metallicity regions for which the stellar winds alone are too weak to allow the formation of WR stars. An example of such an evolution for a 20 $M_\odot$ plus a 15 $M_\odot$ star is shown in Fig. 4. Only the evolution of the primary is indicated. In the present calculations we did not account for rotation. At least for the primary this should not be a too severe problem, because after synchronization, the 20 $M_\odot$ model would have a surface velocity of about 130 km s^{-1} which is a quite moderate velocity. Of course this assumes that the synchronization time is quite short (de Mink et al. 2009; Song et al. 2015) and does not imply any extra-mixing. The case of the secondary is however quite a different story since it may be spun up by accretion of matter coming from the primary.

In Fig. 4, point A is the ZAMS. At point B, the radius of the primary reaches for the first time the Roche limit. The mass transfer episode lasts 2.3 My, and occurs between points B and G . Note that the strong mass losses occurs in two main events. The first occurs between points C and D (loss of a little more than 10 $M_\odot$ in a time of about 0.5 My, thus a time-averaged mass loss rate of 2 10^{-5} $M_\odot$ yr^{-1}). The second event occurs between points E and G (loss of 3.6 $M_\odot$ in about 0.1 My, thus a time-averaged mass loss rate of 3.6 10^{-5} $M_\odot$ yr^{-1}). During these mass transfer events, the mass loss rates due to Roche Lobe Overflow can be up to 56 times stronger than the wind mass loss rates. The strong mass loss due to the first event makes the track to decrease in luminosity (evolution from C to D in 0.5 My). At the end of the core hydrogen burning the star contracts and the evolution goes from D to E and x in about 1.2 My. The point x corresponds to the end of the core H-burning phase. After the core H-burning phase, the core contracts, the envelope expands by mirror effects (evolution from x to F in about 1 My). The core helium burning begins in y, still in a mass transfer episode. In y, the star can be considered as a Wolf Rayet star of the WNL type according to the usual global criteria[1]. Due to strong mass losses, which reduce the H-rich envelope, the star evolves in the blue region of the HRD. From G to H, the luminosity decreases again a lot. During that phase, the total mass of the primary decreases by only 0.27 $M_\odot$, but it removes H-rich layers and the mass of hydrogen has an important impact on the radius of the star (see e.g. Fig. 5 and 10 in respectively Groh et al. 2013; Meynet et al. 2015a). When the core, at the end of the core He-burning phase begins to contract, the envelope expands (evolution from H to z). In z the star enters into the WNE phase according to the global criteria[2]. The evolution from z to J corresponds to the contraction phase between the end of the core helium burning phase and the beginning of the core carbon phase. At J, the star has reached its final position in the HRD.

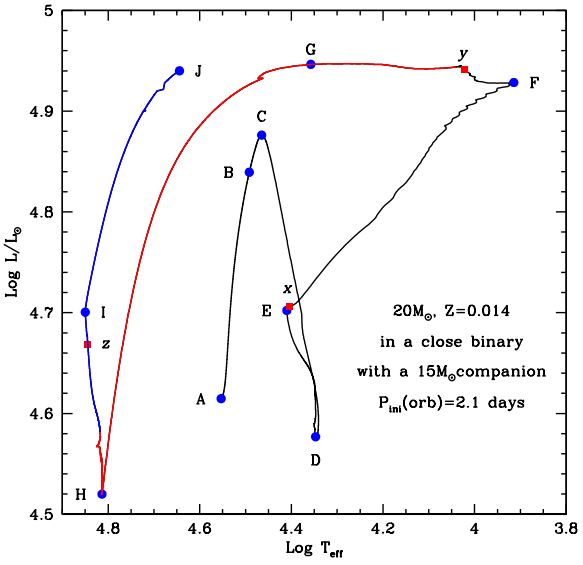

Fig. 4: Evolutionary track in the theoretical HR diagram for a primary of 20 $M_\odot$ in a close binary system with a 15 $M_\odot$ star. The initial orbital period is 2.1 days. The metallicity is solar. The red, respectively the blue part of the track correspond to the WNL and WNE phases as defined by global properties of the stellar models (see text for the description of the letters). The model is from Barblan (private communication).

The close binary evolution described above can therefore produce WR stars. Starting from larger orbital periods shifts the mass transfer at later time, may not produce WR stars and may give birth to redder positions for the progenitors of the core collapse supernova. We obtain that the upper limit for

[1]One considers a star to enter the WR phase when its mass fraction of hydrogen at the surface becomes inferior to 0.3 and the logarithm of the effective temperature is higher than 4.0.

[2]WNE are WR stars defined by the absence of hydrogen at the surface and the usual signatures of CNO processed matter like a high nitrogen abundance.

obtaining WR stars for systems composed of a 20 and a 15 $M_\odot$ is around 6.2 days. All systems with shorter orbital period are predicted to produce some WR stars at a given point.

The duration of the WR phase shown in Fig. 4 is a little longer than 1 My, thus quite significant. For comparison, a rotating single 60 $M_\odot$ model at solar metallicity is predicted to be a WR star during 0.9 My (Georgy et al. 2012). While this kind of evolution might indeed occur in nature, there are a few arguments indicating that it is probably not too frequent. Let us just mention three of them below. First, in case such an evolution would be common enough, one should find single-aged massive star populations where both red supergiants, originating from single or wide binary systems, and WR stars, coming from close binary systems, are observed. At the moment, the stellar clusters at the centre of the Galaxy (Liermann et al. 2012) and Westerlund 1 (Clark et al. 2005) present evidences for hosting both WR stars and red supergiants. In general however this is not the case. Second, such an evolution would produce low luminous WNL and WNE stars. At the present time, the observed lowest luminosities for these two types of stars are respectively 5.25 and 5.3 in Log $L/L_\odot$, while here we would have WN and WNE stars with luminosities below 4.9. A way out of this dilemma is either that the frequency of such an evolution is quite small, or that the WR star is hidden in the light of its more luminous companion. This last point can be checked, and will be discussed in a future paper (Barblan et al. in preparation). Third, such an evolution would also produce blue supergiants (actually not the evolution presented in Fig. 4 but close binary evolution with longer orbital periods). Blue supergiants, after the mass transfer, will show a much smaller surface gravity than those coming from stages before the mass transfer. One will have therefore that the post mass transfer blue supergiants will populate a region of the flux weighted gravity luminosity relation that is not compatible with the present day observations (Meynet et al. 2015b). Another and final point we would like to mention here is the following: interestingly, while the close binary scenario can produce low luminous WN stars, it fails in producing low luminous WC stars (at least from the evolution of the primary). According to the observed sample by Sander et al. (2012), the lowest luminous WC stars have luminosities around 4.95. The end point of the evolution shown in Fig. 4 is still far from being a WC stars. It would still need to lose 1.5 $M_\odot$. Thus unless there is strong underestimates of the mass losses, there is no chance to produce low luminous WC stars through this channel for the mass range considered here. This leaves open the question of the origin of these low luminous WC stars.

References

Aerts, C. 2008, in IAU Symposium, Vol. 250, IAU Symposium, ed. F. Bresolin, P. A. Crowther, & J. Puls, 237–244

Brott, I., de Mink, S. E., Cantiello, M., et al. 2011, A&A, 530, A115

Clark, J. S., Negueruela, I., Crowther, P. A., & Goodwin, S. P. 2005, A&A, 434, 949

de Mink, S. E., Cantiello, M., Langer, N., et al. 2009, A&A, 497, 243

Ekström, S., Georgy, C., Eggenberger, P., et al. 2012, A&A, 537, A146

Fuller, J., Cantiello, M., Lecoanet, D., & Quataert, E. 2015, ApJ, 810, 101

Georgy, C., Ekström, S., Granada, A., et al. 2013, A&A, 553, A24

Georgy, C., Ekström, S., Meynet, G., et al. 2012, A&A, 542, A29

Groh, J. H., Meynet, G., Ekström, S., & Georgy, C. 2014, A&A, 564, A30

Groh, J. H., Meynet, G., Georgy, C., & Ekström, S. 2013, A&A, 558, A131

Heger, A., Woosley, S. E., & Spruit, H. C. 2005, ApJ, 626, 350

Liermann, A., Hamann, W.-R., & Oskinova, L. M. 2012, A&A, 540, A14

Maeder, A. & Meynet, G. 2005, A&A, 440, 1041

Maeder, A. & Meynet, G. 2012, Reviews of Modern Physics, 84, 25

Maeder, A. & Meynet, G. 2014, ApJ, 793, 123

Meynet, G., Chomienne, V., Ekström, S., et al. 2015a, A&A, 575, A60

Meynet, G., Kudritzki, R.-P., & Georgy, C. 2015b, A&A, 581, A36

Meynet, G. & Maeder, A. 2005, A&A, 429, 581

Sander, A., Hamann, W.-R., & Todt, H. 2012, A&A, 540, A144

Song, H. F., Maeder, A., Meynet, G., et al. 2013, A&A, 556, A100

Song, H. F., Meynet, G., Maeder, A., Ekstrom, S., & Eggenberger, P. 2015, ArXiv e-prints

Spruit, H. C. 2002, A&A, 381, 923

Suijs, M. P. L., Langer, N., Poelarends, A.-J., et al. 2008, A&A, 481, L87

Szécsi, D., Langer, N., Yoon, S.-C., et al. 2015, A&A, 581, A15

Zahn, J.-P. 1992, A&A, 265, 115

Zahn, J.-P., Brun, A. S., & Mathis, S. 2007, A&A, 474, 145

Anthony (Tony) Moffat: A new idea in hot luminous stars that has arisen recently (Cantiello et al. 2009) is subsurface convection. Is this important for your models?

Georges Meynet: Indeed in our models we obtain such a subsurface convective zone (see Maeder et al. 2008, A&A 479, L37). There is a possibility that convection plays a role in accelerating the stellar winds and in producing the clumps in the winds. Indeed, matter accelerated in the wind continously goes through the convection zone in a dynamical process. More details can be found in the above referenced paper.

Gloria Koenigsberger: a) Would you please explain again the mechanism for mixing in a rigidly rotating star?
b) How does the meridional circulation behave in the presence of an external gravitational field, as in the case of a binary companion?

Georges Meynet: In a rigidly rotating star, mixing is due to meridional currents which have quite high velocities in this case. An extended gravitational field, if strong enough, deforms the star and as such can likely trigger meridional currents. At the moment, this case has not been studied. Only deformation by the axial rotation of the star itself has been so far considered.

Wolf-Rayet Stars
W.-R. Hamann, A. Sander, H. Todt, eds.
Potsdam: Univ.-Verlag, 2015
URL: http://nbn-resolving.de/urn:nbn:de:kobv:517-opus4-84268

Do rapidly-rotating massive stars at low metallicity form Wolf–Rayet stars?

D. Szécsi[1], N. Langer[1], D. Sanyal[1], C. J. Evans[2], J. M. Bestenlehner[3] & F. Raucq[4]
[1] *Argelander-Institut für Astronomie der Universität Bonn, Germany*
[2] *UK Astronomy Technology Centre, Royal Observatory Edinburgh, UK*
[3] *Max Planck Institute for Astronomy, Heidelberg, Germany*
[4] *Institut d'Astrophysique, Liege University, Belgium*

The evolution of massive stars is strongly influenced by their initial chemical composition. We have computed rapidly-rotating massive star models with low metallicity (∼1/50 $Z_\odot$) that evolve chemically homogeneously and have optically-thin winds during the main sequence evolution. These luminous and hot stars are predicted to emit intense mid- and far-UV radiation, but without the broad emission lines that characterize WR stars with optically-thick winds. We show that such Transparent Wind UV-Intense (TWUIN) stars may be responsible for the high number of He II ionizing photons observed in metal-poor dwarf galaxies, such as I Zw 18. We find that these TWUIN stars are possible long-duration gamma-ray burst progenitors.

1 Stellar evolution at low Z

Massive stars at very low metallicity (1/50 $Z_\odot$) evolve differently to those at solar Z (Meynet & Maeder 2002; Brott et al. 2011; Yoon et al. 2012; Yusof et al. 2013). We have computed low-Z stellar evolutionary models in the mass range 9–300 $M_\odot$ and with initial rotational velocities between 0–600 km/s (Szécsi et al. 2015). Fig. 1 shows a representative sample of the computed tracks in the Hertzsprung-Russell (HR) diagram. The slow rotators (< 200 km/s) follow the normal evolutionary path which proceeds redwards from the zero-age main-sequence (ZAMS). After core-hydrogen burning, these stars develop a distinct core-envelope structure (i.e. no enhanced mixing between the core and the surface), burn helium on the red-supergiant branch and would explode as Type IIp supernovae (Langer 2012; Yoon et al. 2012; Szécsi et al. 2015).

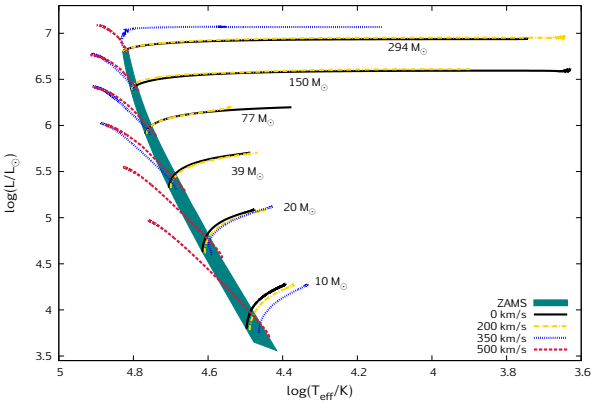

Fig. 1: Evolutionary tracks in the HR diagram during the core-hydrogen-burning phase for models with initial masses between 10–294 $M_\odot$ (see labels) and initial rotational velocities of 0, 200, 350 and 500 km s^{-1}, with a composition of 1/50 $Z_\odot$ (Szécsi et al. 2015). The green shading identifies the zero-age main-sequence.

On the other hand, the fast rotators (> 300 km/s) evolve bluewards from the ZAMS, and undergo chemically-homogeneous evolution. In this case, the mixing timescale is significantly shorter than the main-sequence lifetime of these stars, so all the nuclear burning products are mixed throughout the star. These stars stay compact and hot, spending their post-main-sequence lifetimes as fast rotating helium stars and would, according to the collapsar scenario, explode as long-duration gamma-ray bursts (lGRBs) (Yoon & Langer 2005; Woosley & Heger 2006; Yoon et al. 2006; Brott et al. 2011; Szécsi et al. 2015).

In this work, we aim to understand the observational properties of the potential lGRB progenitor stars during their main sequence lifetimes.

2 Transparent Wind UV-Intense (TWUIN) stars

2.1 TWUIN stars are not WR stars

Chemically-homogeneously-evolving stars were so far understood to be WR stars during their main-sequence evolution based on their position in the HR diagram (on the hot side of the ZAMS) and their surface composition (enhanced helium abundance). However, WR stars have optically thick winds which lead to the spectral emission lines observed, so in order to decide if chemically-homogeneously-evolving

stars are WR stars or not, one needs to analyse their wind properties.

We have estimated the optical depth of the wind (τ) in the chemically-homogeneously-evolving stars in our simulations[1] following Langer (1989). Fig. 2 shows the HR diagram of these stellar models with the wind optical depth colour coded. During most of their main-sequence lifetimes, these stellar models have *optically-thin winds* (i.e. $\tau \lesssim 1$). Therefore, they are not expected to show the broad emission lines in their spectra that characterize WR-type stars. On the other hand, they have luminosities up to 10^7 $L_\odot$ and surface temperatures up to 80 kK. Therefore, they emit intense UV radiation and photoionize their surroundings. To highlight that these hot stars with weak winds would look different from classical WR stars, we call them Transparent Wind Ultraviolet Intense (TWUIN) stars.

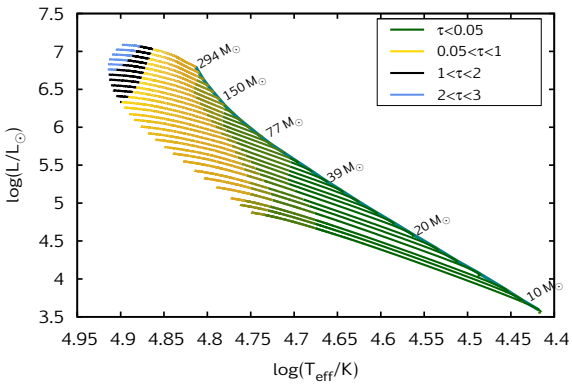

Fig. 2: HR diagram of low-Z stellar models with v_{ini}=500 km s^{-1} (chemically-homogeneous evolution) and masses between 9–294 $M_\odot$. Only the core-hydrogen burning phase is plotted (cf. Fig. 4). The colouring marks the wind optical depth τ according to Langer (1989). See Szécsi et al. (2015) for more details.

TWUIN stars are rapidly-rotating, main-sequence stars which are undergoing chemically-homogeneous evolution and have $\tau \lesssim 1$, predicted by our stellar simulations with low-Z (1/50 $Z_\odot \sim$ 1/10 Z_{SMC}). Based on the empirical distribution of rotational velocities for O stars in the Small Magellanic Cloud (SMC) by Mokiem et al. (2006), we expect that at least 10%, but possibly more, of the massive stars in a given starburst would be influenced by chemically-homogeneous evolution in a 1/50 $Z_\odot$ environment.

2.2 Ionizing photons in I Zw 18

I Zw 18 is a blue compact dwarf galaxy (Legrand et al. 1997; Aloisi et al. 1999; Izotov et al. 1999; Schaerer et al. 1999; Shirazi & Brinchmann 2012; Kehrig et al. 2013) with very low metal content (12+log(O/H)=7.17 $\rightarrow$ $Z_{IZw18} \simeq$ 1/50 $Z_\odot$, Lebouteiller et al. 2013). Kehrig et al. (2015) observed I Zw 18 and found an unusually high He II photon flux of $Q(\mathrm{He\,II})^{obs} \approx 10^{50}$ s^{-1}, which could not be attributed to the rather small WR stellar population in this galaxy (Crowther & Hadfield 2006). Kehrig et al. (2015) therefore proposed that Pop III stars could be responsible for the corresponding ionizing radiation (see also Heap et al. 2015). However, while the gas in I Zw 18 is very metal poor, it is not primordial, so the presence of Pop III stars in I Zw 18 is debatable.

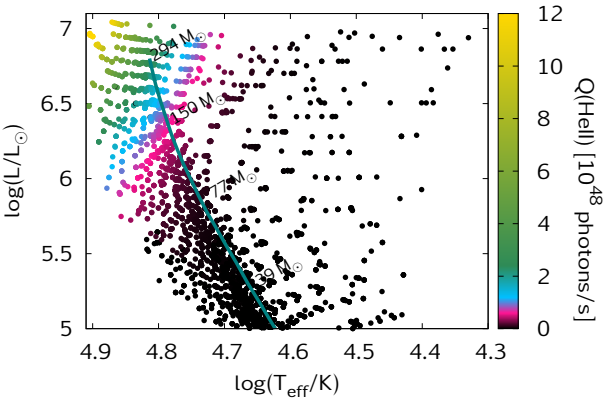

Fig. 3: Dots of equal timesteps (10^5 yr) of our low-Z stellar models (both, slow and fast rotators) in the HR diagram. The thick green line marks the ZAMS. The colouring represents the photon number rate in the He II continuum produced by our models, based on the black body approximation (cf. Szécsi et al. 2015). TWUIN stars are left from the ZAMS; the most massive of them emit as much as 10^{49} He II ionizing photons per second.

In our simulations, the fast rotators evolve chemically homogeneously and become TWUIN stars during their main-sequence lifetime. According to Fig. 3, the hottest and most luminous of the TWUIN stars (~300 $M_\odot$) produce a He II ionizing flux in the order of 10^{49} photons s^{-1}. This means that the total He II flux, $Q(\mathrm{He\,II})^{obs}$ observed in I Zw 18 could be produced by just a few very massive TWUIN stars.

It may be more likely that the observed ionizing flux is produced by TWUIN stars of ~100 $M_\odot$, which emit a He II ionizing flux of about 5×10^{48} pho-

[1] We use the prescription of Hamann et al. (1995) for the winds of our models with reduction by a factor of 10 as suggested by Yoon et al. (2006), as this reduction gives a mass-loss rate comparable to the most commonly adopted one by Nugis & Lamers (2000) (see Fig. 1. of Yoon 2015). The Hamann et al. (1995) prescription is applied together with a metallicity dependence of $\dot{M} \sim Z^{0.86}$ (Vink et al. 2001).

tons s^{-1}. Consequently, about 20 TWUIN stars with 100 $M_\odot$ could explain the observations. Given that the star formation rate for I Zw 18 is about 0.1 $M_\odot$ yr^{-1} (Lebouteiller et al. 2013), this number of TWUIN star appears quite plausible (Szécsi et al. 2015).

2.3 The post-MS phase

TWUIN stars are expected to spend their post-main-sequence evolution as WR stars with optically-thick winds, see Fig. 4. This finding is in accordance with our interpretation of the observations of I Zw 18: while during core hydrogen burning these models are in the TWUIN star phase, but during their post-main-sequence lifetime they would constitute the small WR population found in the galaxy.

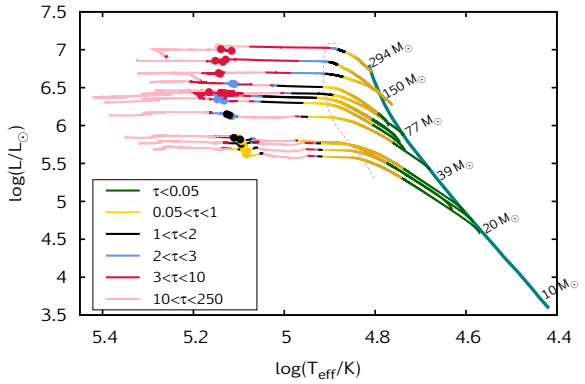

Fig. 4: HR diagram depicting the post-main-sequence phase of the TWUIN stars (v_{ini}=500 km/s). The thick green line marks the ZAMS, the thin dashed line marks the end of core hydrogen burning. The colouring indicates the wind optical depth τ according to Langer (1989). Dots mark approximately where the stars burn helium in the core.

3 Conclusions

We have presented stellar evolutionary predictions for massive stars at the composition of the dwarf galaxy I Zw 18. We found that the main-sequence stars populate both sides of the ZAMS. Our fast rotating stars, which may comprise more than 10% of all massive stars, evolve chemically homogeneously and bluewards in the HR diagram. We call them TWUIN stars and note that they are not WR stars in the classical sense. Due to their extremely high effective temperatures and the optically-thin winds, TWUIN stars would have very high ionizing fluxes. We argue that the measured He II flux of I Zw 18 as well as weakness of Wolf-Rayet features is compatible with a population of TWUIN stars in this galaxy.

The TWUIN stars, which have weak winds because of their low metal content, are possible lGRB progenitors, as they do not lose enough angular momentum in the wind. Our conclusion is that the high HeII flux observed in dwarf galaxies can be a signpost for upcoming lGRBs in these objects. Additionally, the observed high HeII flux may argue that chemically-homogeneous evolution, which leads to the TWUIN stars, is indeed happening in nature.

References

Aloisi, A., Tosi, M., & Greggio, L. 1999, ApJ, 118, 302
Brott, I., de Mink, S. E., Cantiello, M., et al. 2011, A&A, 530, A115
Crowther, P. A. & Hadfield, L. J. 2006, A&A, 449, 711
Hamann, W.-R., Koesterke, L., & Wessolowski, U. 1995, A&A, 299, 151
Heap, S., Bouret, J.-C., & Hubeny, I. 2015, ArXiv e-print 1504.02742
Izotov, Y., Papaderos, P., Thuan, T., et al. 1999, unpublished
Kehrig, C., Pérez-Montero, E., Vílchez, J. M., et al. 2013, MNRAS, 432, 2731
Kehrig, C., Vílchez, J. M., Pérez-Montero, E., et al. 2015, ApJ, 801, L28
Langer, N. 1989, A&A, 210, 93
Langer, N. 2012, ARA&A, 50, 107
Lebouteiller, V., Heap, S., Hubeny, I., & Kunth, D. 2013, A&A, 553, A16
Legrand, F., Kunth, D., Roy, J.-R., Mas-Hesse, J. M., & Walsh, J. R. 1997, A&A, 326, L17
Meynet, G. & Maeder, A. 2002, A&A, 390, 561
Mokiem, M. R., de Koter, A., Evans, C. J., et al. 2006, A&A, 456, 1131
Nugis, T. & Lamers, H. J. G. L. M. 2000, A&A, 360, 227
Schaerer, D., Contini, T., & Kunth, D. 1999, A&A, 341, 399
Shirazi, M. & Brinchmann, J. 2012, MNRAS, 421, 1043
Szécsi, D., Langer, N., Yoon, S.-C., et al. 2015, A&A (accepted), [arXiv:1506.09132]
Vink, J., de Koter, A., & Lamers, H. 2001, A&A, 369, 574
Woosley, S. & Heger, A. 2006, ApJ, 637, 914
Yoon, S.-C. 2015, PASA, 32, 15
Yoon, S.-C., Dierks, A., & Langer, N. 2012, A&A, 542, A113
Yoon, S.-C. & Langer, N. 2005, A&A, 443, 643
Yoon, S.-C., Langer, N., & Norman, C. 2006, A&A, 460, 199
Yusof, N., Hirschi, R., Meynet, G., et al. 2013, MNRAS, 433, 1114

Jose Groh: 1) Are you assuming a Langer et al. (1989) relationship for estimating the wind optical depth (i.e. β=2, v_{inf}=2000 km/s)?

2) Also, have you estimated the LGRB rate if they all indeed come from chemically-homogeneous stars?

Dorottya Szécsi: 1) Yes.

2) Yes, and we found that our results are consistent with the study of Yoon et al. (2006), who found a very similar threshold rotational velocity for chemically-homogeneous evolution for stars below 60 $M_\odot$ as the present work. While we shall present the post-main-sequence evolution of our models in a forthcoming study, from our models we can expect a similar ratio of long-duration GRBs to supernovae of the order of 1–3% as Yoon et al. (2006).

Paul Crowther: A couple of dozen fast rotator very massive stars (100 $M_\odot$+) are required to reproduce $Q_2(He^2+) \sim 10^{50}$ in I Zw 18. But this requires that *all* VMSs are fast rotators given its 30 Doradus-like (i.e. 0.1 $M_\odot^{out}$ yr^{-1}) star formation rate (Izotov et al. 1999), doesn't it?

Dorottya Szécsi: We have calculated that, assuming a star formation rate of 0.1 $M_\odot$/yr, about 10–20% of the massive stars need to be fast rotators (i.e. chemically-homogeneously evolving stars) in order to explain the observed He II flux. Indeed, based on the empirical distribution of rotational velocities for O stars in the SMC by Mokiem et al. (2006), up to 20% of the very massive stars could undergo chemically-homogeneous evolution.

Carolina Kehrig: Which are the highest values of He II/H(β) (i.e. Q(He II)/Q(H)) predicted by your most-massive hottest models?

Dorottya Szécsi: Our hottest TWUIN star model with $M_{ini} = 294\,M_\odot$ predicts a value of $\log[Q(\text{He II})/Q(\text{H})] = -1.75$.

Wolf-Rayet Stars
W.-R. Hamann, A. Sander, H. Todt, eds.
Potsdam: Univ.-Verlag, 2015
URL: http://nbn-resolving.de/urn:nbn:de:kobv:517-opus4-84268

The impact of rotation on the line profiles of Wolf-Rayet stars

T. Shenar[1], **W.-R. Hamann**[1] **& H. Todt**[1]
[1] *Universität Potsdam, Germany*

The distribution of angular momentum in massive stars is a critical component of their evolution, yet not much is known on the rotation velocities of Wolf-Rayet stars. There are various indications that rapidly rotating Wolf-Rayet stars should exist. Unfortunately, due to their expanding atmospheres, rotational velocities of Wolf-Rayet stars are very difficult to measure. In this work, we model the effects of rotation on the atmospheres of Wolf-Rayet stars by implementing a 3D integration scheme in the PoWR code. We further investigate whether the peculiar spectra of five Wolf-Rayet stars may imply rapid rotation, infer the corresponding rotation parameters, and discuss the implications of our results. We find that rotation helps to reproduce the unique spectra analyzed here. However, if rotation is indeed involved, the inferred rotational velocities at the stellar surface are large ($\sim 200\,$km/s), and the implied co-rotation radii ($\sim 10 R_*$) suggest the existence of very strong photospheric magnetic fields ($\sim 20\,$kG).

1 Introduction

The rotation rates of Wolf-Rayet (WR) stars are crucial in the context of the evolution of massive stars (e.g. Meynet & Maeder 2005; Georgy et al. 2014). Rotation dramatically affects the chemical stratification of the star due to rotationally induced mixing (e.g. Heger & Langer 2000), surface deformations (von Zeipel 1924; Bjorkman & Cassinelli 1993), and may provide extra driving of the stellar wind (Friend & Abbott 1986). Furthermore, WR stars with rapidly rotating cores have been proposed as progenitors of long-duration gamma-ray bursts (LGRBs) by various authors, relying on the collapsar model of Woosley (1993).

Recent spectroscopic studies performed with the non-LTE Potsdam Wolf-Rayet (PoWR) model atmosphere code potentially imply the existence of rapidly rotating WR stars. Hamann et al. (2006) and Hainich et al. (2014), who performed extensive spectroscopic studies of a total sample of ~ 180 WN stars, made use of a flux-convolution with a rotation profile in order to reproduce the broad and round emission lines of a few WR stars in their samples. The sample of WN stars portraying these unique broad profiles composes a galactic WR star, WR 2, and four WR stars residing in the Large Magellanic Cloud (LMC): BAT99 7, 51, 88, and 94. To emphasize the striking uniqueness of these spectra, we show a comparison (Fig. 1) between the observed spectra of two WN4b stars residing in the LMC: BAT99 7 (solid blue line), which is in the round-lined star sample, and BAT99 134 (dashed green line). Note the distinct qualitative difference between the two spectra – and this despite their identical spectral class! Out of hundreds of WR stars previously analyzed, only a handful exhibit such exceptional features. We note that Chené et al. (in prep.) claim to have been able to reproduce the spectrum of WR 2 without assuming any rotation.

A few WR stars have been observed to show periodic photometric variations which may be attributed to so called co-rotating interaction regions (CIRs) in the wind (Marchenko & Moffat 1998; Cranmer & Owocki 1996; Chené & St-Louis 2005). Rotation may also lead to a the departure from spherical symmetry which can be detected with polarimetry via the so-called line effect (e.g. Harries et al. 1998), i.e. an enhanced polarization of the continuum radiation relative to that of emission lines. Yet rotational broadening of spectral lines remains the most direct method to detect and calculate rotational velocities of stars. Alas, a simple flux convolution of rotation profiles cannot be applied to WR spectra because they are formed in extended atmospheres. To model rotation in expanding atmospheres, an accurate, 3D integration of the emerging intensities is needed. In these proceedings, which are heavily based on published results by Shenar et al. (2014), we shortly describe the modeling of rotation in expanding atmospheres, and discuss the modeling results.

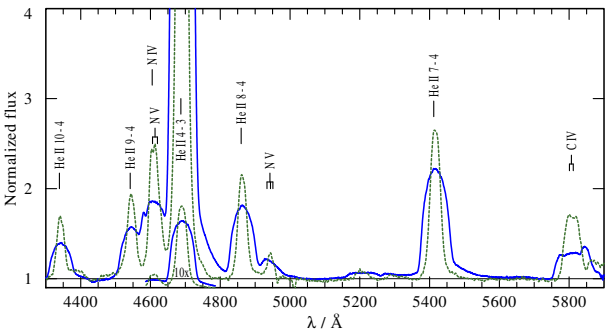

Fig. 1: Comparison between the observed optical spectra of two WN4b stars in the LMC: BAT99 134 (dashed green line), and BAT99 7 (solid blue line).

2 Modeling the effect of rotation on WR spectra

The modeling in this work is performed using the non-LTE model atmosphere PoWR code. A description of the assumptions (spherical symmetry, stationary mass-loss) and methods used in the code is given by Gräfener et al. (2002) and Hamann & Gräfener (2004). The rotational velocity field adopted here is divided into two radial domains: (a) the co-rotating domain $r \leq R_{\rm cor}$, where we postulate the existence of a radius $R_{\rm cor}$ larger or equal to the stellar surface R_*, up to which the wind co-rotates with the star (constant angular velocity), and (b) the outer domain $r > R_{\rm cor}$, where the only forces present are radial, and where the angular momentum is therefore conserved.

Rotation is modeled here only during the formal integration of the emergent intensities, i.e. any possible effect of rotation on the population numbers of the wind plasma are ignored. A thorough discussion of the assumptions and their justifications can be found in Shenar et al. (2014). The structure of the assumed velocity field implies a linear increase of the ϕ-component of the wind velocity up to $r = R_{\rm cor}$, and a sharp decrease of $1/r$ beyond the co-rotation radius due to angular momentum conservation.

3 Results and discussion

A systematic test of the influence of the two free parameters, $v \sin i$ and $R_{\rm cor}$, reveals that even rapid rotation bears no notable influence when no co-rotation of the stellar wind is assumed (i.e. $R_{\rm cor} = R_*$.). The reason is that the majority of lines are formed far above the stellar surface ($r \sim 10\,R_*$), where the rotational velocity becomes very small due to angular momentum conservation. This is thoroughly illustrated in Sect. 4.2 in Shenar et al. (2014).

Generally, the co-rotation radii are found to be of the order of $10\,R_*$, and the co-rotation velocities of the order of 2000 km/s. The implied rotation velocities at the surface of the stars are therefore of the order of 200 km/s. In Fig. 2, we show an example for the effect of rotation for two stars in our sample, BAT99 94 (upper panels) and 88 (lower panels). The model including rotation (dotted red lines) is compared to the non-rotating model (dashed black line) and to the observations (solid blue lines). Generally, suitable rotation parameters help to reproduce the round and broad appearance of the spectral lines. The detailed results of the rotation parameters are given in Shenar et al. (2014). Below, we discuss the general character of the results, their implications, and their plausibility.

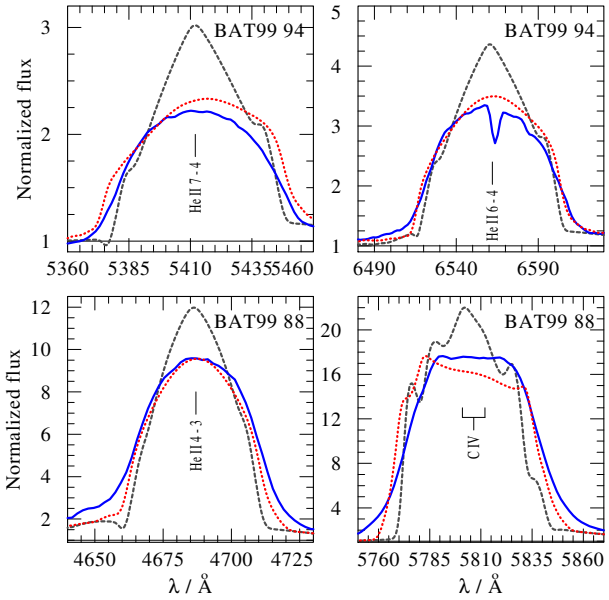

Fig. 2: Comparison between synthetic spectra calculated with rotation (dotted red line) and without rotation (dashed black line) with the observations (solid blue line) for two He II lines belonging to BAT99 94 and 88.

3.1 Rapid rotation

While it conceivable that the WR stars would rotate with velocities of the order of 200 km/s at their surface, the velocities found at the co-rotation radii exceed the local escape velocities by far. One would thus expect to be able to observe significant deviations from spherical symmetry in our sample.

A common method to detect asymmetry in stellar winds is by searching for the so-called line effect (e.g. Schulte-Ladbeck et al. 1991; Harries et al. 1998). Chené et al. (in prep.) extensively analyzed polarimetric data of WR 2 and did not find any linear line depolarization down to the 0.05% noise level, and attribute the 3% linear polarization detected by Akras et al. (2013) to scattering off grains in the interstellar matter. The non-detection of the line effect in WR 2 thus challenges its rapid rotation suggested in this work. As thoroughly discussed in Sect. 5.3 in Shenar et al. (2014), although relatively little scattering occurs in the outermost wind layers, their asymmetry is likely to cause a net continuum polarization to a certain extent. However, the net polarization is very hard to estimate without consistent modeling, and it is not a-priori clear that the resulting asymmetries would have measurable consequences. We therefore stress the need for modeling polarized radiative transfer in co-rotating atmospheres. Whether an obvious contradiction between the polarimetric data and the rotation hypothesized here arises remains to be seen.

3.2 Large co-rotation radii

The postulated co-rotation of the wind is motivated by the possible existence of strong magnetic fields in WR stars. Using some simple assumptions on the postulated magnetic field geometry, is possible to estimate the stellar magnetic field B_* necessary to confine the matter up to a given co-rotation radius (see Sect. 5.4 in Shenar et al. 2014). The magnetic field estimates turn out to be very large, of the order of 20 kG at the photosphere ($\tau_{\rm Ross} \sim 2/3$).

Admittedly, the inferred magnetic fields are very strong. Nevertheless, a couple of OB stars were observed to exhibit strong magnetic fields of several kG (see Nazé 2013, for a review on the topic), with one star even reaching a value of ~ 20 kG (cf. Wade et al. 2012). Since these stars are recognized as progenitors of WR stars, it is plausible that some WR stars can have photospheric magnetic fields of at least this order of magnitude. Taking this reasoning one step further, magnetic fields of magnetars, recognized to be the descendents of WR stars (e.g. Gaensler et al. 2005), often reach values of $10^{14} - 10^{15}$ G (e.g. Esposito et al. 2009). However, to date, any attempts to detect global magnetic larger than several 100 G fields in WR stars have failed (e.g. Kholtygin et al. 2011; de la Chevrotière et al. 2013).

4 Summary

To summarize, among the ~ 180 WN stars analyzed in the Galaxy and in the LMC, we identified five stars (one galactic, four LMC) whose spectra exhibit exceptionally broad and round emission line profiles. It has been suggested that these profiles might indicate rapid rotation (Hamann et al. 2006). Motivated by this and by the lack of alternative explanations, we extended our code to properly handle rotation in expanding atmospheres of hot stars. The modeling of rotation in expanding atmospheres can have a variety of applications, as illustrated by Hillier et al. (2012) for the case of O stars and by Hainich et al. (2015) for the case of WR stars.

We find that rotation helps to reproduce the unique spectra analyzed here. However, the plausibility of the implied rotational velocities and magnetic fields is challenged by other studies. Future observations of the remaining stars in our sample, especially spectropolarimetric ones which could potentially detect the existence of magnetic fields in the sample stars, could help to support, or disprove, the hypothesis brought to test here.

References

Akras, S., Ramirez Velez, J., Hiriart, D., & Lopez, J. M. 2013, in Massive Stars: From alpha to Omega, Conference held June 2013, Rhodes, Greece, id. 53

Bjorkman, J. E. & Cassinelli, J. P. 1993, ApJ, 409, 429

Chené, A.-N. & St-Louis, N. 2005, JRASC, 99, 132

Cranmer, S. R. & Owocki, S. P. 1996, ApJ, 462, 469

de la Chevrotière, A., St-Louis, N., Moffat, A. F. J., & the MiMeS Collaboration. 2013, ApJ, 764, 171

Esposito, P., Burgay, M., Possenti, A., et al. 2009, MNRAS, 399, L44

Friend, D. B. & Abbott, D. C. 1986, ApJ, 311, 701

Gaensler, B. M., McClure-Griffiths, N. M., Oey, M. S., et al. 2005, ApJ, 620, L95

Georgy, C., Granada, A., Ekström, S., et al. 2014, A&A, 566, A21

Gräfener, G., Koesterke, L., & Hamann, W.-R. 2002, A&A, 387, 244

Hainich, R., Pasemann, D., Todt, H., et al. 2015, A&A, 581, A21

Hainich, R., Rühling, U., Todt, H., et al. 2014, A&A, 565, A27

Hamann, W.-R. & Gräfener, G. 2004, A&A, 427, 697

Hamann, W.-R., Gräfener, G., & Liermann, A. 2006, A&A, 457, 1015

Harries, T. J., Hillier, D. J., & Howarth, I. D. 1998, MNRAS, 296, 1072

Heger, A. & Langer, N. 2000, ApJ, 544, 1016

Hillier, D. J., Bouret, J.-C., Lanz, T., & Busche, J. R. 2012, MNRAS, 426, 1043

Kholtygin, A. F., Fabrika, S. N., Rusomarov, N., et al. 2011, Astronomische Nachrichten, 332, 1008

Marchenko, S. V. & Moffat, A. F. J. 1998, ApJ, 499, L195

Meynet, G. & Maeder, A. 2005, A&A, 429, 581

Nazé, Y. 2013, ArXiv e-prints 1306.6753

Schulte-Ladbeck, R. E., Nordsieck, K. H., Taylor, M., et al. 1991, ApJ, 382, 301

Shenar, T., Hamann, W.-R., & Todt, H. 2014, A&A, 562, A118

von Zeipel, H. 1924, MNRAS, 84, 665

Wade, G. A., Maíz Apellániz, J., Martins, F., et al. 2012, MNRAS, 425, 1278

Woosley, S. E. 1993, ApJ, 405, 273

Philip Massey: Some WRs have intrinsic absorption lines, such as HD 193077 (WR 138), a star that has very high $v \sin i$ (500 km/s) as shown from a Fourier analysis of the absorption (Massey 1980, ApJ, 236, 526). Do these stars help at all?

Tomer Shenar: WR 138 has reported low-amplitude radial velocity measurements, suggesting it may be an eccentric, long-term WR+B binary (Lamontagne et al. 1982, ApJ, 253, 230, and following studies). Hamann et al. (2006, ApJ, 457, 1015) associate the He I absorption lines in the star with a companion, so there is a good chance the measured rotation corresponds to the companion (but this requires further study). Generally, absorption lines intrinsic to a WR star are natural candidates for probing rotation at the surface, but given that these lines will probably be associated with H I / He II, pressure-broadening, in combination with the very uncertain gravities of WR stars, may cause problems here.

Philip Massey: There is a nice summery of the history of RV studies of WR 138 by Palate et al. (2013). There is evidence of a 1550 day period (see the discussion by Palate et al. 2013, A&A, 560, A27) in the emission line velocities, but the amplitude is low and the radial velocities have not been measured consistently. I now have data on this star extending over a decade, the results of which will be discussed elsewhere. In the meanwhile it is worth noting that if the punitive companion is an OB star, its $v \sin i$ of 500 km/s is uniquely high. That seems quite a coincidence, doesn't it?

Tomer Shenar: This is indeed a challenge, but there are resolutions that come to mind. (Perhaps the companion is a binary itself?) It won't be necessarily easier to account for such a high rotation velocity in a single WR star, and it would be even harder to explain the presence of He I lines in its spectrum. I'm expecting those new results which will be discussed elsewhere!

Dominik Bomans: How rare are these round emission line WR stars?

Tomer Shenar: 1 out of the 63 Galactic WNs analyzed by Hamann et al. (2006, A&A, 457, 1015) and 4 out of the 102 LMC WNs analyzed by Hainich et al. (2014, A&A, 565, 27) are found to show these unique profiles (WR 2, BAT99 7, 51, 88, and 94). Sander et al. (2012, A&A, 540, 144) reported roundish profiles for two out of the four Galactic WO stars (WR 102 and 142), but the profiles are not as extreme, and Frank Tramper could reproduce them using standard assumptions in his PhD thesis. So, pretty rare!

Anthony (Tony) Moffat: In fact Chené et al. did find low-level, but clear spectral variation due to clumping, pointing to a high terminal velocity in WR 2 that is not compatible with your much lower value.

Tomer Shenar: Admittedly, the soon-to-be-published study by Chené et al. poses many challenges to the hypothesis of rotation in WR 2, and I wouldn't like to continue backing this hypothesis if Chené et al. do indeed manage to reproduce the profiles using standard assumptions, as they claim in their paper. I'm not sure about this specific argument though: It seems that the derivation of clump velocities performed by Chené et al. is heavily based on the assumption that the velocity field in the wind consists solely of a radial outflow (as implied by their Eq. 4).

Tomer Shenar (with microphone) asking a question. Also visible in this picture are A. Liermann (left, standing), A. E. Lynas-Gray (left, sitting), and H. Todt (right, sitting).

Wolf-Rayet Stars
W.-R. Hamann, A. Sander, H. Todt, eds.
Potsdam: Univ.-Verlag, 2015
URL: http://nbn-resolving.de/urn:nbn:de:kobv:517-opus4-84268

Helium stars: Towards an understanding of Wolf–Rayet evolution

L. A. S. McClelland[1] **& J. J. Eldridge**[1]
[1] *University of Auckland, New Zealand*

There are outstanding problems in trying to reproduce the observed nature of Wolf–Rayet stars from theoretical stellar models. We have investigated the effects of uncertainties, such as composition and mass-loss rate, on the evolution and structure of Wolf–Rayet stars and their lower mass brethren. We find that the normal Conti scenario needs to be altered, with different WR types being due to different initial masses as well as different stages of evolution.

1 Introduction

Wolf–Rayet (WR) stars are massive helium-burning stars that, through strong mass loss, have lost all or most of their hydrogen envelopes leaving a partially or fully exposed helium core. We have generated a grid of pure helium star models at various metallicities and shall only study the evolution from onset of core-helium burning onwards.

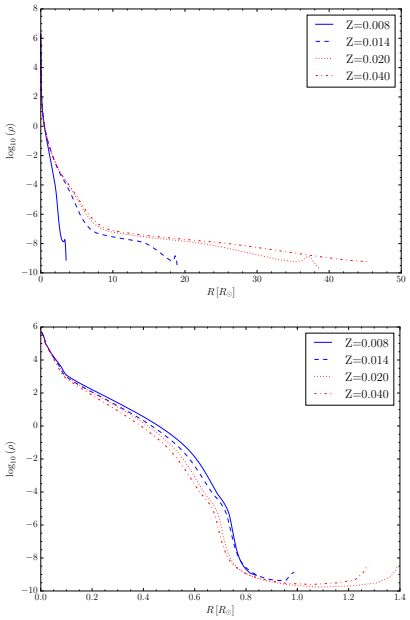

Fig. 1: Density profile of a 3 and 15 $M_\odot$ helium star (top and bottom, respectively) at the end of shell-helium burning for different metallicities.

2 Computational method

2.1 Construction of the Models

To investigate the evolution of helium stars, we have constructed a grid of hydrogen-free models. We make use of the Cambridge STARS evolutionary code. Originally developed by Eggleton (1971), it has been modified by various groups; herein, we employ the version described by Stancliffe & Eldridge (2009).

We make our selection of metallicities based on the expected environments of WR stars: $Z = 0.008$ for the Large Magellanic Cloud; $Z = 0.014$ and $Z = 0.02$ being, respectively, "new" and "old" solar metallicity; and $Z = 0.04$, double "old" solar. To clarify the selection regarding solar metallicity, we have utilised the solar abundance determinations from Grevesse & Sauval (1998) ("old" solar) and Asplund et al. (2009) ("new" solar). A comparison of evolution between models of "old" and "new" solar compositions shows very little difference, and in light of this, we prefer "old" solar abundances for use in our models. Our preference for using "old" solar abundance agrees with the nearby cosmic abundance standard from Nieva & Przybilla (2012).

2.2 Mass-loss Scheme

We employ a mass-loss scheme, outlined in Eldridge & Vink (2006), which is derived from Nugis & Lamers (2000):

$$\dot{M}_Z \propto \dot{M}\beta \left(\frac{Z}{Z_\odot}\right)^{\frac{1}{2}}, \qquad (1)$$

where $\dot{M}$ is taken from Eldridge & Vink (2006), Z is the metallicity of the model, and $Z_\odot$ is solar metallicity. To test the effect of varying the mass-loss rate on the evolution of a model, we introduce a parameter, β. We may use this parameter to estimate the evolution of the helium star model if, before the hydrogen envelope were removed, more helium burning had occurred. For example in the case of $\beta = 1$, the hydrogen envelope is removed before the beginning of helium burning, so the tracks represent the greatest possible effect of mass loss on the models. Thus, more helium mass would be lost from the WR stars. However for $\beta = 0$, the evolution towards the end of the track represents how the star would appear if the hydrogen envelope were removed near the end of helium burning.

3 Results

We may divide our helium star models into two categories: low mass ("helium-giant type"), and high mass ("Wolf–Rayet type").

3.1 Low-mass helium stars

Low-mass ($< 8\mathrm{M}_\odot$) helium star models evolve as "helium giants". A helium giant has a stellar structure that is analogous to that of a red-giant star: a dense core region with an expansive envelope (see top panel of Fig. 1).

3.2 High-mass helium stars

High-mass ($> 8\mathrm{M}_\odot$) helium star models evolve as "traditional" Wolf–Rayet stars, having characteristic high temperatures due to strong mass loss (Crowther 2007). The structure of a high-mass helium star differs from that of a low-mass helium star by the properties of its envelope: an extended region of near-constant density with a large density inversion at the surface (see bottom panel of Fig. 1). The density inversion sits atop the extended envelope structure of the high-mass helium star models, and due to the stellar interior reaching the phase space of the iron-opacity peak (Gräfener et al. 2012), is affected by metallicity.

4 Populations of helium stars

In Figure 2 we present our models compared to observed WR stars on the Hertzsprung–Russell diagram. Observational data is taken from Hamann et al. (2006); Sander et al. (2012), for Galactic WN and WC stars; Hainich et al. (2014), for Large Magellanic Cloud (LMC) WN stars; and Tramper et al. (2013, 2015), for WO stars. In our work, we attempt to reproduce the observed locations of WR stars.

4.1 WN stars

Observed early-type WN stars lie near the HeZAMS for massive helium stars and are, generally, in good agreement with helium star models above $\approx 10\mathrm{M}_\odot$. However, the agreement is not so favourable for observed late-type WN stars. These WN stars have stellar temperatures that are far cooler than temperatures at the HeZAMS, and their locations cannot be reproduced using models with $\beta > 0$.

Without mass loss ($\beta = 0$), we see an interesting result: the higher mass helium star models do, indeed, cross the region of observed (hydrogen-free) late-type WN stars for solar metallicity ("old" and "new"). A small amount of mass loss will remove the outer layers of the envelope and expose the hot interior of the model. Thus, without mass loss, the model swells due to inflation and the surface temperature decreases.

4.2 WC/WO stars

The expected locations of WC stars (marked in solid blue lines) are in very poor agreement with the positions of observed WC stars. As first suggested by Sander et al. (2012) in their analyses of Galactic WC stars, the Conti scenario (Conti 1975) is insufficient at explaining this discrepancy. We note from Fig. 2 that low-mass helium models can reproduce the observed locations of early- and late-type WC stars.

The observed WO stars in Fig. 2 occupy locations on the HR diagram that are hotter and more luminous than the observed WC stars, implying a higher stellar mass for WO stars. We find the observed WO stars in a region predicted by our high-mass models.

5 Discussion

In light of our work, we can draw some firm conclusions about certain aspects of WR star evolution and speculate about others.

First, WO stars are what we have always considered to be WC stars in stellar models. They are the progeny of the most massive WN stars ($M_{\mathrm{He,i}} \gtrsim 10\mathrm{M}_\odot$) that have suffered significant mass loss and are the hottest WR stars. Due to their significant mass loss, WO stars are likely to explode as Type Ic supernovae at any metallicity. However, these massive stars are also likely to form black holes at core collapse, so it is unknown as to whether they produce visible supernovae (e.g., Smartt 2015).

Second, WC stars evolve from less massive stars ($M_{\mathrm{He,i}} \lesssim 10\mathrm{M}_\odot$). The evolution of these stars could be described either as an inflationary effect occurring towards the end of their lives or as them becoming helium giants. The WC stars experience increased mass loss as they evolve; a consequence of a decrease in surface gravity allowing material on the surface to be removed more efficiently. The expansion of the envelope, whether through inflation or a helium-giant phase, is metallicity dependent. For low metallicities, the stars would retain a small fraction of hydrogen in their envelopes, and would not be identified as WC stars. This is in agreement with the lack of observed WC stars at low metallicity. We note the WC stars are unlikely to be the evolutionary end-points of the typical WN stars observed. They are more likely to arise from lower mass objects that we have yet to find; the recently identified and very faint WN3/O3 stars discovered by Massey et al. (2015) are also possible candidates.

In summary, we have created a series of helium star models at various metallicities and mass-loss rates. The models are available for download on the BPASS website (http://bpass.auckland.ac.nz).

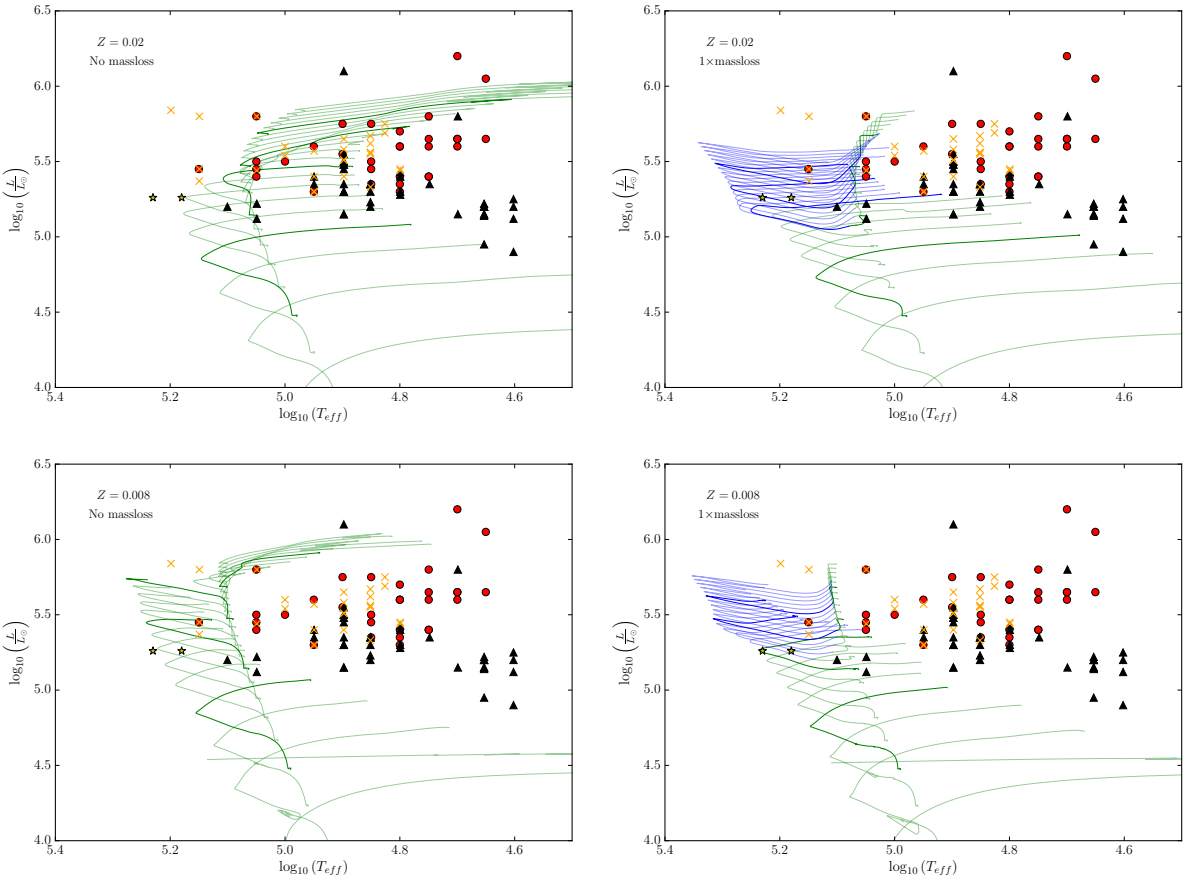

Fig. 2: HR diagram of our evolved models. For clarity, models with initial masses of 5, 10, 15 and 20 $M_\odot$ are made thicker. Observed WR star locations are marked as follows: Galactic WN, red circles; Galactic WC, black triangles; WO, yellow stars; and LMC WN, orange saltires. All observed stars are hydrogen-free. The phase of WR mass loss is indicated, WN (solid, green line) and WC (solid, blue line); non-WR mass loss is shown with solid, black lines. Mass-loss rate and metallicity are noted on the plots.

Future areas of research include incorporating the inflation of Gräfener et al. (2012) into the model evolution, and increasing the resolution of the model grids

References

Asplund, M., Grevesse, N., Sauval, A. J., & Scott, P. 2009, ARA&A, 47, 481

Conti, P. 1975, Memoires of the Societe Royale des Sciences de Liege, 9, 193

Crowther, P. A. 2007, ARA&A, 45, 177

Eggleton, P. P. 1971, MNRAS, 151, 351

Eldridge, J. J. & Vink, J. S. 2006, A&A, 452, 295

Gräfener, G., Owocki, S. P., & Vink, J. S. 2012, A&A, 538, A40

Grevesse, N. & Sauval, A. J. 1998, Space Sci. Rev., 85, 161

Hainich, R., Rühling, U., Todt, H., et al. 2014, A&A, 565, A27

Hamann, W.-R., Gräfener, G., & Liermann, A. 2006, A&A, 457, 1015

Massey, P., Neugent, K. F., Morrell, N., & John Hillier, D. 2015, in IAU Symposium, Vol. 307, IAU Symposium, 64–69

Nieva, M.-F. & Przybilla, N. 2012, A&A, 539, A143

Nugis, T. & Lamers, H. J. G. L. M. 2000, A&A, 360, 227

Sander, A., Hamann, W.-R., & Todt, H. 2012, A&A, 540, A144

Smartt, S. J. 2015, ArXiv e-prints

Stancliffe, R. J. & Eldridge, J. J. 2009, MNRAS, 396, 1699

Tramper, F., Gräfener, G., Hartoog, O. E., et al. 2013, A&A, 559, A72

Tramper, F., Straal, S. M., Gräfener, G., et al. 2015, in IAU Symposium, Vol. 307, IAU Symposium, 144–145

D. John Hillier: *(also to John Eldridge)* Do you expect WCs that arise in binary evolution to be slow rotators? Most WC stars show no evidence for polarization.

John Eldridge: Binary WC stars would be expected to be slow rotators. Especially if they have expanded as, by conservation of momentum, they would also spin down. Although, if they are in binaries, we don't know how strong the tides would be.

Norbert Langer: In your comparison to observations, you should not include the pre-MS He stars or the cool He-giant phase, as they are very short lived.

Liam McClelland: The post-helium-burning lifetime of low-mass helium stars (the He giants) is comparable to the helium-burning lifetime of the more massive stars.

Philip Massey: Is there a problem with the scarcity of WOs and this result?

Liam McClelland: The scarcity of WO stars is consistent with the short lifetime of that phase.

Liam McClelland (l.) listens to the question from Phil Massey

Wolf-Rayet Stars
W.-R. Hamann, A. Sander, H. Todt, eds.
Potsdam: Univ.-Verlag, 2015
URL: http://nbn-resolving.de/urn:nbn:de:kobv:517-opus4-84268

Instabilities in the envelope of Wolf-Rayet stars

L. Grassitelli[1], N. Langer[1], D. Sanyal[1], L. Fossati[1,2] & J. M. Bestenlehner[1,3]
[1] *Argelander Institute for Astronomy, Universität Bonn, Germany*
[2] *Space Research Institute, Austrian Academy of Sciences, Graz, Austria*
[3] *Max-Planck-Institute for Astronomy, Heidelberg, Germany*

Wolf-Rayet stars are very hot stars close to the Eddington limit. In the conditions encountered in their radiation pressure dominated outer layers several instabilities are expected to arise. These instabilities could influence both the dynamic of their optically thick winds and the observed spectral lines introducing small and large scale variability. We investigate the conditions in the convective envelopes of our helium star models and relate them to the appearance of a high number of stochastic density inhomogeneities, i.e. clumping in the optically thick wind. We also investigate the pulsational stability of these envelope, considering the effect of the high stellar wind mass loss rates.

1 Introduction

The late stages of the evolution of galactic massive stars are characterized by a very high mass loss via stellar wind (Chiosi & Maeder 1986; Langer 2012). During the helium burning stage massive stars become very hot and their stellar wind is so dense that it can enshroud the hydrostatic layers and dominate the spectra of these objects with broad emission lines. Wolf-Rayet stars (WR) of the subclass WNE are thought to be helium burning stars that, due to their high mass loss rate have lost almost all their hydrogen rich envelope (Chiosi & Maeder 1986; Langer 2012). While the energy production due to the 3-α process makes their core convective, most of the WR envelope is expected to be radiative (see Fig.1). In the very outer layers at the base of their optically thick wind a convective zone is expected to arise.

This convective zone (FeCZ) is due to the recombination of iron and iron-group elements, which significantly increase the opacity at the temperature $\log(T) \approx 5.3$ which is thought to be of crucial importance for the driving of the wind (see Fig.1, Hamann et al. 2006; Owocki 2015). The FeCZ is characterized by the proximity to the Eddington limit (cf. Langer et al., this volume), a density inversion (Gräfener et al. 2012; Sanyal et al. 2015) and a very small convective flux. Cantiello et al. (2009) and Grassitelli et al. (2015) argued that the propagated effects of turbulent convection in the subsurface convective zones is likely the origin of the observed small and large scale velocity fields at the photosphere of massive main sequence stars, namely the micro- and macro-turbulence.

It has been observed that WR spectra show the presence of systematic variability in the form of emission sub-peaks. These emission sub-peaks are thought to be the signature of a high number of density inhomogeneities, or clumps, in the wind of WR stars (Moffat et al. 1988; Lépine & Moffat 1999). Given the stochastic nature of the phenomenon and the fact that it is thought to originate at the base of the wind (Owocki 2015), we investigate the connection between the conditions in the outer hydrostatic layers and the small-scale variability of the spectral lines, in order to connect the effects of convection to the appearance of wind clumping.

In addition to this, according to theoretical works we can expect another kind of periodic variability to appear in the low density envelope of WR stars, the *strange mode* pulsations (Glatzel et al. 1993). However there is no observational evidence for pulsations in WN stars so far, except for WR123 (Chené & Moffat 2011) which presents a 10 h period which is by far larger than the expected periods. We investigate the so far neglected influence of mass loss onto the pulsational stability of our WR models.

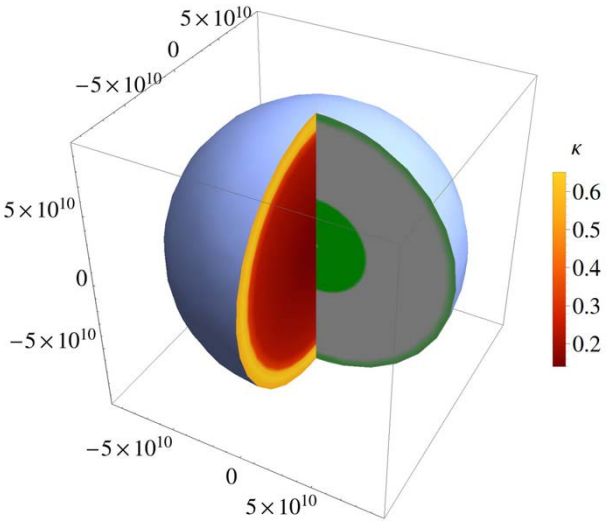

Fig. 1: 3D spatial projection (in cm) of the interior of a 1D 16 $M_\odot$ helium star. The right section shows in green the convective zones and in gray the radiative one, while the left section shows color coded the opacity of stellar matter according to the color bar on the right.

2 Method

We computed a set of chemically homogeneous helium zero age main sequence (He-ZAMS) stellar

models from 2 to 17 $M_\odot$ with BEC, the Bonn 1-D hydrodynamical stellar evolution code (Heger et al. 2000; Petrovic et al. 2006; Brott et al. 2011). It includes up-to-date physics, adopts the Mixing-Length Theory (MLT) for convection (Böhm-Vitense 1958), mass loss via stellar wind according to Nugis & Lamers (2000) and a metallicity Z=0.02. The models were computed with outer boundary conditions given by the assumption of a plane parallel gray atmosphere.

Goldreich & Kumar (1990) considered the interaction between the convective eddies and the overlying radiative layers as a possible driving mechanism for travelling gravity-waves. Cantiello et al. (2009) applied this concept to the sub-surface convective zones of massive main sequence stars introducing an estimate of the upper limit of the induced velocity field at the surface, based on a conservation of energy argument. This writes:

$$v_s \leq \langle v_c \rangle \sqrt{M_c \frac{\rho_c}{\rho_s}} \quad , \qquad (1)$$

where v_s is the upper limit for the expected velocity field at the surface, M_c is the Mach number, ρ_c and ρ_s are the densities at the outer convective border and at the surface, respectively, and $\langle v_c \rangle$ is the averaged convective velocity in the last mixing-length λ_p of the FeCZ. We consider the isothermal sound speed in defining the Mach number because of the small ratio between the thermal and dynamical time scales.

3 Results

All the computed He-ZAMS models in the mass range 2−17 $M_\odot$ have a convective region close to the surface. Starting from the 6 $M_\odot$ model, all the more massive helium star models are inflated with $\Gamma \approx 1$ and a density inversion (Sanyal et al. 2015). The radial extent of the inflated region increases in the more massive models and, despite its small mass, typically of the order of 10^{-8} $M_\odot$, it can account 6% of the total radius in the 17 $M_\odot$ model.

3.1 Sub-surface convection

The convective velocities within the FeCZ are low ($\lesssim$ 5 km/s) for the less massive ($\leq$ 10 $M_\odot$) helium star models. As the luminosity-to-mass ratio increases in the more massive models, the convective velocities become of the order of the local sound speed, i.e. 10 − 20 km/s. Consequently the averaged convective velocities in the last mixing-length sharply increase in the models with $M > 10$ $M_\odot$, inducing therefore a turbulent velocity field at the surface that approaches the local sound speed in the more massive models (see Fig.2). Such a surface turbulent velocity field induced by convection is thought to be able to trigger the formation of clumps in the WR wind.

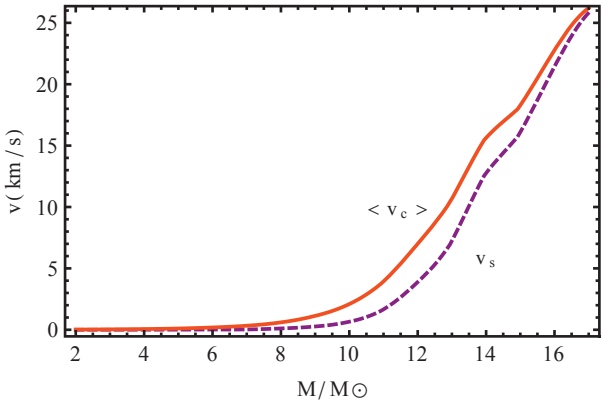

Fig. 2: Average velocity (red solid line, $\langle v_c \rangle$) of the convective elements at the top of the convective zone and expected surface velocity fluctuations (purple dashed line, v_s) as a function of stellar masses.

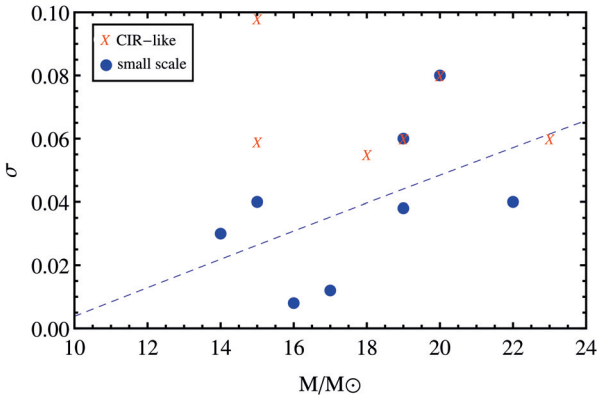

Fig. 3: Rms variability relative to the line strength σ as a function of mass of the Galactic H-free WN stars. Red crosses correspond to CIR-type variability, while the blue dots correspond to the small-scale variability in WN stars. Data are taken from St-Louis et al. (2009); Chené & St-Louis (2011); Michaux et al. (2014). The linear fit in blue dashed is computed considering only the blue dots.

In order to test this hypothesis, but being unable to directly observe the hydrostatic layers veiled by the optically thick winds, we have to rely on indirect evidences. Therefore we compare our prediction of an increased turbulent velocity field at the surface in the more massive models to the observed small-scale variability in a sample of H-free single WN stars. We collect the results of St-Louis et al. (2009), Chené & St-Louis (2011), and Michaux et al. (2014), in particular the rms variability across the HeII spectral lines relative to the local line strength σ, which is considered as an indication of the intensity of clumping, and investigate σ as a function of the WR mass estimated by Hamann et al. (2006).

We note however that spectra showing a dominant large-scale variability, the so called corotating interaction regions (Dessart & Chesneau 2002; St-Louis et al. 2009), have been excluded, assuming for this kind of periodic variability an origin not directly related to the convective motion.

Our results, plotted in Fig.3 show that an increased variability as a function of mass is found. Moreover, the zero point of the linear fit matches our prediction of an increased variability occurring only above M $\approx$ 10 $M_\odot$. However these results have to be taken with cautious due to the small sample and the relatively small number of spectra available to derive the values of σ (St-Louis et al., in prep.).

3.2 Pulsations

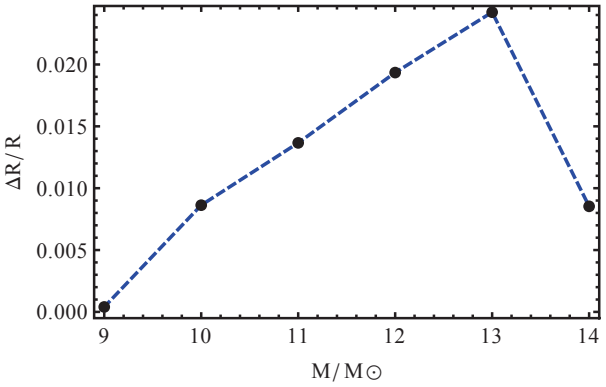

Fig. 4: Amplitude of the saturated pulsations appearing in the helium star models. The decreasing amplitude above 13$M_\odot$ is believed to be an effect of the increased mass-loss rate.

A sub-sample of our He-ZAMS model shows instability to pulsations. The small ratio between the local thermal-to-dynamical time scale in the envelope of WR stars rules out thermal mechanisms (as the κ-mechanism) as the origin of these pulsations, but refer to strange modes (Glatzel et al. 1993). These pulsations appear in the mass range $9 - 14$ $M_\odot$ in our models, and their periods match well those of the lowest unstable order in the models of Glatzel et al. (1993).

Their normalized radial amplitudes $\Delta R/R$ are shown in Fig. 4, where we can see an increase in the pulsational amplitude from the 9 $M_\odot$ to the 13 $M_\odot$ model, followed by a decrease in the case of the 14 $M_\odot$ models, after which the models are stable. However Glatzel et al. (1993) predict also the more massive models to be unstable to pulsation, and indeed the more massive models do show instability to pulsations, but only in the computations in which mass loss was neglected. In fact, the 14 $M_\odot$ model does show higher amplitudes (of the order of $\Delta R/R \approx 0.03$) when mass loss is not included in the calculations. The same works for the higher mass models, which are unstable to also higher order modes only when mass loss via stellar wind is not included.

We therefore conclude that the high mass loss rates have a stabilizing effect on these pulsations, starting from the 14 $M_\odot$ model. This may help to understand the lack of observational evidences for pulsations in the very late stage of the evolution of stars with high luminosity-to-mass ratio. Furthermore, the computed luminosity variation due to pulsations is very small, typically $10^{-2}\,L_\odot$, which could be masked by the small and large scale variability present in the winds of WR stars. It is important to note that the velocities associated to these pulsations are significantly supersonic, up to 140 km/s, therefore an observational spectroscopical signature could be expected.

References

Böhm-Vitense, E. 1958, ZAp, 46, 108

Brott, I., de Mink, S. E., Cantiello, M., et al. 2011, A&A, 530, A115

Cantiello, M., Langer, N., Brott, I., et al. 2009, A&A, 499, 279

Chené, A.-N. & Moffat, A. F. J. 2011, in IAU Symposium, Vol. 272, IAU Symposium, ed. C. Neiner, G. Wade, G. Meynet, & G. Peters, 445–450

Chené, A.-N. & St-Louis, N. 2011, ApJ, 736, 140

Chiosi, C. & Maeder, A. 1986, ARA&A, 24, 329

Dessart, L. & Chesneau, O. 2002, A&A, 395, 209

Glatzel, W., Kiriakidis, M., & Fricke, K. J. 1993, MNRAS, 262, L7

Goldreich, P. & Kumar, P. 1990, ApJ, 363, 694

Gräfener, G., Owocki, S. P., & Vink, J. S. 2012, A&A, 538, A40

Grassitelli, L., Fossati, L., Simon-Diaz, S., et al. 2015, ApJ, 808, L31

Hamann, W.-R., Gräfener, G., & Liermann, A. 2006, A&A, 457, 1015

Heger, A., Langer, N., & Woosley, S. E. 2000, ApJ, 528, 368

Langer, N. 2012, ARA&A, 50, 107

Lépine, S. & Moffat, A. F. J. 1999, ApJ, 514, 909

Michaux, Y. J. L., Moffat, A. F. J., Chené, A.-N., & St-Louis, N. 2014, MNRAS, 440, 2

Moffat, A. F. J., Drissen, L., Lamontagne, R., & Robert, C. 1988, ApJ, 334, 1038

Nugis, T. & Lamers, H. J. G. L. M. 2000, A&A, 360, 227

Owocki, S. P. 2015, in Astrophysics and Space Science Library, Vol. 412, Astrophysics and Space Science Library, ed. J. S. Vink, 113

Petrovic, J., Pols, O., & Langer, N. 2006, A&A, 450, 219

Sanyal, D., Grassitelli, L., Langer, N., & Bestenlehner, J. M. 2015, A&A, 580, A20

St-Louis, N., Chené, A.-N., Schnurr, O., & Nicol, M.-H. 2009, ApJ, 698, 1951

Gloria Koenigsberger: In a binary system, oscillations can be excited. So, can we speculate that these oscillation modes in your talk can subsist even if the star has a high mass-loss rate?

Luca Grassitelli: It could, although I am not aware of neither theoretical nor observational evidences of pulsations for binary systems. The message that, however, we can take from these results is that these pulsations have high surface velocities that could be detected even in the case of optically thick winds. I think that the lack of observational evidences favours a stabilizing effect of the wind scenario.

Wolf-Rayet Stars
W.-R. Hamann, A. Sander, H. Todt, eds.
Potsdam: Univ.-Verlag, 2015
URL: http://nbn-resolving.de/urn:nbn:de:kobv:517-opus4-84268

WR Time Series Photometry: A Forest of Possibilities

H. Pablo[1], A. F. J. Moffat[1] & the *MOST* team
[1] *Université de Montréal, Canada*

We take a comprehensive look at Wolf Rayet photometric variability using the *MOST* satellite. This sample, consisting of 6 WR stars and 6 WC stars defies all typical photometric analysis. We do, however, confirm the presence of unusual periodic signals resembling sawtooth waves which are present in 11 out of 12 stars in this sample.

1 Introduction

The Wolf-Rayet (WR) phenomenon, or evolutionary phase, is by its very nature most easily identifiable spectroscopically. The intense winds result in large emission line features that are quite unique. Therefore it is not hard to understand why the many of the breakthroughs in our understanding of these stars has been a result of spectroscopic analysis. While this is important, one look at the abstracts listed in this proceedings will show a very obvious gap in observations and study: photometry.

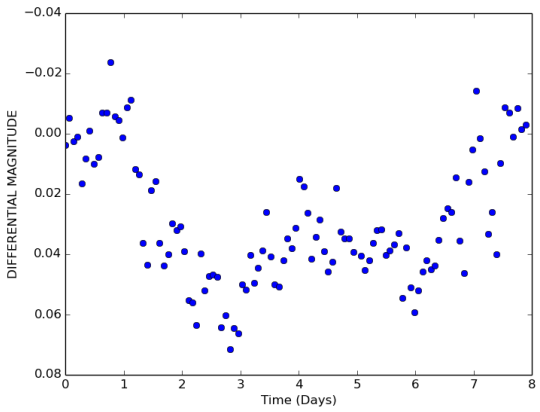

Fig. 1: False eclipse from WR 71. This eclipse has the longest duration lasting ≈ 8 days.

This is mainly because large scale photometric studies of multiple WR stars over long time periods just simply hasn't been done until the onset of the Canadian space telescope *MOST*. From its observations we have been able to say rather definitively that WR stars are all variable at some level. Unfortunately though, the photometry is not as insightful as hoped. The variations in the data have been attributed to a variety of things including spots, pulsations, and atmospheric eclipses (David-Uraz et al. 2012; Lefèvre et al. 2005; Chené et al. 2011). One thing that hasn't been found though is any sense of uniformity. There are as many causes of photometric variation as there are published papers. This is not to say that these explanations are incorrect, but rather that they lack cohesion.

In this proceedings our aim is to find similarities and/or links between the photometric variability of all 12 WR stars in the *MOST* archive, including those which have already been published. First we apply a full frequency analysis looking for evidence of pulsational modes. Next we search for similarities in the 1/f noise associated with these stars. Finally, as a last resort we apply phenomenological classification to the photometric variability observed and discuss the results.

2 Data & Observations

We obtained optical photometry with the *MOST* microsatellite that houses a 15-cm Maksutov telescope through a custom broad-band filter covering 3500–7500 Å. The sun-synchronous polar orbit has a period of 101.4 minutes ($f = 14.20$ d^{-1}), which enables uninterrupted observations for up to eight weeks for targets in the continuous viewing zone. A pre-launch summary of the mission is given by Walker et al. (2003).

The sample consisted of 12 targets, 6 of WC type and 6 of WN type all chosen because they are in the limited window of MOST observability, are relatively bright, and in most cases were already known to be highly variable. These data were then extracted using the technique of Reegen et al. (2006). Specific information for each target is given in Table 1. The instrumental scatter according to what we know about *MOST* is close to 1 mmag per *MOST*-orbit bin for the WR stars of the magnitude that were observed. This is much lower than what is given in Table 1, which is a measure of the raw, un-binned light curve.

3 Photometric Analysis

3.1 Looking for Pulsations

In order to search for pulsational signals we first did a full frequency analysis of every target in our sample. The method we used is called prewhitening. In this method we took the fourier transform of our target, identified and fit the largest peak, and then removed a sinusoid matching the peak's fit parameters from the data. This process was then repeated until the peaks fall below our significance threshold

Tab. 1: *MOST* Observations. The point to point scatter is a measure of the raw observation precision, but can be biased by real variations in the data.

Target	Sp. Type	V Mag	Start Date (JD-2450000)	Length (Days)	Scatter (Mag)
WR 71	WN6	10.1	6806	27	0.00911
WR 92	WC9	10.2	6092	26	0.00792
WR 103	WC9d	8.7	3535	37	0.00688
WR 110	WN5	9.9	5812	30	0.00266
WR 111	WC5	7.8	3892	23	0.00100
WR 113	WC8+O8-9IV	9.1	5009	45	0.00350
WR 113	WC8+O8-9IV	9.1	5361	28	0.00311
WR 115	WN6	11.84	5720	38	0.00811
WR 119	WC9d	12.43	6454	48	0.00978
WR 120	WN7	12.28	5720	38	0.01428
WR 121	WC9d	11.9	6455	47	0.00908
WR 123	WN8	11.12	3174	38	0.01281
WR 124	WN8h	11.5	4651	32	0.01066

of 4 sigma. This was done using Period04 (Lenz & Breger 2005).

Using the lists of frequencies that were found, we looked for the most typical sign of pulsations: spacings. Regular pulsations often show common spacings either in frequency (p-modes) or period (g-modes). As it was not clear what type of pulsations would be expected we searched for both. At first glance the results seemed to be promising as we found 5 stars with strong evidence of period spacing and 3 stars with evidence for frequency spacing. However, it was difficult to explain the presence of both p-modes and g-modes in this dataset. In addition, there were no apparent correlations between spectral type, radius, or any other fundamental parameter and the frequency or period spacings we found. It is important to note that this does not rule out pulsations entirely for each individual star, but it makes it unlikely to be a common source of variation for all WR stars.

3.2 Signal in the Noise

While the peaks in the Fourier transform were hard to quantify, they were not the only source of variability present. Something that occurs often in the Fourier regime is the presence of the so called 1/f noise which is where the mean level of the transform increases as you got to lower and lower frequencies. Although it is often referred to as noise it can be evidence for specific astronomical signals such as flickering on the surface of the star (Stanishev et al. 2002). It's form is given by

$$P(f) = \frac{C}{1 + (2\pi f)^{\gamma}} \quad (1)$$

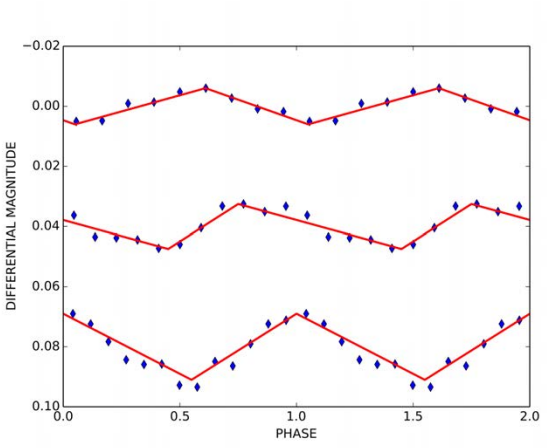

Fig. 2: Phased and binned data from WR 71 (top and middle) and WR 103 (bottom) in blue with periods of 0.73 d, 1.63 d, 0.59 d respectively. In red is an overlay of a sawtooth wave with different slopes for each wave. It is important to note that the red line is not a fit to the data, and is only present to show how well this form matches the observed data.

We fit the Fourier Transform for each star and compared the results of the fit to fundamental parameters found in Hamann et al. (2006) & Sander et al. (2012). The only significant result was a confirmation of Michaux et al. (2014) that the size of the variation is inversely dependent on temperature.

4 Morphological Classification

The conclusions from the previous sections have shown us that the intrinsic variability was either too

transient or non-sinusoidal for Fourier methods to be of much use. Therefore, we turned to looking for inherent similarities between the light curves themselves. While this method does not a priori provide any physical insight, our first priority was to find commonalities in the data.

4.1 False Eclipses

One of the most obvious variations that was apparent in 4 out of 12 light curves is the presence of eclipse like structures. They never happened more than once per dataset and were typically the largest variations present. However, while they looked fairly similar to an eclipse (see Fig. 1) the length was abnormally long, on the order of several days.

Even if these dips were periodic they were much too long to belong to the presence of a companion star. We also considered the presence of large clumps as they could block a significant amount of light as they pass into the line of sight. However, while the depth of the eclipse is relatively consistent with this phenomenon, the wind speed is far too great for such an eclipse to last for several days. One thing that did seem apparent though, was that these eclipses were uncorrelated with the other variations seen in the light curves.

4.2 Unusual Waves

In addition to these false eclipses, we had a large amount of semi-periodic transient variability which appeared in every single light curve. Under close examination of a small section of one of these light curves we noticed something strange; the presence of a unique repeatable triangular or sawtooth shape (see Fig. 2).

While we originally ignored this as a consequence of a poorly sampled sine wave, closer examination of all light curves revealed that this simply could not be the case. Further investigation of several other unrelated *MOST* light curves did not reveal this unique shape making it unlikely to be of instrumental origin. In addition, this same shape was present once or multiple times in 11 of 12 targets at a variety of different periods. The only noticeable difference between these waves was the slope of the waves' rise and fall.

In addition, we see the presence of two other unique wave forms referred to as the w-wave and the reverse w-wave due to their w-like shapes. The w-wave and reverse w-wave, though not pictured due to lack of space, occur with slightly less regularity appearing in 3 out of 12 and 2 out of 12 light curves respectively. However, their singular appearance makes it likely that they are real phenomena.

5 Discussion & Future Work

We have used the largest space-based photometric dataset of WR stars which exists to determine similarities between these stars in a search for underlying physics. It is abundantly clear that the normal mechanisms attributed to most stars such as pulsations are not sufficient to adequately describe their variability. However, though our current understanding does not predict what the variability in these objects is, it is most certainly correlated. The fact that their are consistent, unique, repeatable shapes indicates that their is a common source which responsible this triangular and w shaped variability.

The only issue is that this variability is so unusual that the underlying cause is unclear. While it is quite easy to speculate that these odd shapes are related to light propagation through a wind, what the original cause could be or what interactions cause these unique but repeatable shapes is currently nearly impossible to say. There are simply too many possibilities and a lack of viable theories to test them against. Therefore, we choose not to make wild or unfounded claims as to the possible nature of these variations and instead present simply what we see.

While models are likely far in the future, we do hope to characterize these data more rigorously. This includes fitting the slopes of the triangular waves and seeing if there are any correlations with parameters such as radius or spectral type. We also eagerly await the presence of the Gamma Velorum, a WR recently observed photometrically with the BRITE-constellation project for 6 months in two filters. This data set will be unprecedented and hopefully help our understanding of WRs stars in our sample.

References

Chené, A. N., Moffat, A. F. J. Cameron, C., et al. 2011, 735, 34

David-Uraz, A. Moffat, A. F. J. Chené, A. N. et al. 2012, MNRAS, 426, 1720

Hamann, W. R. and Gräfener, G. and Liermann, A. 2006, A&A, 457, 1015

Lefèvre, L. Marchenko, S. V. Moffat, A. F. J. et al. 2005, ApJ, 634, 109L

Lenz P., Breger M. 2005, CoAst, 146, 53

Michaux, Y. J. L. Moffat, A. F. J. Chené, A.-N. & St-Louis, N. 2014, MNRAS, 440, 2

Reegen, P., Kallinger, T., Frast, D., et al. 2006, MNRAS, 367, 417

Sander, A. and Hamann, W. R. and Todt, H. 2012, A&A, 540, A144

Stanishev, V., Kraicheva, Z., Boffin, H. M. J., & Genkov, V. 2002, å, 394, 625

Walker, G., Matthews, J., Kuschnig, R., et al. 2003, PASP, 115, 1023

Norbert Langer: What timescales can you probe with your data?

Herbert Pablo: This depends largely on whether or not the target can be viewed continuously or for only part of each *MOST* orbit (which is more common). In the latter case we will always bin on the orbital period (0.0704 d). Therefore, in all cases we are sensitive to periods which are greater than 0.14 d.

Peredur Williams: How much of the scatter in your light curves is intrinsic to the star and how much is instrumental?

Herbert Pablo: If we bin on the *MOST* orbital period then the precision of each point is typically less than 1 mmag for all the stars sampled. The point to point scatter can be quite a bit higher, but as we are talking about long periods (greater than 0.5 d) binning is quite appropriate. Therefore we can believe variations that are at least a mmag in amplitude.

Wolf-Rayet Stars
W.-R. Hamann, A. Sander, H. Todt, eds.
Potsdam: Univ.-Verlag, 2015
URL: http://nbn-resolving.de/urn:nbn:de:kobv:517-opus4-84268

A new mechanism for long long-term pulsations of hot stars?

T. Shacham[1], I. Idan[2] & N. J. Shaviv[1,3]
[1] *Racah Inst. of physics, Hebrew University of Jerusalem, Jerusalem 91904, Israel*
[2] *Dept. of Physics, Israel Institute of Technology, Haifa 32000, Israel*
[3] *Institute for Advanced Study, Einstein Drive, Princeton, NJ 08540, USA*

We suggest several ideas which when combined could lead to a new mechanism for long-term pulsations of very hot and luminous stars. These involve the interplay between convection, radiation, atmospheric clumping and winds, which collectively feed back to stellar expansion and contraction. We discuss these ideas and point out the future work required in order to fill in the blanks.

1 Introduction

The current understanding of stellar pulsations is based on the following scenario: a star contracts, the opacity of a certain layer increases, and radiation is trapped beneath. If sufficient radiation pressure manages to build up, the star will begin to expand, thus reducing the opacity and releasing the radiation. Due to the reduction in radiative pressure, the star will contract and so on.

The κ-mechanism is a well know example of such opacity related pulsations.[1] The link between the stellar contraction and increase in opacity is found in partially ionised layers, whose opacity is proportional to the temperature (as opposed to inversely proportional, which is usually the case). If there exists such a layer with a sufficient heat capacity, pulsations could occur.[2] The timescale for such pulsations is the dynamic timescale, $1/\sqrt{G\rho}$.

In very hot, massive stars, the partially ionised layers are either absent altogether or very close to the surface, in which case the density is very low and so is the heat capacity. Any κ-mechanism oscillations are therefore expected to be damped.[3] These stars may also exhibit pulsations of much longer timescales – the S-Dor pulsations, see e.g. Vink (2012).

In attempt to understand years-scale pulsations of very hot stars, we propose a new mechanism for stellar pulsations, which falls into the previously described generalised class of opacity related pulsations. It is depicted in Fig. 1.

The suggested mechanism, as this note, consists of several components. First is the coupling between convection and radiation, reviewed in Sect. 2. Second is the coupling between radiation and opacity, presented in Sect. 3. Third, and most important, is the connection between opacity and winds, proposed in Sect. 4. Finally, in Sect. 5 we point out well defined questions and the future toolbox required in order to answer them.

2 Between convection and radiation

As argued by Shaviv (2000), even if a region is unstable to convection – as is expected in atmospheres of super Eddington stars – if the radiative flux is *too* high the convective efficiency might be significantly lower than the mixing-length-theory (MLT; Vitense 1953, Böhm-Vitense 1958) prediction. Simply put, if the thermal energy flux is lower than the radiative flux, convection will be effectively choked.

Consider a gas element with a specific energy ε and height H. The energy density gradient, which scales as $\nabla E \sim \rho\varepsilon/H$ gives rise to a radiative flux given by

$$\mathbf{F}_{\rm rad} = -\frac{1}{3}\frac{c}{\kappa\rho}\nabla E \sim \frac{c\varepsilon}{\kappa H}, \tag{1}$$

which exceeds the maximal convective flux

$$\mathbf{F}_{\rm conv} = v_{\rm sound}\rho\varepsilon \tag{2}$$

when

$$H\rho\kappa \equiv h < c/v_{\rm sound}. \tag{3}$$

Here we defined h to be the *optical width* of the layer. Above the surface which satisfies relation (3), which we refer to as the *last convective surface* (LCS), convection could be safely ignored.

3 Between radiation and opacity

The only known explanation for stable super-Eddington states is that radiation can force the atmosphere to become inhomogeneous due to hydrodynamical instabilities, which operate at Eddington

[1] For a review see, e.g., Maeder (2009); Cox (1974).
[2] Admittedly, this is a rather simplified description. Even if the thermodynamical conditions for amplification of pulsations are locally satisfied, a careful analysis should weigh in the damping effect of the surroundings.
[3] An exception to this statement is the strange mode instability which "enhances" the κ-mechanism, but relevant to short-term variations – see e.g. Saio et al. (2013).

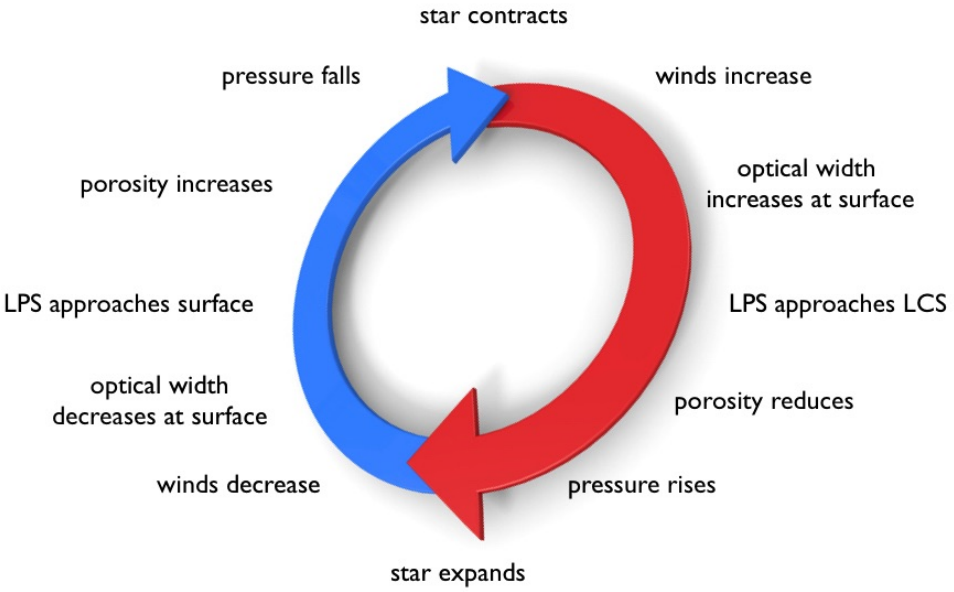

Fig. 1: The proposed pulsation mechanism consists of this cycle of events.

ratios of $\Gamma \gtrsim 0.8$. These were first predicted in Shaviv (2001) and seen in recent simulations (Takeuchi et al. 2013).

The clumping of the atmosphere reduces the opacity on macroscopic distances.[4] Due to the mixing nature of convection, the hydrodynamical instabilities could result in clumping only above the last convective surface.

At very low optical depths, the clumps will "smear" as radiation could easily escape. Therefore, the *last porous surface* (LPS), is located where $h \sim 1$. In steady state winds, the sonic surface and last porous surface will coincide.

A necessary condition for the existence of clumps is that the last convective surface and last porous surface be separated by at least a few scale heights.[5] Since

$$-\int_{LCS}^{LPS} \frac{dr}{H(r)} = \ln\left(\frac{P|_{LCS}}{P|_{LPS}}\right) > \text{a few}, \quad (4)$$

the pressure at the LPS must be significantly lower than at the LCS. Therefore, a change in pressure at the sonic surface will effect the opacity beneath it. Such changes of pressure are expected to follow changes in mass loss.

4 Between opacity and winds

Consider a contraction of a star with thick continuum driven winds – the mass loss is expected to increase. This would reflect in the conditions at the sonic point; an increase in mass loss would increase the pressure, and push the sonic point towards higher optical depths. The LPS would approach the LCS, eventually closing the window for porosity. The subsequent rise in opacity will translate to a rise in pressure, followed by expansion.

There are two regimes which are usually dealt with separately; one where the winds reach infinity with a velocity comparable to the escape velocity at the sonic surface, and the other where the winds stagnate and fall back down (the "photon tired" regime). The pulsations we aim to describe here reside in the transition between the two regimes, where the energy in the winds is comparable to the luminosity. As every super-Eddington star with heavy winds necessarily passes through this stage, such pulsations

[4] In this case, macroscopic stands for "of the order of the scale height".

[5] The length scale of the smearing of the clumps, at both the last porous surface and last convective surface, is of the order of a scale height.

are rather generic.

Whether or not these oscillations are damped or not, depends on the height of energy barrier due to the column depth of the cumulative winds. The amount of mass which must accumulate above the sonic surface in order to have significant feedback to the structure of the star, dictates the time scale of the pulsations. As this amount is proportional to the luminosity of the star, so will be the period of the pulsations.

A modulation of the pulsations could be due to hysteresis in the porosity phase transition of the atmosphere. We do not yet know how this phase transition depends on radial velocity.

5 Summary

In this wonderful conference, we proposed several ideas that may eventually assemble the long-term pulsations mechanism behind the S-Dor phenomena.

In order to further investigate these ideas, several questions should be answered:

1. What is the dependence of the convective efficiency on the radiative flux?
2. How does the atmosphere clump; what are the parameters of the porosity phase transition, hysteresis etc.?
3. What is the profile of interaction between clumping and convection?
4. How do the boundary conditions at the surface depend on mass loss? and finally,
5. What region of parameter space supports pulsations?

Acknowledgements: This research was supported by the Prof. A. Pazy research foundation. NJS also thanks the IBM Einstein Fellowship support by the IAS.

References

Böhm-Vitense, E. 1958, ZAp, 46, 108

Cox, J. P. 1974, Reports on Progress in Physics, 37, 563

Maeder, A. 2009, Physics, Formation and Evolution of Rotating Stars (Springer)

Saio, H., Georgy, C., & Meynet, G. 2013, in Astronomical Society of the Pacific Conference Series, Vol. 479, Progress in Physics of the Sun and Stars: A New Era in Helio- and Asteroseismology, ed. H. Shibahashi & A. E. Lynas-Gray, 47

Shaviv, N. J. 2000, ApJ, 532, L137

Shaviv, N. J. 2001, ApJ, 549, 1093

Takeuchi, S., Ohsuga, K., & Mineshige, S. 2013, PASJ, 65, 88

Vink, J. S. 2012, Astrophysics and Space Science Library, Vol. 384, Eta Carinae and the Luminous Blue Variables, ed. K. Davidson & R. M. Humphreys (Springer US), 221–247

Vitense, E. 1953, ZAp, 32, 135

Norbert Langer: I cannot see how you could obtain periods much longer than the dynamical timescale.

Tomer Shacham: The wind intensity is coupled to the amount of ejected mass, which accumulates during timescales much longer than the dynamical timescale.

Stephen Ro: Your illustration shows an efficiently convective region smoothly transitioning into an inefficient region. In more massive WR stars, the iron convection zone is inefficient and exists above a radiative envelope. How do these instabilities apply here?

Tomer Shacham: The instabilities exist only above the last convective surface, and only when the profile of the gamma factor can support them. Once they begin to operate, the convective structure of the outer layers changes (and winds start blowing).

Wolf-Rayet Stars
W.-R. Hamann, A. Sander, H. Todt, eds.
Potsdam: Univ.-Verlag, 2015
URL: http://nbn-resolving.de/urn:nbn:de:kobv:517-opus4-84268

Envelope inflation in Wolf-Rayet stars and extended supernova shock breakout signals

D. Sanyal, T. J. Moriya & N. Langer
Argelander-Institut für Astronomie, Universität Bonn, Germany

Massive, luminous stars reaching the Eddington limit in their interiors develop very dilute, extended envelopes. This effect is called envelope *inflation*. If the progenitors of Type Ib/c supernovae, which are believed to be Wolf-Rayet (WR) stars, have inflated envelopes then the shock breakout signals diffuse in them and can extend their rise times significantly. We show that our inflated, hydrogen-free, WR stellar models with a radius of $\sim R_\odot$ can have shock breakout signals longer than $\sim 60\,s$. The puzzlingly long shock breakout signal observed in the Type Ib SN 2008D can be explained by an inflated progenitor envelope, and more such events might argue in favour of existence of inflated envelopes in general.

1 Stellar envelope inflation

Inflation refers to the extremely dilute, loosely-bound envelopes that massive, luminous stars develop in the course of their evolution (Ishii et al. 1999; Petrovic et al. 2006; Sanyal et al. 2015, Langer et al., this volume). A typical inflated envelope is shown in Fig. 1, which corresponds to an evolved hydrogen-free 7.8 $M_\odot$ model burning carbon in the core. Such ubiquitous hydrostatic structures result from stellar layers reaching the Eddington limit in the interior of the star, facilitated by the peak in opacity at $T \approx 200\,000$ K, the so-called iron opacity bump. For more details on the appropriate definition of the Eddington limit, we refer to Sanyal et al. (2015) and Langer et al. (this volume).

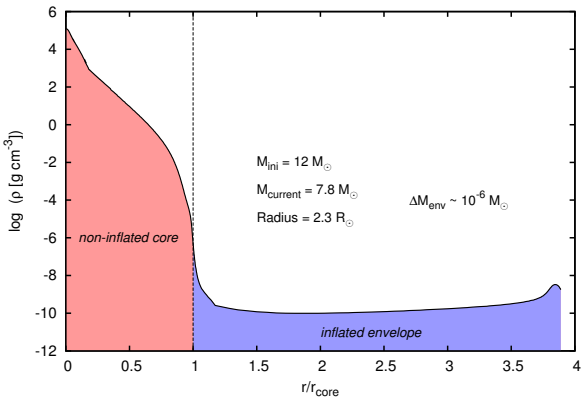

Fig. 1: Density profile of a 7.8 $M_\odot$ hydrogen-free stellar model with $T_{\rm eff} = 82\,700$ K and $\log(L/L_\odot) = 5.35$, showing an inflated envelope (shaded blue) and a density inversion. The radial co-ordinate has been normalised by the non-inflated core radius ($r_{\rm core}$) of 0.6 $R_\odot$.

Stellar layers approaching the Eddington luminosity become convectively unstable (Langer 1997) but convection, of course, does not contribute to the radiative acceleration. However, the fraction of the total flux transported by convection in these WR stars, according to standard MLT, is negligibly small. Hence, whether or not the layers will hit the Eddington limit and inflate the envelope, does not depends critically on the theory of convective energy transport used to model the stars.

As we can see from Fig. 1, the mass contained in the inflated envelope is a tiny fraction of the stellar mass, $\Delta M_{\rm env} \approx 10^{-6}\,M_\odot$. However, for cool supergiants, the mass in the inflated envelopes can be as high as a few solar masses, see Sanyal et al. (2015) for details.

2 Stellar models of WR stars

We modelled WR stars as non-rotating, hydrogen-free helium stars and evolved them through core-helium buring to the onset of core-carbon burning, using the 1-D stellar evolution code BEC (see Heger et al. 2000; Brott et al. 2011; Moriya et al. 2015, for details). We computed two sets of models, with initial masses 10 $M_\odot$ and 12 $M_\odot$, and a metal composition that of the Sun (Brott et al. 2011). In particular, we used the OPAL opacity tables (Iglesias & Rogers 1996) for our computations and used the standard Mixing-Length-Theory (MLT) to model convective zones, with $\alpha_{\rm MLT} = 1.5$. The mass-loss rate prescription from Nugis & Lamers (2000) was applied. The resulting structure (e.g. Fig. 1) will resemble a SN Type Ib progenitor because no significant changes in the stellar structure is expected in the remaining lifetime until the explosion.

The evolutionary tracks of the aforementioned models, in the H-R diagram, is shown in Fig. 2. Both the helium zero age main sequence models are marginally inflated. As a consequence of the applied mass loss, they decrease in luminosity during the core helium-burning phase. After helium is exhausted in the core, the stars begin to contract and become hotter and brighter. The models are hardly inflated during this phase because the Fe-group opacity bump is only partially contained inside the stars. These are probably related to the WO stars (cf. Tramper et al., this volume). When the

helium-shell ignites, the evolutionary tracks eventually move toward cooler temperatures because of the mirror principle. As the models become cooler, they become significantly inflated and exhibit a pronounced core-halo structure, as shown in Fig. 3 (cf. Moriya et al. 2015).

3 Shock breakout in inflated stellar envelopes

The shock breakout occurs when the dynamical timescale of the shock propagation in the unshocked envelope, i.e. $t_{\rm dyn} \simeq \Delta R/v_{\rm sh}$ becomes comparable to the diffusion timescale in the envelope, i.e. $t_{\rm diff} \simeq \tau \Delta R/c$, where $v_{\rm sh}$ is the shock velocity and τ is the optical depth in the remaining unshocked envelope (Weaver 1976). Therefore, the shock breakout condition can be expressed as: $\tau \simeq c/v_{\rm sh}$.

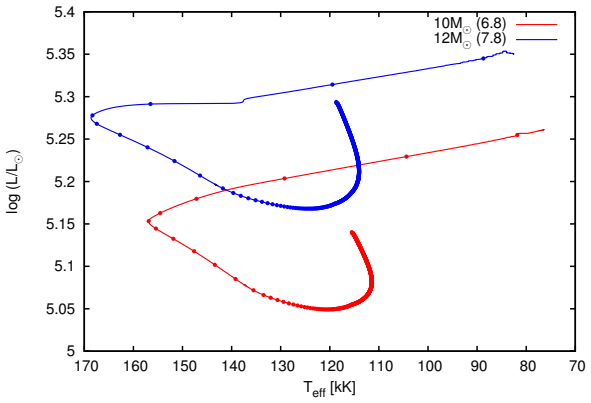

Fig. 2: Stellar evolutionary tracks of our 10 $M_\odot$ and 12 $M_\odot$ solar-metallicity helium-star models from the He-ZAMS until core-carbon ignition.

For a model in which the shock breakout condition is fulfilled very close to the stellar surface, ΔR is very small, such that $t_{\rm diff} \ll t_{\rm lc}$, where $t_{\rm lc} \simeq R_\star/c$ is the light-crossing time. Assuming a shock velocity of 20 000 km s^{-1}, in the case of the polytropic model shown in Fig. 3, the light-crossing time $t_{\rm lc}$ is 5.6 s whereas the diffusion time is only 0.5 s, meaning that the shock breakout duration is determined by $t_{\rm lc}$.

On the other hand, in an inflated stellar model, the shock breakout happens relatively deep inside the envelope, making ΔR quite large, such that $t_{\rm diff} \gg t_{\rm lc}$. In Fig. 4, we plot the optical depth in the interior of our stellar models and show that ΔR can be as large as $\sim R_\odot$. In such a situation, the rise time of the shock breakout signals will be determined by the diffusion time. The subsequent light curve is expected to decline exponentially with an e-folding timescale of the diffusion time due to the photon diffusion in the shocked envelope (Moriya et al. 2015). Table 1 summarises the different timescales involved in inflated and un-inflated models.

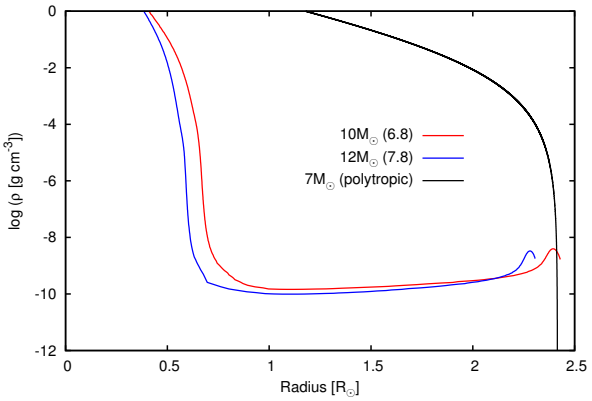

Fig. 3: Density structure of our last computed models, with initial masses of 10 $M_\odot$ and 12 $M_\odot$. The final masses are indicated in parentheses, in units of a solar mass. The density structure of a 7 $M_\odot$ polytropic model (polytropic index = 3) without an inflated envelope is also shown.

SN 2008D: The X-ray light curve of the Type Ib SN 2008D was serendipitously observed by Soderberg et al. (2008) with the *SWIFT* satellite, and is the only direct detection of a SN shock breakout so far. The total shock breakout duration was 300 seconds with a rise time of $\sim$ 60 seconds. If we assume the shock brekout duration was dominated by $t_{\rm lc}$, as is done in the literature, then it implies a WR progenitor radius of 130 $R_\odot$, which is much larger than predicted by stellar evolutionary models. On the other hand, our inflated model with a radius of $\sim$ 2 $R_\odot$ can naturally explain the long rise time of SN 2008D. The estimated SN ejecta mass is 3$-$7 $M_\odot$ (Soderberg et al. 2008; Mazzali et al. 2008; Bersten et al. 2013) which is consistent with the final masses of our models (after subtracting the remnant mass of the neutron star). The mass-loss rates of our models (7×10^{-6} M$_\odot$ yr^{-1}) are also consistent with that estimated from radio observations (7×10^{-6} M$_\odot$ yr^{-1}, Soderberg et al. 2008).

The shock velocity at shock breakout has been suggested to be $\sim$ 30 000 km s^{-1} for WR stars (e.g., Nakar & Sari 2010), but these studies assume a steeply declining density profile as in the case of the polytropic model. Hydrodynamic modelling of shock propagation in inflated envelopes is needed to estimate the shock velocity at breakout.

There have been other models proposed for explaining the long shock breakout signal of SN 2008D, like the thick wind model by Svirski & Nakar (2014) which assumes a high mass-loss rate of $\sim$ 10^{-4} M$_\odot$ yr^{-1} a few days prior to the explosion,

and the supernova ejecta expanding through the optically-thick wind.

Tab. 1: A comparison of the properties and the relevant timescales of our computed models. The shock breakout rise time of SN 2008D was ~ 60 seconds.

Mass ($M_\odot$)	$t_{\rm lc}$ (s)	$t_{\rm diff}$ (s)	$R_\star$ ($R_\odot$)
6.8	5.67	14	2.43
7.8	5.38	50	2.31
7.0 (Polytropic)	5.60	0.5	2.40

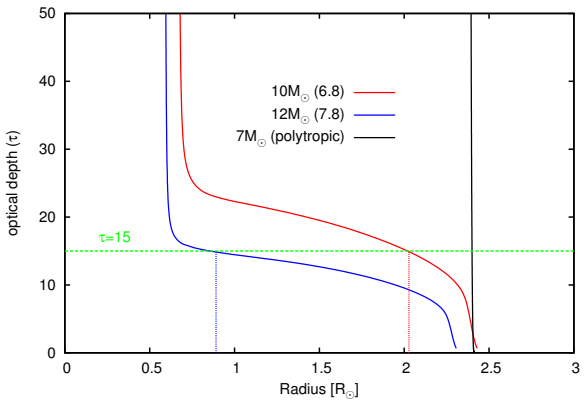

Fig. 4: The run of optical depth τ in our models. For computing τ in the polytropic model, a constant opacity coefficient of $0.2\,{\rm cm}^2\,{\rm g}^{-1}$ was used. The green dashed line at $\tau = 15$ is drawn for convenience. The blue and red dotted lines show where in the stellar envelope shock breakout happens.

4 Conclusions

We have shown that if WR type supernova progenitors have inflated envelopes, then the rise times of supernova shock breakout signals can be extended because the shock breakout can then occur within the low-density envelopes. The long diffusion time of the inflated envelopes makes the shock breakout rise times long. Even if a SN progenitor has a radius on the order of the solar radius whose light-crossing time is a few seconds, the rise time of the shock breakout signals can be ~ 60 s because of the inflated envelope. Our inflated model can simultaneously explain the mysterious long shock breakout rise time, the ejecta mass, the mass-loss rate estimate right before explosion, and the shock velocity in SN 2008D.

The inflated envelope is a generic feature of luminous, mass stars and can have an array of observational consequences. It leads to cooler effective temperatures, higher spin-down rates in rotating stars, and less massive supernova progenitors. It has been argued in the literature (Gräfener et al. 2012) that inflated WR envelopes can address the WR radius problem. A recent study of galactic OB stars by Castro et al. (2014) indicates that inflated envelopes do exist in nature. Furthermore, core-hydrogen burning stars evolving to temperatures below ~ 8000 K can be expected to have massive inflated envelopes and might be related to LBV giant eruptions (Sanyal et al. 2015).

References

Bersten, M. C., Tanaka, M., Tominaga, N., Benvenuto, O. G., & Nomoto, K. 2013, ApJ, 767, 143
Brott, I., de Mink, S. E., Cantiello, M., et al. 2011, A&A, 530, A115
Castro, N., Fossati, L., Langer, N., et al. 2014, A&A, 570, L13
Gräfener, G., Owocki, S. P., & Vink, J. S. 2012, A&A, 538, A40
Heger, A., Langer, N., & Woosley, S. E. 2000, ApJ, 528, 368
Iglesias, C. A. & Rogers, F. J. 1996, ApJ, 464, 943
Ishii, M., Ueno, M., & Kato, M. 1999, PASJ, 51, 417
Langer, N. 1997, in Astronomical Society of the Pacific Conference Series, Vol. 120, Luminous Blue Variables: Massive Stars in Transition, ed. A. Nota & H. Lamers, 83
Mazzali, P. A., Valenti, S., Della Valle, M., et al. 2008, Science, 321, 1185
Moriya, T. J., Sanyal, D., & Langer, N. 2015, A&A, 575, L10
Nakar, E. & Sari, R. 2010, ApJ, 725, 904
Nugis, T. & Lamers, H. J. G. L. M. 2000, A&A, 360, 227
Petrovic, J., Pols, O., & Langer, N. 2006, A&A, 450, 219
Sanyal, D., Grassitelli, L., Langer, N., & Bestenlehner, J. M. 2015, Accepted in A&A
Soderberg, A. M., Berger, E., Page, K. L., et al. 2008, Nature, 453, 469
Svirski, G. & Nakar, E. 2014, ApJ, 788, L14
Weaver, T. A. 1976, ApJS, 32, 233

Stephen Ro: The SN2008D pre-SN flash was observed in X-rays by Chandra, which implies a mildly relativistic shock was responsible. Your assumption of a 20,000 km/s shock speed seems to be very small and incompatible. Can you explain this?

Debashis Sanyal: The implications of a mildly relativistic shock comes from the assumption of a steeply declining density profile of the progenitor, which is not the case in our model. The flat density structure in the inflated envelope might decelerate the shock significantly, and hence hydrodynamical modelling in inflated envelopes is required to estimate the shock breakout velocity. The later shock velocity of $0.25c$ observed by Soderberg et al. (2008) with *Chandra* might also not correspond to the actual shock velocity at breakout because the shock could have accelerated post-breakout due to the steep density gradient between the stellar surface and the low density wind.

Vikram Dwarkadas: One of the problems with SN2008D was that the X-ray flux of the flash was quite low, if it was a flash. From your parameters, you could use this to calculate the X-ray flux of the flash, and see if it matches.

Wolf-Rayet Stars
W.-R. Hamann, A. Sander, H. Todt, eds.
Potsdam: Univ.-Verlag, 2015
URL: http://nbn-resolving.de/urn:nbn:de:kobv:517-opus4-84268

Massive star population synthesis with binaries

D. Vanbeveren[1,2], & N. Mennekens[1]
[1] *Vrije Universiteit Brussel, Brussels, Belgium*
[2] *K.U. Leuven, Louvain, Belgium*

We first give a short historical overview with some key facts of massive star population synthesis with binaries. We then discuss binary population codes and focus on two ingredients which are important for massive star population synthesis and which may be different in different codes. Population simulations with binaries is the third part where we consider the initial massive binary frequency, the RSG/WR and WC/WN and SNII/SNIbc number ratio's, the probable initial rotational velocity distribution of massive stars.

1 Introduction

It is generally accepted that most of the Wolf-Rayet stars are massive hydrogen deficient core helium burning stars. Some WNL stars (using the original abbreviation-definition of Vanbeveren and Conti, 1980) may be core hydrogen burning objects. They are not considered in the present paper. In the late sixties and seventies Roche lobe overflow (RLOF) in binaries was considered as a most plausible process capable to remove the hydrogen rich layers of a star. Furthermore, at the massive star conference in 1971 in Buenos Aires, Kuhi (1973) presented statistical arguments to conclude that all galactic WR stars may be binary components. At the same time large observational data sets became available of X-ray binaries and together with the WR argument it made flourish massive close binary evolution. Some protagonists are B. Paczynski, E. van den Heuvel, I. Iben, A. Tutukov, L. Yungelson, C. De Loore and the Brussels gang. Interested readers may find many massive binary evolution studies published in this period.

The early seventies are also characterised by important breakthroughs in the study of stellar winds of massive stars (e.g., Castor et al. 1975) and the question was raised whether or not WR stars could form via massive single star evolution, single stars that lose their hydrogen rich envelope by stellar winds (the Conti scenario, Conti, 1976). Chiosi et al. (1978) were among the first to demonstrate that this is indeed possible, but it still had to be shown that WR single stars exist (remember Kuhi, 1971). Vanbeveren and Conti (1980) reconsidered the galactic census of WR binaries. They concluded that the Kuhi statistics is biased and that the real galactic WR+OB frequency is no more than 30–40%, a percentage that still holds today.

Since 1980 large evolutionary data sets of massive single stars and binaries were calculated and with these data sets in combination with a description of the different processes that govern binary evolution (e.g., the effect of the supernova explosion on orbital parameters, the treatment of binary mergers, the treatment of the effect on orbital parameters of mass loss from the system during the RLOF, etc.) it became possible to predict theoretically how a massive star population would look like. It was realized that a comparison with the observed population yields important information in order to understand the physics of massive star/binary evolution.

Meurs and van den Heuvel (1989) are probably among the first authors to study in some detail the massive star population including binaries. The authors focussed on the number of evolved early type close binaries in the Galaxy, in particular the X-ray binary population.

Portegies Zwart and Verbunt (1996) introduced the skeleton of what would later on become the population code SeBa used in dynamical N-body simulations. In 1996 they used it to discuss the population of massive binaries with compact companions.

The investigation of the effects of binaries on the population of O-type and WR-type stars also started by the end of the previous millennium (Dalton and Sarazin 1995; Vanbeveren 1995; Vanbeveren et al. 1997; De Donder et al. 1997). A detailed description of the Brussels massive star population code was given in Vanbeveren et al. (1998a = Paper I) (see also Vanbeveren et al. 1998b for an extended review) and it was applied in order to predict the galactic number ratios WR/O, WR+OB/WR, WC/WN, O and WR stars with a compact companion, O and WR runaway stars, O and WR single stars but with a binary origin, O and WR single stars originating from a merged binary, the number of real O and WR single stars, etc. Furthermore, De Donder and Vanbeveren (2004) studied the effects of binaries on the chemical evolution of galaxies and it was therefore necessary in order to extend the code so that it was capable to predict the temporal evolution of the massive star/binary population as a function of metallicity Z.

Since 1998 other research groups wrote massive star+binary population codes with various degree of sophistication, e.g., Nelemans et al. (2001) and Toonen et al. (2012) substantially updated SeBa, Izzard et al. (2004, Binary_c) simulated the population of core collapse supernovae and gamma-ray bursts, Belczynski et al. (2008, Startrack) focussed on relativistic binaries with an application to future gravitational wave detectors. Eldridge et al. (2008) also presented simulations of massive star populations as a function of Z using an extensive grid of

single and binary evolutionary computations.

Spectral synthesis is a powerful tool in order to investigate extragalactic young massive starburst regions in general, the O and WR spectral features in these starbursts in particular. Starburst99 (Leitherer et al. 1999) is extremely useful for galaxies with active star formation but it has to be kept in mind that it does not account for the presence/evolution of massive binaries. The effect of binaries on the spectral synthesis of young starbursts was a main research topic in Brussels (Van Bever et al. 1999; Van Bever and Vanbeveren 2000, 2003; Belkus et al. 2003) and repeated by Eldridge and Stanway (2009) who essentially confirmed the Brussels results.

De Mink et al. (2013, 2014) introduced an important parameter in massive star population studies: rotation. They showed that the observed distribution of rotation velocities in O-type stars can be explained entirely by the process of RLOF and the possible spin-up of mass gainers/binary mergers.

In the line of the work of De Mink et al. a study of the rotation velocities of the O-type companions in WR+O binaries may be most illuminating and may help to answer the question if RLOF and mass transfer happened in WR+O progenitors. Mike Shara, Tony Moffat, Gregor Rauw, Dany Vanbeveren et al. just started an observational project aiming at determining these rotational velocities in as many WR+O binaries as possible. We invite everybody interested in joining the "et al.".

2 Massive single star + binary population synthesis codes

The Brussels population code has been described in detail in the list of papers given in the introduction and very recent updates are discussed in Mennekens and Vanbeveren (2014). Rather than repeating all the basic ingredients (once more) we prefer to highlight two ingredients which may be different in different codes: the initial-final mass relation and the LBV/RSG stellar wind mass loss rate formalism.

2.1 The initial-final mass relationship

Some codes (e.g., Nelemans et al. 2001; Izzard et al. 2004; Belczynski et al. 2008; De Mink et al. 2013) use single star interpolation formulae proposed by Hurley et al. (2000) and binary-evolutionary algorithms described by Tout et al. (1997) and Hurley et al. (2002). Other codes (e.g., Eldridge et al. 2008; the Brussels code) use an extended library of detailed binary evolutionary computations. The latter two codes and the codes based on the algorithmic method predict massive star populations that differ mainly in the absolute number of mass gainers of interacting-binaries but the differences are not critical and do not affect overall conclusions made in the papers cited above. A much more severe difference is related to the initial mass-final mass relation ship. As was discussed by Mennekens and Vanbeveren (2014) for stars with initial mass $\geq$ 20 $M_\odot$ the final masses are significantly larger in Hurley et al. based codes than in the Brussels code, possibly due to different stellar wind mass loss rate formalisms and/or alternative convective core overshooting prescriptions during core hydrogen burning. Note that a similar effect is visible in the intermediate mass range (Toonen et al. 2014). Unfortunately, this difference plays a critical role for the predicted population of binaries with at least one compact companion, even more for systems consisting of two compact stars, and as shown by Mennekens and Vanbeveren (2014) also for the predictions of the detection rates of gravitational wave observatories.

2.2 The stellar wind mass loss rate formalism during the LBV and the RSG phase

LBV. The Brussels code adopts the LBV scenario of massive binaries as has been introduced by Vanbeveren (1991). It states that the LBV phase is a common evolutionary phase of the most massive stars and that the LBV mass loss rate suppresses the RLOF/common envelope phase in case Br / case Bc / case C binaries when the mass loser has a mass higher than $\approx$40 $M_\odot$ (see also Mennekens and Vanbeveren, 2014, for a recent argumentation). However, when this mass loser is a member of a case A binary, the star will lose most of its hydrogen rich layers due to RLOF prior to the LBV phase and it is tempting then to assume that the LBV phase does not happen. A case A binary in this high mass range then follows a more canonical evolutionary scenario where the case A RLOF is followed by case Br RLOF. Mennekens and Vanbeveren (2014) demonstrated that the way how LBV mass loss is implemented in population codes has an enormous effect on the predicted merger rates of double compact star binaries (primarily double black hole binaries are affected) and thus also on the predicted detection rates of forthcoming advanced LIGO detectors.

Note that the story would be completely different if the LBV phenomenon would appear to be related to massive binary mergers.

RSG. Since the early days when scientist started to investigate the effects of stellar winds on massive star evolution, very conservative formalisms were used in order to study the effects of the RSG wind. Most common was the formalism proposed by de Jager et al. (1988). However, based on observations of Feast (1992), Bressan (1994) concluded that the mass loss rate during the RSG phase of an LMC 20 $M_\odot$ star could be a factor 10 larger than predicted by the

de Jager et al. formalism. Vanbeveren (1995) was among the first to investigate the effect of these larger rates on the evolution of $20 - 25\,M_\odot$ single stars. It was concluded that as a consequence of RSG mass loss a 20–25 $M_\odot$ single star may become a WR star. A more throughout discussion of evolutionary computations of massive single stars with the alternative RSG rates and the effect on the overall WR population was presented in Paper I. Salasnich et al. (1999) also re-investigated the effect of new RSG mass loss rates on the evolution of massive stars and essentially arrived at similar conclusions. Note that these alternative RSG rates also significantly affect the evolution of case C binaries, the RSG scenario as it was described in the Vanbeveren et al. papers which states that RSG mass loss may suppress the RLOF in Case C massive binaries. About 15–20 years after the papers of Bressan and Vanbeveren larger RSG rates were also implemented in the Geneva single star evolutionary code (Ekström et al. 2012; Meynet et al. 2015). In the latter paper it was concluded that enhanced mass-loss rates during the RSG phase have little impact on the WR population, contrary to the simulations made in Brussels. The difference between the Geneva and Brussels results is most probably due to the post-RSG mass loss rates used in both codes. To illustrate let us consider a $20\,M_\odot$ star. When due to the larger RSG rates this star has lost about 10 $M_\odot$ during the RSG phase, it leaves the RSG region and starts evolving to the blue part of the HR-diagram. The Geneva code calculates the further evolution by using blue supergiant mass loss rates (Vink-rates) and the star never becomes a WR star. However, although the star still has a rather high hydrogen content in its atmosphere at the moment it leaves the RSG phase (typically $X_{atm} \approx 0.5$), the models have an internal structure similar to WNL stars. In Brussels we therefore decided to continue the further post-RSG evolution by using typical WNL mass loss rates rather than blue supergiant rates. As a consequence the star loses its remaining hydrogen rich layers, becomes a WNE (also here we use the original nomenclature of Vanbeveren and Conti, 1980) and eventually a WC star. The discussion of post-RSG mass loss rates remains open but at least with the Brussels suggestion it is possible to explain the low luminosity WC stars as observed by Sander et al. (2012). In section 3.2 we will add additional support for higher RSG mass loss rates.

3 Massive single star + binary population synthesis simulations

Note that in this section we only consider population simulations where binaries are included.

3.1 The initial massive binary frequency

First, it is important to realize that accounting for all the physical processes that determine the evolution of binaries, the massive binary frequency (in a population of stars where star formation has been going on for at least a few million years) is smaller that the binary frequency at birth (on the ZAMS). In all the population simulations that we published since Paper I it is assumed that the massive binary frequency (binaries with initial period ≤ 10 yr) at birth $f \geq 0.7$. This latter value is based on the following argumentation. By studying a sample of 67 bright O-type stars Garmany et al. (1980) concluded that 33% ($\pm$13%) are primary of a close binary with mass ratio > 0.2 and period $P \leq 100$ days. As discussed in Paper I a population of O-type stars in a field of continuous star formation consists of real single stars, interacting binaries with periods up to 10 years, mergers looking like singles, post-supernova single O-type mass gainers, etc. Therefore, to recover the results of Garmany et al. (1980) with a population synthesis simulation we had to start with an initial binary frequency $f \geq 0.7$.

As was outlined in the introduction, the observed WR+OB binary frequency (in the Galaxy) seems to be not larger than 30-40%. But also a population of WR stars in a region where star formation is continuous consists of real WR single stars, WR+OB binaries, WR stars resulting from binary mergers, single WR stars resulting from post-SN single OB-type mass gainers etc. and also here we had to start with a very high initial binary frequency in order to explain the observed WR+OB frequency.

Recent observations of O-type stars in young clusters seem to confirm a high massive binary fraction (Sana et al. 2008, 2009, 2011, 2012; Rauw et al. 2009) and they propose a value $\geq$ 50%. A similar exercise as the one made in Paper I (and summarized above) was done by De Mink et al. (2014) but using the observations discussed by H. Sana et al.. Also De Mink et al. concluded that in order to recover the observed $\geq$ 50 % massive binary frequency of H. Sana and co-workers, one has to start with an initial binary frequency $\geq$ 70%.

3.2 the RSG/WR number ratio as function of Z

RSG winds significantly affect the RSG-timescale of a massive star and depending on the post-RSG mass loss formalism (see section 2.2), they also significantly affect the WR-timescale. The RSG (and post-RSG) mass loss formalism therefore significantly affects the predicted RSG/WR number ratio. Remark that our population code is the only single star + binary code that includes the effects of the alternative RSG mass loss rates as discussed above. Fig. 1 compares predicted and observed RSG/WR number ratios as function of Z. The observations come from

Massey (2003) with updates as reviewed by Massey et al. (2013). The predictions holds for a population with a binary frequency at birth = 70%. The dashed line is based on the simulation of Eldridge et al. (2008), the full lines are the Brussels predictions (predictions depend on parameters who's values are subject to some uncertainty; varying the values of these parameters yields a maximum and a minimum RSG/WR number ratio, resp. the upper line and the lower line in Fig. 1). The main difference between the simulation of Eldridge et al. and the Brussels one is the RSG mass loss formalism and we are inclined to conclude that the prediction with the alternative (higher) RSG rates fits the observations better, supporting the conclusion of section 2.2.

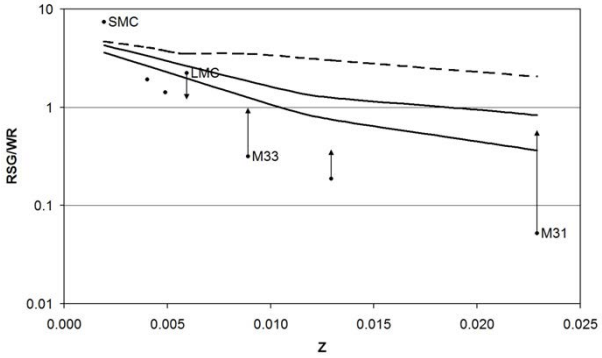

Fig. 1: A comparison between the observed and predicted RSG/WR number ratio as function of Z. The observations are those reviewed by Massey (2003) and the arrows indicate updates as discussed by Massey et al. (2013). The dashed line is the prediction proposed by Eldridge et al. (2008), the full lines are the maximum/minimum (see text) predictions made with the Brussels code.

3.3 The WC/WN number ratio as function of Z

L. Smith (1973) argued that metallicity might be responsible for the relative absence of WCs in the Magellanic Clouds, but without understanding the physical mechanism. Vanbeveren and Conti (1980) were among the first to link the effect of Z on stellar wind mass loss and the WC/WN-Z dependence. Detailed population simulations (with binaries) were presented by Vanbeveren et al. (2007) and Eldridge et al. (2008) and compared to observations. It was concluded that correspondence is rather satisfactory. In both studies the observations were those discussed by Massey (2003). It can readily be checked that recent updates (Neugent et al. 2013) do not significantly change the overall conclusions made in the two population studies cited above.

3.4 The SNII and SNIbc population

Studies of the effect of binaries on the population of SNII and SNIbc are numerous and go back to the very beginning of massive binary evolution research. Interested readers may consider Tutukov et al. (1992), Podsiadlowski et al. (1992), Joss et al. (1992), De Donder and Vanbeveren (1998, 2003, 2004), Belczynski et al. (2002) and references therein. Some more recent work essentially confirms the earlier results. One of the conclusions is that most of the progenitors of SN Ibc are massive binary components with an initial mass ≥ 10 $M_\odot$, e.g. most of the progenitors of SN Ibc do not have an initial mass $\geq$ 25-30 $M_\odot$ and thus most of the progenitors of SN Ibc are not WR stars. Moreover, since the population of SN II and SN Ibc depends so much on the massive interacting binary population, one may wonder whether SN-population differences between different types of galaxies may reflect differences in the population of these massive binaries.

De Donder and Vanbeveren (1998) compared the overall (cosmological) observed SN II and SN Ibc population with population simulations and it was concluded that the overall cosmological massive interacting binary frequency should be about 50%.

3.5 The initial rotational velocity distribution

The observed rotational velocities of O-type stars in the Galaxy has been discussed by Conti and Ebbets (1977), Penny (1996), and in Paper I. An analysis of these observations in terms of massive single star and close binary evolution was presented in Vanbeveren (2009). It was concluded that a majority of massive O-type stars are born as relatively slow rotators with an average < 200 km/s rather than the 300 km/s used by the Geneva team. The rotation velocity distribution proposed in the papers cited above shows that there is a significant group of rapidly-rotating O-type stars but many of the stars in this latter group are runaways with a peculiar space velocity > 30 km/s. This means that many of them do not have a canonical single star history but are the product of binary evolution (binary mergers, spun-up binary mass gainers, mergers due to dynamical interaction in dense clusters). The latter paper then suggested the following: *if one asks whether or not rotation is important for stellar evolution, the answer is yes but perhaps mainly in the framework of binary evolution (rapidly-rotating mass gainers and binary mergers) or in the framework of dynamics in dense clusters where stars collide, merge and become rapid rotators.*

Within the VLT-Flames Tarantula survey Ramirez-Agudelo et al. (2013) investigated the rotational velocities of the O-type stars in 30 Dor and obtained a distribution which is very similar as the

one proposed for the Galaxy in the papers listed above.

De Mink et al. (2013) implemented rotation and the evolution of rotation in a population code of single stars and of close binaries. They concluded that starting with an initial population of slowly rotating massive stars (average velocity = 100 km/s), the observed rotational velocity distribution (the one discussed in the papers cited above) can be recovered by properly accounting for all processes that affect the rotation in single star and binary evolution. Therefore (in line with the suggestion of Vanbeveren, 2009 cited above) it can not be excluded that most massive O-type stars are born as slow rotators, much slower than the average value adopted by the Geneva team in their standard evolutionary calculations. If this is true then one may be inclined to conclude that *the overall evolution of massive single stars and of most of the binary components prior to the onset of RLOF hardly depends on rotation.*

4 Conclusions

We like to end this paper with an advice and an overall conclusion.

Advice (not only for young scientists): before starting a research topic, try to get a literature overview that is as complete as possible and do not forget that also in the previous millennium interesting studies have been published.

Conclusion: a theoretical population study of massive stars where binaries are ignored may have an academic value but may be far from reality.

References

Belczynski, K., et al. 2002, ApJ, 572, 407
Belczynski, K., et al. 2008, ApJS, 174, 223
Belkus, H., et al. 2003, A&A, 400, 429
Bressan, A. 1994, in Meeting: Evolution of massive stars, 373
Castor, J. et al. 1975, ApJ, 195, 157
Chiosi, C., et al. 1978, A&A, 63, 103
Conti, P. 1976, MSRSL 9, 193
Conti, P., Ebbets, D. 1977, ApJ, 213, 438
Dalton, W., Sarazin, C. 1995, ApJ, 448, 369
De Donder, E., Vanbeveren, D. 1998, A&A, 333, 557
De Donder, E., Vanbeveren, D. 2003, NewA, 8, 415
De Donder, E., Vanbeveren, D. 2004, NewA Review, 48, 861
De Donder, E., et al. 1997, 318, 812
De Jager, C., et al. 1988, A&AS, 72, 259
De Mink, S., et al. 2013, ApJ, 764, 166
De Mink, S., et al. 2014, ApJ, 782, 7
Ekstrom, S., et al. 2012, A&A, 537, A146
Eldridge, J., Stanway, E. 2009, MNRAS, 400, 1019
Eldridge, et al. 2008, MNRAS, 384, 1109
Feast, M. 1992, in Proceedings of the International Colloquium, 18
Garmany, C., et al. 1980, ApJ, 242, 1063
Hurley, J., et al. 2000, MNRAS, 315, 543
Hurley, J., et al. 2002, MNRAS, 329, 897
Izzard, R., et al. 2004, MNRAS, 350, 407
Joss, P., et al. 1992, IAUS, 151, 523
Kuhi, L. 1973, IAUS, 49, 205
Leitherer, C., et al. 1999, ApJS, 123, 3
Massey, P. 2003, ARA&A, 41, 15
Massey, P., et al. 2013, Massive Stars: From α to Ω
Mennekens, N., Vanbeveren, D. 2014, A&A, 564, A134
Meurs, E., Van den Heuvel, E. 1989, A&A, 226, 88
Meynet, G., et al. 2015, A&A, 575, A60
Nelemans, G., et al. 2001, A&A, 365, 491
Neugent, K., et al. 2013, Massive Stars: From α to Ω
Penny, L. 1996, Ph.D. Thesis, Georgia State University
Podsiadlowski, P., et al. 1992, ApJ, 391, 246
Portegies Zwart, S., Verbunt, F. 1996, A&A, 309, 179
Ramirez-Agudelo, O., et al. 2013, A&A, 560, A29
Rauw, G., et al. 2009, MNRAS, 398, 1582
Salasnich, B., et al. 1999, A&A, 342, 131
Sana, H., et al. 2008, MNRAS, 386, 447
Sana, H., et al. 2009, MNRAS, 400, 1479
Sana, H., et al. 2011, MNRAS, 416, 817
Sana, H., et al. 2012, Sci, 337, 444
Sander, A., et al. 2012, A&A, 540, A144
Smith, L. 1973, IAUS, 49, 228
Toonen, S., et al.. 2012, A&A, 546, A70
Toonen, S., et al. 2014, A&A, 562, A14
Tout, C., et al. 1997, MNRAS, 291, 732
Tutukov, A., et al. 1992, ApJ, 386, 197
Van Bever, J., Vanbeveren, D. 2000, A&A, 358, 462
Van Bever, J., Vanbeveren, D. 2003, A&A, 400, 63
Van Bever, et al. 1999, NewA, 4, 173
Vanbeveren, D. 1991, A&A, 252, 159
Vanbeveren, D. 1995, A&A, 294, 107
Vanbeveren, D. 2009, NewA Review, 53, 27
Vanbeveren, D., Conti, P. 1980, A&A, 88, 230
Vanbeveren, D., et al. 1997, A&A, 317, 487
Vanbeveren, D., et al. (Paper I) 1998a, NewA, 3, 443
Vanbeveren, D., et al. 1998b, A&A Review, 9, 63
Vanbeveren, D., et al. 2007, ApJ, 662, 107

Philip Massey: I have a comment and a question. First, J. J. Eldridge made the point yesterday that we really have to worry about "duplicity" and not "binary/not-binary". I took this to mean that there is a range of properties of binaries, including mass ratios and orbital separations, that are going to affect to what degree the stars will interact, if at all. In other words, simply saying that "all massive stars are in binaries" doesn't actually mean that we have to worry about binary evolution: maybe we do, and maybe we don't. One greatly overestimates the fraction of stars that will interact by assuming that all massive stars go through a RSG phase (see, e.g., Sana et al. 2012). So, while binary evolution may be important, you don't demonstrate that by just saying, "All massive stars are born in binaries!" My question is, why have you cherry-picked the observational data with which to compare? You show my WC/WN ratios from 2003 to compare with your models, but we've done a lot of work to improve these numbers over the past 12 years. The same is true for the number of RSGs to WRs.

Dany Vanbeveren: Let me start with your question: my talk is a review, so when referring to Eldridge et al. (2008) I used the data that they used namely those of your ARA&A paper of 2003. However, for the written version I promise to add a few observation-updates and I leave it to the interested reader to decide if conclusions remain valid.

What about the comment. It is easy to show that most of the massive binaries (and massive here means binaries with primary mass $\geq 10\,M_\odot$) with initial period ≤ 10 years are interacting. Even more: the value 10 years is based on the assumption that the star is in a circular orbit and this needs not to be the case (we know from observations that the larger the binary period the more eccentric the orbit). So, binaries with a period much larger than 10 years may still be interacting binaries. When one considers massive binaries with primary masses larger than, say, $20\,\mathrm{M}_\odot$, there the RSG scenario may be at work (see the paper) stating that binaries where the RSG phase (with larger RSG mass loss rates) happens before the RLOF will start will not interact. Still (based on detailed population simulations) it can be concluded that at least 60–70% of the massive binaries with primary mass $> 20\,M_\odot$ and initial period < 10 years will interact. Last but maybe not least: binaries with primary masses $> 40\,M_\odot$. Here the LBV scenario may be at work (see again the paper), e.g., when the binary period is such the the primary turns into an LBV before the RLOF can start, the latter may be avoided and the binary then can be considered as non-interacting. A significant fraction of binaries in this mass range may therefore be non-interacting (may be all except case A binaries). The LBV story would of course be completely different if the LBV phenomenon is linked to binary merging rather than a general evolutionary phase of a very massive star. Note that the RSG/LBV scenario is accounted for in the Brussels binary population code (already since 1998) but this is not true for all existing codes.

Cyril Georgy: A comment about the mixing in massive stars. In current stellar evolution codes including rotation, rotational mixing (of chemicals and of angular momentum) is parametrised, and is not a prediction of the models. It is thus not possible so far to argue that a star rotating at 100 km/s will not mix. It may be the case, or not.

Tony Moffat: You told me earlier in this meeting that you need RSGs with higher M-dots to make RLOF work in medium-period binaries ($P \approx 50$–$3000\,\mathrm{d}$) with $M_\mathrm{i} = 25$–$40\,M_\odot$ for the primary. But where are such RSGs? We don't see them: the observed upper mass limit for RSG is $25\,M_\odot$ (Massey et al. 2007+). You also said that we don't see such RSG, not because they don't exist, but because the lifetimes (a few 10^4 years) are so short. But among the large samples of known RSG, this time is *not* too short to prevent us from seeing them I would say. Those RSGs that we do see have lifetimes of several 10^4 years, too, and we have no trouble seeing them.

Dany Vanbeveren: This looks like a misunderstanding. If the period of a binary is such that the primary fills its Roche lobe before an eventual RSG will happen, this RSG phase will be avoided. However, when the period is such that an eventual RSG phase will happen before the RLOF can start (of the order of 1000 days depending on the initial mass of the primary), the latter may not start at all (the RSG scenario of massive binaries as explained in the paper). A general theorem of binary evolution sounds as follows: when a star still has the tendency to expand at the moment that it fill its Roche lobe when the star is a binary component, then the RLOF will happen.

About the upper mass limit of RSG: this can indeed be due to the fact that stars above this mass limit do not become RSG, but I wonder whether or not one can exclude the fact that this apparent upper mass limit is due to the combination of IMF-arguments and the fact that the RSG-lifetime becomes shorter the larger the stellar mass.

Dany Vanbeveren asking a question

The conference audience shortly before leaving for the excursion

The Big Refractor of the Astrophysical Observatory Potsdam

Wolf-Rayet Stars
W.-R. Hamann, A. Sander, H. Todt, eds.
Potsdam: Univ.-Verlag, 2015
URL: http://nbn-resolving.de/urn:nbn:de:kobv:517-opus4-84268

The missing Wolf-Rayet X-ray binary systems

M. Munoz[1], A. F. J. Moffat [1], G. M. Hill[2], N. D. Richardson[1], & H. Pablo[1]
[1] *Université de Montréal, Canada*
[2] *W. M. Keck Observatory, Hawaii*

We investigate the rarity of the Wolf-Rayet X-ray binaries (WRXRBs) in contrast to their predecessors, the high mass X-ray binaries (HMXRBs). Recent studies suggest that common envelope (CE) mergers during the evolution of a HMXRBs may be responsible (Linden et al. 2012). We conduct a binary population synthesis to generate a population of HMXRBs mimicking the Galactic sample and vary the efficiency parameter during the CE phase to match the current WRXRB to HMXRB ratio. We find that ∼50% of systems must merge to match observational constraints.

1 Introduction

Current Wolf-Rayet (WR) evolution theories agree that WR stars originate from O-type main sequence stars. Thus, we expect a commonplace O+O binary system to evolve into an O+cc, a high mass x-ray binary, and eventually to a WR+cc system. Yet, while the number of known O + cc is significant, the number of detected WR+cc systems is much lower than predicted. In fact, while there are a total of 114 confirmed HMXRBs (Liu et al. 2006) in our Galaxy, there is only a single confirmed WR+cc binary: Cyg X-3 (Tutukov et al. 2013).

To explain this discrepancy, the evolution of an HMXRB to a WRXRB is presumably halted by a CE merger. The goal is to produce a sufficient number of massive OB binaries to obtain 114 HMXRBs and adjust the efficiency parameter such that the merger rate of the HMXRBs is compatible with the observed number of WRXRBs.

2 Computational method

2.1 Initial binary population

Assuming zero eccentricity, the synthetic binaries can be synthesized with the aid of three probability distribution functions (PDFs): 1) the Salpeter initial mass function to determine the mass of the primary, m_1 2) empirical mass ratio to determine the mass of the secondary, m_2 3) Öpiks law to determine the orbital period, P. Respectively, the PDFs are:

$$\begin{aligned} f(m_1) &\propto m_1^{-2.35} \\ f(q) &\propto 1 \\ f(P) &\propto 1/P \end{aligned} \tag{1}$$

where $q = m_2/m_1$. The masses will range from 8 $M_\odot$, the minimum threshold for massive stars to undergo a supernova explosion, to 100 $M_\odot$, the maximum capacity in the binary evolution code (see section 2.2), and the period from 2 to 3000 days. Any system with a period less than 2 days is expected to merge and binary interaction is insignificant above 3000 days.

2.2 Binary Evolution

The generated binaries are evolved with a binary evolution code from Hurley et al. (2002). The initial masses and periods obtained in (1) will serve as input parameters. It is necessary to determine the distribution of supernova kicks and the efficiency parameter of the CE phase as they play an important role in the evolution of a HMXRB.

2.2.1 Supernova kicks

Asymmetric supernova (SN) explosions may impart an additional kick to a binary system. This may encourage the binary to disrupt or even help stabilize the orbit. Modelling SN kicks is therefore essential in massive binary evolution.

The direction of the kicks is presumed to be random. As for its magnitude, neutron star (NS) natal kicks are modeled with a Maxwellian distribution peaked at 300 km/s. Black hole (BH) kicks are assumed to obey reduced NS kicks owing to conservation of momentum (Repetto et al. 2012). For example, a 10 $M_\odot$ BH will receive ∼60% the kick of a 1.4 $M_\odot$ NS.

2.2.2 Common envelope evolution

If mass transfer occurs on dynamical timescales, faster than the compact object can accrete, then the excess matter will lead to the formation of a common envelope (CE) around both stars. As the compact companion orbits around the donor's core, the envelope creates a drag force on the two stars that dissipates their angular momentum and causes them to spiral in. The outcome of this scenario is either a successful ejection of the CE or a merger.

As the stars spiral in, if enough gravitational energy is released and converted to kinetic energy into the envelope, the CE may be blown away. However, as there are non-conservative forces, some energy will be lost. The survivability of the system depends on its efficiency in transferring orbital energy into the envelope.

Treatment of the CE evolution in Hurley et al. (2002) introduces two free parameters: $\alpha_{\rm CE}$, the

efficiency, and λ, a corrective term in the envelope's binding energy that depends the donor's mass-density structure. It is common practice to set λ at 0.5 (de Kool 1990) and the efficiency typically varies from 0 to 1. Therefore, in this study, λ is left constant at this default value and only $\alpha_{\rm CE}$ was varied.

3 Results

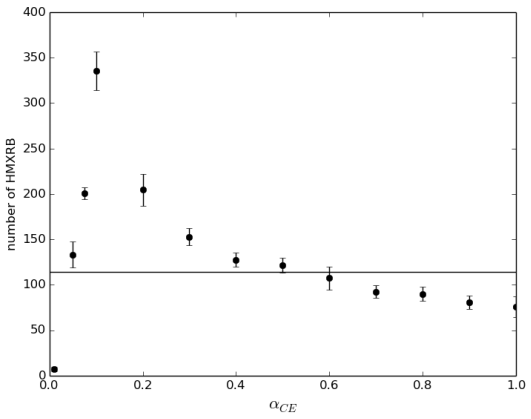

Fig. 1: Number of HMXRBs as a function of the efficiency. The number of initial synthetic binaries is kept constant at 12000. The solid horizontal line indicates the cut off for 114 HMXRBs.

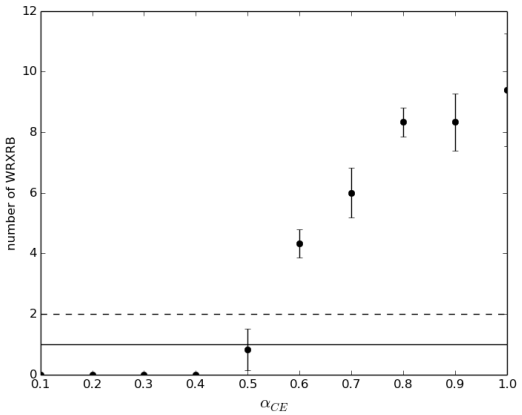

Fig. 2: Number of WRXRBs as a function of the efficiency. The number of initial synthetic binaries is adjusted to produce roughly 114 HMXRBs. The solid and dashed horizontal lines respectively correspond to the thresholds for 1 WRXRB (Cyg X-3) and 2 WRXRBs (Cyg X-3 and possibly another unidentified WRXRB, such as WR 148).

In Figure 1 we illustrate how the efficiency parameter effects the number of resulting HMXRBs with a constant initial population of 12000 binaries. The efficiency ranged from 0 to 1 with an increment of 0.1.

Similarly, depicted in Figure 2 is the number of WRXRB for a given efficiency. For each value of $\alpha_{\rm CE}$, the initial population of generated OB binaries is calibrated (by trial and error) to ensure that there are $\sim$114 HMXRBs.

4 Discussion

Of interest is the value of $\alpha_{\rm CE}$ to require all but a single HMXRB to merge from an initial sample of 114 HMXRBs. However, obtaining a constant population of 114 HMXRBs is difficult because it is sensitive to the efficiency. This indicates that there may be a CE phase prior to the SN of the original primary. If this were the case, then intuitively one would expect the number of HMXRBs to decrease as the efficiency drops. And yet, as seen in Figure 1, the number of HMXRBs appear to rise for $\alpha_{\rm CE}$ decreasing to 0.1.

A CE phase, while both stars are still on the main sequence, has an unprecedented effect on the disruption rate of a binary subsequent to a SN. As the efficiency drops, the pre-SN binaries that survive a CE phase (if a CE phase occurs) will have a much reduced orbital separation. As a result, these tighter binaries will have a better chance of surviving the first SN, thus creating more HMXRBs. This is valid for an efficiency between 0.1 and 1. However, below $\alpha_{\rm CE} = 0.1$, the energy conversion isn't efficient enough for the binaries to survive the pre-SN CE phase and so the number of HMXRBs decline rapidly.

The surviving HMXRBs face another hurdle. Their evolution and fate is often subject to a CE phase once again. This is because unstable mass transfer is easily triggered if the binary components have a large mass ratio (i.e. $q \geqslant 1$). This is most likely the case for puffy OB stars orbiting around a compact object. Binaries that are successful at ejecting their CE can have their orbital separations drastically reduced by up to a factor of 100 (Tauris & van den Heuvel 2006). This can explain Cyg X-3's extremely short period of 4.8 hours.

Considering the typical lifetimes of a WR compared to its O-star progenitors, we would expect around 10% of the HMXRBs to evolve into WRXRBs. Thus naively, if there were no CE mergers, we would predict $\sim$11 WRXRB in the Galaxy. This is what is shown in Figure 2 at 100 % efficiency (within error). As suspected, the number of WRXRBs decreases along with the efficiency. Below 40% efficiency, all HMXRBs have merged and there are no WRXRBs. Setting $\alpha_{\rm CE}$ to 0.5 allows us to obtain the ideal merger rate.

These results are valid in the assumption that $\lambda = 0.5$. However, the true determination of this coefficient is still subject to much debate. Nevertheless, we are fortunate that the CE evolution depends on the product $\alpha_{\rm CE}\lambda$ and not on the individual values themselves. Therefore, if λ is ever better constrained, the validity of this work is not changed as long as $\alpha_{\rm CE}$ is adjusted so that the quantity $\alpha_{\rm CE}\lambda$ remains equal to 0.25.

5 Conclusion and future work

We demonstrated how the transition from HMXRB to WRXRB can be impeded due to unstable mass transfer which leads to the formation of a common envelope. The apparent lack of WRXRB in comparison to the number of HMXRB can hence be explained by CE mergers. We obtain an efficieny of 0.5 during the CE phase to reproduce the current WRXRB to HMXRB ratio.

It is important to note that this study relies on the premise that Cyg X-3 is the only WRXRB in our galaxy. There are however other candidates worthy of investigation, namely WR 148 (HD 197406). WR 148 is a single lined spectroscopic binary classified as a WN8h + B3IV/BH (Hamann et al. 2006). To determine the nature of the companion we have obtained high signal to noise spectra (above 1000 per pixel in the continuum once combined) from the Keck observatory with the ESI spectrograph, providing a range of 3900 Å to 10900 Å. A meticulous study of these spectra is currently underway.

References

de Kool, M. 1990, ApJ, 358, 189

Hamann, W.-R., Gräfener, G., & Liermann, A. 2006, A&A, 457, 1015

Hurley, J. R., Tout, C. A., & Pols, O. R. 2002, MNRAS, 329, 897

Linden, T., Valsecchi, F., & Kalogera, V. 2012, ApJ, 748, 114

Liu, Q. Z., van Paradijs, J., & van den Heuvel, E. P. J. 2006, A&A, 455, 1165

Repetto, S., Davies, M. B., & Sigurdsson, S. 2012, MNRAS, 425, 2799

Tauris, T. M. & van den Heuvel, E. P. J. 2006, Formation and evolution of compact stellar X-ray sources, ed. W. H. G. Lewin & M. van der Klis, 623–665

Tutukov, A. V., Fedorova, A. V., & Cherepashchuk, A. M. 2013, Astronomy Reports, 57, 657

Jennifer L. Hoffman: How sure are we that only one WR+cc binary exists in our Galaxy? Could we have missed a couple?

Melissa Muñoz: It is unlikely because while gas might hide many such systems, it is transparent to X-rays, which are prominent in X-ray binaries. However, there are a couple of unique cases, such as WR 148, which may in fact have compact companions.

Wolf-Rayet Stars
W.-R. Hamann, A. Sander, H. Todt, eds.
Potsdam: Univ.-Verlag, 2015
URL: http://nbn-resolving.de/urn:nbn:de:kobv:517-opus4-84268

Wolf-Rayet stars as an evolved stage of stellar life

C. Georgy[1], S. Ekström[2], R. Hirschi[1], G. Meynet[2], J. H. Groh[2], & P. Eggenberger[2]
[1] *Astrophysics group, EPSAM, Keele University, Lennard-Jones Labs, Keele, ST5 5BG, UK*
[2] *Geneva Observatory, University of Geneva, Chemin des Maillettes 51, 1290 Versoix, Switzerland*

Wolf-Rayet (WR) stars, as they are advanced stages of the life of massive stars, provide a good test for various physical processes involved in the modelling of massive stars, such as rotation and mass loss. In this paper, we show the outputs of the latest grids of single massive stars computed with the Geneva stellar evolution code, and compare them with some observations. We present a short discussion on the shortcomings of single stars models and we also briefly discuss the impact of binarity on the WR populations.

1 Introduction

Wolf-Rayet (WR) stars are known to be the very advanced stages of the life of massive stars (Conti 1976). These stars exhibit at their surface signs of hydrogen burning products through CNO cycle (for the WN stars) or even of helium burning products (Crowther 2007). To explain the existence of such objects, elements that are produced in the centre of a massive stars have to appear at the surface. This can be achieve by two different ways: a) internal mixing inside that star, allowing for transporting chemical elements from the place where they are produced to the surface, b) mass loss, that progressively remove the external layer of the star, and can ultimately uncover deep regions of the star, where nuclear burning previously occurred.

Internal mixing can be induced by the convective movements of matter in the convective regions, or by any other kind of mixing process in the radiative regions, such as rotational mixing (e.g. Zahn 1992). Mass loss can be due either by stellar winds, or by mass transfer in close binaries.

In this paper, we present preliminary results showing what are the expected WR stars population in the single massive star scenario, at different metallicities. The assumptions made in our computations and the chosen prescriptions are shortly reminded in section 2. Then, the various mass limits and number ratio of WR subtypes are presented in section 3. Finally, we briefly discuss the interesting challenges that need to be resolved to make progresses in that field.

2 Ingredients of the stellar models

The results presented in this paper were obtained by analysing the models from Ekström et al. (2012), Georgy et al. (2013), and Eggenberger et al. (in prep.). The computations were performed using the Geneva stellar evolution code (Eggenberger et al. 2008). Here is a brief summary of the assumed physical ingredients and prescriptions we used.

Convective zones are determined with the Schwarzschild criterion. For hydrogen and helium burning cores, a penetrative overshoot is assumed, which extends over a fraction $d_{\rm over}$ of the pressure scale height at the formal edge of the convective core. Inside the convective zones, the mixing is assumed to be instantaneous. In the inner regions, convection is assumed to be adiabatic, while in the external envelope, the thermal gradient is computed in the framework of the mixing-length theory (MLT Böhm-Vitense 1958). The free parameter $d_{\rm over}$ is calibrated at solar metallicity, by reproducing the width of the main sequence (MS) at around $1.7\,M_{\odot}$ (Ekström et al. 2012). The value of the α parameter appearing in the MLT is calibrated on a solar model.

Rotation is included in the framework of the "shellular" rotation approximation (Zahn 1992; Meynet & Maeder 1997; Maeder & Zahn 1998). The transport of angular momentum is computed with both the advective and diffusive term (Zahn 1992), while the transport of chemical elements is a purely diffusive process (Chaboyer & Zahn 1992). In this context, two diffusion coefficients are required. In our works, we use $D_{\rm h}$ from Zahn (1992) and $D_{\rm shear}$ from Maeder (1997). This choice best reproduces the presence of Cepheid loops at solar metallicity. The free parameter appearing in the formulation of $D_{\rm shear}$ is calibrated in order to reproduce the observed enrichment of stars in the range of 10 to $20\,M_{\odot}$ at solar metallicity (Ekström et al. 2012).

The mass-loss prescriptions and metallicity dependence are described in Ekström et al. (2012) and Georgy et al. (2013). An enhanced mass-loss rate (by a factor of 3) is used for red supergiant stars (RSG) above $20\,M_{\odot}$ (see discussion in Georgy 2012; Georgy et al. 2012).

In this work, we use the following criteria to classify the WR stars (Georgy et al. 2012). We consider that a star is a WR stars when its $\log(T_{\rm eff})$ is above 4., and its surface mass fraction is smaller than 0.3. A WR star with more than 10^{-5} as surface H mass fraction is a WNL star. If the surface hydrogen abundances drops below 10^{-5}, we have a WNE star if the surface nitrogen abundance is bigger than the carbon one, and a WC star otherwise. These are obviously rough criteria, but they have the advantage that they can be computed with standard outputs from stellar evolution models. A more

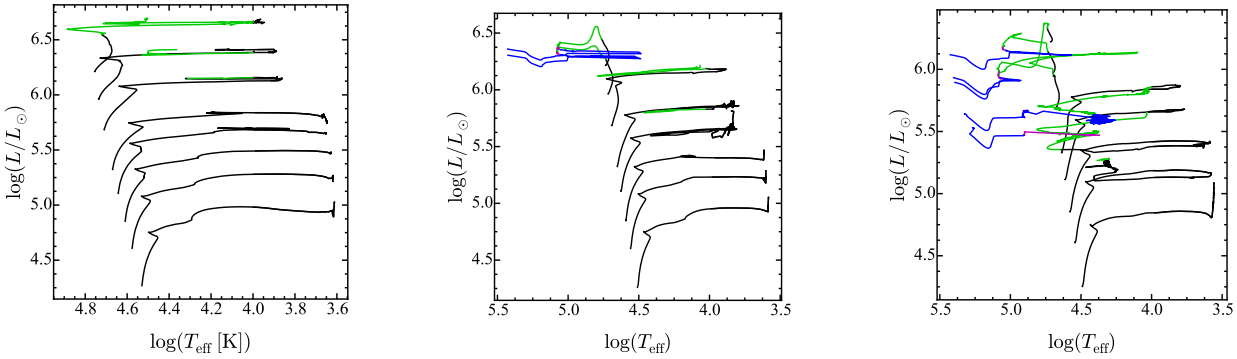

Fig. 1: HRD of rotating massive star models: $Z = 0.002$ (SMC, *left panel*), $Z = 0.006$ (LMC, *middle panel*), and $Z = 0.014$ (solar, *right pannel*). In each panel, models from $15\,M_\odot$ (bottom track) to $120\,M_\odot$ (top track) are shown. The different WR stages are indicated in colour: WNL (green), WNE (purple) and WC (blue). The initial rotation velocity is 40% of the critical one. Models are taken from Georgy et al. (2012) for $Z = 0.002$, Eggenberger et al. (in prep.) for $Z = 0.006$ and Ekström et al. (2012) for $Z = 0.014$.

detailed classification would require the modelling of the emergent spectrum (taking into account the winds), and this is so far not possible during the computation runtime. Such spectrum modelling in a post-processing approach has shown that a classification based on the aspect of the spectrum leads to significant differences (Groh et al. 2014).

3 Wolf-Rayet stars from single star models

Figure 1 shows the Hertzsprung-Russell diagram (HRD) for our latest models of massive stars, for 15, 20, 25, 32, 40, 60, 85, and $120\,M_\odot$, at three metallicities: $Z = 0.002$ (*left panel*), corresponding to the metallicity of the Small Magellanic Cloud, $Z = 0.006$ (*middle panel*), corresponding to the Large Magellanic Cloud one, and finally solar metallicity $Z = 0.014$ (*right panel*). The successive WR stages are highlighted with different colours: the WNL phase is shown in green, the WNE one in purple, and the WC one in blue.

A direct consequence of the weakness of the stellar winds at lower metallicity (Vink et al. 2001; Eldridge & Vink 2006) is that it becomes more and more difficult to produce WR stars when metallicity is decreasing. Moreover, at solar metallicity, our models spend a longer time in the RSG phase, allowing them to lose a lot of mass, and helping them to cross the HRD towards the WR phase at lower mass (around $20\,M_\odot$, see also Vanbeveren et al. 1998).

The minimal masses to enter into a given WR phase are given in Table 1. At solar and LMC metallicities, all WR types are accessible to single star models. Note however that the WC subtype occurs only for very massive stars at the LMC metallicity, while at solar Z, models more massive that about $27\,M_\odot$ are able to reach this stage. Moreover, these stars are found at luminosities higher than $\log(L) \sim 5.3$ at $Z_\odot$ and $\log(L) \sim 6.2$ at $Z_{\rm LMC}$. At the metallicity of the SMC, the radiative stellar winds are too weak to produce stars more evolved than the WNL phase, and no stars without hydrogen at the surface are expected from our models. The minimal mass to produce a WR star progressively shift from about $20\,M_\odot$ at $Z_\odot$ to more than $50\,M_\odot$ at the SMC metallicity. Above these masses, the endpoint of the evolution of our models are thus WR stars from our simple classification scheme (see however Groh et al. 2013b,c). It is not yet clear what would be the final fate of this kind of stars in terms of supernova explosion (type Ibc, failed supernova, direct collapse? See Heger et al. 2003; Dessart et al. 2011; Groh et al. 2013a; Bersten et al. 2014).

	O-star	WNL	WNE	WC
Solar	$15.8\,M_\odot$	$20.0\,M_\odot$	$25.3\,M_\odot$	$27.0\,M_\odot$
LMC	$14.2\,M_\odot$	$32.1\,M_\odot$	$60.8\,M_\odot$	$63.1\,M_\odot$
SMC	$12.6\,M_\odot$	$53.5\,M_\odot$	–	–

Tab. 1: Minimal mass to enter into a given phase. Results at $Z_\odot$ are taken from Georgy et al. (2012).

The expected ratio of WR stars to O-type stars, as well as subtype ratios, are shown in Table 2, in the constant star formation context. These numbers confirm that the number of WR stars with respect to O-type stars is decreasing with decreasing metallicity. The fraction of WC star is also expected to decrease at low metallicity, as well as the WC/WN ratio. Comparison with the observation at solar metallicity was presented in Georgy et al. (2012). Our results showed that in order to reproduce the observed ratio, WR stars should originate from a stellar population containing about 50% of

	WR/O-stars	WNL/WR	WNE/WR	WN/WR	WC/WR	WC/WN
Solar	0.066	0.687	0.022	0.709	0.291	0.409
LMC	0.016	0.887	0.005	0.892	0.108	0.121
SMC	0.006	1.000	0.000	0.000	0.000	0.000

Tab. 2: Various type ratios. Values at $Z_\odot$ are taken from Georgy et al. (2012).

binaries, in good agreement with results from more elaborated synthetic binary population codes (Vanbeveren et al. 1998; Eldridge et al. 2008). Note also that our WC/WN ratio reproduce reasonably well the observed trend at different metallicities (Neugent et al. 2012).

4 Discussion

Since a few years, it became clear that massive star populations contain a significant fraction of binary stars (e.g. Sana et al. 2012). It is thus important to know what are the physical mechanisms responsible for the appearance of the WR phenomenon (or subtypes), and what is linked to binary evolution or not. Recent observations of Galactic WC stars show a significant number of such kind of stars at surprisingly low luminosities ($\log(L) \sim 5.2$, Sander et al. 2012). These stars are hard to form through single star channel, even with a strong mass-loss rate during the RSG phase (Georgy 2012; Meynet et al. 2015), except if we assume that the strong mass loss continues *after* the RSG phase (Vanbeveren et al. 1998). On the other hand, they are routinely produced through the binary channel (Eldridge et al. 2008, 2013).

The relatively high number of high luminosity WNL stars with a large fraction of hydrogen on their surface (e.g. Hainich et al. 2014) on the other hand points to the need of accounting for a proper treatment of the internal mixing of the star, particularly inside the radiative zones (Georgy et al. 2012). This illustrates the need of a correct treatment of the physics of *single* massive star, that definitely intervenes as well in the modelling of binary evolution.

Acknowledgements

CG and RH acknowledge support from the European Research Council under the European Union's Seventh Framework Programme (FP/2007-2013) / ERC Grant Agreement n. 306901.

References

Bersten, M. C., Benvenuto, O. G., Folatelli, G., et al. 2014, AJ, 148, 68
Böhm-Vitense, E. 1958, ZAp, 46, 108
Chaboyer, B. & Zahn, J. 1992, A&A, 253, 173
Conti, P. S. 1976, Memoires of the Societe Royale des Sciences de Liege, 9, 193
Crowther, P. A. 2007, ARA&A, 45, 177
Dessart, L., Hillier, D. J., Livne, E., et al. 2011, MNRAS, 414, 2985
Eggenberger, P., Meynet, G., Maeder, A., et al. 2008, Ap&SS, 316, 43
Ekström, S., Georgy, C., Eggenberger, P., et al. 2012, A&A, 537, A146
Eldridge, J. J., Fraser, M., Smartt, S. J., Maund, J. R., & Crockett, R. M. 2013, MNRAS, 436, 774
Eldridge, J. J., Izzard, R. G., & Tout, C. A. 2008, MNRAS, 384, 1109
Eldridge, J. J. & Vink, J. S. 2006, A&A, 452, 295
Georgy, C. 2012, A&A, 538, L8
Georgy, C., Ekström, S., Eggenberger, P., et al. 2013, A&A, 558, A103
Georgy, C., Ekström, S., Meynet, G., et al. 2012, A&A, 542, A29
Groh, J. H., Georgy, C., & Ekström, S. 2013a, A&A, 558, L1
Groh, J. H., Meynet, G., & Ekström, S. 2013b, A&A, 550, L7
Groh, J. H., Meynet, G., Ekström, S., & Georgy, C. 2014, A&A, 564, A30
Groh, J. H., Meynet, G., Georgy, C., & Ekström, S. 2013c, A&A, 558, A131
Hainich, R., Rühling, U., Todt, H., et al. 2014, A&A, 565, A27
Heger, A., Fryer, C. L., Woosley, S. E., Langer, N., & Hartmann, D. H. 2003, ApJ, 591, 288
Maeder, A. 1997, A&A, 321, 134
Maeder, A. & Zahn, J.-P. 1998, A&A, 334, 1000
Meynet, G., Chomienne, V., Ekström, S., et al. 2015, A&A, 575, A60
Meynet, G. & Maeder, A. 1997, A&A, 321, 465
Neugent, K. F., Massey, P., & Georgy, C. 2012, ApJ, 759, 11
Sana, H., de Mink, S. E., de Koter, A., et al. 2012, Science, 337, 444
Sander, A., Hamann, W.-R., & Todt, H. 2012, A&A, 540, A144
Vanbeveren, D., De Donder, E., van Bever, J., van Rensbergen, W., & De Loore, C. 1998, New A, 3, 443
Vink, J. S., de Koter, A., & Lamers, H. J. G. L. M. 2001, A&A, 369, 574
Zahn, J.-P. 1992, A&A, 265, 115

Thomas Madura: I was wondering if you could comment on the effect of the LBV phase on your results, e.g., large burst of mass loss.

Cyril Georgy: This could indeed change the results shown here. For example, a massive ejection can help entering the WR phase sooner, or at lower mass. Generally, the numbers I showed are extremely dependent on the various mass-loss rates adopted for the computation, that are sometimes not well known (for example, the RSG or LBV mass-loss rates).

Claus Leitherer: The agreement between observed and predicted WR subtype ratios seems to worsen rather than improve with rotation. Are you concerned about this?

Cyril Georgy: The main point here is that the number of WR in general (not the subtypes) is much better reproduced by rotating than non-rotating models. The results I showed were only for the purpose of presenting what our models are able (or not) to do, knowing that they suffer from a lot of uncertainties (physics of convection/rotation, mass loss, classification into a given type on the basis of surface abundances and not spectrum, and impact of a significant population coming from the binary channel).

Gloria Koenigsberger: Could you comment on the internal velocity structure used for these calculations? How is the Ω-profile chosen?

Cyril Georgy: Our models follow the time evolution of the internal Ω-profile in the framework of the "shellular rotation" (see the contribution by G. Meynet). However, we do not include a strong internal coupling, as it would be for example by considering the effect of an internal Tayler-Spruit dynamo. We have thus differential rotation in the radial direction, producing shear mixing.

The Ω-profile is set to be flat on the zero-age main sequence, and is then evolved self-consistently during the stellar life, under the combined effects of internal transport, and angular momentum removal due to the stellar winds.

Vikram Dwarkadas: Can you use the number of type Ib/c SNe to infer whether rotating or non-rotating stars are more likely to give rise to the Ib/c population. Or at least infer whether single or binary stars are more likely progenitors.

Cyril Georgy: Due to the fact that a significant fraction of these progenitors should come from the binary channel, it is hard to use them to constrain the physics of rotation. The study of the lightcurves, however, can help to infer the mass of the ejecta, and thus, the mass of the progenitor (see the contribution by L. Dessart). As far as I know, current studies indicate that the mass of the ejecta is rather small, favouring binary progenitor.

Wolf-Rayet Stars
W.-R. Hamann, A. Sander, H. Todt, eds.
Potsdam: Univ.-Verlag, 2015
URL: http://nbn-resolving.de/urn:nbn:de:kobv:517-opus4-84268

Properties of LEGUS Clusters Obtained with Different Massive-Star Evolutionary Tracks.

A. Wofford[1], S. Charlot[1] & J. J. Eldridge[2]
[1] *Institut d'Astrophysique de Paris, CNRS, UMR 7095, Sorbonne Universités, UPMC Univ Paris 6, France*
[2] *University of Auckland, New Zealand*

We compute spectral libraries for populations of coeval stars using state-of-the-art massive-star evolutionary tracks that account for different astrophysics including rotation and close-binarity. Our synthetic spectra account for stellar and nebular contributions. We use our models to obtain $E(B-V)$, age, and mass for six clusters in spiral galaxy NGC 1566, which have ages of < 50 Myr and masses of $> 5\times10^4\ M_\odot$ according to standard models. NGC 1566 was observed from the NUV to the I-band as part of the imaging Treasury *HST* program LEGUS: Legacy Extragalactic UV Survey. We aim to establish i) if the models provide reasonable fits to the data, ii) how well the models and photometry are able to constrain the cluster properties, and iii) how different the properties obtained with different models are.

1 Introduction

Determining extinction-corrected ages and masses for large samples of individual young massive clusters (YMCs) in a wide range of galaxy environments is essential for investigating cluster formation and evolution, characterizing the star-cluster age and mass functions of galaxies, and studying the star formation histories of galaxies (Calzetti et al. 2015). The task of observing large samples of clusters in galaxies with a wide range of properties was recently completed by *HST*'s LEGUS program (PID 13364; Calzetti et al. 2015), which consists of high spatial resolution ($\sim$ 0.07") images of portions of 50 nearby ($\leq$ 13 Mpc) galaxies taken with the UVIS channel of the Wide Field Camera Three (WFC3) in broad band filters F275W (2704 Å), F336W (3355 Å), F438W (4325 Å), F555W (5308 Å), and F814W (8024 Å). The survey includes galaxies of different morphological types and spans factors of $\sim 10^3$ in both SFR and sSFR, $\sim 10^4$ in stellar mass ($\sim 10^7 - 10^{11}\ M_\odot$), and $\sim 10^2$ in oxygen abundance (12+log(O/H)=7.2-9.2).

At the distances of LEGUS galaxies ($3-13$ Mpc), the cores of YMCs are unresolved. In such cases, a standard technique for deriving cluster properties is the comparison of observed and computed broad-band fluxes. With regards to populations of massive stars, at fixed star formation history and initial mass function (IMF), uncertainties in synthetic spectral energy distributions (SEDs) are arguably dominated by uncertainties in massive-star evolutionary tracks (Leitherer et al. 2014). In recent years, independent groups in Padova, Geneva, and Auckland, working on massive star evolution have attempted to reproduce three key observational constraints. First, the blue loops that are observed in the color-magnitude diagrams of nearby metal-poor dwarf irregular star-forming galaxies. Second, nitrogen enhancements are observed on the surfaces of main sequence stars of typically $15\ M_\odot$ (Hunter et al. 2009). Finally, it is now well established that massive stars are in binary systems with close to 70% of them interacting over the course of their evolution (Langer 2012; Sana et al. 2012; Sana et al. 2013). Processes that occur during the evolution of binaries include envelope stripping from the binary, accretion of mass by the secondary, or even complete mergers (de Mink et al. 2014). In this contribution we aim to motivate the importance of pinning down massive star evolution of which Wolf-Rayet stars are an important component.

2 Sample & Observations

We select six YMCs in galaxy NGC 1566 with ages of ≤ 50 Myr, which ensures the presence of massive stars; masses of $\geq 5\times10^4$ $M_\odot$, which mitigates the effect of the stochastic sampling of the stellar initial mass function (IMF, Cerviño & Luridiana 2004); and metallicity close to solar ($Z = 0.014$, Asplund et al. 2009), for which tracks from Padova, Geneva, and Auckland are available. Figure 1 shows the LEGUS NUV image of the galaxy and locations of clusters. We avoid the AGN at the center. We use labels from the LEGUS catalogue. The pixel scale of WFC3/UVIS is 0.039 arcsec/pixel. Photometry is performed with a circular aperture of 4 pixels in radius, with the background measured within an annulus of 7 pixels in inner radius and 1 pixel in width (for more details see Adamo et al., in prep.).

3 Models & Method

We obtain the color excess $E(B-V)$, mass $M_{\rm cl}$, and age t of individual YMCs by comparing observed and synthetic photometry in the five LEGUS bands. For the stellar component, we use instantaneous star formation, an initial stellar mass of $M_{\rm cl} = 10^6\ M_\odot$, and a Kroupa (2001) IMF in the

range $0.1-100\,M_{\odot}$. We test the most recent Padova tracks for single non-rotating stars (Bressan et al. 2012, Chen et al. 2014b in prep.), Geneva tracks for single non-rotating and single rotating stars (Ekström et al. 2012), and Auckland tracks for single non-rotating stars and interacting binary stars (Eldridge et al. in prep.). The rotating Geneva tracks are at 40% of the break-up velocity on the zero-age main sequence. None of these tracks that are mentioned so far include pre-main-sequence stars, and this should be taken as a limitation to our approach. The tracks from different cities are implemented in different spectral synthesis codes which are `Galaxev` (Bruzual & Charlot 2003; Charlot & Bruzual in prep.), `Starburst99` (Leitherer et al. 1999; Leitherer et al. 2014), and `BPASS` (Eldridge et al. in prep.), respectively. Hereafter we refer to models that use these tracks as Pn, Gn, Gr, An, and Ab, respectively. In addition to the evolution tracks, a main ingredient of spectral population synthesis are the spectra of the individual stars, which in our case are theoretical. Given that we use low-resolution spectra in order to compute broad-band fluxes, we do not expect differences in atmospheres to significantly affect our results. For Wolf-Rayet stars, all models use the PoWR models (Gräfener et al. 2002; Hamann & Gräfener 2003; Hamann & Gräfener 2004). For the nebular component we use version 13.03 of photoionization code `Cloudy` and parameters as in Zackrisson et al. (2011). We attenuate the model SEDs using the Milky Way extinction curve of Mathis (1990), a foreground dust geometry, and equal attenuation of the nebular gas and stellar continuum. The range of $E(B-V)$ values is from 0 to 3, in steps of 0.01 mag, while it is 6 to 9 in steps of 0.1 for $\log(t/\mathrm{yr})$. Thus, for a given metallicity (Z), IMF, and set of tracks, the number of models is 9331. We use Bayesian inference to derive the cluster properties. The cluster mass is a normalization constant between the observation and model. For each cluster property, i.e., $E(B-V)$, $M_{\rm cl}$, and t we record two values, the best-fit or minimum χ^2 value, and the median of the marginal probability distribution function. We use flat priors in $E(B-V)$, $\log(M_{\rm cl})$, and $\log(t)$. Our errors around the median correspond to the 16th and 84th percentiles.

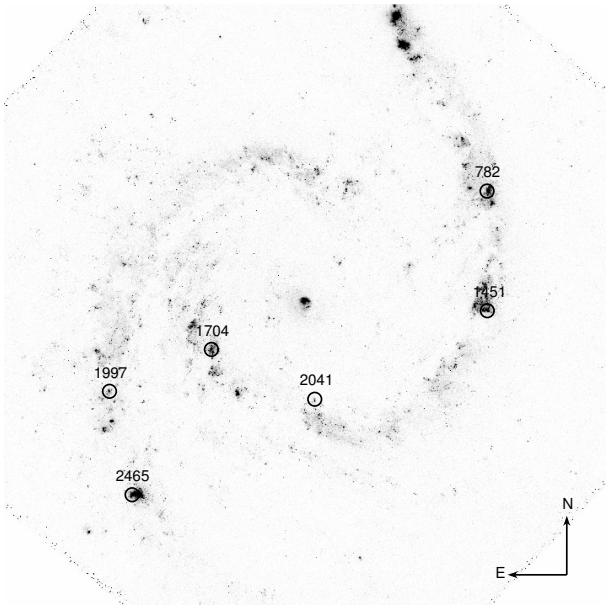

Fig. 1: F275W LEGUS image of NGC 1566. We mark the locations of clusters with circles of radius 1.6" or ∼100 pc. Photometry was extracted from circles of radius 10 times smaller. North is up and east is to the left.

4 Summary of Results

i) How well do the models fit the data? 5/6 clusters show very similar spectral shapes, except for the most reddened one. We find that for all clusters, best-fit models based on any of the tracks are able to fit the observations within the observational error bar in at least 3/5 of bands. Thus, overall the models are successful in fitting the LEGUS data. In addition, surprisingly, there is a slight preference for the Ab (binary models), which present the most degrees of freedom.

ii) How well do the models constrain the cluster properties given the data? Overall, the marginal PDFs of $E(B-V)$ are single peaked and this is the best constrained quantity. A few exceptions are the PDFs of clusters 1997 and 2041 derived from Gn or Gr models, which present multiple peaks. For the masses and ages, the marginal PDFs present multiple peaks more frequently, but there are cases were these properties are well constrained.

iii) How different are the properties obtained with the different models? Based on medians of the PDFs, the ranges of $E(B-V)$, $M_{\rm cl}$, and t found for the six clusters follow: $E(B-V) = 0.02-0.63$ mag, $M_{\rm cl}/10^4\,M_{\odot} = 1.9-11.0$, and $t/\mathrm{Myr} = 2-5$. For comparison, the ranges of properties derived from older standard models used to select the clusters are: $E(B-V) = 0.0-0.76$ mag, $M_{\rm cl}/10^4\,M_{\odot} = 5.9-14.2$, and $t/\mathrm{Myr} = 1-15$. Figures 2 to 4 show comparisons between the median values of $E(B-V)$, $M_{\rm cl}$, and t derived with the different models. Since there is a slight preference for the Ab models, we plot the Ab models on the x-axis. For $E(B-V)$, all models agree on which is the most reddened cluster. In addition, in general, models are in agreement with each other within the model error-bars. We note that Gr models are systematically offset relative to the Ab models, and yield larger values of $E(B-V)$. For $M_{\rm cl}$, all models agree on which are the least and most massive clusters, but the models are in general disagreement on the absolute value of the cluster mass within the model error bars. In addition, the

Ab models result in lower masses relative to the rest of models except the Gr models. Finally, for age, all models agree on which are the youngest (2041) and oldest (1704). The youngest is also the most reddened, which makes sense if the cluster is still partially enshrouded in its natal cloud. Wether the models agree on the ages within the model error bars depends on the cluster and pair of models. The Gr models clearly yield the oldest ages.

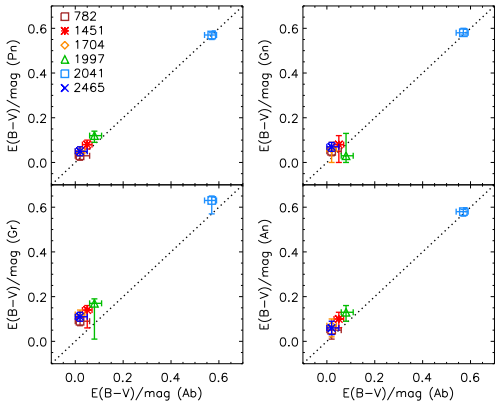

Fig. 2: Comparison of median $E(B-V)$ values obtained with models that use different massive-star evolutionary tracks. The different symbols represent the different clusters, as indicated in the legend. On the x-axis, we always plot results based on the Ab models. On the y-axis, we plot results based on the Pn, Gn, Gr, or An models, depending on the panel.

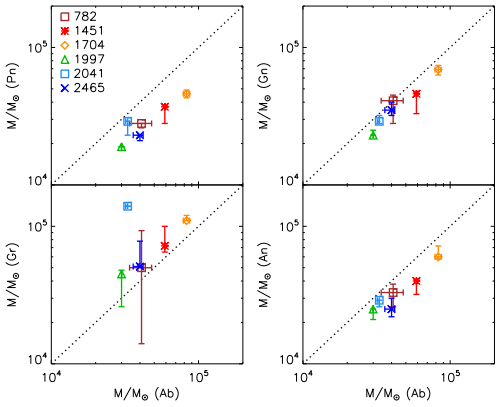

Fig. 3: Similar to Figure 2 but for the mass of clusters.

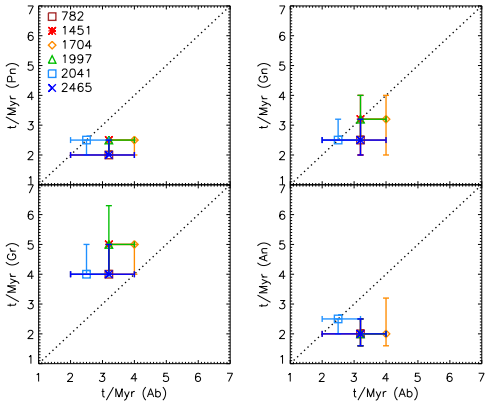

Fig. 4: Similar to Figure 2 but for the age of clusters.

A. Wofford acknowledges support from the ERC via an Advanced Grant under grant agreement no. 321323-NEOGAL.

References

Asplund, M., Grevesse, N., Sauval, A. J., & Scott, P. 2009, ARA&A, 47, 481
Bressan, A., Marigo, P., Girardi, L., et al. 2012, MNRAS, 427, 127
Bruzual, G. & Charlot, S. 2003, MNRAS, 344, 1000
Calzetti, D., Lee, J. C., Sabbi, E., et al. 2015, AJ, 149, 51
Cerviño, M. & Luridiana, V. 2004, A&A, 413, 145
de Mink, S. E., Sana, H., Langer, N., Izzard, R. G., & Schneider, F. R. N. 2014, ApJ, 782, 7
Ekström, S., Georgy, C., Eggenberger, P., et al. 2012, A&A, 537, A146
Gräfener, G., Koesterke, L., & Hamann, W.-R. 2002, A&A, 387, 244
Hamann, W.-R. & Gräfener, G. 2003, A&A, 410, 993
Hamann, W.-R. & Gräfener, G. 2004, A&A, 427, 697
Hunter, I., Brott, I., Langer, N., et al. 2009, A&A, 496, 841
Langer, N. 2012, ARA&A, 50, 107
Leitherer, C., Ekström, S., Meynet, G., et al. 2014, ApJS, 212, 14
Leitherer, C., Schaerer, D., Goldader, J. D., et al. 1999, ApJS, 123, 3
Mathis, J. S. 1990, ARA&A, 28, 37
Sana, H., de Koter, A., de Mink, S. E., et al. 2013, A&A, 550, A107
Sana, H., de Mink, S. E., de Koter, A., et al. 2012, Science, 337, 444
Zackrisson, E., Rydberg, C.-E., Schaerer, D., Östlin, G., & Tuli, M. 2011, ApJ, 740, 13

Dominik Bomans: Did I understand correctly, that the oldest and most massive cluster is the most reddened? Would one not expect that massive older clusters would clear out of dust?

Adia Wofford: The oldest and most massive is not the most reddened one.

Kimberly Sokal: Why did you choose an upper mass cutoff of $100\,M_{\odot}$? Isn't that rather low for these clusters?

Adia Wofford: The choice of the upper mass limit was driven by the fact that the standard models used by the LEGUS collaboration use an upper mass limit of $100\,M_{\odot}$. For easier comparison with these models, we also adopted $100\,M_{\odot}$ for the rest of the models.

Dorottya Szécsi: How do you know that the difference of your output (the factor 2 and 3) is attributed to the difference between the stellar evolutionary models and not to that between the stellar atmosphere models?

Adia Wofford: We use low resolution spectra to compute the magnitutes in LEGUS filters. In addition, the LEGUS filters are broad-band filters. Differences in the ionizing fluxes predicted by different massive star evolutionary tracks have a bigger effect on the predicted magnitutes.

Aida Wofford (r.) after her talk, passing the microphone to Jose Groh (l.)

Wolf-Rayet Stars
W.-R. Hamann, A. Sander, H. Todt, eds.
Potsdam: Univ.-Verlag, 2015
URL: http://nbn-resolving.de/urn:nbn:de:kobv:517-opus4-84268

The end stages of massive star evolution: WR stars as SN Ibc progenitors

J. H. Groh[1]
[1] *Geneva Observatory, Geneva University, Versoix, Switzerland*

The morphological appearance of massive stars across their post-Main Sequence evolution and before the SN event is very uncertain, both from a theoretical and observational perspective. We recently developed coupled stellar evolution and atmospheric modeling of stars done with the Geneva and CMFGEN codes, for initial masses between 9 and 120 $M_{\odot}$. We are able to predict the observables such as the high-resolution spectrum and broadband photometry. Here I discuss how the spectrum of a massive star changes across its evolution and before death, with focus on the WR stage. Our models indicate that single stars with initial masses larger than 30 $M_{\odot}$ end their lives as WR stars. Depending on rotation, the spectrum of the star can either be that of a WN or WO subtype at the pre-SN stage. Our models allow, for the first time, direct comparison between predictions from stellar evolution models and observations of SN progenitors.

1 The need for combined stellar evolution and atmospheric modeling

Massive stars are essential constituents of stellar populations and galaxies in the near and far Universe. They are among the most important sources of ionizing photons, energy, and some chemical species, which are ejected into the interstellar medium through powerful stellar winds and during their extraordinary deaths as supernovae (SN) and long gamma-ray bursts (GRB). For these reasons, massive stars are often depicted as cosmic engines, because they are directly or indirectly related to most of the major areas of astrophysical research.

Despite their importance, our current understanding of massive stars is still limited. This inconvenient shortcoming can be explained by many reasons, such as uncertainties related to mass loss, rotation, binary interaction, and how to compare observations and models of massive stars. Here we focus on this last topic.

Our understanding of different classes of stars is often built by comparing evolutionary models and observations. However, mass loss may affect the spectra, magnitudes, and colors of massive stars, thus making the comparison between evolutionary models and observations a challenge. In addition to luminosity, effective temperature, and surface gravity, the observables of massive stars can be strongly influenced by a radiatively driven stellar wind that is characteristic of these stars. The effects of mass loss on the observables depend on the initial mass and metallicity, since they are in general more noticeable in MS stars with large initial masses, during the post-MS phase, and at high metallicities. When the wind density is significant, such as in Wolf-Rayet (WR) stars, the mass-loss rate, wind clumping, wind terminal velocity, and velocity law have a strong impact on the spectral morphology. This makes the analysis of massive stars a difficult task, and obtaining their fundamental parameters, such as luminosity and effective temperature, is subject to the uncertainties that comes from our limited understanding of mass loss and clumping. Furthermore, the definition of effective temperature of massive stars with dense winds is problematic and, while referring to an optical depth surface, it does not relate to a hydrostatic surface. This is caused by the atmosphere becoming extended, with the extension being larger the stronger the wind is. Stellar evolution models are able to predict the stellar parameters only up to the stellar hydrostatic surface, which is not directly reached by the observations of massive stars when a dense stellar wind is present. Since current evolutionary models do not thoroughly simulate the physical mechanisms happening at the atmosphere and wind, model predictions of the evolution of massive stars are difficult to be directly compared to observed quantities, such as a spectrum or a photometric measurement.

To improve the comparison between models and observations of massive stars, we recently devised coupled calculations of stellar evolution with the Geneva code and atmospheric and wind modeling with the CMFGEN code. This approach opens up the possibility to investigate stellar evolution based not only on interior properties, but also from a spectroscopic point of view. Essentially, the atmospheric models allow the physical quantities predicted by the stellar evolution model to be directly compared to observed features.

2 Predicting the look of stars at the pre-SN stage

Our group recently analyzed the properties of massive stars just before the SN explosion in a series of papers (Groh et al. 2013b,c,a, 2014; Groh 2014). Our models indicate that rotating stars with initial mass

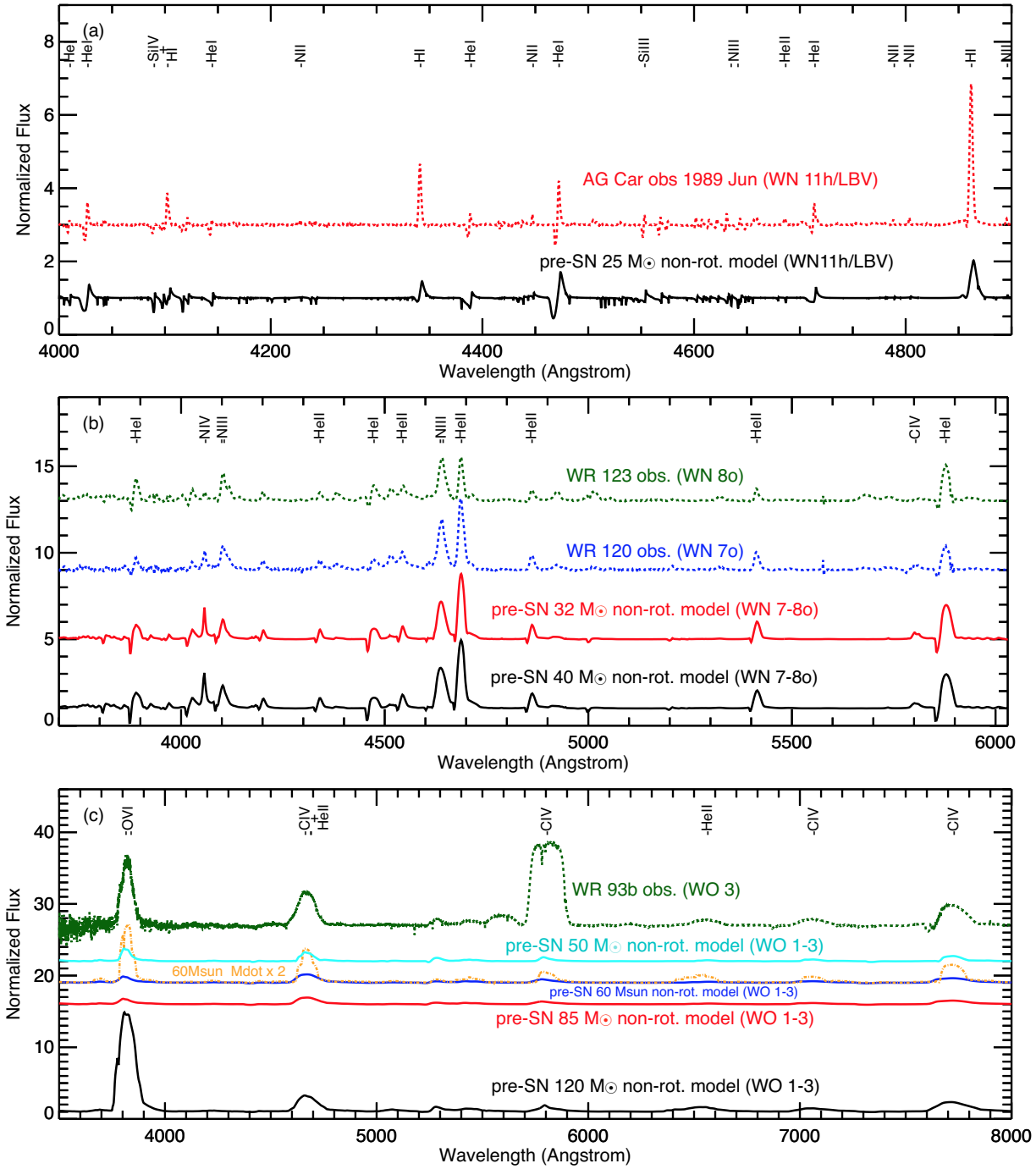

Fig. 1: Montage of the synthetic optical spectra of massive stars at the pre-SN stage from non-rotating stellar evolution models. Observations of stars with similar spectral type (dashed) are shown to support the spectroscopic classifications. The strongest spectral features are indicated. The spectra have been offset in flux for better visualization. *(a)*: The 25 $M_{\odot}$ model (black), which has a WN11h/LBV spectral type. The 1989 June observations of the LBV AG Car (red) are also shown, when it showed a WN11h spectral type Smith et al. (1994); Stahl et al. (2001); Groh et al. (2009). *(b)*: The 32 $M_{\odot}$ (red) and 40 $M_{\odot}$ (black) models, which have spectral type WN7–8o, are compared to observations of Galactic WN7o (WR120) and WN8o (WR123) stars, form the catalogue of Hamann et al. (1995). *(c)*: The 50 $M_{\odot}$ (cyan), 60 $M_{\odot}$ (blue), 85 $M_{\odot}$ (red), and 120 $M_{\odot}$ (black) models, which have WO1–3 spectral type. The spectrum of the 60 $M_{\odot}$ model with the mass-loss rate enhanced by a factor of two at the pre-SN stage is shown (orange dot-dashed). The optical spectrum of the Galactic WO 3 star WR 93b (green, from Drew et al. 2004) is also displayed.

($M_{\rm ini}$) in the range 20–25 $M_\odot$ surprisingly end their lives as luminous blue variable (LBV) stars. The fate of single massive stars with $M_{\rm ini} = 9 - 120$ $M_\odot$ was investigated in Groh et al. (2013c), where we showed that massive stars, depending on their initial mass and rotation, can explode as red supergiants (RSG), yellow hypergiants (YHG), LBVs, and Wolf-Rayet (WR) stars of the WN and WO subtype. We applied these models to investigate the nature of the candidate progenitor of the SN Ib iPTF13bvn, concluding that a single WR star with initial mass $\sim 31-35$ $M_\odot$ could explain the properties of the progenitor (Groh et al. 2013a). Figure 1 presents a subset of synthetic spectra of massive stars at the pre-SN stage for non-rotating models.

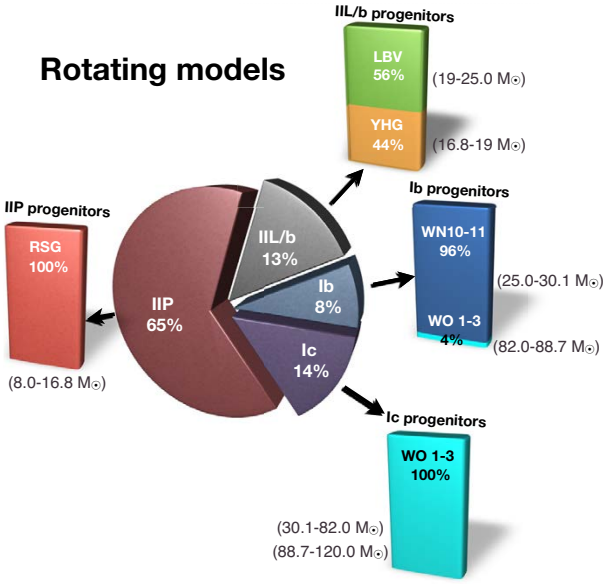

Fig. 2: Diagram illustrating, for different core-collapse SN types, their relative rates and the types of progenitors and their respective frequencies. Initial mass ranges (indicated in parenthesis) and SN types are based on the criteria outlined in Georgy et al. (2012), assuming that the minimum amount of He in the ejecta to produce a SN Ib is 0.6 $M_\odot$. We show here the predictions for non-rotating models.

Figure 2 shows the different channels that link the spectral types of SN progenitors to the core-collapse SN types according to our models. For rotating models, we obtained the following types of SN progenitors: WO1–3 ($M_{\rm ini} \geq 32$ $M_\odot$), WN10–11 ($25 < M_{\rm ini} < 32 M_\odot$), LBV ($20 \leq M_{\rm ini} \leq 25$ $M_\odot$), G1 Ia$^+$ ($18 < M_{\rm ini} < 20$ $M_\odot$), and RSGs ($9 \leq M_{\rm ini} \leq 18$ $M_\odot$). For non-rotating models, we found spectral types WO1–3 ($M_{\rm ini} > 40$ $M_\odot$), WN7–8 ($25 < M_{\rm ini} \leq 40$ $M_\odot$), WN11h/LBV ($20 < M_{\rm ini} \leq 25 M_\odot$), and RSGs ($9 \leq M_{\rm ini} \leq 20$ $M_\odot$). Our rotating models indicate that SN IIP progenitors are all RSG, SN IIL/b progenitors are 56% LBVs and 44% YHGs, SN Ib progenitors are 96% WN10-11 and 4% WOs, and SN Ic progenitors are all WO stars. We find that not necessarily the most massive and luminous SN progenitors are the brighter ones in a given filter, since this depends on their luminosity, temperature, wind density, and how the spectral energy distribution compares to a filter bandpass. We find that SN IIP progenitors (RSGs) are bright in the $RIJHK_S$ filters and faint in the UB filters. SN IIL/b progenitors (LBVs and YHGs), and SN Ib progenitors (WNs) are relatively bright in optical/infrared filters, while SN Ic progenitors (WOs) are faint in all optical filters.

To conclude, our analyses showed that it is crucial to produce an output spectrum out of evolutionary calculations to properly interpret the observations of massive stars at different evolutionary stages, in particular those with dense winds such as WR stars.

References

Drew, J. E., Barlow, M. J., Unruh, Y. C., et al. 2004, MNRAS, 351, 206
Georgy, C., Ekström, S., Meynet, G., et al. 2012, A&A, 542, A29
Groh, J. H. 2014, A&A, 572, L11
Groh, J. H., Georgy, C., & Ekström, S. 2013a, A&A, 558, L1
Groh, J. H., Hillier, D. J., Damineli, A., et al. 2009, ApJ, 698, 1698
Groh, J. H., Meynet, G., & Ekström, S. 2013b, A&A, 550, L7
Groh, J. H., Meynet, G., Ekström, S., & Georgy, C. 2014, A&A, 564, A30
Groh, J. H., Meynet, G., Georgy, C., & Ekström, S. 2013c, A&A, 558, A131
Hamann, W.-R., Koesterke, L., & Wessolowski, U. 1995, A&AS, 113, 459
Smith, L. J., Crowther, P. A., & Prinja, R. K. 1994, A&A, 281, 833
Stahl, O., Jankovics, I., Kovács, J., et al. 2001, A&A, 375, 54

Vikram Dwarkadas: There is considerable observational evidence that RSG stars above $9\,M_\odot$ do not give rise to II-P SNe. You manage to fit that in your latest models. What has changed? What happens to RSG stars $> 19\,M_\odot$? What SNe do they rise to, and does it agree with the SN rate?

Jose Groh: The main change is the increased $\dot{M}$ for the most luminous RSGs due to being close to the Eddington limit. These stars evolve back to the blue and potentially explode as type IIb or IIn (or II-L even). We still have to look at the SN rates predicted by models.

Francisco (Paco) Najarro: 1) Apart from the lack of WOs there was also a lack of WNLs. Are they coming from a different channel?
2) Is your $T_{\rm eff}$ measure at $\tau = 20$ or $\tau = 2/3$?

Jose Groh: 1) We think they come from less massive stars in the $\sim$ 28–45 $M_\odot$ range. 2) The ones I showed are quoting $T_{\rm eff}$ at 2/3, which I think is more appropriate for comparing observations and models. Using T_* is very dangerous since the non wind-corrected $T_{\rm eff}$ quoted by the models have little to do with T_* derived from spectroscopic analyses.

Jose Groh (with microphone) asking a question. Also visible in this picture are F. Najarro (left, sitting), M. Corcoran (standing behind Jose), and A. Liermann (right, standing).

Wolf-Rayet Stars
W.-R. Hamann, A. Sander, H. Todt, eds.
Potsdam: Univ.-Verlag, 2015
URL: http://nbn-resolving.de/urn:nbn:de:kobv:517-opus4-84268

The stellar Eddington limit

N. Langer, D. Sanyal, L. Grassitelli, D. Szécsi
Universität Bonn, Germany

It is often assumed that when stars reach their Eddington limit, strong outflows are initiated, and that this happens only for extreme stellar masses. We discuss here that in models of up to $500\,M_\odot$, the Eddington limit is never reached at the stellar surface. Instead, we argue that the Eddington limit is reached inside the stellar envelope in hydrogen-rich stars above $\sim 30\,M_\odot$ and in Wolf-Rayet stars above $\sim 7\,M_\odot$, with drastic effects for their struture and stability.

1 Introduction

Massive stars are powerful engines and strongly affect the evolution of star forming galaxies throughout cosmic time (Langer 2012, Szécsi et al. 2015). In particular the most massive ones produce copious amounts of ionising photons (Doran et al., 2013), emit powerful stellar winds (Kudritzki & Puls, 2000, Smith 2014) and are thought to produce the most energetic and spectacular stellar explosions, as pair-instability supernovae (Kozyreva et al., 2014), superluminous supernovae (Gal-Yam et al. 2009), and long-duration gamma-ray bursts (Larsson et al., 2007, Raskin et al., 2008).

2 The Eddington limit in main sequence stars

The most massive stars are close to the so called Eddington limit. The Eddington luminosity is traditionally considered as the maximum luminosity which a star may have to avoid that the radiative acceleration at its surface exceeds gravity, when considering only electron scattering as opacity source (Eddington 1926):

$$L_{\rm e} = 4\pi cGM/\kappa_{\rm e}. \qquad (1)$$

Massive main sequence stars, which we understand here as those which undergo core hydrogen burning, have a much higher luminosity than the Sun, as they are known to obey a simple mass-luminosity relation, $L \sim M^\alpha$, with $\alpha > 1$. However, whereas this relation is very steep for low mass stars ($\alpha \simeq 5$), it is shown in Kippenhahn & Weigert (1990) that $\alpha \to 1$ for $M \to \infty$, and Köhler et al. (2015) find $\alpha \simeq 1.1$ for $M = 500\,M_\odot$. In fact, Kato (1986) showed that zero-age main sequence models computed only with the electron scattering opacity do reach the Eddington limit at a mass of about $\sim 10^5\,M_\odot$. Whereas it is debated in the literature whether real main sequence stars do reach the Eddington-limit (Langer 1998, Crowther et al. 2010, Maeder et al. 2012, Langer & Kudritzki 2014, Bestenlehner et al., 2014), we argue below that this is indeed the case.

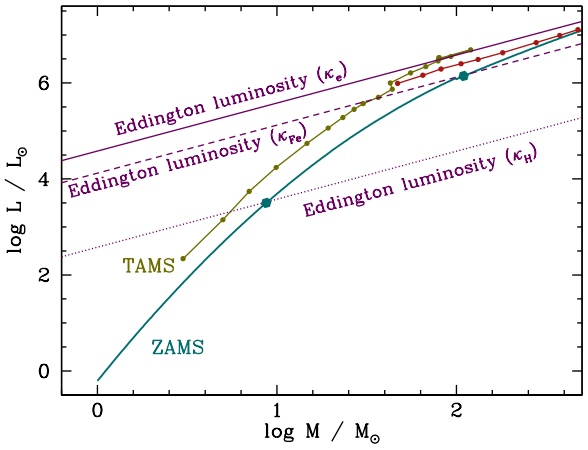

Fig. 1: The stellar Eddington limit (cf., Eqs. 1 and 2) in the mass-luminosity plane, assuming three different dominant opacity sources. The first one, referring to the electron scattering opacity κ_e (full-drawn straight line), is valid for a Solar hydrogen and helium mass fraction and assuming complete ionisation, such that $\kappa_{\rm e} \simeq 0.34\,{\rm cm^2\,g^{-1}}$. The second one (dashed straight line) refers to a Rosseland mean opacity dominated by iron, assumed here as $\kappa_{\rm Fe} \simeq 1\,{\rm cm^2\,g^{-1}}$. The third one (dotted straight line) refers to the Rosseland mean opacity in the hydrogen recombination zone and is assumed here as $\kappa_{\rm H} \simeq 100\,{\rm cm^2\,g^{-1}}$ (see text). The curved blue line gives the location of zero-age main sequence stellar models, with dots marking the crossing of the H- and Fe-Eddington limit. The brown line marks the terminal-age main sequence (TAMS) location of the models of Brott et al. (2011) and Köhler et al. (2015) for LMC composition rotating initially with $\sim 100\,{\rm km/s}$, and the red line marks those models at which a surface helium enrichment is starting to occur.

Figure 1 illustrates the situation in the mass-luminosity plane. The zero age main sequence (ZAMS) bends such that the electron-scattering Eddington limit is only met far outside the figure. I.e., real massive stars never encounter this limit. However, the true opacity can be substantially larger than the electron scattering opacity. We thus follow Sanyal et al. (2015; SGLB15) and define a local

Eddington luminosity anywhere inside the star as

$$L_{\rm Edd}(r) = 4\pi cGM(r)/\kappa(r), \qquad (2)$$

where r is the radial coordinate and $\kappa(r)$ now represents the local Rosseland mean opacity. We consider $L_{\rm Edd}$ locally inside the star, since SGLB15 showed that, again, the condition $L = L_{\rm Edd}$ according to Eq. (2) is not met by any stellar model of Köhler et al. (2015) at the stellar surface. This implies that, based on these models, we do not expect stars of up to $500\,{\rm M}_\odot$ to drive a super-Eddington wind.

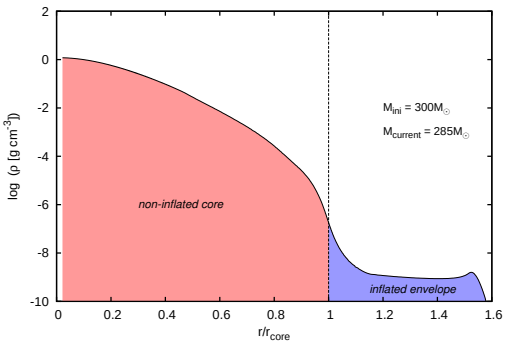

Fig. 2: Density profile of a non-rotating $285\,{\rm M}_\odot$ star with $T_{\rm eff} = 46600\,{\rm K}$ and $\log(L/L_\odot) = 6.8$, showing an inflated envelope and a density inversion. The X-axis has been normalised by the core radius $r_{\rm core}$ of $25.3\,{\rm R}_\odot$.

However, when assuming that even in hot stars, the Rosseland mean opacity may become as large as $1\,{\rm cm}^2\,{\rm g}^{-1}$ due to the iron opacity peak (cf., fig. 9 in SGLB15), the Eddington luminosity according to Eq. (2) is about a factor of three smaller than that according to Eq. (1). Correspondingly, the ZAMS line crosses it at about $M = 100\,{\rm M}_\odot$ (upper blue dot in Fig. 1). When looking at the luminosity increase during core hydrogen burning by including the terminal age main sequence (TAMS) in Fig. 1, we see that even core hydrogen burning stars with $M = 30\,{\rm M}_\odot$ may violate the local Eddington limit in their envelopes. The iron opacity peak is metallicity and density dependent, such that the corresponding Eddington limit is only approximate. However, we show below that the expectation derived from Fig. 1 is actually met by detailed stellar models.

The largest opacities are found in the hydrogen recombination zones of cool stars. Thus, for illustration, we plot a third Eddington limit in Fig. 1, which is again approximate, by assuming $\kappa_{\rm H} = 100\,{\rm cm}^2\,{\rm g}^{-1}$, which then we expect to be violated by cool giants with $M \gtrsim 5\,{\rm M}_\odot$.

SGLB15 demonstrated that when the local radiative luminosity in the stellar envelope exceeds the Eddington luminosity as defined by Eq. (2), the envelope inflates, as shown for an example in Fig. 2. As the iron opacity decreases for lower densities, inflation leads to an increase of the Eddington luminosity and generally stops for the hot models when the Eddington limit is not violated any more. Figure 3 shows that, for LMC metallicity, inflation occurs for $\log L/{\rm L}_\odot \gtrsim 5.5$, and exceeds a factor of 2 for models which are located to the right of the hot edge of the S Doradus instability strip (see also Gräfener et al. 2012).

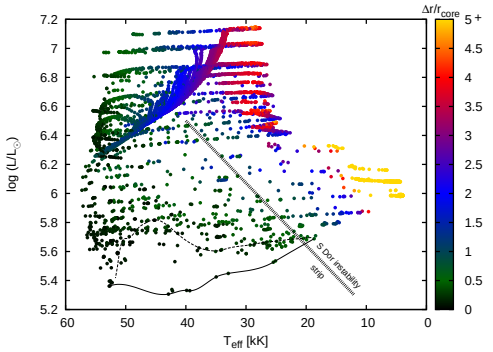

Fig. 3: Hertzsprung-Russell diagram showing core-hydrogen burning inflated models from the LMC grid of Köhler et al. (2015). The color indicates the degree of inflation as defined through $\Delta r/r_{\rm core}$, where r is the stellar radius, $r_{\rm core}$ would be the stellar radius if inflation was absent, and $\Delta r = r - r_{\rm core}$ (cf., Fig. 2). Dots corresponding to models with $\Delta r/r_{\rm core} > 5$ are colored in yellow. Below the solid black line, no inflated models are found, and above the dotted black all models were found to be inflated. The hot part of the S Dor instability strip (Smith et al., 2004) is also marked. Cf., SGLB15.

Since the inflated envelopes are convectively unstable (Langer 1997), and the convectively transported fraction of the stellar luminosity does not contribute to the inflation, the extent of inflation depends on the assumed convection theory. The shown results are obtained with the standard Mixing Length Theory (cf. SGLB15).

Observational evidence for inflation in Galactic main sequence stars, as predicted by the extremely extended main sequence band for $5.5 \lesssim \log L/{\rm L}_\odot \lesssim 6.5$ of the Köhler et al. (2015) models, is found in fig. 5 of Clark et al. (2014) and fig. 1 of Castro et al. (2015). These figures show an abundance of B supergiants which is unexpected if they would have to be explained by core helium burning stars. The inflated envelopes are also likely to be pulsationally unstable (cf. Grassitelli et al., this volume), which may lead to observable consequences.

Inflated stars may be found well below the quoted Eddington luminosities for various reasons. E.g., stars which lost a significant amount of their hydrogen-rich envelope to a wind or to a close binary companion will, to first order, keep their luminosity, but since their mass is reduced their Eddington luminosity will be reduced. Similarly, rotation may reduce the Eddington luminosity (Langer 1997, 1998), even though its effect is latitude dependent and vanishes at the poles. SGLB15 suggested that latitude dependent inflation may give rise to the B[e] phenomenon in supergiants (Zickgraf et al. 1985).

3 The Eddington limit in Wolf-Rayet stars

So far, the effect of envelope inflation has been discussed most extensively for Wolf-Rayet stars (Ishii et al. 1999, Petrovic et al. 2006, Gräfener et al. 2012). Figure 4 demonstrates the situation in the HR diagram on the basis of zero-age helium star models. Using standard Rosseland mean opacities, we find inflation to occur for models above $\sim 7\,M_\odot$ at solar metallicity (Grassitelli et al., this volume), and above $\sim 12\,M_\odot$ for the SMC metallicity.

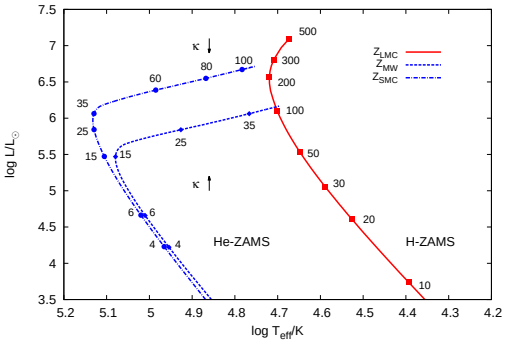

Fig. 4: Zero-age main sequence of the models of Köhler et al. (2015) for LMC metallicity (full drawn red line) together with lines for zero-age main sequence helium star models for Galactic (blue, dashed line) and SMC (blue, dash-dotted line) metallicity. Labelled dots represent masses in units of the Solar mass. The labels "$\kappa \downarrow$" and "$\kappa \uparrow$" indicate the vertical shift in the kink of the He-ZAMS lines if the opacity in the inflated stars would decrease (the Eddington luminosity would move up) or increase (the Eddington-limit would move down), respectively.

It has been suggested that the opacity in the inflated layer may come down because of porosity effects (Owocki et al. 2004), which would lead to an increase of the Eddington-luminosity and to an occurrence of the kink in the He-ZAMS at higher luminosity. An increase of the opacity has been suggested, on the other hand, by Gräfener et al. (2012), as this might lead to a better agreement of the surface temperatures of Wolf-Rayet stars with the observations. We conclude that the main parameters of the Wolf-Rayet stars are strongly affected by their proximity to the Eddington limit.

References

Bestenlehner J M, Gräfener G, Vink J S, et al., 2004, A&A, 570, A38

Brott I, de Mink S E, Cantiello M, et al., 2011, A&A, 530, A115

Crowther P A, Schnurr O., Hirschi R., et al. 2010, MNRAS, 408, 731

Doran E.I., Crowther P.A., de Koter, A., et al., 2013, A&A, 558, A134

Eddington A.S., 1926, The Internal Constitution of Stars

Gal-Yam A, Mazzali P, Ofek E O, et al., 2009, Nature, 462, 624

Gräfener G, Owocki, S P, Vink, J S 2012, A&A, 538, A40

Ishii M, Ueno M, Kato M, 1999, PASJ, 51, 417

Kato M, 1986, Ap&SS, 119, 57

Kippenhahn R., Weigert A., 1990, Stellar Structure and Evolution (Springer, Berlin)

Köhler K., Langer N., de Koter A., et al., 2015, A&A,

Kozyreva A, Blinnikov S, Langer N, Yoon S-C, 2014, A&A, 566, A146

Kudritzki R.-P., Puls, J, 2000, ARA&A, 38, 613

Langer N, 1997, in ASP Conf. Ser. Vol. 120, p. 83

Langer N, 1998, A&A, 329, 551

Langer N, 2012, ARA&A, 50, 107

Langer N., Kudritzki R P, 2014, A&A, 564, A52

Larsson J, Levan A J, Davies M B, Fruchter A S, 2007, MNRAS, 376, 1285

Maeder A, Georgy C, Meynet G, Ekström, S. 2012, A&A, 539, A110

Owocki S P, Gayley K G, Shaviv N J, 2004, ApJ, 616, 525

Petrovic J, Pols O, Langer N. 2006, A&A, 450, 219

Raskin C, Scannapieco E, Rhoads J, Della Valle M, 2008, ApJ, 689, 358

Sanyal D., Grassitelli L., Langer N., Bestenlehner J.M., 2015, A&A, 580, A20

Smith N, 2014, ARA&A, 52, 487

Smith N, Vink J S, de Koter A. 2004, ApJ, 615, 475

Szécsi D., Langer N., Yoon, S.-C., et al., 2015, A&A, 581, A15

Zickgraf F-J, Wolf B., Stahl O., et al., 1985, A&A, 143, 421

Dany Vanbeveren: What is the effect of a companion on the inflation?

Norbert Langer: The companion may suck off the inflated envelope (RLOF), but it will regrow, such that the mass transfer rate will be close to the critical mass-loss rate above which inflation is supressed.

Wolf-Rayet Stars
W.-R. Hamann, A. Sander, H. Todt, eds.
Potsdam: Univ.-Verlag, 2015
URL: http://nbn-resolving.de/urn:nbn:de:kobv:517-opus4-84268

Wolf-Rayet stars as supernova progenitors

L. Dessart
Laboratoire Lagrange, UMR7293, Université Nice Sophia-Antipolis, CNRS, Observatoire de la Côte d'Azur, 06300 Nice, France.

In this review, I discuss the suitability of massive star progenitors, evolved in isolation or in interacting binaries, for the production of observed supernovae (SNe) IIb, Ib, Ic. These SN types can be explained through variations in composition. The critical need of non-thermal effects to produce He I lines favours low-mass He-rich ejecta (in which ^{56}Ni can be more easily mixed with He) for the production of SNe IIb/Ib, which thus may arise preferentially from moderate-mass donors in interacting binaries. SNe Ic may instead arise from higher mass progenitors, He-poor or not, because their larger CO cores prevent efficient non-thermal excitation of He I lines. However, current single star evolution models tend to produce Wolf-Rayet (WR) stars at death that have a final mass of $> 10\,M_\odot$. Single WR star explosion models produce ejecta that are too massive to match the observed light curve widths and rise times of SNe IIb/Ib/Ic, unless their kinetic energy is *systematically and far greater* than the canonical value of 10^{51} erg. Future work is needed to evaluate the energy/mass degeneracy in light curve properties. Alternatively, a greater mass loss during the WR phase, perhaps in the form of eruptions, as evidenced in SNe Ibn, may reduce the final WR mass. If viable, such explosions would nonetheless favour a SN Ic, not a Ib.

1 Introduction

Since the 80's, supernovae (SNe) Ibc have been associated with the explosion of Wolf-Rayet (WR) stars, resulting from either the single-star or binary-star evolution scenario (see, e.g., Wheeler & Levreault 1985; Ensman & Woosley 1988; Podsiadlowski et al. 1992; Woosley et al. 1995; Crowther 2007; Yoon et al. 2010; Georgy et al. 2012). Their spectroscopic classification as type IIb (presence of both H I and He I lines), Ib (H I lines absent, but presence of He I lines), and Ic (absence of both H I and He I lines) is commonly associated with distinct composition mixtures, hence tied to explosions of WNh, WN, and WC/WO stars, respectively.

SNe owe their extreme luminosity to their large photospheric radii ($\sim 10^{15}$ cm), while their photospheres are cool (5–10 kK). Their radiative flux emerges primarily within the optical range, exhibiting spectral signatures from neutral and once-ionised species. Broad spectral lines reflect the fast expansion of the emitting layers, of the order of 5000–15000 km s^{-1}, depending on time and object. Their spectra are initially composed of P-Cygni profiles, often affected by line overlap due to fast expansion and line blanketing. After a few months and the transition to the nebular phase, the spectra exhibit primarily symmetric broad profiles associated with forbidden lines, while the continuum flux disappears. This evolution from early to late times allows a full scanning of the progenitor envelope, from the surface layers during the photospheric phase to the core layers in the nebular phase.

Both single and close-binary evolution can produce stars with a pre-SN composition compatible with the spectral signatures of SNe IIb, Ib, and Ic. Here, I highlight important differences between them, in particular the pre-SN chemical stratification (e.g., for the production of He I lines) and the final mass (e.g., to match the light curve properties).

2 Numerical tools

With the exception of super-massive stars, all stars more massive initially than $\approx 8\,M_\odot$ eventually form a degenerate core, which inevitably collapses when reaching the Chandrasekhar mass. This gravitational collapse is dynamical and lasts few 100 ms. As the innermost regions reach nuclear density, the material becomes incompressible and the core "bounces". A shock wave forms, but following energy losses (neutrino emission, photo-dissociation), it quickly stalls and turns into a stationary accretion shock. A successful core-collapse SN (CCSN) results if fresh energy (probably in the form of neutrinos) is pumped into the post-shock region, to drive the shock outward all the way to the surface (Woosley & Janka 2005). After shock breakout, radiation pressure gradients accelerate the ejecta until homologous expansion is reached, i.e., all mass shells move at constant speed. In addition, explosive nucleosynthesis behind the shock (where temperatures are $\sim 5\times 10^9$ K during the first second) produce some ^{56}Ni and Si-group elements.

To extract information from SN radiation requires solving an energy problem for a fast-expanding shock-heated stellar envelope. The evolution is controlled by cooling (expansion of all mass shells; radiation leakage from the photosphere), heating (primarily from the radioactive decay of ^{56}Ni, whose half life is comparable to the expansion time scale of the ejecta; recombination), and transport (primarily through the photospheric region).

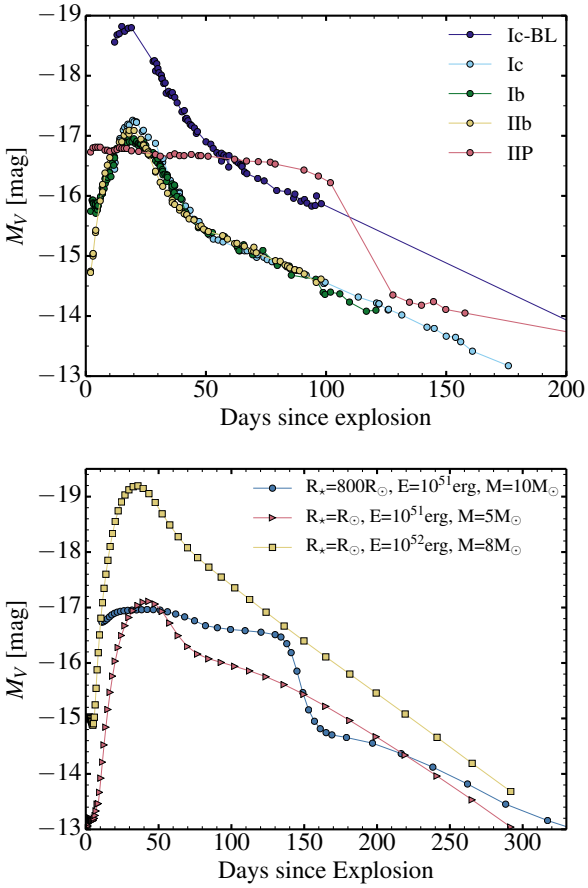

Fig. 1: *Left:* Representative observed light curves for a type II-Plateau (1999em; Leonard et al. 2002), a IIb (2011dh; Pastorello et al. 2009), a Ib (2008D; Modjaz et al. 2009), a Ic (2007gr; Valenti et al. 2008b), and a broad-line Ic (2003jd; Valenti et al. 2008a). *Right:* Light curve diversity obtained with CMFGEN by varying the progenitor massive star and explosion properties (for details, see Dessart et al. 2011, 2013; Dessart et al. in prep.).

One physically consistent approach is to first follow the star (either single or binary) from the main sequence to core collapse with a stellar evolution code (e.g., MESA, Paxton et al. 2015). The dynamical phase of the explosion is then simulated with a radiation-hydrodynamics code (e.g., V1D; Livne 1993; Dessart et al. 2010), using an artificial trigger (piston, thermal bomb), and stopped when homologous expansion is established. The final step is to follow the evolution of the ejecta and the radiation until late times, e.g., with the non local thermodynamic equilibrium (non-LTE) radiative transfer code CMFGEN (Hillier & Miller 1998; Dessart & Hillier 2010; Hillier & Dessart 2012). The code treats time dependence (Dessart & Hillier 2008) and non-thermal processes (Li et al. 2012; Dessart et al. 2012), a unique asset to model SNe IIb/Ib/Ic. It computes the emergent spectrum from the far-UV to the far-IR, thereby allowing a direct comparison to observed multi-band light curves and multi-epoch spectra.

3 Diversity of CCSN light curves

CCSNe exhibit two distinct light curve morphologies. One presents an extended plateau (which in fact may show a range of slopes; Anderson et al. 2014) of about 100 d, the other a bell shape. Both have a typical V-band brightness at maximum of -17 mag (top panel of Fig. 1), which corresponds to a bolometric luminosity of the order of a few $10^8\,L_\odot$.

SNe IIb, Ib, and Ic light curves show a relative uniformity in width (about 20–30 d) and in rise time to optical maximum (about 20–30 d) (Drout et al. 2011). Broad-lined type Ic, characterised by greater-than-average line profile widths, are, in addition, globally more luminous.

These various light curve morphologies are qualitatively well understood (Falk & Arnett 1977; Ensman & Woosley 1988). A large progenitor radius, as typically found in red-supergiant (RSG) stars, is essential to reduce expansion cooling and produce a sustained brightness for a few months, as seen in type II-Plateau SNe. In these, the SN radiation stems from the release of shock-deposited energy. For smaller stars like a WR, the SN luminosity is powered primarily by radioactive decay of ^{56}Ni and ^{56}Co (this power source affects SN II-Plateau light curves too, but primarily at nebular times).

It is therefore chiefly the variation in progenitor radius, rather than mass, that differentiates CCSN light curves (Dessart et al. 2011). The bottom panel of Fig. 1 illustrates the good agreement between more recent models and the observed diversity of CCSN light curves.

4 Constraints from spectra

Figure 2 shows one set of models (others may exist) suitable to produce the types IIb, Ib, and Ic. The properties of these models (see Yoon et al. 2010 and Dessart et al. 2015 for details) are as follows. The SN IIb corresponds to the explosion of the He-rich primary from an initial 5 d-period $16\,M_\odot \oplus 14\,M_\odot$ binary system (model 3p65Ax1). The pre-SN star has $0.005\,M_\odot$ of H at its surface. The SN Ib corresponds to the explosion of the He-rich primary from an initial 10 d-period $25\,M_\odot \oplus 24\,M_\odot$ binary system (model 6p5Ax1). The SNe Ic corresponds to the explosion of the CO-rich He-poor primary from an initial 3 d-period $60\,M_\odot \oplus 40\,M_\odot$ binary system (model 5p11Ax1). The SN IIb/Ib/Ic spectral diversity can thus be well explained by the changes in composition in the spectrum formation region.

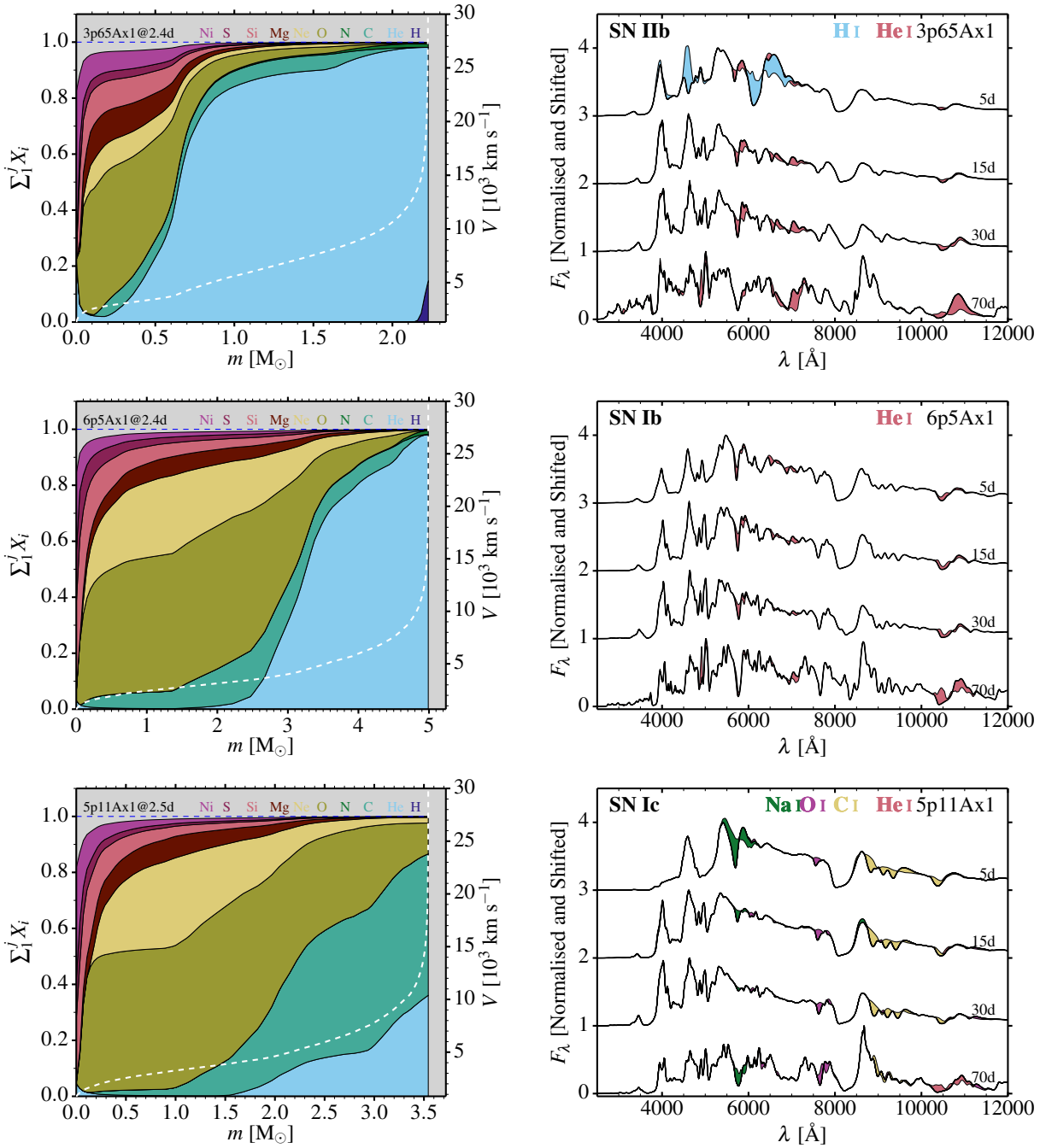

Fig. 2: *Left:* Chemical stratification in mass space for 3 ejecta (the dashed line corresponds to the velocity) suitable to produce a SN IIb (top), a Ib (middle), and a Ic (bottom) – see Dessart et al. (2015) for details. *Right:* Multi-epoch synthetic spectra calculated with CMFGEN and corresponding to the models shown at left. The color coding corresponds to the flux associated with selected ions.

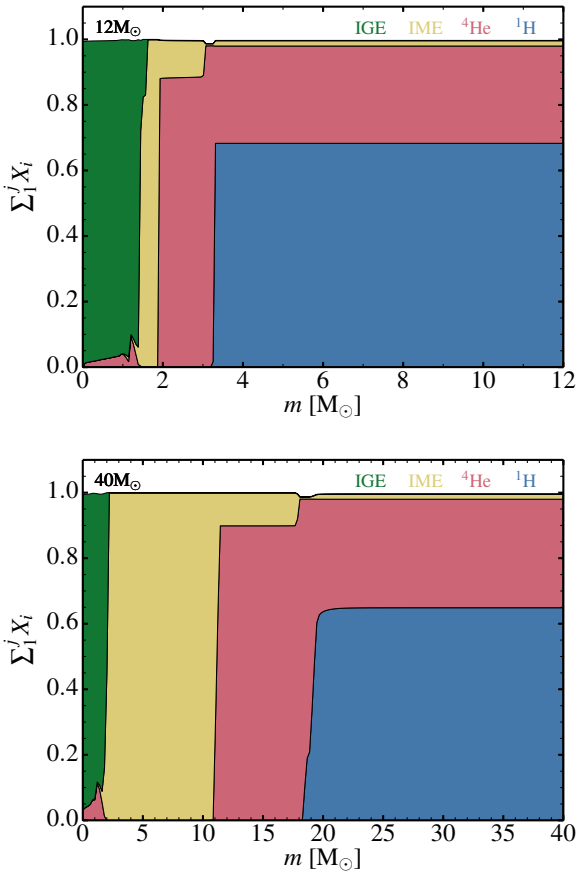

Fig. 3: Illustration of the pre-SN chemical stratification in mass space computed by MESA for a $12\,M_\odot$ and a $40\,M_\odot$ single massive star. IME (IGE) corresponds here to the cumulative mass fraction of intermediate-mass (iron-group) elements. The pre-SN evolution is computed with mass loss disabled.

However, a key problem concerns the production of He I lines. In massive stars (e.g., OB, WR), the photospheric temperatures are large enough to partially ionise He and produce He I and/or He II lines. The cool photospheric temperature of CCSNe prevents this. For example, in SN II-Plateau from RSG star explosions, He I lines are present during the first 2–3 weeks after explosion (when the photosphere is hot), but absent at the recombination epoch (when the photosphere is cool), although the RSG H-rich envelope is $\approx 35\%$ He by mass (Dessart et al. 2008). For the same reason, in SNe IIb, Ib, Ic, He I lines may be absent, even if He is present.

γ-rays emitted by ^{56}Ni–^{56}Co decay produce, through Compton scattering and absorption, high energy electrons that modify the non-LTE state of the gas. The associated non-thermal effects can in theory produce a strong He I line spectrum even at low temperature (Lucy 1991). But the process works only if significant ^{56}Ni is mixed with the He-rich material (Dessart et al. 2012). Because of this sensitivity, a SN IIb/Ib requires both the presence of a large amount of He and the efficient mixing of ^{56}Ni and He. It is not adequate to postulate a SN IIb/Ib classification based solely on the presence of He at the progenitor surface.

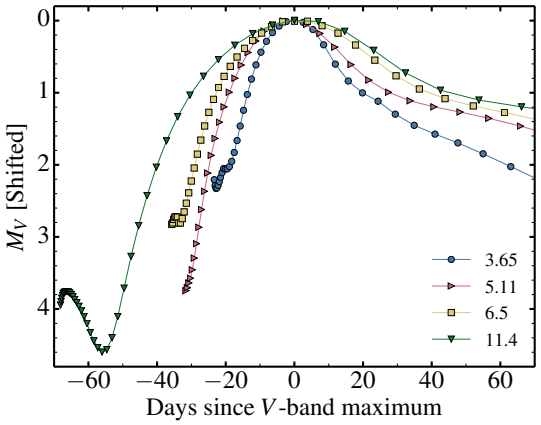

Fig. 4: SNe IIb/Ib/Ic V-band light curves (shifted vertically to peak at 0 mag) for $\approx 10^{51}$ erg explosions of progenitors arising from moderate-mass interacting binaries (the pre-SN masses are 3.65, 5.11, and $6.5\,M_\odot$) and from a single $40\,M_\odot$ massive star (pre-SN mass of $11.4\,M_\odot$) – see Dessart et al. (2015) for details.

5 Chemical stratification at death

Let us now inspect the pre-SN envelope structure of massive stars at death (Fig. 3) and ask what mass loss is needed to produce the distinct chemical stratifications responsible for the various SN types discussed above.

For the $12\,M_\odot$ model, wind mass loss in a RSG phase would produce a progenitor suitable for a $\approx 10\,M_\odot$ ejecta SN II-Plateau. Mass transfer in an interacting binary could get rid of the H-rich envelope and may produce a $\approx 4\,M_\odot$ bare He core, suitable for a SN IIb/Ib progenitor (see Fig. 2). Weak mixing might instead produce a SN IIc/Ic (see Dessart et al. 2012).

For the $40\,M_\odot$ model, whatever the mass loss, a SN IIb/Ib would require the ejection of $\approx 20\,M_\odot$, although the large CO core would strongly inhibit the non-thermal excitation of He in this case, favouring a SN Ic classification. In contrast, the ejection of a fraction of the CO core would suffice to produce a SN Ic (ejecta mass $< 10\,M_\odot$).

We can test the validity of these ejecta masses by confronting the associated light curve properties to observations. For that purpose, we now turn to stellar evolution models with mass loss enabled, through mass transfer in a binary system and/or a wind.

6 Constraints from light curves

Figure 4 shows the V-band light curves computed with CMFGEN for models 3p65Ax1, 5p11Ax1, 6p5Ax1 (produced by binary-star evolution – see Fig. 2), together with the explosion of a single $40\,M_\odot$ star that dies as a $11.4\,M_\odot$ WC star. The ejecta kinetic energy is $\approx 10^{51}$ erg for all 4 models.

Is is evident that these light curve widths are compatible with the observed ones, of 20–30 d (Drout et al. 2011), only for the lower mass ejecta models. The mismatch of the higher mass ejecta model reveals the fundamental discrepancy of single WRs (at least, as produced presently in the literature) to match the properties of observed SNe Ibc. In contrast, moderate-mass massive stars in binaries that shed their envelope through mass transfer can produce lower mass ejecta compatible with SN Ibc light curve properties. These objects are quite unlike the typical massive WR stars studied by the massive star community (Crowther 2007).

It is however possible to reconcile massive single WR stars as SN Ibc progenitors. First, one may invoke a larger WR mass loss rate than presently used in the stellar evolution calculations, perhaps in connection to non-steady mass loss observed in SNe Ibn (Pastorello et al. 2007). This would facilitate the trimming of the He core and may allow a reduction of the final mass to a few $M_\odot$. Another option is to consider that more massive WRs explode and yield ejecta with a systematically larger kinetic energy. Indeed, SN Ibc light curves show a degeneracy with the ratio of kinetic energy over mass (E/M). It is in fact hard to distinguish spectroscopically and photometrically two WR star explosions with a similar E/M (Dessart et al. 2015, in prep.). Both options would, however, make such explosions a SN Ic rather than a SN Ib. Whatever the alternative, single massive WR stars should not produce the SNe IIb/Ib we observe, which should instead arise primarily from moderate mass massive stars in interacting binaries.

An alternate fate of WR stars is that a SN shock explodes the star, but a large fraction of the CO core material falls back onto the neutron star, leading to black hole formation. This trimming of the inner envelope/ejecta would likely deplete the ejecta of its ^{56}Ni-rich material, producing a SN without a ^{56}Ni-powered peak. The shock breakout signal should, however, be detectable in such a "dark" SN.

References

Anderson, J. P., González-Gaitán, S., Hamuy, M., et al. 2014, ApJ, 786, 67

Crowther, P. A. 2007, ARA&A, 45, 177

Dessart, L., Blondin, S., Brown, P. J., et al. 2008, ApJ, 675, 644

Dessart, L. & Hillier, D. J. 2008, MNRAS, 383, 57

Dessart, L. & Hillier, D. J. 2010, MNRAS, 405, 2141

Dessart, L., Hillier, D. J., Li, C., & Woosley, S. 2012, MNRAS, 424, 2139

Dessart, L., Hillier, D. J., Livne, E., et al. 2011, MNRAS, 414, 2985

Dessart, L., Hillier, D. J., Waldman, R., & Livne, E. 2013, MNRAS, 433, 1745

Dessart, L., Hillier, D. J., Woosley, S., et al. 2015, ArXiv:1507.07783

Dessart, L., Livne, E., & Waldman, R. 2010, MNRAS, 408, 827

Drout, M. R., Soderberg, A. M., Gal-Yam, A., et al. 2011, ApJ, 741, 97

Ensman, L. M. & Woosley, S. E. 1988, ApJ, 333, 754

Falk, S. W. & Arnett, W. D. 1977, ApJS, 33, 515

Georgy, C., Ekström, S., Meynet, G., et al. 2012, A&A, 542, A29

Hillier, D. J. & Dessart, L. 2012, MNRAS, 424, 252

Hillier, D. J. & Miller, D. L. 1998, ApJ, 496, 407

Leonard, D. C., Filippenko, A. V., Gates, E. L., et al. 2002, PASP, 114, 35

Li, C., Hillier, D. J., & Dessart, L. 2012, MNRAS, 426, 1671

Livne, E. 1993, ApJ, 412, 634

Lucy, L. B. 1991, ApJ, 383, 308

Modjaz, M., Li, W., Butler, N., et al. 2009, ApJ, 702, 226

Pastorello, A., Smartt, S. J., Mattila, S., et al. 2007, Nature, 447, 829

Pastorello, A., Valenti, S., Zampieri, L., et al. 2009, MNRAS, 394, 2266

Paxton, B., Marchant, P., Schwab, J., et al. 2015, ArXiv:1506.03146

Podsiadlowski, P., Joss, P. C., & Hsu, J. J. L. 1992, ApJ, 391, 246

Valenti, S., Benetti, S., Cappellaro, E., et al. 2008a, MNRAS, 383, 1485

Valenti, S., Elias-Rosa, N., Taubenberger, S., et al. 2008b, ApJ, 673, L155

Wheeler, J. C. & Levreault, R. 1985, ApJ, 294, L17

Woosley, S. & Janka, T. 2005, Nature Physics, 1, 147

Woosley, S. E., Langer, N., & Weaver, T. A. 1995, ApJ, 448, 315

Yoon, S., Woosley, S. E., & Langer, N. 2010, ApJ, 725, 940

Paul Crowther: What does the fact that energetic SNe Ic tend to be rare in giant metal rich hosts and common in dwarf metal poor galaxies tell us about the explosions of massive Wolf-Rayet stars?

Luc Dessart: Highly energetic explosions require a large energy per unit mass in the associated ejecta, significantly greater than the standard for SNe Ibc. This suggests a more efficient engine at the origin of the explosion. A potential explanation is that the higher explosion energy occur from progenitors with a fast-spinning pre-collapse iron core. After collapse, these may turn into a ms-period proto-neutron star, which holds of the order of 10^{52} erg of rotational energy, and this may boost the explosion energy to values far greater than typically expected from standard SNe powered by neutrino energy deposition alone. This larger angular momentum budget in pre-collapse iron cores may exist only at lower metallicity and permit these energetic SNe Ic in dwarf hosts.

Single massive Wolf-Rayet stars are characterized by a large total binding energy, and very flat density profiles above the iron core. Such a structure presents a challenge for explosion because of the large accretion rate during the first second after collapse. So, an intriguing possibility is that single massive Wolf-Rayet stars have a greater tendency to explode in such environments because of the greater explosion energy delivered by faster-spinning cores. In contrast, a standard enery *deposition* (i.e., without the additional contribution from rotation), may simply fail in a massive Wolf-Rayet star.

Jose Groh: It seems that many conclusions on the fate of massive stars depend on the determination of the ejected mass. Could you clarify how the ejected masses are obtained and their uncertainties?

Luc Dessart: One approach is to use a simplistic one-zone diffusion model of the light curve and an estimated expansion rate of the ejecta to determine the explosion properties (this approach derives from the early work of Arnett 1982). This approach is attractive because of its simplicity but it bears numerous uncertainties (fixed opacity independent of composition and ionization; uniform density etc.). Despite these uncertainties, results based on this approach suggest that SNe Ibc ejecta have a low mass of about 2–3 $M_\odot$, while highly energetic SNe Ic are more massive.

The other approach is to do detailed time-dependent radiative transfer calculations of the spectra and light curves. As presented in this talk, ejecta masses of 2–3 $M_\odot$ are confirmed if one invokes a standard ejecta kinetic energy of 10^{51} erg. For that same energy, a 10 $M_\odot$ ejecta from a more massive WR star produces a broader light curve in disagreement with the observed narrower light curves of SNe Ibc. As I emphasize in this talk, light curve and spectral properties have some degeneracy, e.g., ejecta with the same E/M show relatively similar properties.

Overall, and in particular for SNe Ic, it is possible that inferred ejecta masses are not known to better than a factor of two.

WR-type central stars of PNe

Wolf-Rayet Stars
W.-R. Hamann, A. Sander, H. Todt, eds.
Potsdam: Univ.-Verlag, 2015
URL: http://nbn-resolving.de/urn:nbn:de:kobv:517-opus4-84268

Wolf-Rayet central stars of planetary nebulae

H. Todt[1] **& W.-R. Hamann**[1]
[1] *Universität Potsdam, Germany*

A significant number of the central stars of planetary nebulae (CSPNe) are hydrogen-deficient, showing a chemical composition of helium, carbon, and oxygen. Most of them exhibit Wolf-Rayet-like emission line spectra, similar to those of the massive WC Pop I stars, and are therefore classified as of spectral type [WC]. In the last years, CSPNe of other Wolf-Rayet spectral subtypes have been identified, namely PB 8, which is of spectral type [WN/C], and IC 4663 and Abell 48, which are of spectral type [WN].

We review spectral analyses of Wolf-Rayet type central stars of different evolutionary stages and discuss the results in the context of stellar evolution. Especially we consider the question of a common evolutionary channel for [WC] stars. The constraints on the formation of [WN] or [WC/N] subtype stars will also be addressed.

1 Introduction

Central stars of planetary nebulae (CSPNe) are evolved low-mass stars in the phase after the asymptotic giant branch (AGB) and before the white dwarf (WD) stage. The outer envelope of the former AGB star was shed off by a slow but strong AGB wind and is then swept up by a fast stellar wind of the CSPN. As the star evolves towards higher surface temperatures the surrounding material gets ionized as soon as the star reaches $T \approx 25\,000$ K and a PN gets visible.

While most of the low mass stars stay hydrogen-rich on their surface throughout their life, there exist a considerable fraction of post-AGB stars with H-deficient surface composition. Almost all H-deficient CSPNe exhibit spectra with strong carbon and helium lines (see Fig. 1), indicating that their surface is composed predominantly by these elements (e.g. Górny & Tylenda 2000; Werner & Heber 1991). As these objects show spectra very similar to the massive WC stars, they are classified as [WC], where the brackets distinguish them from their massive counterparts, as suggest by van der Hucht.

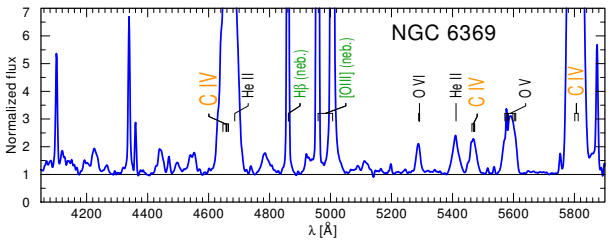

Fig. 1: NGC 6369: optical spectrum of a [WC4] type CS

Closely related to the [WC] stars are the PG 1159 stars, whose spectra are characterized by an absorption trough at about 4680 Å formed by C IV and He II lines. The corresponding gravity is of the order of $\log g = 7$. They are named after their prototype PG 1159-035 and show a strong excess in the UV (e.g. GALEX) due to their high temperatures. As their surface composition is rich in carbon and oxygen, they are considered as the descendants of the [WC] stars. This idea of an evolutionary link was corroborated by the discovery of the [WC]-PG 1159 stars Abell 30 and Abell 78, which exhibit weak emission *and* absorption lines of carbon, oxygen, and helium.

The first calculations of the post-AGB phase were performed by Paczyński (1970, 1971). In his models the surface composition remains H-rich throughout the evolution of the post-AGB object. An interesting feature of the late AGB evolution phase is the occurrence of a thermo-nuclear instability of the helium-burning shell – below the hydrogen-burning shell –, the so-called thermal pulse (TP).

The discovery of H-deficient, C-rich knots in the PNe of A 30 and A 78 (Hazard et al. 1980; Greenstein 1981; Jacoby & Ford 1983) motivated the idea of the born-again scenario (Iben et al. 1983; Iben 1984), where a TP occurs when the post-AGB star is already on the WD cooling track (Very Late TP), and the star is thrown back to the AGB regime. One should note that already Schoenberner (1979) encountered TPs *after* the AGB phase in his numerical simulations.

In this "classical" born-again scenario by Iben & MacDonald (1995) the H-rich envelope is removed *during the 2nd* post-AGB phase, resulting in a He-rich surface composition with $X_{\rm H} \approx 0.03$, $X_{\rm He} \approx 0.76$, $X_{\rm C} \approx 0.15$, $X_{\rm O} \approx 0.01$, and $X_{\rm N} \approx 0.05$.

However, first quantitative spectral analyses of PG 1159 stars (Werner et al. 1991), Abell 78 (Werner & Koesterke 1992) and [WCL] stars (Leuenhagen et al. 1996) raised the following problems (cf. Werner 2001) with this born-again scenario: [WCL] stars are relatively cool, i.e. young post-AGB stars, so the hydrogen must have been removed already *on* the AGB. The low expansion velocities of the H-free knots in Abell 30 and Abell 78 imply that the ejection happened during a low surface gravity phase, i.e. during the AGB phase. Moreover, the atmospheres of PG 1159 and [WC] stars are found to be rich in oxygen ($\approx 15\%$), whereas the models predict high amounts of oxygen only at the bottom of the

He-rich intershell region, but max. 3% at the surface.

These problems can be solved when additionally to the simultaneous mixing and burning in the models also diffusive overshoot (Freytag et al. 1996) is taken into account. Such models develop an efficient dredge-up (Herwig et al. 1997, 1999) and result in a carbon and oxygen enriched surface composition.

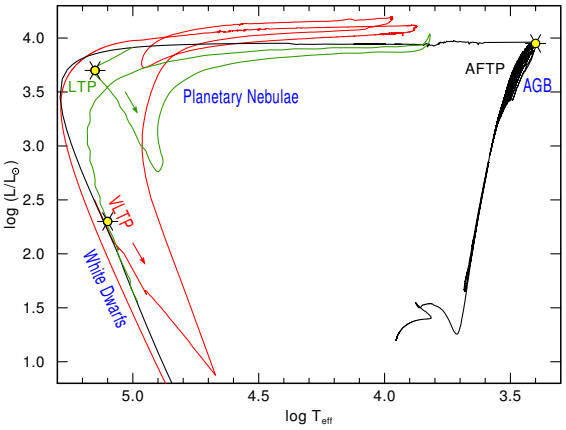

Fig. 2: Stellar evolutionary tracks for AGB final thermal pulse (black line, beginning from the ZAMS for $M_{\rm ini} = 2\,M_\odot$ Herwig 2001), late thermal pulse (green line, for $M_{\rm ini} = 3\,M_\odot$ Blöcker 1995), and very late thermal pulse (red line, for $M_{\rm ini} = 2\,M_\odot$ Herwig 2001)

Depending on the time at which these TPs occur (cf. Fig. 2), they can lead to an efficient subsequent dredge-ups of processed intershell material which is than displayed at the surface. An AGB final thermal pulse (AFTP) occurs at the tip of the AGB and a late thermal pulse (LTP) occurs just before the stars enters the White Dwarf cooling track.

While hydrogen is only diluted by intershell material in the case of the AFTP and LTP, it is completely burned in the VLTP scenario. Moreover, nitrogen and neon are also produced in the VLTP up to a mass fraction of a few percent (cf. Fig. 3).

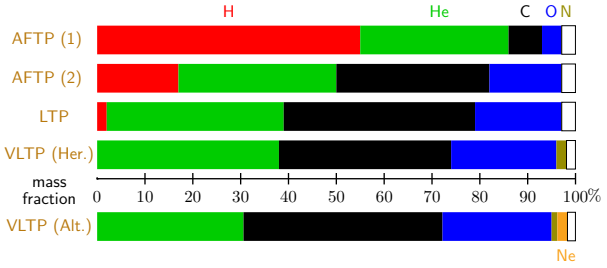

Fig. 3: Expected abundance patterns for [WC] stars from stellar evolutionary models. Upper panel: Herwig (2001); lower panel: Althaus et al. (2005)

2 Spectral analyses of [WC] stars

Analogously to the spectral subtypes of the massive WC stars, the [WC] subtypes form a sequence where the hottest objects, i.e. those showing He II and C IV lines, belong to the early-type [WC] stars ([WCE]) and the cooler ones with He I and C II, C III lines belong to the late-type [WC] stars ([WCL]).

Previous analyses of [WCL] and [WCE] stars, based on optical and UV spectra, resulted in systematically different abundances of He and C for these subtypes.

For the majority of the [WCL] stars, analyzed e.g. by Leuenhagen & Hamann (1994); Leuenhagen et al. (1996); Leuenhagen & Hamann (1998), 13 objects, Marcolino et al. (2007), two objects, and De Marco & Crowther (1998, 1999), three objects, a C:He:O abundance ratio of about 50:40:10 (by mass) was found. Only for three [WCL] stars De Marco et al. (2001) and Crowther et al. (2003) found $X_{\rm C} < X_{\rm He}$. Their models accounted also for density inhomogeneities and line blanketing due to the iron group elements. Leuenhagen & Hamann (1998) also inferred enhanced $(1-4\,\%)$ neon and nitrogen abundances in six of their objects.

Koesterke & Hamann (1997a,b) analyzed 12 [WCE] stars, and derived a typical abundance ratio C:He:O of 30:60:10. Crowther et al. (2003) and Marcolino et al. (2007) studied two [WCE] stars each and found almost equal mass fractions of carbon and helium, similar to the result of an analysis of the extragalactic [WCE] star LMC-SMP 61 by Stasińska et al. (2004) and to the findings for two objects in the sample of Keller et al. (2014), whose analyses are based on UV spectra only. The other two [WCE] stars in the sample of Keller et al. (2014) have an abundance ratio similar to that found by Koesterke & Hamann (1997a,b).

Hydrogen. Hydrogen could in principal help to distinguish between the VLTP and AFTP/LTP scenario, but it is hard to detect, as in [WC] stars hydrogen emission lines are always blended with He II lines, often outshone by nebular emission lines, and generally weak in [WCE] stars. However, in the [WCL] stars IRAS 21282+5050, Hen 2-113 (Leuenhagen & Hamann 1998), and M 4-18 (De Marco & Crowther 1999) evidences for stellar hydrogen were found, based on the analysis of the broad wings of the Hα emission line.

Iron. Iron depletion would be an evidence to the s-process nucleosynthesis (neutron capture) in the former AGB star. Such deficiency was derived for LMC-SMP 61, where $X_{\rm Fe} = \frac{1}{6} X_{\rm Fe,\,LMC}$ and was also claimed by Marcolino et al. (2007) and Keller et al. (2014). However, only 10 % iron depletion due to neutron capture is predicted. For PG 1159 stars the originally claimed iron depletion was later revoked by the detection of Fe VIII / X lines (Werner et al. 2010, 2011).

Nitrogen, Neon. The detection of super-solar neon abundances was already claimed for [WCL] stars. For the hotter [WCE] stars only few lines lie in the optical range, Werner et al. (2007) identified some Ne VIII lines, but as the oscillator strengths of the corresponding transitions are only estimated, they are not useful for abundance determinations. Herald et al. (2005) discovered a strong Ne VII line in the FUSE range at 973.3 Å, which is not too sensitive to the mass-loss rate and can therefore be used for abundance determinations. A surface abundance of neon of the order of a few percent can be obtained not only via a VLTP, but also via an LTP (Miller Bertolami, priv. comm.).

A more unambiguous imprint of the VLTP is the presence of a considerable amount of nitrogen ($> 0.1\%$ by mass). For the [WCE] stars the nitrogen abundance can be reliably inferred from the optical emission lines of N V at 4604/4620 Å and 4934/4945 Å. Keller et al. (2014) found enhanced, i.e. $1-4\%$, Ne and N abundances for all of their objects, whereas Marcolino et al. (2007) found $X_{\rm N} < 0.1\%$.

Clumping in WR-CSPN. As shown by Hillier (1991), the clumpiness of WR star atmospheres can be estimated from the strength of electron scattering (e.s.) line wings. However, the degree of density inhomogeneities (microclumping) in [WC] star winds is generally hard to determine, because in the normalized spectrum the e.s. line wings are much weaker than for massive WC stars. This may help to distinguish between massive and low-mass WR stars, as mentioned in Todt et al. (2008) and Todt et al. (2013). Unfortunately, the stellar spectra are contaminated with nebular emission lines which often outshine the e.s. wings.

3 [WC]-PG 1159 stars

As the spectra of [WC]-PG 1159 stars show both, photospheric absorption lines and wind emission lines, previous analyses by either plan-parallel or pure wind models were limited. The analyses by Leuenhagen et al. (1993) of Abell 30 and Abell 78 were based on pure wind models and resulted in abundance patterns similar to those for [WCL] stars, i.e. with C : He : O : N=50 : 33 : 15 : 2 (Abell 78) and C:He:O:N=40 : 41 : 15 : 4 (Abell 30).

Results of improved analyses (Guerrero et al. 2012; Toalá et al. 2015), which account for pressure broadened absorption lines as well as Doppler broadened wind lines ($v_\infty \approx 4000$ km/s) revised the carbon abundances downwards to a more [WCE]-like chemical composition, i.e. C : He : O : N = 20 : 63 : 15 : 1.5 for Abell 30 and C : He : O : N : Ne : F = $30 : 55 : 10 : 1.5 : 4 : 1.3 \times 10^{-5}$ for Abell 78. The abundances of N and Ne are consistent with predictions for the VLTP, which is the suggested evolutionary channel for both objects.

4 [WN] central stars

While the low-mass spectral twins of the massive WC stars have been known since the discovery of the first WC stars, it was until recently not clear whether there also exist [WN] central stars, i.e., CSPNe whose spectra resemble those of the massive WN stars. At least this was not expected from the stellar evolutionary models of Herwig (2001) and Althaus et al. (2005).

4.1 PMR 5 - a [WN] suspect

The earliest claim for the discovery of a [WN] central star was by Morgan et al. (2003), who observed the highly reddened ($E_{\rm B-V} = 3$ mag) object PMR 5, which shows a WN spectrum (subtype WN6) and a round nebula. However, it is not clear, whether this is a PN or ring nebula around a massive WR star. While the electron density is consistent with a PN, the expansion velocity of $v_{\rm exp} = 165$ km/s is rather unusual for a PN, but typical for a ring nebula. Moreover, the luminosity distance is consistent with a massive WR star. For a typical CSPN luminosity of $L/L_\odot = 6000$ PMR 5 would be located at a distance of 0.5 kpc and at a height of 6 pc above the Galatic plane, while for a typical luminosity of a massive WN star PMR 5 would be at 2.9 kpc away and 35 pc above the Galactic plane. Hence, both locations are consistent with the corresponding type of star. However, a reddening of $E_{\rm B\text{-}V} = 3$ mag is rather untypical for a distance of only 500 pc. A spectral analysis based on the published spectrum revealed a chemical composition of a typical WNh star, but with a large mass fraction of N ($\approx 10\%$). Overall, chemistry and $v_{\rm exp}$ point to a massive WN star with a ring nebula.

4.2 PB 8 - a [WN/C] star

The CS PB 8 was classified as [WC 5-6] by Acker & Neiner (2003) based on a low-resolution spectrum. A spectral analysis based on a high resolution spectrum, (Todt et al. 2010) revealed that this object has a stellar temperature of about 50 kK and an unusual composition with He:H:C:N:O=55:40:1:1:1 by mass and resembles spectroscopically a massive WN/C star.

Due to its unknown distance, also L is unknown, so whether this star is a true [WN/C] CS can only be inferred indirectly.

The nebula analysis by García-Rojas et al. (2009) yield values for $T_{\rm e}$ and $n_{\rm e}$ which are typical for young PNe, as well as the small $v_{\rm exp} \approx 30$ km/s. Regarding the luminosity distance, one finds that for a CSPN

with $L/L_\odot = 6000$, PB 8 would be at a distance of 4.2 kpc and at a height of 300 pc above the Galactic plane, whereas a massive WR star would have at least $L/L_\odot = 2 \times 10^5$, and so at least a distance of 24 kpc and a height of 1.7 kpc above the Galatic plane. This is a rather untypical location for a massive WR star. So, PB 8 is indeed a CSPN.

We also considered the possibility that PB 8 may be a binary. Although this can not be excluded completely, it is rather unlikely as there were no shifts of radial velocities of spectral lines detected (Méndez 1989) and the nebula appears spherically symmetric, also in velocity space.

4.3 IC 4663 - [WNE] type CS

The first "pure" [WN] was discovered by Miszalski et al. (2012). Their spectral analysis based on an optical spectrum revealed that IC 4663 is an almost hydrogen-free ($< 2\,\%$ by mass) [WN] star, whose wind consists to 95 % of helium with only 0.8% nitrogen. Interestingly it is of early spectral subtype ([WN3]) with a temperature of about 140 kK and a relatively low mass-loss rate of about $2\times10^{-8}\,M_\odot\,\mathrm{a}^{-1}$. Miszalski et al. (2012) showed that if IC 4663 were a massive WN star it would be at an implausible distance of 58 kpc and more than 8 kpc below the Galactic plane. Moreover, they discovered an AGB halo around IC 4663, proving it is a CSPN.

4.4 Abell 48

The CS Abell 48 was found to have a helium-rich (85%) wind with about 10% hydrogen, and a nitrogen abundance of about 5% (Todt et al. 2013; Frew et al. 2014). From the nebula analysis (line ratios of S II and Hα, as in Riesgo-Tirado & López 2002) it was concluded that Abell 48 is indeed a CSPN. This is also consistent with the measured extinction and its significant proper motion - Abell 48 is a runaway.

5 Discussion

The evolutionary channel by which [WC] stars are formed is still unclear. Neither the VLTP nor the AFTP or LTP scenario yield a consistent picture. While the observed super-solar nitrogen abundances can be explained by the VLTP scenario, the corresponding PNe are much younger than predicted by this scenario. Moreover, within the [WCE] sample the nitrogen abundances vary from solar to a few percent. The AFTP scenario would better fit to the derived ages of the PNe, but the observed abundances, especially of hydrogen and nitrogen, are not matched by stellar evolutionary models.

Regarding the systematic differences of the C:He ratio between [WCE] and [WCL] stars in previous analyses it is even unclear whether the suggested evolutionary sequence AGB → [WCL] → [WCE] → [WC]-PG1159 → PG1159 → non-DA WD (e.g. Werner & Heber 1991) is appropriate. Further analyses with updated models on larger wavelength ranges with more spectral lines may resolve the discrepancy. Note, for example, that the born-again object V605 Aql (Clayton et al. 2006) has apparently evolved directly from the VLTP to the [WCE] stage.

The situation is even more puzzling for the [WN] stars. None of the recent late TP scenarios predicts the observed surface compositions of PB 8, IC 4663, and Abell 48. It was speculated whether these objects belong to an alternative evolutionary sequence [WN] → O(He) (Werner 2012) or that [WN] stars are O(He) stars with higher masses (Reindl et al. 2014), evolving from RCB or sdO(He) stars, which might be merger products of non-DA WDs. However, the merger scenario seems to be rather unlikely due to the long timescales involved, which are incompatible with the observed low ages of the PNe of the [WN] stars. Moreover, PB 8 and Abell 48 also contain hydrogen while the assumed progenitors are H-free.

Note that the "classical" born-again scenario by Iben & MacDonald (1995) yields abundances that are somehow similar to the observed ones.

Another remaining questions is how H-deficient central stars become [WR] stars, or: Why do they have so strong winds?

For massive WNL stars Gräfener & Hamann (2008) demonstrated that it is the proximity to the Eddington limit, i.e. high L/M ratios of $\approx 15\,000 - 30\,000$ (in solar units), which determines the strength of the stellar wind.

For CSPNe in general, $L/M \approx 3\,000 - 30\,000$ in average (e.g. 15 000 for LMC-SMP61, with assumed $M = 0.6\,M_\odot$), although for most CSPNe the individual distances are unknown, and so are L and M.

For stellar models with $M_\mathrm{ini} > 2M_\odot$ the ratio L/M for H-rich CSPNe is about the same as for H-deficient CSPNe (Miller Bertolami & Althaus 2006) and model calculations show that the most massive H-rich CSPNe are already close to the Eddington limit (Miller Bertolami 2015). Moreover, some of the H-rich CSPNe, like NGC 6543, show WR features in their spectra and are therefore classified as of type WR-O(f).

In our wind models with fixed $L = 6000\,L_\odot$ and $M = 0.6\,M_\odot$, the wind efficiency $\eta = \dot{M}v_\infty/(L/c)$ is always smaller than 1 (for a β-law with $\beta = 1$ and $\dot{M} \approx 10^{-7}\,M_\odot/\mathrm{a}$) and the only hydrodynamically consistent model of a [WCE] star, NGC 6905, by Gräfener et al. (2008) needed strong clumping with $D = 100$. It may be that additional opacity is provided by enriched s-process elements (produced on the AGB), which are not included in our models, as the atomic data are hardly available.

References

Acker, A. & Neiner, C. 2003, A&A, 403, 659

Althaus, L. G., Serenelli, A. M., Panei, J. A., et al. 2005, A&A, 435, 631

Blöcker, T. 1995, A&A, 299, 755

Clayton, G. C., Kerber, F., Pirzkal, N., et al. 2006, ApJ, 646, L69

Crowther, P. A., Abbott, J. B., Hillier, D. J., & De Marco, O. 2003, in IAU Symposium, Vol. 209, Planetary Nebulae, ed. S. Kwok, M. Dopita, & R. Sutherland, 243

De Marco, O. & Crowther, P. A. 1998, MNRAS, 296, 419

De Marco, O. & Crowther, P. A. 1999, MNRAS, 306, 931

De Marco, O., Crowther, P. A., Barlow, M. J., Clayton, G. C., & de Koter, A. 2001, MNRAS, 328, 527

Frew, D. J., Bojičić, I. S., Parker, Q. A., et al. 2014, MNRAS, 440, 1345

Freytag, B., Ludwig, H.-G., & Steffen, M. 1996, A&A, 313, 497

García-Rojas, J., Peña, M., & Peimbert, A. 2009, A&A, 496, 139

Górny, S. K. & Tylenda, R. 2000, A&A, 362, 1008

Gräfener, G. & Hamann, W.-R. 2008, A&A, 482, 945

Gräfener, G., Hamann, W.-R., & Todt, H. 2008, in ASPCS, Vol. 391, Hydrogen-Deficient Stars, ed. A. Werner & T. Rauch, 99

Greenstein, J. L. 1981, ApJ, 245, 124

Guerrero, M. A., Ruiz, N., Hamann, W.-R., et al. 2012, ApJ, 755, 129

Hazard, C., Terlevich, R., Ferland, G., Morton, D. C., & Sargent, W. L. W. 1980, Nature, 285, 463

Herald, J. E., Bianchi, L., & Hillier, D. J. 2005, ApJ, 627, 424

Herwig, F. 2001, Ap&SS, 275, 15

Herwig, F., Blöcker, T., Langer, N., & Driebe, T. 1999, A&A, 349, L5

Herwig, F., Bloecker, T., Schoenberner, D., & El Eid, M. 1997, A&A, 324, L81

Hillier, D. J. 1991, A&A, 247, 455

Iben, Jr., I. 1984, ApJ, 277, 333

Iben, Jr., I., Kaler, J. B., Truran, J. W., & Renzini, A. 1983, ApJ, 264, 605

Iben, Jr., I. & MacDonald, J. 1995, in Lecture Notes in Physics, Berlin Springer Verlag, Vol. 443, White Dwarfs, ed. D. Koester & K. Werner, 48

Jacoby, G. H. & Ford, H. C. 1983, ApJ, 266, 298

Keller, G. R., Bianchi, L., & Maciel, W. J. 2014, MNRAS, 442, 1379

Koesterke, L. & Hamann, W.-R. 1997a, in IAU Symposium, Vol. 180, Planetary Nebulae, ed. H. J. Habing & H. J. G. L. M. Lamers, 114

Koesterke, L. & Hamann, W.-R. 1997b, A&A, 320, 91

Leuenhagen, U. & Hamann, W.-R. 1994, A&A, 283, 567

Leuenhagen, U. & Hamann, W.-R. 1998, A&A, 330, 265

Leuenhagen, U., Hamann, W.-R., & Jeffery, C. S. 1996, A&A, 312, 167

Leuenhagen, U., Koesterke, L., & Hamann, W.-R. 1993, Acta Astron., 43, 329

Marcolino, W. L. F., Hillier, D. J., de Araujo, F. X., & Pereira, C. B. 2007, ApJ, 654, 1068

Méndez, R. H. 1989, in IAU Symposium, Vol. 131, Planetary Nebulae, ed. S. Torres-Peimbert, 261–272

Miller Bertolami, M. M. 2015, in ASPCS, Vol. 493, 19th European Workshop on White Dwarfs, ed. P. Dufour, P. Bergeron, & G. Fontaine, 83

Miller Bertolami, M. M. & Althaus, L. G. 2006, A&A, 454, 845

Miszalski, B., Crowther, P. A., De Marco, O., et al. 2012, MNRAS, 423, 934

Morgan, D. H., Parker, Q. A., & Cohen, M. 2003, MNRAS, 346, 719

Paczyński, B. 1970, Acta Astron., 20, 47

Paczyński, B. 1971, Acta Astron., 21, 417

Reindl, N., Rauch, T., Werner, K., Kruk, J. W., & Todt, H. 2014, A&A, 566, A116

Riesgo-Tirado, H. & López, J. A. 2002, in RMxAC, ed. W. J. Henney, J. Franco, & M. Martos, Vol. 12, 174–174

Schoenberner, D. 1979, A&A, 79, 108

Stasińska, G., Gräfener, G., Peña, M., et al. 2004, A&A, 413, 329

Toalá, J. A., Guerrero, M. A., Todt, H., et al. 2015, ApJ, 799, 67

Todt, H., Hamann, W.-R., & Gräfener, G. 2008, in Clumping in Hot-Star Winds, ed. W.-R. Hamann, A. Feldmeier, & L. M. Oskinova, 251

Todt, H., Kniazev, A. Y., Gvaramadze, V. V., et al. 2013, MNRAS, 430, 2302

Todt, H., Peña, M., Hamann, W.-R., & Gräfener, G. 2010, A&A, 515, A83

Werner, K. 2001, Ap&SS, 275, 27

Werner, K. 2012, in IAU Symposium, Vol. 283, IAU Symposium, 196–203

Werner, K. & Heber, U. 1991, A&A, 247, 476

Werner, K., Heber, U., & Hunger, K. 1991, A&A, 244, 437

Werner, K. & Koesterke, L. 1992, in Lecture Notes in Physics, Berlin Springer Verlag, Vol. 401, The Atmospheres of Early-Type Stars, ed. U. Heber & C. S. Jeffery, 288

Werner, K., Rauch, T., & Kruk, J. W. 2007, A&A, 474, 591

Werner, K., Rauch, T., & Kruk, J. W. 2010, ApJ, 719, L32

Werner, K., Rauch, T., Kruk, J. W., & Kurucz, R. L. 2011, A&A, 531, A146

Martin Guerrero: Do planetary nebulae with [WR] CSPNe have more complex morphologies? Could this be related to the stellar wind of [WR] stars?

Helge Todt: I am not an expert on PNe in general, but it seems that PNe with [WR] central stars have similar morphologies to other PNe.

Marcelo Miguel Miller Bertolami: One should be careful when comparing the ^{16}O abundances of [WC] and PG1159 stars with the "predictions" of the models. In fact, there are *no true predictions* for ^{16}O from stellar evolution models of LTP and VLTP scenarios. This is because the oxygen abundance is completely dependent on the intensity of diffusive extra mixing during the whole TP-AGB which is indeed calibrated to reproduce the O abundance of PG 1159 stars.

Wolf-Rayet Stars
W.-R. Hamann, A. Sander, H. Todt, eds.
Potsdam: Univ.-Verlag, 2015
URL: http://nbn-resolving.de/urn:nbn:de:kobv:517-opus4-84268

Post-common-envelope Wolf-Rayet central stars of planetary nebulae

B. Miszalski[1,2], R. Manick[3] & V. McBride[1,4]
[1] *South African Astronomical Observatory, South Africa*
[2] *Southern African Large Telescope Foundation, South Africa*
[3] *KU Leuven, Belgium*
[4] *University of Cape Town, South Africa*

Nearly 50 post-common-envelope (post-CE) close binary central stars of planetary nebulae (CSPNe) are now known. Most contain either main sequence or white dwarf (WD) companions that orbit the WD primary in around 0.1–1.0 days. Only PN G222.8−04.2 and NGC 5189 have post-CE CSPNe with a Wolf-Rayet star primary (denoted [WR]), the low-mass analogues of massive Wolf-Rayet stars. It is not well understood how H-deficient [WR] CSPNe form, even though they are relatively common, appearing in over 100 PNe. The discovery and characterisation of post-CE [WR] CSPNe is essential to determine whether proposed binary formation scenarios are feasible to explain this enigmatic class of stars. The existence of post-CE [WR] binaries alone suggests binary mergers are not necessarily a pathway to form [WR] stars. Here we give an overview of the initial results of a radial velocity monitoring programme of [WR] CSPNe to search for new binaries. We discuss the motivation for the survey and the associated strong selection effects. The mass functions determined for PN G222.8−04.2 and NGC 5189, together with literature photometric variability data of other [WR] CSPNe, suggest that of the post-CE [WR] CSPNe yet to be found, most will have WD or subdwarf O/B-type companions in wider orbits than typical post-CE CSPNe (several days or months c.f. less than a day).

1 Close binary central stars of Planetary Nebulae

Planetary nebulae (PNe) are the ionised gaseous envelopes ejected by low to intermediate mass stars (1–8 $M_{\odot}$) at the end of the asymptotic giant branch (AGB) phase. The origin of the myriad shapes observed in PNe is a difficult problem that has persisted for several decades (Balick & Frank 2002). The most promising solution is now understood to be stellar or even sub-stellar companions (De Marco 2009). Observational evidence for binarity in PNe was relatively modest with pioneering photometric monitoring surveys producing around a dozen examples (Bond 2000). Most of these have orbital periods of 0.1–1.0 d and have therefore passed through the common-envelope (CE) phase (Ivanova et al. 2013). As the ejected CE is still visible as the PN with an age of $\sim 10^4$ years, post-CE central stars of planetary nebulae (CSPNe) are the youngest probes we have of the very short (unobserved) and poorly understood CE interaction.

To realise the potential of post-CE CSPNe as a population to address problems concerning CE evolution, as well as the shaping mechanism of PNe, a statistically significant sample must be gathered. Miszalski et al. (2008, 2009a) leveraged the large areal coverage, high time cadence and high sensitivity of I-band photometry from the microlensing survey OGLE-III (Udalski et al. 2008) to discover several more post-CE CSPNe. A major result from this work is that around 1 in 5 PNe have a post-CE CSPN, consistent with earlier estimates (Bond 2000). High-quality imaging of the enlarged sample has revealed post-CE PNe often show collimated outflows or jets, low-ionisation filaments and rings, as well as bipolar morphologies (Miszalski et al. 2009b). These morphological features have since been successfully used to target PNe with similar morphologies to discover several more post-CE binaries (Miszalski et al. 2011b; Jones 2015), bringing the total to nearly 50 binaries (Jones 2015).

The population of post-CE CSPNe mostly consists of white dwarf (WD) primaries with main sequence (MS) secondaries, however several double degenerate (DD) systems are also known (e.g. Tovmassian et al. 2010; Boffin et al. 2012; Santander-García et al. 2015). Photometric variability of WDMS CSPNe is often dominated by a large sinusoidal irradiation effect, produced by the heating of the hemisphere of the secondary facing the primary. Also present in post-CE CSPNe lightcurves are eclipses and ellipsoidal variability, the latter mostly occurring in DD systems. The optical photometric monitoring technique used in most surveys for post-CE CSPNe has introduced significant selection effects into the known population. Firstly, there is a strong bias against finding WDMS binaries with orbital periods >1 d since the irradiation effect amplitude decreases rapidly with increasing orbital separation (De Marco et al. 2008). Secondly, DD systems are under-represented since they (a) do not usually produce an irradiation effect, and (b) require a close orbital separation to produce ellipsoidal variability or eclipses. Radial velocity (RV) monitoring is therefore the only reliable technique to establish if a post-CE CSPN is present (e.g. Boffin et al. 2012).

2 Binary status of Wolf-Rayet central stars

Over a hundred PNe have H-deficient Wolf-Rayet central stars (denoted [WR]), the low-mass ($M \sim 0.6$ $M_{\odot}$) spectroscopic mimics of massive WR stars (see the review of Todt & Hamann (2015), these proceedings). The origin of [WR] stars remains elusive, especially given the recent discovery of two bona-fide [WN] stars whose extremely He-rich atmospheres may be better explained by a merger scenario, rather than the traditional scenarios used to explain [WC] star formation (Miszalski et al. 2012; Todt et al. 2013). Some binary formation scenarios have been proposed (e.g. De Marco & Soker 2002), but there are currently too few known binaries to further develop these scenarios. The only known [WR] binaries are PN G222.8−04.2 ([WC7], Hajduk et al. 2010) and NGC 5189 ([WO1], Manick et al. 2015) with respective orbital periods of 1.26 and 4.05 d.

Why are there so few post-CE [WR] CSPNe known? The answer lies in the previous reliance on photometric monitoring to find post-CE CSPNe. At least 37 early-type [WC] stars and related H-deficient stars have been monitored photometrically by Ciardullo & Bond (1996) and González Pérez et al. (2006). Some were found to be non-radial pulsators, but no variability was found that could be attributed to a binary companion. Indeed, since 15–20% of PNe have post-CE CSPNe (Bond 2000; Miszalski et al. 2009a), then we would have expected ∼5–7 post-CE [WR] CSPNe to have been found. These non-detections exclude the presence of post-CE [WR] binaries in the sample with MS companions since they would have produced a very large amplitude irradiation effect as in e.g. Corradi et al. (2011) and Miszalski et al. (2011a).

3 A new approach: RV monitoring of [WR] stars

RV monitoring is a tried and tested method to discover massive WR binaries (e.g. Foellmi et al. 2003), so there is no reason not to suspect it would work for [WR] stars. Our approach is to take several spectra of each object with a resolution of ∼2Å and signal-to-noise > 40 in the continuum. We are using SpCCD on the SAAO 1.9-m telescope for the brightest targets and the Robert Stobie Spectrograph (RSS) on the Southern African Large Telescope (SALT) for fainter targets. We then follow the cross-correlation procedure of Foellmi et al. (2003) to derive the RV measurements. Initial results have been published in Manick et al. (2015). No periodic variability was found in PMR 2, Hen 2-99, NGC 5315, Hen 2-113 and Hen 3-1333, whereas we found periodic variability of 4.04 d in NGC 5189. Additional higher quality SALT observations have since ruled out the previously suspected variability in Hen 2-99 and NGC 5315.

Figure 1 presents an updated RV curve for NGC 5189 containing 12 additional spectra, resulting in a revised period of 4.05 d, as well as our preliminary RV curve for PN G222.8−04.2. The measured RV amplitudes for NGC 5189 and PN G222.8−04.2 are 54 ± 4 and 184 ± 8 km s^{-1}, respectively. As the orbital inclinations of both objects are unknown, we present a list of possible companion masses in Tab. 1. An evolved WD companion is most likely present in NGC 5189, similar to that in Fleming 1 (Boffin et al. 2012). In the case of PN G222.8−04.2, if the unusually high RV amplitude is not an artefact of the cross-correlation technique, then we may suspect the companion to be a subdwarf O/B-type star, perhaps similar to that found in NGC 6026 (Hillwig et al. 2010). Polarimetric observations and spatiokinematic modelling (e.g. Sabin et al. 2012) would be desirable to constrain the inclinations of both objects.

Tab. 1: Companion mass estimates for a variety of orbital inclination angles assuming $M_1 = 0.6$ $M_{\odot}$.

i (°)	M_2 (NGC 5189)	M_2 (PN G222.8−04.2)
30	1.30±0.20	7.60±0.70
40	0.80±0.10	4.10±0.20
50	0.59±0.04	2.70±0.10
60	0.50±0.02	2.10±0.10
70	0.44±0.01	1.80±0.10
80	0.42±0.01	1.60±0.03
90	0.40±0.01	1.60±0.04

4 Summary

We have started to conduct RV monitoring of several [WR] CSPNe to search for post-CE [WR] binaries. These binaries are needed to provide the first accurate distance-independent stellar parameters for [WR] stars, as well as to inform the still enigmatic formation scenarios regarding [WR] stars. We have increased the known sample of post-CE [WR] binaries to two with the discovery of a 4.05 d orbital period in NGC 5189 (Manick et al. 2015), an object long suspected of harbouring a binary CSPN (Phillips & Reay 1983) because of its peculiar morphology (Sabin et al. 2012). Its morphology is typical of post-CE PNe and in particular bears close resemblance to the post-CE PN NGC 6326 (Miszalski et al. 2011c). Furthermore, we have presented a preliminary RV curve for PN G222.8−04.2 that will form the basis of a more detailed study to be presented elsewhere.

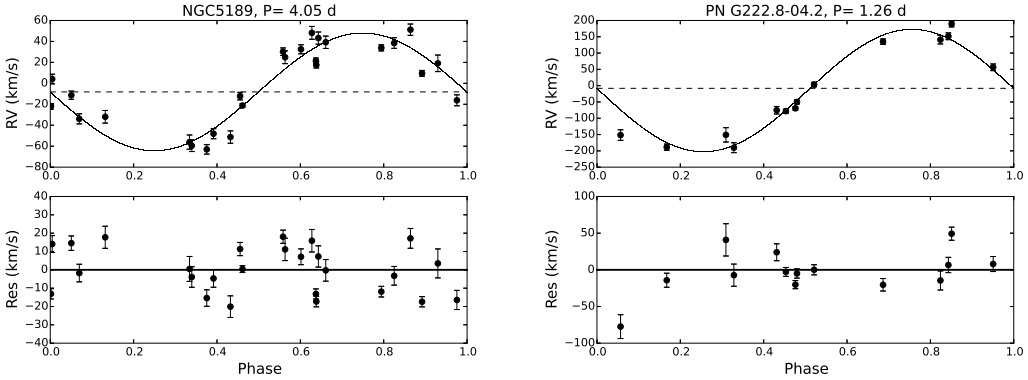

Fig. 1: SALT RSS RV curves of NGC 5189 (left upper panel, 26 epochs) and PN G222.8−04.2 (right upper panel, 14 epochs) fitted with circular orbits (solid curve). The residuals (lower panels) show a larger amplitude scatter than seen in non-[WR] post-CE CSPNe (e.g. Boffin et al. 2012), but is consistent with wind variability that is also encountered in massive WR RV curves (e.g. Foellmi et al. 2003). The larger residuals in PN G222.8−04.2 are probably the result of the cross-correlation method reacting to the high degree of line profile variability.

The anomalously large 4.05 d orbital period for NGC 5189 suggests that the orbital periods of other post-CE [WR] CSPNe may also be several days or months. This may be a result of the [WR] primary and its extended atmosphere requiring more space in its orbit. Such binaries can only be found from RV monitoring and much work remains to find them. If this is correct, then we would expect close binaries containing the progeny of [WC] stars, PG1159 stars, to have similarly wide orbits.

This work incorporates SALT observations taken under programmes 2013-2-RSA-005 and 2014-2-SCI-060. We thank Tony Moffat for helpful discussions.

References

Balick, B. & Frank, A. 2002, ARA&A, 40, 439
Boffin, H. M. J., Miszalski, B., Rauch, T., et al. 2012, Science, 338, 773
Bond, H. E. 2000, in Astronomical Society of the Pacific Conference Series, Vol. 199, Asymmetrical Planetary Nebulae II: From Origins to Microstructures, ed. J. H. Kastner, N. Soker, & S. Rappaport, 115
Ciardullo, R. & Bond, H. E. 1996, AJ, 111, 2332
Corradi, R. L. M., Sabin, L., Miszalski, B., et al. 2011, MNRAS, 410, 1349
De Marco, O. 2009, PASP, 121, 316
De Marco, O., Hillwig, T. C., & Smith, A. J. 2008, AJ, 136, 323
De Marco, O. & Soker, N. 2002, PASP, 114, 602
Foellmi, C., Moffat, A. F. J., & Guerrero, M. A. 2003, MNRAS, 338, 360
González Pérez, J. M., Solheim, J.-E., & Kamben, R. 2006, A&A, 454, 527
Hajduk, M., Zijlstra, A. A., & Gesicki, K. 2010, MNRAS, 406, 626
Hillwig, T. C., Bond, H. E., Afşar, M., & De Marco, O. 2010, AJ, 140, 319
Ivanova, N., Justham, S., Chen, X., et al. 2013, A&A Rev., 21, 59
Jones, D. 2015, arXiv:1507.05447
Manick, R., Miszalski, B., & McBride, V. 2015, MNRAS, 448, 1789
Miszalski, B., Acker, A., Moffat, A. F. J., Parker, Q. A., & Udalski, A. 2008, A&A, 488, L79
Miszalski, B., Acker, A., Moffat, A. F. J., Parker, Q. A., & Udalski, A. 2009a, A&A, 496, 813
Miszalski, B., Acker, A., Parker, Q. A., & Moffat, A. F. J. 2009b, A&A, 505, 249
Miszalski, B., Corradi, R. L. M., Boffin, H. M. J., et al. 2011a, MNRAS, 413, 1264
Miszalski, B., Corradi, R. L. M., Jones, D., et al. 2011b, in Asymmetric Planetary Nebulae 5 Conference, 328
Miszalski, B., Crowther, P. A., De Marco, O., et al. 2012, MNRAS, 423, 934
Miszalski, B., Jones, D., Rodríguez-Gil, P., et al. 2011c, A&A, 531, A158
Phillips, J. P. & Reay, N. K. 1983, A&A, 117, 33
Sabin, L., Vázquez, R., López, J. A., García-Díaz, M. T., & Ramos-Larios, G. 2012, Rev. Mexicana Astron. Astrofis., 48, 165
Santander-García, M., Rodríguez-Gil, P., Corradi, R. L. M., et al. 2015, Nature, 519, 63
Todt, H. & Hamann, W.-R. 2015, these proceedings
Todt, H., Kniazev, A. Y., Gvaramadze, V. V., et al. 2013, MNRAS, 430, 2302
Tovmassian, G., Yungelson, L., Rauch, T., et al. 2010, ApJ, 714, 178
Udalski, A., Szymanski, M. K., Soszynski, I., & Poleski, R. 2008, Acta Astron., 58, 69

Vikram Dwarkadas: I am a bit suspicious of the correlation between morphology and binarity. Are you saying that single stars should give only spherical (circular) PNe? Are there exceptions? Are there any nebulae which show jets and other structures where you did *not* find a binary? What does it mean?

Brent Miszalski: Yes, there have been some and these could potentially be wider binaries or mergers. That said, we've had considerable success finding new close binaries based on these trends, the stronges of which are jets, so they do seem to hold up to scruting.

Generally, it is believed that spherical/elliptical PNe are formed by single stars, but this has not been fully explored yet.

Gloria Koenigsberger: Among the light curves you showed, are there eclipses? Have radii been determined?

Brent Miszalski: Yes, several of the known systems have eclipses and many have been modelled to determine accurate orbital parameters including stellar radii.

Norbert Langer: Even if the PNe show jets, couldn't the central stars be single? As many central stars are *very* short period binaries, one would expect that many others would have merged in the common envelope (CE) phase.

Brent Miszalski: Yes, that is a possibility covered by jet models, e.g. a shredded companion in Nordhaus et al. (2006). A merger would be consistent with non-detection of close binaries, but is exceptionally difficult to prove observationally.

Dany Vanbeveren: Lev Yungelson once claimed that finding one in a 1000 double WDs with a combined mass $\geq 1.4\,M_{\odot}$ that will merge within a Hubble time will highly increase the probability that the double degenerate (DD) scenario is a very valuable scenario to form SN Ia. It is fantastic that you found the candidate.

Brent Miszalski (center) with Andy Pollock (left) and Victor Gómez-Gonzáles (right)

Wolf-Rayet Stars
W.-R. Hamann, A. Sander, H. Todt, eds.
Potsdam: Univ.-Verlag, 2015
URL: http://nbn-resolving.de/urn:nbn:de:kobv:517-opus4-84268

Planetary nebulae and Their Central Stars in X-rays

M. A. Guerrero[1]
[1] *Instituto de Astrofísica de Andalucía, IAA-CSIC, Spain*

Two types of X-ray sources are mostly found in planetary nebulae (PNe): point sources at their central stars and diffuse emission inside hot bubbles. Here we describe these two types of sources based on the most recent observations obtained in the framework of the *Chandra* Planetary Nebula Survey, ChanPlaNS, an X-ray survey targeting a volume-limited sample of PNe. Diffuse X-ray emission is found preferentially in young PNe with sharp, closed inner shells. Point sources of X-ray emission at the central stars reveal magnetically active binary companions and shock-in stellar winds.

1 High-Energy Processes in PNe

Planetary nebulae (PNe) are the result of the evolution of low- and intermediate-mass stars, i.e., those with initial masses in the range $1 - 8\,M_{\odot}$. These stars evolve through the asymptotic giant branch (AGB) phase losing mass through a slow (10–30 km s^{-1}) and dense wind that clears the interstellar medium. Once the star evolves off towards the post-AGB phase, it develops a fast wind ($v_{\infty} \simeq 500$–4000 km s^{-1}; e.g., Guerrero & De Marco 2013) that interacts with the previously ejected AGB material. This wind-wind interaction results in a double-shock pattern: a forward shock sweeps up the AGB material, producing a sharp shell, whereas a backward shock thermalizes and heats the fast wind, creating an adiabatically shocked "hot bubble" with temperatures 10^7–10^8 K. At the same time, the newly exposed stellar core (CSPNe) begins to ionize the swept-up AGB material, creating a PN (Kwok et al. 1978; Balick 1987).

The physical processes that lower the temperature of the gas within the hot bubble take place at its outer interface with the cold (10^4 K) nebular shell. Instabilities formed in the wind-wind interaction zone break up the swept-up shell into dense clumps and filaments that locally absorb heat inside the outer edge of the hot bubble and inject cold material into it (Stute & Sahai 2006; Toalá & Arthur 2014). Thermal conduction can boost these effects, additionally reducing the temperature of the shocked stellar wind and favoring the evaporation of cold nebular material into the hot bubble (e.g., Soker 1994; Steffen et al. 2008; Toalá & Arthur 2014,2015).

The central stars of PNe (CSPNe) are also expected to be sources of X-ray emission. Hot CSPNe with effective temperature in excess of 100,000 K exhibit photospheric emission in the soft X-ray domain (e.g., NGC 6853, Hoare et al. 1995). Otherwise, the coronal emission from an unresolved late-type companion star can produce (harder) X-ray emission (e.g., the G5 III companion of the CSPN of LoTr 5, Montez et al. 2010). Finally, the variability in the stellar wind of the CSPNe can also produce shocks, resulting in shock-in winds as is the case of massive OB and Wolf-Rayet stars (Lucy & White 1980; Gayley & Owocki 1995).

Fig. 1: *Chandra* X-ray (blue) and *HST* optical Hα (red) and [N II] (green) composite-color picture of NGC 6543. This PN shows diffuse X-ray emission inside the innermost nebular shell and a point-source of X-ray emission at its CSPN (Chu et al. 2001; Guerrero et al. 2001).

2 X-ray Observations of PNe

Early *Einstein*, *EXOSAT*, and *ROSAT* observations of PNe resulted in many cases in misidentifications of the emitting source and ambiguous interpretation of the emission mechanism. These problems were emphasized in 2001 by a comprehensive analysis of the entire *ROSAT* archive of pointed observations of over 60 PNe (Guerrero et al. 2000). The few detections of diffuse X-ray emission indicated that this emission is not universal among PNe or that their X-ray luminosities had to be much lower than predicted.

Far better more sensitive, *Chandra* and *XMM-Newton* observations have revealed the presence of diffuse X-ray emission within PNe (Figure 1), lending strong support to the interacting stellar winds

model of PN formation (e.g., Kastner et al. 2000; Guerrero et al. 2002). *Chandra* has been particularly successful in the detection of point-sources at CSPNe (Guerrero et al. 2001; Ruiz et al. 2013).

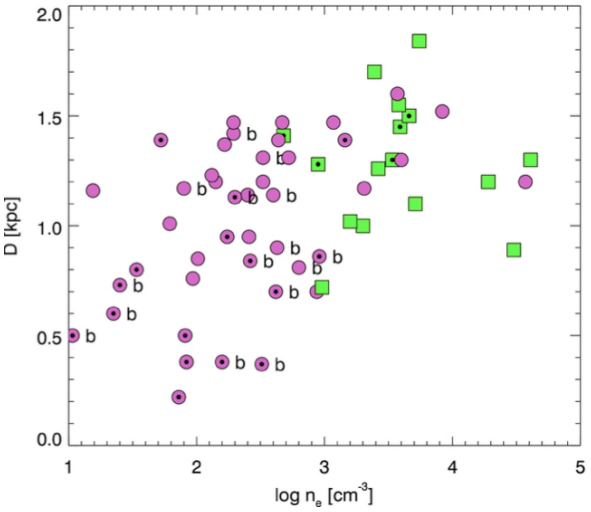

Fig. 2: Distribution with distance and density of the ChanPlaNS detections (green) and non-detections (purple) of diffuse X-ray emission among PNe. A point inside the symbol indicates that the CSPN also emits in X-rays. The "b" letter indicates the bipolar morphology of the PN. Adapted from Freeman et al. (2014).

Building over multiple programs for X-ray observation of individual sources, the PN community has joined efforts into the *Chandra* Planetary Nebulae Survey (ChanPlaNS) aiming at the X-ray study of a volume-limited sample of PNe within 1.5 kpc of the Sun. So far, ChanPlaNS has been awarded with a Cycle 12 Program and a Cycle 14 Large Project to observe 45 PNe with total observing times $\simeq$1 Msec. Including archival *Chandra* observations, the present sample of ChanPlaNS PNe amounts up to 60 sources. ChanPlaNS has provided important insight into the X-ray emission from PNe (Kastner et al. 2012; Freeman et al. 2014) and their CSPNe (Montez et al. 2015).

2.1 Hot Bubbles in PNe

Diffuse X-ray emission has now been detected in almost 20 PNe (Freeman et al. 2014). This emission is preferentially found in PNe with sharp, closed inner shells and is rarely associated with bipolar PNe (Gruendl et al. 2006). Diffuse X-rays are mostly associated with compact ($\lesssim$0.15 pc in radius) and high nebular electron densities ($\gtrsim$2500 cm^{-3}, see Figure 2). This suggests that the detection of diffuse X-ray emission is limited to relatively young ($\lesssim$5,000 yrs) PNe (Ruiz et al. 2013; Freeman et al. 2014). The X-ray-emitting gas has temperatures (1–3)$\times10^6$ K (Ruiz et al. 2013, and references therein), well below the expectations from adiabatic shocks.

2.2 Point-Sources at CSPNe

ChanPlaNS has also detected point-sources at the CSPNe of $\sim$20 PNe (Montez et al. 2015). Some of these detections correspond to the soft photospheric emission from hot CSPNe, but in most cases they display relatively hard, $\gtrsim$0.5 keV X-ray emission. The plasma properties and energetic budget allow us to identify at least two different types of X-ray sources among CSPNe.

The X-ray luminosity of CSPNe (Figure 3) reveals a group of CSPNe that follows the typical X-ray to bolometric luminosity relationship of massive stars, $L_{\rm X}/L_{\rm bol} \simeq 10^{-7}$. The X-ray emission in massive stars is caused by shocks inside their unstable radiatively-driven stellar winds, the so-called shock-in winds. A similar physical scenario may cause the "hard" X-ray emission in CSPNe, as their stellar winds are also known to exhibit variability (Prinja et al. 2007; Guerrero & De Marco 2013).

The other group of CSPNe show X-ray luminosities above the $L_{\rm X}/L_{\rm bol} \simeq 10^{-7}$ relationship. In these cases, there is either evidence of binarity or the properties of the X-ray emission, indicating plasmas at higher temperatures, are similar to those from active companion stars (Montez et al. 2015). In those cases, the X-ray emission is enhanced up to the critical limit $L_{\rm X}/L_{\rm bol} \simeq 10^{-3}$, suggesting that during the binary evolution the CSPN transferred angular momentum to the companion to spin up its rotation rate and increase its coronal activity.

2.3 Other Sources of X-rays in PNe

Besides the diffuse X-ray emission from hot bubbles and point-source emission from CSPN, there are two other sources of X-ray emission in PNe. Born-again PNe, with their rejuvenated fast stellar winds blowing away highly processed material, have revealed to be sources of soft diffuse X-ray emission. Complex wind-interaction processes and even charge-exchange reactions can be responsible for this emission (Guerrero et al. 2012; Toalá et al. 2015).

X-ray emission can be caused by strong shocks associated to fast collimated outflows, as those seen, e.g., in IC 4634 (Guerrero et al. 2008). So far, however, only the fast, 1000 km s^{-1} collimated outflow of Hen 3-1475 has been detected by its X-ray emission (Sahai et al. 2003).

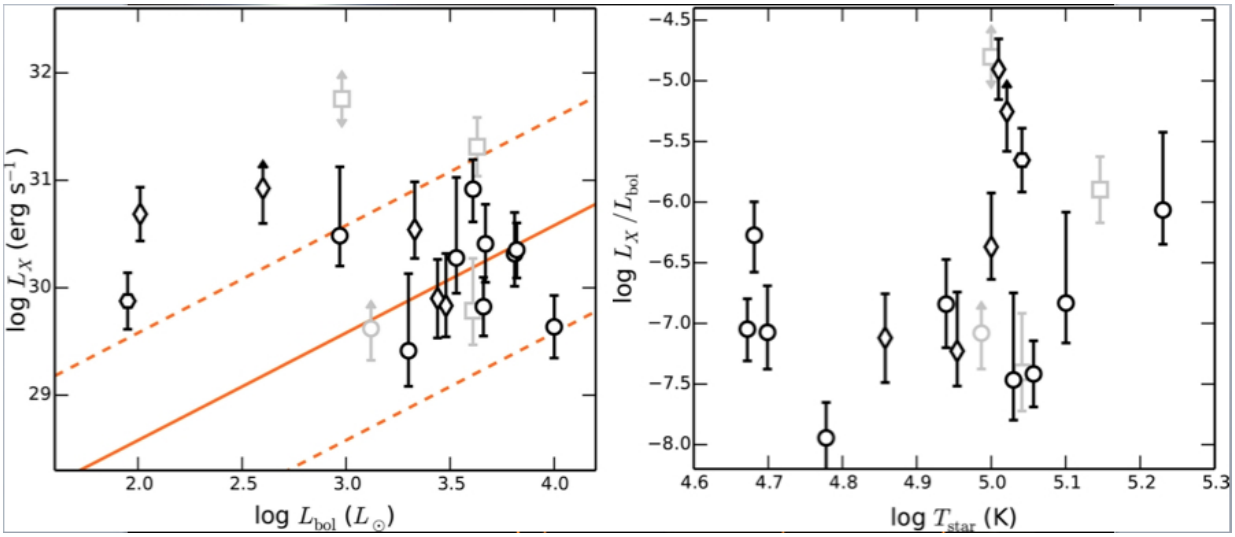

Fig. 3: X-ray luminosity of the CSPNe in the ChanPlaNS sample plotted with respect to the star bolometric luminosity (left) and effective temperature (right).

3 Future X-ray Observations of PNe

Most of our knowledge about the hot gas content of PNe comes from low-dispersion CCD spectroscopy. To date, high-dispersion X-ray spectroscopy has only been obtained for two PNe, BD+30°3639 (Yu et al. 2009) and NGC 6543 (Guerrero et al. 2015). These observations provide invaluable information. The high-dispersion *Chandra* LETG observation of BD+30°3639 shows bright H-like resonance lines of O VIII and C VI and He-like triplets of Ne IX and O VII, but weak/absent lines of N VII. This indicates that the chemical abundances of the hot gas are similar to those of the [WC] central star, i.e. mixing is not operating. In the future, *Athena* XIFU will allow routinely high-dispersion X-ray spectroscopic observations of a large number of PNe to test the efficiency of heat conduction and mixing inside the hot bubbles of PNe.

References

Balick, B. 1987, AJ, 94, 671
Chu, Y.-H., Guerrero, M.A., Gruendl, R.A., Williams, R.M., & Kaler, J.B. 2001, ApJ, 553, L69
Freeman, M., Montez, R., Jr., Kastner, J.H., et al. 2014, ApJ, 794, 99
Gayley, K.G., & Owocki, S.P. 1995, ApJ, 446, 801
Gruendl, R.A., Guerrero, M.A., Chu, Y.-H., Williams, R.M. 2006, ApJ, 653, 339
Guerrero, M.A., Chu, Y.-H., & Gruendl, R.A. 2000, ApJS, 129, 295
Guerrero, M.A., Chu, Y.-H., Gruendl, R.A., Williams, R.M., & Kaler, J.B. 2001, ApJ, 553, L55
Guerrero, M.A., Gruendl, R.A., & Chu, Y.-H. 2002, A&A, 387, L1
Guerrero, M.A., & De Marco, O. 2013, A&A, 553, 126
Guerrero, M.A., Miranda, L.F., Riera, A. 2008, ApJ, 683, 272
Guerrero, M.A., Ruiz, N., Hamann, W.-R. et al. 2012, ApJ, 755, 129
Hoare, Melvin G.; Barstow, Martin A.; Werner, Klaus; Fleming, Thomas A. 1995, MNRAS, 273, 812
Kastner, J.H., Montez, R., Jr, Balick, B. et al. 2012, AJ, 144, 58
Kastner, J.H., Soker, N., Vrtilek, S.D., Dgani, R. 2000, ApJ, 545, L57
Kwok, S., Purton, C.R., & Fitzgerald, P.M. 1978, ApJ, 219, L125
Lucy, L.B., & White, R.L. 1980, ApJ, 241, 300
Montez, R., Jr., De Marco, O., Kastner, J.H., Chu, Y.-H. 2010, ApJ, 721, 1820
Montez, R., Jr., Kastner, J.H., Balick, B. 2015, ApJ, 800, 8
Prinja, R.K., Hodges, S.E., Massa, D.L., Fullerton, A.W., Burnley, A.W. 2007, MNRAS, 382, 299
Ruiz, N., Chu, Y.-H., Gruendl, R.A., Guerrero, M.A., Jacob, R., Schönberner, D., & Steffen, M. 2013, ApJ, 767, 35
Sahai, R., Kastner, J.H., Frank, A., Morris, M., & Blackman, E.G. 2003, ApJ, 599, 87
Stute, M., & Sahai, R. 2006, ApJ, 651, 882
Toalá, J.A., & Arthur, S.J. 2014, MNRAS, 443, 3486
Toalá, J.A., & Arthur, S.J. 2015, submitted to MNRAS
Toalá, J.A., Guerrero, M.A., Todt, H. et al. 2015, ApJ, 799, 67
Yu, Y.S., Nordon, R., Kastner, J.H. et al. 2009, ApJ, 690, 440

Kenji Hamaguchi: Do you see any correlation of the temperature of the diffuse plasma with stellar wind velocity?

Martín Guerrero: Not really. The plasma temperature tends quickly to an asymptotic value at 1-2 $\times$ 10^6 K. The reason is that the bubble grows and the stellar wind mechanical luminosity diminishes, even though its terminal velocity increases.

Vikram Dwarkadas: Have you seen any correlation between X-ray emission and binarity, or morphological features that suggest binarity (as in Brent's talk)? Have you looked for this in your sample?

Martín Guerrero: The sample of binary CSPNe is very recent, so there is very little overlap with the ChanPlaNS sample. Binary CSPNe evolve so that they produce broken nebular shells which cannot contain the hot gas inside.

Gloria Koenigsberger: Is NGC 6543 a binary?

Martín Guerrero: The precessing-like jet features point to a binary star, but so far there is no direct evidence. B. Miszalski confirms this point from this RV studies. These can be difficulted by wind variability.

WR colliding winds, dust

Wolf-Rayet Stars
W.-R. Hamann, A. Sander, H. Todt, eds.
Potsdam: Univ.-Verlag, 2015
URL: http://nbn-resolving.de/urn:nbn:de:kobv:517-opus4-84268

Dust formation in carbon-rich Wolf-Rayet colliding winds

I. Cherchneff
Departement Physik, Universität Basel, Switzerland

Carbon-rich Wolf-Rayet stars are efficient carbon dust makers. Despite the strong evidence for dust formation in these objects provided by infrared thermal emission from dust, the routes to nucleation and condensation and the physical conditions required for dust production are still poorly understood. We discuss here the potential routes to carbon dust and the possible locations conducive to dust formation in the colliding winds of WC binaries.

1 Introduction

An infrared (IR) excess radiated by circumstellar dust grains was detected decades ago in the wind of the most evolved, carbon-rich Wolf-Rayet (WC) stars (Allen et al. 1972; Gehrz & Hackwell 1974; Cohen et al. 1975). WC stars are characterised by strong mass loss, emission lines of ionised carbon and relatively low effective temperatures for evolved massive stars. Dust was only detected in the latest sub-types (WC7-WC9) of the WC sequence and the spectral energy distribution (SED) was reproduced by assuming graphite as a potential condensate located in a circumstellar shell (Williams et al. 1987). Photometric data often reveal variability in the IR emission indicative of an episodic dust formation event, like in the case of WR 140 (Williams et al. 1978, 1987) and WR 137 (Williams et al. 1985). These dust production events are periodic and relates to binarity and the nature of the orbit. Both WR 140 and WR 137 are binary systems with eccentric orbits and dust forms at periastron passage where the stellar winds collide and induce shocks and gas density enhancement in the wake of the shocked region. Several successive dust formation events have been observed in WR140 at times corresponding to the system orbiting period of ~ 8 years (Monnier et al. 2002; Williams et al. 2009).

While some WC stars appear as periodic dust makers, others seem to form dust steadily, as the prototype star WR 104, which shows spiral dust plumes. These plumes or pinwheels were first observed by Tuthill et al. (1999, 2008) in the near-IR, and orbit parameters were deduced from the geometry of the pinwheels. The analysis revealed that WR 104 was characterised by a circular orbit (Tuthill et al. 2008). Furthermore, the IR flux dis not show significant variability over long epochs, which suggested the dust formation rate was steady and constant at all orbital phases (Tuthill et al. 2008). Typical dust formation rates for both episodic and constant dust makers are in the range $10^{-9} - 10^{-6}$ $M_{\odot}$/yr. The percentage of carbon depleted in dust is $\sim 1\%$ for most stars (Cohen 1991; Zubko 1998). These rather modest rates argue for a negligible contribution of WC stars to the dust budget in galaxies, although their contribution may increase at high redshift (Dwek & Cherchneff 2011).

Despite the wealth of IR data of dust thermal emission in WC winds, we have yet no clue on the exact nature of the dust and how it so efficiently forms. The WC wind environment is harsh. Intense ultraviolet (UV) stellar radiation fields pervade the steady winds while shocks control the wind-collision region (WCR). The growth of carbon grains was studied by Zubko et al. (1992) and Zubko (1998). These studies considered the growth of small charged grains with supra-thermal velocities in a shell located at a large distance from the star and assumed the growth occurred from carbon ions impinging on the charged grains. However, no clue was provided as to how the initial population of small carbon grains formed in the first place. The final grain size was in the range $90 - 200$ Å. In contrast, the modelling of mid-IR imaging of WC systems indicates the presence of much larger grains. In the case of WR 112, a massive episodic dust maker, Marchenko et al. (2002) derive a grain radius of ~ 0.5 μm, in line with the size value derived from ISO data (Chiar & Tielens 2001).

Another study based on a chemical kinetic approach showed that the formation of carbon dust at large radii in the homogeneous wind was unlikely (Cherchneff et al. 2000). The study considered both neutral and ion chemical processes as well as photoprocesses induced by the stellar radiation field. Owing to the low gas densities at large radii, the ionisation fraction of the gas remained high and the chemistry was inefficient at building up molecules and dust clusters. An increase by several orders of magnitude of the gas density led to the formation of chemical species and very small clusters. Therefore, clumps or high density regions in the wind are a prerequisite to the production of dust in WC stars, and these dense regions are naturally found in the shocked environment of the WCR. Interestingly, a recent study of the formation of dust in the gas ejected by core-collapse supernovae leads to a similar conclusion: a clumpy ejecta is required to explain the production of the large amount of dust recently detected in supernova remnants (Sarangi & Cherchneff 2015).

In this review, we discuss the types of carbon clusters that form in WC stars, the possible chemical

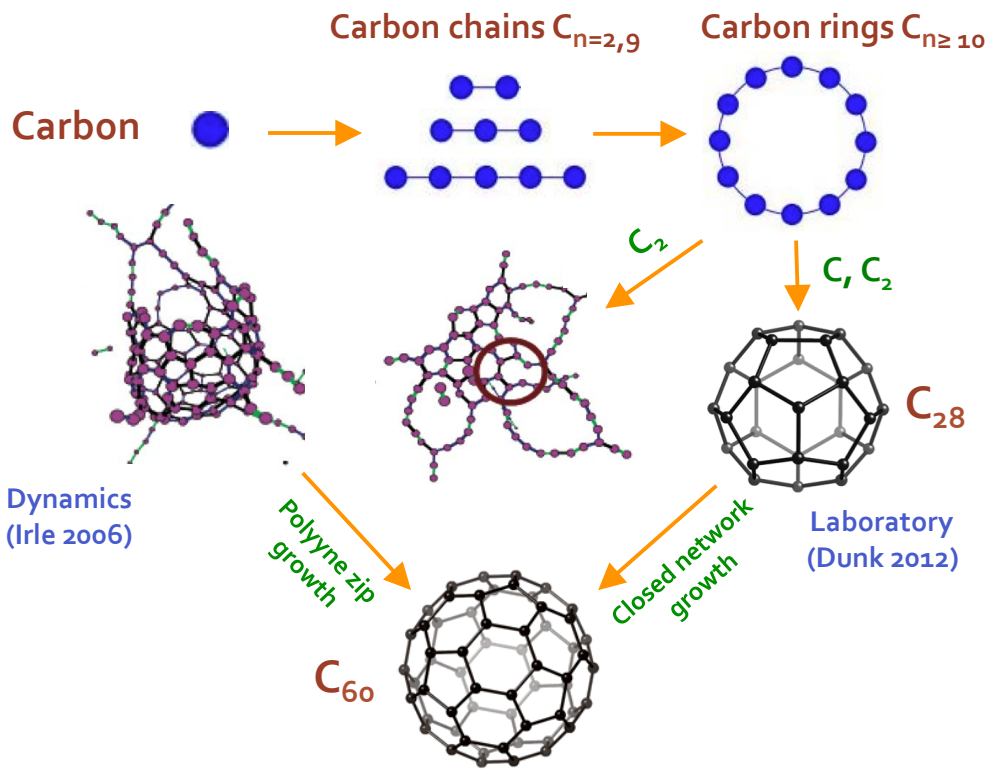

Fig. 1: Carbon cluster intermediates and routes involved in the synthesis of fullerene, C_{60}, for a hydrogen-poor environment.

routes leading to dust, and the gas conditions required for dust nucleation and condensation in the WCR.

2 The routes to carbon dust

Because a WC star has ripped off most of its hydrogen envelope, the WC wind is primarily helium- and carbon-rich. In laboratory experiments and under hydrogen-poor conditions, carbon grains form from a sequence of specific chemical routes that lead to the nucleation of carbon clusters. These routes resemble the formation pathways of the closed-cage carbon clusters of fullerenes that were first identified in a condensing carbon vapour devoid of hydrogen by Kroto et al. (1985). As shown in Figure 1, neutral carbon atoms react through radiative association reactions to form the first carbon chain molecules, which are linear until they reach C_{10}. For the latter, a monocyclic ring has the lowest energy and is thus the most stable structure (Jones 1999). These rings continue to grow through reaction and inclusion of atomic carbon and C_2 in their structure. A recent study of laser-induced carbon vapour condensation by Dunk et al. (2012a) shows that the smallest fullerene molecule is C_{28}, which contains four units of triple-fused pentagons arranged in tetrahedral symmetry. This small stable closed cage continues to growth to larger sizes through the closed network growth mechanism proposed and tested in the laboratory by Dunk et al. (2012b). In this scenario, the inclusion of C_2 molecules into the cage with no cage rupture controls the fullerene growth.

Other carbon cluster growth processes have been proposed by dynamic studies (Irle et al. 2006), whereby the steady addition of C_2 molecules through irreversible processes under non equilibrium conditions and at high gas temperature (2000 K) leads to the formation of mixed aromatic-cyclic carbon clusters as illustrated in Figure 1. Nucleation of polycyclic structures from entangled polyyne chains first happens, followed by growth supported by ring condensation of carbon chains and ring attachment to the hexagon and pentagon containing nucleus, and finally, the cage closure where polyyne chains reach over the opening and close the structures.

It is not yet clear if these two formation paths ex-

clude one another. The absence of hydrogen fosters the synthesis of carbon chains and rings, with the possible creation of aromatic units. The detection of several sub-peaks along with the clear signature of carbon rings in mass spectra may indicate that clusters including aromatic structures also form in carbon vapour experiments (Dunk et al. 2012a). In any case, these routes will prevail in the hydrogen-poor WC stellar winds.

The companion of WC stars is usually an O-type star. The possibility of some hydrogen being present in the WCR gas may thus not be excluded. Hydrogen would occupy the valence bonds of small carbon chains and lead to the formation of hydrocarbons, including acetylene, C_2H_2. The formation processes of soot in acetylenic flames involve the recombination of propargyl radicals (C_3H_3) to form phenyl (C_6H_5) and benzene (C_6H_6), the growth of polycyclic aromatic hydrocarbons (PAHs) through acetylene addition and hydrogen abstraction, and PAH coalescence and coagulation to produce amorphous carbon grains (Cherchneff 2011). Therefore, a dual chemistry may take place in WC colliding winds, which includes the pure carbon routes leading to fullerenes and the aromatic pathways leading to the formation of small amorphous carbon clusters. These clusters will further grow from coalescence, coagulation, and the deposition of atoms, ions, and chemical species on the surface once a critical grain size of several tens of Ångströms is reached.

In the context of WC stars, these chemical routes to carbon remain speculative but are supported by a few observations of the aromatic C-C stretch transitions at ~ 6.2 μm and ~ 7.7 μm detected in absorption and emission in WR 104, WR 118, WR 112 and WR 48a (Chiar & Tielens 2001; Chiar et al. 2002).

3 The wind-collision region

With stellar temperatures of ~ 20000 K for the latest WC types, the UV radiation field that pervades the wind is strong and most helium and all carbon atoms are ionised at 2 $R_\star$(van Der Hucht et al. 1986). The presence of helium ions in the wind is detrimental to the synthesis of molecules and strongly inhibits the nucleation stage of dust formation in any circumstellar environment (Lepp et al. 1990; Cherchneff et al. 2000; Sarangi & Cherchneff 2013). Therefore, the production of molecules and dust clusters from the gas phase is severely hampered.

The efficient dust production by WC stars points to locations where the gas ionisation fraction remains low, the densities are high and the gas temperatures are sufficiently low. These conditions are found in the wake of the WCR as shown in Figure 2, which illustrates the geometry of the WCR in a plane perpendicular to the orbit of the binary system (Williams 2010). In regions of the compressed wind that are downstream from the stagnation point, the gas is expected to have densities higher than those of the homogeneous WC wind.

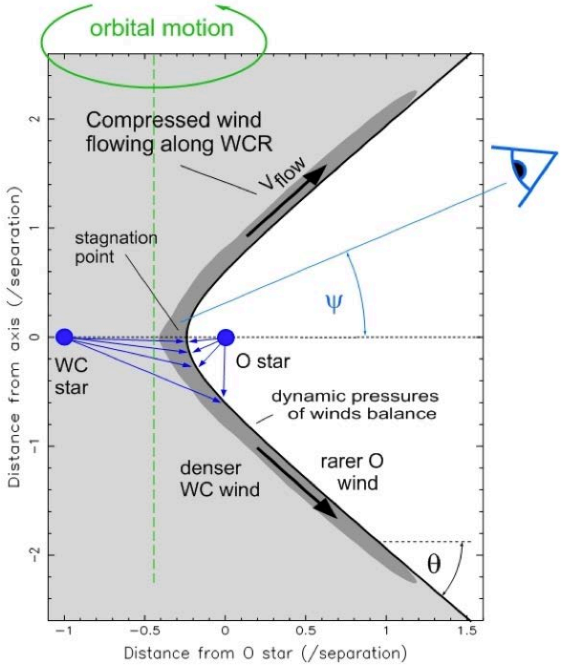

Fig. 2: The wind colliding region in the plane perpendicular to the orbit [taken from Williams (2010)]. The dust forms downstream from the compressed wind flow.

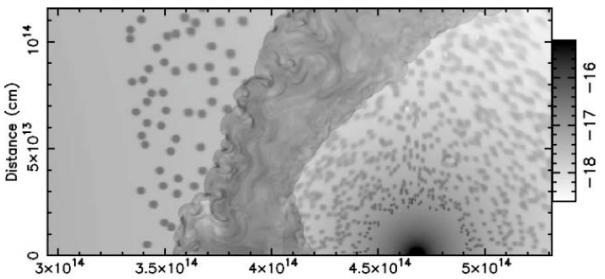

Fig. 3: Gas density in the wind-collision region of WR 140 [taken from Pittard (2007)]. Both stellar winds are clumpy.

Figure 3 represents the WCR of the WR 140 binary from the hydrodynamical study by Pittard (2007). Both stellar winds are assumed to be

clumpy and the study follows the evolution of the inhomogeneities in the WCR. The turbulent regions of the compressed wind are shown in dark grey, and are characterised by gas densities in the range $\sim 10^6 - 10^8\,\mathrm{cm}^{-3}$. These values are sufficient to drive the recombination of helium ions and the nucleation of carbon dust by radiative association processes, which are usually temperature independent (Cherchneff et al. 2000). Therefore, when the downstream post-shock gas temperature drops to values in the range $1000 - 2000\,\mathrm{K}$ for which vaporisation of carbon dust can be excluded, carbon grains will likely nucleate and grow by coalescence, coagulation and surface deposition of carbon atoms and ions.

An interesting point resulting from the study by Pittard (2007) relates to mixing in the WCR. According to the model, the inhomogeneities initially present in the clumpy wind of WR140 (shown on the left-hand side of Figure 3) are disrupted by the WCR, which tends to smooth out the clumps initially present in both winds. If so, hydrogen-poor gas will mix with hydrogen-rich gas in the WCR. Such a mixing will drive the dual chemistry controlling carbon dust formation as described in §2. Depending on the location in the WCR, some regions will be richer in hydrogen than others, and will trigger the formation of acetylene, hydrocarbons and aromatic species, as in the shocked wind of carbon-rich AGB stars (Cherchneff 2012). Another important component acting on the WCR is the stellar radiation field of the companion star, which penetrates the WCR and generates photo-processes that play an active role in the local carbon chemistry. These photo-processes will generate a chemistry controlled by ions and radicals, which will have an uncertain impact on the nucleation of carbon dust. Warm, dense media sheltered from harsh radiation field are usually cradles of dust production, so the regions penetrated by intense UV radiation may not be conducive to dust formation, whatever their hydrogen content.

Hydrogen will not only affect the chemistry of carbon dust but the entire gas chemistry in the WCR. The occurrence of hydrogen in the WCR will trigger a chemistry that resembles that of the carbon-rich zone of supernova ejecta. There, Raleigh-Taylor instabilities induced by the explosion have mixed some hydrogen from the supergiant wind with the heavy elements, including carbon, that are present in the outermost ejecta zone. Species such as CO, CS and HCO^+ have recently been detected with ALMA in the young supernova remnant SN1987A (Matsuura, private communication). The molecules CO and CS were predicted to form in physico-chemical models of the outermost, hydrogen-free ejecta zone of supernova explosions (Sarangi & Cherchneff 2013), and similarly, these two molecules have been predicted to be present in the dense WC winds (Cherchneff et al. 2000). The chemistry responsible for the build up of molecules, carbon clusters and dust in the WCR should then be complex and include neutral-neutral and ion-molecule processes in hydrogen-poor or -rich gas.

4 Outlook

If the WCR in WC binaries is efficient at producing carbon dust, the evolution and fate of these grains are still unclear. Marchenko et al. (2002) derived that ~ 20 % of the grains formed in the innermost region of WR 112 survived to the outermost arcs. Destruction of grains may be the result of the strong UV radiation field combined with sputtering due to the high drift velocities of charged grains (Zubko 1998). Despite the lack of study of dust formation and destruction in the WCR of WC stars, results from supernova studies show that carbon is resilient to sputtering in shocks (Nozawa et al. 2010; Silvia et al. 2010; Biscaro & Cherchneff 2015). Therefore, WCR-produced carbon grains that are larger than several hundreds of Ångströms will likely be incorporated to the local interstellar gas.

The synthesis of molecules such as CO and CS is predicted to go hand in hand with that of dust in the post-shocked gas of WCRs. By-products of dust condensation (fullerenes, aromatics) might also be present in the gas phase. Yet no detection of molecular species has been reported for dust-forming WC stars. Observational attempts to characterise the molecular content of the wind-collision region of WC binaries are therefore highly desirable.

References

Allen, D. A., Swings, J. P. & Harvey, P. M. 1972, A&A, 20, 333
Biscaro, C., & Cherchneff, I. 2015, A&A, submitted
Cherchneff, I., Le Teuff, Y.H., Williams, P.M., & Tielens, A.G.G.M. 2000, A&A, 357, 572
Cherchneff, I. 2011, EAS, 46, 177
Cherchneff, I. 2012, A&A, 545, A12
Chiar, J. E., & Tielens, A.G.G.M. 2001, ApJ, 550, L207
Chiar, J. E., Peeters, E. & Tielens, A.G.G.M., 2001, ApJ, 550, L207
Cohen, M., Kuhi, L. V. & Barlow, M. J. 1975, A&A, 40, 291
Cohen, M. 1991, IAUS 143, 323
Dwek, E., & Cherchneff, I. 2011, ApJ, 727, 63
Dunk, P. W., Kaiser, N. K., Mulet-Gas, M. et al.. 2012a, J. Am. Chem. Soc. 2012, 134, 9380
Dunk, P. W., Kaiser, N. K., Hendrickson, C. L et al. 2012b, Nature Communications, 3, 855
Gehrz, R. D., & Hackwell, J.A. 1974, ApJ, 194, 619
Irle, S., Zheng, G., Wang, Z. & Morokuma, K. 2006, J. Phys. Chem., 110, 14531

Jones, R O. 1999, J.Chem.Phys., 110(11), 5189
Kroto, H.W., Health, J.R., O'Brien, S.C., Curl & R.F. B Smalley, R.E. 1985, Nature, 318, 162
Lepp, S., Dalgarno, A. & McCray R. 1990, ApJ, 358, 262
Marchenko, S. V, Moffat, A. F. J. & Vacca W. D. 2001, ApJ, 565, L59
Monnier, J D., Tuthill, P. G. & Danchi, W. C. 2002, ApJ, 567, 137
Nozawa, T., Kozasa, T., & Nozomu, T. 2010, ApJ, 713, 356
Pittard, J M. 2007, ApJ, 660, L141
Sarangi, A. & Cherchneff, I. 2013, ApJ, 776, 107
Sarangi, A. & Cherchneff, I. 2015, A&A, 575, 95
Silvia, D. W., Smith, B. D. & Shull, J. M. 2010, ApJ, 715, 1575
Tuthill P. G., Monnier J.D. & Danchi W.C., 1999, Nature, 398, 486
Tuthill P. G., Monnier J.D., Lawrance N. et al., 2008, ApJ, 675, 698
van der Hucht K., Cassinelli J.P. & Williams P.M., 1986, A&A 168, 111
Williams, P. M., Beattie, D. H., Lee, T. J. et al. 1978, MNRAS, 185, 467
Williams, P. M., Longmore, A. J., van der Hucht, K. A., et al. 1985, MNRAS, 215, 23
Williams, P. M., van der Hucht, K. A. & The, P. S. 1985, A&A, 182, 91
Williams, P. M., Marchenko, S. V., Marston, A. P et al. 2009, MNRAS, 395, 1749
Williams, P. M. 2010, in "Stellar Winds in Interaction", editors T. Eversberg and J.H. Knapen, Arrábida.
Zubko, V. G., Marchenko, S. V. & Nugis, T. 1992, A&AT, 3, 131
Zubko, V. G. 1998, MNRAS, 295, 109

Wolf-Rayet Stars
W.-R. Hamann, A. Sander, H. Todt, eds.
Potsdam: Univ.-Verlag, 2015
URL: http://nbn-resolving.de/urn:nbn:de:kobv:517-opus4-84268

The colliding-wind WC9+OB system WR 65 and dust formation by WR stars

P. M. Williams[1] **& K. A. van der Hucht**[2]
[1] *University of Edinburgh, Royal Observatory, Edinburgh, United Kingdom*
[2] *SRON Utrecht and University of Amsterdam, The Netherlands*

Observations of the WC9+OB system WR 65 in the infrared show variations of its dust emission consistent with a period near 4.8 yr, suggesting formation in a colliding-wind binary (CWB) having an elliptical orbit. If we adopt the IR maximum as zero phase, the times of X-ray maximum count and minimum extinction to the hard component measured by Oskinova & Hamann fall at phases 0.4–0.5, when the separation of the WC9 and OB stars is greatest. We consider WR 65 in the context of other WC8–9 + OB stars showing dust emission.

1 Identification of WR 65 as a colliding-wind binary

From 1.2–9.7-μm infrared (IR) photometry, Williams et al. (1987) found that WR 65 (LSS 3319), like most of the then-known WC9 stars, had a circumstellar dust cloud which, in this case, absorbed and re-emitted about 3% of its stellar flux in the IR.

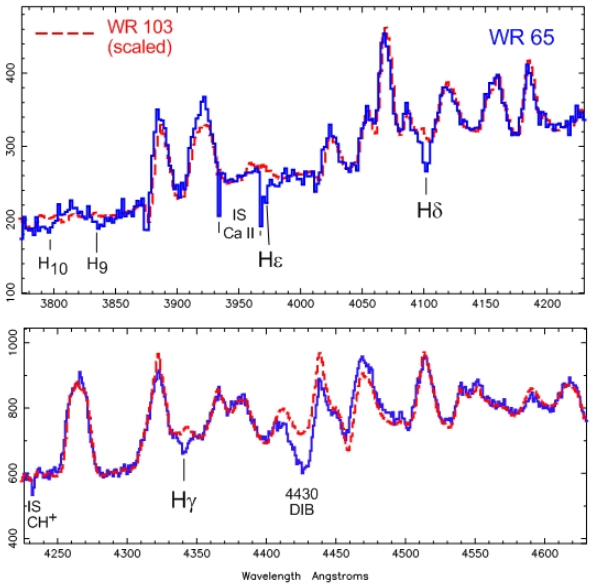

Fig. 1: Spectra of WR 65 and WR 103 observed with the ESO EMMI on the NTT. The interstellar lines in WR 65 are stronger on account of its higher reddening ($A_v \simeq 7.6$).

Spurred by the episodic formation of dust by the WC7+O5 binary WR 140 (Williams et al. 1990) at periastron when its components reached a critical separation, we suggested (Williams & van der Hucht 1992) that the persistent WC8–9 dust makers might also be binaries, but in circular orbits having stellar separations conducive to dust formation – as beautifully confirmed by the rotating dust 'pinwheel' made by the prototypical WC9 dust maker WR 104 (Tuthill et al. 1999) – and we began a spectroscopic survey of WC9 stars in the blue using the SAAO 1.9-m telescope and the ESO NTT to search for absorption lines attributable to OB companions. Amongst the WC9 stars found (Williams et al. 2005) to show Balmer absorption lines in their spectra was WR 65 (Fig. 1), making it a candidate SB2. From dilution of the WC9 emission-line spectrum, van der Hucht (2001) suggested that the OB star was 0.4 mag. brighter than the WC9 star.

Evidence that WR 65 might be a colliding-wind binary came from the variable X-ray emission observed by Oskinova & Hamann (2008). They fitted a $2T2N_H$ plasma model, and found that the column density to the 'hard' component varied with epoch, consistent with the movement of an embedded colliding-wind source in the WC9 wind.

We therefore examined the IR photometric history of WR 65. Besides the 1983 observations in Williams et al. (1987) and those by Pitault et al. (1983) in 1982, eight more sets of $JHKL$ photometry were observed at ESO during 1990–93 as part of another programme. Four of these observations were taken on successive nights in 1991 and the last of them shows brightening (0.09-mag. in JHK, less in L and M), suggesting a mini-outburst like those observed from WR 137 (Williams et al. 2001). Latterly, iJK_s were observed in the DENIS survey (Epchtein et al. 1999) in 1998 and JHK_s in the 2MASS survey (Skrutskie et al. 2006) in 1999. These J and K_s magnitudes are significantly brighter than any of the earlier J and K, suggesting occurrence of an IR maximum in 1998–99. For comparison with the L data, we determined [3.6] magnitudes from the pipeline-processed *Spitzer* IRAC frames observed in 2004 and 2012. We searched for a period in these rather sparse data following Lafler & Kinman (1965). As the dates of the DENIS and 2MASS K_s band observations were different from those of the [3.6] magnitudes, there is a small difference in the cadence of the K/K_s and $L/[3.6]$ datasets and we sought matching minima in the L–K statistic Θ from both of them. This is shown in Fig. 2, from which we adopt a tentative period of 4.8±0.2 yr.

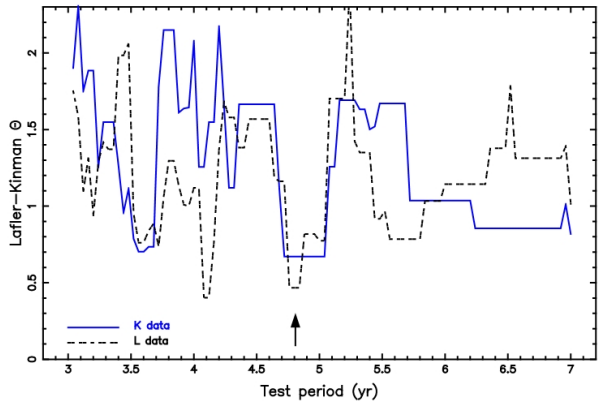

Fig. 2: Lafler-Kinman period search on K and L-band photometry with adopted 4.8-yr period marked (↑).

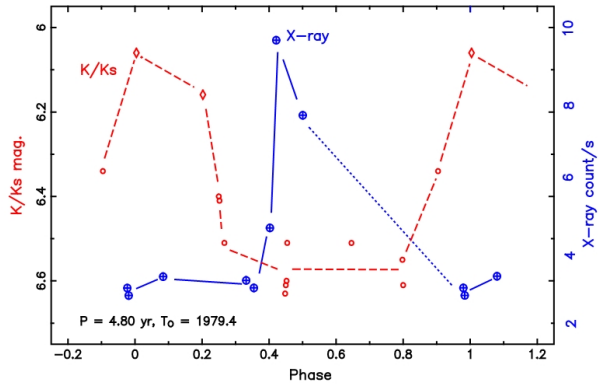

Fig. 3: IR K (○) and K_s (◇) photometry together with X-ray count rates (⊕) from Oskinova & Hamann (2008), all phased to a period of 4.8 yr and taking 1979.4 as zero. (The straight lines joining the observations are drawn just to guide the eye.)

The phased IR (K) magnitudes and X-ray count rates are plotted in Fig. 3 using our IR period of 4.8 yr and arbitrarily adopting $T_0 = 1979.4$, so as to place the brightest IR flux, the DENIS observation, at phase zero. The IR maximum is broad but poorly defined; more IR observations are needed to define the IR light curve and period. At minimum, the IR spectral energy distribution (SED) still shows dust emission. The X-ray emission remains faint during IR maximum, when the wind-collision source would have been most deeply buried in the WC9 wind. The rise to X-ray maximum corresponding to minimum column density to the 'hard' component occurs as the system approaches apastron, but the steepness of the rise suggests that we are observing it through a hole in the WC9 wind formed by the O star wind sweeping through our line-of-sight. Further X-ray observations are needed to define the light curve and map the wind-collision region (WCR). Above all, we need an orbit to allow a comprehensive picture to be developed. The period near 4.8 yr makes WR 65 a tractable source for a study on a reasonable timescale; it is the only WC9 system known to have periodically variable dust emission (cf. Table 1).

Colliding stellar winds can also produce non-thermal radio emission, observable if the WCR lies sufficiently far out in the stellar wind, especially in wide, long period systems. The observable emission may vary during the orbit (Dougherty & Williams 2000) in systems of intermediate period. Our suggested 4.8-yr period lies in that range. The marginal 3.5-cm detection (0.37±0.14 mJy) by Leitherer et al. (1997) is consistent with the free-free emission from the wind of WR 65, 0.35 mJy, which we estimated by scaling the observed flux from γ Vel to the distance (3.3 kpc) of WR 65. The date of the observation corresponds to phase 0.31 on our suggested ephemeris, when the low X-ray flux implies that the wind extinction to the WCR and any non-thermal radio source is still high. We suggest that re-observation at a more favourable phase may well reveal non-thermal radio emission from WR 65.

Tab. 1: Wolf-Rayet stars showing periodic dust emission. The IR photometric periods of WR 140 and WR 137 are supported by RV periods (Fahed et al. 2011; Lefèvre et al. 2005) and that of WR 98a by its pinwheel rotation (Monnier et al. 1999).

WCE (P/yr)	WC7 (P/yr)	WC8 (P/yr)	WC9 (P/yr)
HD 36402	WR 140	WR 98a	**WR 65**
(4.7)[a]	(7.94)[b]	(1.54)[c]	(∼ 4.8)
WR 19	WR 137	WR 48a	
(10.1)[d]	(13.05)[e]	(∼ 32)[f]	

Refs: [a] Williams et al. (2013); [b] Williams et al. (1990); [c] Williams et al. (2003); [d] Veen et al. (1998); [e] Williams et al. (2001); [f] Williams et al. (2012)

2 Relation to other persistent dust-making WC8–9 stars.

From their 'pinwheel' images of WR 104, Tuthill et al. (2008) showed that the dust was made by stars moving in a circular orbit and that the IR flux, and hence dust formation rate, did not vary with orbital phase. Also, the long-term (1982–1997) photometric history of WR 104 from 14 observations show a dispersion of only $\Delta K = 0.04$ mag. We have compiled long-term IR photometric histories of 12 other WC8–9 dust-makers. The only one to show systematic variability is WR 112 (CRL 2104), which may have a period near 12.3 yr (Fig. 4). This period is

consistent with its dust 'pinwheel' and a plausible expansion velocity (Marchenko et al. 2002) with a revised distance ~ 2 kpc (Marchenko & Moffat 2007). The low orbital eccentricity inferred from its dust 'pinwheel' is consistent with the low amplitude of its IR variations compared with those ($\Delta K > 1$) of the high eccentricity binaries WR 140 (Fahed et al. 2011) and WR 19 (Williams et al. 2009).

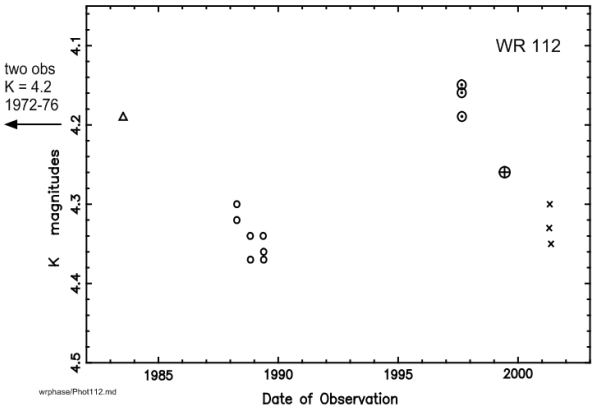

Fig. 4: Photometry of WR 112 from Williams et al. (1987) (△), new observations at ESO (○) and with the Carlos Sánchez IR Telescope (⊙), from the 2MASS Catalogue (⊕) and by Kimeswenger et al. (2004) (×). We do not have dates for the earliest observations by Merrill & Stein (1976) and Allen et al. (1977).

The long-term photometry of another 'heavy' dust maker, WR 118, shows a dispersion $\Delta K = 0.11$ mag. but with no apparent periodicity. Two other dust-making WC9 stars found to have Balmer absorption lines (Williams et al. 2005), WR 59 and WR 69, have smaller dispersions in their photometric histories and we suggest that they are binaries in (near) circular orbits. The same might apply to other WC9 stars showing steady dust emission, which might be undetected binaries, especially if the WC9 stars are more luminous than currently thought, making it harder to detect composite spectra. There is a strong case for RV studies of these objects to search for orbital motion.

References

Allen, D. A., Hyland, A. R., Longmore, A. J., et al. 1977, ApJ, 217, 108

Dougherty, S. M. & Williams, P. M. 2000, MNRAS, 319, 1005

Epchtein, N., Deul, E., Derriere, S., et al. 1999, A&A, 349, 236

Fahed, R., Moffat, A. F. J., Zorec, J., et al. 2011, MNRAS, 418, 2

Kimeswenger, S., Lederle, C., Richichi, A., et al. 2004, A&A, 413, 1037

Lafler, J. & Kinman, T. D. 1965, ApJS, 11, 216

Lefèvre, L., Marchenko, S. V., Lépine, S., et al. 2005, MNRAS, 360, 141

Leitherer, C., Chapman, J. M., & Koribalski, B. 1997, ApJ, 481, 898

Marchenko, S. V. & Moffat, A. F. J. 2007, in Astronomical Society of the Pacific Conference Series, Vol. 367, Massive Stars in Interactive Binaries, ed. N. St.-Louis & A. F. J. Moffat, 213

Marchenko, S. V., Moffat, A. F. J., Vacca, W. D., Côté, S., & Doyon, R. 2002, ApJ, 565, L59

Merrill, K. M. & Stein, W. A. 1976, PASP, 88, 874

Monnier, J. D., Tuthill, P. G., & Danchi, W. C. 1999, ApJ, 525, L97

Oskinova, L. M. & Hamann, W.-R. 2008, MNRAS, 390, L78

Pitault, A., Epchtein, N., Gomez, A. E., & Lortet, M. C. 1983, A&A, 120, 53

Skrutskie, M. F., Cutri, R. M., Stiening, R., et al. 2006, AJ, 131, 1163

Tuthill, P. G., Monnier, J. D., & Danchi, W. C. 1999, Nature, 398, 487

Tuthill, P. G., Monnier, J. D., Lawrance, N., et al. 2008, ApJ, 675, 698

van der Hucht, K. A. 2001, New A Rev., 45, 135

Veen, P. M., van der Hucht, K. A., Williams, P. M., et al. 1998, A&A, 339, L45

Williams, M. & van der Hucht, K. A. 1992, in Astronomical Society of the Pacific Conference Series, Vol. 22, Nonisotropic and Variable Outflows from Stars, ed. L. Drissen, C. Leitherer, & A. Nota, 269

Williams, P. M., Chu, Y.-H., Gruendl, R. A., & Guerrero, M. A. 2013, MNRAS, 431, 1160

Williams, P. M., Kidger, M. R., van der Hucht, K. A., et al. 2001, MNRAS, 324, 156

Williams, P. M., Rauw, G., & van der Hucht, K. A. 2009, MNRAS, 395, 2221

Williams, P. M., van der Hucht, K. A., Morris, P. W., & Marang, F. 2003, in IAU Symposium, Vol. 212, A Massive Star Odyssey: From Main Sequence to Supernova, ed. K. van der Hucht, A. Herrero, & C. Esteban, 115

Williams, P. M., van der Hucht, K. A., Pollock, A. M. T., et al. 1990, MNRAS, 243, 662

Williams, P. M., van der Hucht, K. A., & Rauw, G. 2005, in Massive Stars and High-Energy Emission in OB Associations, ed. G. Rauw, Y. Nazé, R. Blomme, & E. Gosset, 65–68

Williams, P. M., van der Hucht, K. A., & Thé, P. S. 1987, A&A, 182, 91

Williams, P. M., van der Hucht, K. A., van Wyk, F., et al. 2012, MNRAS, 420, 2526

Andy Pollock: Does the correlation between ΔK and e imply common physical conditions at periastron?

Peredur Williams: I think it is more a question of the contrast of conditions between periastron and the rest of the orbit.

Anthony (Tony) Moffat: In recent NIR surveys for Galactic WR stars, a large number of WC9 stars is showing up in the central part of the Galaxy. This may lead to a more significant source of dust in the Galaxy than thought previously. Do you agree?

Peredur Williams: Yes, there are dust makers amongst the newly discovered WC9 stars, but to get the significance of the contributions of WC9 stars to dust in the Galaxy, I would want to know the number of AGB stars in the same volume.

Wolf-Rayet Stars
W.-R. Hamann, A. Sander, H. Todt, eds.
Potsdam: Univ.-Verlag, 2015
URL: http://nbn-resolving.de/urn:nbn:de:kobv:517-opus4-84268

Modelling colliding wind binaries in 2D

T. Hendrix & R. Keppens
CmPA, Department of Mathematics, KU Leuven, Celestijnenlaan 200B, 3001 Leuven, Belgium

We look at how the dynamics of colliding wind binaries (CWB) can be investigated in 2D, and how several parameters influence the dynamics of the small scale structures inside the colliding wind and the shocked regions, as well as in how the dynamics influence the shape of the collision region at large distances. The parameters we adopt are based on the binary system WR98a, one of the few Wolf-Rayet (WR) dusty pinwheels known.

1 Physical setup

We model the binary system WR98a based on the information available from current observations. The system was identified to contain a WC8 or WC9 star (Williams 1995). Monnier (1999) revealed that WR98a forms a "pinwheel nebula" in infrared, suggesting an OB type companion. We model the WR star as a WC9 subtype and use a mass of $M_{\rm WR} = 10M_\odot$ (Sander 2012), mass-loss rate $\dot{M}_{\rm WR} = 0.5 \times 10^{-5}$ M$_\odot$ yr^{-1} (Monnier 2002), and wind velocity $v_{\infty,\rm WR} = 900$ km s^{-1} (Williams 1995). The OB type companion is less constrained. We assume $M_{\rm OB} = 18M_\odot$, $\dot{M}_{\rm OB} = 0.5 \times 10^{-7}$ M$_\odot$ yr^{-1}, and $v_{\infty,\rm OB} = 2000$ km s^{-1}. The momentum flux ratio of the winds is then $\eta = \dot{M}_{\rm OB} v_{\infty,\rm OB} / \dot{M}_{\rm WR} v_{\infty,\rm WR} = 2.22 \times 10^{-2}$, thus the WR outflow dominates. With an orbital period of 565 days (Williams 2003), the semi-major axis length of the orbit is $a = 6.08 \times 10^{13}$ cm.

2 Numerical setup

Following the methodology we employed in Hendrix & Keppens (2014) and Hendrix (2015), we use the gas+dust hydrodynamics module of the `MPI-AMRVAC` code. The dynamics is described by using the coupled gas+dust fluid equations (see Hendrix & Keppens 2014; Porth 2014). Additionally, optically thin radiative cooling of the gas fluid is taken into account in several simulations as an additional term to the energy equation (van Marle & Keppens 2011). In the outflow of WR stars the high metallicity strongly enhances the radiative cooling. We use an adequately adapted table by Mellema & Lundqvist (2002). The physical domain between x,$y \in$ [-160a,160a] is simulated on a Cartesian grid with an effective resolution of 81920×81920 by using 11 adaptive mesh refinement (AMR) levels. The winds are introduced through boundaries at the terminal radii (5×10^{12} cm and 3×10^{12} cm for the WR and OB star, respectively). The stars follow their (counter-clockwise) Keplerian orbit. We use two tracer fluids that are advected with the flow to separately track the material ejected by the stars. The mixing of WR and OB material can be quantified by the product of the tracers.

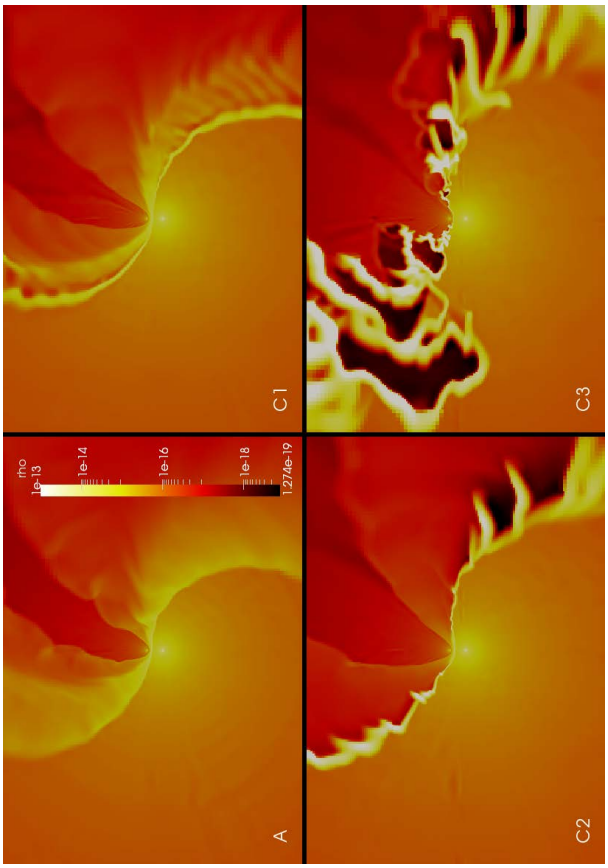

Fig. 1: Densities in A and 3 versions of C with reduced cooling at $t = 0.25$. The region shown is the central (8×10^{14} cm) × (5.6×10^{14} cm).

3 (Ir)relevance of 2D simulations

A model of a colliding wind binary can be seen to be inherently 3D due to the orbital motion of two stars and the non-axisymmetric interaction of the stellar winds. Nevertheless, the question can be asked to which degree it would be useful to consider a similar model in 2D. Due to the non-axisymmetric features the model is preferentially evaluated in a Cartesian grid. This however means that the outflow, for which the density in our model is calibrated at the terminal velocity radius, is no longer physically representative in 2D. In practice this means that density and

pressure patterns may not correspond to the structures in 3D. For colliding wind binary simulations this specifically has influence on the density structures (and contrasts). Radiative cooling is strongly influenced in these cases. 3D simulations will be discussed in Hendrix et al. (2015), however when compared to 2D simulations we see that radiative cooling produces great differences in the obtained results. Nevertheless, 2D simulations are less demanding, and therefore many dynamical simulations of WR (and other) binaries are performed in 2D. Typically, to obtain results that are more comparable to full 3D setups, η is altered so that $\eta_{2D} = \sqrt{\eta_{3D}}$. In this way, the contact discontinuity (CD) of the wind collision shock is located at the same distance between the stars in 2D as in 3D. While this is typically done to obtain a shock location and structure resembling the 3D situation (close to the wind collision region (WCR)), the actual physical correctness of the values is given up. In the following we use 2D simulations to investigate the importance of several parameters on the formation of structures in the WCR and the subsequent outflow. Table 1 gives an overview of the parameters used.

Tab. 1: Parameters in the simulations: the adiabatic index γ, the ellipticity of the orbit (ϵ), the physical domain size (x and y axis length), radiative cooling (C) or not (NC), and the number of AMR levels. Model C represents 3 simulations with altered cooling.

	A	B	C	D	E
γ	5/3	4/3	5/3	4/3	5/3
ϵ	zero	zero	zero	0.7	zero
Domain	$320a$	$320a$	$320a$	$1280a$	$1280a$
Cooling	NC	NC	C	NC	NC
levels	11	11	11	13	13

3.1 Radiative cooling

In 2D, partly due to the switching from η to $\sqrt{\eta}$, densities are typically higher, and therefore the effect of radiative cooling is strongly enhanced. This results in spurious instabilities, something which may not be seen in 3D. To obtain shock structures comparable to those in 3D and to investigate the effect of radiative cooling, we artificially lower the cooling rate to a factor ω. Figure 1 gives a comparison at $t = 0.25$ between setup A and the different cases of C with ω=0.01, 0.05, and 0.2. When going from no cooling to the weakest cooling, ω=0.01, we see that the cooling compresses the region between the WR-shock and the CD. Also, instabilities cause this region (specifically on the trailing arm) to collapse in dense ripples with lower density regions in between. When cooling is further enhanced ($\omega = 0.05$, case C2) the WR-shock and the CD have fully collapsed and produce a compressed region with significantly enhanced densities. Ripples can be seen to form barbed structures in both the trailing and leading shock, however the effect is stronger in the trailing arm where an alternating high and low density pattern forms. The density ratio in these regions is as strong as 5–6 orders of magnitude. For even higher cooling ($\omega = 0.2$, case C3) the instabilities are even further enhanced. The high density structures form a broad region as they move out due to random unstable motions when the thermal instability takes place. If we would increase cooling even further, the motion of the thermal unstable wind collision zone can become so violent that the shock region temporarily or continuously starts to move between (and over) the two stars. Such movement may result in strong mass removal from the stellar surface.

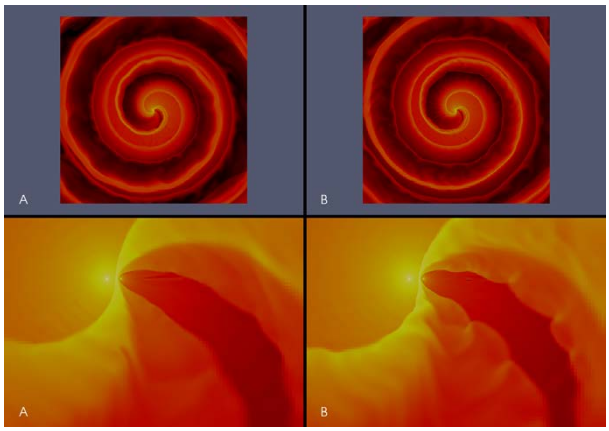

Fig. 2: Densities in A and B at $t = 3.0$, using the same colour scale as figure 1. The top figures show the full domain, the bottom figures are zoomed in near the binary.

A 3D setup of C with $\omega = 1.0$ results in structures in between C2 and C3. The effect of cooling on the dynamics and structure formation in CWB is found to be of great importance to realistically model the WCR in CWB. Local density enhancements due to thermal instabilities are of great importance towards obtaining dust formation. While typical WR wind conditions are unlikely to form significant amounts of dust, density enhancements due to shocks and radiative cooling enhance the formation rate.

3.2 The adiabatic index γ

We are interested to see if a change from $\gamma = 5/3$ (typically assumed in similar setups) to $\gamma = 4/3$ influences the structure formation and mimics some of the effects typically associated with radiative cooling. Figure 2 compares setups A and B at $t = 3.0$. Results can be seen to be similar. The large scale structures and densities in the spirals are nearly identical. If we look at the inner WCR (shown in the bottom panels of figure 2) we see that B with

$\gamma = 4/3$ is slightly more unstable, producing "knots" on the OB-shock and high densities ripples on the CD. While the rippling instabilities B are similar as to cases with weak cooling ($\omega = 0.01$ in section 3.1), the effect is less strong. The ripples of the CD produces visible patterns on the large scale, however their effect on the large scale evolution is small.

3.3 Ellipticity

In the simulation D with elliptic orbit, the periastron passage occurs when the OB star is left of the WR star in the images. While the ellipticity in simulation D is significant at $\epsilon = 0.7$, except for being slightly lopsided, few important differences are seen between setups D and E. While average densities are higher on the periastron side than the apastron side, the density range is similar and no additional high density structures are formed. The density asymmetry is an effect of the orbital velocity of the OB star. This pattern has previously been predicted by the dynamical model of Parkin & Pittard (2008), however only the location of the CD is calculated in their model. A combination of cooling with ellipticity may potentially introduce stronger differences as the effectiveness of the thermal instability may vary based on orbital phase.

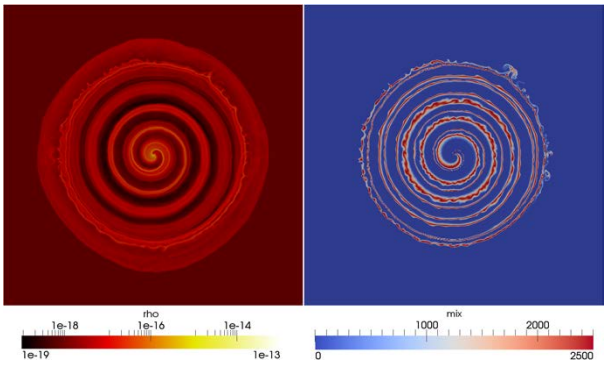

Fig. 3: Density profile (left) and the mixing (right) in E at $t = 6.3$. The entire physical domain is shown.

3.4 Mixing and large scale structures

The mixing zones, shown on large scale in figure 3 and closer to the binary in figure 4, are located around the CD. On the leading edge mixing is closely bound to the CD, while on the trailing edge a broad mixing layer is seen. High velocity and low density material is injected by the OB star. It is confined between the two CDs, causing the low density spiral pattern in figure 3. Because of the velocity shear between the two wind regions the CD is prone to Kelvin-Helmholtz instabilities (KHI). The wind motion is mostly radial. The transverse velocity $\vec{v} - (\vec{v} \cdot \hat{r})\hat{r}$ is parallel to the spiral pattern at larger distances. Interestingly the confined OB material has a much stronger transverse component: while 98% of the velocity of the WR wind is radial, this is only 75–87% for the OB wind. Furthermore, the confined OB material has a significant transverse velocity difference with the surrounding material, which causes shearing along the CD. After one spiral winding the mixing layer along the trailing CD begins to show the onset of a KHI. Nevertheless, on larger scale we see that the spiral stays stable. This extends the findings of Lamberts (2012), who found that a comparable setup was stable in their smaller domain.

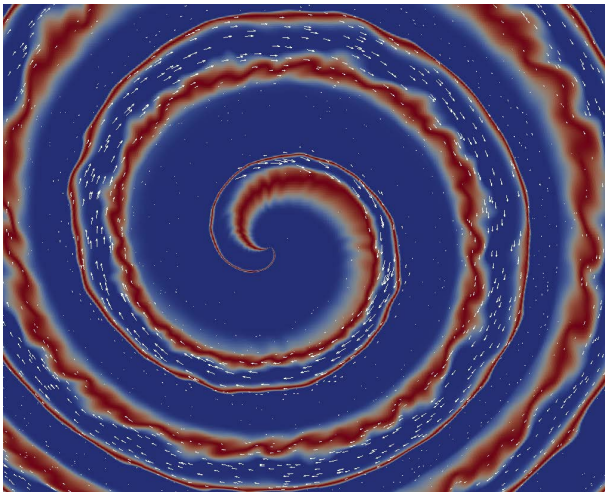

Fig. 4: Mixing in the central region of E at $t = 6.75$. The colour scale is the same as in figure 3.

References

Hendrix, T. & Keppens, R. 2014, A&A, 562, A114
Hendrix, T., van Marle, A. J., Keppens, R., Camps, P., & Meliani, Z. 2015, in preparation
Hendrix, T. e. a. 2015, A&A, 575, A110
Lamberts, A. e. a. 2012, A&A, 546, A60
Mellema, G. & Lundqvist, P. 2002, A&A, 394, 901
Monnier, J. D. e. a. 1999, ApJ, 525, L97
Monnier, J. D. e. a. 2002, ApJ, 566, 399
Parkin, E. R. & Pittard, J. M. 2008, MNRAS, 388, 1047
Porth, O. e. a. 2014, ApJS, 214, 4
Sander, A. e. a. 2012, A&A, 540, A144
van Marle, A. J. & Keppens, R. 2011, Computers and Fluids, 42, 44
Williams, P. M. e. a. 1995, MNRAS, 275, 889
Williams, P. M. e. a. 2003, in IAU Symposium, Vol. 212, , 115

Andy Pollock: Is the hot shocked gas also formed here encased by the dust spiral which might account for the absence of observed X-rays from many of these systems?

Tom Hendrix: No, I don't think that is the case in general, as the X-ray source is probably located in between the stars in the wind collision region, while dust is formed much further away in the interaction region (at 20 AU from the stars in these simulations).

Jesús A. Toalá: Why do you have the dust-emission zone coincident with the lowest density region? It seems weird for me!

Tom Hendrix: We see that the dust is formed in the inner wind collision region at the contact discontinuity (CD) where material from the two stars is being mixed. In this region the densities are high. However, at larger distances (further out than the outer dust forming limit), these regions are perturbed by instabilities. The dust, which was formed at the CD surrounding the low-density region, is then transported and mixed into the low-density region at larger distances. Hence, the presence of the dust in the low-density region is a result of dynamics, and the dust is not formed in the low-density region.

Jose Groh: If I understood correctly, your plan is to do post-processing radiative transfer using the output of the hydrodynamic simulations. But wouldn't you expect feedback effects from the dust onto the hydrodynamics?

Tom Hendrix: Yes! The dust, which is dynamically taken into account as an additional fluid in these simulation, influences the dynamics of the system, certainly when the dust-to-gas mass density ratios are as high as observed here (up to 0.33). In a recent paper (Hendrix & Keppens 2014, A&A, 562, A114) we demonstrated that dust can stabilise the Kelvin-Helmholtz instability (KHI) under certain conditions, and that the KHI strongly influences the density distribution of dust. We have not yet investigated the effect of dust on the other instabilities seen in the setup in full detail (thin-shell instability, Rayleigh-Taylor instability, and Richtmyer-Meshkov), but also there an effect on the dynamics can be expected depending on the setup.

Wolf-Rayet Stars
W.-R. Hamann, A. Sander, H. Todt, eds.
Potsdam: Univ.-Verlag, 2015
URL: http://nbn-resolving.de/urn:nbn:de:kobv:517-opus4-84268

Shaping the outflows of Wolf-Rayet stars

S. Mohamed[1], J. Mackey[2], N. Langer[2] & Ph. Podsiadlowski[3]
[1]*South African Astronomical Observatory, PO Box 9, Observatory 7935, Cape Town, South Africa*
[2]*Argelander Institut für Astronomie, Auf dem Hügel 71, Bonn D-53121, Germany*
[3]*Department of Astrophysics, University of Oxford, Keble Road, Oxford OX1 3RH, UK*

Wolf-Rayet (WR) stars lose copious amounts of mass and momentum through dense stellar winds. The interaction of these outflows with their surroundings results in highly structured and complex circumstellar environments, often featuring knots, arcs, shells and spirals. Recent improvements in computational power and techniques have led to the development of detailed, multi-dimensional simulations that have given new insight into the origin of these structures, and better understanding of the physical mechanisms driving their formation. We review three of the main mechanisms that shape the outflows of WR stars:

- interaction with the interstellar medium (ISM), i.e., wind-ISM interactions;
- interaction with a stellar wind, either from a previous phase of evolution or the wind from a companion star, i.e., wind-wind interactions;
- and interaction with a companion star that has a weak or insignificant outflow (e.g., a compact companion such as a neutron star or black hole), i.e., wind-companion interactions.

We also highlight the broader implications and impact of these circumstellar structures for related phenomena, e.g., for X-ray binaries and Gamma-ray bursts.

1 Introduction

Massive stars have dense, powerful stellar winds, particularly in the final stages of evolution during which mass-loss rates can be as large as $10^{-4}\mathrm{M}_\odot\,\mathrm{yr}^{-1}$ and winds as fast $3\,000\,\mathrm{km\,s}^{-1}$ (Lamers & Cassinelli 1999). These outflows not only remove mass from the outer layers of the star, but also carry away angular momentum. Both these effects can dramatically change the subsequent evolution of the star, determining its lifetime, the type of supernova (SN), if any, it will produce, and whether it will leave behind a neutron star or a black hole (Langer 2012; Smith 2014). The outflows also have a tremendous impact on the circumstellar environment, injecting large amounts of kinetic energy, and gas that is enriched with nuclear processed material and dust grains. Consequently, understanding the mass-loss process is crucial for stellar evolution calculations and population estimates alike, and also has broader implications for other areas in astronomy, e.g., affecting feedback and star formation, or the dust content and chemical evolution of galaxies.

The mass-loss mechanism and the nature of the stellar outflows, however, changes significantly as the stars evolve (see e.g., Lamers & Cassinelli 1999, and references therein). Massive O stars have radiatively driven, fast winds before passing through a red supergiant (RSG) or Luminous Blue Variable (LBV) phase where the winds are an order of magnitude slower and the mechanism that drives the outflows is less well understood. For the former, a combination of convective motions, pulsations, and radiation pressure on dust are thought to play a role, whereas the mass loss from LBVs is thought to be more episodic, giant eruptions. Eventually the stars transition to the Wolf-Rayet (WR) phase where the winds are once again radiatively driven, fast and hot. Each of these evolutionary transitions coupled with both internal and external processes (e.g., stellar and ISM magnetic fields; background radiation fields (such as from clusters) or from a companion; outflows from the ISM or a companion; stellar rotation or merger with a companion) results in the formation of complex circumstellar structures. Advances in both the resolution and sensitivity of the observations have revealed these structures in unprecedented detail. Similarly, advances in computing power have now made it possible to include a large number of physical processes in multi-dimensional models, enabling a more direct comparison with the observations.

In this review, we discuss three of the above processes that shape the outflows of massive stars, namely wind-ISM interactions, i.e., interaction of stellar outflows with the ISM; wind-wind interactions where the stellar wind collides with material either from a previous phase of evolution or the wind of a companion star; and wind-companion interactions where the outflow is shaped by a companion star that has a weak or insignificant outflow (e.g., a compact companion such as a neutron star or black hole). In Sec. 2, we highlight the role wind-ISM and wind-wind interactions play in the formation of 'ring nebulae' and bow shock arcs. The formation of spirals and equatorial, disk-like outflows through interaction with a binary companion are discussed in Sec. 3. We conclude by highlighting areas for further development and exploration in Sec. 4.

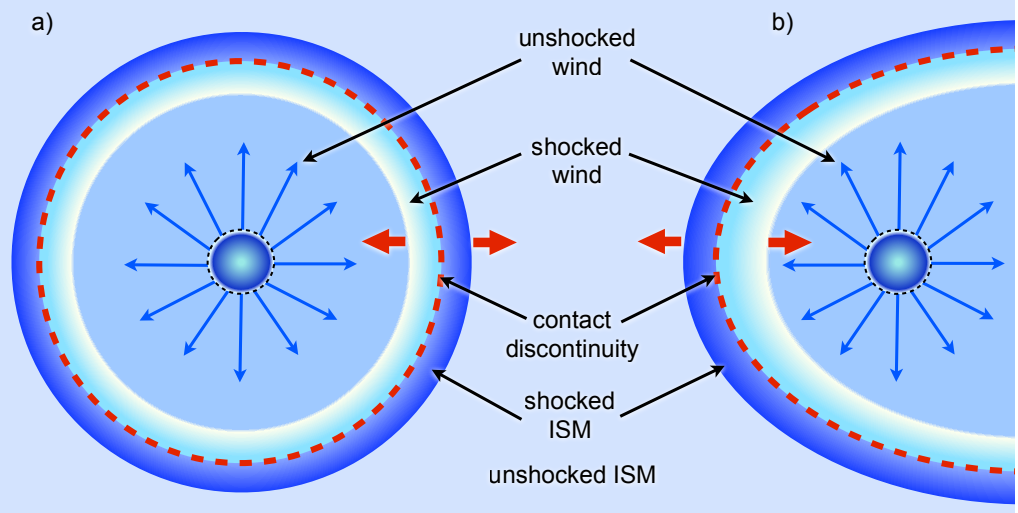

Fig. 1: The equilibrium morphology of the double shock structures that develop due to the supersonic interaction of a stellar outflow with its circumstellar environment. Four regions can be identified: the unshocked and shocked stellar wind separated from the shocked and unshocked surrounding medium (in this case the ISM) by a contact discontinuity. [a] If the star is stationary with respect to the surrounding medium, a ring-like shock structure forms, whereas, [b] if there is relative motion between the star and its environment, a cometary-shaped structure known as a bow shock results, with the apex pointing in the direction of motion. Note, the appearance of the latter depends on the viewing angle, e.g., if the relative motion is along the line-of-sight, the structure observed will look like [a] (see text for discussion). In both [a] and [b] the short, thick arrows in the direction of the ISM and unshocked stellar wind are the forward and reverse shocks, respectively.

2 The formation of ring and bow shock nebulae

When a stellar outflow encounters slower moving, dense circumstellar gas (either ISM or material ejected during an earlier phase of evolution), it sweeps up the material into a shell. As a result of the collision, the material in the interaction zone heats up and wants to expand, in the forward direction into the surrounding medium, driving a forward shock, and into the non-shocked wind material, resulting in a reverse shock. For a star that is non-stationary with respect to its surroundings, the shocks are distorted into a cometary arc-like structure known as a bow shock, pointing in the direction of motion (Weaver et al. 1977; Wilkin 1996; Lamers & Cassinelli 1999). The equilibrium, global morphology of ring and bow shock nebulae is shown in Fig. 1 (note that similar structures, planetary nebulae, are found around low/intermediate mass stars – see Guerrero et al., these proceedings).

The nebulae around WR stars are observed from radio to X-ray wavelengths (Gruendl et al. 2000; Arthur 2007; Toalá et al. 2015, and references therein). The detailed structure depends strongly on the properties (e.g., density, velocity, temperature, ionization degree etc.) of the material swept up by the WR wind, as demonstrated by, for example, models of WR-RSG versus WR-LBV wind interactions (e.g., García-Segura et al. 1996a,b; van Marle & Keppens 2012). The collision with slower, higher density RSG winds results in more highly radiative, unstable shocks than the faster, more ionized LBV winds. Similarly, wind-ISM interactions with fast winds are generally more stable than bow shocks with slow winds (Dgani et al. 1996). In addition to the Raleigh-Taylor instabilities that dominate wind-wind interactions, Kelvin-Helmholtz instabilities resulting from the shear induced by the stellar motion feature prominently in the bow shock models, as well as various thin shell instabilities (Brighenti & D'Ercole 1995; Blondin & Koerwer 1998). One of the most spectacular examples of a runaway WR star is WR 124, the star is moving at $180\,\mathrm{km\,s^{-1}}$ away from us (van der Sluys & Lamers 2003). Thus, the nebula around the star, M1-67, is a bow shock seen almost face-on (i.e. inclination close to 90°, cf. Fig. 2).

Several numerical studies of both wind-wind and wind-ISM interactions have used stellar evolution models as input for the time-evolution of the wind, from O star to WR phases (e.g., Dwarkadas 2007; Toalá & Arthur 2011, and review by Arthur et al., these proceedings). The result is the formation of multiple ring nebulae created with each successive slow-fast wind transition, a time-dependent trace of the mass lost over a star's life that could be used to constrain stellar evolution models. Simulated

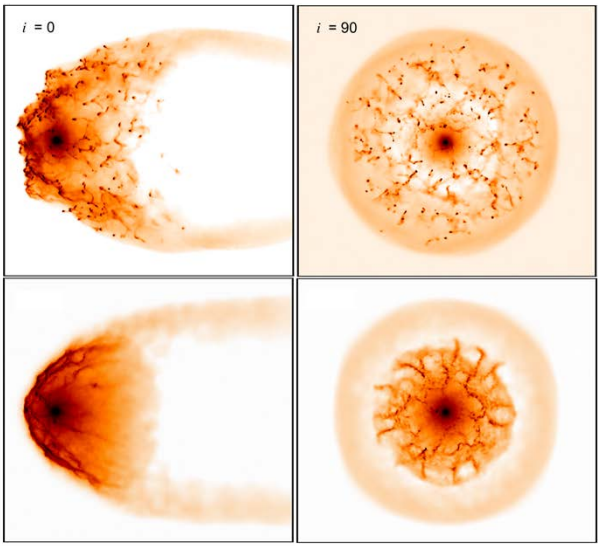

Fig. 2: 3D models of a RSG wind-ISM interaction: Hydrogen column densities (on a logarithmic scale) after 76 000 years seen at different inclination angles, i. The mass-loss rate ($3.1\times10^{-6}\,M_\odot\,yr^{-1}$) and RSG wind velocity ($17\,km\,s^{-1}$) were kept constant, however, the ISM densities and stellar velocities, are $1.5\,cm^{-3}$ and $32\,km\,s^{-1}$[top], and $0.3\,cm^{-3}$ and $73\,km\,s^{-1}$ [bottom], respectively (see Mohamed et al. 2012a, for details).

elemental abundances or ionization levels compared to the observed nebulae can also be used to constrain the properties of the central source.

These circumstellar structures also have implications for supernovae explosions and Gamma-ray bursts (GRBs); the interaction with the rings and bow shocks creates radio, X-ray and optical brightening signatures in the light curves and narrow lines in the spectra (e.g., Brighenti & D'Ercole 1994; Eldridge et al. 2006, 2011; van Marle et al. 2006; Dwarkadas 2007; Mackey et al. 2014; Meyer et al. 2015). Comparing models to observations of SNe remnants and GRB afterglows can help constrain the nature of the progenitors of the explosions (e.g., van Veelen et al. 2009, found that the progenitor of Cas A is unlikely to have gone through a WR phase).

3 The formation of spirals and equatorial outflows

The above discussion focused primarily on single stars, however, the majority of massive stars are in binaries (Sana et al. 2012). Systems in which both components have dense, supersonic winds are known as colliding wind binaries (WR examples typically have an O star companion); the collision of their outflows results in a double shock structure separated by a contact discontinuity. The momentum flux ratio, $\eta = \dot{M}_1 v_1 / \dot{M}_2 v_2$, gives a good indication of the global morphology of the shocks; for $\eta = 1$ the location of the contact discontinuity is equi-distant between the two stars, whereas for $\eta \neq 1$, the contact discontinuity forms a cone-like structure that wraps around one of the stars and through orbital motion forms a larger-scale spiral structure around the system (e.g., Stevens et al. 1992).

As was the case for the rings and bow shocks, the detailed morphology of this wind-wind interaction region depends strongly on the excitation and growth of instabilities. In adiabatic simulations, Kelvin-Helmholtz instabilities result from the shear triggered by the orbital motion even when the stellar winds are identical (Lemaster et al. 2007; Lamberts et al. 2012). For very different stellar wind velocities, the instability becomes so violent that the spiral structure is completely destroyed (Lamberts et al. 2012). Adiabatic models are appropriate for wide binaries where the shock interaction is weak and the post-shock gas does not cool efficiently. However, if the dynamical timescale is short compared to the cooling timescale in one or both of the shock regions, then rapid cooling will give rise to thin shell instabilities (Stevens et al. 1992).

The compressed material in the inter-shock regions also radiates strongly from radio to X-rays; non-thermal emission is also detected in some cases indicating the presence of magnetic fields and particle acceleration (see Russell et al., Gosset et al., and Falceta-Goncalves et al., these proceedings for further details). A subset of these binaries also form dust, e.g., WR 104 and the other pinwheel nebulae in the Quintuplet cluster – infrared spiral structures found around carbon-rich WR (WC) stars (Tuthill 2006; Tuthill et al. 2008). While the radiation at X-ray wavelengths is not surprising since the shock temperatures are $\sim 1.2\,v^2_{\rm wind}$ keV (where $v_{\rm wind}$ is in units of $10^8\,cm\,s^{-1}$, Stevens et al. 1992), infrared emission from dust grains in the harsh shock environment was unexpected.

The formation of dust grains requires sufficient densities and temperatures to form precursor molecules and small clusters which then coagulate to create larger grains. Strong cooling, instabilities and clumps in the intershock region may provide the required density and shielding from the harsh radiation field. Furthermore, mixing between H-rich material from a companion and the carbon-rich WR wind may be necessary for the chemical paths to form the precursors. As the mixing due to instabilities occurs on a macroscopic rather than microscopic scale, one possible solution is the destruction of clumps in the intershock region (Pittard 2007, Cherchneff et al., Williams et al., Hendrix et al., these proceedings).

Highly eccentric binaries show strong variations in their light curves and line profiles with orbital phase, e.g., WR 140. The system forms dust period-

ically at periastron passage (when the shock interaction, hence density increase is greatest), while the radio and X-ray emission also vary as the extinction along the line-of-sight changes (e.g., Williams et al. 2009). The strength of the shock interaction can also be affected by a close companion with a strong radiation field; e.g., radiative inhibition reduces the pre-shock wind velocity, hence the collision and the subsequent X-ray emission are weaker, e.g., in V444 Cyg (Stevens & Pollock 1994; Gayley et al. 1997).

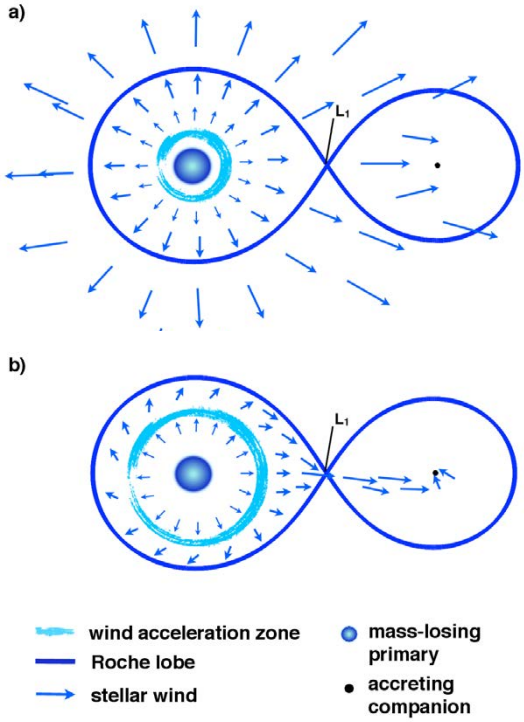

Fig. 3: Schematic diagram of mass transfer in detached binary systems where one of the stars is losing mass via a stellar wind. [a] Standard BHL wind accretion: if the wind acceleration radius is small compared to the RL radius (a wide binary), the wind will reach terminal velocity well before reaching the RL surface and escape, forming a largely spherically symmetric outflow. [b] WRLOF: if the radius of the wind acceleration zone is a significant fraction of the RL radius (e.g., binary separation is small), the dense stellar wind fills the RL and flows towards the companion through the inner Lagrangian point, L1, producing a highly aspherical outflow.

In massive binaries, mass and angular momentum transfer may occur via Roche-Lobe OverFlow (RLOF). If one of the stars fills its Roche lobe (RL) material is transferred to the companion through the inner Lagrangian point, L1. This is likely for short period systems in which the radiation and momentum of the companion's wind does not significantly affect the RL stream, however in wider systems, where the density of the accretion stream is comparable to that in the companion's stellar wind, transfer is inhibited (Dessart et al. 2003). Such binary interactions may play an important role in the formation of some WR stars (Petrovic et al. 2005).

Wind accretion occurs in wide systems when the companion star does not have a strong stellar wind of its own, instead it moves through the WR wind and accretes a small fraction, typically ∼few percent. This mechanism powers systems such as high-mass X-ray binaries where the companion is usually a neutron star or a black hole. Although WR stars have fast, $\gtrsim 1000\,\mathrm{km\,s^{-1}}$, winds, results from self-consistent hydrodynamic models of WC stars showed that to drive the wind, two radiative acceleration zones, and a sufficiently high stellar temperature are necessary (Gräfener & Hamann 2005). This extended acceleration process means that an alternative mass transfer mode, Wind RLOF (WRLOF) (Mohamed 2010, PhD thesis; Mohamed & Podsiadlowski 2012b), may be possible for WR binaries, see Fig. 3. This mode occurs for wind interacting systems where the wind velocity at the RL surface is below the escape speed at that radius; in this case, the dense stellar wind, rather than the star itself, fills the RL and is channelled into the potential well of the companion through L1. Thus, for WR binaries where the acceleration zone is a significant fraction of the RL radius, WRLOF will result in high mass-transfer rates and aspherical outflow geometries.

A spiral structure (of non-accreted material) would also form in this case, however, it would be focused toward the orbital plane resulting in an equatorial outflow. This is one mechanism proposed for the focused outflow in systems such as Cyg X-3 (WR+compact companion) or the formation of the unusual N-rich outflow around WR 122, NaSt1 (Mauerhan et al. 2015). The NaSt1 disk-like outflow shows hints of spiral arms; this substructure and central infrared emission may indicate that the system is a binary (rotation and/or magnetic fields may also play a role). The high mass-transfer rates could lead to spin-up of the accretor which in turn would affect the accretion process and could halt it altogether. The interplay of these complex processes is significant for several related systems, such as SNe, GRBs and bipolar LBVs (e.g., the equatorial outflows may help collimate the ejecta during outbursts).

4 Summary

Models of stellar wind interactions with the ISM, material lost in previous phases of evolution or a nearby companion can broadly explain the formation of rings, bow shock arcs, spirals and equatorial outflows observed around massive stars. These circumstellar structures hold clues both to their mass-loss history and to their final fate.

There are still, however, a large number of complications and uncertainties with both the numeri-

cal approaches and physical processes. For example, the enhancement or suppression of instabilities can be influenced by the numerical methods used, e.g., the number of dimensions (2D vs 3D, e.g., Blondin & Koerwer 1998), resolution or type of solver (e.g., Lamberts et al. (2012) found that the Lax-Friedrichs Riemann solver suppresses instabilities in van Marle et al. (2011) while the shocks in their 2D calculations align with the grid, artificially enhancing them). Physical processes such as radiative cooling, thermal conduction, and the stellar radiation field will also affect the shape of the outflow (e.g., Raga et al. 1997; Toalá & Arthur 2011; Meyer et al. 2015). Another example, already highlighted above, is the highly uncertain process of dust formation.

Further complications result as the winds themselves will be shaped by other processes resulting in strong deviations from a smooth, homogeneous, spherical continuous outflow, e.g., the radiation and stellar magnetic fields, pulsations, and rotation produce latitude dependent winds such as disk-like outflows, co-rotating interaction regions, other wind inhomogeneities such as internal shocks, clumping, porosity, and time-dependent episodic ejections (Cranmer & Owocki 1996; Townsend 1997; Feldmeier & Owocki 1998; Ud-Doula et al. 2008, Küker et al., these proceedings). Environmental inhomogeneities will also play a role including density/velocity gradients in the surroundings as well as ISM radiation and magnetic fields. Finally, binary interactions remain uncertain, as a companion can have a marked effect on the stellar outflow depending on the mass, separation, phase of evolution and luminosity, e.g., interactions may lead to mergers, or spin-up which have important implications for understanding, e.g., GRBs and SN 1987A.

References

Arthur, S. J. 2007, in Diffuse Matter from Star Forming Regions to Active Galaxies (Dordrecht: Springer Netherlands), 183–204

Blondin, J. M. & Koerwer, J. F. 1998, New A, 3, 571

Brighenti, F. & D'Ercole, A. 1994, MNRAS, 270, 65

Brighenti, F. & D'Ercole, A. 1995, MNRAS, 277, 53

Cranmer, S. R. & Owocki, S. P. 1996, ApJ, 462, 469

Dessart, L., Langer, N., & Petrovic, J. 2003, A&A, 404, 991

Dgani, R., van Buren, D., & Noriega-Crespo, A. 1996, ApJ, 461, 927

Dwarkadas, V. V. 2007, ApJ, 667, 226

Eldridge, J. J., Genet, F., Daigne, F., & Mochkovitch, R. 2006, MNRAS, 367, 186

Eldridge, J. J., Langer, N., & Tout, C. A. 2011, MNRAS, 414, 3501

Feldmeier, A. & Owocki, S. 1998, Ap&SS, 260, 113

García-Segura, G., Mac Low, M.-M., & Langer, N. 1996a, A&A, 305, 229

García-Segura, G., Langer, N., & Mac Low, M.-M. 1996b, A&A, 316, 133

Gayley, K. G., Owocki, S. P., & Cranmer, S. R. 1997, ApJ, 475, 786

Gräfener, G. & Hamann, W. 2005, A&A, 432, 633

Gruendl, R. A., Chu, Y.-H., Dunne, B. C., & Points, S. D. 2000, ApJ, 120, 2670

Lamberts, A., Dubus, G., Lesur, G., & Fromang, S. 2012, A&A, 546, A60

Lamers, H. & Cassinelli, J. 1999, Introduction to Stellar Winds (Cambridge University Press)

Langer, N. 2012, ARA&A, 50, 107

Lemaster, M. N., Stone, J. M., & Gardiner, T. A. 2007, ApJ, 662, 582

Mackey, J., Mohamed, S., Gvaramadze, V. V., et al. 2014, Nature, 512, 282

Mauerhan, J., Smith, N., Van Dyk, S. D., et al. 2015, MNRAS, 450, 2551

Meyer, D. M. A., Langer, N., Mackey, J., Velázquez, P. F., & Gusdorf, A. 2015, MNRAS, 450, 3080

Mohamed, S., Mackey, J., & Langer, N. 2012a, A&A, 541, A1

Mohamed, S. & Podsiadlowski, P. 2012b, Baltic Astronomy, 21, 88

Petrovic, J., Langer, N., & van der Hucht, K. A. 2005, A&A, 435, 1013

Pittard, J. M. 2007, ApJ, 660, L141

Raga, A. C., Noriega-Crespo, A., Cantó, J., et al. 1997, Rev. Mexicana Astron. Astrofis., 33, 73

Sana, H., de Mink, S. E., de Koter, A., et al. 2012, Science, 337, 444

Smith, N. 2014, ARA&A, 52, 487

Stevens, I. R., Blondin, J. M., & Pollock, A. 1992, ApJ, 386, 265

Stevens, I. R. & Pollock, A. 1994, MNRAS, 269, 226

Toalá, J. A. & Arthur, S. J. 2011, ApJ, 737, 100

Toalá, J. A., Guerrero, M. A., Ramos-Larios, G., & Guzmán, V. 2015, A&A, 578, 66

Townsend, R. H. D. 1997, MNRAS, 284, 839

Tuthill, P. 2006, Science, 313, 935

Tuthill, P. G. and Monnier, J. D., Lawrance, N. et al. 2008, ApJ, 675, 698

Ud-Doula, A., Owocki, S. P., & Townsend, R. H. D. 2008, MNRAS, 385, 97

van der Sluys, M. & Lamers, H. 2003, A&A, 398, 181

van Marle, A. J., Langer, N., Achterberg, A., & García-Segura, G. 2006, A&A, 460, 105

van Marle, A. J., Keppens, R., & Meliani, Z. 2011, A&A, 527, A3

van Marle, A. J. & Keppens, R. 2012, A&A, 547, A3

van Veelen, B., Langer, N., Vink, J., García-Segura, G., & van Marle, A. J. 2009, A&A, 503, 495

Weaver, R., McCray, R., Castor, J., Shapiro, P., & Moore, R. 1977, ApJ, 218, 377

Wilkin, F. P. 1996, ApJ, 459, L31

Williams, P. M., Marchenko, S. V., Marston, A. P., et al. 2009, MNRAS, 395, 1749

Michael Corcoran: How would the bow shock structure be altered if the moving WR system is a binary?

Shazrene Mohamed: A lot would depend on the orbital parameters; if they were such that the circumbinary outflow is not spherically symmetric but rather more equatorial, it could change the global morphology of the bow shock considerably. Other effects of binarity include the additional mass, velocity structure and luminosity from the companion, the possible presence of dust or magnetic fields, which may change the size of the bow shock, and the cooling/heating rates of the material and therefore affect the growth of instabilities.

Andy Pollock: In low density collisonless plasmas, it is presumably difficult to maintain a contact discontinuity. Would this change the instability properties of the interface?

Shazrene Mohamed: I imagine that you may get similar types of instabilities but the physical processes leading to the favourable conditions for their excitation and growth may be quite different, e.g., ram pressure and thin shell instabilities.

Paul Crowther: NaSt1 is a very interesting system but the X-ray alone (cf. single WR 18) do not necessarily point to a (current) binary colliding wind origin.

Shazrene Mohamed: Yes, that is correct, the disk-like outflow could also be produced by other processes, e.g., rotation or magnetic fields. However, the core is dusty and the hints of "spiral arms" are suggestive of a binary interaction.

Wolf-Rayet Stars
W.-R. Hamann, A. Sander, H. Todt, eds.
Potsdam: Univ.-Verlag, 2015
URL: http://nbn-resolving.de/urn:nbn:de:kobv:517-opus4-84268

Magnetic fields, non-thermal radiation and particle acceleration in colliding winds of WR-O stars

D. Falceta-Gonçalves[1]
[1]*Escola de Artes, Ciências e Humanidades, Universidade de São Paulo, Rua Arlindo Bettio 1000, CEP 03828-000, São Paulo, Brazil*

Non-thermal emission has been detected in WR-stars for many years at long wavelengths spectral range, in general attributed to synchrotron emission. Two key ingredients are needed to explain such emissions, namely magnetic fields and relativistic particles. Particles can be accelerated to relativistic speeds by Fermi processes at strong shocks. Therefore, strong synchrotron emission is usually attributed to WR binarity. The magnetic field may also be amplified at shocks, however the actual picture of the magnetic field geometry, intensity, and its role on the acceleration of particles at WR binary systems is still unclear. In this work we discuss the recent developments in MHD modelling of wind-wind collision regions by means of numerical simulations, and the coupled particle acceleration processes related.

1 Introduction

Wolf-Rayet (WR) stars represent a phase of the evolution of a massive star. Most of these objects are known to be in binary systems, making them a very interesting laboratory for the study of shocks in the space. This because the winds of massive stars are fast ($u_{\rm wind} \sim 1000 - 3000 {\rm km\ s^{-1}}$) and, in the case of luminous blue variables (LBVs) and WR stars, very massive as well ($\dot{M} \sim 10^{-7} - 10^{-4} {\rm M_\odot\ yr^{-1}}$). When two (or more) massive stars form an orbiting system their winds are likely to shock violently, resulting in a vast sort of interesting phenomena, e.g. strong x-ray emission and high energy physics (see e.g. Eichler & Usov 1993; Pittard & Dougherty 2006; Abraham & Falceta-Gonçalves 2010; Reitberger et al. 2014).

Among the most intriguing processes involving shocks at massive binary systems is particle acceleration. Synchrotron emission at large wavelengths have been observed in several WR binaries, revealing both the existence of relativistic particles and strong magnetic fields. Since current models of particle acceleration depends on the magnetization of the shocks, the study of the evolution of the magnetic fields in wind-wind collision regions is crucial.

In this work we present the main results of recent magneto-hydrodynamical numerical simulations of wind-wind collisions. We also briefly discuss the implications of such modelling on the understanding of particle acceleration in such objects.

2 Modelling

In order to obtain the dynamical evolution of the shock region of the massive binary system we have employed a number of magneto-hydrodynamical (MHD) numerical simulations. The simulations were performed solving the set of ideal MHD equations, in conservative form, as performed in Falceta-Gonçalves & Abraham (2012). The set of equations is complete with an explicit equation for the radiative cooling. Two distinct setups were studied, namely the cases where radiative cooling were neglected and included, for comparison. These different setups correspond to the cases where the cooling time is longer, or shorter, respectively, to the dynamical timescales of the flows at the shock region.

The initial setup used was chosen to represent the system of η Carinae, with wind mass loss rates for the two stars as $\dot{M}_1 \sim 2 \times 10^{-4}$ ${\rm M_\odot\ yr^{-1}}$ and $\dot{M}_2 \simeq 10^{-5}$ ${\rm M_\odot\ yr^{-1}}$, and wind terminal velocity $v_1 \sim 700$ km ${\rm s^{-1}}$ and $v_2 \simeq 3 \times 10^3$ km ${\rm s^{-1}}$, respectively (Falceta-Gonçalves et al. 2005; Abraham et al. 2005a,b; Abraham & Falceta-Gonçalves 2007; Falceta-Gonçalves et al. 2008). The orbit is set with a major semi-axis $a = 15$AU and eccentricity $e = 0.9$. The magnetic field of both stars is initially set as a dipole with surface polar intensity $B_0 = 1$G, weak compared to the thermal and kinetic terms of the winds.

3 Results

The numerical integration of each model was performed for 2 complete orbital periods, which corresponds to approximately 11 years. Irrespectively to the model, the amplification of magnetic field at the shock has been shown to be larger than the values predicted by the Rankine-Hugoniot jump conditions (Rocha da Silva et al. 2015). This occurs because the R-H jump conditions are computed for 1D solution of conservation equations, while the shock is multidimensional. It was already shown in Falceta-Gonçalves & Abraham (2012) that the flow of the post-shocked gas occurs mostly parallel to the field lines, reducing the local pressure and allowing further compression of the magnetic fields at the shock layers. Also, in the cases of strong cooling, this compression occurs even further, resulting in magnetic fields orders of magnitude larger that the predicted by R-H jump conditions.

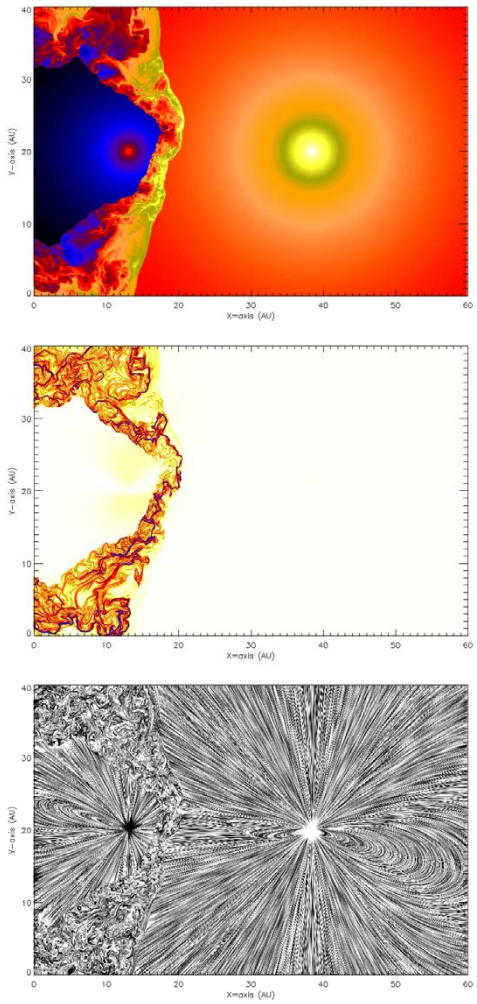

Fig. 1: Central slices of density (top), magnetic energy density (central) and line integral convolution of magnetic field orientation (bottom), for phase 0.5 (apastron).

In Figure 1 we present the central slice of the model with radiative cooling at orbital phase 0.5, i.e. near apastron. The maps are shown for density (top), magnetic energy density (central) and line integral convolution (LIC) for the magnetic field orientation (bottom). The top panel shows that the standard picture of a two shock layers separated by a contact discontinuity is broken. Here the entrainment of material among the two layers is very efficient, as a consequence of the Nonlinear Thin Layer Instability. Several observations of the wind-wind collision region of massive binaries indicate them to be turbulent (Falceta-Gonçalves et al. 2006). This mixing property of turbulent flows is also responsible for the complex geometry of the magnetic field lines at the shock. Instead of accumulating at the contact discontinuity (Rocha da Silva et al. 2015), high magnetic energy density regions are mixed, as shown in the central panel of this figure.

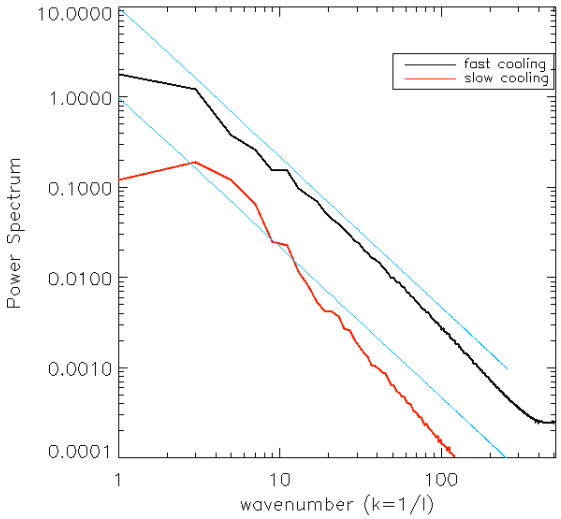

Fig. 2: Power spectrum of magnetic field for two different models, with and without radiative cooling included. Effects of cooling include the growth of local instabilities (e.g. nonlinear thin-layer instability) and turbulent dynamics.

The magnetic field orientation at the shock is absolutely chaotic, as seen in the bottom panel of Figure 1. Here we show the line integral convolution LIC technique applied for the magnetic field lines. The texture shown represents the orientation of the field lines, which are kept approximately dipolar for the surroundings of the stars. At the shock, one would expect a field parallel to the shock structure. Indeed, this is standard result for the adiabatic model. In the cooled case, turbulence at the shock region results in very complex geometry of B-field lines. The scaling of such complex distribution of magnetic field can be obtained from its power spectrum.

The turbulent power spectra of the magnetic field at the shock region obtained for the adiabatic and cooled models are shown in Figure 2. The plot shows the power spectra obtained for the adiabatic and cooled models, and the reference line for Kolmogorov scaling ($P_k \propto k^{-5/3}$). It is clear that the cooled model presents much larger power of turbulent components that the adiabatic model. Also, the slope obtained for the cooled model resembles well the typical energy cascade of Kolmogorov's turbulence, while the adiabatic model shows a steeper spectrum, as a consequence of a dominance of the more uniform (sheath-like) component (Falceta-Gonçalves et al. 2014).

3.1 B-n correlation at wind-wind shock regions

The correlation between the magnetic field energy density and the local gas density is typically used once equipartition between the magnetic and particle kinetics is assumed. This has been largely used by theorists so far in order to model the levels of magnetization of shock regions, as well as to predict the high energy content of particle distributions. However, as shown in Figure 3, the correlation between B and the gas density n is far from trivial.

Three clustering are visible, representing the stellar winds and the shocked region. The more diffuse and highly magnetized cluster of density corresponds to the shock. It is clear that any attempt to fit a $B \propto n^{\alpha}$ correlation is unsuccessful (Burkhart et al. 2009). Therefore, in order to properly model, for instance, the synchrotron emission from massive binaries, one needs to fully evolve the magnetic field as well as the acceleration of particles self-consistently.

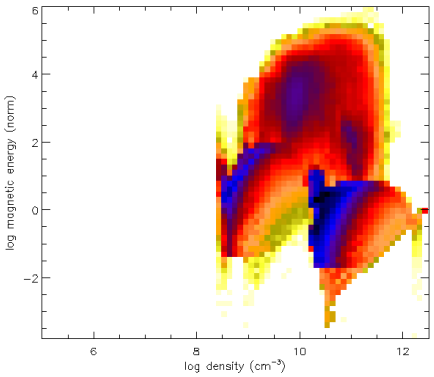

Fig. 3: 2D histogram of the model for the correlation between local density and the magnetic energy density. In general, assumption of equipartition $B^2 \propto \rho$ is used for the description of the non=thermal component of the shock region (see text), however we show that the situation is far more complex.

3.2 Particle acceleration

As pointed by Eichler & Usov (1993), the shock region of massive binaries may be ideal for particle acceleration to relativistic speeds. First order Fermi acceleration is commonly employed in such systems, which is efficient once the shock structure is uniform. If after each shock crossing the energy of the particle increases by a factor $\delta E/E \sim 2U/3c$, where U represents the upstream flow velocity, we obtain – for the parameters of our simulations – an acceleration timescale (from keV to TeV) of $\tau_{\rm acc} \sim 10^4 - 10^5$s. Unfortunately, this is slow compared to particle diffusion time ($\tau_{\rm diff} \sim L/v_{\rm part}$), or even for collisions. Therefore, for the model of the system of eta Carinae, the 1st order Fermi process is not dominant.

However, we have shown that the shocked region is very turbulent. In such an environment particles should be accelerated to relativistic either by the 2nd order Fermi process or by electric fields arising from turbulent reconnection zones. In the 2nd order process the acceleration occurs as random collisions within the shock region, i.e. diffusion at timescales $\tau_{\rm acc} \sim Lc/ < \delta v^2 >$. For the turbulence parameters obtained from the simulations, $< \delta v^2 >^{1/2} \sim$ 100km s^{-1} at $L \sim 10^9$cm, we obtained fast initial acceleration and saturation of relativistic particles with $N(E)dE \propto (E^{-2} - E^{-1})dE$, at maximum energy of $1 - 10$TeV.

References

Abraham, Z. & Falceta-Gonçalves, D. 2007, MNRAS, 378, 309

Abraham, Z. & Falceta-Gonçalves, D. 2010, MNRAS, 401, 687

Abraham, Z., Falceta-Gonçalves, D., Dominici, T., Caproni, A., & Jatenco-Pereira, V. 2005a, MNRAS, 364, 922

Abraham, Z., Falceta-Gonçalves, D., Dominici, T. P., et al. 2005b, A&A, 437, 977

Burkhart, B., Falceta-Gonçalves, D., Kowal, G., & Lazarian, A. 2009, ApJ, 693, 250

Eichler, D. & Usov, V. 1993, ApJ, 402, 271

Falceta-Gonçalves, D. & Abraham, Z. 2012, MNRAS, 423, 1562

Falceta-Gonçalves, D., Abraham, Z., & Jatenco-Pereira, V. 2006, MNRAS, 371, 1295

Falceta-Gonçalves, D., Abraham, Z., & Jatenco-Pereira, V. 2008, MNRAS, 383, 258

Falceta-Gonçalves, D., Jatenco-Pereira, V., & Abraham, Z. 2005, MNRAS, 357, 895

Falceta-Gonçalves, D., Kowal, G., Falgarone, E., & Chian, A. C.-L. 2014, Nonlinear Processes in Geophysics, 21, 587

Pittard, J. M. & Dougherty, S. M. 2006, MNRAS, 372, 801

Reitberger, K., Kissmann, R., Reimer, A., & Reimer, O. 2014, ApJ, 789, 87

Rocha da Silva, G., Falceta-Gonçalves, D., Kowal, G., & de Gouveia Dal Pino, E. M. 2015, MNRAS, 446, 104


HD
Ad

X-rays and WR stars

Wolf-Rayet Stars
W.-R. Hamann, A. Sander, H. Todt, eds.
Potsdam: Univ.-Verlag, 2015
URL: http://nbn-resolving.de/urn:nbn:de:kobv:517-opus4-84268

X-ray emission from single WR stars

L. M. Oskinova[1]
[1] *Universität Potsdam, Germany*

In this review I briefly summarize our knowledge of the X-ray emission from single WN, WC, and WO stars. These stars have relatively modest X-ray luminosities, typically not exceeding $1\,L_\odot$. The analysis of X-ray spectra usually reveals thermal plasma with temperatures reaching a few $\times 10$ MK. X-ray variability is detected in some WN stars. At present we don't fully understand how X-ray radiation in produced in WR stars, albeit there are some promising research avenues, such as the presence of CIRs in the winds of some stars. To fully understand WR stars we need to unravel mechanisms of X-ray production in their winds.

1 X-rays from WR stars: history

The discovery of X-ray emission from WR-stars was among the first results achieved by the *Einstein* X-ray observatory (Seward et al. 1979). This confirmed the theoretical prediction that WR stars, specifically WR binaries, are X-ray sources (Cherepashchuk 1976). Pollock (1987b) summarized the *Einstein* observations of WR stars and outlined their key X-ray properties. From the analysis of the observations it was concluded that (*i*) the X-ray brightest WR stars are often massive binaries; (*ii*) single WR stars are usually faint; (*iii*) the WN stars are on average more X-ray bright than WC stars. These conclusions remains valid today.

The *Rosat* X-ray telescope performed an all sky survey. Besides increasing the number of detected WR stars, it also obtained X-ray spectra and light curves for some key targets (e.g. Willis & Stevens 1996). A preliminary X-ray catalog of WR stars was presented by Pollock et al. (1995). For single WR stars no correlation between X-ray luminosity and their bolometric luminosity or wind momentum was found (Wessolowski 1996). This result was later on confirmed by the detailed studies (Ignace & Oskinova 1999; Ignace et al. 2000).

The ASCA X-ray telescope observed four WR stars in great details, yielding X-ray spectra and light-curves. Monitoring of massive binaries revealed the unambiguous evidence that the X-rays are produced in the wind-wind collision zone (e.g. Stevens et al. 1996). Other X-ray observatories, such as EXOSAT, also contributed to the studies of X-rays from WR-type stars (e.g. Williams et al. 1987).

Today, a fleet of X-ray telescopes operating in space routinely observes WR stars. Modern X-ray telescopes have broad pass-bands and significantly improved sensitivity, spectral and spatial resolution. Among these telescopes, *Chandra* and *XMM-Newton* have unprecedented capabilities allowing in depth studies of the formation and propagation of X-rays in WR stars. The future also looks bright in X-rays with new missions such as Spektrum-Röntgen-Gamma (SRG), Astro-H, and Athena being under development.

2 General properties of X-rays from WR stars

Luminosity. The lack of correlation between X-ray and bolometric luminosity of WR stars is in a strong contrast to O-type stars. The X-ray luminosities of the latter are $L_{\rm X} \approx 10^{-7} L_{\rm bol}$ (Pallavicini et al. 1981). This correlation holds for single as well as for binary O stars (Oskinova 2005; Nazé 2009). The origin of this correlation in O stars is not yet understood and might be related to the properties of shocks or to magnetic effects (Oskinova et al. 2011; Owocki et al. 2013). As can be seen in Fig. 1, the X-ray luminosities of WN-type stars are diverse. While WN binaries seem to show a trend similar to the O+OB binaries, the putatively single WN stars have X-ray luminosities that differ by orders of magnitude. Overall, the X-ray luminosities of WN stars do not significantly exceed $\sim 10^{34}\,{\rm erg\,s^{-1}}$ with binaries being on average more X-ray bright.

Variability. The X-ray monitoring of WR stars revealed that single as well as binary stars are X-ray variable. The X-ray variability of binaries is on the orbital period time scale and is well documented, studied, and understood (among most recent papers, e.g. Pandey et al. 2014; Lomax et al. 2015; Zhekov & Skinner 2015). The sample of single WR stars that were monitored in X-rays is significantly smaller. Data of high fidelity exist so far only for WR6 (Ignace et al. 2013). This WN4 star shows X-ray variability on the level of 20% and with a characteristic period similar to the 3.766 day period well known from the optical (e.g. Morel et al. 1997), but is not in phase. This is quite similar to the X-ray variability observed in single O-type stars (e.g. Oskinova et al. 2001; Nazé et al. 2013). The origin of the X-ray variability is likely related to the presence of corotating interaction regions (CIRs) in the stellar winds (Chené et al. 2011; Massa et al. 2014).

Temperature. Already *Einstein* and *Rosat* observations revealed that X-ray spectra of WR stars can be described as thermal. In binaries, the ionization balance could be out of equilibrium and shocks could be collisionless (Pollock et al. 2005; Zhekov 2007). In single stars, the X-ray spectra were, so far, well reproduced by multi-temperature thermal plasmas in

collisional equilibrium. Temperatures between 1 MK up to 50 MK are found from spectral analyses, with the emission measures of cooler plasma components being larger than that of hotter ones (the differential emission measure declines with temperature) (Skinner et al. 2002a,b, 2010; Ignace et al. 2003; Oskinova et al. 2012).

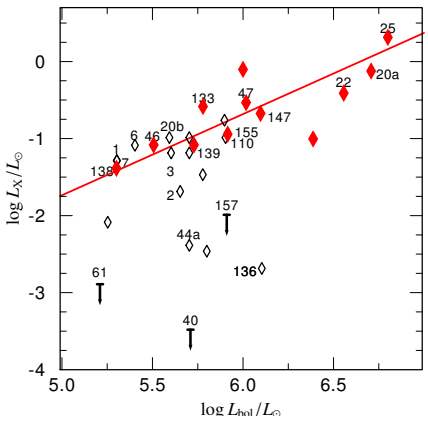

Fig. 1: L_X vs. L_{bol} for WN stars. Black empty diamonds denote single stars, while red filled diamonds denote binaries (Oskinova 2005; Gosset et al. 2005; Skinner et al. 2012; Zhekov 2012). The straight line shows the correlation for O-star binaries (Oskinova 2005).

3 X-ray production in WR stars

The present day sophisticated models are capable to describe and explain the X-ray emission from WR binaries (e.g. Stevens et al. 1992; Pittard & Dougherty 2006; Zhekov 2012; Parkin & Sim 2013; Rauw & Naze 2015). Albeit the exact physics is not yet fully understood, it is beyond reasonable doubt that the bulk of X-rays in the majority of WR binaries is produced in the wind-wind collisions zone.

The situation is very different for single WR stars. There are neither theories nor quantitative models explaining the production of X-rays in the winds of these stars, albeit there is no shortage of scenarios. Among them:

(i) X-ray emission in some "normal" WR stars could be due to the wind accretion on a compact object (White & Long 1986). Modern observations do not support this scenario. The observed X-ray properties of WR stars differ significantly from the X-ray emission of high-mass X-ray binaries. Only a few WR stars with relativistic companions are known, and their X-ray properties do not resemble those of single WR stars (Barnard et al. 2008).

(ii) The binarity idea was further examined by Skinner et al. (2002a) who suggested that a WR wind shocking onto a otherwise unseen close stellar companion could be responsible for the X-ray emission in at least some apparently single WR stars. There are a number of arguments questioning this scenario. For instance, new deep X-ray observations show no spectral signatures characteristic for low-mass stars. The X-ray variability patterns also do not support this scenario (Oskinova et al. 2012; Ignace et al. 2013).

(iii) Particle acceleration in shocks. According to this scenario, a population of relativistic electrons accelerated in the wind shocks is responsible for the generation of X- and γ-rays via inverse Compton scattering (e.g. Pollock 1987a). It seems that this mechanism may indeed operate in colliding wind binaries, however no observational evidence in its support was so far found in single WR stars.

(iv) If a strong dipolar magnetic field is present, it may confine stellar winds and lead to strong shocks at the magnetic equator (Babel & Montmerle 1997). Albeit this mechanism is sometimes considered in the literature to explain the X-ray emission from WR stars, no strong magnetic fields capable to confine powerful WR-winds were detected so far (de la Chevrotière et al. 2014, Hubrig et al. 2016, in press). Nevertheless, even if the wind confinement model does not explain X-rays from WR stars, the role of magnetism for the X-ray generation cannot be ruled out. E.g. a strong magnetic field was suspected in a few peculiar WR stars, such as WR2 (Shenar et al. 2014), but their X-ray properties are not outstanding (Oskinova 2005; Skinner et al. 2010).

(v) Shock heating due to line-driven wind instabilities (LDI) is often invoked to explain X-ray emission from OB-type stars (Feldmeier et al. 1997). Gayley & Owocki (1995) showed that multiple scattering in dense WR winds reduces this instability. However, the residual instability may still lead to clumping of WR winds. These authors did not address X-ray emission from WR stars, i.e. they did not show that the instability in WR winds is sufficient to drive strong shocks where the plasma can be heated to a few MK. Yet, it is tempting to draw parallels between WR and OB supergiant X-ray production mechanisms (Gayley 2016, submitted).

(vi) Gayley (2012) hypothesized that the fast wind may ram into the slow moving clumps, whose signatures are observed as moving bumps on top of lines observed in optical WR spectra (Lépine & Moffat 1999). Plasma could be heated in the resulting shocks. This is an interesting scenario that shall be tested by detailed modeling and observations.

(vii) Observations confirm that corotating interaction regions (CIRs) are present in WR winds (Chené & St-Louis 2011). Their origin is not fully understood but may be related to the presence of surface magnetic fields (Michaux et al. 2014). Mullan (1984); Chené et al. (2011) and Ignace et al. (2013) invoked CIRs to explain the X-ray generation in WR winds. The detailed hydrodynamic models of the CIRs in OB winds (Cranmer & Owocki 1996; Lobel

& Blomme 2008) are so far isothermal, so it remains to be seen whether CIRs can be the origin of X-rays from OB star winds. For the WR winds, to our knowledge, no hydrodynamic modeling of CIRs was performed so far. Yet it seems that the CIR scenario is the most promising one to explain the X-ray emission it least in some rotating single WR stars.

4 Propagation of X-rays

The combination of large column densities and high metal abundance makes WR winds very opaque for X-rays (e.g. Ignace & Oskinova 1999). Figure 2 demonstrates that WR winds may remain optically thick for X-rays up to a few $\times 1000\,R_*$. Wind clumping allows X-rays to emerge from somewhat deeper wind layers due to the porosity effects (Shaviv 2000; Feldmeier et al. 2003; Oskinova et al. 2004).

The X-ray field can be included in non-LTE stellar atmosphere models, such a PoWR (Baum et al. 1992) allowing to consistently solve the X-ray transfer in WR winds. This has important implications for applying X-ray spectral diagnostics, such as the widely used ratios of forbidden to intercombination lines in the X-ray spectra of He-like ions (Leutenegger et al. 2006; Waldron & Cassinelli 2007, Huenemoerder et al. 2016, in press).

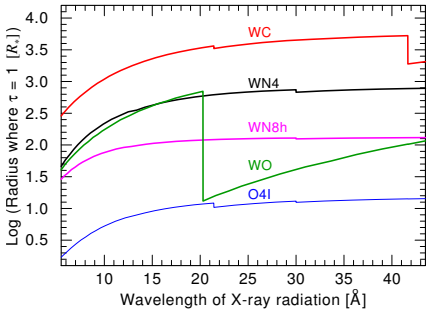

Fig. 2: Radius where the continuum optical depth reaches unity, as predicted by PoWR models for the "cool" wind component in different WR stars and an O-supergiant, in dependence on wavelength.

5 X-rays from WNE stars

Hydrogen free early-type WN stars (WNEs) occupy a distinct region in the HRD and have rather similar stellar parameters (Hamann et al. 2006). It appears that the X-ray properties of WNEs are also similar. The rate of X-ray detections of WNE stars is quite high – all stars that were observed so far with pointing observations were detected. Those WNE stars have similar X-ray luminosities ($L_{\rm X} \approx 2 \ldots 6 \times 10^{32}\,{\rm erg\,s^{-1}}$). Their X-ray temperatures are also similar, with the emission measure weighted average temperature of $\langle T \rangle \approx 5\,{\rm MK}$. The parameter $R_{\rm t}$ (see its definition and discussion in Hamann et al. 2006, or in these Proceedings) is used to characterize the emission measure of WR winds. Figure 3 shows an interesting trend between the X-ray luminosity of WNE stars and their $R_{\rm t}$. The presence of such trend implies that the generations of X-rays is an intrinsic property of stellar winds.

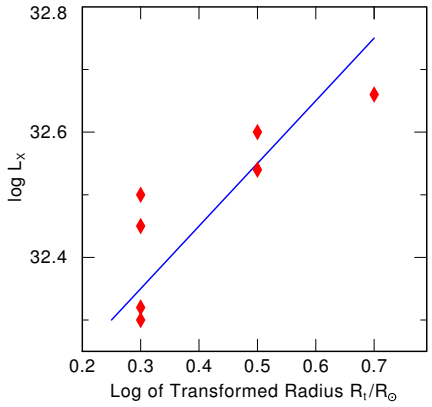

Fig. 3: X-ray luminosity versus transformed radius $R_{\rm t}$ for a sample of WNE stars (red diamonds). The values are from Skinner et al. (2002a,b, 2010); Ignace et al. (2003); Oskinova (2005); Hamann et al. (2006). The straight blue line shows a linear regression fit.

A high-resolution X-ray spectrum is available, so far, for only one single WR star, WR6 (WN4) (see also D. Huenemoerder, these proceedings). Its spectra were obtained by both *XMM-Newton* (Oskinova et al. 2012) and *Chandra* (Huenemoerder et al. 2016, submitted). The abundances in X-ray emitting plasma are consistent with WNE abundances, e.g. no oxygen lines are detectable. This provides a strong argument against a non-degenerate binary component scenario. The X-ray lines are broad, blue-shifted, and have a characteristic shape as expected when the radiation forms in outer wind and suffers strong continuum absorption (Macfarlane et al. 1991; Ignace 2001). The analysis of line ratios in He-like ions confirms that the radiation is formed far out in the wind. Even the hottest plasma is formed at more than tens stellar radii. The spectral analysis reveals that X-ray emitting gas must be present even at $> 1000\,R_*$. Such very extended spatial distribution is very difficult to reconcile with the predictions of the LDI models developed for O stars. Interestingly, there are indications that the fluorescent Fe Kα line is present in the X-ray spectrum. This indicates that dense and cool matter coexists with the hot plasma.

6 X-rays from WNL stars

Late type WN stars (WNLs) have on average higher bolometric luminosities and slower winds than WNE stars (e.g. Sanders et al. 1985). Some WNLs may be descendants of more massive progenitors than WNEs, while others may be on earlier evolutionary stage (Crowther et al. 1995; Hamann et al. 2006). Gosset et al. (2005) obtained deep *XMM-Newton* observations of WR40 (WN8h) and its nebula, but neither was detected in X-rays. The wind of WR40 is more transparent for X-rays than the wind of WR1 (WN4) (see corresponding curves in Fig. 2), yet the later is > 100 times more X-ray luminous than the former. On the other hand, the WN9h star WR79a was detected with $L_{\rm X} \approx 10^{32}\,{\rm erg\,s^{-1}}$ (Oskinova 2005). Its low resolution X-ray spectrum bears similarities with spectra of WNEs, i.e. a relatively high-temperature component ($T \sim 30\,{\rm MK}$) is present (Skinner et al. 2012). Other WNLs well observed in X-rays are WR78 (WR7h) ($L_{\rm X} \approx 10^{31}\,{\rm erg\,s^{-1}}$ Pollock et al. 1995; Wessolowski 1996; Oskinova 2005, note that Skinner et al. (2012) report an order of magnitude higher luminosity for this object) and WR136 (WN6(h)) ($L_{\rm X} \approx 10^{31}\,{\rm erg\,s^{-1}}$, Wrigge et al. 1994; Pollock et al. 1995; Ignace et al. 2000). Thus, while some WNLs are not detected in X-rays, others appear to be relatively X-ray luminous.

7 X-rays from WC and WO stars

Rauw et al. (2015) discovered X-rays from the WC4 star WR144, making it the first single WC star detected in X-rays. Its low X-ray luminosity ($L_{\rm X} \approx 10^{30}\,{\rm erg\,s^{-1}}$) corroborates Oskinova et al. (2003)'s conclusion that WC stars are intrinsically X-ray faint, likely because of the high opacity of their stellar winds (see Fig. 2). On the other hand, known WC binaries are bright X-ray sources (e.g. Schild et al. 2004; Pollock et al. 2005; Zhekov et al. 2011). Hence, X-rays provide a convenient indication of binarity: X-ray bright WC stars should be colliding wind binaries. This makes X-rays observations a very useful diagnostic tool to search for binaries among WC populations (Clark et al. 2008; Oskinova & Hamann 2008; Hyodo et al. 2008; Mauerhan et al. 2011; Nebot Gómez-Morán et al. 2015).

WO stars represent a very advanced evolutionary stage of massive stars shortly before their supernova explosion. The WO winds are the fastest among all non-degenerate stars (Sander et al. 2012; Tramper et al. 2015). Their wind opacity for X-rays is less than that in WC stars (see Fig. 2), therefore X-rays may reach an observer. Oskinova et al. (2009) reported the first discovery of X-ray emission from this important type of objects. They detected the WO2 star WR142 using *XMM-Newton*. This X-ray source identification was confirmed with *Chandra*'s superb angular resolution (Sokal et al. 2010). The X-ray luminosity of WR142 is not very high ($L_{\rm X} \approx 10^{31}\,{\rm erg\,s^{-1}}$), while its X-ray spectrum is quite hard (with $T_{\rm X} > 100\,{\rm MK}$). WO stars are basically bare stellar cores and might expose magnetic fields (Fuller et al. 2015). This and other scenarios were considered in Oskinova et al. (2009), while Sokal et al. (2010) suggested the possibility of inverse Compton scattering or a binary companion.

8 Summary

All types of single WR stars emit X-rays. Their X-ray luminosities are orders of magnitude lower than in persistent high-mass X-ray binaries. The X-ray spectra appear to be thermal, with very hot plasma of a few$\times 10\,{\rm MK}$ being present along with cooler components. The mechanisms responsible for X-ray generation are not yet understood. Promising scenarios include an LDI-like mechanisms, interactions of wind streams with blobs, and CIRs. New observations and modeling shall uncover how X-rays are generated in winds of single WR stars.

References

Babel, J. & Montmerle, T. 1997, A&A, 323, 121

Barnard, R., Clark, J. S., & Kolb, U. C. 2008, A&A, 488, 697

Baum, E., Hamann, W.-R., Koesterke, L., & Wessolowski, U. 1992, A&A, 266, 402

Chené, A.-N., Moffat, A. F. J., Cameron, C., et al. 2011, ApJ, 735, 34

Chené, A.-N. & St-Louis, N. 2011, ApJ, 736, 140

Cherepashchuk, A. M. 1976, Soviet Astronomy Letters, 2, 138

Clark, J. S., Muno, M. P., Negueruela, I., et al. 2008, A&A, 477, 147

Cranmer, S. R. & Owocki, S. P. 1996, ApJ, 462, 469

Crowther, P. A., Smith, L. J., Hillier, D. J., & Schmutz, W. 1995, A&A, 293, 427

de la Chevrotière, A., St-Louis, N., Moffat, A. F. J., & MiMeS Collaboration. 2014, ApJ, 781, 73

Feldmeier, A., Oskinova, L., & Hamann, W.-R. 2003, A&A, 403, 217

Feldmeier, A., Puls, J., & Pauldrach, A. W. A. 1997, A&A, 322, 878

Fuller, J., Cantiello, M., Stello, D., Garcia, R. A., & Bildsten, L. 2015, ArXiv e-prints

Gayley, K. G. 2012, in Astronomical Society of the Pacific Conference Series, Vol. 465, Proceedings of a Scientific Meeting in Honor of Anthony F. J. Moffat, ed. L. Drissen, C. Robert, N. St-Louis, & A. F. J. Moffat, 140

Gayley, K. G. & Owocki, S. P. 1995, ApJ, 446, 801

Gosset, E., Nazé, Y., Claeskens, J.-F., et al. 2005, A&A, 429, 685

Hamann, W.-R., Gräfener, G., & Liermann, A. 2006, A&A, 457, 1015
Hyodo, Y., Tsujimoto, M., Koyama, K., et al. 2008, PASJ, 60, 173
Ignace, R. 2001, ApJ, 549, L119
Ignace, R., Gayley, K. G., Hamann, W.-R., et al. 2013, ApJ, 775, 29
Ignace, R. & Oskinova, L. M. 1999, A&A, 348, L45
Ignace, R., Oskinova, L. M., & Brown, J. C. 2003, A&A, 408, 353
Ignace, R., Oskinova, L. M., & Foullon, C. 2000, MNRAS, 318, 214
Lépine, S. & Moffat, A. F. J. 1999, ApJ, 514, 909
Leutenegger, M. A., Paerels, F. B. S., Kahn, S. M., & Cohen, D. H. 2006, ApJ, 650, 1096
Lobel, A. & Blomme, R. 2008, ApJ, 678, 408
Lomax, J. R., Nazé, Y., Hoffman, J. L., et al. 2015, A&A, 573, A43
Macfarlane, J. J., Cassinelli, J. P., Welsh, B. Y., et al. 1991, ApJ, 380, 564
Massa, D., Oskinova, L., Fullerton, A. W., et al. 2014, MNRAS, 441, 2173
Mauerhan, J. C., Van Dyk, S. D., & Morris, P. W. 2011, AJ, 142, 40
Michaux, Y. J. L., Moffat, A. F. J., Chené, A.-N., & St-Louis, N. 2014, MNRAS, 440, 2
Morel, T., St-Louis, N., & Marchenko, S. V. 1997, ApJ, 482, 470
Mullan, D. J. 1984, ApJ, 283, 303
Nazé, Y. 2009, A&A, 506, 1055
Nazé, Y., Oskinova, L. M., & Gosset, E. 2013, ApJ, 763, 143
Nebot Gómez-Morán, A., Motch, C., Pineau, F.-X., et al. 2015, MNRAS, 452, 884
Oskinova, L. M. 2005, MNRAS, 361, 679
Oskinova, L. M., Clarke, D., & Pollock, A. M. T. 2001, A&A, 378, L21
Oskinova, L. M., Feldmeier, A., & Hamann, W.-R. 2004, A&A, 422, 675
Oskinova, L. M., Gayley, K. G., Hamann, W.-R., et al. 2012, ApJ, 747, L25
Oskinova, L. M. & Hamann, W.-R. 2008, MNRAS, 390, L78
Oskinova, L. M., Hamann, W.-R., Cassinelli, J. P., Brown, J. C., & Todt, H. 2011, Astronomische Nachrichten, 332, 988
Oskinova, L. M., Hamann, W.-R., Feldmeier, A., Ignace, R., & Chu, Y.-H. 2009, ApJ, 693, L44
Oskinova, L. M., Ignace, R., Hamann, W.-R., Pollock, A. M. T., & Brown, J. C. 2003, A&A, 402, 755
Owocki, S. P., Sundqvist, J. O., Cohen, D. H., & Gayley, K. G. 2013, MNRAS, 429, 3379
Pallavicini, R., Golub, L., Rosner, R., et al. 1981, ApJ, 248, 279
Pandey, J. C., Pandey, S. B., & Karmakar, S. 2014, ApJ, 788, 84
Parkin, E. R. & Sim, S. A. 2013, ApJ, 767, 114
Pittard, J. M. & Dougherty, S. M. 2006, MNRAS, 372, 801
Pollock, A. M. T. 1987a, A&A, 171, 135
Pollock, A. M. T. 1987b, ApJ, 320, 283
Pollock, A. M. T., Corcoran, M. F., Stevens, I. R., & Williams, P. M. 2005, ApJ, 629, 482
Pollock, A. M. T., Haberl, F., & Corcoran, M. F. 1995, in IAU Symposium, Vol. 163, Wolf-Rayet Stars: Binaries; Colliding Winds; Evolution, ed. K. A. van der Hucht & P. M. Williams, 512
Rauw, G. & Naze, Y. 2015, ArXiv e-prints
Rauw, G., Nazé, Y., Wright, N. J., et al. 2015, ApJS, 221, 1
Sander, A., Hamann, W.-R., & Todt, H. 2012, A&A, 540, A144
Sanders, W. T., Cassinelli, J. P., Myers, R. V., & van der Hucht, K. A. 1985, ApJ, 288, 756
Schild, H., Güdel, M., Mewe, R., et al. 2004, A&A, 422, 177
Seward, F. D., Forman, W. R., Giacconi, R., et al. 1979, ApJ, 234, L55
Shaviv, N. J. 2000, ApJ, 532, L137
Shenar, T., Hamann, W.-R., & Todt, H. 2014, A&A, 562, A118
Skinner, S. L., Zhekov, S. A., Güdel, M., & Schmutz, W. 2002a, ApJ, 579, 764
Skinner, S. L., Zhekov, S. A., Güdel, M., & Schmutz, W. 2002b, ApJ, 572, 477
Skinner, S. L., Zhekov, S. A., Güdel, M., Schmutz, W., & Sokal, K. R. 2010, AJ, 139, 825
Skinner, S. L., Zhekov, S. A., Güdel, M., Schmutz, W., & Sokal, K. R. 2012, AJ, 143, 116
Sokal, K. R., Skinner, S. L., Zhekov, S. A., Güdel, M., & Schmutz, W. 2010, ApJ, 715, 1327
Stevens, I. R., Blondin, J. M., & Pollock, A. M. T. 1992, ApJ, 386, 265
Stevens, I. R., Corcoran, M. F., Willis, A. J., et al. 1996, MNRAS, 283, 589
Tramper, F., Straal, S. M., Sanyal, D., et al. 2015, A&A, 581, A110
Waldron, W. L. & Cassinelli, J. P. 2007, ApJ, 668, 456
Wessolowski, U. 1996, in Roentgenstrahlung from the Universe, ed. H. U. Zimmermann, J. Trümper, & H. Yorke, 75–76
White, R. L. & Long, K. S. 1986, ApJ, 310, 832
Williams, P. M., van der Hucht, K. A., & The, P. S. 1987, QJRAS, 28, 248
Willis, A. J. & Stevens, I. R. 1996, A&A, 310, 577
Wrigge, M., Wendker, H. J., & Wisotzki, L. 1994, A&A, 286, 219
Zhekov, S. A. 2007, MNRAS, 382, 886
Zhekov, S. A. 2012, MNRAS, 422, 1332
Zhekov, S. A., Gagné, M., & Skinner, S. L. 2011, ApJ, 727, L17
Zhekov, S. A. & Skinner, S. L. 2015, MNRAS, 452, 872

Tomer Shenar: Is it possible to observe indirect "products" of X-rays (e.g. O VI lines in O-star spectra) even if the X-ray emission itself cannot be observed (because it is fully absorbed in the wind)?

Lidia Oskinova: I would think that the answer is "yes". Perhaps we shall search in more detail the spectra of single WC stars for the signatures of 'over-ionization' that can be attributed to the X-rays that are produced but fully absorbed in the winds.

Andy Pollock: Does the conclusion that X-rays can be produced in situ far from the wind acceleration zone suggest that the same might happen in O stars?

Lidia Oskinova: Good question. From high-resolution X-ray spectroscopy of O-stars we have evidence that the bulk of X-ray emitting gas in these stars is produced very close to the stellar surface. Therefore, I would say, it looks quite likely that the mechanisms that produce X-rays in O and WR stars may be different.

Kenji Hamaguchi: Do X-ray light curves of WRs tend to show stochastic variations (such as flares) or cyclic (to the binary orbit)?

Lidia Oskinova: To my knowledge, single WR stars do not show stochastic X-ray variability on the observable level. But these stars show some X-ray variability on time-scale of days. It might be cyclic, but more data are needed to confirm it. WR-stars that are members of binary systems typically show cyclic X-ray variability associated with orbital motion.

Wolf-Rayet Stars
W.-R. Hamann, A. Sander, H. Todt, eds.
Potsdam: Univ.-Verlag, 2015
URL: http://nbn-resolving.de/urn:nbn:de:kobv:517-opus4-84268

High Resolution X-Ray Spectra of WR 6

D. Huenemoerder[1], K. Gayley[2], W.-R. Hamann[3], R. Ignace[4], J. Nichols[5], L. M. Oskinova[3], A. M. T. Pollock[6], N. Schulz[1]
[1] *MIT Kavli Institute*; [2] *Univ. Iowa*; [3] *Univ. Potsdam*; [4] *East Tennessee State Univ.*; [5] *Smithosonian Astrophysical Obs.*; [6] *ESA, & University of Sheffield*

As WR 6 is a putatively single WN4 star, and is relatively bright ($V = 6.9$), it is an ideal case for studying the wind mechanisms in these extremely luminous stars. To obtain higher resolution spectra at higher energy (above 1 keV) than previously obtained with the XMM/Newton RGS, we have observed WR 6 with the Chandra High Energy Transmission Grating Spectrometer for 450 ks. We have resolved emission lines of S, Si, Mg, Ne, and Fe, which all show a "fin"-shaped profile, characteristic of a self-absorbed uniformly expanding shell. Steep blue edges gives robust maximal expansion velocities of about 2000 km/s, somewhat larger than the 1700 km/s derived from UV lines. The He-like lines all indicate that X-ray emitting plasmas are far from the photosphere – even at the higher energies where opacity is lowest – as was also the case for the longer wavelength lines observed with XMM-Newton/RGS. Abundances determined from X-ray spectral modeling indicate enhancements consistent with nucleosynthesis. The star was also variable in X-rays and in simultaneous optical photometry obtained with *Chandra* aspect camera, but not coherently with the optically known period of 3.765 days.

1 Introduction

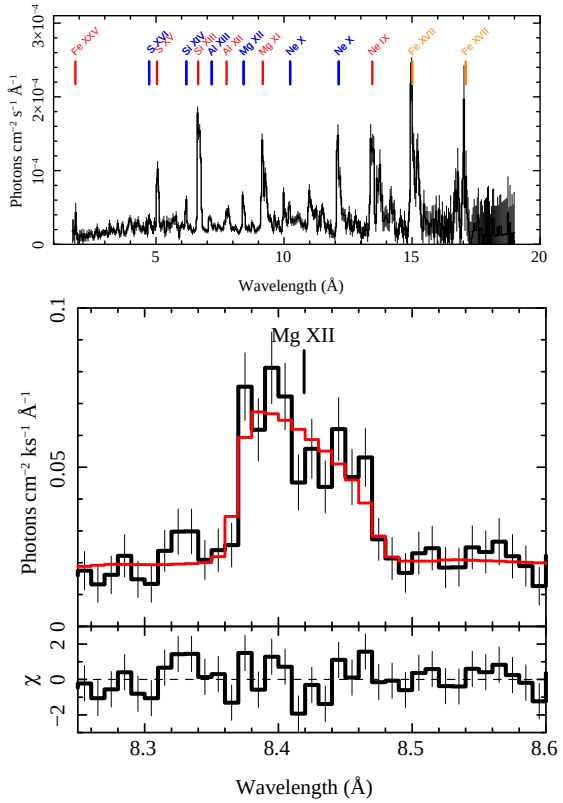

Fig. 1: The HETG spectrum (top) shows lines from H- (blue) and He-like (red) as well as Fe L-shell lines (orange). The lines have a "fin"-shaped profile (bottom) implying constant spherical expansion, as fit (red) to the Mg XII line (black), whose center is labeled. Residuals are shown in the lower sub-panel.

Wolf-Rayet stars are among the most massive and luminous of stars, whose rapid, dense winds and ultimate supernova detonations can contribute significantly to interstellar medium energetics, dynamics, and composition on large scales. Hence it is important to understand their winds and mass-loss rates. Such is usually done through optical and UV spectroscopy (Hamann et al. 2006; Hillier & Miller 1998). X-rays also tell an important story because supersonic winds can generate high temperature shocks. X-ray line strengths and profiles are key diagnostics of high energy processes occurring in the winds of WR-stars.

Hot star winds are thought to be the product of line-driven radiation pressure and dynamical instabilities which occur within the the acceleration zone which extends a few stellar radii above the photosphere (Lucy & White 1980; Krtička et al. 2009). This leads to broad lines (Ignace 2001; Owocki & Cohen 2001), and exposure to UV-intense radiation can destroy He-like forbidden lines, giving a valuable diagnostic on X-ray source location (Blumenthal et al. 1972; Waldron & Cassinelli 2001).

WR stars' massive winds are also thought to be line-driven and to have embedded shocks (Gayley & Owocki 1995). The high mass-loss rates, coupled with more compact distance scales and similar wind velocities as O-stars ($\sim 1000\,\mathrm{km\,s^{-1}}$), implies that WR stars have much denser winds than O stars, leading to higher optical depth, a feature we exploited in our analysis of X-ray profiles.

2 Characteristics of WR 6

WR 6 (EZ CMa), spectral type WN 4, is visually bright ($V = 6.9$; van der Hucht 2001), and has a distance of 1.8 kpc (Howarth & Schmutz 1995). There is no detectable trace of hydrogen in its atmo-

sphere and wind (Hamann & Koesterke 1998). WR 6 has a well established and consistent photometric period of 3.7650 d, though the modulation itself is highly variable in amplitude and phase (Georgiev et al. 1999; Robert et al. 1992; Lamontagne et al. 1986). Based on its radio and X-ray properties (Dougherty & Williams 2000; Oskinova 2005; Skinner et al. 2002), the star is considered to be single, and is not suspected of having a magnetically confined wind since it has no detected global magnetic field (de la Chevrotière et al. 2013). Other fundamental parameters of WR 6 can be found in Hamann et al. (2006).

3 Observations & Analysis

We observed WR 6 with the Chandra/HETG spectrometer (Canizares et al. 2005) in 2013 for a total of 440 ks (dataset identifiers 14533–5). The spectra cover the range from 1–30 Å with resolving powers ranging from 100 to 1000 (depending on wavelength and grating type). The data were reprocessed with standard CIAO programs (Fruscione et al. 2006, version 4.6) to apply the most recent calibrations (calibration database, version 4.5.9). Figure 1 (top panel) shows an overview of the flux spectrum.

The lines are fully resolved and appear non-Gaussian. For WR winds it is natural to expect line profiles that sample the asymptotic flow, because the winds are quite dense such that continuum optical depth unity in photoabsorption of X-ray emission is expected to be at relatively large radii. We have adopted the analytic line profile form valid in the limit of $\tau_c \gg 1$ from Ignace (2001): $f(w_z) = f_0 \left(\sqrt{1-w_z^2}\,/\arccos(-w_z)\right)^{1+q}$ where f_0 is a normalization constant and the dimensionless scaled velocity along the line-of-sight is $w_z = (c/v_\infty)(\lambda/\lambda_0 - 1)$ for a line having rest wavelength λ_0. We assumed that the emissivity per volume varies as density squared (i.e., collisional ionization equilibrium), but introduced an additional term in the form of r^{-q} ($q > -1$), which serves to modify the shape of the profile from a pure density squared case in order to represent a number of possible effects, such as a volume filling factor or an X-ray temperature distribution that depend on radius. Different q values are allowed for different lines. Figure 1 (bottom panel) shows a fit to Mg XII, a strong, relatively isolated line. All the lines share this shape, yielding a robust value for $v_\infty = 1950 \pm 20\,\mathrm{km\,s^{-1}}$. There is no trend with wavelength in contrast to that seen very strongly in thinner OB-star winds (e.g., ζ Oph Cassinelli et al. 2001). There is a hint of a trend for q with wavelength, largely driven by the RGS, but otherwise consistent with $q = -0.3 \pm 0.1$.

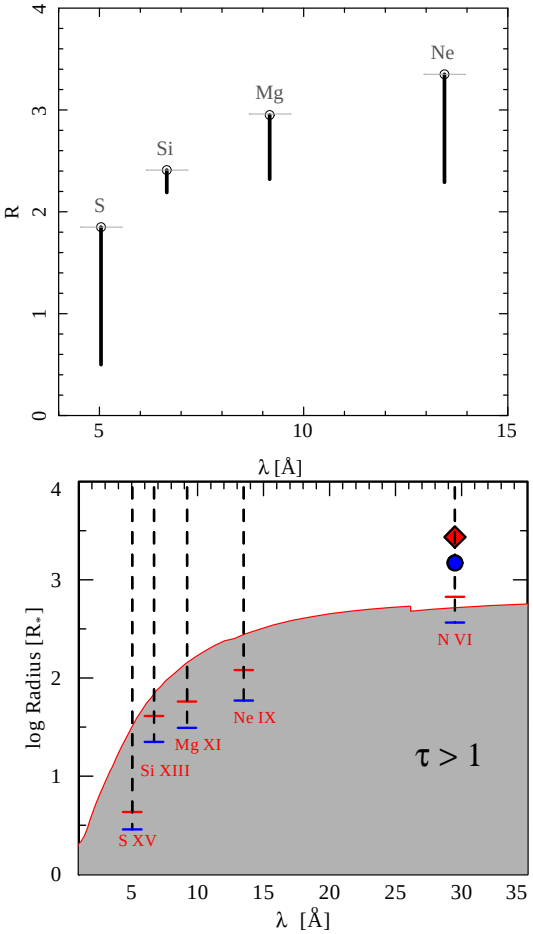

Fig. 2: The He-like $R = f/i$ ratios (top) are at their theoretically maximum values. Black bars show 90% confidence lower limits. Derived radii (bottom) for the lower limits under assumptions of localized (upper red bars) or distributed (lower blue bars) emission are all at large radii. The gray region shows where the continuum opacity exceeds 1. The N VI value is from XMM/Newton RGS, which also has fit results below the maximal R (diamond and circle).

The He-like line ratios are sensitive to UV photoexcitation and can be used to estimate the radii where X-rays are formed (Gabriel & Jordan 1969; Blumenthal et al. 1972; Waldron & Cassinelli 2007). Figure 2 shows our measurements of the R-ratio (forbidden to intercombination flux ratio, or f/i) for several ions (top panel). The best fit values are all at the un-photoexcited limit, indicating that X-rays are emitted far from the intense UV field. Using the 90% confidence limits in conjunction with a detailed model atmosphere for WR 6 of Hamann & Gräfener (2004) we determined the minimum radii of formation (Figure 2 lower panel). These are also generally at large radii, assuming either that the X-rays all form at one radius, or that they are distributed

above some onset radius.

While global modeling of the X-ray spectrum is difficult, due to the presence of both emission and absorption distributed in a likely clumpy wind, our provisional absorbed APEC model is useful in characterizing the X-ray spectrum. We added to the model of Oskinova et al. (2012) a higher temperature component apropos of the higher hard sensitivity of HETG. Comparing model and data revealed large residuals in *both* the Na X and Na XI regions which we could only reduce through a large enhancement ($\sim 7\times$) of the Na abundance. Figure 3 shows this spectral region and our fit. We could not explain the residuals by Fe blends, nor weak lines found in other spectra but not in the atomic database. We conclude that Na is indeed enhanced, and we suggest that this is a result of the Ne-Na nuclear cycle (Cavanna et al. 2014) and is diagnostic of the evolved state of WR 6.

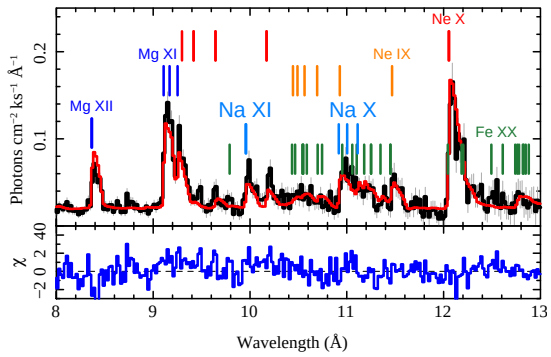

Fig. 3: To fit the HETG spectrum in the 10Å region, we required an enhanced Na abundance by about a factor of 7. We show the observed spectrum (black) and a 4-temperature APEC model (red), and residuals (blue). Some line positions are marked at the blue edge of the profile, and have vertical offsets and color-coding by element and ion (or in the case of Fe, several ions from XVII – XXIV are included).

4 Conclusions

The line profiles are consistent with production of X-rays in an optically thick photoabsorbing wind from a region of constant spherical expansion, far outside the acceleration zone where embedded wind shocks are thought to effectively generate X-rays in OB-stars. In WR 6, we cannot observe this zone.

The He-like line ratios are consistent with the line profile modeling assumptions and localize the emergent emission throughout radii larger than 10–300 R_*.

Presence of enhanced Na lines is indicative of nucleosynthesis. X-ray spectra such as this may be a good way to probe evolutionary states through relative abundances of Ne, Na, Al, and Mg.

Acknowledgements: This work was supported by NASA through the Smithsonian Astrophysical Observatory under contract NAS8-03060 via Chandra Awards GO3-14003A and GO5-16009A to MIT (DPH), GO3-14003D to ETSU (RI), GO3-14003B to SAO (JN), and GO3-13003C to UI (KGG). LO thanks the DLR grant 50 OR 1302.

References

Blumenthal, G. R., Drake, G. W. F., & Tucker, W. H. 1972, ApJ, 172, 205
Canizares, C. R., Davis, J. E., Dewey, D., et al. 2005, PASP, 117, 1144
Cassinelli, J. P., Miller, N. A., Waldron, W. L., MacFarlane, J. J., & Cohen, D. H. 2001, ApJ, 554, L55
Cavanna, F., Depalo, R., Menzel, M.-L., et al. 2014, European Physical Journal A, 50, 179
de la Chevrotière, A., St-Louis, N., Moffat, A. F. J., & the MiMeS Collaboration. 2013, ApJ, 764, 171
Dougherty, S. M. & Williams, P. M. 2000, MNRAS, 319, 1005
Fruscione, A., McDowell, J. C., Allen, G. E., et al. 2006, in Presented at the Society of Photo-Optical Instrumentation Engineers (SPIE) Conference, Vol. 6270, SPIE Conference Series
Gabriel, A. H. & Jordan, C. 1969, MNRAS, 145, 241
Gayley, K. G. & Owocki, S. P. 1995, ApJ, 446, 801
Georgiev, L. N., Koenigsberger, G., Ivanov, M. M., St.-Louis, N., & Cardona, O. 1999, A&A, 347, 583
Hamann, W.-R. & Gräfener, G. 2004, A&A, 427, 697
Hamann, W.-R., Gräfener, G., & Liermann, A. 2006, A&A, 457, 1015
Hamann, W.-R. & Koesterke, L. 1998, A&A, 333, 251
Hillier, D. J. & Miller, D. L. 1998, ApJ, 496, 407
Howarth, I. D. & Schmutz, W. 1995, A&A, 294, 529
Ignace, R. 2001, ApJ, 549, L119
Krtička, J., Feldmeier, A., Oskinova, L. M., Kubát, J., & Hamann, W.-R. 2009, A&A, 508, 841
Lamontagne, R., Moffat, A. F. J., & Lamarre, A. 1986, AJ, 91, 925
Lucy, L. B. & White, R. L. 1980, ApJ, 241, 300
Oskinova, L. M. 2005, MNRAS, 361, 679
Oskinova, L. M., Gayley, K. G., Hamann, W.-R., et al. 2012, ApJ, 747, L25
Owocki, S. P. & Cohen, D. H. 2001, ApJ, 559, 1108
Robert, C., Moffat, A. F. J., Drissen, L., et al. 1992, ApJ, 397, 277
Skinner, S. L., Zhekov, S. A., Güdel, M., & Schmutz, W. 2002, ApJ, 579, 764
van der Hucht, K. A. 2001, New A Rev., 45, 135
Waldron, W. L. & Cassinelli, J. P. 2001, ApJ, 548, L45
Waldron, W. L. & Cassinelli, J. P. 2007, ApJ, 668, 456

D. John Hillier: Calculations by Prantzos et al (Prantzos, N., Doom, C., de Loore, C., & Arnould, M. 1986, ApJ, 304, 695) show that in LBVs and WN stars sodium can be enhanced by a factor of 2 to 4. This can probably explain the enhanced sodium derived from the X-ray spectrum of HD 50896 (WR6).

Michael Corcoran: The X-ray data show that the X-ray emission in WR 6 is far from the star, yet it's variable which suggests that it arises from a relatively small region far from the star. Any comments?

David Huenemoerder: The X-ray modulation is small (about 15%), and has similar amplitude in both the Chandra and XMM (Oskinova et al. 2012). data. The variability is not coherent in phase. We don't know what causes the variability, and are looking for time-resolved spectral changes in the high-resolution spectrum. There is an heuristic model invoking co-rotating interaction region (CIR) propagating spiral structures which can qualitatively describe this type of X-ray variability (Ignace et al. 2013).

Anthony (Tony) Moffat: According to the CIR models of Cranmer & Owocki (1996) the maximum shock velocities reach 500 km/s, so moderately hard X-rays only.

David Huenemoerder: Such a shock velocity would only be sufficient to produce soft X-rays ($\sim$ 2 MK). There is plasma at this temperature in EZ CMa, but there is also significantly hotter plasma, reaching about 40 MK.

Götz Gräfener: WR 6 shows line-depolarization which may indicate a wind anisotropy or DACs (Discrete Absorption Components). Do you think that the latter could explain the X-ray variability?

David Huenemoerder: Yes, possibly. But if related to DACs, coherent structures would need to exist far out in the X-ray emitting wind.

(Ignace et al. 2013 presented a phenomenological model using co-rotating interaction regions to qualitatively explain X-ray variability seen in the XMM observations of WR 6.)

Wolf-Rayet Stars
W.-R. Hamann, A. Sander, H. Todt, eds.
Potsdam: Univ.-Verlag, 2015
URL: http://nbn-resolving.de/urn:nbn:de:kobv:517-opus4-84268

Studies of WR+O colliding-wind binaries

E. Gosset
F.R.S.-FNRS & Institut d'Astrophysique et de Géophysique, Université de Liège, Belgium

Two of the main physical parameters that govern the massive star evolution, the mass and the mass-loss rate, are still poorly determined from the observational point of view. Only binary systems could provide well constrained masses and colliding-wind binaries could bring some constraints on the mass-loss rate. Therefore, colliding-wind binaries turn out to be very promising objects. In this framework, we present detailed studies of basic observational data obtained with the *XMM-Newton* facility and combined with ground-based observations and other data. We expose the results for two particularly interesting WR+O colliding-wind binaries: WR 22 and WR 21a.

1 Introduction

Massive stars (OBs and their descendants WR stars) are very important objects that play a major role in the chemical evolution of galaxies, but also in the dynamical evolution through their influence, positive or negative, on star formation and through the shaping of their environment. Despite this importance, several aspects of their live remain poorly known. Two of the main parameters that govern their evolution, the mass and the mass-loss rate, are still poorly determined from the observational point of view. A good observational determination of masses can only be obtained through the study of binary systems. In massive systems, the winds of both components do collide somewhere in-between the two stars. This collision zone, at least near its apex, is then emitting in the X-ray domain. The shape of the collision zone is dependent on the relative importance of individual winds, possibly providing constraints on the relative mass-loss rates. The X-ray flux characteristics are dependent on the wind and their variations along the orbital cycle bear also information on the individual mass-loss rates. Therefore WR+O and O+O colliding-wind binaries are key objects to constrain evolution of massive stars.

From the formation point of view, the origin and the nature of the most massive stars are also poorly known. In the quest of young massive stars, some astronomers are studying the O2 and O3 stars. However, some people think that, very early, the very massive stars appear as disguised in hydrogen-rich, late WN stars even if they are still in the core-hydrogen-burning evolutionary status. These stars of spectral type WNLh are now recognized as key objects to understand the beginning of the evolution of massive stars. Some of these objects are also belonging to binary systems. In the following, we will illustrate the potentialities of the WNLh+O systems by reporting some results of the study of two of them: WR 22 that we observed and studied some time ago and WR 21a which in some sense is a newcomer in the game.

2 The case of WR 22

WR 22 is a WN7h+O binary star with a period of 80.33 days. Actually, this star has been the first discovered WR+O binary system where the mass of the WR turned out to be strongly in excess of the O one (Rauw et al. 1996). Concomitantly, this primary WNLh star was recognized as strongly massive with a keplerian mass somewhere between 56 and 72 $M_\odot$ (Rauw et al. 1996; Schweickhardt et al. 1999). If at 72 $M_\odot$, the star is most probably not a pure WR but rather a core-H burning object (Rauw et al. 1995, and references therein). WR 22 has been observed with the *XMM-Newton* facility and its X-ray lightcurve tentatively interpreted (Gosset et al. 2009). This lightcurve presents no variation in the hard band, whereas some variable absorption is detected in the soft and middle band. Indeed, the system is eccentric and roughly seen from the apastron side. When the O star goes from apastron to periastron, it is going deeper and deeper into the WR wind. Therefore, the two possible X-ray sources (the O star itself and the collision apex situated very close to the O star on the main axis of the binary) are also diving into the WR wind. Thus, the X-ray emission should be more and more absorbed, which seems to be the case. This configuration offers the possibility to perform some scanning of the WR wind structure.

In the following, we will restrict ourselves to the problem of the mass-loss rate of the WR star that can be deduced from the absorbing column. Assuming a classical velocity law for the wind, it is possible to express the density in the wind as a function of the distance to the WR. The various intervening parameters are the velocity law, the radius of the WR and the mass-loss rate. The last one is the most important one. The absorbing column can be estimated by integrating, along the line of sight from the observer to the X-ray emission zone, the density being estimated at each step as a function of the distance to the WR. Gosset et al. (2009) performed the work and concluded that the adopted mass-loss rate was a factor of two too large to explain the observed soft X-ray absorption. These conclusions could result from a too simple model used by Gosset et al. (2009). However, a more sophisticated model based

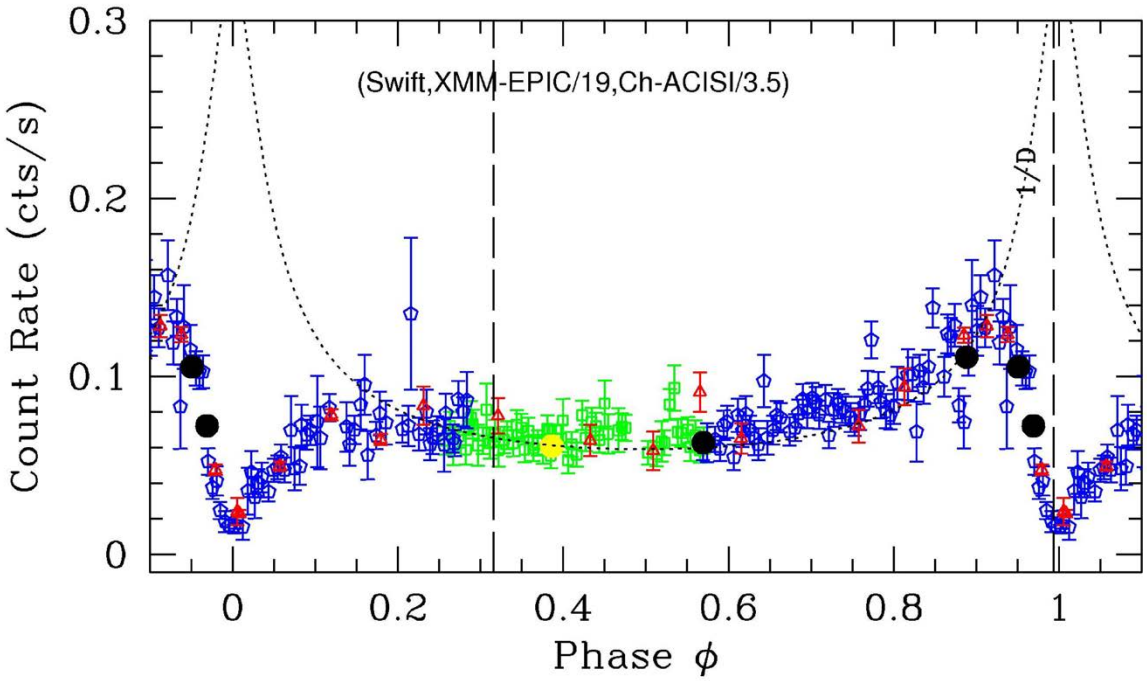

Fig. 1: The X-ray lightcurve of the massive binary system WR 21a presented under the form of count rates as a function of the binary phase. Periastron is at phase 0.0. The filled black circles represent the *XMM-Newton* count rates (divided by 19) whereas the yellow filled circle is from *Chandra* count rates (divided by 3.5). The *Swift* ones are plotted as red triangles for the year 2013, as green squares for the year 2014 and as blue pentagons for 2015. The error-bars represent 1σ standard deviation. The vertical dashed lines mark the position of both conjunctions. The dotted curve is illustrative and represents the canonical $1/D$ evolution of the count rates (see text for details).

on 3D hydrodynamical simulations, arrived from this point of view to similar conclusions (Parkin & Gosset 2011). Two problems occur: the models predict a too large X-ray emission and a too large absorbing column (about a factor of two).

At the time of these works, we supposed that the WN itself was not emitting in the X-ray domain, leading to a lower limit constraint on the fitted mass-loss rate. In addition, since then, WR 22 was observed by the *Chandra* facility in the framework of the CCCP project (Townsley et al. 2011). Within the *XMM-Newton* point spread function, there is actually three sources. The two additional ones were responsible for one fifth of the flux. Therefore, the conclusions needed critical revision.

The *Chandra* observation took place at phase 0.85. We estimated the expected fluxes of WR 22 at that phase from our *XMM-Newton* data. We computed 20% of that flux and attributed this value to the two neighbouring objects. We considered that this contribution is constant and performed again all the fits. The column densities deduced in this way are not strongly different from the previously published ones. A marked exception concerns the spectrum at phase 0.994. In this case, an increase of the column density by 60% is noticed, reaching even 100% if the constant emission component is softer. We also attempted to consider an emission from the WN component of maximum 0.59×10^{-13} erg cm^{-2} s^{-1} (Gosset et al. 2009). In principle, the maximum flux limit could be ten times lower. An increase of the column density is also observed but never markedly exceeding the predicted column (see Fig. 10 of Gosset et al. 2009). Again this does not apply to the observations at phase 0.994 which is impossible to fit properly. We can conclude that the presence of the two neighbouring objects and the possibility to attribute some constant flux to the WN component (the possible WN intrinsic emission does not vary along the orbital cycle), lead to a possible increase of the column densities derived from the fit of the *XMM-Newton* data, by a factor of two but no more. No further information can be extracted from the low S/N spectrum at phase 0.994. Therefore, we can conclude that the derived column density could be in agreement with the physical parameters adopted by Gosset et al. (2009) provided we accept to attribute some emission to the WN component.

3 The new case of WR 21a

In the same context, another very interesting object is WR 21a. The study presented here results from a collaborative work with Y. Nazé; all the details can be found in the related publication (Gosset & Nazé 2015). The object was spectroscopically studied by Niemela et al. (2008) and more recently by Tramper et al. (2015). WR 21a is a WN5h+O3V binary system with an eccentricity $e = 0.693$, and bearing minimum masses of 65.3 and 36.6 $M_\odot$, respectively. If the minimum mass of the O star is scaled to the expected mass for an O3V one, the mass associated to the WN5h object could easily reach 80–100 $M_\odot$ or more. The system is oriented, compared to the observer, in roughly the same manner than WR 22; its inclination based on the minimum masses should be around 58°.8. This system has originally been detected as an X-ray source. Therefore, we decided to observe it with the *XMM-Newton* facility. Four 30 ks exposures took place at phases $\phi = 0.57$, 0.89, 0.95 and 0.97. The resulting spectra can be fitted by a two-component optically-thin thermal plasma emission with kT = 0.8 keV and 3.0 keV. These temperatures do not seem to vary over the orbital cycle except for a small marginal decrease while going to periastron. Concerning the X-ray lightcurve, we complemented our data with archival *Swift* and *Chandra* data (see also Sugawara et al. 2015). Fig. 1 presents the evolution of the count rates in the total band (0.4–10.0 keV) as a function of the orbital phase. From phase 0.2 to phase 0.8, the curve is not varying too much but from phase 0.8 to 0.9, an increase of the flux is clearly present. This corresponds to a behaviour in $1/D$ (where D is the binary separation). This behaviour is typical of eccentric systems where the nearing of the system is accompanied by a proportional increase of the flux if the postshock material is behaving adiabatically. This behaviour is unexpected for WR 21a. When approaching the conjunction ($\phi = 0.9935$) and periastron, the flux starts to decrease. The behaviour of the hard band is slightly different from the one of the soft band. This renders the various fits less trustable than in the case of WR 22. Apparently, a more important absorbing column density (expected near conjunction) is able to explain the decrease in the soft band, but not the entire variation in the hard band. Most probably, a disruption of the shock or a crash of it on the O surface are possible explanations. The recovery of the decrease is not so rapid and the lightcurve seems to exhibit a marked hysteresis effect. The full recovery occurs at $\phi = 0.2$ only. It is also interesting to notice that there is no particular variation around $\phi = 0.346$ that corresponds to the other conjunction. A preliminary estimation of the mass-loss rate of the WN5h star leads to a value similar to the one first adopted for WR 22.

4 Conclusion

We presented detailed studies of two very interesting binary systems. These systems are composed of a primary star of type WNLh and of an O component. The WNLh stars are particularly massive as securely determined from the binarity and keplerian laws. Such systems also harbour a collision of the wind that provides further information on them and particularly on the relative mass-loss rates. The orbital movement of these eccentric systems offers the possibility to scan the envelope of the WR component while the O star is diving in it. Such studies should help us to understand the origin and the true nature of these extreme stars and to provide constraints on their evolution.

References

Gosset, E., & Nazé, Y. 2015, submitted

Gosset, E., Nazé, Y., Sana, H., Rauw, G., Vreux, J.-M. 2009, A&A, 508, 805

Niemela, V.S., Gamen, R.C., Barbá, R.H., et al. 2008, MNRAS, 389, 1447

Parkin, E.R., & Gosset, E. 2011, A&A, 530, A119

Rauw, G., Vreux, J.-M., Gosset, E., Hutsemékers, D., Magain, P. 2005, LIACo, 32, 463

Rauw, G., Vreux, J.-M., Gosset, E., Hutsemékers, D., Magain, P., Rochowicz, K. 1996, A&A, 306, 771

Schweickhardt, J., Schmutz, W., Stahl, O., Szeifert, Th., & Wolf, B. 1999, 347, 127

Sugawara, Y., Tsuboi, Y., Maeda, Y., Pollock, A.M.T., Williams, P.M. 2015, these proceedings

Townsley, L.K., Broos, P.S., Corcoran, M.F., et al. 2011, ApJS, 184, 1

Tramper, F., Sana, H., Fitzsimons, N.E., et al. 2015, submitted

Götz Gräfener: Your results for WR 22 seem to agree very well with hydrodynamic models by Gräfener & Hamann (2008).

Eric Gosset: Really? I do not know this paper. I guess you are speaking of hydrodynamic models for the wind of the WNLh component alone. The agreement between our observations and your predictions indicates that we are on the verge of getting accurate values for the mass-loss rates of this kind of star

Wolf-Rayet Stars
W.-R. Hamann, A. Sander, H. Todt, eds.
Potsdam: Univ.-Verlag, 2015
URL: http://nbn-resolving.de/urn:nbn:de:kobv:517-opus4-84268

Hydrodynamic and radiative transfer modeling of X-ray emission from colliding WR winds: WR 140 & the Galactic center

C. M. P. Russell[1], M. F. Corcoran[1,2], J. Cuadra[3], S. P. Owocki[4], Q. D. Wang[5], K. Hamaguchi[1,6], Y. Sugawara[7], A. M. T. Pollock[8] & T. R. Kallman[1]
[1] *X-ray Astrophysics Laboratory, NASA/GSFC, USA*
[2] *University Space Research Association, USA*
[3] *Pontificia Universidad Católica de Chile, Chile*
[4] *University of Delaware, USA*
[5] *University of Massachusetts Amherst, USA*
[6] *University of Maryland, Baltimore County, USA*
[7] *Chuo University, Japan*
[8] *University of Sheffield, England*

Colliding Wolf-Rayet (WR) winds produce thermal X-ray emission widely observed by X-ray telescopes. In wide WR+O binaries, such as WR 140, the X-ray flux is tied to the orbital phase, and is a direct probe of the winds' properties. In the Galactic center, ∼30 WRs orbit the super massive black hole (SMBH) within ∼10", leading to a smorgasbord of wind-wind collisions. To model the X-ray emission of WR 140 and the Galactic center, we perform 3D hydrodynamic simulations to trace the complex gaseous flows, and then carry out 3D radiative transfer calculations to compute the variable X-ray spectra. The model WR 140 *RXTE* light curve matches the data well for all phases except the X-ray minimum associated with periastron, while the model spectra agree with the *RXTE* hardness ratio and the shape of the *Suzaku* observations throughout the orbit. The Galactic center model of the *Chandra* flux and spectral shape match well in the region $r \leq 3$", but the model flux falls off too rapidly beyond this radius.

1 Introduction

The supersonic speeds and high mass-loss rates of WR winds lead to their collisions generating strong signatures of thermal X-ray emission. These observations, which have been performed by a wide variety of X-ray telescopes, yield important information about these WR winds since they cause both the X-ray emission and absorption. To disentangle the physical properties that lead to the observed thermal X-ray observations, we use 3D hydrodynamic simulations to determine the complex density and temperature structure of the interacting winds, and then perform 3D X-ray radiative transfer calculations to match the model X-ray emission to the observations, refining the models if necessary. Here we present our work on WR 140 and the Galactic center.

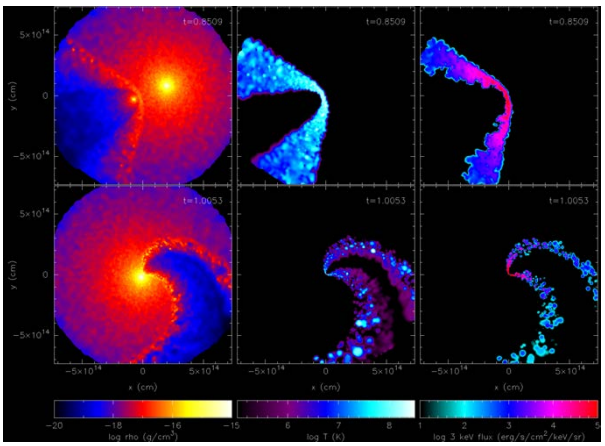

Fig. 1: WR 140 density (left), temperature (center), and 3 keV X-rays (right) in the orbital plane at phase 0.85 (top) and 0.005 (bottom).

2 WR 140

WR 140 is the canonical long-period, highly eccentric, colliding wind binary (CWB). The binary's X-ray flux (Corcoran et al. 2011) show strong variation locked to the orbital period; the flux is ∼ 1/(separation) as expected for adiabatic shocks (Stevens et al. 1992), except around periastron where the flux drops and the spectra hardens.

Fig. 1 shows the density, temperature, and 3 keV X-ray emission in the orbital plane of the 3D smoothed particle hydrodynamics (SPH) simulation of WR 140. The winds accelerate from their stellar surfaces according to a $\beta = 1$ velocity law, $v(r) = v_\infty(1 - R/r)$. The abundances of the two winds, which enter the SPH simulations via the mean molecular weight and the radiative cooling rates from `Spex` (Schure et al. 2009), are from Asplund et al. (2009) for the O4-5 star and from Crowther (2007) for the WC7 star, namely $X_{\rm He} = 0.6$, $X_{\rm C} = 0.31$, and $X_{\rm O}$=0.07. The radiative transfer calculation also uses the abundances for the X-ray emissivites, which come from the `APEC` model (Smith et al. 2001) in `XSpec` (Arnaud 1996), and the wind

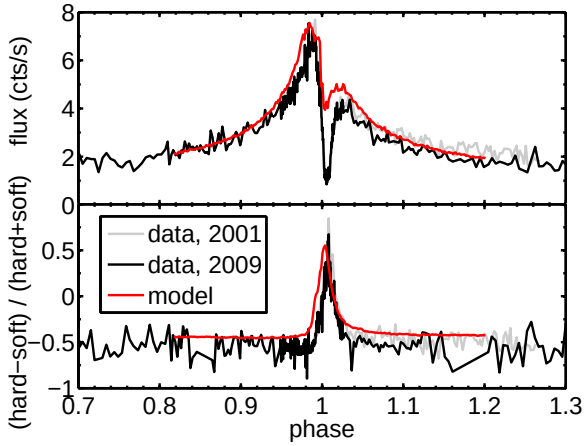

Fig. 2: *RXTE* light curve (top) and hardness ratio (bottom) comparing the data when periastron occurred in 2001 (gray), in 2009 (black), and the model (red).

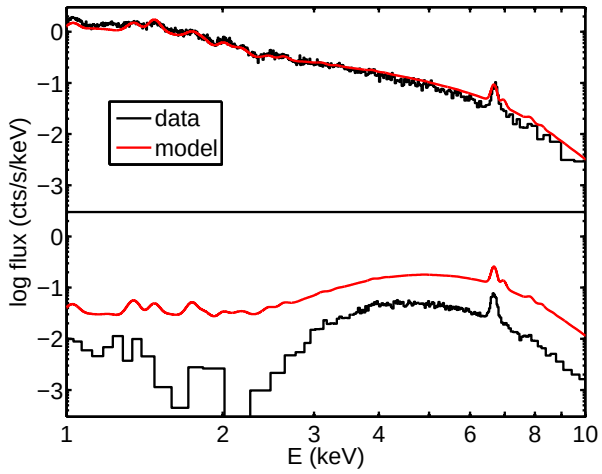

Fig. 3: *Suzaku* XIS spectra at phase 0.904 (top) and 1.000 (bottom). The observations are from Sugawara et al. (2015).

opacities, which come from `windtabs` (Leutenegger et al. 2010). The ISM opacities are from `TBabs` (Wilms et al. 2000), and the basis of the radiative transfer calculation is the SPH visualization program `Splash` (Price 2007).

Fig. 2 shows the *RXTE* 2–10 keV light curve and hardness ratio comparing the 7.5 keV and 3 keV channels, while Fig. 3 shows the *Suzaku* spectra on the rise to maximum and at periastron. The model X-ray flux, in absolute units, matches well for the majority of the orbit, but does not decrease enough around periastron. On the other hand, the hardness ratio and spectral shapes match well throughout the orbit, so a gray reduction in flux at periastron is needed to improve the models.

One possibility is to reduce the O-star wind around periastron so it carves out a smaller cavity in the WC wind, thus making less of the WC wind shock. This will not alter the pre-shock speed of the WC wind, but will reduce its X-ray flux at all energies. Parkin & Sim (2013), based on this phenomena occurring in X-ray binaries (Stevens & Kallman 1990), explored how wind-wind collision X-rays could reduce the wind strength by ionizing its acceleration region, though the colliding-wind X-rays are not strong enough to ionize the O-star wind in WR 140. Alternatively, the hot radiation from the WC star itself could provide the source of the ionizing photons, which will be explored in future work.

3 Galactic center

Cuadra et al. (2008) used the SPH code `Gadget-2` to follow the orbits of the 30 WR stars within 12" (1"∼0.04 pc) of the SMBH at the Galactic center from 1100 years ago to the present day, all while these stars are ejecting their wind material. The simulation volume quickly fills up to form an ambient medium of 'old' ejected material, into which the 'new' ejected material creates bowshocks (spherical bubbles) around the fast- (slow-) moving WR stars. This hot post-shocked gas emits thermal X-rays.

Following the *Chandra* X-ray Visionary Project of the Galactic center (Wang et al. 2013), Cuadra et al. (2015) improved the hydrodynamic simulations by incorporating several SMBH outflow models potentially associated with the radiatively inefficient accretion flow. These range from an outflow of $v = 10\,000$ km/s and $\dot{M}_{\rm out} = \dot{M}_{\rm accrete}$ over the entire simulation time, to an outburst of $v = 10\,000$ km/s and $\dot{M}_{\rm out} = 10^{-4}\,M_\odot$/yr lasting from 400 to 100 years ago as suggested by X-ray light echo observations (Ponti et al. 2010).

To anchor these simulations in observations, we perform the same X-ray radiative transfer calculation as with WR 140, except that we use the following abundances for the various WR spectral types: the WC8-9 stars have the same WC abundance as the WC7 in WR 140, the WN5-7 stars have WN6 abundances from Onifer et al. (2008), and the WN8-9 stars have WN8 abundances from the `CMFGEN` website. Figure 4 shows the 1–9 keV *Chandra* ACIS-S HETG 0th order image of the central ±6″ for the three models. To account for the PSF, we fold the model images through a 0.5″ FWHM Gaussian.

Since the model does not include the swath from the pulsar wind nebulae in the upper right portion of the plot, nor any point-like emission from the SMBH, the valid region of comparison is the remaining diffuse emission. The no-feedback model matches well the region from just beyond the SMBH's influence to ∼ 3″ in radius, but then falls off much more quickly than the data farther out. Also,

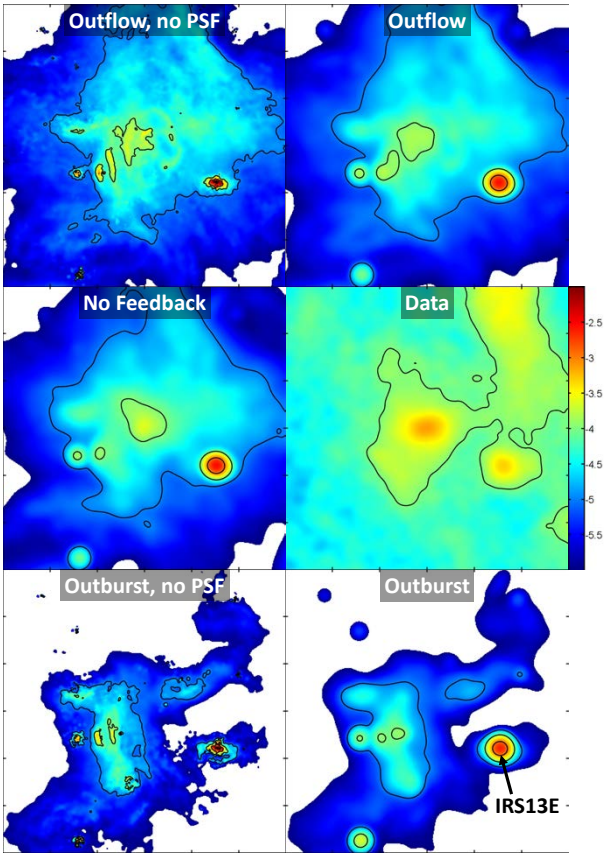

Fig. 4: *Chandra* 1–9 keV images (±6″) of the Galactic center with various SMBH feedback models. The images with the PSF folding are directly comparable to the data. The color bar units are the log of cts/s/arcsec^2. The image color is white below the color bar range.

there are a few stars whose immediate vicinities have too large an X-ray flux compared to the observations, the brightest of which is the IRS13E cluster, which contains two closely located WR stars. The outflow model slightly increases the X-ray emission, which is expected since more energy is being added to the simulation, while the outburst model significantly decreases the X-rays through clearing the hot, X-ray-producing gas out of the simulation volume. It is excluded as a viable feedback model.

Figure 5 shows the X-ray spectra from a 2″–5″ ring (excluding IRS13E). The shape of all feedback models match the data well for $n_H = 1.5{\times}10^{23}\mathrm{cm}^{-2}$, consistent with the value from analyzing the SMBH emission in the *Chandra* data (Wang et al. 2013).

To improve the viable models, the IRS13E flux can be decreased by lowering one or both wind strengths, or increasing the stellar separation. Increasing the diffuse emission beyond $\sim 3''$, but not below this radius, is more challenging since increasing mass loss rates will also increase the central X-ray emission, while raising wind speeds will make the spectra harder. More ambient gas in the outer regions would improve the models since the adiabatic WR shocks

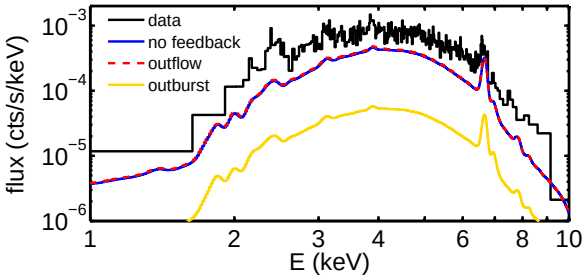

Fig. 5: *Chandra* spectra of the Galactic center.

will occur closer to their star, increasing their emission according to $\sim 1/d_{\mathrm{shock}}$. Depending on their locations, the SMBH-orbiting O stars might provide this extra gas, and will be included in future work.

References

Arnaud, K. A. 1996, in Astronomical Society of the Pacific Conference Series, Vol. 101, Astronomical Data Analysis Software and Systems V, ed. G. H. Jacoby & J. Barnes, 17

Asplund, M., Grevesse, N., Sauval, A. J., & Scott, P. 2009, ARA&A, 47, 481

Corcoran, M. F., Pollock, A. M. T., Hamaguchi, K., & Russell, C. 2011, ArXiv e-prints

Crowther, P. A. 2007, ARA&A, 45, 177

Cuadra, J., Nayakshin, S., & Martins, F. 2008, MNRAS, 383, 458

Cuadra, J., Nayakshin, S., & Wang, Q. D. 2015, MNRAS, 450, 277

Leutenegger, M. A., Cohen, D. H., Zsargó, J., et al. 2010, ApJ, 719, 1767

Onifer, A., Heger, A., & Abdallah, J. 2008, in Astronomical Society of the Pacific Conference Series, Vol. 391, Hydrogen-Deficient Stars, ed. A. Werner & T. Rauch, 305

Parkin, E. R. & Sim, S. A. 2013, ApJ, 767, 114

Ponti, G., Terrier, R., Goldwurm, A., Belanger, G., & Trap, G. 2010, ApJ, 714, 732

Price, D. J. 2007, PASA, 24, 159

Schure, K. M., Kosenko, D., Kaastra, J. S., Keppens, R., & Vink, J. 2009, A&A, 508, 751

Smith, R. K., Brickhouse, N. S., Liedahl, D. A., & Raymond, J. C. 2001, ApJ, 556, L91

Stevens, I. R., Blondin, J. M., & Pollock, A. M. T. 1992, ApJ, 386, 265

Stevens, I. R. & Kallman, T. R. 1990, ApJ, 365, 321

Sugawara, Y., Maeda, Y., Tsuboi, Y., et al. 2015, ArXiv e-prints

Wang, Q. D., Nowak, M. A., Markoff, S. B., et al. 2013, Science, 341, 981

Wilms, J., Allen, A., & McCray, R. 2000, ApJ, 542, 914

Andy Pollock: What improvements, especially related to shocks, do you expect from the improved "pressure-entropy" SPH method?

Christopher Russell: For the adiabatic shocks, which are comparably large and well resolved, I do not expect much difference in the results. So I don't expect much of the X-ray results I presented to change. But for radiative shocks, which are comparably thin, the instabilities that arise in them have been shown to be better modeled in the new method. The reason is the volume parameterization in the current method is the particle mass over the particle density, so the discontinuous-at-a-shock density is in the denominator. The new method uses a volume parameterization that puts the pressure in the denominator, which is continuous across a shock. This improvement might come into play at periastron of WR 140 depending on the exact parameters of the system, including the abundance – and hence the cooling function – of the WC wind.

Anthony (Tony) Moffat: Using clump trajectories, we (Moffatt & Lepine 1999) derived empirical values of $\beta \approx 10$ in the outer wind of many strong-wind WR stars (the O star ζ Pup gave $\beta \approx 1$ with the same technique). What is the justification for adopting $\beta \approx 1$ in the outer wind of WR 140 in your simulations?

Christopher Russell: Well, the most important β to get correct is for the O star wind since the wind-wind collision occurs much closer to it than the WC star. I am aware the WR β's can be larger, but I only recall a value of up to $\beta \approx 3$, which analytic estimates of the ram pressure balance show will not make that much difference in the pre-shock WR wind velocity. So I guess that's why we stuck with $\beta = 1$ in the sims. On the other hand, $\beta \approx 10$ seems like it should have a noticeably lower pre-shock velocity, as well as a denser wind. Both of these effects would soften the spectra at periastron, so while the model's overall flux level might be in better agreement with the observations, the spectral shape will probably be worse. Of course the β-law parameterization is also predicated on having a reliable WR radius. But I will look into the effects of $\beta \approx 10$ more, thank-you.

WR nebulae

Wolf-Rayet Stars
W.-R. Hamann, A. Sander, H. Todt, eds.
Potsdam: Univ.-Verlag, 2015
URL: http://nbn-resolving.de/urn:nbn:de:kobv:517-opus4-84268

Wolf-Rayet nebulae and the wind-interstellar medium interaction

S. J. Arthur[1]
[1]*Instituto de Radioastronomía y Astrofísica, UNAM, México*

I review our current understanding of the interaction between a Wolf-Rayet star's fast wind and the surrounding medium, and discuss to what extent the predictions of numerical simulations coincide with multiwavelength observations of Wolf-Rayet nebulae. Through a series of examples, I illustrate how changing the input physics affects the results of the numerical simulations. Finally, I discuss how numerical simulations together with multiwavelength observations of these objects allow us to unpick the previous mass-loss history of massive stars.

1 Introduction

Shells of optical nebulosity around Wolf-Rayet (WR) stars were originally identified as a class of object by Johnson & Hogg (1965). Kinematical data showed these shells to be expanding with respect to the stellar position and were interpreted in terms of a stellar wind interaction with the surrounding medium (Avedisova 1972), since the WR stars were known to have powerful stellar winds. Chu and collaborators originally classified known nebulae around WR in terms of their [OIII] and Hα morphologies (Chu 1981). The nebulae were classified as radiatively excited (essentially HII regions), ejecta nebulae or wind-blown bubbles. The ejecta nebulae are all related to WN8 stars (e.g., RCW 58), while the wind-blown bubbles are found mainly around WNE stars (e.g., S 308 and NGC 6888). A revised classification scheme (Gruendl et al. 2000) took into account the relative positions of the Hα and [OIII] emission, which can be either coincident, or in many cases the bright, clumpy Hα emission is interior to the [OIII] front.

2 Formation of Wolf-Rayet Nebulae

The general formation scenario for WR wind-blown bubbles was explained in a series of papers by García-Segura et al. (1996a,b) in terms of interacting winds. Numerical simulations were used to explore the interaction between the fast WR wind and the slow, dense wind ejected during a previous red supergiant (RSG) or luminous blue variable (LBV) evolutionary phase of the central star. Instabilities, which form at the contact discontinuity, lead to the formation of clumps and filaments composed of swept-up slow wind material that move outwards as the nebula expands. Even in these purely hydrodynamic models, useful comparisons can be made with WR nebulae such as RCW 58 and S 308. On the timescale of a few tens of thousands of years, nebulae of around 4 pc radius are formed, with expansion velocities similar to those reported from observations (50–100 km s^{-1}; Chu 1983).

Freyer et al. (2003) and Freyer et al. (2006) explored the interaction between massive stars and their environment with radiation-hydrodynamics models. Although their simulations were much lower resolution, in order to include the main sequence bubble, they found the same sorts of instabilities as García-Segura et al. (1996a,b). Furthermore, they found that the ionizing radiation emitted by the massive star is important for the energy balance of the surrounding ISM.

3 Radiation-Hydrodynamics Simulations

High-resolution, radiation-hydrodynamics simulations were carried out by Toalá & Arthur (2011) with the aim of testing 3 sets of stellar evolution models to see if the differences between the models would lead to notable observable differences in the surrounding circumstellar nebulae. They used the 40 and 60$M_\odot$ "Geneva Group" models of Meynet & Maeder (2003), both with and without stellar rotation (denoted MMROT and MM, respectively), and the corresponding STARS models (Eldridge & Tout 2004), where solar metallicity is assumed in each case. The star's radius, luminosity, surface temperature and surface gravity were used to assign a stellar wind velocity and ionizing photon rate to each time point of the evolution models using the Starburst99 code (Leitherer et al. 1999). The wind velocity and ionizing photon rate are important for the formation of the surrounding circumstellar nebulae.

The initial interstellar medium for these simulations was assumed to be uniform with a density of $n = 100$ cm^{-3} and a temperature of $T = 100$ K. In practice, WR stars begin their lives in a dense molecular cloud, often in a cluster environment. Their immediate surroundings will be affected by the ionizing radiation and stellar winds of the other cluster stars, as well as by any large scale density gradients due to the molecular cloud (Arnal & Cappa 1996). Furthermore, several WR stars are classed as runaways and have an important velocity with respect to their ambient medium (see, e.g., Reyes-Iturbide, these proceedings).

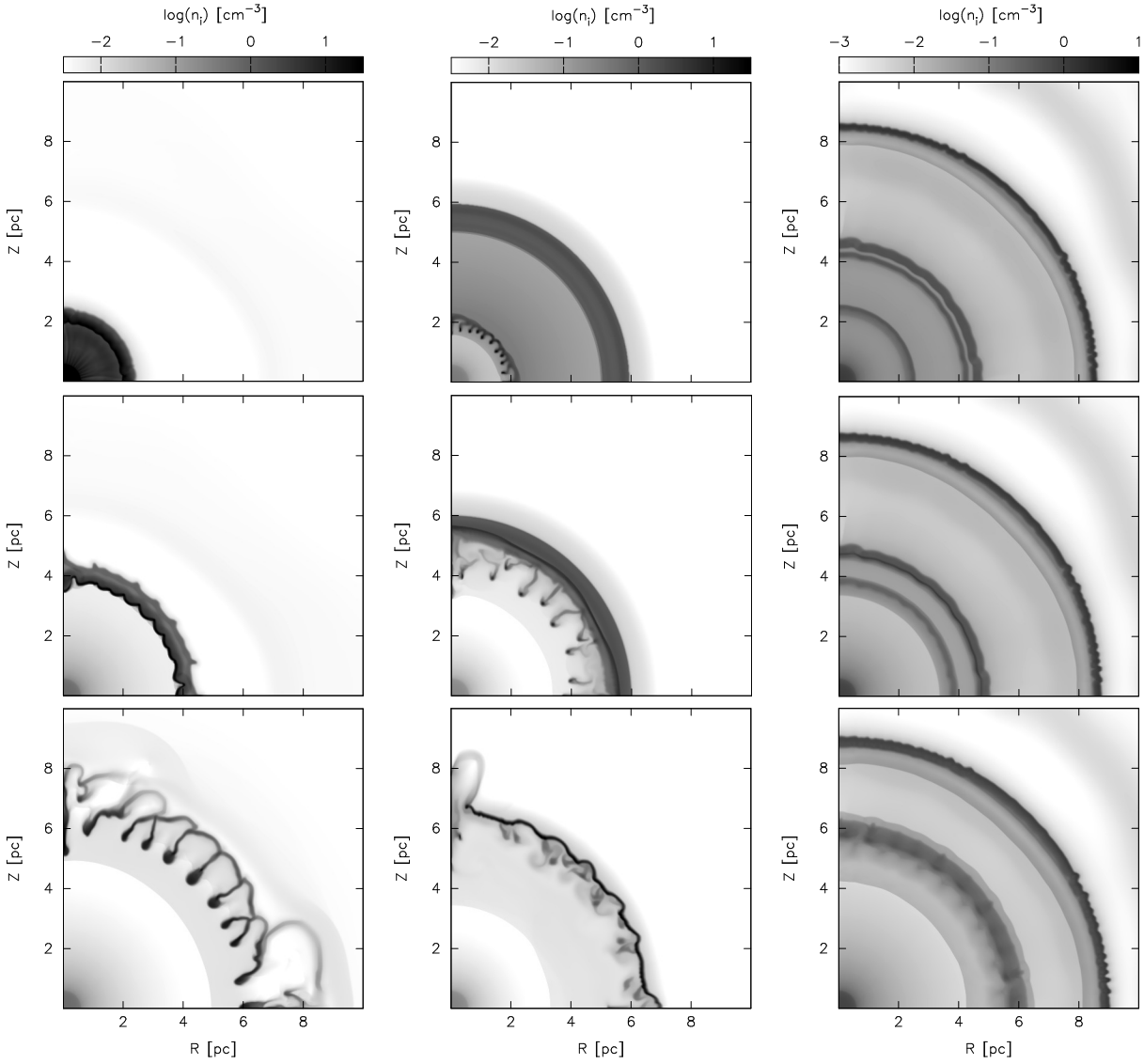

Fig. 1: Number density of ions in the r-z plane at different times after the onset of the WR stage for 3 different stellar evolution models: left - STARS (at 39800, 65900, 86000 yrs), centre - MM (at 10600, 22600, 32650 yrs), right - MMROT (at 6800, 8800, 12800 yrs). Figure adapted from Toalá & Arthur (2011). See text for details of the stellar evolution models.

Results from numerical simulations of the $40M_{\odot}$ case, corresponding to a progenitor RSG star, are shown in Figure 1. The different timescales and mass-loss rates for the period of intense mass loss immediately prior to the onset of the WR stage lead to notable differences in the wind-blown bubbles and nebulae. The stellar wind mass-loss histories of the different stellar evolution models are shown in Figure 2. These are empirical mass-loss rates, assigned according to the surface temperature, abundances and gravity of the star.

The stellar evolution models for the $40M_{\odot}$ initial mass star show that the star could evolve into either a red or yellow supergiant after leaving the main sequence. If the star becomes a yellow supergiant (YSG), the wind velocities will be of order $V_{\rm YSG} \sim 75\,{\rm km\,s^{-1}}$ (Humphreys 2010), which are higher than the velocities of red supergiant winds ($V_{\rm RSG} \sim 10\,{\rm km\,s^{-1}}$), and material that leaves the stellar surface of a YSG will get much further from the star than for a RSG in the same period of time. If the main shell of circumstellar material is dense and slow moving (the STARS models), thin-shell instabilities due to efficient cooling in the material swept up by the shock ahead of the fast wind plasma lead to the formation of clumps close to the

star, which then slowly move outwards, resulting in a small, dense, long-lived clumpy nebula. On the other hand, faster moving circumstellar material, such as is found around the models with rotation (MMROT), leads to a young, tenuous, large-diameter nebula without dense clumps.

A 3D, purely hydrodynamical, numerical study of the interaction of the WR fast wind with the surrounding circumstellar medium (CSM) formed by a progenitor RSG or LBV star was carried out by van Marle & Keppens (2012), with the assumption that the CSM was completely photoionized. They found similar results to Toalá & Arthur (2011) in that when there is a large amount of CSM material close to the star, such as occurs during a short-lived LBV stage, the resulting wind-blown bubble forms instabilities close to the star and soon after the onset of the fast wind, which leads to the sort of clumpy wind-blown bubble seen in RCW 58. On the other hand, a longer period of less intense mass loss, such as occurs during a RSG or YSG stage, leads to less fine structure. The main differences between 3D simulations and 2D simulations are that the instabilities form faster in the 3D case and so at a given time more structure is apparent in the 3D simulation results than in the 2D results.

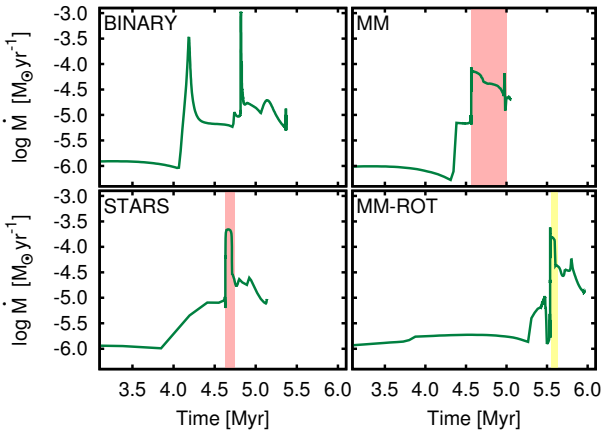

Fig. 2: Mass-loss rate against time for the STARS models and the Meynet & Maeder (2003) models with and without stellar rotation. A binary evolution model obtained from the BPASS website (Eldridge & Stanway 2009) is also included. The regions highlighted in red correspond to the range of time when the star would be considered a red supergiant, due to its low effective temperature. Similarly, the region highlighted in yellow would correspond to a yellow supergiant stage.

Numerical simulations can be used to predict the X-ray emission from the hot gas in the wind-blown bubbles (Toalá & Arthur 2011; Dwarkadas & Rosenberg 2013). The plasma immediately behind the adiabatic shock in the fast wind is too hot ($T \simeq 1.5 \times 10^7 (V_\mathrm{w}/1000\,\mathrm{km\,s^{-1}})^2$ K) and tenuous ($n \sim 0.01$ cm^{-3}) to be responsible for the observed diffuse X-ray emission, which has a typical temperature of $T_\mathrm{X} \sim 10^6$ K and density $n \sim 1$ cm^{-3} (Chu 2008). Instead, processes such as heat diffusion and thermal evaporation of the swept-up shell, or turbulent mixing layers around the clumps and filaments at the interface between the hot, shocked stellar wind and the warm (10^4 K), photoionized nebular material must be present in order to produce the substantial quantities of intermediate temperature and density gas required by the observations.

4 Toy Models

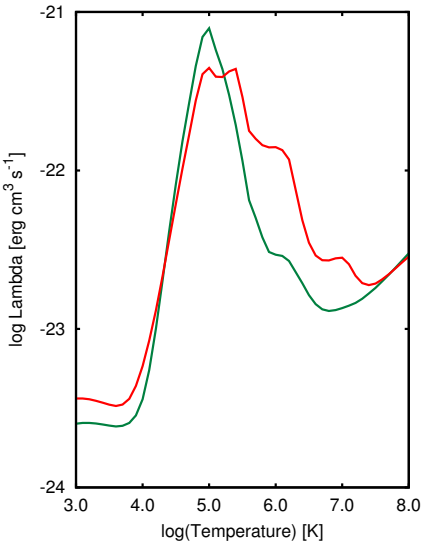

Fig. 3: Cooling rate as a function of temperature for photoionized gas with typical ISM abundances (red) and for gas with the nebular abundances of NGC 6888 (green) and the stellar photoionizing flux of WR 136.

In addition to the stellar evolution models, with their different timescales, mass-loss rates and derived fast stellar wind velocities, other factors affect the results of numerical simulations of WR wind-blown bubbles. For example, the chemical abundances in the gas heated by shock waves affect the cooling rate, which is important for the formation of clumps and filaments due to instabilities in the swept-up, radiatively cooling nebular gas. The optical nebulae around WR stars are generally found to have enhanced nitrogen and reduced oxygen abundances compared to solar values, consistent with the circumstellar material having been enriched with CNO products before being expelled from the star in a dense, slow wind (Fernández-Martín et al. 2012; Mesa-Delgado et al. 2014; Reyes-Pérez et al. 2015). The central star is the exposed stellar nucleus and thus the fast stellar wind will have different abundances on its surface to those in the nebula. In Figure 3 the cooling rates for ISM abundances and

abundances appropriate to the NGC 6888 WR nebula are shown, where the photoionizing flux of the central star WR 136 has been taken from the Potsdam Wolf-Rayet star models (Hamann & Gräfener 2004). The WR abundances lead to a higher cooling rate around 10^5 K and a lower cooling rate for million degree gas.

Another factor contributing to shaping the wind bubble could be the angular distribution of dense circumstellar material, expelled during the previous RSG, YSG or LBV stage. The bipolar nebula around the LBV Eta Carina is an obvious case, while recent ALMA observations towards the red supergiant VY Canis Majoris show that cool, dusty material is being ejected non-isotropically in directed streams (O'Gorman et al. 2015) that must persist for several tens of years in order to achieve their current extent. The density of this gas is highly inhomogeneous.

In Figure 5 snapshots from a set of numerical simulations starting from the same initial conditions but with different input physics or spatial distribution of gas are shown. The initial density distribution corresponds to a steady RSG wind with velocity 15 km s^{-1} which has expelled 15$M_\odot$ of material over 200,000 yrs. The fast wind has a wind velocity of 1600 km s^{-1} and mass-loss rate of $\dot{M}_{\rm WR} = 7 \times 10^{-5} M_\odot$ yr^{-1}. The star has an ionizing photon rate and effective temperature like that of the WNE star WR 136 and the standard model adopts abundances appropriate to the WR nebula NGC 6888. The size of the computational box is 4 pc square and the images show the number density of the ionized gas in the simulations after 18,000 yrs. Although the models without conduction look similar, some differences are apparent: changing the cooling curve (i.e., abundances) affects the thickness of the region where the shocked fast stellar wind and the swept-up CSM material mix in the turbulence around the filaments and clumps produced when the contact discontinuity corrugates due to instabilities. The thickness of the interaction region is greater for the higher metallicity simulations. The densities in the clumps themselves, which can recombine if the density becomes high enough, are also affected by the metallicity, since condensation is more rapid if the cooling rate is higher. On the other hand, thermal conduction leads to almost total evaporation of the clumps of CSM material for the set of parameters used in these toy models.

5 Non-equilibrium Shock Models

It has been postulated, for example by Moore, Hester & Scowen (2000), that cooling out of collisional ionization equilibrium behind the shock wave propagating into the dense CSM is responsible for the differences in position between the sharply defined [OIII] skin and the clumpier, interior Hα emission observed in some WR wind bubbles (those classified as types II, II and IV, e.g., S 308, RCW 58 and NGC 6888, in the scheme of Gruendl et al. (2000)). In order to test this idea, a series of models of instantaneously heated gas cooling out of equilibrium was run using the Cloudy photoionization code (Ferland et al. 2013). The requirement is that the gas reach a final photoionization equilibrium temperature of 10^4 K with a number density $n = 100$ cm^{-3}. This situation can be achieved over different time and lengthscales depending on the assumed pre-shock density and shock velocity responsible for the instantaneous heating of the gas (see Fig. 4). Slower velocity shocks cause less heating and a quick evolution to photoionization equilibrium but require a dense ambient medium. Faster shocks propagating into a more tenuous medium can reach photoionization equilibrium on lengthscales of up to 0.1 pc.

Although these models are rather unsophisticated, they do suggest that non-equilibrium cooling behind 70 – 150 km s^{-1} shock waves propagating into CSM material with densities between 0.3 and 3 cm^{-3} can explain the discrepancy in position between the [OIII] and the Hα emitting material seen in the observations. This range of velocities is consistent with the expansion velocities obtained for WR nebulae, both from radial velocities obtained from optical spectroscopy (Chu 1983) and from absorption features in IUE spectra of some WR stars, which are attributed to an expanding shell of gas around the central object (Smith, Willis & Wilson 1980).

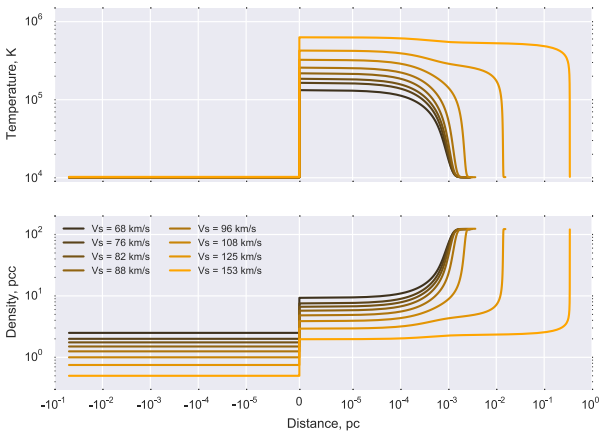

Fig. 4: Cooling regions behind shock waves for a range of shock velocities and initial densities. The requirement is to arrive at a state of photoionization equilibrium at 10^4 K and density $n = 100$ cm^{-3}.

6 Conclusions

The 2D hydrodynamic and radiation-hydrodynamic simulations developed over the past 20 years can explain WR wind bubbles in general terms. However,

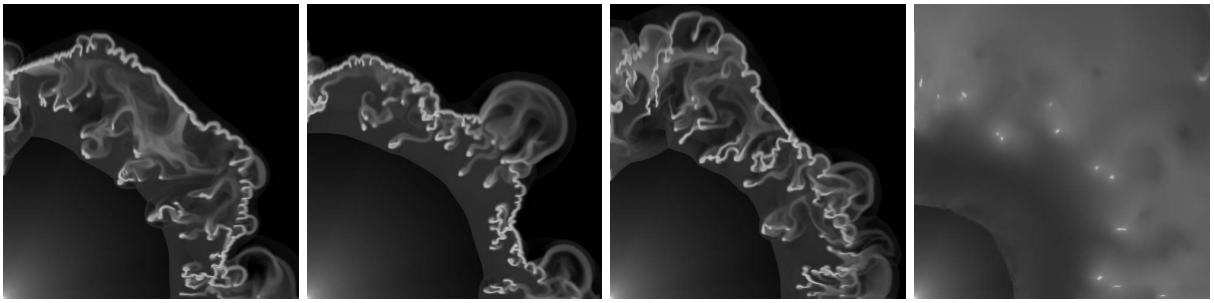

Fig. 5: Simulations starting from the same initial conditions but using different input physics: left - standard model with WR abundances; centre-left - ISM abundances; centre-right - non-spherical CSM; right - thermal conduction.

stellar evolution models are important for determining the mass loss in the RSG, YSG or LBV stage immediately prior to the onset of the fast wind and the velocity and spatial distribution of the CSM gas is important for the structure of the final nebulae.

Multiwavelength observations can constrain the models. For example, optical observations can determine the abundances, photoionization equilibrium state and cooling distances in the shocked and photoionized nebular gas. Mid-infrared observations are principally due to photon reprocessing by dust grains and can highlight the shock position and delimit the size of the wind bubble. X-ray observations are useful for determining the amount of mixing of swept-up nebular material into the hot, shocked fast wind plasma but only 3 objects have been detected so far.

The interaction of the fast wind with the environment of the WR star is responsible for a whole range of hydrodynamical phenomena, including shock waves, instabilities and mixing. A combination of high-resolution radiation-hydrodynamical simulations together with multiwavelength observations provides a laboratory for studying these processes and also for casting light on the stellar evolution process, which formed the circumstellar medium into which the fast wind expands.

The development of high-resolution 3D models with a full range of physical processes, such as radiative transfer, thermal conduction, and interaction with dust grains, would be extremely useful for disentangling the various puzzles in the interpretation of multiwavelength observations of wind-blown bubbles around WR stars.

7 Acknowledgements

SJA would like to thank Will Henney for running the non-equilibrium shock models discussed in § 5. Thanks are also due to Jesús Toalá for many discussions about numerical simulations and diffuse X-ray emission. SJA acknowledges support from UNAM through DGAPA-PAPIIT project IN101713.

References

Arnal E. M., Cappa C. E., 1996, MNRAS, 279, 788
Avedisova V. S., 1972, SvA, 15, 708
Chu Y.-H., 1981, ApJ, 249, 195
Chu Y.-H., 1983, ApJ, 269, 202
Chu Y.-H., 2008, IAUS, 250, 341
Dwarkadas V. V., Rosenberg D. L., 2013, HEDP, 9, 226
Eldridge J. J., Stanway E. R., 2009, MNRAS, 400, 1019
Eldridge, J. J., & Tout, C. A. 2004, MNRAS, 353, 87
Ferland G. J., et al., 2013, RMxAA, 49, 137
Fernández-Martín A., Martín-Gordón D., Vílchez J. M., Pérez Montero E., Riera A., Sánchez S. F., 2012, A&A, 541, A119
Freyer, T., Hensler, G., & Yorke, H. W. 2003, ApJ, 594, 888
Freyer, T., Hensler, G., & Yorke, H. W. 2006, ApJ, 638, 262
García-Segura, G., Langer, N., & Mac Low, M.-M. 1996a, A&A, 316, 133
García-Segura, G., Mac Low, M.-M., & Langer, N. 1996b, A&A, 305, 229
Gruendl, R. A., Chu, Y.-H., Dunne, B. C., & Points, S. D. 2000, AJ, 120, 2670
Hamann W.-R., Gräfener G., 2004, A&A, 427, 697
Humphreys R. M., 2010, ASPC, 425, 247
Johnson H. M., Hogg D. E., 1965, ApJ, 142, 1033
Leitherer C., et al., 1999, ApJS, 123, 3
Mesa-Delgado A., Esteban C., García-Rojas J., Reyes-Pérez J., Morisset C., Bresolin F., 2014, ApJ, 785, 100
Meynet, G., & Maeder, A. 2003, A&A, 404, 975
Moore B. D., Hester J. J., Scowen P. A., 2000, AJ, 119, 2991
O'Gorman E., et al., 2015, A&A, 573, L1
Reyes-Pérez J., Morisset C., Peña M., Mesa-Delgado A., 2015, MNRAS, 452, 1764
Smith L. J., Willis A. J., Wilson R., 1980, MNRAS, 191, 339
Toalá J. A., Arthur S. J., 2011, ApJ, 737, 100
van Marle A. J., Keppens R., 2012, A&A, 547, A3

Georges Meynet: Are there any evidences from the shape of the nebulae around WR stars that some of them are runaway stars?

Jane Arthur: Yes: in the case of a runaway star you would expect a bow shock to form ahead of the star, which forms at a stand-off distance where the ram pressure balances the shocked stellar wind pressure. We would expect the bow shock to be bright in emission lines. In the downstream direction, the stellar wind shock would be a lot further from the star and the swept-up CSM would not emit so brightly. There is evidence for such asymmetrical nebulae in objects such as M1-67 around WR 124.

Kerstin Weis: It looks like you treat the wind in the LBV phase as a steady smooth flow. In an S Dor cycle however, the wind changes $v_{\rm Wind}$ and $\dot{M}$ on a 10 to 50 yrs timescale. How would this change your results?

Jane Arthur: For simplicity, in our calculations the winds in all stages have been assumed to be isotropic. In our detailed calculations, we do take into account the time variation of the wind mass-loss rate and terminal velocity in accordance with the underlying stellar evolution models, but even so, the resolution is of order 100 years in the fastest varying stages. The effect of such a fast-varying wind as you mention is that many shells of material will be formed close to the star, however, slower shells will be overtaken by fast material coming up behind and the net result will be a shell dominated by the fastest velocity and the finer details of the mass loss will be erased.

Wolf-Rayet Stars
W.-R. Hamann, A. Sander, H. Todt, eds.
Potsdam: Univ.-Verlag, 2015
URL: http://nbn-resolving.de/urn:nbn:de:kobv:517-opus4-84268

A consistent spectral model of WR 136 and its associated bubble NGC 6888

J. Reyes-Pérez[1], C. Morisset[1], M. Penã[1] & A. Mesa-Delgado[2]
[1]*Instituto de Astronomía, Universidad Nacional Autónoma de México, México*
2*Instituto de Astrofísica, Facultad de Física, Pontificia Universidad Católica de Chile*

We analyse whether a stellar atmosphere model computed with the code CMFGEN provides an optimal description of the stellar observations of WR 136 and simultaneously reproduces the nebular observations of NGC 6888, such as the ionization degree, which is modelled with the pyCloudy code. All the observational material available (far and near UV and optical spectra) were used to constrain such models. We found that the stellar temperature T_*, at $\tau = 20$, can be in a range between 70 000 and 110 000 K, but when using the nebula as an additional restriction, we found that the stellar models with $T_* \sim 70\ 000$ K represent the best solution for both, the star and the nebula.

1 Introduction

NGC 6888 is an emission nebula associated with the Wolf-Rayet star WR 136 with spectral type WN6(h), and both have been already studied in several wavelength ranges from X-rays to radio emission, but all the previous works focus only on the modelling of the star or the nebula but not both simultaneously. This is why we focus in a semiempirical method based in the self-consistent modelling of the star and its associated nebula. It is logical to proceed in this way because the nebula associated to the star is naturally an additional restriction to the stellar atmosphere model, because the nebula can tell us about the ionizing ultraviolet photons coming from the star and then reprocessed and re-emitted with low energy through recombination and collisional processes.

2 Observational restrictions

The main analysis in this work is based on the optical observations of the star WR 136, the nebula using the REOSC echelle spectrograph (Levine & Chakrabarty 1994) attached to the 2.1-m telescope at the Observatorio Astronómico Nacional (OAN) in San Pedro Mártir, B. C. México. In addition to the optical spectra of WR 136, we retrived several reduced IUE spectra and from the *FUSE* satellite observational program C097.

3 Stellar atmosphere models of WR 136

To model the observed stellar spectra of WR 136, in the UV and optical ranges, we used the CMFGEN code (Hillier & Miller 1998).

For the stellar models computed in this study, the input values used to constrain the model atmosphere for WR 136 were the mass-loss rate $\dot{M}$, the terminal wind velocity V_∞, the stellar luminosity L, the hydrostatic radius of the star R_* (at optical depth τ equal to 20) and the chemical composition.

As the modelled spectral features do not respond linearly to the input parameters, we calculated a grid of models in order to find the more appropriated models which reproduce most of the observed spectral signatures. From this grid, we obtained *star1* which fits very well most of the stellar spectral characteristics. This model is presented in Table 1. In addition we also show in this table models from the literature, as Hamann et al. (2006) (hereafter HGL06) and Crowther & Smith (1996) ones.

The main difference between *star1* and the model reported by HGL06 is the stellar radius R_* which in our case has a low value of 1.5 $R_\odot$ (compared to the value of 3.34 $R_\odot$ by HGL06) leading to a higher stellar temperature T_* of 110 kK. Additionally the chemical composition, represented by the values of X and Y, is different. These differences indicate that it could exist more than one solution for a stellar model of a WR star as both, *star1* and HGL06 model, reproduce similarly well the stellar spectrum (see Fig. 68 by HGL06). This apparent degeneracy has already been remarked in a study of WR stars modelling by Hillier (1991).

To investigate this degeneracy we searched for other CMFGEN models that could fit the stellar observations. In a simple manner we used interpolated values between the model *star1* and the HGL06 model for the radius, the clumping factor (f_V) and the hydrogen and helium fractions by mass, X and Y. The result is model *star2* which has an effective temperature of 90 000 K (its characteristics are presented too in Table 1). Model *star2* reproduces the stellar spectrum similarly well as *star1*. It is presented in Fig. 1, in green.

We computed two additional models. The first is *star3* which basically uses HGL06 model parameters but it was calculated with the CMFGEN code. Model *star3* reproduces very well the results of HGL06 model, which shows that CMFGEN and the Potsdam WR model atmosphere code are equivalent. The last one is model *star4* which is almost the same as *star3* but calculated with the β value equal to 2, leading

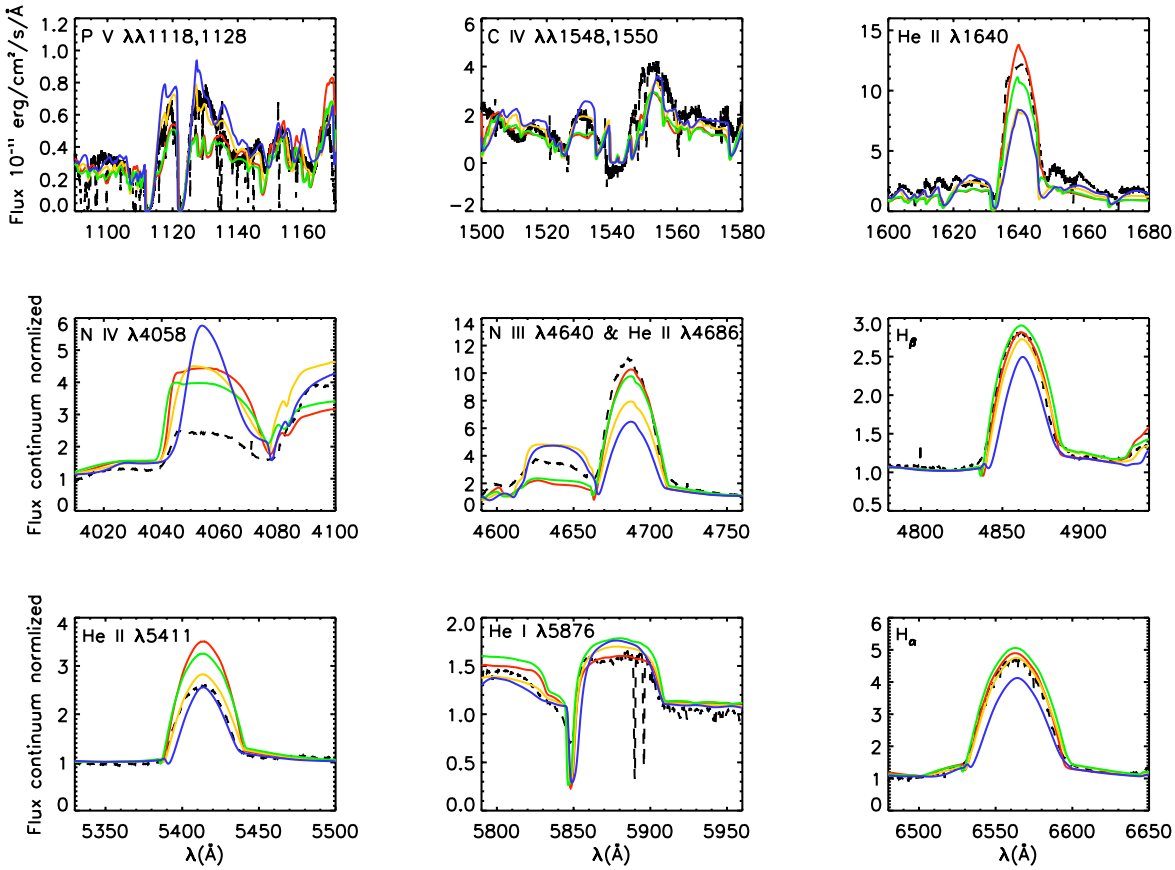

Fig. 1: Selected lines from the observed spectra to constrain the models. In each plot the dashed black line is the observed spectrum; red, green, yellow and blue lines are respectively the *star1, star2, star3* and *star4* models obtained through the CMFGEN code but reddened. The optical spectrum is shown as flux-normalized.

to a lower $T_{2/3}$ value because the wind region becomes more extended. Models *star3* and *star4* reproduce fairly well the observed stellar continuum and many spectral features (lines yellow and blue in Fig. 1). The differences among all these models appear mainly in the He lines, where the He II/He I line ratio is well reproduced when considering an effective temperature of 110 000 K but it is understimated when the effective temperature is reduced, i.e., at a lower stellar temperature the stellar He I lines are stronger and the stellar He II lines become weaker than observed.

All the stellar model characteristics are presented in Table 1.

4 NGC 6888 as an additional restriction

The key difference between the stellar models comes from the far UV region of the spectra, whose UV photons are absorbed by the nebula (between 1.0 and $\sim$ 7.0 Ryd). This difference is clear when we compare the models with a blackbody with the same temperature than the modelled spectra, 70 000 or even 46 000 K, we would see an excess of UV photons which would lead to a much more ionized nebula, contrary to the high absorption of the UV photons emitted by the star, due to the presence of the stellar wind (Reyes-Pérez et al. 2015).

Owing to there are not stellar observations in the far UV to discriminate which stellar model is reproducing the real spectral energy distribution of the star WR 136, it is necessary to add an external restriction. In this case, such additional restriction is the associated nebula NGC 6888 that is highly sensitive to this UV ionizing radiation. To reproduce the optical spectra of NGC 6888 we computed a photoionization model using the pyCloudy package (Morisset 2013) based on the 1D photoionization code Cloudy (Ferland et al. 1998). As we aim to build a consistent model of the system we used as ionizing sources the stellar atmosphere models of the star WR 136, as calculated with the CMFGEN code and described in §3.

Tab. 1: Stellar model parameters

Model	R_* $[R_\odot]$	$\log L$ $[L_\odot]$	$\log \dot{M}$ $[M_\odot \mathrm{yr}^{-1}]$	V_∞ [km s^{-1}]	T_* [kK]	$T_{2/3}$ [kK]	β	f_V	X	Y
This work *star1*	1.50	5.45	-4.63	1550	110	55	2	0.1	0.016	0.95
This work *star2*	2.10	5.40	-4.95	1550	90	48.30	1	0.175	0.068	0.91
This work *star3*	3.38	5.40	-4.95	1550	70	45.91	1	0.25	0.12	0.86
This work *star4*	3.38	5.40	-4.95	1550	70	42.26	2	0.25	0.12	0.86
HGL06	3.34	5.40	-4.95	1600	70.8	...	1	0.25	0.12	0.86
Crowther & Smith (1996)	5.00	5.30	-3.91	1750	55.7	28				

The results of the photionization model show that, under the assumptions made for this model (Reyes-Pérez et al. 2015) and using *star1* as ionizing source, the observed line fluxes are not well reproduced. In particular the lines from highly ionized elements (O^{++}, Ar^{++}) are extremely overpredicted. The fact that the ionization of the nebula is strongly overpredicted could be due to a too high stellar effective temperature, because the only way to reproduce the observed low line intensity of high ionized elements is to consider a star with a temperature lower than the value derived for model *star1*, i.e., we must deal with their energy of ionization photons.

The predicted emission lines improve very much and fit well the observations when we use the model *star3* which has $T_* = 70\,000$ K, indicating that the star WR 136 emits the UV ionizing photons corresponding to a star with this low effective temperature. The details about the photoionization model and its results can be found in Reyes-Pérez et al. (2015)

5 Conclusions

We computed several atmosphere models using the code CMFGEN to reproduce the stellar observations of WR 136. The characteristics of the star such as L, $\dot{M}$ and V_∞ agree with the values found by other authors, i.e., HGL06 and Crowther & Smith (1996).

We find that models with very different effective temperature, T_* from 70 000 K to 110 000 K, can reproduce fairly well the stellar continuum and several emission lines. Therefore there is a degeneracy in atmosphere models, than apparently is due to our misunderstanding of the structure of the wind velocity field.

To decide which stellar model produces the correct UV amount of ionizing photons coming from WR 136, we computed a photoionization model for the associated ring nebula NGC 6888, using the SED produced by the stellar models. This led us to conclude that WR 136 follows better the spectral behaviour of a star with a T_* of 70 kK.

6 Acknowledgements

This work received partial financial support from UNAM PAPIIT IN109614 and CONACyT CB-2010/153985. The FUSE and IUE data presented in this paper were obtained from the Multimission Archive at the Space Telescope Science Institute (MAST). STScI is operated by the Association of Universities for Research in Astronomy, Inc., under NASA contract NAS5-26555. Support for MAST for non-HST data is provided by the NASA Office of Space Science via grant NAG5-7584 and by other grants and contracts.

References

Crowther, P. A. & Smith, L. J. 1996, A&A, 305, 541

Ferland, G. J., Korista, K. T., Verner, D. A., et al. 1998, PASP, 110, 761

Hamann, W. R., Gräfener, G., & Liermann, A. 2006, A&A, 457, 1015

Hillier, D. J. 1991, Wolf-Rayet Stars and Interrelations with Other Massive Stars in Galaxies: Proceedings of the 143rd Symposium of the International Astronomical Union, 143, 59

Hillier, D. J. & Miller, D. L. 1998, ApJ, 496, 407

Levine, S. & Chakrabarty, D. 1994, Technical Report MU-94-04, Instituto de Astronomía, Universidad Nacional Autónoma de México

Morisset, C. 2013, sites.google.com/site/cloudy3d

Reyes-Pérez, J., Morisset, C., Peña, M., & Mesa-Delgado, A. 2015, MNRAS, 452, 1764

Andreas Sander: The position of WR 136 in the analyses of Hamann et al. (2006) is already close to the degeneracy region. Of course the hidden inner part of the velocity field is something that is important and might cause additional degeneracy between atmosphere models, but it seems that already a large fraction of the spectrum is formed in the wind of WR 136. Therefore I would not trust the particular value of T_* so much.

Franciso (Paco) Najarro: Are your assumed oxygen and silicon abundances (both well above 10^{-3} by mass) a bit too high for that spectral type?

Jonnathan Reyes-Pérez: I think it is not the case. The oxygen and silicon are similar to those published by van der Hucht et al. (1986) for WN stars, and recently Skinner et al. (2010) have constrained the silicon abundance using X-ray observation performed for WR 136.

Wolf-Rayet Stars
W.-R. Hamann, A. Sander, H. Todt, eds.
Potsdam: Univ.-Verlag, 2015
URL: http://nbn-resolving.de/urn:nbn:de:kobv:517-opus4-84268

Ring Nebulae: Tracers of the CNO Nucleosynthesis

A. Mesa-Delgado[1], C. Esteban[2] & J. García-Rojas[2]
[1]*Instituto de Astrofísica, Facultad de Física, Pontificia Universidad Católica de Chile, Av. Vicuña Mackenna 4860, 782-0436 Macul, Santiago, Chile*
[2]*Instituto de Astrofísica de Canarias, E-38200 La Laguna, Tenerife, Spain*

Preliminary results are presented from spectroscopic data in the optical range of the Galactic ring nebulae NGC 6888, G2.4+1.4, RCW 58 and Sh2-308. Deep observations with long exposure times were carried out at the 6.5m Clay Telescope and at the 10.4m Gran Telescopio Canarias. In NGC 6888, recombination lines of C II, O II and N II are detected with signal-to-noise ratios higher than 8. The chemical content of NGC 6888 is discussed within the chemical enrichment predicted by evolution models of massive stars. For all nebulae, a forthcoming work will content in-depth details about observations, analysis and final results (Esteban et al. 2015, in prep.).

1 Introduction

Half a century has already passed since Johnson & Hogg (1965) pointed out the possible link between stellar evolution and the presence of fuzzy-filamentary, ring-like shells around Wolf-Rayet stars. Today, the origin and evolution of ring nebulae is certainly much better understood within the evolution of massive stars around and above 20 $M_{\odot}$. These circumstellar bubbles of ionized gas actually represent material of the surrounding medium swept up during the mass loss episodes experienced by their massive progenitors (see e.g. Weaver et al. 1977; Freyer et al. 2006; Toalá & Arthur 2011). A genuine phenomena that emerges from the interaction between the stellar wind and the environment, whose large-scale effects are observed in the chemical history of star-forming galaxies (e.g. López-Sánchez & Esteban 2010).

The classification of ring nebulae includes an interesting group: the ejected and wind-blown types as defined by Chu (1981). These ring nebulae show the presence of processed stellar material in their chemical composition. An enrichment process is behind these chemical traces. Through efficient dredge-up and mixing processes boosted by deep convective layers, nucleosynthetic products are transported from the stellar core to the surface. These products are mainly ejected during the post-main sequence, especially in the red supergiant (RSG), luminous blue variable (LBV) and Wolf-Rayet (WR) phases. This particular group of ring nebulae stands as powerful channels of information connected to the chemical history of previous evolutionary stages. Thus, their study is a unique approach to test our knowledge about massive stars, looking for a consistent picture between both stellar and nebular stories.

Because of their inherent low surface brightness ($F(H\beta) \leq 10^{-15}$ erg/s/cm^2/arcsec^2), the study of ring nebulae from their emission line spectra is indeed a challenging task. In the early 90s, Esteban and collaborators presented the first systematic study of the chemical composition of 11 Galactic ring nebulae (e.g. Esteban et al. 1992). From deep spectroscopic data obtained from 2.5–4m telescope classes, these authors conducted a comprehensive analysis about the history of the stellar progenitors from the constraints given by the nebular story (Esteban et al. 1993). More recently, and mainly using a 3.5m telescope, Stock et al. (2011) have enhanced the sample of studied ring nebulae so far, even adding 3 ring nebulae of the Magellan Clouds. Consistently, the results show that ring nebulae containing stellar ejecta present overabundances of He and N, and a deficiency of O. A substantial fraction of O is transformed into N in the stellar interior via the activation of the ON chain and the He excess that remains until the activation of the 3α reactions. This enrichment pattern is in agreement with the stellar nucleosynthesis of the H-burning through the CNO cycle during the main sequence of massive stars.

For decades, a dramatic lack of reliable determinations of C abundances in any ring nebulae has hindered the full knowledge of the CNO cycle trace. The main spectral lines of C are either faint and challenging for detection as the recombination line C II 4267 Å, or either inaccessible from ground telescopes, requiring space facilities, as the doublet C III] 1907+09 Å. Recently, our research group reviewed the chemical composition of NGC 6888 with an improved accuracy (Mesa-Delgado et al. 2014; hereinafter, MD14) and reported the first detection of the C II optical feature in this proto-typical ring nebula that is confirmed in this work.

The present proceeding represents a preliminary *taste* of our renewed interest in reviewing the chemical composition of the brightest Galactic ring nebulae as revealed by deep spectroscopic observations with 6.5m and 10.4m telescopes. The final results will appear in a forthcoming work, including in-depth details about observations and analysis (Esteban et al. 2015, in prep.).

2 Observations

Making use of northern and southern facilities, we have collected the deepest spectroscopic data of the group of Galactic ring nebulae NGC 6888, G2.4+1.4, RCW 58 and Sh2-308. On the one hand, NGC 6888

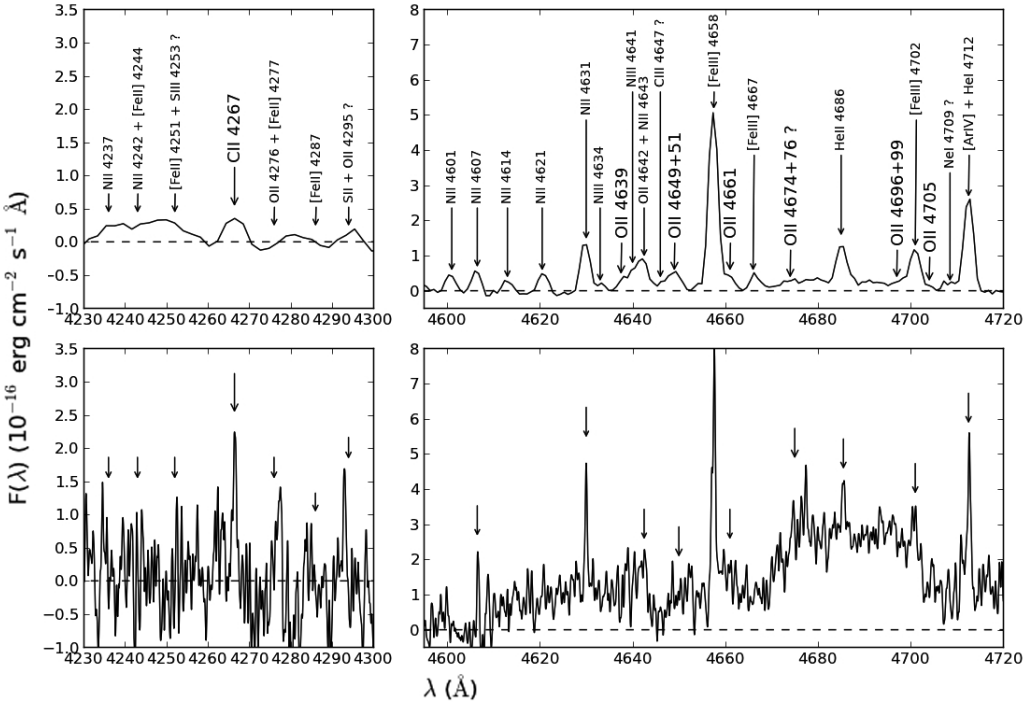

Fig. 1: Sections of NGC 6888 spectra. Top: detections of recombination lines of C II, O II, N II and N III from OSIRIS observations (Esteban et al. 2015, in prep.). Bottom: lower-limit detections of C II, N II and other features from HDS observations (MD14). The dashed lines represent the average continuum.

and G2.4+1.4 were observed with the OSIRIS spectrograph at the 10.4m Gran Telescopio Canarias. Within its capabilities, this spectrograph provides a slit of 7′.4 along the spatial direction, allowing us to simultaneously target multiple nebular areas and bright knots. On the other hand, single slit positions were observed on the brightest zones of G2.4 + 1.4, RCW 58 and Sh2-308 using the Magellan Echellette (MagE) spectrograph at the 6.5m Clay Telescope. In all cases, extractions of knot sizes, 3″ to 8″, were considered to maximize the signal-to-noise ratio of the final spectra. The two-observation campaigns were carried out with a slit width of 1″, covering the optical range with a spectral resolution of about 3000. Total exposure times of 1.4 hours were used in the OSIRIS observations, while times between 1.2 and 2.5 hours were used in MagE.

At first look, the outstanding quality and depth of these new observational data are well remarkable in the spectrum of NGC 6888. In Fig. 1, we compare the HDS spectra of NGC 6888 (MD14) with the recent OSIRIS observations. Both spectra represent similar extracted areas of about 1″ × 4″, located in positions on the bright arc to the northwest of the central star WR136, with similar integration times of 1.4 hours. The comparison is centered in the spectral ranges populated by recombination lines (RLs) of heavy-elements, and clearly reveals the superior result of the OSIRIS observations. The C II 4267 Å is well detected in this new dataset with a signal of about 8 over the continuum noise (σ). Almost featureless in the HDS observations, the O II RLs appears blended among them and other lines. The eight transitions constituting the O II multiplet 1 seem to be detected, where the brightest features are blended at 4649+51 Å with a signal of about 17σ. N II and N III RLs are also detected, though their emission may be affected by continuum pumping (Escalante & Morisset 2005). The high-ionization feature of He II 4686 Å is also detected, making plausible the detection of the C III line at 4647 Å, the brightest feature of the transition $3s^3S$–$3p^3P^0$.

3 Preliminary results

The analysis of emission line spectra allows us to determine the chemical composition of these ring nebulae. Using the traditional methodology, He abundances are calculated from dereddened flux ratios of He I and He II RLs, while chemical abundances of O, N and Ne are derived from collisionally excited lines (CELs). This chemical analysis is based on reliable detections ($> 30\sigma$) of the temperature-sensitive auroral lines of [O III] and [N II], allowing us to calculate total abundances of He, N, and O with high

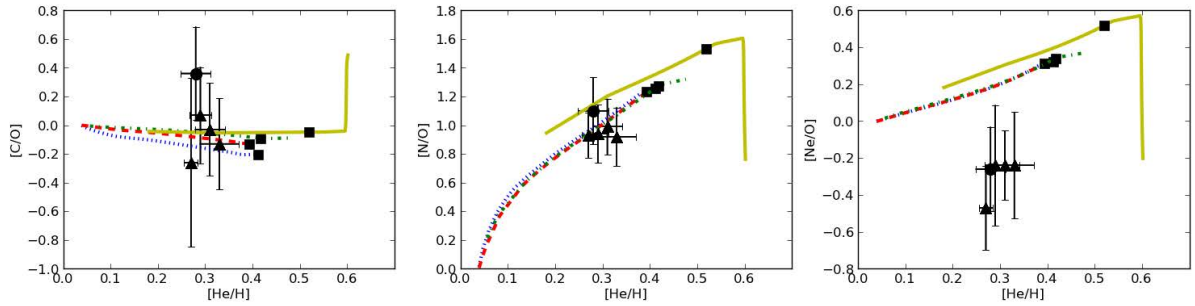

Fig. 2: Abundance ratios of C/O, N/O and Ne/O as a function of the He enrichment in NGC 6888. The zero points are referenced to the solar abundances as adopted by the Geneva models (Ekström et al. 2012). Lines represent the enrichment predictions of non-rotational evolution models of massive stars since the RSG onset (see details in MD14). The masses are: 25 $M_\odot$ (blue-dotted line), 32 $M_\odot$ (red-dashed line), 40 $M_\odot$ (green-dotted-dashed line), and 50 $M_\odot$ (yellow-straight line). The square is the onset of the WR phase for each model. Observational data are presented with error bars: triangles represent OSIRIS observations and circles correspond to the MD14 study.

accuracy ($\leq 25\%$) in such faint objects as ring nebulae. The first results confirm the chemical enrichment previously reported in Sh2-308 and RCW 58, as well as the absence of enrichment in G2.4 + 1.4 (see Esteban et al. 1992).

In NGC 6888, both the new analysis of four OSIRIS extractions and the previous work by MD14 confirm the chemical enrichment by CNO cycle products. The final abundances derived by these studies are shown in Fig. 2 together to the chemical enrichment traces predicted by the Geneva models for non-rotational evolution of stars with masses of 25, 32, 40 and 50 $M_\odot$ (Ekström et al. 2012). These multi-positional analysis do not show any significant real abundance spread, favoring the presence of chemically homogeneous material within uncertainties. For instance, the optimal accuracy reached in the He abundances points out that, if chemical inhomogeneities may be presented in NGC 6888, they would produce chemical variations lower than 1% across the nebula.

For the first time in an ejecta nebula, the C/O abundance pattern is determined in a consistent manner from good detections of C II and O II RLs. In comparison with the OSIRIS results, we find that the C abundance derived by MD14 actually represents a higher limit (the highest C/O ratio in Fig. 2). Then, we estimate that the mean [C/O] ratio is essentially 0, consistent with the solar reference within the abundance errors. It is also consistent with the model predictions, where no C is produced in the CNO synthesis. In Fig. 2, the N enrichment becomes quite clear exploring the [N/O] ratio, which shows an average value of about 1. Certainly, the Ne/O ratio presents a puzzling behavior. An average value of -0.3 is observed in the [Ne/O] ratio, much lower than the predicted Ne enrichment by the models. As MD14 suggested, this behavior might be related to a higher efficiency of the NeNa cycle, higher than the assumed by current models, which also seems to correlate with the observations of Na deficiencies in the surface of yellow giant stars (Denissenkov 2005). Finally, combining the abundance ratios of C/O, N/O and He/H and the characteristic lifetime of massive stars in the WR phase to develop such a bubble as NGC 6888 (see MD14), we constraint the mass of the stellar progenitor to be of about 40 $M_\odot$.

Acknowledgments: A.M.D. acknowledges support from the FONDECYT project 3140383. C.E.L. and J.G.R. acknowledge funding by MINECO under project AYA2011-22614.

References

Chu, Y.-H. 1981, ApJ, 249, 195
Denissenkov, P. A. 2005, ApJ, 622, 1058
Ekström, S., et al. 2012, A&A, 537, A146
Escalante, V. & Morisset, C. 2005, MNRAS, 361, 813
Esteban, C., et al. 1993, A&A, 272, 299
Esteban, C., et al. 1992, A&A, 259, 629
Freyer, T., Hensler, G., & Yorke, H. W. 2006, ApJ, 638, 262
Johnson, H. M. & Hogg, D. E. 1965, ApJ, 142, 1033
López-Sánchez, Á. R. & Esteban, C. 2010, A&A, 517, A85
Mesa-Delgado, A., et al. 2014, ApJ, 785, 100
Stock, D. J., Barlow, M. J., & Wesson, R. 2011, MNRAS, 418, 2532
Toalá, J. A. & Arthur, S. J. 2011, ApJ, 737, 100
Weaver, R., et al. 1977, ApJ, 218, 377

Georges Meynet: Are there lines of Na that could be used to see whether the abundance of sodium is enhanced?

Adal Mesa-Delgado: Sadly, there are no Na emission lines in the optical range that could be used to determine the Na abundance and its possible enhancement.

David Huenemoerder: Regarding your question about whether the Ne-Na nucleosynthesis cycle could be more efficient than models predict, our Chandra high-resolution X-ray spectrum of WR 6 (my talk yesterday) requires a substantial enhancement of the Na abundance to fit the observed Na X and Na XI emission lines, by an amount which also seems larger than the nominally expected enhancements. We also have strong Ne emission lines in the X-ray spectra, so this suggests that careful analysis of abundances or ratios would be very interesting.

Wolf-Rayet Stars
W.-R. Hamann, A. Sander, H. Todt, eds.
Potsdam: Univ.-Verlag, 2015
URL: http://nbn-resolving.de/urn:nbn:de:kobv:517-opus4-84268

X-ray Emission from Ionized Wind-Bubbles around Wolf-Rayet Stars

V. V. Dwarkadas[1] & D. Rosenberg[2]
[1] *Astronomy and Astrophysics, University of Chicago*
[2] *Oak Ridge National Laboratory*

Using a code that employs a self-consistent method for computing the effects of photoionization on circumstellar gas dynamics, we model the formation of wind-driven nebulae around massive Wolf-Rayet (W-R) stars. Our algorithm incorporates a simplified model of the photo-ionization source, computes the fractional ionization of hydrogen due to the photoionizing flux and recombination, and determines self-consistently the energy balance due to ionization, photo-heating and radiative cooling. We take into account changes in stellar properties and mass-loss over the star's evolution. Our multi-dimensional simulations clearly reveal the presence of strong ionization front instabilities. Using various X-ray emission models, and abundances consistent with those derived for W-R nebulae, we compute the X-ray flux and spectra from our wind bubble models. We show the evolution of the X-ray spectral features with time over the evolution of the star, taking the absorption of the X-rays by the ionized bubble into account. Our simulated X-ray spectra compare reasonably well with observed spectra of Wolf-Rayet bubbles. They suggest that X-ray nebulae around massive stars may not be easily detectable, consistent with observations.

1 Introduction:

Massive stars (> 8 M$_\odot$) lose mass throughout their lifetime, via winds and eruptions, before ending their lives in a cataclysmic supernova (SN) explosion. The interaction of this material with the surrounding medium creates vast wind-blown cavities surrounded by a dense shell, referred to as wind-blown bubbles. As the star evolves through various stages, the mass-loss parameters will change, affecting the structure of the bubble. When the star finally explodes, the resulting SN shock wave will expand within the bubble, and the dynamics and kinematics of the shock wave will depend on the bubble parameters (Dwarkadas 2005, 2007a,b). Similarly, the relativistic blast waves associated with gamma-ray bursts are expected to expand within wind bubbles surrounding Wolf-Rayet (W-R) stars. Using an ionization-gasdynamics code, AVATAR, we compute the structure and evolution of the wind-blown bubbles around massive stars. Using the ISIS package, we compute the X-ray spectrum from the simulations as would be observed by the Chandra satellite, and compare to observational data.

2 The AVATAR Code:

We have further developed a code that combines photoionization from the star with the gasdynamics, and used it to compute the structure of wind bubbles around massive stars. The method operator splits the contribution due to photoionization effects from the usual gas dynamics, and utilizes a backward-Euler scheme together with a Newton-Raphson iteration procedure for achieving a solution. The effects of geometrical dilution and of column absorption of radiation are considered. The gasdynamic algorithm makes use of a multidimensional covariant implementation of well established Eulerian finite difference algorithms (Rosenberg 1995). A second-order (van Leer) monotonic transport algorithm is used for advection of total mass and the neutral component, and a third order piecewise parabolic scheme is available. Tabulated functions are used to compute the collisional ionization rate and cooling function. Shocks are treated using an artificial viscosity. Grid expansion is available to study flow over distance scales spanning several orders of magnitude. The algorithm incorporates a simplified model of the photo-ionization source, computes the fractional ionization of hydrogen due to the photo-ionizing flux and recombination, and determines self-consistently the energy balance due to ionization, photo-heating and radiative cooling. In this, our method is superior to that of other calculations, such as Garcia-Segura et al. (1996); van Marle et al. (2005), who use the on-the-spot approximation and do not take the recombination time into account. It is comparable to the work of Toalá & Arthur (2011).

3 Evolution of the Wind-Blown bubble around a 40 M$_\odot$ star:

A model for a 40 $M_\odot$ star using the AVATAR code is shown in Figure 1. Stellar parameters are adapted from van Marle et al. (2005). The evolution of the star can be divided into 3 main phases. An inhomogeneous pressure and density distribution develops in the main-sequence (MS) stage, accompanied by vorticity deposition near the inner shock. The inclusion of photo-ionization results in the formation of a dense, lower temperature ($\sim 10^4$ K) region of ionized material outside the wind bubble during the

MS phase. The nebula is fully ionized, and the ionization front is trapped in the dense shell, which is unstable to ionization instabilities. In the red supergiant (RSG) stage the surface temperature of the star decreases considerably. Consequently the ionizing radiation drops considerably and recombination reduces the ionization fraction to $\sim 40\%$, although this goes up again in the W-R stage. The high-density RSG wind is followed by a higher momentum W-R wind which breaks up the RSG shell, scattering the dense material into a turbulent W-R nebula.

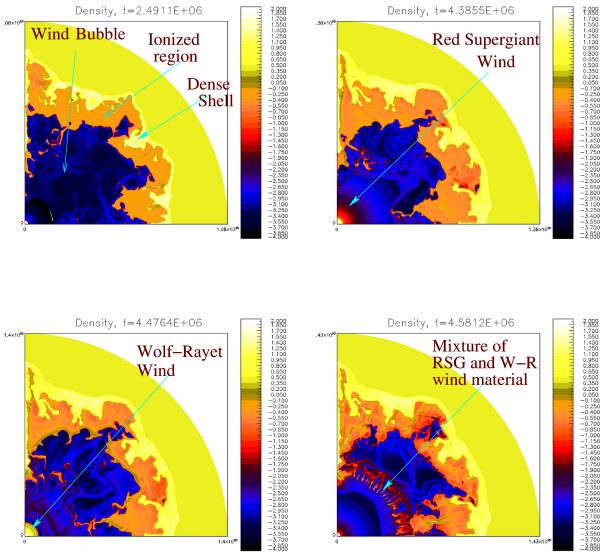

Fig. 1: Density snapshots from calculation of wind bubble evolution around 40 $M_\odot$ star (600 × 400 zones), computed with AVATAR with expanding grid (Dwarkadas & Rosenberg 2013). Time increases from left to right and top to bottom, and is listed at the top of each plot.

We can use the simulations to illustrate the regions from which the X-ray flux arises. We assume that thermal bremsstrahlung is the dominant contributor to the X-ray flux, although line emission will also play a role. The flux is then proportional to $n_e^2 T^{1/2}$ where n_e is the density and T the temperature. We show maps of this quantity at various times in Figure 2. The normalization is arbitrary, however they are all normalized to the same scale. Only zones having temperature $T > 10^6$ K are assumed to emit X-rays. The densest clumps do not contribute because their temperature is lower than 10^6 K. It is clear that the highest X-ray flux arises in the W-R stage, and that the highest levels of X-ray emission emanate from very small regions.

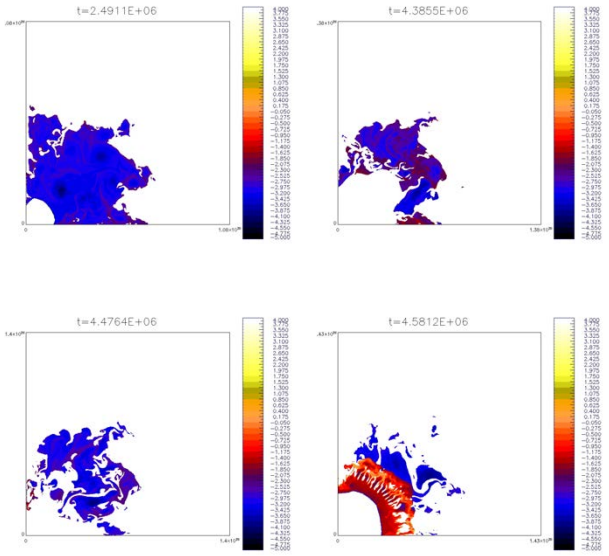

Fig. 2: Maps showing the area from which X-ray emission arises from the bubble in Figure 1. An increase of the X-ray flux in the W-R stage is seen.

4 THE X-RAY SPECTRUM OF THE BUBBLE:

In order to calculate the X-ray emission accurately, we use the ISIS package (Houck & Denicola 2000). The data are read into ISIS, the spectrum calculated for every zone, taking the absorption outside that zone into account, and added together. A point source is assumed. We use the VMEKAL model in XSPEC to model the spectrum, since it is the one most commonly used to fit the observed X-ray spectra. Herein we present (Figure 3) X-ray spectra as would be detected by the Chandra ACIS instrument for an object at 1.5kpc distance, integrated over 50,000s. Foreground absorption of 2×10^{20} cm^{-2} is added to absorption due to the neutral material surrounding the bubble, which varies, and can be as high as 2×10^{21} cm^{-2} (total $N_{\rm H}$ in units of 10^{22} cm^{-2}). Line broadening is based on the underlying fluid velocity. Solar abundances (Anders & Grevesse 1989) are used for the MS and RSG stages. Abundances in the W-R phase are from Chu et al. (2003) for the W-R bubble S308.

Our spectra are comparable in shape and temperature to observed spectra (Figure 4). Our simulations show that the X-ray emission in the MS phase is generally too weak to be detected by current X-ray satellites. It is higher in the W-R stage, but still difficult to detect. The X-ray emission depends strongly on the density within the bubble, which is a function of the density of the material around the

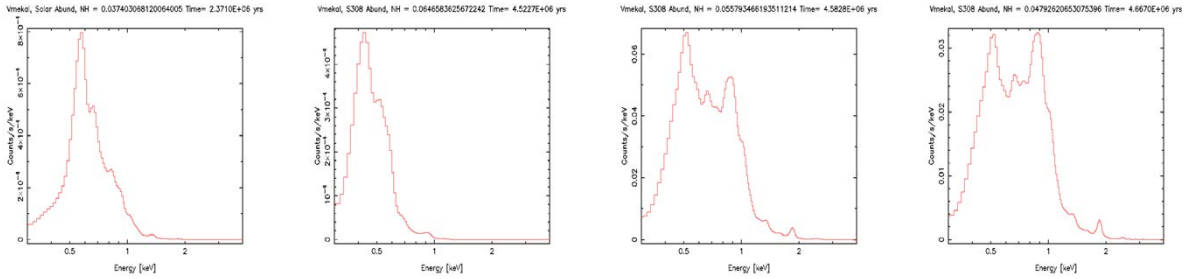

Fig. 3: Simulated X-ray spectra for a point source calculated from the simulation shown in Figure 1. The leftmost image is from the MS phase, the next three are from the W-R phase. Note that as time increases in the W-R stage, the intensity of the spectrum (counts/sec/keV) also increases.

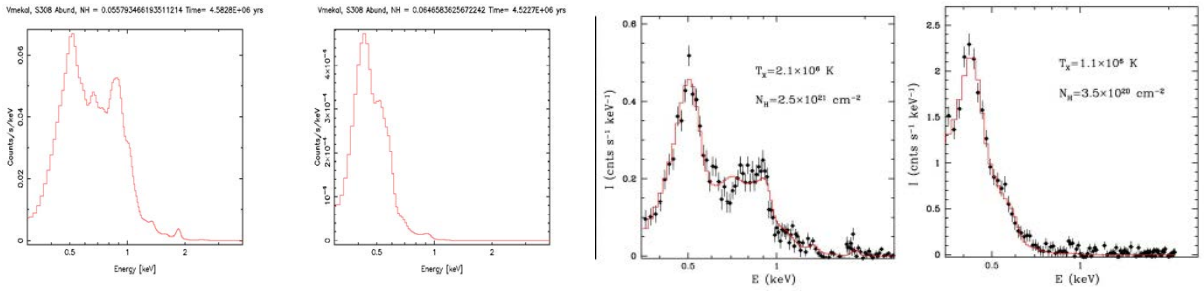

Fig. 4: Simulated and Observed spectra. Panel 1 resembles observed Chandra spectrum for NGC 6888 (panel 3) and Panel 2 XMM spectrum of S308 (panel 4), from Chu et al. (2006). Although the spectral shapes are similar, the counts are significantly lower in our simulated spectra as compared to the data. This seems to be generally true over all our simulations, in agreement with the fact that diffuse X-ray emission is not generally observed.

nebula. Thus it is possible that a higher ambient density leads to a higher intensity, although unless it was all ionized the absorption would correspondingly increase. The general low intensity is in agreement with observations, which have only detected 3 W-R nebulae, and no MS nebulae around massive stars (Chu et al. 2006; Toalá et al. 2014, 2015).

Acknowledgements: Support for VVD is provided by Chandra grants TM9-0001X and TM5-16001X issued by the CXO, which is operated by SAO for and on behalf of NASA under contract NAS8-03060. DR acknowledges resources of the OLCF at ORNL, which is supported by the Office of Science of the U.S. DOE under Contract No. DE-AC05-00OR22725.

References

Anders, E. & Grevesse, N. 1989, Geochim. Cosmochim. Acta, 53, 197

Chu, Y.-H., Gruendl, R. A., & Guerrero, M. A. 2006, in ESA Special Publication, Vol. 604, The X-ray Universe 2005, ed. A. Wilson, 363

Chu, Y.-H., Guerrero, M. A., Gruendl, R. A., García-Segura, G., & Wendker, H. J. 2003, ApJ, 599, 1189

Dwarkadas, V. V. 2005, ApJ, 630, 892

Dwarkadas, V. V. 2007a, in Revista Mexicana de Astronomia y Astrofisica Conference Series, Vol. 30, 49–56

Dwarkadas, V. V. 2007b, ApJ, 667, 226

Dwarkadas, V. V. & Rosenberg, D. L. 2013, High Energy Density Physics, 9, 226

Garcia-Segura, G., Langer, N., & Mac Low, M.-M. 1996, A&A, 316, 133

Houck, J. C. & Denicola, L. A. 2000, in Astronomical Society of the Pacific Conference Series, Vol. 216, Astronomical Data Analysis Software and Systems IX, ed. N. Manset, C. Veillet, & D. Crabtree, 591

Rosenberg, D. L. 1995, PhD thesis, The University of North Carolina at Chapel Hill

Toalá, J. A. & Arthur, S. J. 2011, ApJ, 737, 100

Toalá, J. A., Guerrero, M. A., Chu, Y.-H., & Gruendl, R. A. 2015, MNRAS, 446, 1083

Toalá, J. A., Guerrero, M. A., Gruendl, R. A., & Chu, Y.-H. 2014, AJ, 147, 30

van Marle, A. J., Langer, N., & García-Segura, G. 2005, A&A, 444, 837

Anthony Marston: Can you say how different your simulations would be if you used an LBV rather than an RSG as an intermediate phase of evolution?

Vikram Dwarkadas: The main difference in our simulations would be due to the wind properties between an LBV and a RSG. LBV wind properties are not that well defined. The wind velocities are higher than RSGs, in the range of 100–200 km/s, which means that the winds would expand further than RSG winds. However, since the density varies inversely as the wind velocity, this would reduce the density of the winds compared to the RSG phase, for equivalent mass-loss rate. Decreasing density would result in higher temperatures. The wind mass-loss rates could vary. If the mass-loss rates were equivalent then the RSG wind would be slower and more dense, and presumably more unstable. Some LBVs in eruption could achieve very high mass-loss rates, much higher than RSG wind mass-loss rates, although this would not last for a long time. This could considerably increase the total mass output in this phase. Furthermore, the momentum of the winds would be much higher, perhaps comparable to the subsequent W-R wind, which would then not be able to break up the shell easily and mix the material over the entire nebula.

Wolf-Rayet Stars
W.-R. Hamann, A. Sander, H. Todt, eds.
Potsdam: Univ.-Verlag, 2015
URL: http://nbn-resolving.de/urn:nbn:de:kobv:517-opus4-84268

Diffuse X-ray Emission within Wolf-Rayet Nebulae

J. A. Toalá[1], M. A. Guerrero[1], Y.-H. Chu[2], S. J. Arthur[3] & R. A. Gruendl[4]
[1] *Instituto de Astrofísica de Andalucía, IAA-CSIC, Granada, Spain*
[2] *Institute of Astronomy and Astrophysics, Academia Sinica (ASIAA), Taipei, Taiwan*
[3] *Centro de Radioastronomía y Astrofísica, UNAM, Campus Morelia, Mexico*
[4] *Department of Astronomy, University of Illinois, Urbana, IL, USA*

We discuss our most recent findings on the diffuse X-ray emission within Wolf-Rayet (WR) nebulae. The best-quality X-ray observations of these objects are those performed by *XMM-Newton* and *Chandra* towards S 308, NGC 2359, and NGC 6888. Even though these three WR nebulae might have different formation scenarios, they all share similar characteristics: i) the main plasma temperatures of the X-ray-emitting gas is found to be T=[1–2]$\times10^6$ K, ii) the diffuse X-ray emission is confined inside the [O III] shell, and iii) their X-ray luminosities and electron densities in the 0.3–2.0 keV energy range are $L_{\rm X}$ $\approx10^{33}$–10^{34} erg s^{-1} and $n_{\rm e}$ $\approx$0.1–1 cm^{-3}. These properties and the nebular-like abundances of the hot gas suggest mixing and/or thermal conduction is taking an important rôle reducing the temperature of the hot bubble.

1 Introduction

Massive stars represent the main source of feedback that govern the physics of the Interstellar Medium (ISM). The most massive stars ($M_{\rm i}$ $\gtrsim$25 M$_\odot$) will evolve through the red supergiant or yellow supergiant (RSG or YSG) or luminous blue variable (LBV) phase depositing up to half their masses into the ISM, to finally become Wolf-Rayet (WR) stars (e.g., Ekström et al. 2012, and references therein). During the intermediate RSG/YSG or LBV phase, the star develops a slow and dense wind ($\dot{M}$=10^{-4}–10^{-3} M$_\odot$ yr^{-1}, v_∞=10–100 km s^{-1}) with no significant UV flux. The final WR phase is characterized by a strong wind ($\dot{M}$=10^{-5} M$_\odot$ yr^{-1}, v_∞=1500 km s^{-1}) that sweeps up, shocks, and compresses the RSG/LBV slow material, while a newly developed ionising photon flux ionises the material. This combination of effects will lead to the formation of the so-called WR nebulae (or ring nebulae).

Before the current generation of X-ray satellites (e.g., *XMM-Newton*, *Chandra*, and *Suzaku*) the only WR nebulae reported to harbor diffuse X-ray emission were S 308 and NGC 6888 around WR 6 and WR 136, respectively (see, e.g., Wrigge 1999; Wrigge et al. 2005) but with low resolution X-ray maps. The reported plasma temperatures and X-ray luminosities of the X-ray-emitting gas were T $\approx10^6$ K and $L_{\rm X}$ $\approx10^{34}$ erg s^{-1}, respectively.

In this talk we review the most recent *Chandra* and *XMM-Newton* observations towards S 308, NGC 2359, and NGC 6888 around WR 6, WR 7 and WR 136, respectively.

2 On the origin of the diffuse X-ray emission

An adiabatically shocked stellar wind can form a hot bubble inside a nebula with an estimated temperature of $k_{\rm B}T = 3\mu m_{\rm H} v_\infty^2/16$ (see Dyson & Williams 1997), where μ is the mean particle mass for fully ionised gas, $m_{\rm H}$ is the hydrogen mass, and $k_{\rm B}$ is the Boltzmann's constant. That is, for the estimated stellar wind velocities of WR 6 and WR 136 of v_∞ $\approx$1700 km s^{-1} (Hamann et al. 2006), hot bubbles with temperatures of T $\sim10^7$–10^8 K are expected, which are in clear mismatch with the observed X-ray temperatures.

It was always argued that thermal conduction between the outer cold (10^4 K) nebular material and the hot bubble would lead to temperatures as those as reported by X-ray observations. In particular, the often cited work of Weaver et al. (1977), which assumes classical thermal conduction (e.g., Spitzer 1962), predicts higher luminosity values than those observed ($L_{\rm X}$ $\geqslant10^{35}$ erg s^{-1}). Recent numerical studies have shed light into this problem showing that as a result of the slow-wind/fast-wind interaction, the swept up shell will break up due to the formation of Rayleigh-Taylor and thin shell instabilities and will be a source of mass, reducing the temperature of the hot bubble, raising the density to observed values, and reproducing the observed X-ray luminosities (Toalá & Arthur 2011; Dwarkadas & Rosenberg 2013).

3 Notes on individual objects

To date, five WR nebulae have been reported in the literature to be observed with the current generation of X-ray satellites: S 308, NGC 2359, RCW 58, and NGC 6888 around WR 6, WR 7, WR 40, and WR 136, respectively, and the WR nebula around WR 16, but only diffuse X-ray emission has been detected in S 308, NGC 2359, and NGC 6888 (see Figure 1). In this section we will present a summary of the best-quality X-ray observations towards these three objects as performed with *XMM-Newton* and *Chandra* satellites.

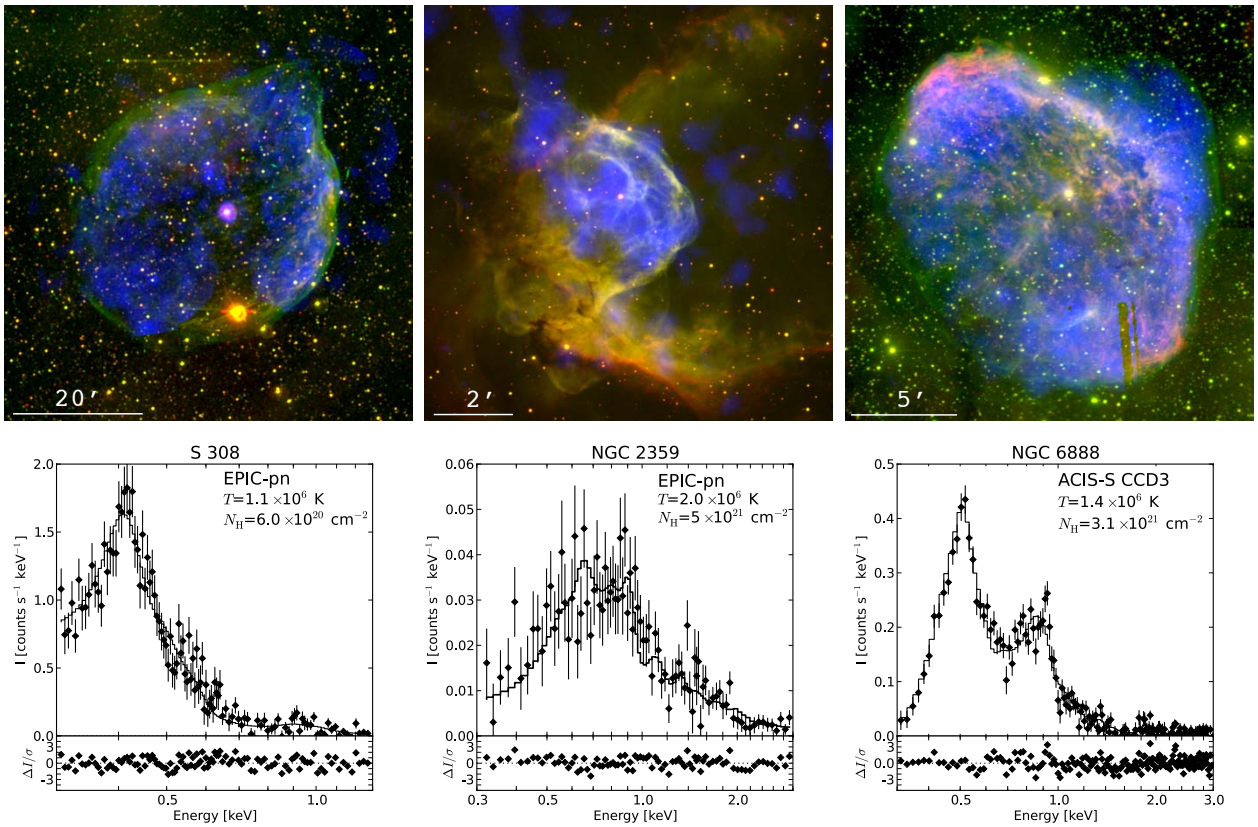

Fig. 1: X-ray emission from the WR nebulae S 308 (left panels), NGC 2359 (central panels), and NGC 6888 (right panels) around WR 6, WR 7 and WR 136, respectively. Top panels: Colour-composite pictures. Red, green, and blue correspond to the Hα, [O III], and diffuse X-ray emission as detected by *XMM-Newton*. Bottom panels: Background-subtracted spectra of the diffuse X-ray emission overplotted with their best-fit optically thin plasma model (solid line).

3.1 S 308 (WR 6)

S 308 around WR 6 is a nearly spherical nebula with an angular size of $\sim$40′ (in diameter) rendering it the most extended object of this class. Because of this, it had to be observed with 4 *XMM-Newton* pointings that mapped 90% of its total extension. The diffuse X-ray emission was found to be confined by the [O III] emission and displays a clear limb-brightened morphology (Toalá et al. 2012, see Figure 1 – upper left panel). The EPIC-pn background-subtracted spectrum presented in Fig. 1-bottom left panel shows that it is mainly dominated by the He-like triplet of N VI at 0.43 keV declining towards higher energies.

Toalá et al. (2012) presented a spectral study of S 308 concluding that spectra extracted from different regions can be modeled by an optically thin plasma model with nebular abundances and a main temperature of T=1.1×10^6 K. The averaged luminosity and rms electron density are $L_{\rm X}$=2×10^{33} erg s^{-1} and $n_{\rm e}$=0.1 cm^{-3}.

Toalá & Arthur (2011) argued that the most probable scenario formation of this nebula is that the central star, WR 6, might have evolved through a YSG phase in order to create such an extended nebula ($\sim$9 in radius) using a stellar evolution model with initial mass of 40 M$_\odot$ and initial rotation of 300 km s^{-1} (Meynet & Maeder 2003).

3.2 NGC 2359 (WR 7)

The WR nebula NGC 2359 presents an interesting morphology: it displays a main central bubble with several blisters and filaments (see Fig. 1, upper central panel). The X-ray-emitting gas seems to fill the main cavity and the northeast blister. It is probable that this is also the case for the southeast blister, but molecular material in the line of sight towards this region precludes a clear view of the total distribution of the X-ray-emitting gas (see Rizzo et al. 2003, and references therein). Furthermore, as different velocity components have been reported by Rizzo et al. (2003) and the complex shape of the nebula points

out an eruptive and non-isotropic origin as an LBV (Toalá et al. 2015a).

The EPIC-pn background-subtracted spectrum presents a broad peak around 0.5–0.9 keV, with two apparent maxima at 0.65 keV and ∼0.9 keV (Fig. 1, bottom central panel). Toalá et al. (2015a) estimated a main temperature of T=2×10^6 K adopting nebular abundances. The luminosity and rms electron density were estimated to be $L_{\rm X}$=2×10^{33} erg s^{-1} and $n_{\rm e}$ $\lesssim$0.6 cm^{-3}.

3.3 NGC 6888 (WR 136)

NGC 6888 is the most studied WR nebula in optical and X-rays. Its Hα emission shows a nearly elliptical distribution of clumps but the [O III] emission reveals a more spherical morphology with a blowout towards the northwest (Fig. 1, upper right panel). Toalá et al. (2014) reported the study of the spectral properties as observed with *Chandra* ACIS-S CCD#3 and #4. Even though the spectral responses of these CCDs are not the same and the observations only covered 60% of the nebula, they manage to derive the physical parameters of the X-ray-emitting gas. Toalá et al. (2014) argued that there should be an extra maximum in the spatial distribution of the X-ray emission towards the northwest blowout.

The *Chandra* ACIS-S CCD#3 spectrum shows that there are two main components, one at the N VII at 0.5 keV and a secondary peak at 0.7–0.9 keV which could be associated to the Fe complex and Ne lines (see Fig. 1, bottom right panel). The estimated main plasma temperature was T=1.4×10^6 K assuming an optically thin plasma model with nebular abundances. The luminosity and rms electron density were estimated to be $L_{\rm X}$=7.7×10^{33} erg s^{-1} and $n_{\rm e}$ $\gtrsim$0.4 cm^{-3}.

We have recently obtained *XMM-Newton* observations of this nebula and have confirmed that the distribution of the X-ray-emitting gas presents three maxima: two associated to the caps and an extra spatially correlated to the northwest blowout as suggested by the *Chandra* observations (see Fig. 1, top right panel). The global physical properties of the X-ray emission in NGC 6888 are very similar as those obtained for the *Chandra* observations, but due to the superior spectral capabilities of the EPIC cameras we are able to detect spectral variations (temperature and nitrogen abundance) when studying in detail different regions within the nebula (Toalá et al. in prep.). It is probable that the variations in nitrogen abundance might be due to different mixing efficiencies in different regions of the nebula as suggested by the possible interaction with a cold filament as seen in infrared wavelengths (see discussion by Toalá et al. 2014).

4 Remarks

Even though these three WR nebula might have formed as the result of different stellar evolutionary paths, they all exhibit diffuse X-ray emission with soft temperatures. The main reason of this it is now understood: mixing of nebular material into the hot bubble by instabilities and/or thermal conduction, but the contribution of each effect has not been critically assessed so far. It would be also interesting to test numerically the effect of cooling due to the dust present in the nebula (Toalá et al. 2015b).

It is worth noting that the WR nebulae reported to harbor diffuse X-ray emission have very similar central stars: WN4–6 type stars with terminal wind velocities of v_∞ ≈1700 km s^{-1} and mass-loss rates of $\dot{M}$=2–5×10^{-5} M$_\odot$ yr^{-1} (Hamann et al. 2006). Those that do not exhibit diffuse X-ray emission have WN8h stars (e.g., WR 16 and WR 40) with lower stellar wind velocities (v_∞=650 km s^{-1}) but similar mass-loss rates. In addition, our recently obtained *XMM-Newton* observations of the WR nebula NGC 3199 around WR18 also follow this trend (Toalá et al. in prep.): diffuse X-ray emission is detected in a WR nebula around a WN4-type star (v_∞ ≈1700 km s^{-1}, $\dot{M}$=3×10^{-5} M$_\odot$ yr^{-1}). A detailed analysis on these observations is still lacking in order to assess the physical properties of the diffuse X-ray emission and put it in context with S 308, NGC 2359 and NGC 6888.

References

Dwarkadas, V. V. & Rosenberg, D. L. 2013, High Energy Density Physics, 9, 226

Dyson, J. E. & Williams, D. A. 1997, The physics of the interstellar medium

Ekström, S., Georgy, C., Eggenberger, P., et al. 2012, A&A, 537, A146

Hamann, W.-R., Gräfener, G., & Liermann, A. 2006, A&A, 457, 1015

Meynet, G. & Maeder, A. 2003, A&A, 404, 975

Rizzo, J. R., Martín-Pintado, J., & Desmurs, J.-F. 2003, A&A, 411, 465

Spitzer, L. 1962, Physics of Fully Ionized Gases

Toalá, J. A. & Arthur, S. J. 2011, ApJ, 737, 100

Toalá, J. A., Guerrero, M. A., Chu, Y.-H., & Gruendl, R. A. 2015a, MNRAS, 446, 1083

Toalá, J. A., Guerrero, M. A., Chu, Y.-H., et al. 2012, ApJ, 755, 77

Toalá, J. A., Guerrero, M. A., Gruendl, R. A., & Chu, Y.-H. 2014, AJ, 147, 30

Toalá, J. A., Guerrero, M. A., Ramos-Larios, G., & Guzmán, V. 2015b, A&A, 578, A66

Weaver, R., McCray, R., Castor, J., Shapiro, P., & Moore, R. 1977, ApJ, 218, 377

Wrigge, M. 1999, A&A, 343, 599

Wrigge, M., Chu, Y.-H., Magnier, E. A., & Wendker, H. J. 2005, ApJ, 633, 248

Anthony Marston: Please be careful with NGC 3199. It has ISM abundances and large masses almost certainly *not* associated with ejecta from the star. More likely, the X-rays are associated with a cluster/association of hot stars.

Jesús A. Toalá (left) with session chair Isabelle Cherchneff

Wolf-Rayet Stars
W.-R. Hamann, A. Sander, H. Todt, eds.
Potsdam: Univ.-Verlag, 2015
URL: http://nbn-resolving.de/urn:nbn:de:kobv:517-opus4-84268

The importance of Wolf-Rayet ionization and feedback on super star cluster evolution

K. R. Sokal[1], K. E. Johnson[1], P. Massey[2], & R. Indebetouw[1]
[1] *University of Virginia, United States*
[2] *Lowell Observatory, United States*

The feedback from massive stars is important to super star cluster (SSC) evolution and the timescales on which it occurs. SSCs form embedded in thick material, and eventually, the cluster is cleared out and revealed at optical wavelengths – however, this transition is not well understood. We are investigating this critical SSC evolutionary transition with a multi-wavelength observational campaign. Although previously thought to appear after the cluster has fully removed embedding natal material, we have found that SSCs may host large populations of Wolf-Rayet stars. These evolved stars provide ionization and mechanical feedback that we hypothesize is the tipping point in the combined feedback processes that drive a SSC to emerge. Utilizing optical spectra obtained with the 4m Mayall Telescope at Kitt Peak National Observatory and the 6.5m MMT, we have compiled a sample of embedded SSCs that are likely undergoing this short-lived evolutionary phase and in which we confirm the presence of Wolf-Rayet stars. Early results suggest that WRs may accelerate the cluster emergence.

1 Introduction

The highest concentrations of Wolf-Rayet stars (WRs) are found extragalactically in massive and super star clusters (SSCs). These bright, blue star clusters have masses as high as 10^6 $M_\odot$ and host hundreds to thousands of massive stars, which interact with each other, in a single dense cluster. These regions are thus equivalent to, or more massive than, the closest well-known example R136 in the Large Magellanic Cloud. As SSCs are so rich, these are some of the most extreme regions of star formation.

A cartoon picture of SSC evolution has developed in which SSCs form as scaled-up versions of single massive stars in the Milky Way (Johnson 2002), during which we expect different observable signatures at each stage. A SSC forms from a thick, dense molecular cloud; the proto-SSC is thus embedded in and obscured by an envelope of natal material. Soon, massive stars forming within the cluster ionize this surrounding material. A SSC at this evolutionary stage is detectable as a radio continuum source with thermal emission, which is indicative of this dense young H II region (e.g. Kobulnicky & Johnson 1999). As the stars continue to evolve and more form, feedback will clear out the surrounding material and will ultimately produce an optically visible cluster.

Yet, how these SSCs emerge from the natal envelope is not yet well understood despite implications for the fate of the cluster itself as well as for the nearby environment and host galaxy. For instance, a lack of understanding how the ionizing radiation escapes from individual H II regions may be hindering current cosmic simulations (Paardekooper et al. 2011). The future of a cluster is impacted by the removal of natal gas, as this can effect further star formation efficiencies (even halting further star formation, Baumgardt & Kroupa 2007) and the cluster's ability to stay bound and thus survive (Pfalzner & Kaczmarek 2013). Understanding cluster emergence has been extremely difficult, largely because these are messy environments with many physical mechanisms at play. Feedback processes include: direct stellar radiation; photoionization; pressure from cold, warm (ionized), and hot gas; dust-processed IR radiation; protostellar wind and jets; and later, winds and supernova from massive stars (e.g. Lopez et al. 2011).

Simulations and observations have recently concentrated on identifying the dominant feedback mechanism. However, simulations often are limited in some capacity. Modeled star clusters are typically less massive than SSCs, and the input coupling of the feedback to the cloud material is not yet well founded (Rogers & Pittard 2013). Fortunately, as simulations are becoming more powerful, they are able pull out more details about how clusters emerge: for instance, in comparing the effects of stellar winds versus photoionization. Dale et al. (2014) find that photoionization dominates the energetics during star cluster evolution, yet the additional inclusion of winds is necessary to get observed morphologies of the produced H II region.

Observationally, a consensus on the dominate feedback mechanism has not been reached. Lopez et al. (2011) compares the pressures due to various feedback mechanisms (stellar radiation, dust-processed IR radiation, and the different temperature gas components) and finds that radiation pressure dominates in 30 Dor. Alternatively, an independent study by Pellegrini et al. (2011) concludes that hot gas dominates instead. Moreover, a larger expanded sample of H II regions in the Magellanic Clouds finds that the warm ionized gas pressure dominates (Lopez et al. 2014).

By highlighting an overlooked yet potential source of feedback instead, we provide a fresh look into this important evolutionary transition through the identification of an emerging massive star cluster. This

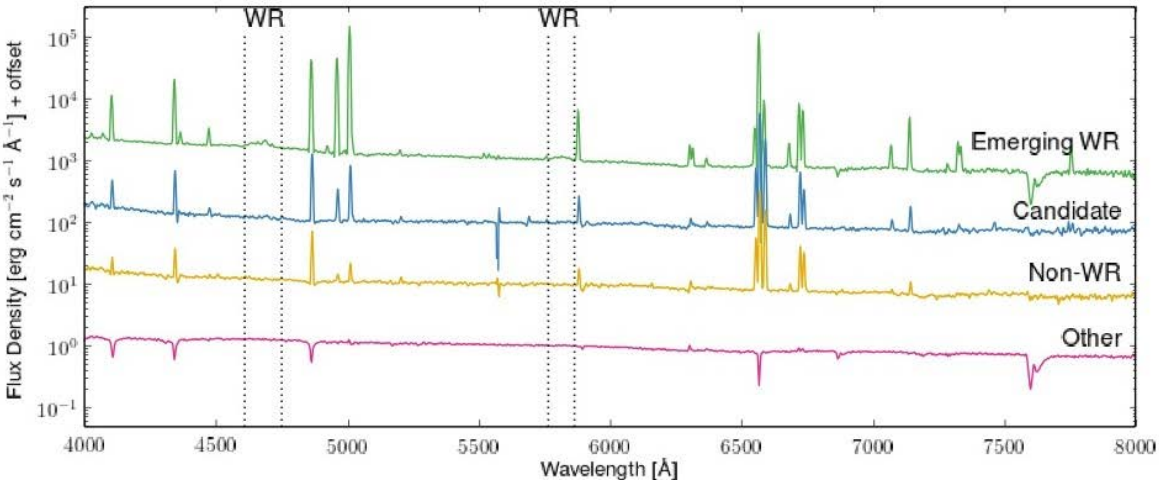

Fig. 1: An example optical spectrum observed with the 4m Mayall Telescope at KPNO and the 6.5m MMT of each type of class within our sample. Dashed lines show where the broad WR features ('bump') lie.

star cluster is a prime example of this phase as enshrouding natal material is being drastically altered and evacuated by a massive star population containing WRs.

2 S26 - discovery of emerging WR clusters

S26 in NGC 4449 was identified as a partially-embedded radio continuum source (Reines et al. 2008) with a thermal emission component. An extragalactic thermal radio detection of an H II region, which is rather rare (Aversa et al. 2011), indicates youth and either vast size or high density. Archival *Hubble Space Telescope* images show that S26 also quite bright optically and currently emerging. When we obtained optical spectra of S26, we discovered a surprising feature know as the WR bump (Reines et al. 2010; Sokal et al. 2015) due to integrated stellar emission from WRs.

Given our previous understanding of timescales, one would not expect for WRs to appear until after a star cluster has emerged. Thus their simultaneous presence with thermal radio emission may suggest that S26 remained embedded until the WRs help it emerge (Sokal et al. 2015). Additional evidence for ongoing feedback is also seen in the infrared SED from archival Spitzer and Herschel Space Telescope images and a possible nebular bipolar outflow in the cluster center (Sokal et al. 2015). Because of S26, we hypothesize that WRs may provide the tipping point in the combined feedback processes that drive a SSC to emerge (Sokal et al. 2015).

3 Finding more emerging WR clusters

3.1 Observational survey

We have carried out an observational survey to identify more clusters like S26. Targeting radio continuum sources with thermal emission similar to S26 in star-forming galaxies, we obtained optical spectra with the 6.5m MMT at the Fred Lawrence Whipple Observatory and the 4m Mayall Telescope at Kitt Peak National Observatory to search for the WR bump. In line with a classification scheme from Whitmore et al. (2014), we find clusters undergoing the emerging phase via detected radio emission, optical continuum, and optical lines. By searching for emerging clusters with WR features, we are looking specifically for 'emerging WR clusters.'

3.2 Success! and classifications

Clear detections of the WR bump are found in many targets – vastly expanding our sample of emerging WR clusters. However, there are many sources in which we do not see a clear WR bump, these range from very different objects, to H II regions without any bump whatsoever, and to sources with possible or only nebular WR features. As such, we have classified our sample of radio-selected sources as 'emerging WR' if the WR bump is detected, 'candidate' if there is a non-significant detection of the WR bump, 'non-WR' if the WR bump is not detected, and 'other' if the spectra do not resemble emission line spectra expected of H II regions (Sokal et al. 2015b, in prep). Example spectra and the distribution of the classes are shown in Fig. 1 and 2.

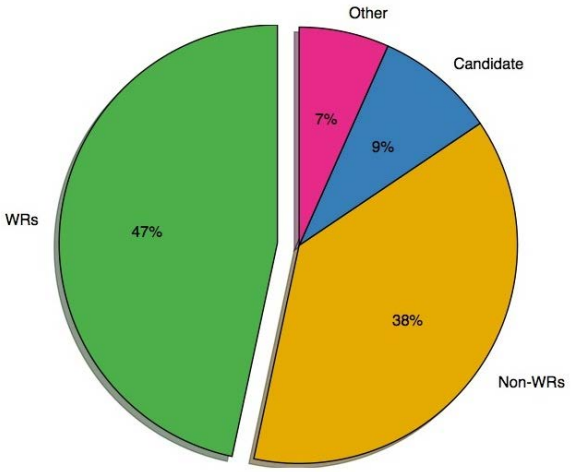

Fig. 2: The distribution of the classes observed in our sample. Emerging WR clusters are the most common amongst the classes, and if the Other class is omitted, these clusters makes up more that 50% of the sample.

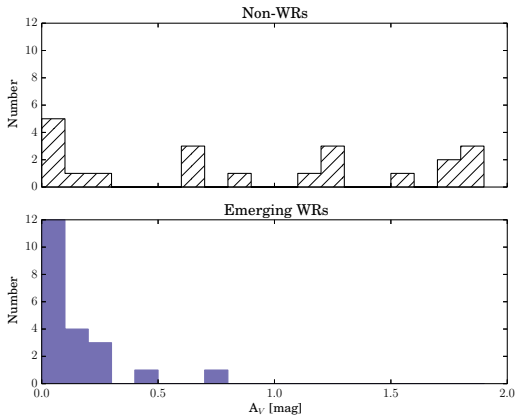

Fig. 3: The measured extinctions of the emerging WR cluster and non-WR cluster classes. We see that sources with WR features are less extincted on average.

3.3 WRs and cluster evolution

With this survey, we have identified 21 emerging WR clusters by searching for the WR bump in a sample of 45 radio-selected sources. We find we do not preferentially detect or observe either the emerging WR cluster class nor the non-WR cluster class. Classes with and without WR features show similar observed luminosity distributions and span the same parameter space in radio properties.

Thus, the observed commonality of the WRs is an important result: a clear detection of the WR bump is observed in ∼50% of our radio-selected sample (see Fig. 2). We note that just like proving single stars are single, it is difficult to prove that WRs are not present in a given integrated spectrum – rather, one can only show that they are. Still, a compelling percentage of the sample hosts WRs.

Moreover, we have found there may be large differences between these two classes.The distribution of cluster ages shows that the emerging WR clusters tend to be younger than sources without WR features. Similarly, the emerging WR clusters in general are found to have lower extinctions, as shown in Figure 3. Our preliminary results suggest the sources with the highest extinctions do not have WRs (are non-WR clusters) and are also older (Sokal et al. 2015b, in prep). This may suggest that clusters without significant populations of WRs remain embedded for longer periods of time than clusters which host WR stars. This scenario is in agreement with the hypothesize derived from S26 by Sokal et al. (2015) that WRs are evolutionally important for a cluster to emerge.

K.R.S. is thankful for support provided by the AAS International Travel Grant, Sigma Xi Grants-In-Aid of Research, and observing support from NOAO. K.E.J. acknowledges support provided by the David and Lucile Packard Foundation.

References

Aversa, A.G., Johnson, K.E., Brogan, C.L., Goss, W.M., & Pisano, D.J. 2011, AJ, 141, 125

Baumgardt, H., & Kroupa, P. 2007, MNRAS, 380, 1589

Dale, J.E., Ngoumou, J., Ercolano, B., & Bonnell, I.A. 2014, MNRAS, 442, 694

Johnson, K.E. 2002, Science, 297, 776

Kobulnicky, H.A. & Johnson, K.E. 1999, ApJ, 527, 154

Lopez, L.A., Krumholz, M.R., Bolatto, A.D., Prochaska, J.X., & Ramirez-Ruiz, E. 2011, ApJ, 731,91

Lopez, L.A., Krumholz, M.R., Bolatto, A.D. et al. 2014, ApJ, 795, 121

Paardekooper, J.-P., Pelupesy, F.I., Altay, G., & Kruip, C.J.H. 2011, A&A, 530, 87

Pellegrini, E.W., Baldwin, J.A., & Ferland, G.J. 2011, ApJ, 738, 34

Pfalzner, S. & Kaczmarek, T. 2013, A&A, 559A, 38

Reines, A.E., Johnson, K.E., & Goss, W.M. 2008, ApJ, 135, 2222

Reines, A.E., Nidever, D., Whelan, D., & Johnson, K.E. 2010, ApJ, 708, 26

Rogers, H., & Pittard, J.M. 2013, MNRAS, 431, 1337

Sokal, K.R., Johnson, K.E., Indebetouw, R., & Reines, A.E. 2015, ApJ, 149, 115

Whitmore, B.C., Brogan, C., Chandar, R. et al. 2014, ApJ, 795, 156

Shweta Srivastava: You mentioned some of the clusters are obscured in radio. At which wavelength and angular resolutions were these clusters observed in radio?

Kimberly Sokal: They are selected from the literature with a variety of observations at different wavelengths. They all included 6 cm observations but then to get the radio spectral index α, some had 20 cm, others 3.4 cm. It is unfortunate, but there are only a handful of galaxies with actually detected, multiple sources.

Joanne Bibby: How do you know that when you see no WR-bump it's just not due to line dilution where the WR emission is hidden by a large continuum?

Kimberly Sokal: Yes, I can't know. Which is why I leave it at "at least 50%" because it really is a lower limit, also can be affected by weak-lined WRs and aperture effects (we heard about this week).

John Eldridge: If you look at your BPT diagram you'll see that it goes right into the area predicted by binary models which and all relevant data is on the website.

Paul Crowther: In view of the spatial resolution achieved at > 2 Mpc distances, the central cluster of 30 Dor (R136) has an age below 2 Myr, yet shows a WR bump from very massive stars whereas a nearby older modest cluster R140 dominates the WR bumps on a scale of 30×30 pc.

Kimberly Sokal: Yes, yes. We hope that with the largest sampling some of that averages out. Apertures and line of side effects are both unavoidable.

Wolf-Rayet Stars
W.-R. Hamann, A. Sander, H. Todt, eds.
Potsdam: Univ.-Verlag, 2015
URL: http://nbn-resolving.de/urn:nbn:de:kobv:517-opus4-84268

The Wolf-Rayet Population and ISM Interaction in Nearby Starbursts

J. R. Walsh[1], A. Monreal-Ibero[2], J. M. Vílchez[3], E. Pérez-Montero[3], J. Iglesias-Páramo[3], C. Sandin[4], M. Relaño[5] & R. Amorín[5]
[1]*European Southern Observatory, Garching, Germany*
[2]*GEPI, Observatoire de Paris, Meudon, France*
[3]*Instituto de Astrofísica de Andalucía – CSIC, Granada, Spain*
[4]*Leibniz-Institut für Astrophysik Potsdam, Germany*
[5]*Departamento de Física Teórica y del Cosmos, Universidad de Granada, Spain*
[6]*INAF-Osservatorio Astronomico di Roma, Italy*

The interaction between massive star formation and gas is a key ingredient in galaxy evolution. Given the level of observational detail currently achievable in nearby starbursts, they constitute ideal laboratories to study interaction process that contribute to global evolution in all types of galaxies. Wolf-Rayet (WR) stars, as an observational marker of high mass star formation, play a pivotal role and their winds can strongly influence the surrounding gas. Imaging spectroscopy of two nearby (<4 Mpc) starbursts, both of which show multiple regions with WR stars, are discussed. The relation between the WR content and the physical and chemical properties of the surrounding ionized gas is explored.

1 Local starbursts as WR laboratories

Nearby blue compact galaxies (BCGs) are the nearest examples of actively starbursting galaxies. They display more vigorous star formation rates and higher gas and stellar mass than the Magellanic Clouds and provide the opportunity to study star formation in low and very low Z environments, comparable to younger, and more active, galaxies at high z. Some of these galaxies display Wolf-Rayet (WR) star features, such as the blue bump around 4650 Å or red bump around 5800 Å, in their integrated spectra and have been named *WR galaxies*. But this is not really a type, but rather a selection effect of viewing a starburst at the time when the high mass stellar content of a single strong starburst is evolving through the H and He burning phases.

Surveys of starburst galaxies to search for WR features in integrated spectra, such as the massive study of SDSS emission line galaxies with EW (Hβ) $\geq$ 2 Å by Brinchmann et al. (2008), show that a small fraction of the emission line galaxies (around 0.2%) exhibit WR features in their integrated spectra. Our approach is to select a few nearby starburst galaxies and study in detail with integral field spectroscopy the interplay between massive star formation and the surrounding gas, the spectral properties of their WR stars and the relation to the general stellar population.

2 Mapping gas and stars in BCGs

Three integral field units (IFUs) have been employed for this study: on the VLT the FLAMES Argus and VIMOS IFU, and on Gemini GMOS. All have subarcsecond spaxel size and fields of view well-matched to map nearby BCGs. Use of an IFU avoids slit biasing resulting from preselection based on surface brightness morphology in line or continuum. Nearby BCGs allow single clusters or super star clusters (SSCs) to be distinguished. From the datacubes, regions can be flexibly delimited based on various parameters, such as line ratios, stellar colour, WR feature, etc. By comparing WR star and emission line properties to resolved stellar photometry, such as from HST imaging in optical and UV, the luminosity, ionizing flux, age and stellar content (WR/O ratio) can be assessed. Studies of two starburst galaxies at <4Mpc, NGC 5253 and NGC 625, are highlighted.

2.1 NGC 5253

NGC 5253 was among the first blue compact galaxies to have a WR feature (blue bump) identified, after He2-10 (Campbell et al. 1986; Walsh & Roy 1987). It is an irregular, low Z (0.5 $Z_\odot$) starburst H II galaxy in Centaurus, at ∼3.8Mpc with many young stellar clusters, including two SSCs (masses $\sim 10^6$ $M_\odot$) in its embedded core. Infrared images show a nucleus with central starburst, a spiral dust feature, a disk of star forming regions and a warped rotating gas disk (observed in H I, H II and CO). It has been suggested that the current starburst activity was initiated by an interacting H I plume from nearby M83 (Kobulnicky & Skillman 2008).

It is still the best observed example of an extended enhanced N region (Walsh & Roy 1989), which is centred on the central SSC. However the other elements, O, He, Ar, S, etc display uniform abundance distribution. With FLAMES Argus (R∼12000) and GMOS IFU (R∼8000), the optical spectra (3500–7300 Å) were observed and lines fluxes and velocities, stellar continuum and line ratios over 12×8″

fields (∼210×130pc) were studied and extinction, electron density (N_e), temperature (T_e) and abundance maps derived (Monreal-Ibero et al. 2010). Fifteen regions were defined based on various criteria, such as blue bump (He II+N III), presence of narrow (nebular) He II line, and young star clusters resolved by HST (Harris et al. 2004), and intercompared (Monreal-Ibero et al. 2012). The occurrence of the red bump was studied with the GMOS IFU data (Westmoquette et al. 2013). An extensive study of ionized He in NGC 5253 (Monreal-Ibero et al. 2013) did not reveal an enhancement of He corresponding to the N enrichment.

The SSC in NGC 5253 presents both blue bump (predominantly WN) and red bump (WC) features, extended N^+/H^+, higher N_e and broad line profiles, the latter suggesting outflow. A second N enriched region was detected in an older (10 Myr) cluster (#3) with no WN signature (but narrow He II emission; the WR red bump has not yet been observed, but the presence of WC stars is predicted). Many regions with distinct WN and or WC features, such as at the position of a UV cluster, and three other regions (W-R 1, 4 and 5) were identified. Figs. 3 and 4 of Westmoquette et al. (2013) and Fig. 10 of Monreal-Ibero et al. (2010) show the location of all identified regions. From the size of the N-enriched region on the SSC (80×35 pc) and the emission line velocities, a timescale for N enrichment of ≤ 1 Myr is estimated.

Four other distinct regions with narrow (nebular?) He II but no clear evidence of very young clusters or blue bump emission were identified (see Fig. 12 in Monreal-Ibero et al. 2010). GMOS observations showed, however, how one of them (He II-1) was spatially associated to red bump emission. After a reinspection of the FLAMES data, it was noticed that the relatively older cluster #3 presented He II nebular emission (see Fig. 1). This has not been reported so far. Interestingly enough, this region is spatially coincident with the secondary area of N enrichment in this galaxy. In a scenario where this enrichment is caused by WR stars, given both the age of the cluster and the extra amount of N in the region, this cluster is a candidate to host evolved/older versions of WR stars (i.e., WC, or even WO, stars). However, the cluster was not observed with GMOS and further spectroscopic observations would be needed to test this hypothesis.

2.2 NGC 625

The Sculptor group dwarf SB galaxy NGC 625 (∼3.9 Mpc), has a similar metallity to NGC 5253 but slightly higher mass $\sim 10^{8.3}$ $M_\odot$, with a central extended starburst. It has a more prominent underlying stellar disk and well-defined (old) radial population gradient. IFU spectroscopy with VIMOS in two fields (R ∼ 3000) reveals five compact regions with WR N III/He II signature (and one with only C IV) without general correspondence with blue stellar continuum peaks.

Data reduction and processing will be presented in a forthcoming contribution (Monreal-Ibero et al., in prep.). A first inspection of the distribution of the WR emission (see Fig. 2) shows that: i) WR emission in this galaxy is extended and shows peaks of emission in multiple locations; ii) the peaks for the *blue bump* emission may or may not coincide with those of the *red bump* emission; iii) in general, these blue/red WR peaks do not necessarily coincide with features in the overall general stellar distribution. The stellar distribution presents several independent peaks of emission. The most important one is associated with the peak of emission in Hα and with the strongest peak of the *blue bump* emission. Additionally, the overall stellar distribution presents some peaks which are associated to a plethora of young (i.e., <20 Myr) stars identified by means of HST broad-band imaging (Cannon et al. 2003; McQuinn et al. 2012). However, no WR emission is found in any of these peaks. In general, the *blue bump* emission is more concentrated and centralized that the *red bump* emission. Indeed the only WR emission detected in region #2 is the red bump; this region is situated at a distance of about 400 pc from the peak of emission in Hα. These results are in accord with the spatially resolved star formation history for the galaxy (McQuinn et al. 2012).

3 General deductions

Nearby starburst galaxies, although few in number, allow a privileged view on the earliest stages of clustered high mass star formation. Although this work is only based on two galaxies, the results refer to 22 WR regions. Monreal-Ibero et al. (2012) summarize the diversity of WR pollution in nearby starburst galaxies. Four cases can be distinguished:

i) No WN or WC stars and no N enrichment (default scenario);

ii) WN and WC stars and N enrichment (NGC 5253, SSC);

iii) WN and/or WC stars and marginal N enrichment (normal scenario; NGC 5253 cluster and possibly NGC 625);

iv) N enrichment and no detectable WN presence, but candidate for WC presence (NGC 5253 cluster #3).

It appears that WR stars can provide N enrichment in special circumstances, but witnessing the process of pollution itself requires fine tuning of conditions, age, confinement, etc.

The presence of narrow He II 4686Å emission also provides several test cases:

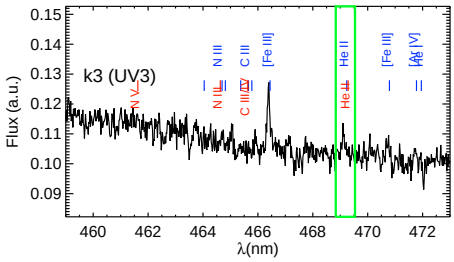

Fig. 1: Spectrum showing nebular He II in the NGC 5253 cluster ♯3. The positions of the nebular emission lines are indicated with blue ticks and labels, while those corresponding to Wolf-Rayet features appear in red. The green rectangle marks the position of the He II nebular emission line.

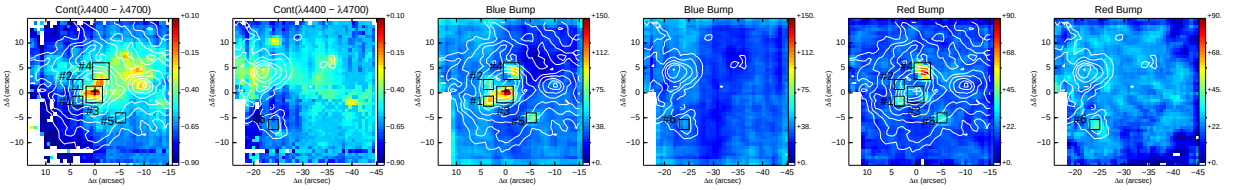

Fig. 2: Maps showing the location of the Wolf-Rayet features with respect to the overall stellar population in NGC 625 (Monreal-Ibero et al. in prep). *Two left maps:* Emission line free stellar continuum. *Two central maps:* WR blue bump emission. *Two right maps:* WR red bump emission. Every map displays contours tracing the observed Hα flux in steps of 0.3 dex as derived from Gaussian fitting. Square apertures used to extract spectra at the locations presenting WR emission are shown and numbered in black and the cross marks the peak of Hα emission. Orientation is north up, east to the left.

i) High EW (Hα) emission, no He II, no WR stars (default scenario);
ii) High EW(Hα) emission, no He II, WN and or WC stars;
iii) He II emission, no WN or WC star broad line signatures;
iv) He II emission, WR and/or WC star presence.

In the absence of other indicators (high velocity shocks, high mass X-ray binaries or clusters with many low mass X-ray binaries), very young massive O stars, or hot late-type WR stars, such as WC and WO, may explain the narrow He II 4686Å emission.

References

Brinchmann, J., Kunth, D., & Durret, F. 2008, A&A, 485, 657

Campbell, A., Terlevich, R., & Melnick, J. 1986, MNRAS, 223, 811

Cannon, J. M., Dohm-Palmer, R. C., Skillman, E. D., et al. 2003, AJ, 126, 2806

Harris, J., Calzetti, D., Gallagher, III, J. S., Smith, D. A., & Conselice, C. J. 2004, ApJ, 603, 503

Kobulnicky, H. A. & Skillman, E. D. 2008, AJ, 135, 527

McQuinn, K. B. W., Skillman, E. D., Dalcanton, J. J., et al. 2012, ApJ, 759, 77

Monreal-Ibero, A., Vílchez, J. M., Walsh, J. R., & Muñoz-Tuñón, C. 2010, A&A, 517, A27

Monreal-Ibero, A., Walsh, J. R., & Vílchez, J. M. 2012, A&A, 544, A60

Monreal-Ibero, A., Walsh, J. R., Westmoquette, M. S., & Vílchez, J. M. 2013, A&A, 553, A57

Walsh, J. R. & Roy, J.-R. 1987, ApJ, 319, L57

Walsh, J. R. & Roy, J.-R. 1989, MNRAS, 239, 297

Westmoquette, M. S., James, B., Monreal-Ibero, A., & Walsh, J. R. 2013, A&A, 550, A88

Carolina Kehrig: Regarding the origin of nebular He II emission, you might be interested in having a look at the paper Kehrig et al. (2015).

Jeremy Walsh: Thank you. This galaxy has much lower metallicity than NGC 5253 and NGC 625 starbursts. I was considering, but a very important datum for exploring the effects of metallicity on WR and ISM interaction.

John Eldridge: I'm going to say binaries again but in this case this is close enough that if you check in HST you might see the source in an image. And that would be the first detection of one of these low mass helium stars.

Jeremy Walsh: At this distance the cluster may be too mesh and difficult to see individual stars.

Yes, true. I'm just thinking of the SN progenitor detections where we can see the progenitors at these distances.

Closing session

Wolf-Rayet Stars
W.-R. Hamann, A. Sander, H. Todt, eds.
Potsdam: Univ.-Verlag, 2015
URL: http://nbn-resolving.de/urn:nbn:de:kobv:517-opus4-84268

Concluding Remarks

P. S. Conti[1]
[1] *JILA, Univ. Colorado, Boulder, CO 80309, USA*

Selected remarks concerning Wolf-Rayet (W-R) stars in the framework of this workshop are given. The rich history of international conferences over the past four or so decades is summarized, important issues concerning W-R stars are considered, and some outstanding problems are reviewed.

I begin briefly with the very first international conference on W-R stars, IAU Symposium #49 held in Buenos Aires, Argentina in 1971. I believe I am the only participant at that meeting who is also at this one; a picture of the participants is shown in Fig. 1. (Curiously, it was not included in those proceedings, but a similar shot at an oblique angle was shown at a 2006 conference in honor of Dr. Virpi Niemela; Niemela 2008).

Three women in the first row, Drs. Neimela, Underhill, and Smith, are well known in the study of W-R stars, and represent ∼10% of the participants at that meeting. There has been a substantial increase of women working on this topic, as may be indicated by the ∼25% fraction attending this conference. Of course, there is still room to go, but I was glad to see that this fraction was similarly represented on the meeting's SOC, the fraction of chairs, and the number of speakers. I was also very pleased to see all of the young people who are presenting their work here.

I would characterize IAUS#49 as both very stimulating, and very frustrating, as most of the senior participants there were unconvinced there were *any* abundance anomalies in these stars, despite the fact that hydrogen lines were either weak or not present. We juniors were much more excited about the new work being done by Paczynski, and others, on "mass exchange binaries," which had the potential to uncover stellar interior products of nuclear reactions (helium, carbon, nitrogen, oxygen) in massive stars as they evolved and interacted. One can get the flavor of the discussions by reading the published proceedings, but I will say in hindsight that much of that material was tedious, repetitive, and, often just plain wrong.

The big issues at that time concerned the evolutionary status of these stars; it appeared to some that perhaps they were pre-main sequence stars with normal composition, to others the spectra suggested highly evolved objects with abundance anomalies consistent with the products of core nuclear reactions visible in the stellar winds. Mass loss rates were, at the time, difficult to determine. Detailed and predictive wind codes, non-LTE, radiative transfer codes, statistical equilibrium calculations were all in the future and by now have been found to be more or less in reasonable agreement with the observations.

For example, it is feasible to predict the WN/WC star ratio, which depends on the initial metal abundance, and compare it with observations of W-R stars in Local Group galaxies in which they have been identified. This prediction seems to hold for all galaxies so far studied, with the possible exception of IC10 (see contribution at this conference by Massey et al. 2015). Furthermore, the W-R/O star ratio ought to be near to 0.1 (the helium to hydrogen burning lifetimes) in a random sample of massive stars; this is much harder to test observationally due to the difficulties in identifying O stars (Massey 2010), although it can be done locally (Conti et al. 1983).

Advances in scientific fields are mostly noted by publications in refereed journals, of which you are all familiar. Not as well known is the role conferences play in advancements in the field. In dealing with W-R stars, and more generally hot massive stars in general, there have been a series of IAU Symposia, which originated in the late 70s on these topics, which were held near to beaches, thus receiving a certain notoriety from the OC of the relevant IAU Commissions judging the proposals. I was involved in organizing the first of these (see below) with the eager participation of my Canadian colleagues. A beach location creates a marvelous level of informality for the interactions of the participants, thus providing an open and often speculative set of conversations. In addition, when one informs ones spouse of the location of the conference, there is often a request to also attend, with the result that strong bonding occurs between the participants families, leading to life-time scientific relationships. Personally, these conferences were a major positive impact on my work over these past four decades.

They were also fun. And do not think that non-beach Symposia are not fun too! Here we have lake water all around us, and I have observed intense personal interactions going on while the formal sessions are not in progress. I have only listed the IAU Symposia, there were also a handful of Colloquia, conferences and Workshops on these topics.

Listing of IAU (Beach) Symposia (IAUS) Involvement with W-Rs:

- **IAUS 83 Mass Loss and Evolution of O-Type Stars,** 5–9 June 1978 Qualicum Beach, Canada.

Fig. 1: Participants at IAU#49: *First Row:* Marita Chidichino, Dora Goniadsky, Virpi Niemela, Anne B. Underhill, M. K. Vainu Bappu, Lindsey F. Smith, Peter S. Conti, Bengt Westerlund, Humberto Gerola. *No Row, at Left:* David J. Van Blerkom, Marcos Emilio Machado, Hugo Gustavo Marraco, Roberto Hugo Mendez, Juhan Frank, Leonard Kuhi. *Second Row:* Gonzalo Alcaíno, Richard N. Thomas, Ana María Hernández, Julio C. Duro, Nolan R. Walborn, Robert J. Altizer, Willem Seggewiss, Robert J. Havlen, Mart De Groot. *Third Row:* H. John Wood, Bohdan Paczynski, ??, Horacio Ghielmetti, Donald C. Morton, Luis Lopez, Jorge Sahade, Hugh M. Johnson.

- **IAUS 99 Symposium on Wolf-Rayet Stars: Observations, Physics, Evolution,** 18–22 September 1982 Cozumel, Mexico.
- **IAUS 116 Luminous Stars and Associations in Galaxies,** 26–31 May 1985 Porto Heli, Greece.
- **IAUS 143 Wolf-Rayet and Other Massive Stars in Galaxies,** 18–22 June 1990 Bali, Indonesia.
- **IAUS 163 Wolf-Rayet Stars: Binaries, Colliding Winds, Evolution,** 2–6 May 1994 Elba, Italy.
- **IAUS 193 Wolf-Rayet Phenomena in Massive Stars and Starburst Galaxies,** 3–7 November 1998 Puerto Vallarta, Mexico.
- **IAUS 212 A Massive Star Odyssey, from Main Sequence to Supernova,** 24–28 June 2002 Lanzarote, Canary Islands, Spain.
- **IAUS 227 Massive Star Birth: A Crossroads of Astrophysics,** 16–20 May 2005 Catania, Italy.
- **IAUS 250 Massive Stars as Cosmic Engines,** 10–14 December 2007, Kauai, Hawaii, USA.

Some of you will recall your own attendance at these meetings, which still resonate in my memories. I hope such pleasures will also be found by the younger of you attending this conference.

Let me now turn to the current status of W-R research concerning their origin and fate. Not to trivialize the latter, it appears clear that when their evolved stellar cores give out of nuclear fuel and cannot support the remaining overlying material the star will collapse, resulting in a supernova! These have been associated with SNe of type Ib and Ic, which collectively have no hydrogen remaining. Many of our colleagues here are working extensively in this area, and so I leave the subject of the deaths of W-Rs in their capable hands, and instead concentrate on the origins question.

For quite some time after the extensive research into the evolution of exchange mass (massive) binaries, it became clear that this was a way to uncover the products of nuclear reactions in their stellar cores. But was it the only way? For this to be

the case, ALL W-R stars had to be binaries, and, furthermore, they had to have had an acceptance of mass from their companions. But was there another "channel"? Here I need to relate a very personal story. In 1975 I was very involved with an observing program at CTIO to obtain high dispersion spectra of all the bright (∼8th mag) southern O type stars (I had already obtained the northern ones at Lick Observatory). I had just obtained spectra of several Of and WN stars in the Carina Nebula, and it popped into my head they looked very similar with absorption lines, and weak to strong W-R WN type emission features of Helium and Nitrogen. But their type of star labels were not the same, rather they were called Of and WN. Was there a connection?

It was already clear from rocket observations pioneered by Don Morton (Morton 1967) that hot massive stars had winds. These stars also contained spectral indicators for winds and perhaps at a level to remove enough material to uncover their cores. I developed and talked about this scenario at the Liege Symposium that year (Conti 1975) and the concept was well received. Thus opened up a single star mass loss channel to produce W-R phenomena.

It has been claimed that all W-R stars are in binary systems, similarly there have been extensive arguments that all massive stars are binaries. I would tend to doubt this as the brightest O star in our sky, Zeta Pup, appears to be single. Furthermore, the brightest W-R, γ^2 Vel, while a binary, has its companion in a several month elliptical orbit. I had always understood that mass exchange led to a circularization of the orbit. Thus how could it have been interacting? For this star, an investigation of the spectrum of the companion O type supergiant (Conti & Smith 1972) revealed *no* anomalies in its lines. In particular, *if* there has been an interaction, nitrogen atoms would have been earlier preferentially been removed from the WC star and deposited on the companion. There is *no* evidence of this. I would like to suggest that other WC binaries with known companions ought to be investigated for evidence of past mass exchange. While clearly the short period ones could have interacted, the mass peeled off the initial primary might well have been completely ejected from the system.

Another important unsettled issue is the role of rotational mixing in massive stars. This might well aid in the mass loss process, in single and in binary stars, thus a channel to provide W-R phenomena. For example, it might affect the Humphreys-Davidson luminosity limit for massive stars, above which stars turn back to the blue and below which they become red supergiants. This affects the minimum mass for W-R star production. Related to his is an unsettled issue of whether or not RSG can end up as W-R stars. The jury is out on this question at present. What is the role of Luminous Blue Variables (LBVs) in W-R production? Are all W-R post LBV stars?

Let me list some outstanding problems still with us in considering our understanding of W-R evolution.

W-R stars ought to define the spiral arms of our galaxy, but typical placement of them does not readily lend itself to clearly defined arms. Also, we live in a barred galaxy, which ought to have *two* well defined arm features. This is not seen in a face-on view. It might be that the distance determinations are still insufficiently accurate to give us a clear picture.

Are massive stars born in isolation? IR imaging of isolated UCHII regions, the precursors of massive O stars typically result is the discovery of fainter stars in the immediate vicinity. Might these objects play a role in further W-R evolution?

In the very luminous galactic cluster Westerlund 1, 23 W-R stars and 3 red supergiants are found. It seems likely given its size that these stars are coeval. But how can this be, given an HD limit? Individual stars may have different rotational mixing properties. Higher values would push more to W-R production and lower values would tend to produce a red supergiants. At a certain time both types might be present together.

Finally, I would like to strongly suggest that someone devise a observation that would demonstrate that a close W-R binary had, indeed, gone through a mass *exchange* to its companion, rather than a mere mass *loss* during the interaction.

In closing, all of us Wolf-Rayet "stars" would like to thank Professor Wolf-Ranier Hamman for conceiving of and organizing this conference.

I am indebted to Nolan Walborn for providing me with the image of the IAUS#49 participants, and Hugo Marraco for their identification. I appreciate the help of Kimberly Sokal for helping me with my oral presentation and Phil Massey for assistance beyond the call of duty in organizing my talk.

References

Conti, P. S. 1975, Memoires of the Societe Royale des Sciences de Liege, 9, 193

Conti, P. S., Garmany, C. D., De Loore, C., & Vanbeveren, D. 1983, ApJ, 274, 302

Conti, P. S. & Smith, L. F. 1972, ApJ, 172, 623

Massey, P. 2010, in Astronomical Society of the Pacific Conference Series, Vol. 425, Hot and Cool: Bridging Gaps in Massive Star Evolution, ed. C. Leitherer, P. D. Bennett, P. W. Morris, & J. T. Van Loon, 3

Massey, P., Neugent, K. F., & Morrell, N. 2015, in Wolf-Rayet Star Workshop, ed. W.-R. Hamann, A. Sander, & H. Todt, in press

Morton, D. C. 1967, ApJ, 150, 535

Niemela, V. S. 2008, in Revista Mexicana de Astronomia y Astrofisica Conf. Series, Vol. 33, 3


Peter Conti

Posters

Wolf-Rayet Stars
W.-R. Hamann, A. Sander, H. Todt, eds.
Potsdam: Univ.-Verlag, 2015
URL: http://nbn-resolving.de/urn:nbn:de:kobv:517-opus4-84268

P Cygni and its Observations at the Abastumani Observatory

S. Beradze[1], N. Kochiashvili[1], R. Natsvlishvili[1], I. Kochiashvili[1,2], E. Janiashvili[1], T. Urushadze[1]& M. Vardosanidze[1]
[1] *Abastumani Astrophysical Observatory, Ilia State University, Georgia*
[2] *Dark Cosmology Centre, Niels Bohr Institute, University of Copenhagen, Denmark*

We found original observations of P Cygni by E. Kharadze and N. Magalashvili in the archives of the Abastumani Observatory. These observations were carried out in the period 1951–1983. Initially they used 29 Cygni as a comparison star, and all observations of P Cygni were processed using this star. On the basis of their calculations, the authors decided that P Cygni may be a W UMa type binary with an orbital period of 0.500565 d, but this hypothesis was not confirmed. The only observations that have been published in the Bulletin of the Abastumani Astrophysical Observatory were those of of 1951–1955. There are whole sets of observational data not only for P Cygni and 29 Cygni, but in the majority of cases also for 36 Cygni in the archives. We recalculated all data (where it was possible) using 36 Cygni as a comparison star. We are presenting UBV light curves of the variable, and also observations made by V. Nikonov in Abastumani in the period 1935–1937.

UBV Observations at the Abastumani Observatory

Investigations of variable stars were performed in the Abastumani Observatory from the very beginning of its establishment (1932). Photoelectric observations of P Cyg were made using the 33 cm reflector during the period 1935–1937 comprising 758 days in total. We emphasize that the increase in brightness for P Cygni was almost 0.3 mag between 1935–1936 (Nikonov 1937).

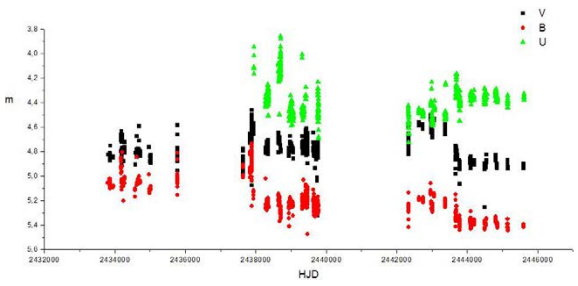

Fig. 1: UBV observations of P Cygni made by E. Kharadze and N. Magalashvili during 1951–1983. 36 Cygni = HD 193369 was used as comparison star.

From 1951 N. Magalashvili and E. Kharadze were regularly observing P Cyg using the 33 cm reflector with an electro-photometer. On the basis of these observations, they concluded that the behavior of the star was similar to W UMa variability, with a period of 0.500565 d and an amplitude of 0.10–0.08 mag (Magalashvili & Kharadze 1967). But W UMa type variability was not confirmed. Presumably, one of the reasons of Magalashvili–Kharadze erroneous conclusions is the complex variability of the star; it is possible that the variability of 12–14 hours does really exist. The latest revision of the observational material fortunately allowed us to re-process the 1951–1967 and 1974–1983 observations and to estimate the true variability picture of P Cygni. After 1968, E. Kharadze and N. Magalashvili used the same filters and the same photometer with the 48 cm Cassegrain telescope. These observations are unpublished, so we recalculated the data using 36 Cyg as comparison star (where it was possible). The UBV data are presented in Fig. 1.

At the first glance, we can see that during 1974–1983 the star dimmed in the U band while it brightened in the B and V bands (the last third part of Fig. 1). The middle part of the figure represents the time interval 1961–1967. Here the colour behavior of the star is different: during brightening in the V band, the star becomes fainter in B and U.

Conclusions

We think that the unpublished observations of P Cygni obtained by E. Kharadze and N. Magalashvili at the Abastumani Observatory are very significant for the following reasons: *1.* they are homogenous observations spanning more than 30 years, which could reveal periodicities in brightness variations; *2.* from the UBV observations it is possible to trace the colour behavior of the star; *3.* the observations by Nikonov, Kharadze and Magalashvili are unique because they are the only existing data of P Cygni observed with UBV filters between 1935 and 1983.

References

Magalashvili, N. L. & Kharadze, E. K. 1967, Information Bulletin on Variable Stars, 210, 1
Nikonov, V. B. 1937, Bulletin onf the Abastumani astrophysical Observatory, 1, 35

Wolf-Rayet Stars
W.-R. Hamann, A. Sander, H. Todt, eds.
Potsdam: Univ.-Verlag, 2015
URL: http://nbn-resolving.de/urn:nbn:de:kobv:517-opus4-84268

Stellar parameters from photometric data for fainter and more distant Wolf-Rayet stars

J. M. Bestenlehner[1,2]
[1] *Max Planck Institute for Astronomy, Heidelberg, Germany*
[2] *Argelander Institute for Astronomy, Bonn, Germany*

Spectroscopy is the preferred way to study the physical and wind properties of Wolf-Rayet (WR) stars, but with decreasing brightness and increasing distance of the object spectroscopy become very expensive. However, photometry still delivers a high signal to noise ratio. Current and past astronomical surveys and space missions provide large data sets, that can be harvested to discover new WR stars and study them over a wide metallicity range with the help of state of the art stellar atmosphere and evolutionary models.

1 Motivation

The large grid of stellar atmosphere models and synthetic spectra (Bestenlehner et al. 2014) has been further extended to higher effective temperatures ($T_{\rm eff}$ from 35 kK to 100 kK) and a wider mass-loss rate range ($\log \dot{M}/(M_{\odot}{\rm yr}^{-1})$ from -6.5 to -3.8). The grid has been computed with the the non-LTE radiative transfer code CMFGEN (Hillier & Miller 1998). For this study I have developed a python code (STellar pARmeterS from pHOTometry, STARSHOT) to extract colours from synthetic spectra using any photometric or self-defined filter system to predict spectral energy distributions (SEDs) and photometric colours of individual stars or stellar populations. These stars or stellar populations can be followed from the formation until the end of their lifetime in combination with evolutionary tracks and stellar initial mass functions.

2 Method

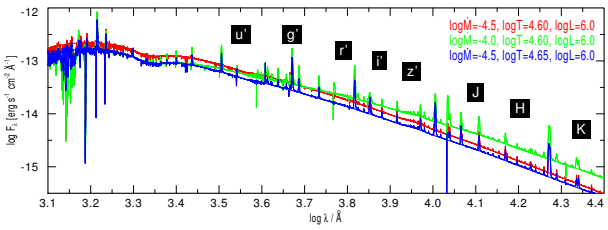

Fig. 1: Spectral energy distribution of models with varying $\dot{M}$ and $T_{\rm eff}$. The central wavelengths of SDSS and 2MASS filters are indicated by black boxes.

STARSHOT can be applied to spatially resolved objects as well as unresolved stellar populations such as multiple stellar systems, star clusters and galaxies. Spatially resolved objects are analysed with a grid search approach by applying reddening laws and minimization techniques. Unresolved clusters or galaxies dominated by WR and/or OB star populations are studied with a population synthesis approach by combining synthetic grid spectra, evolutionary models and initial mass functions. Depending on the input of synthetic spectra and evolutionary models it can be applied to any cluster or galaxy.

With this method it is possible to estimate luminosities, helium abundances, effective temperatures and mass-loss rates. The luminosity is derived from the SED by applying the distance modulus and reddening laws. For example for photometry from the Sloan Digital Sky Survey (SDSS), Helium abundances can be derived from the ratio of the g' (He II λ4686) and r' (H_{α}) magnitudes. The filters are rather broad and the uncertainties are large. $T_{\rm eff}$ is derived from the slope of the SED. The SED varies stronger in the optical than in the near-IR (Rayleigh-Jeans slope, Fig. 1). The uncertainty increases with increasing temperature and mass loss. $\dot{M}$ has a large impact on the SED in the near-IR in particular for optically thick WR winds (Fig. 1). However, the actual $\dot{M}$ cannot be determined. Only the wind density is derived, which is a function of $\dot{M}$, v_{∞}, clumping and β-type velocity law.

3 Goals

This project is in a very early phase and STARSHOT is extensively developed at the current stage. The goals are: 1) to discover new WR stars based on public available data sets without the need of particular designed narrow band filters, 2) to study their mass loss dependence on the Eddington factor over a wide metallicity range from extremely metal poor to very metal rich in addition what has been found by Bestenlehner et al. (2014) in the Large Magellanic Cloud and Vink & Gräfener (2012) for the Arches Cluster in the Milky-Way, 3) to study the chemical self enrichment of WR stars in relation to the mass-loss time-scale, 4) to analyse the properties of WR and star-burst galaxies. The uncertainties are rather large in comparison to spectroscopic studies, but it can be compensated with a large number statistic.

References

Bestenlehner, J. M., Gräfener, G., Vink, J. S., et al. 2014, A&A, 570, A38
Hillier, D. J. & Miller, D. L. 1998, ApJ, 496, 407
Vink, J. S. & Gräfener, G. 2012, ApJ, 751, L34

Wolf-Rayet Stars
W.-R. Hamann, A. Sander, H. Todt, eds.
Potsdam: Univ.-Verlag, 2015
URL: http://nbn-resolving.de/urn:nbn:de:kobv:517-opus4-84268

The Distribution of Massive Stars in M101

J. Bibby[1], M. Shara[2], D. Zurek[2], P. A. Crowther[3], A. F. J. Moffat[4], L. Drissen[5] & M. Wilde[2]

[1] *Jeremiah Horrocks Insitute, University of Central Lancashire* [2] *American Museum of Natural History*
[3] *University of Sheffield* [4] *Université de Montréal* [5] *Université Laval*

75 WR stars and 164 RSGs are identified in a single WFC3 pointing of our M101 survey. We find that within it's large star-forming complex NGC 5462 WR stars are preferentially located in the core whilst RSGs are found in the halo, suggesting two bursts of star-formation. A review of our WR candidates reveals that only ∼30% are detected in the archival broad-band ACS imaging whilst only ∼50% are associated with HII regions.

1 Motivation & Data

The location and relative numbers of Wolf-Rayet (WR) and Red Supergiant (RSG) stars can be used to investigate star-formation history and test theoretical predictions from stellar evolutionary models.

HST/WFC3 imaging of M101 using the F469N filter was used with archival ACS imaging to identify WR and RSG stars. Follow-up Gemini/GMOS spectroscopy was obtained to confirm the WR nature of the candidates. The top spectrum in Fig. 1 indicates at least one early-type WN star whilst the lower spectrum suggests an unresolved cluster hosting both WN and WC subtypes based on the presence and relative strengths of the He IIλ4686, C IIIλ4650 and C IVλ5808 lines. Flux calibration will quantify the total WR population of each source.

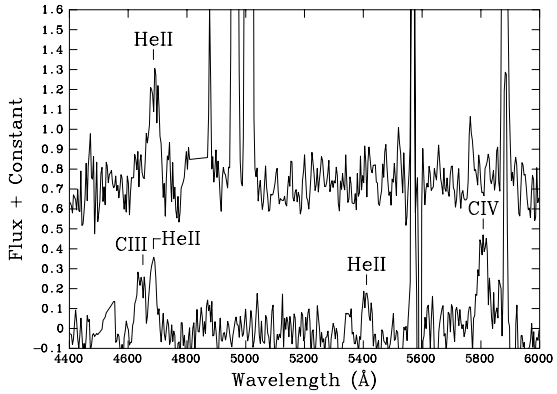

Fig. 1: GMOS spectra of a WNE star (upper) and unresolved WN+WC cluster (lower) in M101.

2 Spatial Distribution of WR Stars

WR stars and RSGs are useful tools in constraining both the age of a star-forming region and the mode of star-formation. Less massive RSGs are indicative of an older population if a single burst of star-formation is assumed. Analysis of the large star-forming complex NGC 5462 in M101 shows that both WR and RSG stars are present.

WR stars are preferentially located in the core of the star-forming cluster which hosts the brightest H II regions. We find the RSG/WR ratio increases from ∼0.4 in the core to ∼5 in the more isolated regions. This supports a conclusion of multiple epochs of star-formation, in agreement with previous work by Drissen et al. (1999).

Previous work finds that ∼70% of ccSNe and ∼75% of WR stars are associated with H II regions (Crowther 2013; Bibby & Crowther 2012). Inspection of ground-based Hα imaging reveals that only ∼50% of these WR candidates are associated with H II regions. Fig. 2 shows that the WR candidates detected in only the F469N filter are evenly distributed across the field, which is unexpected.

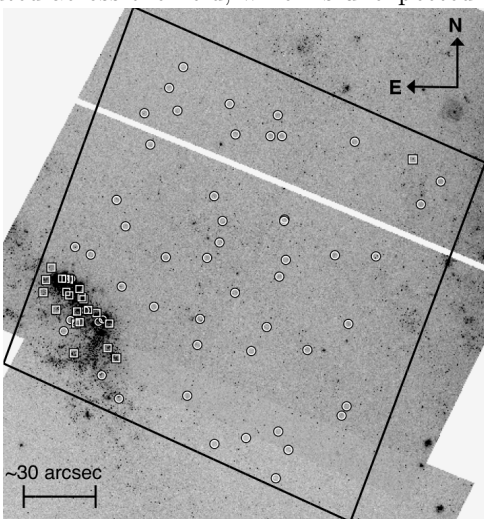

Fig. 2: One WFC3 field of M101. WR candidates detected with a 3σ excess (squares) and F469N detection only (circles) are shown.

This could suggest a low-mass origin for some WR stars, or there could be some contamination in the field. Possible contaminants could include symbiotic stars or planetary nebula, although the magnitudes of the WR candidates appear fainter than one would expect for PN. Inspection of deeper Hα imaging and narrow-band O III imaging will allow us to identify the most likely explanation.

References

Bibby, J. & Crowther, P. 2012, MNRAS, 420, 3483
Crowther, P. 2013, MNRAS, 428, 1927
Drissen, L., Roy, J., Moffat, A., & Shara, M. 1999, AJ, 117, 1249
Shara, M., Bibby, J., Zurek, D., Crowther, P., Moffat, A., & Drissen, L. 2013, AJ, 146, 162
Smith, L., Shara, M., & Moffat, A. 1996, MNRAS, 281, 163

Wolf-Rayet Stars
W.-R. Hamann, A. Sander, H. Todt, eds.
Potsdam: Univ.-Verlag, 2015
URL: http://nbn-resolving.de/urn:nbn:de:kobv:517-opus4-84268

Formation of the infalling Galactic Centre cloud G2 by collision of stellar winds

D. Calderón[1], A. Ballone[2,3], J. Cuadra[1], M. Schartmann[4], A. Burkert[2,3] & S. Gillessen[2]
[1] *Instituto de Astrofísica, Pontificia Universidad Católica de Chile, Chile*
[2] *Max Planck Institute for Extraterrestrial Physics, Germany*
[3] *Universitätssternwarte der Ludwig-Maximilians-Universität, Germany*
[4] *Centre for Astrophysics and Supercomputing, Swinburne University of Technology, Australia*

The gas cloud G2 is currently being tidally disrupted by the Galactic Centre super-massive black hole, Sgr A*. The region around the black hole is populated by $\sim$ 30 Wolf-Rayet stars, which produce strong outflows. Here we explore the possibility that gas clumps like G2 originate from the collision of stellar winds via the *non-linear thin shell instability*.

Gillessen et al. (2012) detected a moving diffuse object, the so-called G2 cloud, on its way toward the central super-massive black hole of our Galaxy. The object might be a gas clump created by the collision of stellar winds from the young stars in the Galactic Centre (Burkert et al. 2012; Schartmann et al. 2012). Although cold dense clumps are produced in SPH simulations performed by Cuadra et al. (2008), it is not clear whether their formation is physical or dominated by numerical artefacts (Hobbs et al. 2013). This work aims to test independently clump formation as the result of colliding stellar winds in the central parsec of the Milky Way. For more details see Calderón et al. (2015).

Colliding wind systems generate dense slabs of shocked gas located between the stars. This slab can become unstable easily if the shocked gas cools down rapidly. In this case, the dominant instability in the slab is the *non-linear thin shell instability* (Lamberts et al. 2011) which was described by Vishniac (1994). The instability results from the misalignment of the thermal pressure within the cold slab (perpendicular to the slab) and the ram pressure of the wind (parallel to the wind direction). Tracking the thermal evolution of the slab after the winds collide, we estimated the time evolution of the unstable wavelength criteria.

Here we present models of identical wind collisions using as input parameters the stellar separation and wind terminal velocity. The mass loss rate was fixed to 10^{-5} $M_\odot$ yr^{-1} as typically observed in Wolf-Rayet stars in the central star cluster. Once we estimated the unstable wavelength range, we computed the mass of the possible clumps assuming spherical symmetry. Our results are shown in Figure 1: clumps with masses of the order of Earth's, i.e., similar to that observed for G2 (Gillessen et al. 2012), are possible, but require short stellar separations and slow winds.

Following the orbits of the known mass-losing star sample within the inner parsec of the Milky Way (Paumard et al. 2006), we found that separations shorter than 10 milli-parsec, which is roughly the required separations to generate thin slabs, do not happen frequently enough. This makes the formation of G2 through colliding winds an unlikely but possible scenario. IRS 16SW and other Wolf-Rayet *binaries* on the other hand are permanently at short stellar separations – it is possible that their winds can be radiative enough to generate such massive clumps in the Galactic Centre. We defer studying these systems numerically to a forthcoming work.

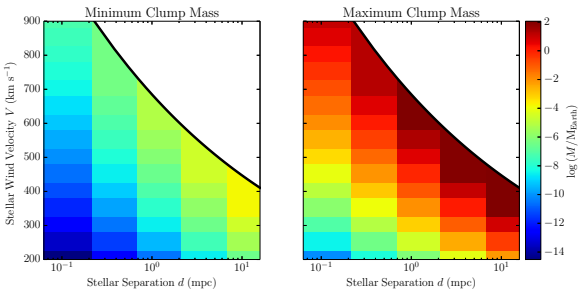

Fig. 1: Range of clump masses (colours) obtained with our model as a function of stellar wind velocity and separation. The left and right panels show the clump mass lower and upper limits, respectively.

References

Burkert, A., Schartmann, M., Alig, C. et al. 2012, ApJ, 750, 58

Calderón, D., Ballone, A., Cuadra, J. et al. 2015, arXiv:1507.07012

Cuadra, J., Nayakshin, S. & Martins, F. 2008, MNRAS, 383, 458

Gillessen, S., Genzel, R., Fritz, T. K. et al. 2012, Nature, 481, 51

Hobbs, A., Read, J., Power, C. & Cole, D. 2013, MNRAS, 434, 1849

Lamberts, A., Fromang, S. & Dubus, G. 2011, MNRAS, 418, 2618

Paumard, T., Genzel, R., Martins, F. et al. 2006, ApJ, 643, 1011

Schartmann, M., Burkert, A., Alig, C. et al. 2012, ApJ, 708, 605

Vishniac, E. T. 1994, ApJ, 428, 186

Wolf-Rayet Stars
W.-R. Hamann, A. Sander, H. Todt, eds.
Potsdam: Univ.-Verlag, 2015
URL: http://nbn-resolving.de/urn:nbn:de:kobv:517-opus4-84268

Results Of The Spectroscopic Analysis Of WR6 Using CMFGEN

A. C. Gormaz-Matamala[1,5,6], A. Hervé[2,3], A.-N. Chené[4], M. Curé[5,6] & R. E. Mennickent[1]
[1] *Departamento de Astronomía, Universidad de Concepción, Concepción, Chile*
[2] *CNRS & Université Montpellier, Place Eugene Bataillon, F-34095 Montpellier, France*
[3] *Astronomical Institute of the ASCR, Fričova 298, 251 65 Ondřejov, Czech Republic*
[4] *Gemini Observatory, Hawaii, USA*
[5] *Instituto de Física y Astronomía, Universidad de Valparaíso, Valparaíso, Chile*
[6] *Centro de Astrofísica, Universidad de Valparaíso.*

Using ESPaDOnS optical spectra of WR6, we search variations on the stellar wind parameters during the different phases of the spectral variations. We use the radiative transfer code CMFGEN (Hillier & Miller 1998) to determine the wind parameters.

Our work gives mean parameters for WR6, $T_{\rm eff} = 55\,$kK, $\dot{M} = 2.7 \times 10^{-5}\,M_\odot$/yr and $v_\infty = 1700\,$km/s. Furthermore the line profiles variations at different phases are the consequence of a variation of mass loss rate and temperature un the winds. Effective temperature reaches 59 kK at the highest intensity, whereas the mass-loss rate decreases to $2.5 \times 10^{-5}\,M_\odot$/yr in that case. On the other hand, effective temperature decreases to 52.5 kK and the mass-loss rate increases to $3 \times 10^{-5}\,M_\odot$/yr when the line profile reach its minimum intensity.

Results confirm the variable nature of the stellar wind, presented in this case on two of its fundamental parameters: temperature and mass-loss; which could be used to constrain the nature of the instability at the basis of the wind.

WR6 shows a large-scale variability observed with a period of $P = 3.77$ days (Lamontagne et al. 1986). Morel et al. (1997) suggested this variability might be caused by Corotating Interaction Regions (CIR) as modelled by Cranmer & Owocki (1996).

The results of our analysis of the mean spectrum and at the maxima and minima line profile intensity phases are presented in Table 1. A comparison to previous studies is also presented.

The variation of HeII line profiles are due to variations of stellar wind properties. Since these line profile variabilities are an observational consequence of the presence of CIRs (Cranmer & Owocki 1996), we suggest the idea that the variations found are due to the difference in the structure of the wind across the different observed faces of WR6 during its rotation.

By the other side, it is known the CIRs are probably produced by instability on the stellar surface (Cranmer & Owocki 1996). In that case, the range of the variations found could be a first-order representation of the CIR physical conditions.

Special acknowledgements to N. St-Louis and A. de la Chevrotière for kindly putting at our disposition the ESPaDOnS spectra. We also thanks to the Deutsche Forschungsgemeinschaft, for supporting our participation in the present Workshop. A. H. is supported by the grant 14-02385S from GA ČR.

References

Cranmer, S. R. & Owocki, S. P. 1996, ApJ, 462, 469

Hamann, W.-R., Gräfener, G., & Liermann, A. 2006, A&A, 457, 1015

Hillier, D. J. & Miller, D. L. 1998, ApJ, 496, 407

Lamontagne, R., Moffat, A. F. J., & Lamarre, A. 1986, AJ, 91, 925

Morel, T., St-Louis, N., & Marchenko, S. V. 1997, ApJ, 489, 470

Morris, P. W., Crowther, P., & Houck, J. R. 2004, ApJ, 154, 413

Tab. 1: Parameters found by the present work for WR6 for mean, lowest profile and highest profile, compared with those determined by Morris et al. (2004) and Hamann et al. (2006).

Parameter	Morris et al.	Hamann et al.	Mean	Lowest Profile	Highest Profile
$T_{\rm eff}$ [kK]	52	54.3	55.0 ± 1.0	52.5 ± 1.5	59 ± 1.5
$\dot{M}[M_\odot/{\rm yr}]$	1.25×10^{-5}	5×10^{-5}	$2.7(\pm 0.2) \times 10^{-5}$	$3(\pm 0.2) \times 10^{-5}$	$2.5(\pm 0.2) \times 10^{-5}$
v_∞ [km/s]	1 800	1 700	$1\,700 \pm 10$	$1\,700 \pm 10$	$1\,700 \pm 10$
f	0.1	0.25	0.09 ± 0.01	0.1 ± 0.01	0.08 ± 0.01
$v_{\rm CL}$	-	-	50 ± 30	50 ± 30	50 ± 30

Wolf-Rayet Stars
W.-R. Hamann, A. Sander, H. Todt, eds.
Potsdam: Univ.-Verlag, 2015
URL: http://nbn-resolving.de/urn:nbn:de:kobv:517-opus4-84268

Inversion of Intensity Profiles for Bubble Emissivity

R. Ignace[1], J. A. Toalá[2] & L. M. Oskinova[3]
[1]*East Tennessee State University, USA*
[2]*Instituto de Astrofisca de Andalucía, Spain*
[3]*Universität Potsdam, Germany*

Under the assumption of spherical symmetry, the run of intensity with impact parameter for a spatially resolved and optically thin bubble can be inverted for an "effective emissivity" as a function of radius. The effective emissivity takes into account instrumental sensitivity and even interstellar absorption. This work was supported by a grant from NASA (G03-14008X).

1 The assumptions

Consider a spherically symmetric and optically thin bubble. For z the observer axis to the star at bubble center, and with p the cylindrical radius (or "impact parameter"), the observed intensity profile for a spatially resolved bubble is given by

$$I_\nu(p) = \int j_\nu(r)\, dz, \tag{1}$$

where j is the emissivity that is strictly a function of radius. This however is the emergent intensity. The measured intensity can be affected by interstellar extinction and instrumental response. So we define an "effective" emissivity $\tilde{j}$, and working with a passband intensity (to increase S/N of the data), this new parameter will be given by

$$\tilde{j}(r) = \frac{1}{A_0} \int\int \Lambda(E,T)\, \frac{dEM}{dT}\, e^{-\tau(E)}\, A(E)\, dE\, dT, \tag{2}$$

where for the case of X-ray emission: Λ is the temperature and energy dependent cooling function, T is temperature, EM is emission measure, dEM/dT is differential emission measure, τ is the energy-dependent interstellar absorption, $A(E)$ is the effective area as representing the X-ray telescope instrumental response, and A_0 is the total energy-integrated area. Our inversion recovers a passband-equivalent emissivity that takes these various factors into account.

2 The solution

Equation (1) is well known to yield an inversion solution in the form of Abel's equation (e.g., Craig & Brown 1986) The formal solution is analytic with

$$\tilde{j}(r) = \frac{-1}{\pi}\, \frac{d}{dr} \int_r^R r\, I(p)\, \frac{dp/p}{\sqrt{p^2 - r^2}}, \tag{3}$$

where R is the bubble radius, and the square root in the denominator acts like geometrical deprojection weighting factor. Note first that the integral for the inversion proceeds from the limb toward the center. Also, the solution ultimately derives from a derivative involving the data. It is well-known that this solution is ill-posed, and quite sensitive to the effects of noise. Applications will therefore generally require the use of regularization techniques.

In practice one would produce $I(p)$ by averaging the intensity in annuli. All things equal, this approach will increase the S/N of the averaged profile as $\sqrt{p}$, which means data toward the limb, where the inversion starts, will be of superior quality (unless $I(p)$ drops precipitously from center to limb), which should make the inversion more stable.

3 Some handy analytic examples

The advantage of inversion techniques is that the data guide the solution, as opposed to forward modeling and fits that ultimately involve preconceived notions regarding the source structure. The disadvantage is having to negotiate the sensitivity of solutions to the data noise.

Some useful insight can be derived from a consideration of simple profiles with analytic solutions. One might for example characterize intensity profiles as "flat" (i.e., uniform), "rounded", "triangular", "double-horned", and so on.

Take for example the case of a flat profile with $I(p) = I_0$, a constant. This implies an effective emissivity of the form

$$\tilde{j}(r) = (I_0/\pi)/\sqrt{R^2 - r^2}, \tag{4}$$

which increases steeply toward the limb. By contrast a parabolic profile with $I(p) = I_0\,(1 - p^2/R^2)$ would have a solution

$$\tilde{j}(r) = (2I_0/\pi R)\, \sqrt{R^2 - r^2}. \tag{5}$$

Interestingly, polynomial fits to $I(p)$ will generally yield these two types of square-root factors along with additional radial dependence and numerical weighting factors that derive from the best fit polynomial to the data.

References

Craig, I. J. D. & Brown, J. C. 1986, Inverse problems in astronomy: A guide to inversion strategies for remotely sensed data

Wolf-Rayet Stars
W.-R. Hamann, A. Sander, H. Todt, eds.
Potsdam: Univ.-Verlag, 2015
URL: http://nbn-resolving.de/urn:nbn:de:kobv:517-opus4-84268

New Galactic Wolf-Rayet Stars

G. Kanarek[1,2], M. Shara[2], J. Faherty[3], D. Zurek[2], & A. F. J. Moffat[4]
[1] *Columbia University, New York, NY, USA*, [2] *American Museum of Natural History, New York, NY, USA*
[3] *Carnegie Institute, Washington, DC, USA*, [4] *Université de Montréal, Montréal, QC, CA*

Over the course of 6 months in 2013, we observed nearly 400 Wolf-Rayet candidates in the Galactic plane. Preliminary results from this dataset are presented.

1 Introduction

In 2005–2006, our group conducted a 300 deg^2 NIR narrowband survey of the Galactic plane (first described in Shara et al. 2009). The vast majority of WR candidates from this survey, at magnitudes of $K \geq 13.5$, still await spectroscopic follow-up. In 2013, nearly 400 WR and PN candidates ($K \leq 13.5$) were observed on the SMARTS 1.5m telescope at CTIO with the Université de Montréal's SIMON spectrograph, and an additional 8 candidates of $14.3 \leq K \leq 14.7$ on the VLT with ISAAC. Reduction and analysis of this large dataset is ongoing; preliminary results are presented here.

2 Candidate Selection

Candidates were selected using a combination of colors from 2MASS (Skrutskie et al. 2006), WISE (Wright et al. 2010), and this NB survey, as per Faherty et al. (2014) and Kanarek et al. (2015) (the latter shown in figure 1), a method that identifies PNe as easily as WR stars.

3 Preliminary Results

Preliminary results are very promising. A number of new objects displaying WR or PN spectral characteristics have been identified; one is shown in figure 2. We have a preliminary success rate of $\sim 75\%$ for PNe and $\sim 50{-}60\%$ for WCs and [WCs]. The full dataset of 400 spectra will comprise a complete catalogue of the remaining WCs in the Galactic plane from $l = -90°$ to $+60°$, $b = \pm 1°$, to a limit of $K = 13.5$. These preliminary results show that future spectroscopic surveys with large NIR telescopes will be able to probe the far side of the Galaxy and identify WR stars and PNe at $K \geq 14$.

References

Faherty, J. K., Shara, M. M., Zurek, D., Kanarek, G., & Moffat, A. F. J. 2014, AJ, 147, 115

Kanarek, G., Shara, M., Faherty, J., Zurek, D., & Moffat, A. 2015, Monthly Notices of the Royal Astronomical Society, 452, 2858

Shara, M. M., Moffat, A. F. J., Gerke, J., et al. 2009, AJ, 138, 402

Skrutskie, M. F., Cutri, R. M., Stiening, R., et al. 2006, AJ, 131, 1163

Wright, E. L., Eisenhardt, P. R. M., Mainzer, A. K., et al. 2010, AJ, 140, 1868

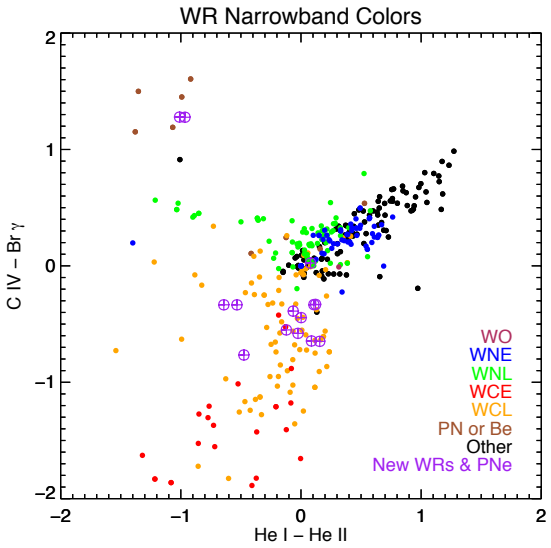

Fig. 1: Color-color plot using the NB magnitudes from the Shara et al. survey. WC stars in particular are very easy to identify.

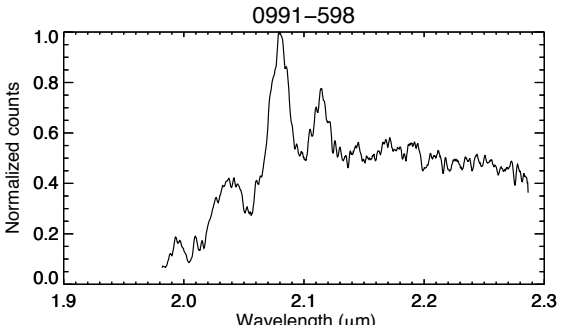

Fig. 2: An example preliminary spectrum of a new WC star (before telluric correction) from the CTIO dataset.

Wolf-Rayet Stars
W.-R. Hamann, A. Sander, H. Todt, eds.
Potsdam: Univ.-Verlag, 2015
URL: http://nbn-resolving.de/urn:nbn:de:kobv:517-opus4-84268

New Photometric Observations of P Cygni

N. Kochiashvili[1], S. Beradze[1], I. Kochiashvili[1 2], R. Natsvlishvili[1]& M. Vardosanidze[1]
[1] *Abastumani Astrophysical Observatory, Ilia State University, Georgia*
[2] *Dark Cosmology Centre, Niels Bohr Institute, University of Copenhagen, Denmark*

We present the results of the new photometric observations of the famous hypergiant P Cygni. New observations were obtained in 2014 using the 48 cm Cassegrain telescope of the Abastumani Astrophysical Observatory, Georgia. We reveal some interesting behaviors of the B,V,R,I light curves, and also report new results on the periodicity of P Cygni's variation. The latter result is based on the analysis of the photometric data (U,B,V filters) collected at the Abastumani Observatory between 1937 and 1983.

Photometric observations of P Cygni in 2014

We observed P Cygni in July 23 – October 20, 2014 with the 48 cm Cassegrain telescope and standard B,V,R,I filters. HD 228793 has been used as a comparison star. We find spectral observations of the star by Alexandre Senterne[1] with the HARPS-N spectrograph, attached to the TNG. During the observations the star underwent light variations with the mean amplitude of approximately 0.1 magnitudes in all pass-bands, and the period of this change was approximately 70 (67.8) days. There is also a relation between brightness and the Hα EW variability. The cause of this feature may be a variability rate of the stellar wind that is very strong, which, on the other hand, maybe due to the pulsation of the star.

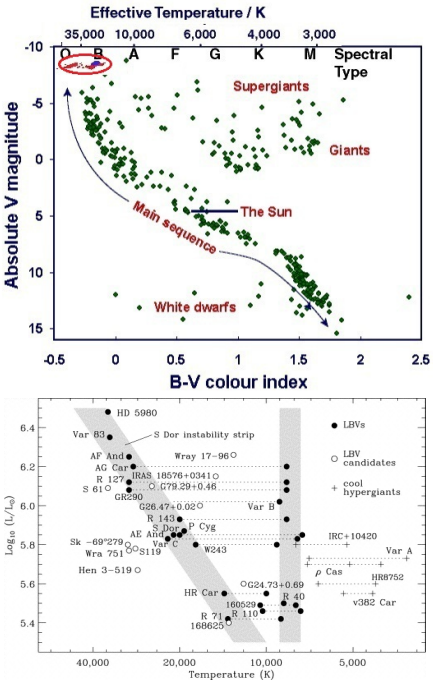

Fig. 1: P Cygni in the HR diagram

Colour behavior of P Cygni

Long-term photometric observations of P Cygni give us the possibility to trace the B-V and U-B colour variability of the star. It is accepted that P Cygni is gradually reddening. But this behavior is very impressive in the observations of Kharadze and Magalashvili, because B-V varies from 0.0 to 0.4. It means that the star seems to be of late A, early F spectral type, with temperature between 7500–9000 K. But according to the 2014 spectral observations by A. Senterne[1], the temperature of P Cygni is $T_{\rm eff}$ = 21000 K ($T_{\rm eff}$ = 18200 K by Najarro et al. 1997). After correcting for the reddening by 0.5 (Najarro 2001), we have B-V values from -0.5 to -0.1 in 1951–1983. In 2014's observations the colour of the star corresponds to the early B-spectral type (B1), and it seems that the problem is resolved. However, the B-V colour shift by $\sim$ 0.55 during 1951–2014 is an observed fact (B-V varied in the range of 0.4–0.55 during the observational run of 2014).

P Cygni's fate

It seems that P Cygni has been a late O-spectral type star at the first half of the 20th century (the top part of the Fig. 1). If the colour behavior of P Cygni will have the same character in future, then in 80–120 years the star will reach the "constant temperature outburst phase" and may undergo the next great eruption, or even supernova explosion. See the bottom part of Fig. 1 (from Smith et al. 2004).

References

Najarro, F. 2001, in Astronomical Society of the Pacific Conference Series, Vol. 233, P Cygni 2000: 400 Years of Progress, ed. M. de Groot & C. Sterken, 133

Najarro, F., Hillier, D. J., & Stahl, O. 1997, A&A, 326, 1117

Smith, N., Vink, J. S., & de Koter, A. 2004, ApJ, 615, 475

[1] http://www.spectro-aras.com/forum/viewtopic.php?f=17&t=996

Wolf-Rayet Stars
W.-R. Hamann, A. Sander, H. Todt, eds.
Potsdam: Univ.-Verlag, 2015
URL: http://nbn-resolving.de/urn:nbn:de:kobv:517-opus4-84268

Modeling of spectral variability of Romano's star

O. Maryeva[1], V. F. Polcaro[2], C. Rossi[3] & R. Viotti[2]
[1] *Special Astrophysical Observatory of the Russian Academy of Sciences*
[2] *Institute for Space Astrophysics and Planetology, INAF, Roma, Italy*
[3] *Universita La Sapienza, Roma, Italy*

We present results of investigation of spectral variability of one of the most interesting massive stars, Romano's star (M33/V532 or GR290), located in the M33 galaxy. Brightness of the star changes together with its spectral class, which varies from WN11 to WN8. Using CMFGEN code we estimated parameters of stellar atmosphere and found that during last ten years bolometric luminosity of the star changed synchronously with stellar magnitude. Our calculations argue in favor of the hypothesis of a post-LBV status of GR290.

We have used the CMFGEN atmospheric modeling code (Hillier & Miller 1998) and new spectral data as well as archival data. In order to see how parameters of GR290 changed with time we constructed nine models for most representative spectra with best quality, obtained between 2002 and 2014. Table 1 lists the parameters of the models, while the model spectra themselves are shown in Figure 1. The main result of this analysis is that **the bolometric luminosity of GR290 is variable**, it is higher during the phases of larger optical brightness. We argue that GR290 is now in a short, and thus very rare transition phase between the LBV state and the W-R nitrogen rich stellar class. More details will be published in the article by V. F. Polcaro, O. Maryeva, R. Nesci, M. Calabresi, A. Chieffi, S. Galleti, R. Gualandi, R. Haver, A. Pasquali, C. Rossi, T. Vasilyeva, R. F. Viotti, which now is in preparation.

We'd like to thank R. Gualandi, R. Haver and M. Calabresi for providing new spectral and photometric data. OM thanks Dynasty Foundation and RFBR (project no. 14-02-31247, 14-02-00291) for support of the study.

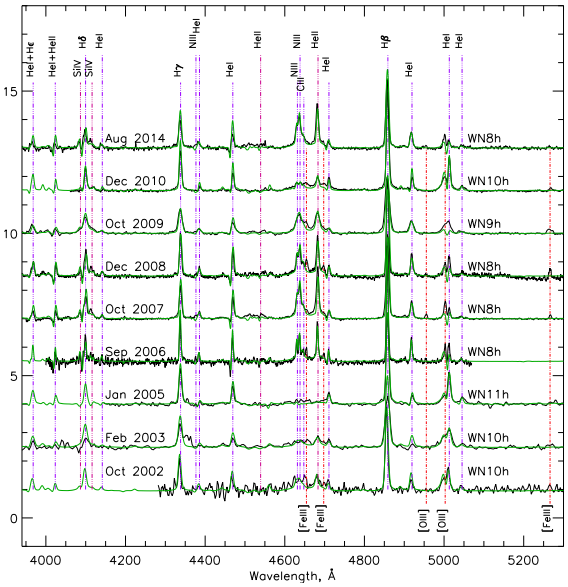

Fig. 1: Normalized optical spectra of GR290 compared with the best-fit CMFGEN models (green line).

Tab. 1: Derived properties of GR290. Hydrogen number fraction relative to helium H/He=1.7 ± 0.2. Filling factor f= 0.2 ± 0.1. In calculations we assume that the distance to the M33 galaxy is $D = 847 \pm 60$ kpc.

Date	V [mag]	Sp. type	$T_{\rm eff}$ [kK]	$R_{2/3}$ [$R_\odot$]	$L_*, 10^5$ [$L_\odot$]	$\dot{M}_{cl}, 10^{-5}$ [$M_\odot$/yr]	v_∞ [km/s]
Oct 2002	17.98	WN10h	27.5	35.4	6.5	2.1	200
Feb 2003	17.70	WN10.5h	28	37	7.5	2.2	200
Feb 2005	17.24	WN11h	23.3	61.2	10	4	200
Sep 2006	18.4	WN8h	31	26	5.5	1.4	200
Oct 2007	18.6	WN8h	33.5	21.6	5.3	1.7	400
Dec 2008	18.31	WN8h	31.5	24.5	5.3	2.0	400
Oct 2009	18.36	WN9h	32	25.2	6	1.7	300
Dec 2010	17.66	WN10h	26.4	43	8	2.6	200
Aug 2014	18.74	WN8h	32.7	22	5.1	1.7	400

References

Hillier, D. J. & Miller, D. L. 1998, ApJ, 496, 407

Wolf-Rayet Stars
W.-R. Hamann, A. Sander, H. Todt, eds.
Potsdam: Univ.-Verlag, 2015
URL: http://nbn-resolving.de/urn:nbn:de:kobv:517-opus4-84268

A not so massive cluster hosting a very massive star

S. Ramírez Alegría[1,2], A.-N. Chené[3], J. Borissova[1,2], R. Kurtev[1,2], C. Navarro[1,2], M. Kuhn[2], J. A. Carballo-Bello[1,2]
[1] *Millennium Institute of Astrophysics, Santiago, Chile*
[2] *Instituto de Astronomía, Valparaíso, Chile* [3] *Gemini Observatory, AURA, USA*

We present the first physical characterization of the young open cluster VVV CL041. We spectroscopically observed the cluster main-sequence stellar population and a very-massive star candidate: WR62-2. CMFGEN modelling to our near-infrared spectra indicates that WR62-2 is a very luminous ($10^{6.4\pm0.2} L_\odot$) and massive ($\sim 80 M_\odot$) star.

The current census of Wolf-Rayet (WR) in the Milky Way is far from complete. For example, there are ∼640 WR stars reported in the online "Galactic Wolf Rayet Catalogue", but we expect over 1900 in our Galaxy (Rosslowe & Crowther 2015). It is also under debate the WR birth-place. We expect their formation in clustered environments, but it is unclear whether it happens in young clusters or associations. Trying to solve this question, we started a search of WR in the cluster candidates catalogue from Borissova et al. (2011), based on images from the ESO Public Survey VVV (Minniti et al. 2010).

Using VVV JHK_S photometry and H-, K-band spectroscopy we determine the cluster distance (via spectroscopic parallax; $d = 4.2 \pm 0.9$ kpc), radius ($r = 0.75'$), age (fitting Geneve-MS and PMS isochrones, Ekström et al. 2012; Siess et al. 2000; age=$1-5$ Myr), and total stellar mass (by integration of Kroupa-IMF, Kroupa 2001, fitted to the cluster mass function; $M_{CL} = (3.1 \pm 0.6) \cdot 10^3 M_\odot$).

The near-IR spectra also revealed part of the cluster main sequence population. We observe 8 stars, and we classify 6 of them as OB-type stars (between O4 V and early B-type). Spectrum of star #8, the brightest star in the decontaminated CMD, displays the Brackett series with strong and broad emission lines. The C IV and N III lines are clearly detected. The Brackett series in emission indicates that hydrogen is still present. Carbon lines are narrow and weak, confirming that it is not a WC. We assigned a spectral type WN8-9h to star #8 (hereafter, WR62-2).

Using the code CMFGEN (Hillier & Miller 1998), we estimate for WR62-2 the effective temperature ($T_{\rm eff} = 34000K$), which indicates a luminosity of ($10^{6.4\pm0.2} L_\odot$) and a initial mass of at least $80 M_\odot$, from the star position in the HR-diagram. The cluster and WR62-2 masses are incompatible with the ($M_{\rm ecl} - m_{\rm max}$) relation (Weidner et al. 2010). A binary merge is a probable mechanism to explain the presence of this very massive star in VVV CL041 and a gas remnant surrounding WR62-2 should be expected in mid-IR.

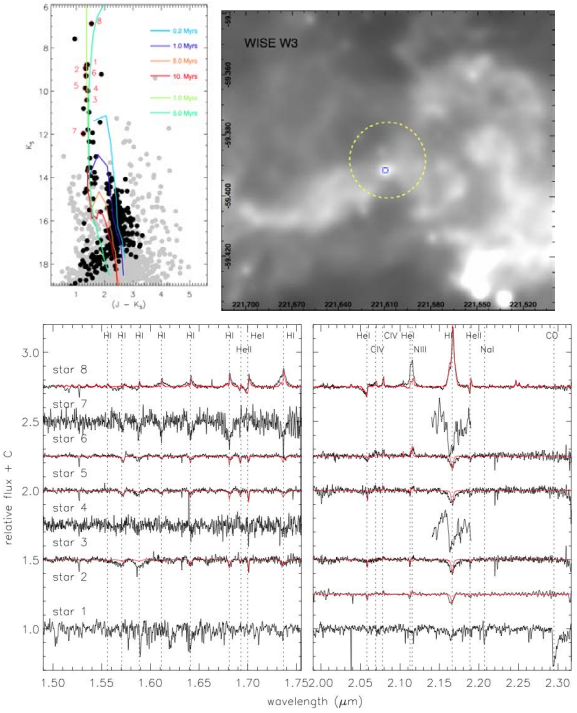

Fig. 1: *Top-left:* VVV CL041 field-star statistically decontaminated CMD. WR62-2 is shown on top of the cluster stellar population sequence. *Top-right:* VVV CL041 mid-IR WISE W3 image. The yellow circle and the blue square show the cluster's and WR62-2 positions. *Bottom:* Near-IR stellar spectra (WR62-2 is shown on top). The CMFGEN models are shown with red lines.

References

Borissova, J., Bonatto, C., Kurtev, R., et al. 2011, A&A, 532, A131
Ekström, S., Georgy, C., Eggenberger, P., et al. 2012, A&A, 537, A146
Hillier, D. J. & Miller, D. L. 1998, ApJ, 496, 407
Kroupa, P. 2001, MNRAS, 322, 231
Minniti, D., Lucas, P. W., Emerson, J. P., et al. 2010, New A, 15, 433
Rosslowe, C. K. & Crowther, P. A. 2015, MNRAS, 447, 2322
Siess, L., Dufour, E., & Forestini, M. 2000, A&A, 358, 593
Weidner, C., Kroupa, P., & Bonnell, I. A. D. 2010, MNRAS, 401, 275

Wolf-Rayet Stars
W.-R. Hamann, A. Sander, H. Todt, eds.
Potsdam: Univ.-Verlag, 2015
URL: http://nbn-resolving.de/urn:nbn:de:kobv:517-opus4-84268

3D numerical model for NGC 6888 Nebula

J. Reyes-Iturbide[1,2], P. F. Velázquez[2] & M. Rosado[3]
[1] *Tecnológico de Estudios Superiores de Tianguistenco. México*
[2] *Instituto de Ciencias Nucleares, UNAM. México*
[3] *Instituto de Astronomía, UNAM. México*

We present 3D numerical simulations of the NGC6888 nebula considering the proper motion and the evolution of the star, from the red supergiant (RSG) to the Wolf-Rayet (WR) phase. Our simulations reproduce the limb-brightened morphology observed in [OIII] and X-ray emission maps. The synthetic maps computed by the numerical simulations show filamentary and clumpy structures produced by instabilities triggered in the interaction between the WR wind and the RSG shell.

1 Numerical simulation

The galactic bubble NGC 6888 is produced by the WR 136 star. This bubble is a case of a limb-brightened, asymmetric structure. The limb-brightening can be caused by a bow-shock produced when the star (in this case the WR 136) moves through the ISM. The WR 136 is a runaway star with a proper motion ~ 75 kms^{-1} .

Taking into account the above, we show numerical simulations which consider the interaction between the WR wind and the bow shock generated during the previous RSG phase (cf. Table 1 for a list of the parameters used in the RSG and WR stages). The emission maps are computed from the 3D numerical simulations taking the y-axis as the line of sight (thus the xz plane represents the plane of the sky). We have carried out 3D numerical simulations with the adaptive mesh refinement Yguazú code (Raga et al. 2000). A computational domain of $256 \times 256 \times 512$ pixels was considered along the x, y, and z axis respectively, with a maximum resolution of 9.7×10^{16} cm.

Tab. 1: Parameters from numerical simulations; where $\dot{M}$ and V_w are mass loss rate and velocity wind from the star, respectively.

parameters	RSG	WR
$\dot{M}[10^{-5}M_\odot yr^{-1}]$	8	3
V_w[km s^{-1}]	75	2000

1.1 Results

- The interaction between the bow shock created by the RSG and the WR wind produce the limb-brightened observed in the NGC 6888 nebula.
- The expansion of the fast WR wind into the slow RSG wind produce the Vishniac and Rayleigh-Taylor instabilities, creating clumpy and filamentary density structures (see Fig. 1).
- The total X-ray luminosity computed from the simulations is 1.9×10^{33}erg s^{-1} in the $[0.4-2.4]$ keV range, which is in agreement with the observed one.

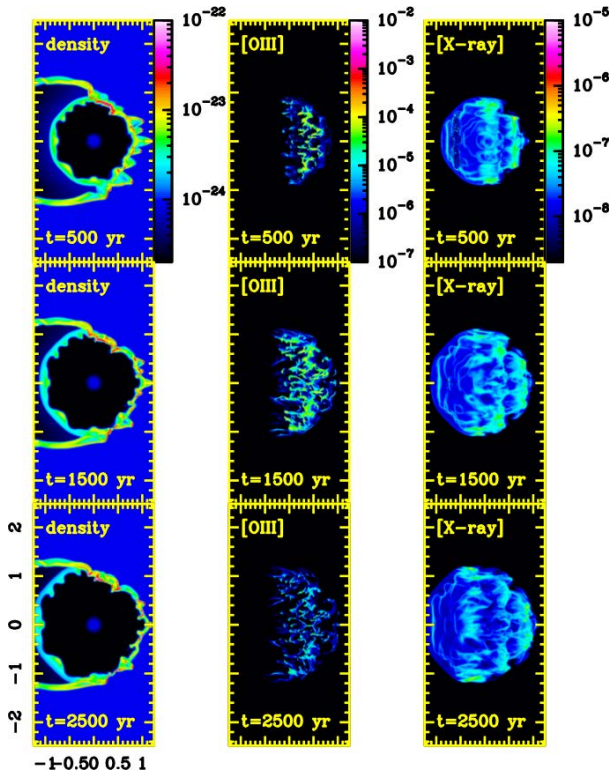

Fig. 1: From left to right (in the XZ plane): cuts of density distribution [g cm^{-3}], [OIII] and thermal X-ray [erg s^{-1} cm^{-2} sr^{-1}] synthetic maps at different evolutionary stages (from top to bottom) of the WR phase.

References

Raga, A. C., Navarro-González, R., & Villagrán-Muniz, M. 2000, Rev. Mexicana Astron. Astrofis., 36, 67

Wolf-Rayet Stars
W.-R. Hamann, A. Sander, H. Todt, eds.
Potsdam: Univ.-Verlag, 2015
URL: http://nbn-resolving.de/urn:nbn:de:kobv:517-opus4-84268

Envelope Inflation or Stellar Wind?

S. Ro[1] **& C. D. Matzner**[1]
[1] *University of Toronto, Canada*

We an optically-thick, transonic, steady wind model for a H-free Wolf-Rayet star. A bifurcation is found across a critical mass loss rate $\dot{M}_b$. Slower winds $\dot{M} < \dot{M}_b$ extend by several hydrostatic stellar radii, reproduce features of envelope inflation from Petrovic et al. (2006) and Gräfener et al. (2012), and are energetically unbound. This work is of particular interest for extended envelopes and winds, radiative hydrodynamic instabilities (eg. wind stagnation, clumping, etc.), and NLTE atmospheric models.

1 Introduction

Understanding the structure of Wolf-Rayet (WR) stars are critical for two reasons. Observationally, WRs have optically-thick winds that extend the photosphere to larger radii (Hamann et al. 2006, Crowther et al. 2006) and obscure basic stellar parameters (e.g. hydrostatic radius, rotation, etc.). This has implications for single and binary evolution, and predict type Ic supernova progenitors, shock breakout and early SN lightcurves, GRB hosts. Stellar models predict significantly inflated stellar envelopes that approach or exceed the Eddington limit (Petrovic et al. 2006; Gräfener et al. 2012). The models are capped by a density (and gas-pressure) inversion to maintain hydrostatic equilibrium.

We find the envelopes must have supersonic velocity fields, if they are to be consistent with a steady WR outflow. Furthermore, they would decelerate and contain multiple sonic points due to the density inversion. It is critical to understand the influence of dynamics as NLTE atmospheric models (e.g. `CMFGEN`; Hillier & Miller 1998 and `PoWR`; Hamann & Gräfener 2004) presume the velocity field is monotonic.

2 Results

We replicate a $23 M_\odot$ helium star with solar metallicity from Gräfener et al. (2012). We continue the integration including dynamical terms at the iron opacity bump in a separate calculation, with the sonic point criteria solved exactly within the Rosseland approximation. The radiative diffusion approximation becomes invalid where line-force amplification (LFA) enhances, and dominates, the wind acceleration. Castor et al. (1975) expresses this condition as an optical depth parameter $t = \sigma_e v_{th} \rho / (dv/dr) < 1$ for line-driven winds, with thermal velocity v_{th} and electron scattering opacity σ_e.

For $\dot{M} > \dot{M}_b$, the wind accelerates monotonically until LFA dominates the acceleration. These winds are expected to successfully escape the star. Weaker winds $\dot{M} < \dot{M}_b$ exhibit structure similar to envelope inflation. For $\dot{M} < 6 \times 10^{-6} M_\odot$/yr, the wind does not accelerate significantly such that $t < 1$, and are thus described adequately by the diffusion approximation. These models decelerate to become subsonic again, and fail to escape.

The minimum mass loss rate to which the extended structure is erased is $\dot{M}_b = 10^{-4.8}$ $M_\odot$ yr^{-1}. This $\dot{M}_b$ does not coincide with the dynamical estimate from Petrovic et al. (2006) nor Gräfener et al. (2012). Instead, we find models $\dot{M} < \dot{M}_b$ become energetically unbound. Such a condition is drawn onto Fig. 1, which clearly bifurcates the set solutions.

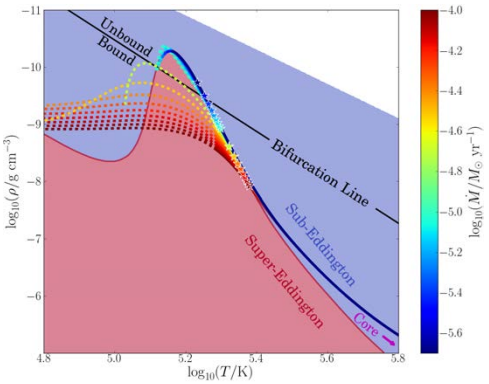

Fig. 1: Figure 3: $(\rho - T)$ map partitioned into sub- and super-Eddington regions (blue and red, respectively). The iron opacity bump is at log $(T/\mathrm{K}) = 5.2$. A Bifurcation Line $e \simeq 4aT^4/3\rho - GM_*/R_* = 0$ is where the energy density exceeds the gravitational potential. R_* is the hydrostatic radius where dynamics are negligible (i.e. $v \ll c_i \simeq 30$ km s^{-1}). Dashed lines are where $t < 1$, which roughly corresponds to $v \gtrsim 125$ km s^{-1}.

References

Castor, J. I., Abbott, D. C., & Klein, R. I. 1975, ApJ, 195, 157
Gräfener, G., Owocki, S. P., & Vink, J. S. 2012, A&A, 538, A40
Hamann, W.-R. & Gräfener, G. 2004, A&A, 427, 697
Hillier, D. J. & Miller, D. L. 1998, ApJ, 496, 407
Petrovic, J., Pols, O., & Langer, N. 2006, A&A, 450, 219

Wolf-Rayet Stars
W.-R. Hamann, A. Sander, H. Todt, eds.
Potsdam: Univ.-Verlag, 2015
URL: http://nbn-resolving.de/urn:nbn:de:kobv:517-opus4-84268

The Wolf-Rayet stars WR 102c and 102ka and their isolation

M. Steinke[1], L. M. Oskinova[1], W.-R. Hamann[1] & A. Sander[1]
[1] *Universität Potsdam, Germany*

While the majority of very massive stars is clearly found in clusters, there are also very massive objects not associated with any cluster, suggesting they may have been born in isolation. In order to gain more insights, we studied the regions around two WR stars in the Galactic Center region. To understand the nature of the potential cluster around massive stars, photometry alone is not sufficient. We therefore used the ESO VLT/SINFONI integral field spectrograph to obtain photometry and spectra for the whole region around our two candidate stars. In total, more than 60 stars have been found and assigned a spectral type.

1 Introduction

It is commonly assumed that massive stars form in clusters or at least associations. Thus, when massive stars are found to be located in isolation, one would expect them to be either in an unknown cluster or be run-away stars that were kicked out from their birth-cluster. The second scenario can have several reasons, e.g. tidal disruption by a strong (external) potential like in the Galactic Center (GC) region or close binary interaction within the parental cluster.

Our first target star, WR 102c, had been discovered about 3 pc outside the Quintuplet cluster (Figer et al. 1999) while the other, WR 102ka, was found far off all known clusters in the region (Homeier et al. 2003).

2 Observations and data reduction

We used the K-Band filter ($\lambda = 2 - 2.45\,\mu$m) of SINFONI in the Near Infrared (NIR) which has a Resolving Power of $R = 4000$. For a clear identification of stars we found a limiting magnitude of $K_\mathrm{s} \approx 14.5$ mag. Our field of view was about 1.3×1.3 pc, centered on WR 102c and 1.3×1.45 pc around WR 102ka, respectively.

The calibration was done by use of B type main-sequence stars of known spectral type, so we could use the Potsdam Wolf-Rayet code for expanding stellar atmospheres (PoWR) to model their spectra. During this process the telluric lines were also removed from the data cubes. For details, see section 2 of Oskinova et al. (2013).

3 Analysis and results

The cool stars were classified accoring to a scheme given by González-Fernández et al. (2008) which mainly makes use of the CO absorption band around $\lambda = 2.29\,\mu$m. That also allowed us to distinguish between super giants and giants.

By use of the PoWR code we analysed the early type stars and found the following results: WR 102c is a hot, evolved, hydrogen-free WN star with typical parameters (see Steinke et al., in prep.). The OB-type stars were found to be main-sequence stars near the turn-off point ranging between 12 and 27 solar masses with temperatures in the order of $15 - 25$ kK. WR 102ka is an Ofpe/WN9-10 star with a relatively low effective temperature of about 25 kK but an unusually high (present day) mass of about $100\,M_\odot$, resulting in a luminosity of $L = 10^{6.5}\,L_\odot$.

4 Summary and conclusions

In total we found 25 stars within a radius of about 1.3 pc around WR 102c, and 37 around WR 102ka in a similarly sized region. From the spectral analysis, including radial velocities, we conclude that the early-type stars of the 102c-field are likely to be members of a common cluster or association while the late-type stars (K and M giants) are identified as field stars of the GC region with a large velocity scatter.

Our observations confirm the isolation of WR 102ka as there is no massive star nearby.

References

Figer, D. F., McLean, I. S., & Morris, M. 1999, ApJ, 514, 202

González-Fernández, C., Cabrera-Lavers, A., Hammersley, P. L., & Garzón, F. 2008, A&A, 479, 131

Homeier, N. L., Blum, R. D., Pasquali, A., Conti, P. S., & Damineli, A. 2003, A&A, 408, 153

Oskinova, L. M., Steinke, M., Hamann, W.-R., et al. 2013, MNRAS, 436, 3357

Wolf-Rayet Stars
W.-R. Hamann, A. Sander, H. Todt, eds.
Potsdam: Univ.-Verlag, 2015
URL: http://nbn-resolving.de/urn:nbn:de:kobv:517-opus4-84268

The *Swift* monitoring of the colliding wind binary WR 21a

Y. Sugawara[1], Y. Tsuboi[1], Y. Maeda[2], A. M. T. Pollock[3], & P. M. Williams[4]
[1] *Chuo University, Japan*
[2] *Institute of Space and Astronautical Science, Japan Aerospace Exploration Agency, Japan*
[3] *University of Sheffield, The United Kingdom*
[4] *Royal Observatory Edinburgh, The United Kingdom*

The X-ray observations of the colliding wind binary WR 21a is reported. The first monitoring performed by *Swift*/XRT in order to reveal the phase-locked variation. Our observations cover 201 different epochs from 2013 October 1 to 2015 January 30 for a total exposure of about 306 ks. It is found for the first time that the luminosity varies roughly in inverse proportion to the separation of the two stars before the X-ray maximum but later drops rapidly toward periastron.

1 Introduction

Colliding wind binary is the best testing ground for plasma shock physics, because plasma properties vary with binary separations. WR 21a is one of the X-ray brightest colliding wind binaries ($e = 0.64$, $P_{\rm orb}$ =31.673 d). These masses are estimated to be $M_{\rm WR} > 87 M_\odot$ (one of the most massive stars) and $M_{\rm O} > 53 M_\odot$ (Niemela et al. 2008).

2 Observation & Results

We requested a target of opportunity (ToO) monitoring with *Swift*. Our observations cover 201 different epochs from 2013 October 1 to 2015 January 30 for a total exposure of about 306 ksec. We used the XRT data products generator (Evans et al. 2009). We found the phase-locked X-ray variation of WR 21a for the first time (Fig. 1).

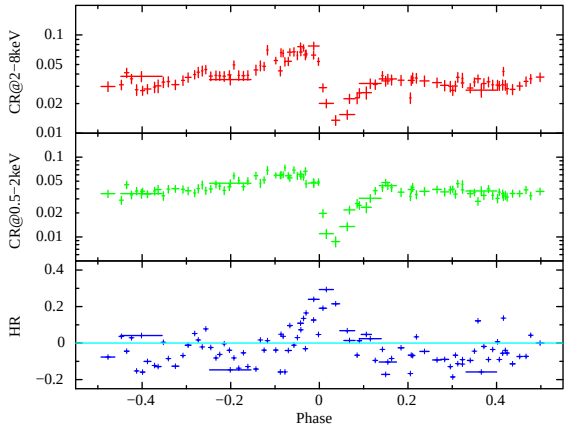

Fig. 1: X-ray light curves. Top: 2–8 keV band. Middle: 0.5–2 keV band. Bottom: Hardness ratio.

According to Stevens et al. (1992), the wind momentum flux ratio affects the intrinsic X-ray luminosity of the colliding wind zone. The solid line of Fig. 2 shows this relation. A part of the X-ray flux drop near the periastron could be explained the change of the plasma shape and occultation by WR star. In addition, the flux difference between pre-periastron and post-periastron could be explained each moving velocity (the difference of wind momentum).

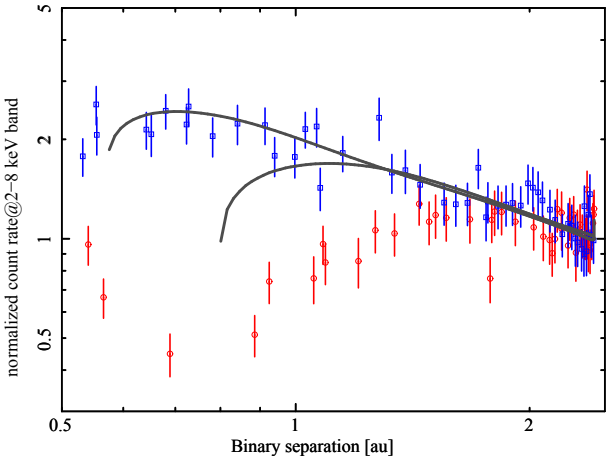

Fig. 2: The separation-luminosity relation of WR 21a. Blue and red shows the pre-periastron data and the post-periastron data, respectively. The black line shows the luminosity relation based on wind momentum ratio.

References

Evans, P. A., Beardmore, A. P., Page, K. L., et al. 2009, MNRAS, 397, 1177
Niemela, V. S., Gamen, R. C., Barbá, R. H., et al. 2008, MNRAS, 389, 1447
Stevens, I. R., Blondin, J. M., & Pollock, A. M. T. 1992, ApJ, 386, 265

From left to right: S. Beradze, D. Calderón Espinoza, A. Gormaz-Matamala, and J.M. Bestenlehner


R. Ignace


G. Kanarek


J. Bibby


N. Kochiashvili


Y. Sugawara

O. Maryeva (l.) and S. Srivastava

J. Reyes Iturbide

S. Ramírez Alegría

S. Ro

M. Steinke

Author Index

A
Aldoretta, E. J., 71, 75
Amorín, R., 341
Arthur, S. J., 315, 333

B
Ballone, A., 356
Barblan, F., 183
Becker, A., 47, 51
Beradze, S., 353, 360
Bestenlehner, J. M., 189, 201, 354
Bibby, J., 355
Bomans, D. J., 47, 51
Bonanos, A., 121
Bonatto, C., 97
Borissova, J., 97, 362
Bouret, J.-C., 97
Bray, J., 177
Brinchmann, J., 55
Burkert, A., 356

C
Calderón, D., 356
Carballo-Bello, J. A., 362
Charlot, S., 233
Chené, A.-N., 97, 357, 362
Cherchneff, I., 269
Chu, Y.-H., 333
Clark, J. S., 105
Clementel, N., 163
Conti, P. S., 347
Corcoran, M. F., 159, 309
Crowther, P. A., 21, 55, 105, 355
Cuadra, J., 309, 356
Curé, M., 357

D
de Koter, A., 109
de la Fuente, D., 113
de Mink, S. E., 109
Dessart, L., 245
Drissen, L., 355
Durret, F., 55
Dwarkadas, V. V., 329

E
Eggenberger, P., 183, 229
Ekström, S., 183, 229
Eldridge, J. J., 177, 197, 233
Esteban, C., 325
Evans, C. J., 189
Eversberg, T., 71, 75

F
Faherty, J., 359
Falceta-Gonçalves, D., 289
Figer, D. F., 113
Fossati, L., 201
Franco, G. A. P., 31

G
García-Rojas, J., 325
Gayley, K., 301
Geballe, T. R., 113
Georgy, C., 183, 229
Gillessen, S., 356
Gómez-González, V. M. A., 43
Gormaz-Matamala, A. C., 357
Gosset, E., 305
Gräfener, G., 109
Grassitelli, L., 201, 241
Groh, J. H., 183, 229, 237
Gruendl, R. A., 333
Guerrero, M. A., 263, 333
Gull, T. R., 149, 163

H
Hainich, R., 117, 125, 139
Hamaguchi, K., 159, 309
Hamann, W.-R., 91, 117, 125, 139, 193, 253, 301, 365
Hendrix, T., 279
Hervé, A., 97, 357
Hill, G. M., 75, 225
Hillier, D. J., 65, 101, 113
Hirschi, R., 229
Hoffman, J. L., 85
Huenemoerder, D., 301

I
Icke, V., 163
Idan, I., 209
Iglesias-Páramo, J., 55, 59, 341
Ignace, R., 301, 358
Indebetouw, R., 337

J
Janardhan, P., 59
Janiashvili, E., 353
Johnson, K. E., 337

K
Kallman, T. R., 309
Kanarek, G., 359
Kantharia, N. G., 59
Kaper, L., 109
Kehrig, C., 55, 59
Keppens, R., 279
Kleemann, B., 51
Knapen, J. H., 71
Kochiashvili, I., 353, 360
Kochiashvili, N., 353, 360
Koenigsberger, G., 171
Kourniotis, M., 121
Kruip, C. J. H., 163
Kubátová, B., 125

Kuhn, M., 97, 362
Küker, M., 143
Kunth, D., 55
Kurtev, R., 97, 362

L
Langer, N., 109, 189, 201, 213, 241, 283
Liermann, A., 129
Lomax, J. R., 85

M
Mackey, J., 283
Madura, T. I., 163
Maeda, Y., 366
Maeder, A., 183
Manick, R., 259
Marston, A. P., 27
Maryeva, O., 361
Massey, P., 35, 101, 337
Matzner, C. D., 364
Mauerhan, J., 27
Mayya, Y. D., 43
McBride, V., 259
McClelland, L. A. S., 177, 197
Mennekens, N., 217
Mennickent, R. E., 357
Mesa-Delgado, A., 321, 325
Meynet, G., 183, 229
Miszalski, B., 259
Moffat, A. F. J., 13, 71, 75, 205, 225, 355, 359
Mohamed, S., 283
Monreal-Ibero, A., 341
Morel, T., 71
Morisset, C., 321
Moriya, T. J., 213
Morrell, N. I., 35, 101
Morris, P. W., 27, 155
Munoz, M., 225

N
Najarro, F., 113, 121
Natsvlishvili, R., 353, 360
Navarro, C., 362
Negueruela, I., 105
Neugent, K. F., 35, 101
Nichols, J., 301

O
Oskinova, L. M., 295, 301, 358, 365
Owocki, S. P., 309

P
Paardekooper, J.-P., 163
Pablo, H., 205, 225
Pasemann, D., 117
Pasquali, A., 51
Penã, M., 321
Pérez-Montero, E., 55, 59, 341
Podsiadlowski, Ph., 283
Polcaro, V. F., 361
Pollock, A. M. T., 301, 309, 366

R
Ramiaramanantsoa, T., 71
Ramírez Alegría, S., 97, 362
Raucq, F., 189
Rauw, G., 71
Relaño, M., 341
Reyes-Iturbide, J., 363
Reyes-Pérez, J., 321
Richardson, N. D., 71, 75, 225
Ro, S., 364
Roman-Lopes, A., 31
Rosado, M., 363
Rosa-González, D., 43
Rosenberg, D., 329
Rossi, C., 361
Rosslowe, C. K., 105
Rühling, U., 117
Russell, C. M. P., 309

S
Sana, H., 109
Sander, A., 125, 139, 365
Sandin, C., 341
Sanmartin, D., 31
Sanyal, D., 109, 189, 201, 213, 241
Schartmann, M., 356
Schulz, N., 301
Shacham, T., 209
Shara, M., 355, 359
Shaviv, N. J., 209
Shenar, T., 125, 139, 193
Sokal, K. R., 337
Song, H. F., 183
Srivastava, S., 59
Stanway, E. R., 177
Steinke, M., 125, 365
St-Louis, N., 71, 75, 79
Straal, S. M., 109
Sugawara, Y., 309, 366
Szécsi, D., 189, 241

T
Teodoro, M., 71
Toalá, J. A., 333, 358
Todt, H., 125, 139, 193, 253
Tramper, F., 109
Tsuboi, Y., 366

U
Urushadze, T., 353

V
van der Hucht, K. A., 275
Van Dyk, S., 27
Vanbeveren, D., 217
Vardosanidze, M., 353, 360
Velázquez, P. F., 363
Vílchez, J. M., 55, 59, 341

Vink, J. S., 109, 133
Viotti, R., 361

W
Walsh, J. R., 341
Wang, Q. D., 309
Weis, K., 47, 51, 167
Wilde, M., 355
Williams, P. M., 275, 366
Wofford, A., 233
Wyrick, D., 97

X
Xiao, L., 177

Z
Zurek, D., 355, 359

Nearly 150 years ago, the French astronomers Charles Wolf and Georges Rayet described stars with very conspicuous spectra that are dominated by bright and broad emission lines. Meanwhile termed Wolf-Rayet Stars after their discoverers, those objects turned out to represent important stages in the life of massive stars.

As the first conference in a long time that was specifically dedicated to Wolf-Rayet stars, an international workshop was held in Potsdam, Germany, from 1.–5. June 2015. About 100 participants, comprising most of the leading experts in the field as well as as many young scientists, gathered for one week of extensive scientific exchange and discussions. Considerable progress has been reported throughout, e. g. on finding such stars, modeling and analyzing their spectra, understanding their evolutionary context, and studying their circumstellar nebulae. While some major questions regarding Wolf-Rayet stars still remain open 150 years after their discovery, it is clear today that these objects are not just interesting stars as such, but also keystones in the evolution of galaxies.

These proceedings summarize the talks and posters presented at the Potsdam Wolf-Rayet workshop. Moreover, they also include the questions, comments, and discussions emerging after each talk, thereby giving a rare overview not only about the research, but also about the current debates and unknowns in the field. The Scientific Organizing Committee (SOC) included Alceste Bonanos (Athens), Paul Crowther (Sheffield), John Eldridge (Auckland), Wolf-Rainer Hamann (Potsdam, Chair), John Hillier (Pittsburgh), Claus Leitherer (Baltimore), Philip Massey (Flagstaff), George Meynet (Geneva), Tony Moffat (Montreal), Nicole St-Louis (Montreal), and Dany Vanbeveren (Brussels).

Potsdam University Press
Online